

REPORT NO. FRA/ORD-80/19

ti

## MEASUREMENTS OF WHEEL/RAIL LOADS ON CLASS 5 TRACK

BATTELLE-COLUMBUS LABORATORIES  
505 King Avenue  
Columbus OH 43201



FEBRUARY 1980

FINAL REPORT

DOCUMENT IS AVAILABLE TO THE PUBLIC  
THROUGH THE NATIONAL TECHNICAL  
INFORMATION SERVICE, SPRINGFIELD,  
VIRGINIA 22161

Prepared for

U.S. DEPARTMENT OF TRANSPORTATION  
FEDERAL RAILROAD ADMINISTRATION  
Office of Research and Development  
Washington DC 20590

**NOTICE**

This document is disseminated under the sponsorship of the Department of Transportation in the interest of information exchange. The United States Government assumes no liability for its contents or use thereof.

**NOTICE**

The United States Government does not endorse products or manufacturers. Trade or manufacturers' names appear herein solely because they are considered essential to the object of this report.

1. Report No. FRA/ORD-80/19		2. Government Accession No.		3. Recipient's Catalog No.	
4. Title and Subtitle MEASUREMENTS OF WHEEL/RAIL LOADS ON CLASS 5 TRACK				5. Report Date February 1980	
				6. Performing Organization Code DTS-744	
7. Author(s) Donald R. Ahlbeck*, Milton R. Johnson**, Harold D. Harrison* and James M. Tuten*				8. Performing Organization Report No. DOT-TSC-FRA-80-6	
9. Performing Organization Name and Address * Battelle-Columbus      ** IIT Research Institute Laboratories                      10 West 35th Street 505 King Avenue                      Chicago IL 60616 Columbus OH 43201                      Subcontractor				10. Work Unit No. (TRAIS) RR919/R0322	
				11. Contract or Grant No. DOT-TSC-1051	
12. Sponsoring Agency Name and Address U.S. Department of Transportation Federal Railroad Administration Office of Research and Development Washington DC 20590				13. Type of Report and Period Covered Final Report Jan 1978-Dec 1978	
				14. Sponsoring Agency Code RRD-32	
15. Supplementary Notes *Under contract to: U.S. Department of Transportation Transportation Systems Center Kendall Square Cambridge MA 02142					
16. Abstract Measurements have been made on two tangent test sections and a curved test section to characterize the wheel/rail load environment on Class 5 track. The tangent-track test sections included a 3-mile length of bolted-joint rail under a 3-mile length of continuous welded rail. Wayside measurements of loads under passing revenue traffic were obtained from randomly located strain gage patterns on the rail, while an instrumented 100-ton freight car was run over the test sections at a range of speeds to define the load spectrum from the vehicle. Joint impact loads were defined from the instrumented wheelset measurements, while special wayside measurements were included to define the influence of wheel flats. Additional measurements were obtained from the on-board instrumentation over a test section that included two 6-degree, 6-inch superelevation curves. This report presents the data obtained from these measurements and describes the wayside and vehicle-borne instrumentation, the experiment design and operation, and the data reduction and analysis approach employed. Statistical summaries of the load environments are presented.					
17. Key Words Wheel/Rail Loads, Load Measurement Techniques, Flat Wheel Impact Loads, Rail Joint Impact Loads, Statistical Description of Wheel/Rail Loads			18. Distribution Statement DOCUMENT IS AVAILABLE TO THE PUBLIC THROUGH THE NATIONAL TECHNICAL INFORMATION SERVICE, SPRINGFIELD, VIRGINIA 22161		
19. Security Classif. (of this report) UNCLASSIFIED		20. Security Classif. (of this page) UNCLASSIFIED		21. No. of Pages 292	
				22. Price	

## PREFACE :

This report was prepared by Battelle's Columbus Laboratories (BCL) and IIT Research Institute (IITRI) under Contract No. DOT-TSC-1051 as part of the Improved Track Structures Research Program managed by the Transportation Systems Center (TSC). This program is sponsored by the Office of Rail Safety Research, Improved Track Structures Research Division, of the Federal Railroad Administration, Washington, D.C.

The overall objective of this contract is to apply existing data analyses and instrumentation to develop a statistical characterization of wheel/rail loads for U.S. railroads, and to evaluate strategies for the reduction of these loads. This report is the second of three prepared under this contract. The first, Report No. FRA-OR&D-76-276, published in November 1976, presented a survey of analytical and experimental methodologies for characterizing wheel/rail loads. In the third report, to be published in early 1980, an overall methodology for characterizing the wheel/rail load environment will be presented. This present report covers the field experimental phase of this contract, during which wheel/rail loads were measured both from way-side and vehicle-borne transducers under representative operational conditions. The resulting data were processed and analyzed, and results are discussed herein. A subsequent report will utilize this data to evaluate several methodologies for characterizing wheel/rail loads and evaluating load-reduction strategies for a variety of traffic and track conditions.

Mr. Donald McConnell and Dr. Herbert Weinstock of the Transportation Systems Center were technical monitors during the time period for this report. Their cooperation and suggestions are gratefully acknowledged. Ken Schueller and Don Skaggs of BCL, Ed Scharres of IITRI, and other staff members deserve recognition for their work on the measurement program. And finally, the enthusiastic cooperation of a large number of people on the Union Pacific Railroad was vital to the success of these experiments. In particular, we would like to acknowledge Dr. Paul Rhine, Charlie Johnson, and Tom Stewart on the test train, Lyle Hamm and Tom Ferguson in Engineering, and Mr. E. A. Krause, whose cooperation provided us the luxury of electrical power and track-circuit warning signals at the instrumentation van.

# METRIC CONVERSION FACTORS

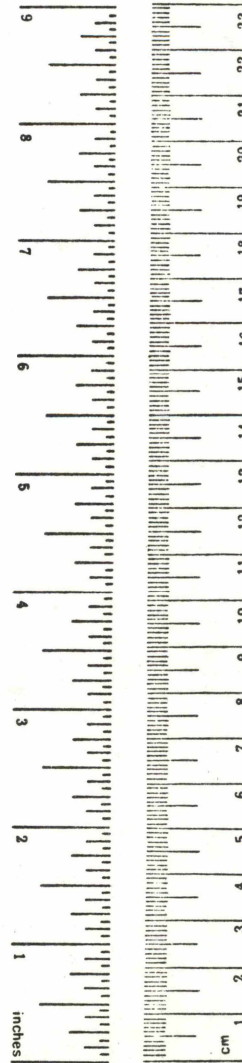
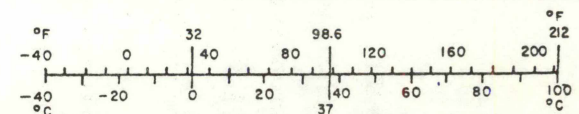
## Approximate Conversions to Metric Measures

Symbol	When You Know	Multiply by	To Find	Symbol
<b>LENGTH</b>				
in	inches	2.5	centimeters	cm
ft	feet	30	centimeters	cm
yd	yards	0.9	meters	m
mi	miles	1.6	kilometers	km
<b>AREA</b>				
in <sup>2</sup>	square inches	6.5	square centimeters	cm <sup>2</sup>
ft <sup>2</sup>	square feet	0.09	square meters	m <sup>2</sup>
yd <sup>2</sup>	square yards	0.8	square meters	m <sup>2</sup>
mi <sup>2</sup>	square miles	2.6	square kilometers	km <sup>2</sup>
	acres	0.4	hectares	ha
<b>MASS (weight)</b>				
oz	ounces	28	grams	g
lb	pounds	0.45	kilograms	kg
	short tons (2000 lb)	0.9	tonnes	t
<b>VOLUME</b>				
tsp	teaspoons	5	milliliters	ml
Tbsp	tablespoons	15	milliliters	ml
fl oz	fluid ounces	30	milliliters	ml
c	cups	0.24	liters	l
pt	pints	0.47	liters	l
qt	quarts	0.95	liters	l
gal	gallons	3.8	liters	l
ft <sup>3</sup>	cubic feet	0.03	cubic meters	m <sup>3</sup>
yd <sup>3</sup>	cubic yards	0.76	cubic meters	m <sup>3</sup>
<b>TEMPERATURE (exact)</b>				
°F	Fahrenheit temperature	5/9 (after subtracting 32)	Celsius temperature	°C

\*1 in = 2.54 (exactly). For other exact conversions and more detailed tables, see NBS Misc. Publ. 286, Units of Weights and Measures, Price \$2.25, SD Catalog No. C13.10:286.

## Approximate Conversions from Metric Measures

Symbol	When You Know	Multiply by	To Find	Symbol
<b>LENGTH</b>				
mm	millimeters	0.04	inches	in
cm	centimeters	0.4	inches	in
m	meters	3.3	feet	ft
m	meters	1.1	yards	yd
km	kilometers	0.6	miles	mi
<b>AREA</b>				
cm <sup>2</sup>	square centimeters	0.16	square inches	in <sup>2</sup>
m <sup>2</sup>	square meters	1.2	square yards	yd <sup>2</sup>
km <sup>2</sup>	square kilometers	0.4	square miles	mi <sup>2</sup>
ha	hectares (10,000 m <sup>2</sup> )	2.5	acres	
<b>MASS (weight)</b>				
g	grams	0.035	ounces	oz
kg	kilograms	2.2	pounds	lb
t	tonnes (1000 kg)	1.1	short tons	
<b>VOLUME</b>				
ml	milliliters	0.03	fluid ounces	fl oz
l	liters	2.1	pints	pt
l	liters	1.06	quarts	qt
l	liters	0.26	gallons	gal
m <sup>3</sup>	cubic meters	35	cubic feet	ft <sup>3</sup>
m <sup>3</sup>	cubic meters	1.3	cubic yards	yd <sup>3</sup>
<b>TEMPERATURE (exact)</b>				
°C	Celsius temperature	9/5 (then add 32)	Fahrenheit temperature	°F



## CONTENTS

<u>Section</u>	<u>Page</u>
1. INTRODUCTION . . . . .	1
1.1 BACKGROUND . . . . .	1
1.2 OBJECTIVES . . . . .	3
2. SUMMARY OF RESULTS AND CONCLUSIONS . . . . .	5
2.1 STATISTICAL DESCRIPTION OF WHEEL/RAIL LOADS . . . . .	5
2.2 EVALUATION OF LOAD MEASUREMENT SYSTEMS . . . . .	10
3. RESULTS OF WAYSIDE MEASUREMENTS . . . . .	13
3.1 WHEEL/RAIL LOADS . . . . .	13
3.1.1 Statistical Analysis of Wheel/Rail Loads . . . . .	13
3.1.1.1 Comparison of Measurement Sites . . . . .	22
3.1.1.2 Comparison of Tangent Track Test Sections . . . . .	27
3.1.1.3 Speed Effects on Tangent Track Sections . . . . .	27
3.1.1.4 Lateral Versus Vertical Load Statistics . . . . .	31
3.1.2 Time-Domain Analysis of Wheel/Rail Loads . . . . .	31
3.1.3 Frequency-Domain Analysis of Wheel/Rail Loads . . . . .	37
3.2 WHEEL/RAIL IMPACT LOADS . . . . .	40
3.2.1 Extended Vertical W/R Load Circuit . . . . .	40
3.2.2 Flat Wheel Impact Loads . . . . .	43
3.2.3 Rail Joint Impact Loads . . . . .	54
3.3 TRACK RESPONSE MEASUREMENTS . . . . .	56
3.3.1 Rail Joint Bolt Hole Strains . . . . .	56
3.3.2 Rail Longitudinal Strains . . . . .	58
3.3.3 Tie Plate Vertical Loads . . . . .	60
3.3.4 Track Deflections . . . . .	62
3.3.5 Track Accelerations . . . . .	64
3.3.5.1 Rail Accelerations, BJR Track . . . . .	66
3.3.5.2 Rail Accelerations, CWR Track . . . . .	66
3.3.5.3 Ground Accelerations, BJR Track . . . . .	66
4. RESULTS OF VEHICLE-BORNE MEASUREMENTS . . . . .	71
4.1 WHEEL/RAIL LOADS . . . . .	71
4.1.1 Statistical Analysis of Wheel/Rail Loads . . . . .	71
4.1.2 Frequency Domain Analysis of Wheel/Rail Loads . . . . .	84
4.1.3 Rail Joint Impact Loads . . . . .	91
4.2 COMPARISON OF W/R LOAD MEASUREMENT SYSTEMS . . . . .	97
5. COMPARISON WITH OTHER TEST DATA . . . . .	102
5.1 WAYSIDE TEST DATA . . . . .	102
5.2 VEHICLE-BORNE TEST DATA . . . . .	105
6. PILOT STUDY TEST DESCRIPTION . . . . .	108
6.1 SITE SELECTION CRITERIA . . . . .	108

## CONTENTS (Continued)

<u>Section</u>	<u>Page</u>
6.2 TEST SECTION TRACK GEOMETRY . . . . .	109
6.2.1 Selection of Test Sections . . . . .	109
6.2.2 Track Geometry Measurements . . . . .	111
6.3 INSTRUMENTED VEHICLE TEST SECTIONS . . . . .	117
6.3.1 BJR Tangent Track . . . . .	117
6.3.2 CWR Tangent Track . . . . .	118
6.3.3 Curved Track . . . . .	119
6.4 WAYSIDE TEST SECTIONS . . . . .	120
6.4.1 Rough Tangent Track . . . . .	120
6.4.2 Smooth Tangent Track . . . . .	120
6.4.3 Curved Track . . . . .	124
6.5 WAYSIDE MEASUREMENTS . . . . .	124
6.5.1 Instrumentation . . . . .	124
6.5.2 Data Acquisition System . . . . .	132
6.5.3 Test Section Layout . . . . .	135
6.5.4 Installation of Transducers . . . . .	138
6.5.5 Calibration . . . . .	138
6.5.6 Wayside Test Operations . . . . .	144
6.6 WAYSIDE DATA ANALYSIS TECHNIQUES AND FORMATS . . . . .	146
6.6.1 Time-Domain Data Analysis . . . . .	146
6.6.2 Frequency-Domain Data Analysis . . . . .	148
6.6.3 Statistical Data Analysis . . . . .	148
6.7 INSTRUMENTED VEHICLE DESCRIPTION . . . . .	156
6.8 VEHICLE-BORNE MEASUREMENTS . . . . .	156
6.8.1 Instrumentation . . . . .	156
6.8.1.1 Side Frame Vertical Load Gages . . . . .	158
6.8.1.2 Axle Bending Moment Gages . . . . .	158
6.8.1.3 Wheel Plate Strain Gage Bridges (Vertical Load) . . . . .	158
6.8.1.4 Wheel Plate Strain Gage Bridges (Lateral Load) . . . . .	163
6.8.1.5 Wheel Plate Strain Gage Bridges (Vertical Load Position) . . . . .	163
6.8.1.6 Wheel Position Indicators . . . . .	163
6.8.1.7 Accelerometers . . . . .	165
6.8.1.8 Event Marker, Correlation Switch . . . . .	165
6.8.1.9 Time Code . . . . .	165
6.8.1.10 Signal Conditioning . . . . .	165
6.8.2 Data Acquisition System . . . . .	166
6.8.3 Installation and Calibration . . . . .	167
6.9 VEHICLE-BORNE DATA ANALYSIS TECHNIQUES AND DATA FORMATS . . . . .	168
6.9.1 Vertical Load at Rail Joints . . . . .	168
6.9.2 Statistical Load Parameters From Instrumented Wheel . . . . .	169
6.9.3 Load Parameters From Instrumented Side Frames and Axles . . . . .	169
6.9.4 Mean Square Spectral Density . . . . .	173

## CONTENTS (Continued)

<u>Section</u>	<u>Page</u>
6.9.5 Data Formats . . . . .	173
7. EVALUATION OF LOAD MEASUREMENT SYSTEMS . . . . .	175
7.1 WAYSIDE INSTRUMENTATION ERROR ANALYSIS . . . . .	175
7.1.1 Lateral Load Measurements . . . . .	175
7.1.2 Vertical Load Measurements . . . . .	179
7.1.3 Extended Vertical Load Circuits . . . . .	181
7.2 VEHICLE-BORNE INSTRUMENTATION ERROR ANALYSIS . . . . .	183
7.3 COMPARISON OF WAYSIDE AND VEHICLE-BORNE MEASUREMENTS . . . . .	185
7.4 RECOMMENDATIONS FOR IMPROVED INSTRUMENTATION . . . . .	190
7.4.1 Wayside Instrumentation . . . . .	190
7.4.2 Vehicle-Borne Instrumentation . . . . .	191
APPENDIX A - STATISTICAL ANALYSIS OF WHEEL/RAIL LOAD DATA . . . . .	193
APPENDIX B - FREQUENCY OF EXCEEDANCE CURVES COMPARING VARIATIONS IN WHEEL/RAIL LOAD MEASUREMENTS AMONG WAYSIDE MEASUREMENT SITES . . . . .	229
APPENDIX C - FREQUENCY OF OCCURRENCE OF LATERAL LOAD AND L/V RATIO VERSUS VERTICAL LOAD, WAYSIDE DATA . . . . .	233
APPENDIX D - FREQUENCY ANALYSIS OF VEHICLE-BORNE WHEEL/RAIL LOAD DATA .	236
APPENDIX E - VEHICLE-BORNE INSTRUMENTATION ERROR ANALYSIS . . . . .	247
APPENDIX F - REPORT OF NEW TECHNOLOGY . . . . .	274
REFERENCES . . . . .	275

## ILLUSTRATIONS

<u>Figure</u>	
3-1.	Variation in Vertical W/R Load Statistics Among Individual Measurement Sites, All Traffic, All Speeds, Tangent BJR Track . . . . . 18
3-2	Peak Lateral W/R Load Statistics for All Traffic, All Speeds, All Measurement Sites (0.6 Kip Load Interval) . . . . . 19
3-3	Peak Vertical W/R Load Statistics for All Traffic, All Speeds, All Measurement Sites (1.2 Kip Load Interval) . . . . . 20

# ILLUSTRATIONS (Continued)

<u>Figure</u>		<u>Page</u>
3-4	Peak L/V Ratio Statistics for All Traffic, All Speeds, All Measurement Sites (0.03 Ratio Interval) . . . . .	21
3-5	Vertical W/R Load Statistics at Two Different Measurement Sites Versus Speed, 100-Ton Freight Cars, Tangent BJR Track . .	25
3-6	Lateral W/R Load Statistics for Tangent Track Test Sections, All Measurement Sites, Empty (<40T GWT) Cars Versus Speed . . .	28
3-7	L/V Ratio Statistics for Tangent Track Test Sections, All Measurement Sites, Empty (<40T GWT) Cars Versus Speed . . . . .	29
3-8	Vertical W/R Load Statistics for Tangent Track Test Sections, All Measurement Sites, 100-Ton Freight Cars Versus Speed . . .	30
3-9	Exceedance Curves for Lateral Versus Vertical Wheel Load, Tangent BJR Track, All Traffic, All Speeds, All Measurement Sites Within Test Section . . . . .	32
3-10	Exceedance Curves for Lateral Versus Vertical Wheel Load, Tangent CWR Track, All Traffic, All Speeds, All Measurement Sites in Test Section . . . . .	33
3-11	Frequency of Exceedance Curves for L/V Ratio Versus Vertical Wheel Load, Tangent BJR Track, All Traffic, All Speeds, All Measurement Sites in Test Section . . . . .	34
3-12	Frequency of Exceedance Curves for L/V Ratio Versus Vertical Wheel Load, Tangent CWR Track, All Traffic, All Speeds, All Measurement Sites . . . . .	35
3-13	Slow Roll-By of Locomotive Axles, Test Section 2 (CWR Track), Showing Vertical Wheel/Rail Loads at Site 3 -- Trailing Truck of 8-Axle DD-35 Locomotive Unit, Westbound . . . . .	36
3-14	Vertical W/R Load Frequency Spectra (PSD) for Typical Freight Train, 68 MPH, CWR Track . . . . .	38
3-15	Vertical W/R Load Frequency Spectrum (PSD) for Typical Freight Train, 64 MPH, Long Measurement Zone at Instrumented Rail Joint . . . . .	39
3-16	Slow Roll-By of Test Train Locomotive (Backing Westbound) Showing Vertical Wheel and Tie Plate Loads at Site 3, Test Section 1 (BJR Track) . . . . .	41

# ILLUSTRATIONS (Continued)

<u>Figure</u>		<u>Page</u>
3-17	Slow Roll-By of Test Car (Backing Westbound) Showing Vertical Wheel Loads and Tie Plate Loads at Site 3, Test Section 1 (BJR Track) . . . . .	42
3-18	Examples of Wheel/Rail Loads Under Normal and Flatted Wheels at Short Measurement Sites, Smooth Tangent Track, Westbound Freight Train at 46 MPH . . . . .	44
3-19	Flat Wheel Impact Within Vertical Continuous Measurement Zone -- Test Section 2, (CWR Track), Adjacent Trucks of 100-Ton Covered Hopper Cars in Wheat Unit Train at 46 MPH . . . . .	45
3-20	Flat Wheel Impact Within Vertical Continuous Measurement Zone -- Test Section 2 (CWR Track), Adjacent Trucks of 100-Ton Hopper Cars, Westbound Train at 40 MPH . . . . .	47
3-21	Frequency of Exceedance of Dynamic Load Increment by Vehicle Categories, All Speeds . . . . .	48
3-22	Percent Wheels From Total Population Generating Dynamic Load Increments Above Given Cut-Off Level . . . . .	49
3-23	Vertical Wheel/Rail Loads Under Instrumented Truck of Test Car (100-Ton Hopper Car), Eastbound at 65 MPH With High-Frequency Wheel Trailing, Test Section 1 (BJR Track), Measurement Site 3 . . . . .	55
3-24	Example of Bolt Hole Strains and Wheel Load at Instrumented Joint, Test Section 1 (BJR Track), Lead Truck of Trailing 8-Axle (DDA-40X) Locomotive Unit, Westbound at 68 MPH . . . . .	59
3-25	Wheel Loads, Longitudinal Strains, and Deflections of Rail During Slow Roll-By of Lead Truck of Locomotive, Test Section 1 (BJR), Site 6 . . . . .	61
3-26	Rail Force/Deflection Curves From Calibration of Wheel/Rail Load Circuits on Tangent Track Sections . . . . .	63
3-27	Rail Vertical Acceleration Power Spectral Density, BJR Track Under Mixed Freight, 60 MPH (10 Averages, 800-Hz Bandwidth) . . . . .	67
3-28	Rail Vertical Acceleration Power Spectral Density, CWR Track Under Mixed Freight, 60 MPH (10 Averages, 800-Hz Bandwidth) . . . . .	68
3-29	Rail Vertical Acceleration Power Spectral Density, CWR Track Under Mixed Freight, 60 MPH (25 Averages, 3200-Hz Bandwidth) . . . . .	69

# ILLUSTRATIONS (Continued)

<u>Figure</u>		<u>Page</u>
3-30	Ground Vertical Acceleration Linear Spectrum, 10 Ft From Centerline of BJR Track Under Empty Unit Train, 48 MPH (20 Averages, 100-Hz Bandwidth) . . . . .	70
4-1	Frequency-of-Exceedance Plots for Vertical Wheel Load From Instrumented Wheel, Tangent BJR Track . . . . .	72
4-2	Frequency-of-Exceedance Plots for Lateral Wheel Load From Instrumented Wheel, Tangent BJR Track . . . . .	73
4-3	Frequency-of-Exceedance Plots for Vertical Wheel Load From Instrumented Wheel, Tangent CWR Track . . . . .	74
4-4	Frequency-of-Exceedance Plots for Lateral Wheel Load From Instrumented Wheel, Tangent CWR Track . . . . .	75
4-5	Frequency-of-Exceedance Plots for Lateral Wheel Load From Instrumented Wheel, Low Rail of 6°00' Curve (6" Superelevation) . . . . .	78
4-6	Frequency-of-Exceedance Plots for Lateral Wheel Load From Instrumented Wheel, High Rail of 5°59' Curve (6" Superelevation) . . . . .	79
4-7	Frequency-of-Exceedance Plots of Lateral Wheel Load From Axle/Side Frame (Low-Frequency) Measurement System Through 6° Curves . . . . .	83
4-8	Frequency Analysis of Vertical Wheel Load, Data From Instrumented Wheel, Trailing Axle of Trailing Truck . . . . .	85
4-9	Frequency Analysis of Lateral Wheel Load, Data From Instrumented Wheel, Trailing Axle of Trailing Truck . . . . .	88
4-10	Frequency Analysis of Vertical Side Frame Force, Westbound (Leading Truck) Runs . . . . .	89
4-11	Frequency Analysis of Vertical Side Frame Force, Eastbound (Trailing Truck) Runs . . . . .	90
4-12	Vertical Wheel Load Record From Instrumented Wheel for 65 MPH Eastbound Run Over BJR Track . . . . .	92
4-13	Frequency of Occurrence of Peak Vertical Wheel Load Due to Joint Impact Versus Train Speed, 100-Ton Freight Car, Trailing Axle, Trailing Truck . . . . .	94

# ILLUSTRATIONS (Continued)

<u>Figure</u>		<u>Page</u>
4-14	Vertical Wheel Load on Instrumented 100-Ton Hopper Car Traversing Rail Joint #50, Eastbound (Trailing Axle), 55 MPH . .	95
4-15	Vertical Wheel Load on Instrumented 100-Ton Hopper Car Traversing Rail Joint #50, Eastbound (Trailing Axle), 65 MPH . .	96
4-16	Representative Wheel/Rail Load Time Histories From High- Frequency Wheel (Leading, South Rail), 35 MPH Westbound Run of Test Train, Tangent BJR Test Section . . . . .	98
4-17	Comparison of High-Frequency Wheel and Low-Frequency System Loads, 35 MPH Westbound Test Run (Instrumented Wheel Leading) Through Tangent BJR Test Section . . . . .	99
4-18	Comparison of Two Lateral Load Measurement Systems at Transient Load Condition, 6°00.4' Curve, Eastbound at 25 MPH . . . . .	101
5-1	Comparison of Vertical Wheel/Rail Load Distributions From Pilot Study With Data Available From Other Sources . . . . .	103
5-2	Comparison of Lateral Wheel/Rail Load Distributions From Pilot Study With Data Available From Florida East Coast Concrete Tie Study . . . . .	104
5-3	Comparison of Vertical Wheel Load Spectra From Pilot Study With 1976 Wheel Stress Study, Operation on UPRR Track at Speeds > 60 MPH . . . . .	106
6-1	Comparison of Average Track Surface Profile Geometry Spectra From BJR and CWR Sections . . . . .	112
6-2	Comparison of Track Crosslevel Geometry Spectra From BJR and CWR Sections . . . . .	113
6-3	Comparison of Track Gage Geometry Spectra From BJR and CWR Sections . . . . .	114
6-4	Comparison of Track Curvature Geometry Spectra From BJR and CWR Sections . . . . .	115
6-5	Track Average Surface and Cross Level Through Trackside Test Section 1, Rough Tangent Track, M.P. 292.4 . . . . .	121
6-6	View of Rough Tangent Test Section (MP 292.4) . . . . .	122

## ILLUSTRATIONS (Continued)

<u>Figure</u>		<u>Page</u>
6-7	Track Average Surface and Cross Level Through Trackside Test Section 2, Smooth Tangent Track, M.P. 207.9 . . . . .	123
6-8	View of Smooth Tangent Test Section (MP 207.9) Looking Toward the West . . . . .	125
6-9	Track Average Surface and Cross Level Through Trackside Test Section 3, Curved Track, M.P. 350.1 . . . . .	126
6-10	View of Curved Track Test Section (MP 350.1) . . . . .	127
6-11	Strain Gage Circuits for Measuring Lateral and Vertical Wheel/Rail Loads . . . . .	129
6-12	Layout of Wheel/Rail Load Transducers for Different Wayside Test Sections . . . . .	130
6-13	Rail Joint Bolt Hole Strain Gages at Site 3, Test Section 1 (South Rail) . . . . .	131
6-14	Location of Longitudinal Strain Gages on Rail, Site 6, Test Sections 1 and 2 . . . . .	131
6-15	Wayside Measurement System Components . . . . .	134
6-16	Layout of Measurement Sites Within Test Sections . . . . .	136
6-17	Typical Installation of Vertical and Lateral Wheel/Rail Load Measurement Gage Patterns . . . . .	139
6-18	View of Load Cell Tie Plates During Installation at Instrumented Rail Joint . . . . .	140
6-19	Calibration Head With Load Cells Used for Field Calibration of Strain Gage Patterns . . . . .	141
6-20	Example of X-Y Plot of Strain Gage Circuit Output Versus Calibration Load Input (From Load Cell), Wheel/Rail Load Study Field Experiments . . . . .	143
6-21	Typical Page from Field Data Log Book . . . . .	145
6-22	Example of Lateral and Vertical Wheel/Rail Loads Generated at Short Measurement Site (Site 5), Smooth Tangent Track (CWR), Westbound Freight Train at 67 MPH . . . . .	147

# ILLUSTRATIONS (Continued)

<u>Figure</u>		<u>Page</u>
6-23	Vertical Wheel/Rail Loads Under Lead Truck of Test Train Locomotive (GP-30), Eastbound at 65 MPH, Test Section 1 (BJR Track), Site 3 . . . . .	149
6-24	Power Spectrum of Rail Acceleration Under Locomotive Units, 60 MPH, Bolted-Joint Rail at Midspan . . . . .	150
6-25	Analog/Digital Data Conversion System . . . . .	152
6-26	Data Processing on CDC 6500 Digital Computer System . . . . .	153
6-27	Example of W/R Load Statistical Curves . . . . .	154
6-28	Transducer Placement on Test Truck . . . . .	160
6-29	Truck Side Frames Strain-Gaged for Vertical Load Measurements (Low-Frequency System) . . . . .	161
6-30	Diagram of Instrumented Wheel/Axle Set Showing Positions of Axle Bending Moment Bridges $M_L$ and $M_R$ . . . . .	162
6-31	Vertical Load Measurement Strain-Gage Bridge . . . . .	164
6-32	Lateral Load Measurement Strain-Gage Bridge . . . . .	164
7-1	Comparison of High-Frequency Wheelset Data With Wayside Data, Vertical Wheel Load at Site 3, 65 MPH Test Run . . . . .	189
B-1	Variations in Vertical W/R Load Statistics Among Measurement Sites, All Traffic, All Speeds . . . . .	230
B-2	Variations in Lateral W/R Load Statistics Among Measurement Sites, All Traffic, All Speeds . . . . .	231
B-3	Variations in L/V Ratio Statistics Among Measurement Sites, All Traffic, All Speeds . . . . .	232
D-1	Frequency Analysis of Vertical Wheel Load From Instrumented Wheel, 35 MPH Eastbound (Trailing Axle) Runs . . . . .	237
D-2	Frequency Analysis of Lateral Wheel Load From Instrumented Wheel, Eastbound (Trailing Axle) Runs, 35 MPH . . . . .	238
D-3	Comparison of Frequency Analysis of Vertical Wheel/Rail Load From High-Frequency and Low-Frequency Systems, Westbound (Leading Axle) Run, 35 MPH on BJR Track Section . . . . .	239

## ILLUSTRATIONS (Continued)

<u>Figure</u>	<u>Page</u>
D-4 Comparison of Frequency Analysis of Vertical Wheel/Rail Load From High-Frequency and Low-Frequency Systems, Westbound (Leading Axle) Run, 35 MPH on CWR Track . . . . .	240
D-5 Frequency Analysis of Lateral Wheel Load From Instrumented Wheel, Westbound (Leading Axle) Runs at 35 MPH . . . . .	241
D-6 Frequency Analysis of Vertical Wheel/Rail Force From Instrumented Side Frames, Eastbound (Trailing Axle) Runs at 35 MPH . . . . .	242
D-7 Frequency Analysis of Vertical Wheel Load From Instrumented Wheel, 45 MPH Runs . . . . .	243
D-8 Frequency Analysis of Lateral Wheel Load From Instrumented Wheel, 45 MPH Runs . . . . .	244
D-9 Frequency Analysis of Vertical Wheel Load From Instrumented Wheel, Eastbound (Trailing Axle) Runs at 55 MPH . . . . .	245
D-10 Frequency Analysis of Lateral Wheel Load From Instrumented Wheel, Eastbound (Trailing Axle) Runs at 55 MPH . . . . .	246
E-1 Results from Calibration of Vertical Wheel Load Bridge . . . . .	249
E-2 Section Through Side-Frame-Pedestal/Roller-Bearing-Adapter Interface . . . . .	265

## TABLES

<u>Table</u>		
2-1 Extreme-Value Lateral Loads and L/V Ratios on Tangent Track Sections, Train Speeds $\geq$ 60 MPH . . . . .		7
2-2 Predicted Extreme-Value Vertical Wheel/Rail Load on 7-Inch Piece of Rail (Away From Joint), Mixed-Freight Traffic . . . . .		8
2-3 Summary of Peak Vertical Wheel Loads for Instrumented Hopper Car Operating Over 50 Rail Joints Through BJR Track Section, Eastbound (Trailing Axle) Runs . . . . .		9
3-1 Average Number of Data Points (Axles) Per Measurement Site . . . . .		14
3-2 Summary of W/R Load Statistics for All Traffic, All Speeds Within Test Sections (Range of Data From Individual Measurement Sites). . . . .		16

# TABLES (Continued)

<u>Table</u>		<u>Page</u>
3-3	Summary of W/R Load Statistics for All Traffic, All Speeds Within Test Sections for Individual Measurement Sites . . . . .	17
3-4	Comparison of Statistical Values for Vertical W/R Loads at Individual Measurement Sites . . . . .	24
3-5	Comparison of Statistical Values for Lateral W/R Loads at Individual Measurement Sites . . . . .	26
3-6	Parameters Describing Vertical Extreme-Value (Flat Wheel) Loads Within CWR Test Section . . . . .	52
3-7.	Comparison of Predicted and Measured Vertical W/R Load Exceedance Levels, CWR Track (All Traffic, All Speeds) . . . . .	52
3-8	Distribution of Dynamic Vertical W/R Loads and Representative Extreme Values Measured Within Extended (35") Zone. . . . .	53
3-9	Speed Effects on Vertical Dynamic Wheel/Rail Loads . . . . .	54
3-10	Comparison of Peak Vertical W/R Load at Joint Zone Vs. Midspan of Rail . . . . .	57
3-11	Track Vertical Stiffness Measurements at Individual Measurement Sites, Tangent Track Sections . . . . .	65
4-1	Statistical Summary of Wheel/Rail Load Characteristics From Vehicle-Borne Measurement Systems, Tangent Track Operation . . . . .	76
4-2	Statistical Summary of Wheel/Rail Load Data From Instrumented Wheel Through Curved Track Test Section (6°, 6" Superelevation) . . . . .	80
4-3	Comparison of High- and Low-Frequency System W/R Load Measurements Through Curved Track Test Section (6° Curve, 6" Superelevation) . . . . .	81
4-4	Rotational Frequencies Associated With 36-Inch Diameter Instrumented Wheel . . . . .	86
4-5	Maximum Vertical Rail Joint Loads for Eastbound (Trailing Axle) Runs Through BJR Tangent Section . . . . .	93
5-1	Comparison of Lateral Wheel/Rail Loads on UPRR and Fast Curved Track . . . . .	107
6-1	Comparison of Track Geometry Roughness of Candidate Test Sections (Peak-to-Peak Exceedances From Plasser Car Data) . . . . .	110

# TABLES (Continued)

<u>Table</u>		<u>Page</u>
6-2	Final Choice of Test Sections for W/R Load Measurements on Union Pacific Railroad . . . . .	110
6-3	Comparison of Track Geometry Standard Deviation Values for Rough and Smooth Tangent Track Sections . . . . .	116
6-4	Differences in Spectral Peaks Due to Harmonics of 39-Ft Rail Length for Tangent Test Sections . . . . .	116
6-5	Description of Curves Within Curved-Track Test Sections, MP 349.5-351.5 . . . . .	119
6-6	Wayside Measurement for Characterization of Wheel/Rail Loads and Track Dynamic Properties . . . . .	133
6-7	Dimensional Layout of Wheel/Rail Load Measurement Transducers on UPRR Test Sections . . . . .	137
6-8	Description of Instrumented 100-Ton Hopper Car . . . . .	157
6-9	Instrumentation Data Channels . . . . .	159
7-1	Comparative Evaluation of Lateral Wheel/Rail Load-Measuring Strain Gage Circuits . . . . .	176
7-2	Description of Physical Parameters for Lateral Wheel/Rail Load Measurement Circuits . . . . .	178
7-3	Description of Physical Parameters, Vertical Wheel/Rail Load-Measuring Circuits . . . . .	180
7-4	Summary of Vehicle-Borne Load Measurement Errors at the One-Standard-Deviation Level . . . . .	184
7-5	Comparison of Wayside and Vehicle Wheel/Rail Load Peaks at Low Rail Instrumented Site, 6° Curve, 6" Superelevation . . .	186
7-6	Comparison of Wayside and Vehicle Wheel/Rail Load Peaks Through Tangent BJR Test Section, South Rail (M.P. 292.4) . .	188
A-1	Statistical Summary of Wayside Wheel/Rail Load Data . . . . .	195
C-1	Frequency of Occurrence of Lateral Vs. Vertical W/R Load . . .	234
C-2	Frequency of Occurrence of L/V Vs. Vertical Wheel/Rail Load From Wayside Data . . . . .	235

## 1. INTRODUCTION

In support of the Federal Railroad Administration (FRA) of the U.S. Department of Transportation, the Transportation Systems Center (TSC) is conducting an Improved Track Systems Research Program. The purpose of this program is to develop engineering data and analysis techniques necessary to design and maintain railroad track with improved safety, reliability and serviceability.

The development of a systematic technique for predicting the reliability of rail and other track components is an important part of the track improvement program. A key factor for all aspects of track performance, particularly the reliability of rail and track components, is the characterization of the rail loading environment. In the context of rail flaw growth and track component fatigue, this characterization is best defined in a statistical sense.

A preliminary survey of available wheel/rail load data conducted under this contract showed that little was available in useable statistical formats. Therefore, in addition to demonstrating wheel/rail load-measuring techniques, the field experimental phase of this contract was aimed at developing wheel/rail loads in statistical formats to characterize typical revenue traffic conditions.

### 1.1 BACKGROUND

A characterization of the rail loading environment is a key factor for all aspects of improved track performance. The quantitative description of rail loads will be used as inputs to studies of cross-tie track improvement, rail stress analysis, rail reliability and failure prediction, as well as other research and testing of rail and track structural components. A preliminary characterization of the wheel/rail load environment was included in the Interim Report [1-1], using published results from a number of sources. However, these data often lack sufficient detail on the measurement conditions

or were presented in formats unsuitable for direct use to validate a load-predictive model or to analyze track strength or fatigue life. The field measurement and data reduction phase of this project was planned to fill in some of the noticeable gaps in the present wheel/rail load characterization to provide a more comprehensive description of the load environment.

Wheel/rail load data gathered during the field measurement program on the Union Pacific Railroad during February of 1978 will be used to exercise and validate the several options of a general methodology for characterizing wheel/rail loads. The purposes of this methodology [1-2] are specifically:

- a. To use an optimum combination of available information (the "data bank") and analytical procedures, along with actual wayside measurements, vehicle-borne measurements, and/or track geometry measurements to characterize the load environment for specified operating conditions over the rail route, and

- b. To estimate the effects of alternate track, vehicle, and/or operating conditions on the load environment.

These extrapolations will be used to evaluate strategies for the reduction of wheel/rail loads associated with particular modes of track degradation. The options of the methodology represent a range of possible procedures that depend upon the extent of the available data base, the feasibility of performing wayside and/or vehicle-borne measurements (including track geometry measurements), and the availability of validated analytical models with the computer facilities to apply them. The exercise of any option will require the following basic steps:

- a. A classification of track into track load categories which have similar load-producing characteristics.

- b. A classification of the traffic into vehicle classes which have similar load-producing characteristics.

- c. The definition of load statistics for a representative section of rail for each vehicle class within several speed bands and for each track load category.

d. A separate definition of load statistics for flat wheels and special track features (joints, crossings, frogs, etc.) which are treated as special track load categories.

e. A compilation of data for each track load category, including variations in traffic mix and seasonal variations.

The measurement program was planned to exercise and validate this general methodology. A description of measurement procedures and a summary of the resulting data are included in this report. The subsequent exercise and validation of the methodology will be contained in the Final Report on this project.

## 1.2 OBJECTIVES

The field measurement and data reduction phase of this project was planned to fulfill two basic objectives:

- a. To provide a comprehensive description of the wheel/rail loads to which the selected track sites and test vehicle are subjected, and
- b. To provide sufficient data to exercise and validate the several options of the methodology for characterization of the wheel/rail load environment.

Because the loads measured from the track and from the vehicle are fundamentally different in character, the specific objectives of the measurements from the two points of view are somewhat different. The primary objectives of the trackside measurements in this pilot study are:

- a. To define the statistical characteristics of wheel/rail loads and L/V ratios for revenue traffic passing the wayside sites.
- b. To determine the statistical characteristics of vertical loads due to wheel flats, and
- c. To demonstrate and evaluate the performance of the trackside measurement system.

On the other hand, the primary objectives of the vehicle-borne measurements in this pilot study are:

- a. To define the statistical characteristics of the wheel/rail loads for the instrumented vehicle operating over specific test sections constituting particular track load categories,

b. To validate several load-predictive vehicle/track models by comparing computed and measured wheel/rail loads and car body accelerations, and

c. To demonstrate and evaluate the performance of the vehicle-borne measurement system.

## 2. SUMMARY OF RESULTS AND CONCLUSIONS

### 2.1 STATISTICAL DESCRIPTION OF WHEEL/RAIL LOADS

Three different sections of wood-tie track on the Union Pacific Railroad were chosen for measurements of wheel/rail loads using both wayside and vehicle-borne instrumentation. These included two sections on the California Division, one a "rough tangent" bolted-joint rail (BJR) track section, the other a "smooth tangent" continuous-welded rail (CWR) track section located in the Mojave Desert. A third section on the Utah Division just north of Las Vegas, Nevada, contained two 6-degree curves. Each of the tangent-track sections provided three miles of relatively homogeneous track for test runs with an instrumented 100-ton hopper car. Wayside instrumentation was located at seven randomly-located sites within 900-ft subsections of each tangent-track section, and within a 600-ft subsection of one 6-degree curve.

Wheel/rail loads were recorded for all revenue traffic over a 7-day period at each tangent-track location. This included priority freight trains operating at speeds up to 79 mph. The tonnage recorded under mixed-freight traffic was approximately 0.37 million gross tons (MGT) at the BJR track location, and 0.45 MGT at the CWR track location. Due to unexpected traffic fluctuations, a significantly higher percentage of loaded 100-ton freight cars passed the CWR track location during that 7-day period, while a higher percentage of empty 100-ton cars was recorded at the BJR track location. While this produced differences in the overall load environment between BJR and CWR track, it did not affect statistical results in the specific vehicle weight subcategories which were used for direct comparisons.

Results from a track geometry survey by the Union Pacific's Plasser-built geometry car were used in choosing the specific test sections. Significant differences (roughly 2-to-1) in the number of exceedances per mile in rail surface greater than 1/4 inch and 1/2 inch were measured between the "rough" and "smooth" sections. However, track geometry measurements from a second geometry car survey did not show significant differences--in fact, the CWR track section was noticeably

rougher in terms of cross level variance, while the BJR track section was slightly rougher in surface, gage and curvature variance. Only the spectral components of the 39-ft staggered joint wavelength of the bolted-rail track showed exceptional differences from the CWR track. Both track sections were well within the Class 5 geometry limits of the Federal Track Safety Standards.

Statistical analyses of wayside wheel/rail load measurements showed only a modest spatial variation in vertical load statistics among the 7 measurement sites at each section. This variation ranged between 10 and 20 percent in vertical load at a given frequency-of-exceedance level. The major difference between the vertical load environments for the BJR and CWR track sections was due to the difference in traffic mix. There would be little difference in the vertical load environment on an "average" piece of rail in the mid-rail region, whether the track is BJR or CWR, for identical mixed-freight traffic. Response of specific types of equipment to components of the 39-ft wavelength on BJR track did cause noticeable differences in the load environment, however. Loaded 100-ton freight cars, for example, exhibited a much higher load variance on BJR track at speeds above 60 mph due to a bounce/pitch response to track geometry. However, locomotives showed higher vertical load variance at higher speeds on the CWR track.

Lateral wheel/rail loads were found to be characterized by two normal (Gaussian) distributions, one due to low-magnitude creep forces, the other due to flanging forces. The number of axles producing flanging forces ranged from 0.7 to 12.0 percent among the seven sites in the BJR section, and from 4.0 to 21.0 percent among the seven sites in the CWR section. At speeds above about 50 mph on tangent track, there was a higher incidence of truck hunting on CWR track, and this caused higher lateral loads and L/V ratios as shown in Table 2-1.

TABLE 2-1. EXTREME-VALUE LATERAL LOADS AND L/V RATIOS ON TANGENT TRACK SECTIONS, TRAIN SPEEDS  $\geq$  60 MPH

	1 Axle in 1000		Maximum Value Recorded	
	Lateral Load (kips)	L/V Ratio	Lateral Load (kips)	L/V Ratio
BJR Track Section	8.2	0.69	16.4	0.97
CWR Track Section	10.4	1.04	21.7	1.51

Lateral loads on BJR track were found to be more-or-less independent of car weight over a 10-to-40-kip range of vertical wheel loads; but on CWR track the lateral loads were noticeably higher for vertical wheel loads in the 10-to-25-kip wheel load range, probably due to hunting of TOFC/COFC flatcars on high-speed freight trains. The L/V ratios for both BJR and CWR sections were highest for the lightly-loaded and empty cars.

Flat wheel impact loads up to 104 kips were measured under revenue traffic. One 97-kip vertical impact produced a peak tie-plate load of 57 kips, or roughly 59 percent transmission of the load to the plate. Cars in the 40-to-70-ton gross weight category (mostly TOFC/COFC flatcars) showed the lowest percentage of wheel flats (2 percent), while cars under 40 tons GWT showed the highest (11 percent). Dynamic loads due to wheel flats on locomotives were observed to increase with speed. However, for freight cars the loads tended to reach a maximum in a lower speed band for the different weight categories. The highest values of flat wheel impact load were found to fall into an exponential distribution superimposed on the normal distribution representing vertical loads for the individual vehicle weight and speed categories. This provides a means for making statistical predictions of extreme-value impact loads for any desired traffic mix and operating speed. The results in Table 2-2 show the predicted loads for a 7-inch length of rail for mixed-freight traffic operating primarily in the 40 to 70 mph speed range.

TABLE 2-2. PREDICTED EXTREME-VALUE VERTICAL WHEEL/RAIL LOAD ON 7-INCH PIECE OF RAIL (AWAY FROM JOINT), MIXED-FREIGHT TRAFFIC

Frequency of Occurrence	Vertical W/R Load (kips)	Average Days Between Occurrence at 25 MGT/year
1 axle in $10^3$	49.4	0.27 days
$10^4$	63.7	2.7
$10^5$	80.0	27.0
$10^6$	96.0	270.0

One rail joint within the wayside zone was instrumented for vertical loads and bolt hole strains. In the process of installing the instrumented tie plates, the joint lost its dip and was nearly level in the unloaded condition. Vertical load measurements showed no evidence of the short duration initial impact load component (less than 1 millisecond) expected for joint dips in the 2-kHz bandwidth considered. The lower frequency component of joint dynamic load (10-20 ms in duration) due to deflection of the softer joint under load was typically up to 25 percent higher than the static wheel load for runs up to 65 mph.

Data for statistical analysis were obtained for one low-rail site on a 6-degree curve. One axle in 1000 generated a lateral load of 14 kips and an L/V ratio of 0.59 on the low rail. Consistently high lateral loads were recorded on the lead inner wheel of heavy cars and locomotives, typically in the 7 to 12-kip range, with most traffic operating slightly under the balance speed of the curve.

A 100-ton, open-top hopper car loaded with crushed rock was instrumented to measure wheel/rail loads during test runs over the three track sections. Runs at speed increments of 10 mph were made from 15 to 65 mph over both tangent-track sections, and at 5 mph increments from 15 to 35 mph over the curved-track section. Statistical analysis of the load data showed a general increase in the variance of load about the mean value with increasing speed, both for vertical and lateral loads. Load variance was substantially higher on the BJR track than on the CWR track, with the standard deviation values ranging from 10 to 20 percent higher. Low-probability, high-amplitude loads, both vertical and lateral, were noticeably higher on the BJR track.

A sequence of 50 rail joints was identified within the BJR track section, and peak wheel loads were tabulated at each joint for the instrumented hopper car operating at several different speeds. These data are summarized in Table 2-3. The static wheel load for the hopper car was 25,000 lb. Speed effects on joint impact loads are quite apparent in these results. Because of data sampling limitations, these maxima represent primarily the "P2" force component.

TABLE 2-3. SUMMARY OF PEAK VERTICAL WHEEL LOADS FOR INSTRUMENTED HOPPER CAR OPERATING OVER 50 RAIL JOINTS THROUGH BJR TRACK SECTION, EASTBOUND (TRAILING AXLE) RUNS

Train Speed (mph)	Mean of Peaks (kips)	St'd Dev of Peaks (kips)	Maximum Load Recorded (kips)	Cumulative Peak Load Level (kips)	
				95%	98%
15	28.7	2.3	39.7	32.3	39.6
25	30.4	2.9	41.2	36.7	41.0
35	30.7	3.8	42.9	38.4	42.8
45	31.5	4.5	46.7	41.4	46.7
55	33.7	7.4	66.3	50.8	66.3
65	35.6	8.8	63.3	60.0	63.3

Analysis of data from measurements through two 6-degree curves having 6-inch superelevation showed the lead inner wheel (low rail) developing the highest lateral loads at the lowest speeds--13.9 kips mean load at 15 mph, with a 1.8-kip standard deviation. Lateral loads on the lead inner wheel decreased with increasing speed, while loads on the lead outer wheel increased, so that, at approximately the balance speed of 38 mph, the lateral loads on the lead outer wheel reached 10.6 kips (1.7-kip standard deviation), and the lateral load on the lead inner wheel reached 7.5 kips (2.2-kip standard deviation). Lateral loads on the trailing wheels ranged from -1.0\* to +1.4 kips on the high rail, and from 4.2 to 3.8 kips on the low rail, for a speed range of 15 to 25 mph.

\* Positive lateral forces tend to move the rail outward from the track centerline.

In conclusion, analysis of both wayside and vehicle-borne data showed that the vertical wheel/rail load environment is similar for the mid-rail region of the BJR and for the entire CWR track under mixed freight traffic. The lateral load environment is more severe on CWR track because of the greater tendency toward severe truck-hunting oscillations. Vehicle-borne measurements on a 100-ton freight car showed that the vertical wheel load environment is statistically more severe on BJR track due to joint impact loads, and the lateral wheel load environment is more severe in response to joint-related track geometry errors.

## 2.2 EVALUATION OF LOAD MEASUREMENT SYSTEMS

Laboratory experiments were conducted with a section of rail strain-gaged in a sufficient number of locations to map the strain field. Results were used to develop an improved lateral wheel/rail load-measuring circuit with reduced sensitivity to vertical load "cross talk". The resulting "base chevron" circuit was chosen from several candidate circuits, based on overall superiority in several categories (see Table 7-1). This circuit was employed during these field experiments with good results. Based on field calibration of 15 total measurement sites, an error analysis shows a circuit sensitivity error within  $\pm 3.2$  percent, and an "uncertainty band" of  $\pm 1.2$  kips based on circuit noise, linearity and hysteresis. A worst-case cross talk error (high lateral load with a 30-kip vertical wheel load) could underestimate the actual lateral load by 1.8 kips, but the normal cross talk error should be well within  $\pm 1$  kip.

The vertical wheel/rail load-measuring circuit, which is the standard rail-web chevron circuit used by ORE experimenters, exhibits excellent linearity, low hysteresis and negligible cross talk. An error analysis based on laboratory experiments and field calibrations predicts a circuit sensitivity error within  $\pm 1$  percent, an "uncertainty band" (primarily circuit electrical noise) of  $\pm 1.7$  kips, and cross talk within  $\pm 0.5$  kips.

Unexpected problems were encountered on the curved-track location due to premature failure of the welded strain gages used for the wheel/rail load circuits. High vibration levels due to flange squeal are the suspected cause of premature fatigue failures of strain gage elements and breakdown

of the MgO dielectric. Improved strain gages using increased dielectric thickness are currently being used in locomotive evaluation tests at the Transportation Test Center, but it is not yet known whether these gages will survive sustained flange squeal on sharp curves.

A finite-element model of a railroad wheel was used to optimize (in terms of sensitivity and cross talk) the location of strain gages for measuring vertical and lateral loads on an instrumented wheel. Theoretical strain curves were verified in laboratory tests before final placement of the gages. These results were used to locate vertical load-measuring circuits that minimized cross talk due to lateral loads or changes in sensitivity due to lateral position of the vertical load. However, optimized lateral load-measuring circuits exhibited excessive cross talk error due to vertical load. To compensate for this, an additional strain gage bridge was used to determine the lateral position of the vertical load. This measurement was then used in data processing to correct the lateral load signal for the vertical cross talk error. Wheel load errors are estimated to be within  $\pm 1.0$  kip when sampled at the point of maximum sensitivity (8 times per revolution), although additional error in lateral load is possible due to the coarse sampling for cross talk/position error correction.

In addition to the instrumented wheel, a "low-frequency" load measuring system consisting of strain gage circuits on the side frames and axles was applied to the test vehicle. An error analysis showed a substantial error in the lateral load signal,  $\pm 2.5$  kips at one-standard-deviation, primarily due to variations in axle bending moment with changes in the line of action of the vertical load through the side frame/bearing adapter interface. The low-frequency system was found to also consistently underestimate the standard deviation of vertical wheel loads by as much as a 2-to-1 ratio because of the attenuation of dynamic loads transmitted from the wheel/rail interface to the instrumented axles and side frames.

Direct comparisons of wayside and vehicle-borne wheel/rail load measurements were made to evaluate the different measurement systems. At the instrumented rail joint zone on the BJR track section, high-resolution (1000 sample/second) reconstructed time histories from the wheel load measurement were compared with oscillograph traces from the wayside. These comparisons showed excellent agreement. For short-zone wayside sites, the

relatively coarse sampling rate for wheel load data (once every 1/8th wheel revolution, or every 14.1 inches) precluded an accurate comparison, particularly on the tangent track. Comparison on the curve showed the low-rail wayside site consistently reading 1 to 3 kips (up to 30 percent) lower than the lateral loads measured by the instrumented wheel. A reasonably good comparison between wayside and instrumented wheel vertical loads was noted on the curve, with error bands overlapping.

Only an indirect evaluation of the frequency range of wayside and vehicle-borne systems was possible. A frequency analysis of wayside W/R load measurements showed negligible load energy above 500 Hz. However, mass attenuation effects of the rail head should not be significant below 2 kHz. High-resolution (4000 samples/second) time histories of joint impact loads on the instrumented wheel indicate wheel plate oscillations above 500 Hz, which imply a frequency limitation on the system of about 200 Hz (i.e., the reconstructed time-histories should be filtered at this frequency to avoid erroneous plate-bending signals). Finally, the low-frequency load-measuring system shows evidence of severe attenuation of vertical loads above roughly 10 Hz, which underestimates load oscillations due to the unsprung mass/track structure resonance (typically 35 to 45 Hz), as well as the higher-frequency joint impact loads.

In conclusion, the rail strain gage circuit for measuring vertical load provides an accurate and well-defined transducer for this purpose. The rail base chevron strain gage circuit is less well understood, has more inherent error in its measurement of lateral loads, and is in need of some further development, particularly in calibration techniques. Strain gage patterns on the wheel plate provide an accurate means for measuring vertical and lateral wheel loads, providing that lateral load measurements are corrected for vertical cross talk errors due to the lateral position of vertical load. A means for processing the wheel strain gage bridge signals into a continuous, real-time measurement of vertical and lateral loads needs to be developed. Measurement of vertical and lateral wheel loads by means of strain-gaged side frames and axles is not recommended because of mass attenuation effects and excessive errors in the load calculations.

### 3. RESULTS OF WAYSIDE MEASUREMENTS

#### 3.1 WHEEL/RAIL LOADS

##### 3.1.1 Statistical Analysis of Wheel/Rail Loads

The generation of frequency-of-occurrence histograms and calculations of mean values and standard deviations for each vehicle and speed category (as discussed in Section 6.6.3) provided the base data for all subsequent data combinations. Appendix A contains a listing of mean value, standard deviation, and accuracy evaluations in terms of the confidence levels for  $\pm 10$  and  $\pm 20$  percent mean value tolerance bands, and the estimated tolerance bands at the 90 and 95 percent confidence levels, for each category of data.

A summary of the average axle count for the individual measurement sites is given in Table 3-1. This summary shows significant differences in the traffic "mix" recorded at the two tangent-track sections. Both test sections were manned for roughly a 7-day period, and both were located west of Las Vegas, with no intervening classification yards or branch lines. It is obvious, however, that substantially more heavy cars ( $\geq 110$  tons gross weight) in coal, wheat, and soda ash unit trains were recorded at the second tangent-track section. On the other hand, substantially more light cars ( $< 40$ T GWT) were recorded at the first section in the 40-49 mph speed band. Other observations on traffic mix and operating practices can be made from this table:

a. Relatively few heavy cars ( $\geq 110$ T GWT) or light cars ( $< 40$ T GWT) are run at speeds above 59 mph. Most of the fast freight trains were priority freight, consisting of flat cars with semi-trailers or containers (TOFC/COFC).

b. A disproportionate number of locomotive axles were recorded in the higher speed bands, reflecting the higher horsepower requirements of the priority freight trains.

c. Few trains were recorded at speeds under 40 mph, and a substantial portion of these data were lost for statistical analysis due to a persistent malfunctioning of wheel detectors at lower train speeds.

TABLE 3-1. AVERAGE NUMBER OF DATA POINTS (AXLES)  
PER MEASUREMENT SITE

I. Rough (BJR) Tangent Track Test Section				
	(1) 40 mph	(2) 40-49	(3) 50-59	(4) 60
(1) Locomotive	122	322	553	715
(2) Car $\geq$ 110T GWT	371	818	342	187
(3) 70T - <110T	86	883	908	1109
(4) 40T - <70T	143	815	1421	3061
(5) <40T	681	2032	4580	1653
II. Smooth (CWR) Tangent Track Test Section				
	(1) 40 mph	(2) 40-49	(3) 50-59	(4) 60
(1) Locomotive	26	365	793	799
(2) Car $\geq$ 110T GWT	77	1854	1874	174
(3) 70T - <110T	90	1222	1243	675
(4) 40T - <70T	63	1015	1960	3637
(5) <40T	30	491	4713	1426
III. Curve Track Test Section Low Rail)				
	(1) 35 mph	(2) 35 mph		
(1) Locomotive	180	256		
(2) Car $\geq$ 110T GWT	202	393		
(3) 70T - <110T	320	312		
(4) 40T - <70T	442	954		
(5) <40T	1272	848		

Few trains were recorded at speeds less than 30 mph or greater than 40 mph, so only two speed bands of approximately 5 mph width were used for curved-track data.

Data in Table 3-2 summarize the range of wheel/rail load statistics for all traffic, all speeds at the individual measurement sites within each test section. Mean values, standard deviations, and 0.1 percent load levels (the load or L/V ratio exceeded by one in 1000 axles) are recorded in this table. W/R load statistics are further expanded in Table 3-3 to show the mean value estimate, tolerance band (at the 95 percent confidence level), and standard deviation for individual measurement sites and for pooled data (all sites). Percent exceedance functions (left-hand graph) and frequency-of-occurrence histograms (right-hand graph) shown in Figure 3-1 illustrate the typical multimodal statistical functions for vertical wheel/rail loads due to the several distinct populations of vehicles in the traffic mixture. Peaks in relative frequency of occurrence can be seen near 8, 18 and 33 kips, with corresponding piecewise-linear segments (each approximating a separate Gaussian distribution) in the exceedance function. While the curve shapes are similar for individual sites, the load level for a particular exceedance probability varies over a 10 to 20 percent range. This is indicative of the effects of spatial variations in track geometry on vertical wheel/rail loads. A complete set of statistical function curves for lateral and vertical wheel/rail forces and L/V ratio for all measurement sites on the tangent track sections are given in Appendix B.

Statistical function curves for pooled data (all measurement sites within each test section) are presented in Figures 3-2 through 3-4. Exceedance curves in Figure 3-2 show that for most wheels on tangent track the lateral loads are near zero or inwardly-directed on the rail. The radical change in the slope of the curves at zero load indicates that the outwardly-directed lateral loads caused by flange contact are a distinct population which is different from the inwardly-directed forces due primarily to creep phenomena. The curves show higher lateral loads (particularly at the low-probability end of the plot) on CWR than on BJR tangent track. On the

TABLE 3-2. SUMMARY OF W/R LOAD STATISTICS FOR ALL TRAFFIC,  
ALL SPEEDS WITHIN TEST SECTIONS (RANGE OF DATA  
FROM INDIVIDUAL MEASUREMENT SITES)

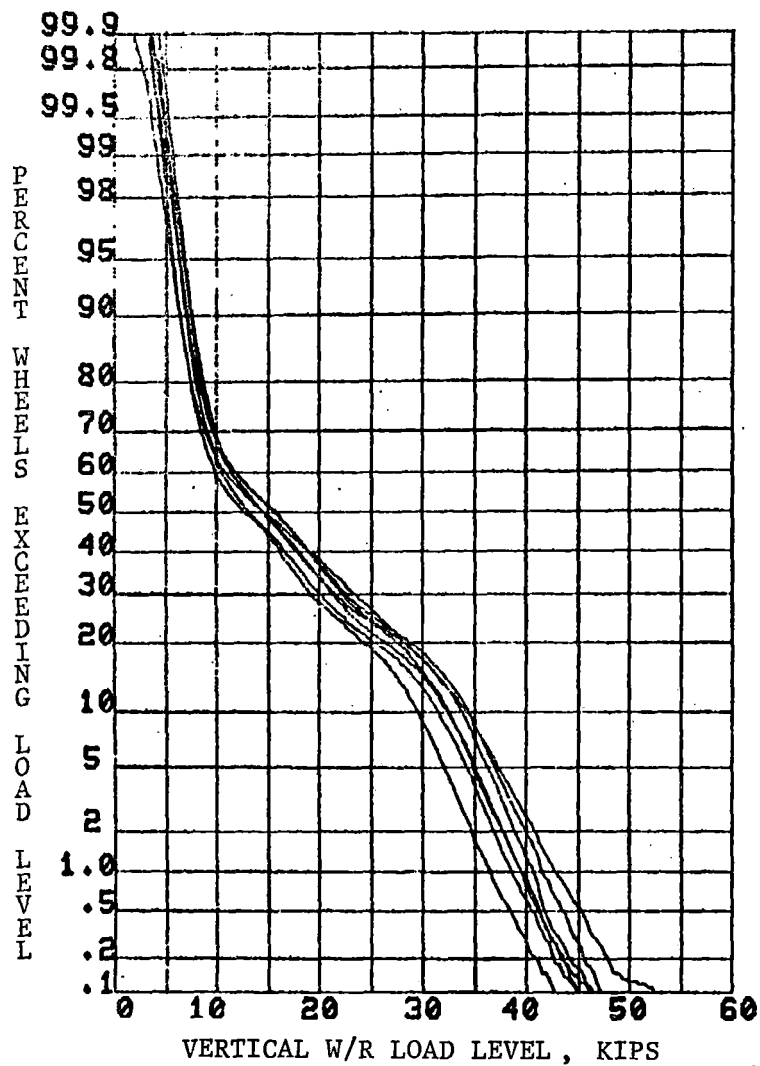
	Test Section BJR Tangent		Test Section CWR Tangent		Test Section 3 Curve, Low Rail
	Min.	Max	Min.	Max	
Lateral W/R Load*					
Mean, kips	-0.65	0.32	-0.48	0.22	2.40
Std Dev, kips	0.85	1.26	1.13	1.38	2.75
0.1% Load, kips	6.0	9.0	7.0	9.5	14
Vertical W/R Load					
Mean, kips	16.6	18.6	18.6	22.4	15.6
Std Dev, kips	8.6	10.7	9.6	11.5	8.12
0.1% Load, kips	42	53	43	53	40
L/V Ratio					
Mean	-0.044	0.014	-0.028	0.016	0.139
Std Dev	0.043	0.073	0.074	0.100	0.133
0.1% Ratio	0.37	0.63	0.55	0.80	0.59

\*Note: Positive lateral load in direction of flange contact.

TABLE 3-3. SUMMARY OF W/R LOAD STATISTICS FOR ALL TRAFFIC, ALL SPEEDS WITHIN TEST SECTIONS  
FOR INDIVIDUAL MEASUREMENT SITES

Site	Lateral, kips		Vertical, kips		L/V Ratio		No. of Data Points
	Mean (95% Tol.)	Std Dev	Mean (95% Tol.)	Std Dev	Mean (95% Tol.)	Std Dev	
Test Section 1, Rough (BJR) Tangent Track							
1	-0.649 (+2.0%)	0.939	17.9 (+0.7%)	9.41	-0.0441 (+2.0%)	0.0630	19715
2	0.315 (+5.4%)	1.26	18.2 (+0.7%)	9.88	0.0135 (+7.3%)	0.0724	21090
3	-0.327 (+4.3%)	1.01	18.2 (+0.7%)	9.63	-0.0226 (+4.1%)	0.0660	19474
4	-0.0079 (+19%)	1.15	16.4 (+0.7%)	8.58	-0.0086 (+11%)	0.0725	22547
5	0.229 (+5.2%)	0.914	18.6 (+0.7%)	10.3	0.0064 (+12%)	0.0577	22285
6	-0.535 (+2.1%)	0.849	18.3 (+0.8%)	10.7	-0.0357 (+1.6%)	0.0434	22486
7	-0.203 (+6.4%)	0.885	16.6 (+0.8%)	9.56	-0.0153 (+5.8%)	0.0606	17734
Pooled	-0.171 (+3.2%)	1.07	17.8 (+0.3%)	9.79	-0.0148 (+2.3%)	0.0658	145331
Test Section 2, Smooth (CWR) Tangent Track							
1	0.219 (+7.4%)	1.28	20.5 (+0.6%)	10.3	0.0164 (+6.7%)	0.0868	24184
2	-0.096 (+17.1%)	1.25	22.4 (+0.7%)	11.5	-0.0062 (+15.6%)	0.0739	22286
3	-0.192 (+8.4%)	1.24	18.8 (+0.7%)	9.83	-0.0147 (+8.0%)	0.0906	22717
4	0.210 (+8.5%)	1.38	18.6 (+0.7%)	9.77	0.0074 (+17.5%)	0.0995	22844
5	-0.486 (+3.1%)	1.13	20.5 (+0.7%)	10.5	-0.0267 (+3.6%)	0.0731	21946
6	-0.152 (+10.9%)	1.27	20.9 (+0.6%)	9.65	-0.0089 (+10.2%)	0.0698	22422
7	0.134 (+12.1%)	1.20	18.9 (+0.7%)	9.96	0.0059 (+21.2%)	0.0927	21043
Pooled	-0.049 (+13.0%)	1.28	20.1 (+0.3%)	10.3	-0.0036 (+11.7%)	0.0856	157442
Test Section 3, Curved Track (6°, 6" Superelevation, low rail)							
7	2.40 (+3.1%)	2.75	15.6 (+1.4%)	8.12	0.139 (+2.6%)	0.133	5179

Note: Positive lateral load in direction of flange contact.



111652 112652 113652 114652 115652 116652 117652

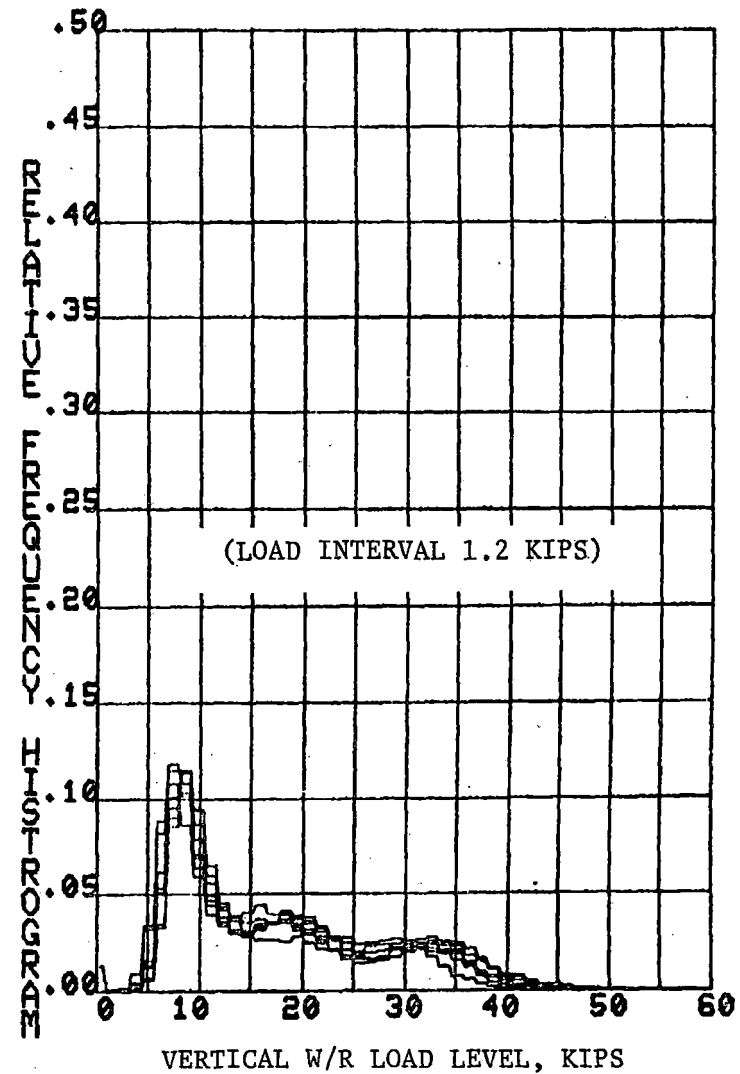
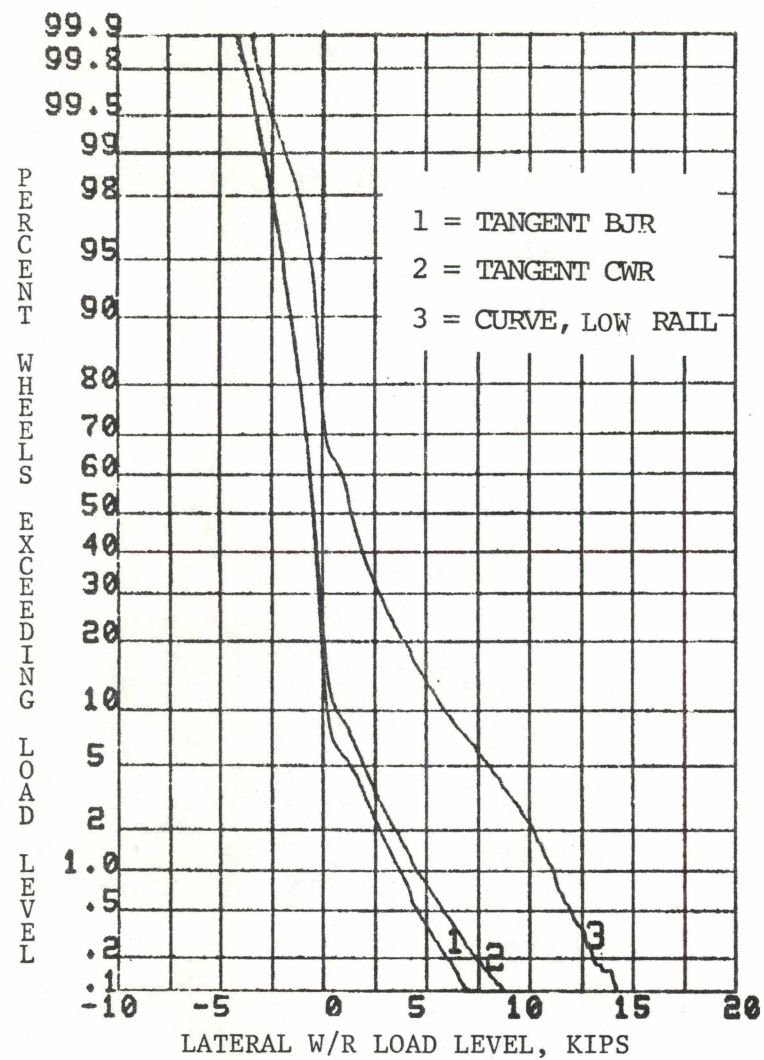


FIGURE 3-1. VARIATION IN VERTICAL W/R LOAD STATISTICS AMONG INDIVIDUAL MEASUREMENT SITES, ALL TRAFFIC, ALL SPEEDS, TANGENT BJR TRACK



118651 128651 138651

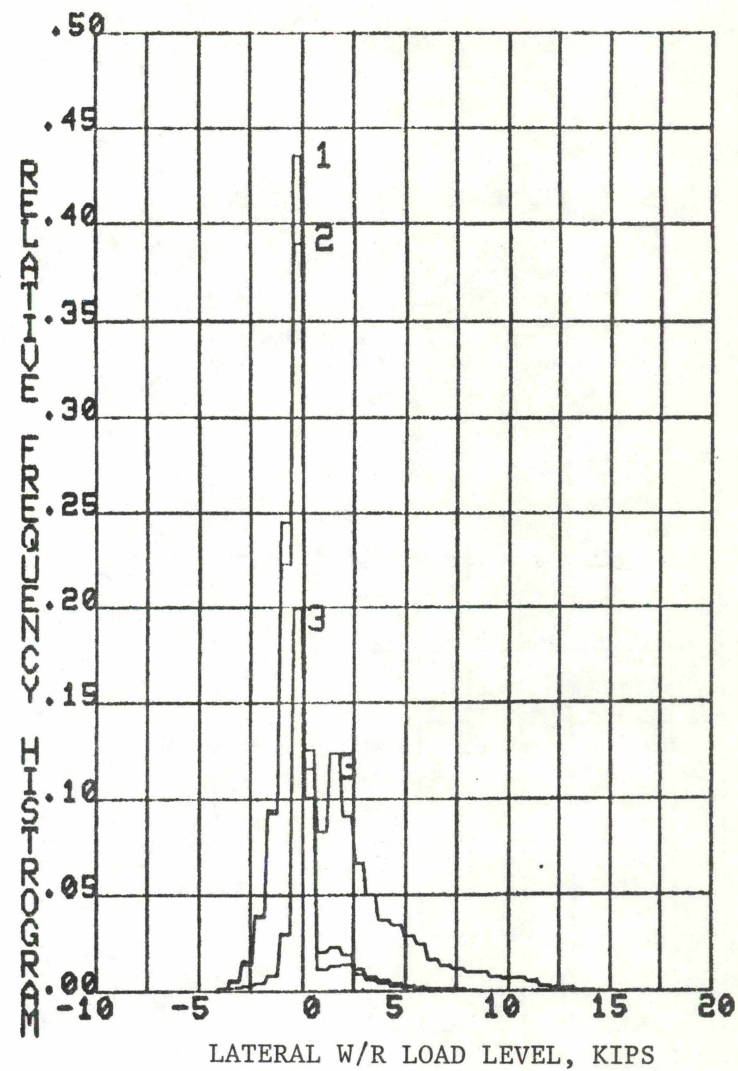


FIGURE 3-2. PEAK LATERAL W/R LOAD STATISTICS FOR ALL TRAFFIC, ALL SPEEDS, ALL MEASUREMENT SITES (0.6 KIP LOAD INTERVAL)

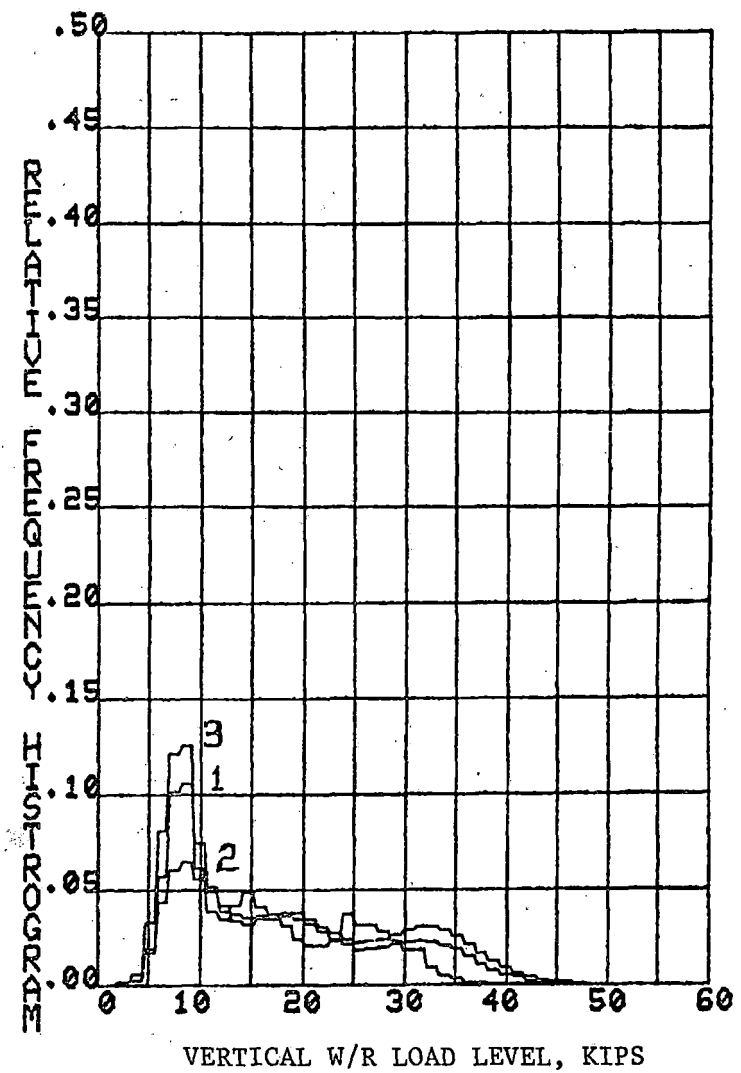
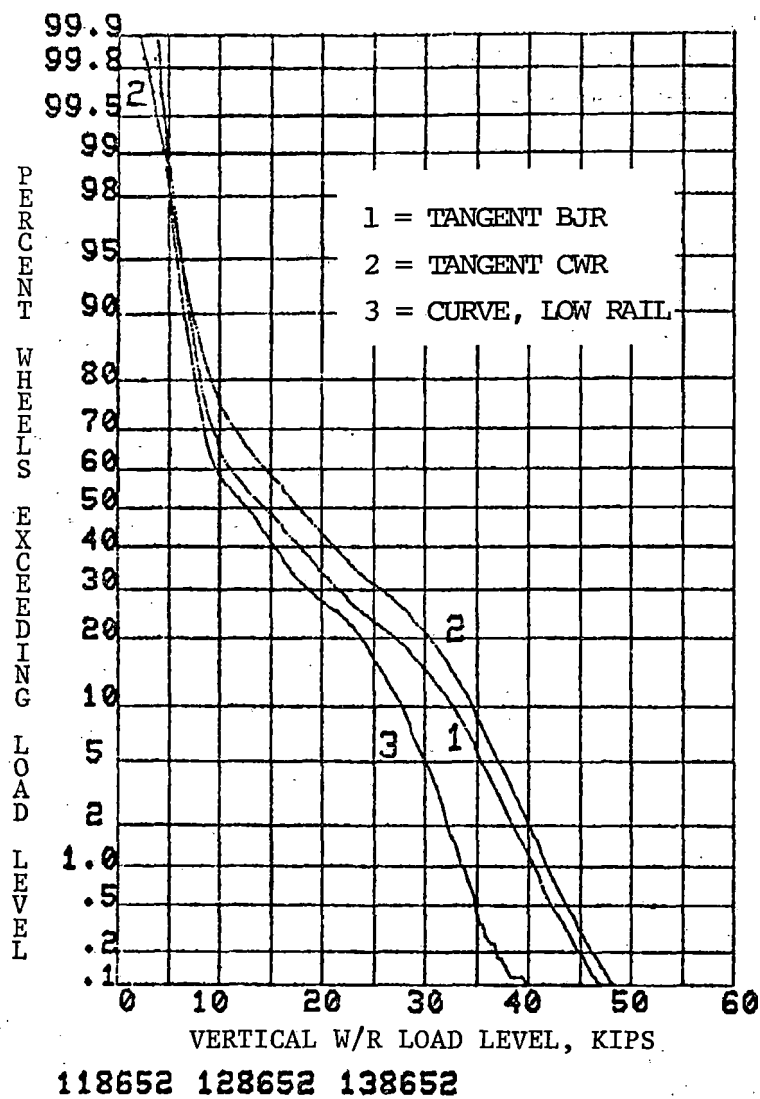
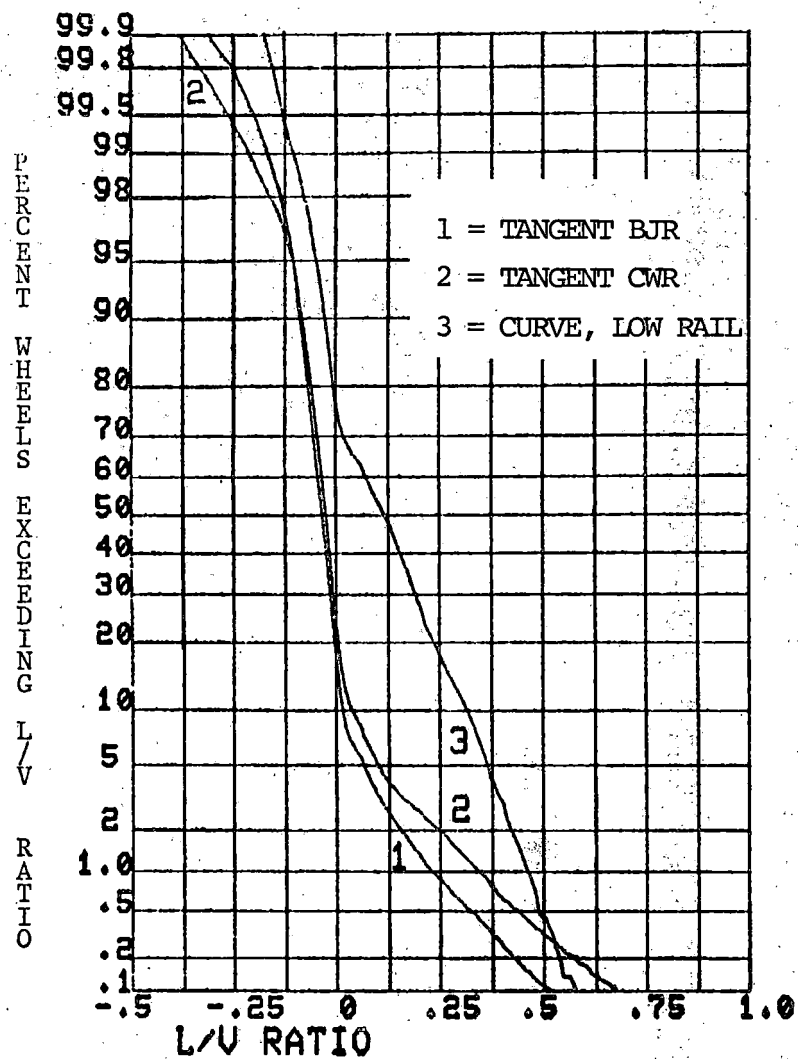


FIGURE 3-3. PEAK VERTICAL W/R LOAD STATISTICS FOR ALL TRAFFIC, ALL SPEEDS, ALL MEASUREMENT SITES (1.2 KIP LOAD INTERVAL)



118653 128653 138653

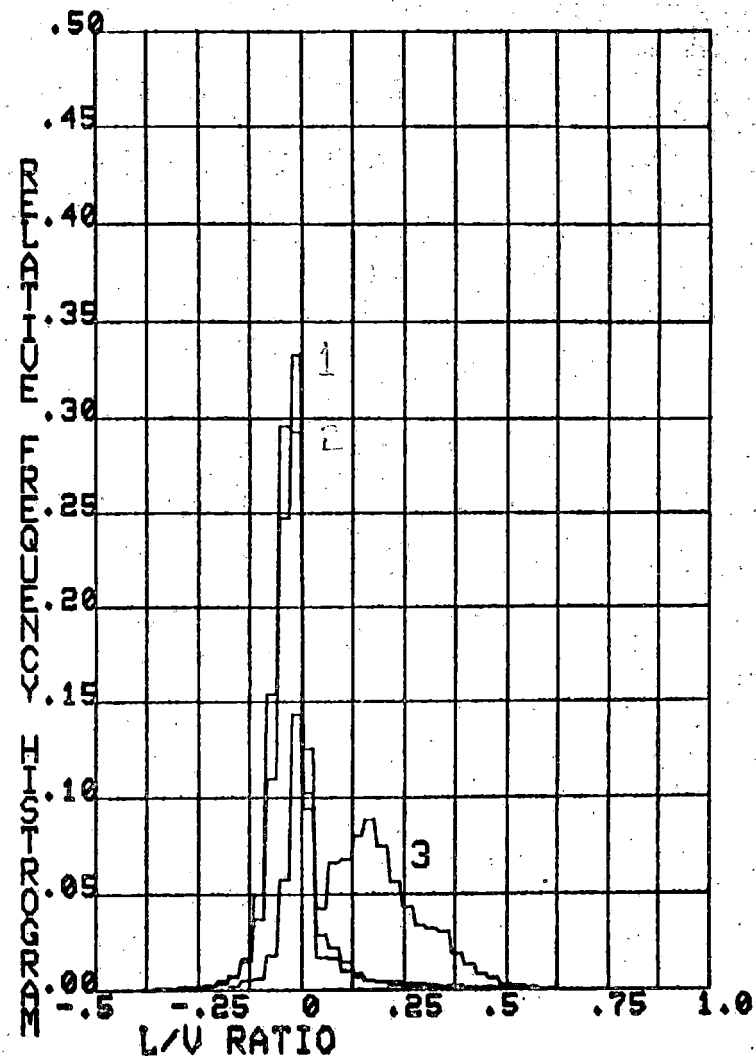


FIGURE 3-4. PEAK L/V RATIO STATISTICS FOR ALL TRAFFIC, ALL SPEEDS, ALL MEASUREMENT SITES ( 0.03 RATIO INTERVAL)

low rail in the curve, approximately 70 percent of the wheels have outwardly-directed lateral forces on the rail. Computer simulation (using BCL's steady-state curving program) shows the lead inner wheel (low rail) lateral creep force to be higher than the lead outer wheel net (flange minus creep) lateral force at below-balance speeds on a 6-degree curve. While extensive head wear was noted at this location on the high rail, the low rail showed no evidence of wear due to flanging.

Statistical data for vertical wheel/rail loads are shown in Figure 3-3 for the three test sections. As noted before, the traffic through the second (smooth tangent) section included a substantially higher number of 100-ton freight cars, which accounts for the higher loads (higher exceedance probability) of this curve. The exceedance curve for vertical load on the low rail shows an apparent shift of load to the high rail on the curve, even though the low rail showed some evidence of head crushing typical of high curvature, high superelevation. The shift is definitely speed-related, although the balance speed on this curve was calculated as 38 mph. A check of locomotive vertical wheel loads (nominally 32 kips) shows the following:

Speed = < 35 mph,	mean = 29.2,	std dev = 4.44 kips
= ≥ 35 mph,	= 27.1,	= 4.45 kips.

Curves for L/V ratio are given in Figure 3-4, and show an interesting sigmoid shape toward the negative (inwardly-directed) L/V end of the plot. This is probably due to a few hollow-worn wheels that can apply substantial lateral forces pulling the rail inward toward the track centerline. Again, a substantially higher probability of exceeding a given L/V ratio is seen for the smooth tangent (CWR) track in comparison with the rougher tangent (BJR) track, which may be attributed to a greater tendency toward hunting instabilities on the CWR track.

3.1.1.1 Comparison of Measurement Sites. One point of great interest in this experimental program is the comparison of individual measurement sites within a given test section, and the variation in loads from one site to another due to track geometry variations. The Japanese [3-1] have determined that six or more points distributed over a distance of 12.5 meters are needed to hold the error within 5 percent (at a 95 percent confidence

level) when measuring loaded freight car weights (vertical wheel loads). For this program seven measurement sites distributed within a 900-ft length were used to provide a tolerance band of less than one standard deviation for mean value estimates, and to provide data on the effects of spatial variations on load statistics.

Locomotive axles were chosen to provide a comparison of sites because of the better load equalization, consistent weight, and more-or-less uniform dynamic response of these vehicles. In addition, values for 100-ton freight cars were also tabulated. A comparison based on vertical wheel loads is given in Table 3-4. Load values from slow roll-by of the test train and of the four SD-40 units of a revenue freight train (24 axles) were examined to check the calibration of sites at Test Section 1, the BJR track. Even this slow roll-by showed a standard deviation of locomotive wheel loads of 8 to 11 percent of the mean value. Site 5 on the BJR track was noted to record loads under locomotives roughly one standard deviation higher than other sites, but to record nearly average loads under 100-ton freight cars. This difference was construed to be a track geometry effect, rather than a problem in calibration of the site.

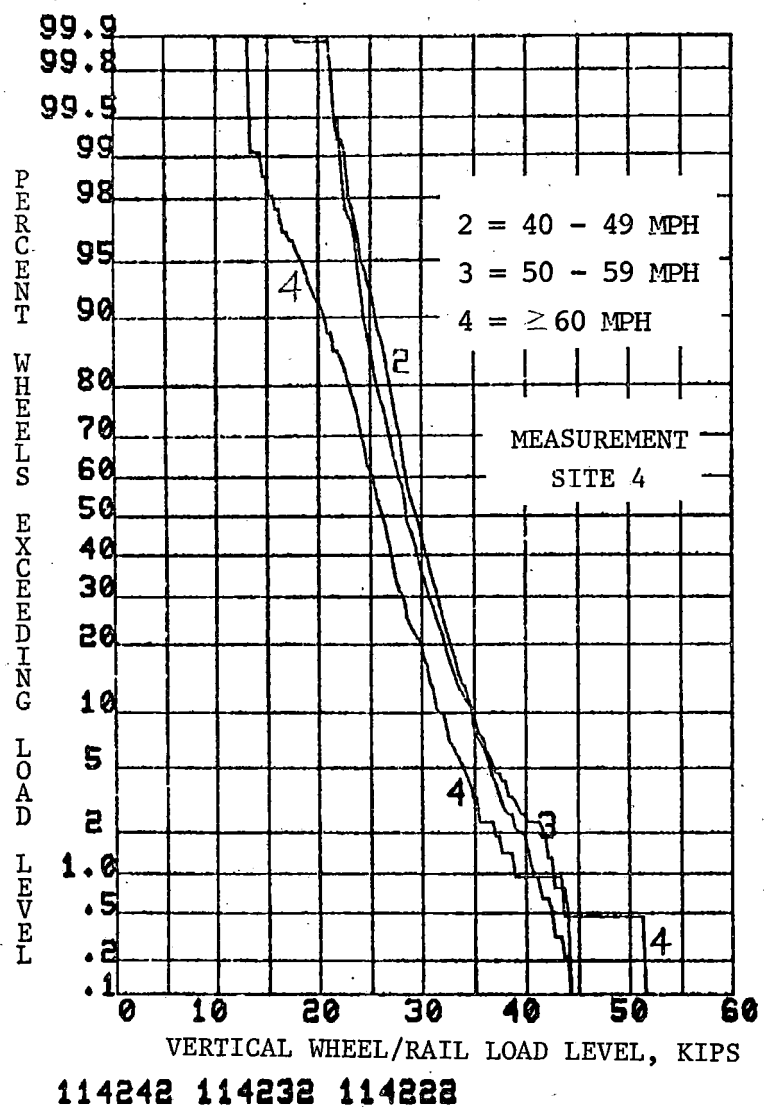
Statistical function curves comparing lateral and vertical loads and L/V ratios for all traffic, all speeds, for the different measurement sites are given in Appendix B. Track geometry variations cause rather startling differences in loads at different sites for particular vehicle categories. For example, in Figure 3-5 the vertical load exceedance curves for 100-ton freight cars in the three speed bands above 40 mph are compared for Sites 4 and 6, BJR track. Site 6 shows a strong increase in maximum vertical loads with speed, while at Site 4 the vertical loads (except for a small percentage of axles) are actually lower in the highest speed band.

Differences in lateral loads generated at the different sites are also found within the exceedance curves (see Appendix B, Figures B-1 and B-2). For example, the curves for BJR track indicate that less than one percent of the axles were "flanging" at Site 2. Lateral loads for locomotives and 100-ton freight cars are characterized by small (generally inward) mean values on the order of 1.0 kips and standard deviation values ranging from 0.6-to-2.2 kips. Comparison by sites is given in Table 3-5.

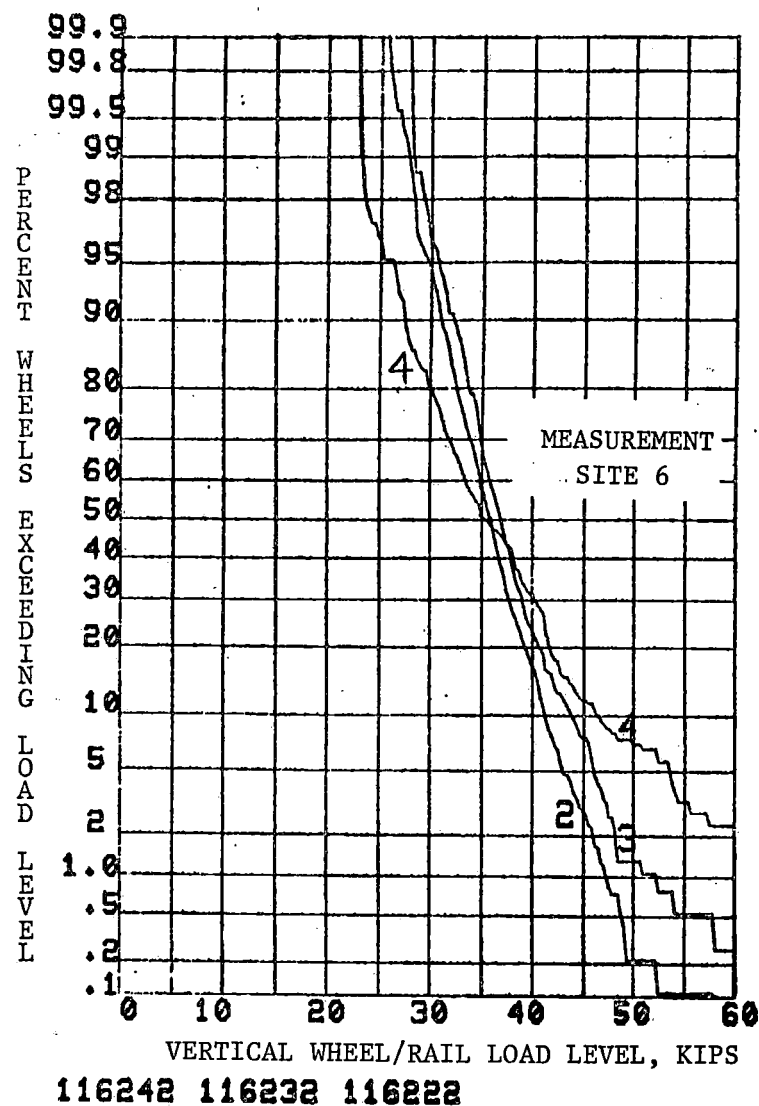
TABLE 3-4. COMPARISON OF STATISTICAL VALUES FOR VERTICAL W/R LOADS  
AT INDIVIDUAL MEASUREMENT SITES

Site	Speed (mph)	Vertical W/R Loads, kips							
		Locomotives				100T Cars			
		BJR Track		CWR Track		BJR Track		CWR Track	
		Mean	Std Dev	Mean	Std Dev	Mean	Std Dev	Mean	Std Dev
1	40-49	34.6	3.50	34.0	3.57	33.6	3.90	34.2	4.12
2		33.9	3.16	37.8	3.49	34.7	3.57	37.9	4.35
3		34.3	3.56	34.2	3.24	33.4	3.93	31.1	3.99
4		31.0	3.08	32.2	3.37	30.4	3.87	31.7	3.92
5		35.9	3.65	35.7	3.19	33.8	4.23	33.1	4.81
6		33.8	3.95	33.7	3.25	36.6	4.14	33.8	4.22
7		33.9	3.72	35.3	3.41	31.0	4.34	31.7	4.14
1	50-59	33.4	3.60	34.5	4.74	33.5	4.13	35.7	4.09
2		35.2	3.69	36.6	4.50	33.0	3.74	37.6	4.20
3		32.1	3.66	33.7	4.46	32.4	4.34	32.4	4.27
4		32.0	3.57	31.9	3.57	29.8	4.19	31.8	4.13
5		35.4	3.57	33.3	3.92	33.4	3.62	35.5	4.17
6		30.4	3.87	34.5	4.04	38.0	4.71	34.3	3.96
7		34.4	3.73	33.1	4.17	30.9	5.46	31.8	3.89
1	>60	33.8	3.80	34.1	5.40	33.8	3.92	33.7	3.82
2		34.3	4.22	37.1	4.62	31.3	5.73	37.0	4.94
3		33.0	4.07	33.2	5.00	32.5	3.41	30.7	4.47
4		31.1	4.01	32.1	4.11	26.8	4.97	29.0	4.10
5		36.1	3.99	32.0	4.74	30.1	7.65	33.5	4.97
6		33.6	5.36	35.0	4.35	37.1	7.94	31.6	4.54
7		34.1	3.66	31.3	4.26	29.1	4.97	28.9	4.47
All	<40	33.5	4.13	34.6	3.33	33.7	4.77	33.2	4.31
All	40-49	33.9	3.81	34.7	3.76	33.4	4.49	33.5	4.77
All	50-59	33.3	4.07	34.0	4.44	33.2	4.91	34.2	4.59
All	>60	33.7	4.44	33.6	5.02	31.5	6.70	31.9	5.20
All	All	33.6	4.19	33.9	4.58	33.2	4.96	33.7	4.72
Mean	*	33.6	3.78	34.1	4.07	32.6	4.58	33.2	4.27
Std Dev	*	1.56	0.45	1.75	0.64	2.72	1.22	2.54	0.33

\*Of all Sites, 3 speed bands given above equally weighted.



MEASUREMENT SITE 4



MEASUREMENT SITE 6

FIGURE 3-5. VERTICAL W/R LOAD STATISTICS AT TWO DIFFERENT MEASUREMENT SITES - VERSUS SPEED, 100-TON FREIGHT CARS, TANGENT BJR TRACK

TABLE 3-5. COMPARISON OF STATISTICAL VALUES FOR LATERAL W/R LOADS  
AT INDIVIDUAL MEASUREMENT SITES

Site	Speed (mph)	Lateral W/R Load, kips**							
		Locomotives				100T Cars			
		BJR Track		CWR Track		BJR Track		CWR Track	
		Mean	Std Dev	Mean	Std Dev	Mean	Std Dev	Mean	Std Dev
1	40-49	-1.46	0.70	-0.34	1.02	-1.18	0.89	-0.39	0.97
2		0.60	1.49	-0.05	1.23	0.53	1.60	-0.63	1.14
3		0.48	1.46	-0.27	0.90	-0.93	1.05	-0.89	0.98
4		-0.29	1.56	0.46	1.40	-0.74	1.43	-0.19	1.33
5		0.43	1.03	-0.86	0.99	0.24	0.89	-1.38	0.94
6		-0.80	0.63	-0.16	1.51	-1.60	0.87	-0.71	1.33
7		-0.69	0.81	0.34	1.35	-0.91	0.78	-0.40	1.04
1	50-59	-1.09	0.95	0.09	1.03	-1.26	0.99	-0.40	1.12
2		-0.03	1.88	0.48	1.13	0.25	1.73	-0.82	1.24
3		-0.97	1.24	-0.21	1.29	-0.91	1.17	-0.92	1.30
4		-0.21	1.74	0.55	1.49	-0.55	1.53	-0.34	1.27
5		0.22	1.10	-0.72	0.92	0.34	1.13	-1.42	1.10
6		-0.55	0.74	-0.11	1.21	-1.50	1.02	-0.88	1.27
7		-0.74	1.30	0.38	1.19	-0.75	1.08	-0.38	1.08
1	>60	-1.29	0.97	0.22	1.11	-1.09	1.44	-0.12	1.12
2		0.49	1.67	0.15	1.11	0.55	2.21	-0.28	1.29
3		-0.67	1.18	-0.25	1.11	-0.78	1.21	-1.12	2.19
4		-0.29	1.64	0.63	1.61	-0.19	1.62	0.98	1.59
5		0.54	1.16	-0.62	1.15	0.23	1.15	-0.91	1.35
6		-0.63	0.71	0.12	1.63	-1.69	1.45	-0.71	1.13
7		-0.60	1.33	0.59	1.23	-0.45	1.09	-0.03	1.05
All	<40	-0.55	1.39	-0.08	1.35	-1.17	1.30	-0.61	0.88
All	40-49	-0.36	1.33	-0.13	1.28	-0.65	1.32	-0.65	1.17
All	50-59	-0.45	1.41	0.00	1.25	-0.60	1.45	-0.74	1.25
All	60-69	-0.34	1.41	0.12	1.36	-0.50	1.64	-0.41	1.48
All	All	-0.40	1.40	0.22	1.31	-0.74	1.40	-0.68	1.22
Mean	*	-0.36	1.20	0.02	1.22	-0.59	1.25	-0.57	1.23
Std Dev	*	0.63	0.38	0.44	0.21	0.71	0.35	0.53	0.27

\*Of all Sites, 3 speed bands given above equally weighted.

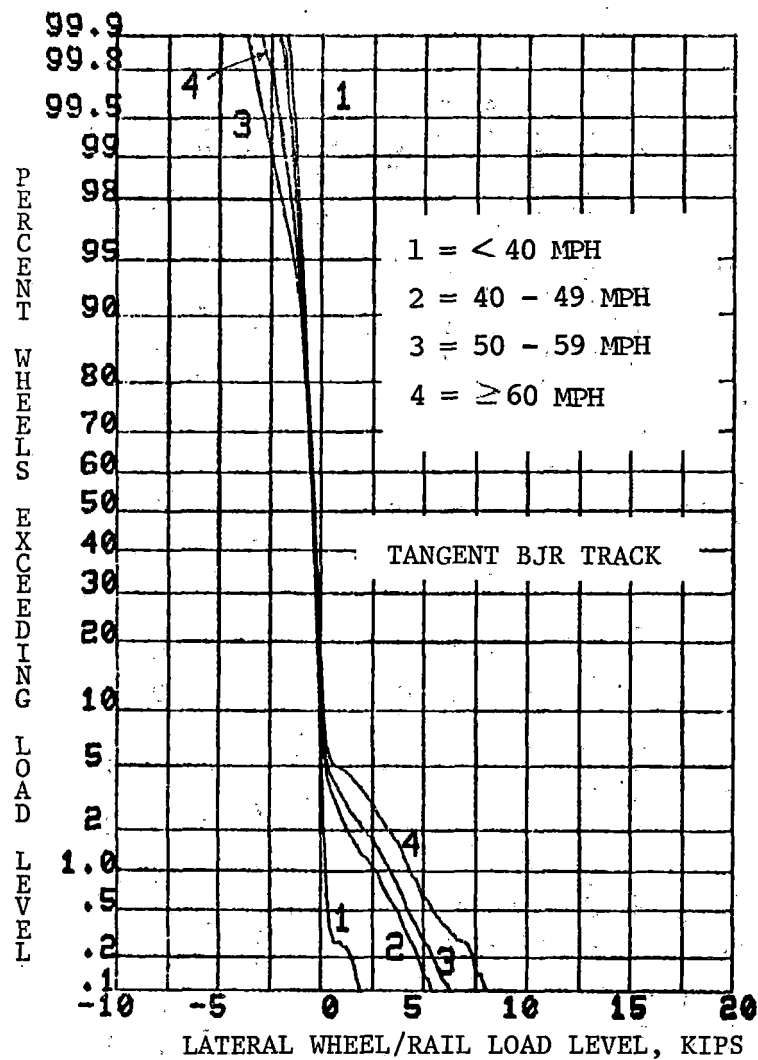
\*\*Positive lateral forces tend to move the rail outward from the track centerline.

3.1.1.2 Comparison of Tangent Track Test Sections. Using the two vehicle categories of locomotives and 100-ton freight cars as a basis for comparison, very little difference can be seen in Table 3-4 in the vertical load environment at the mid-rail region of the two test sections. The locomotives generated generally higher standard deviation values of vertical wheel load at higher speeds on the CWR track; while conversely the 100-ton freight cars generated higher standard deviation values at higher speeds on the BJR track (these forces, of course, measured away from the rail joint region). Overall (all sites, all speeds), the standard deviation values are 9 percent higher for locomotives on CWR track, 5 percent higher for 100-ton cars on BJR track, not including joint impact.

Exceedance curves for all traffic, all speeds, and all sites (Figure 3-2) show that the low-probability lateral forces due to flange contact will be approximately 25 percent higher at a given exceedance level on CWR track than on BJR track. This also appears to be true for lateral loads within the individual vehicle categories.

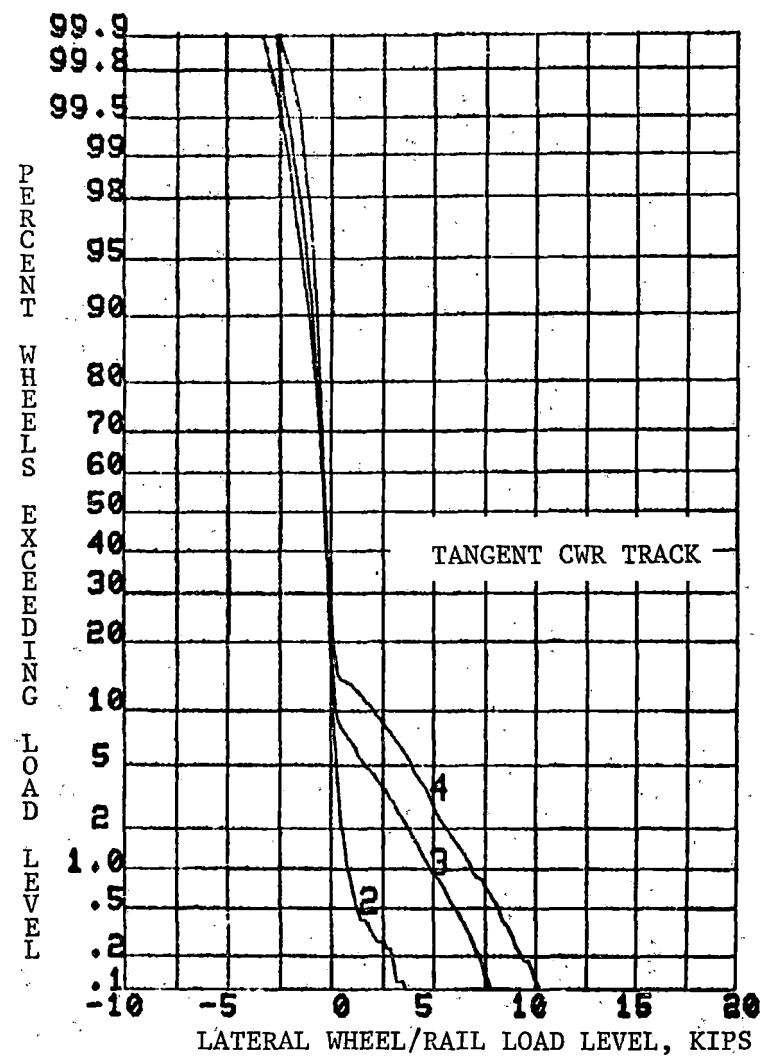
3.1.1.3 Speed Effects on Tangent Track Sections. The most significant difference between the BJR and CWR tangent track sections is the greater tendency for truck hunting to occur on the CWR track, which causes higher lateral loads and L/V ratios. This is illustrated in Figure 3-6 which compares the lateral loads developed by freight cars under 40 tons gross weight in the different speed bands, and in Figure 3-7 which compares L/V ratios. On the CWR track, lateral loads up to 21,700 lb and L/V ratios to 1.51 were recorded; while on BJR track, a maximum lateral load of 16,400 lb and an L/V ratio of 0.97 were recorded. Train speeds were comparable in both test sections, with several freight trains at speeds over 65 mph recorded in each.

The 100-ton freight car has been shown [3-2, 3-3] to have a bounce resonance excited by rail joints at about 60 mph. This is demonstrated in Table 3-4 by an increase in vertical load standard deviation from 4.5 kips in the 40-49-mph speed band to 6.7 kips in the >60-mph speed band. Seen in Figure 3-5 for Site 6, the effect can also be seen in Figure 3-8 for all



118511 118521 118531 118541

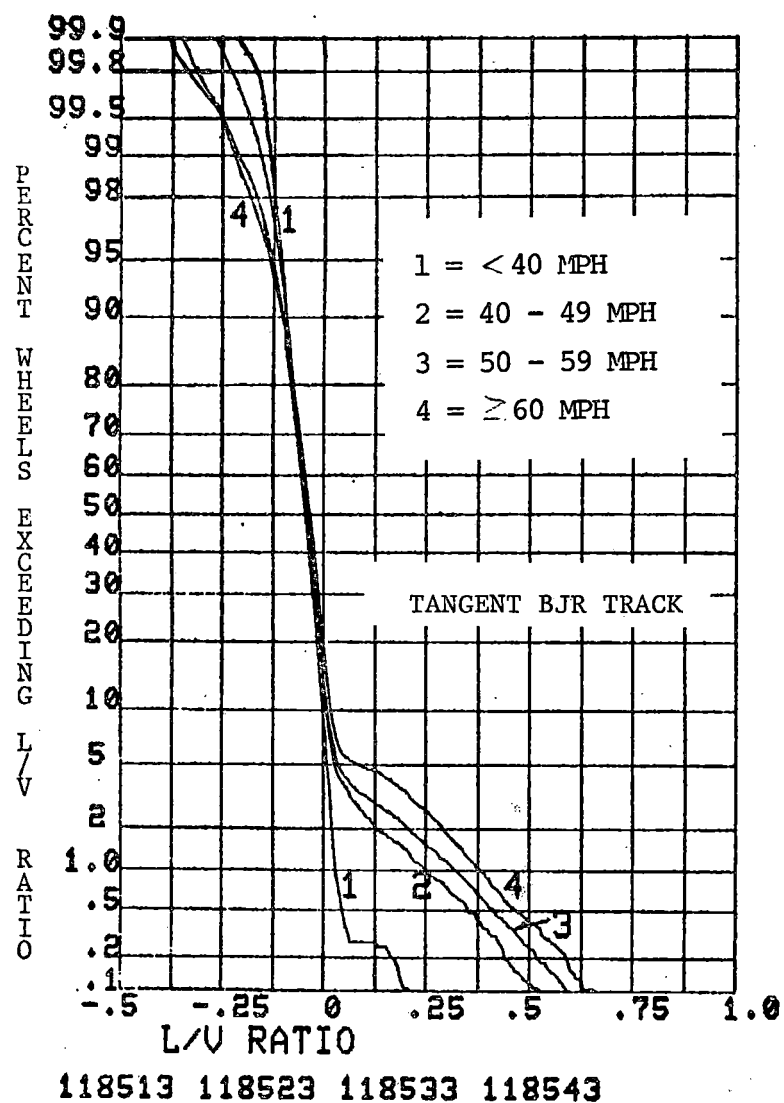
TANGENT BJR TRACK



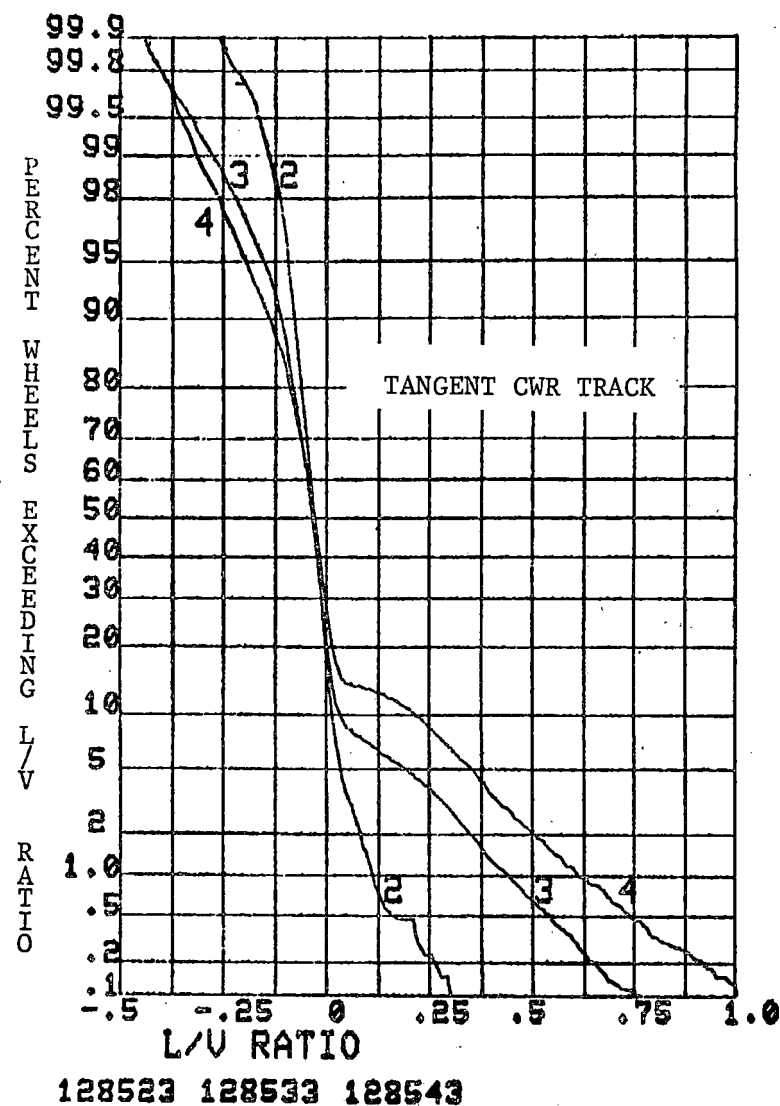
128521 128531 128541

TANGENT CWR TRACK

FIGURE 3-6. LATERAL W/R LOAD STATISTICS FOR TANGENT TRACK TEST SECTIONS, ALL MEASUREMENT SITES, EMPTY (<40T GWT) CARS VERSUS SPEED

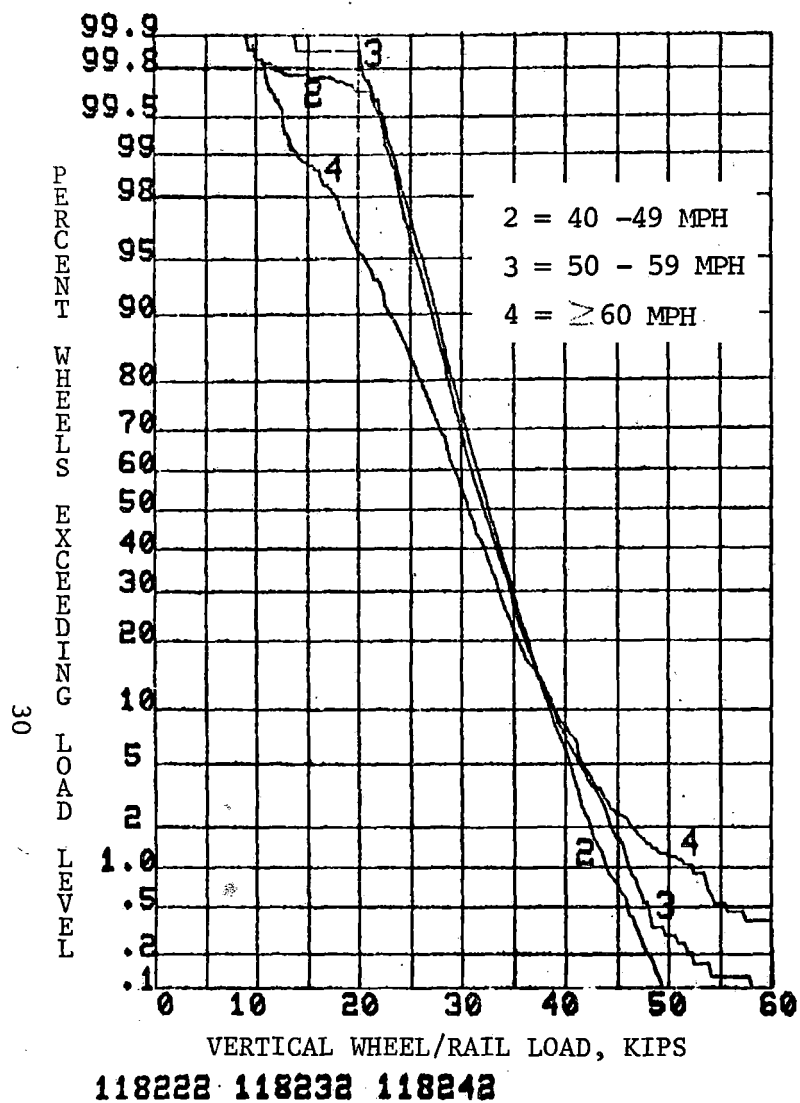


TANGENT BJR TRACK

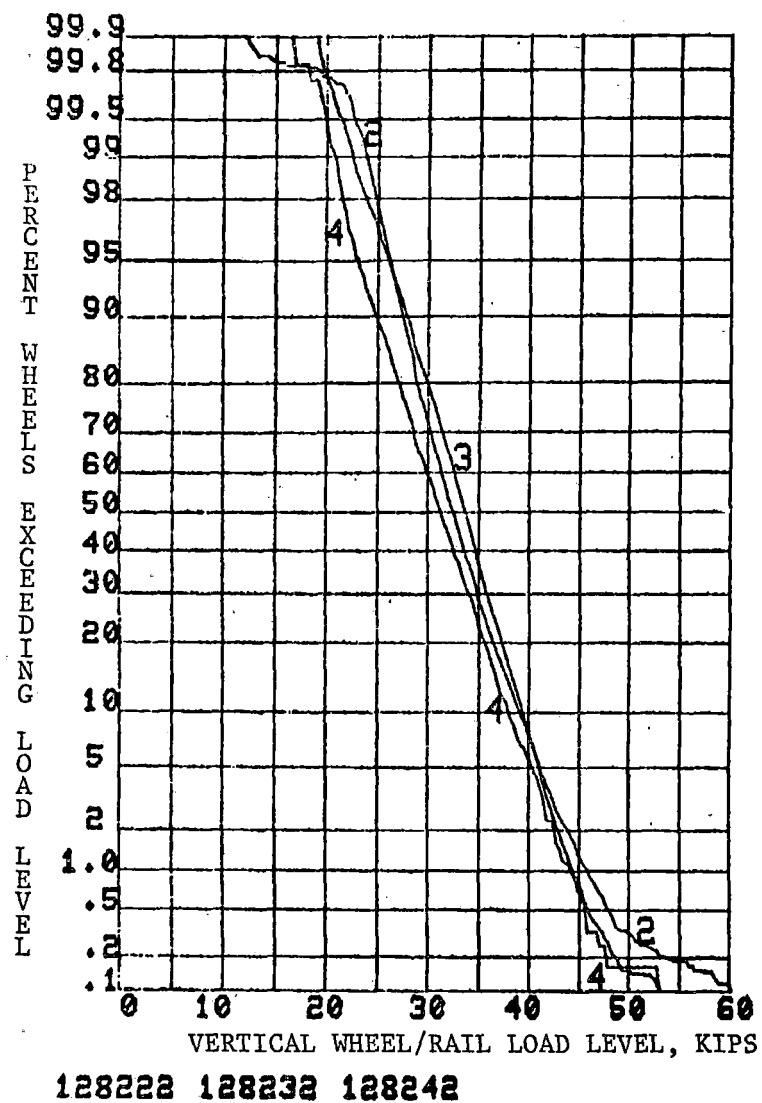


TANGENT CWR TRACK

FIGURE 3-7. L/V RATIO STATISTICS FOR TANGENT TRACK TEST SECTIONS, ALL MEASUREMENT SITES, EMPTY (< 40T GWT) CARS VERSUS SPEED



TANGENT BJR TRACK



TANGENT CWR TRACK

FIGURE 3-8. VERTICAL W/R LOAD STATISTICS FOR TANGENT TRACK TEST SECTIONS, ALL MEASUREMENT SITES, 100-TON FREIGHT CARS VERSUS SPEED

sites in the BJR track section, but is absent in data from the CWR track section. The data for 70-ton cars (70 to 110 tons gross weight) and the lighter cars do not exhibit this resonant effect on BJR track.

3.1.1.4 Lateral Versus Vertical Load Statistics. The simultaneous occurrence of vertical and lateral loads on the rail are of particular interest for rail stress and rail failure investigations. A method for processing this type of load data was to generate frequency-of-occurrence histogram matrices of lateral versus vertical and L/V ratio versus vertical wheel/rail loads. Data were sorted into a matrix of "bins", 2 kips or 0.1 ratio in width of increment by 5-kip vertical load increments. The resulting frequency-of-occurrence tables of L versus V, or L/V versus V for the three test sections are given in Appendix C. Exceedance curves for the 0.1, 0.5 and 1.0 percent frequency of occurrence levels derived from these tables are shown in Figures 3-9 through 3-12 for the tangent track sections. Again, significant differences in both lateral loads and L/V ratios can be seen in comparing the BJR and CWR track sections due to the greater degree of truck hunting by light cars on CWR track. Note that data for wheel vertical loads above 45 kips is limited in number, resulting in a progressively lower confidence level.

#### 3.1.2 Time-Domain Analysis of Wheel/Rail Loads

The joint and CWR "continuous" vertical load measurement zones provided a sample of wheel load 30 milliseconds or greater in length (depending on speed) for each passing axle (this is discussed in Section 6.6.1). A more detailed discussion of these measurement zones is contained in Section 3.2 on flat wheel impact loads.

While the time-domain analysis was primarily limited to a qualitative assessment of load measurements, some interesting load response phenomena were observed in the process. One of these is shown in Figure 3-13, which shows the north and south rail wheel loads (long and short

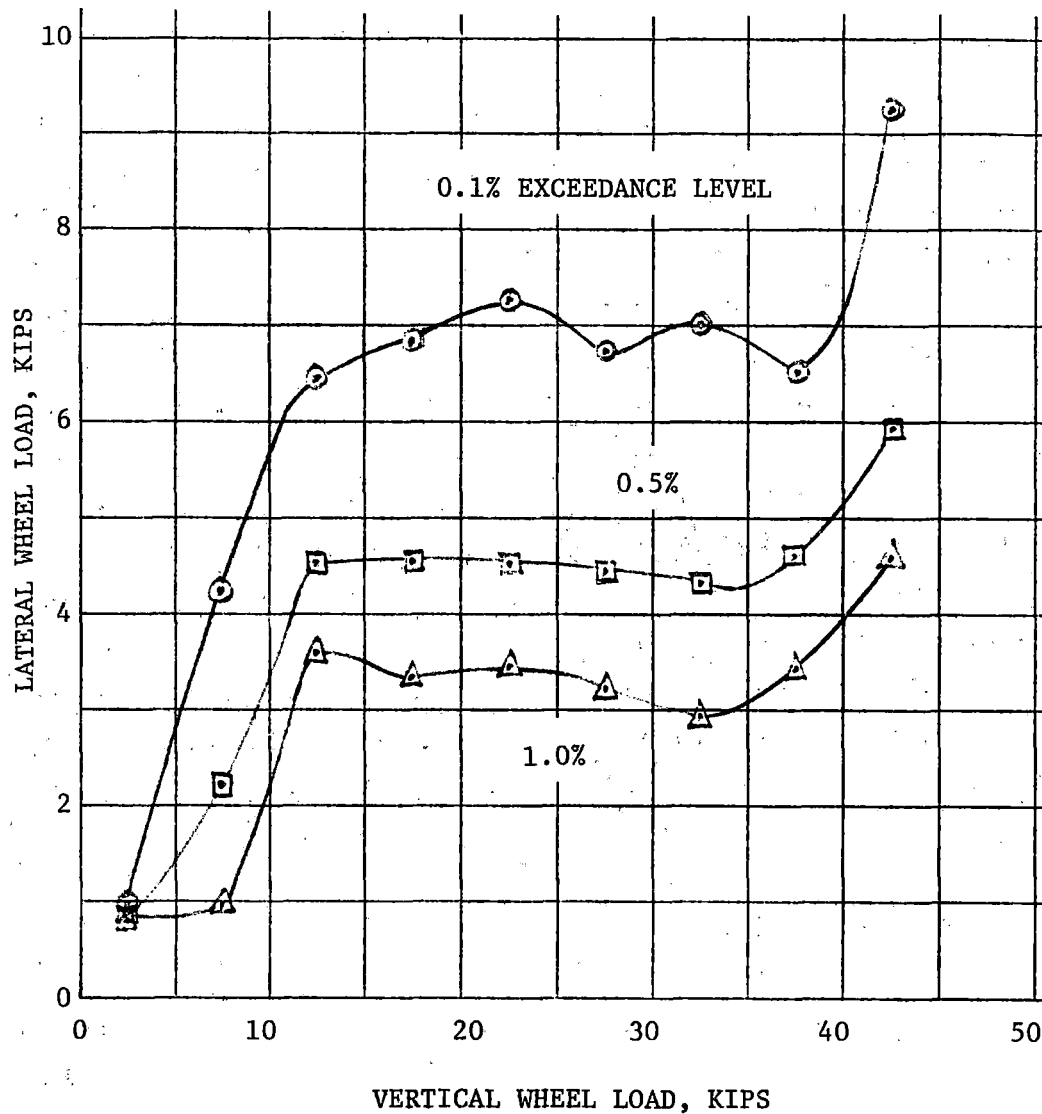


FIGURE 3-9. EXCEEDANCE CURVES FOR LATERAL VERSUS VERTICAL WHEEL LOAD, TANGENT BJR TRACK, ALL TRAFFIC, ALL SPEEDS, ALL MEASUREMENT SITES WITHIN TEST SECTION

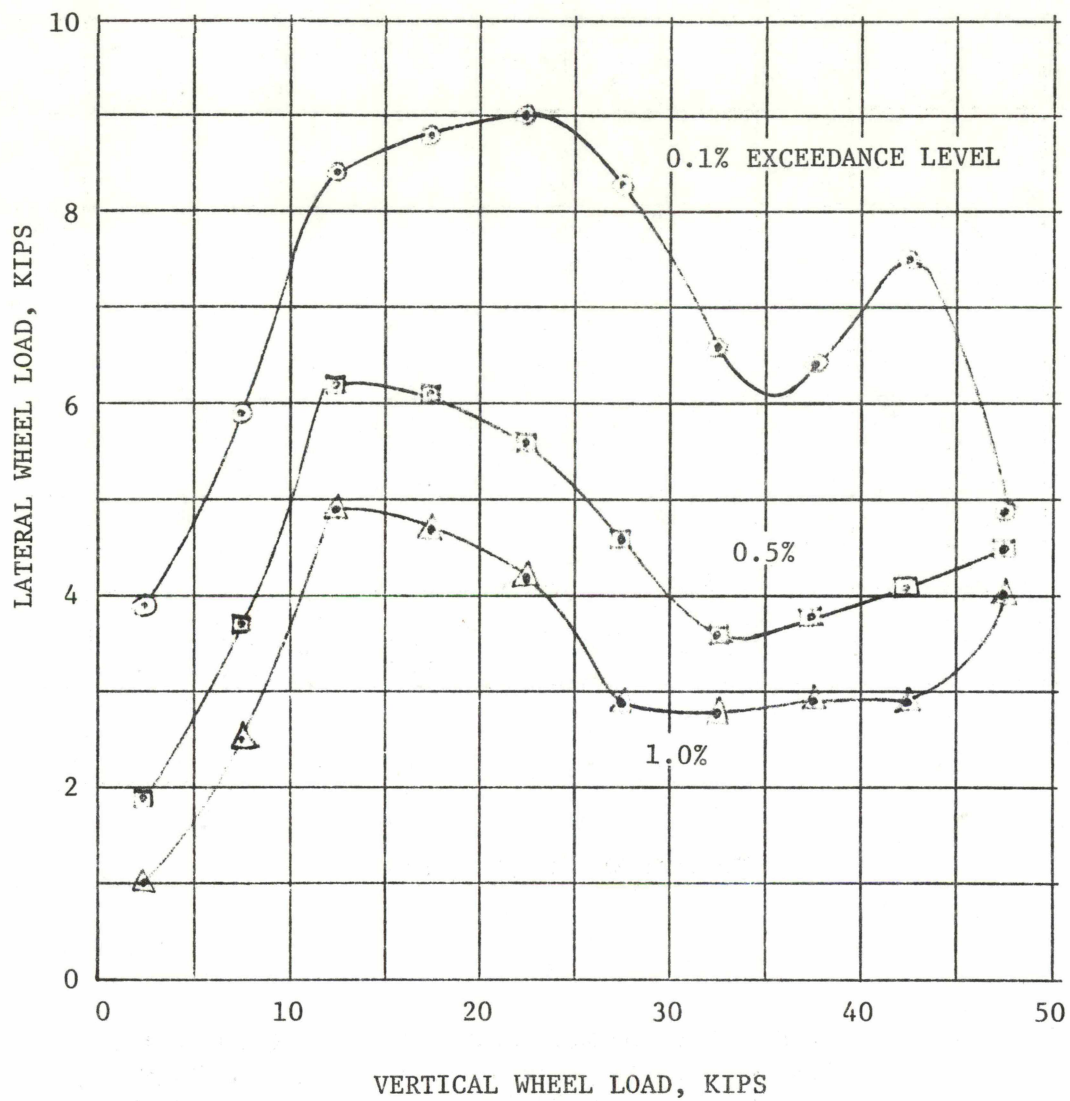


FIGURE 3-10. EXCEEDANCE CURVES FOR LATERAL VERSUS VERTICAL WHEEL LOAD, TANGENT CWR TRACK, ALL TRAFFIC, ALL SPEEDS, ALL MEASUREMENT SITES IN TEST SECTION

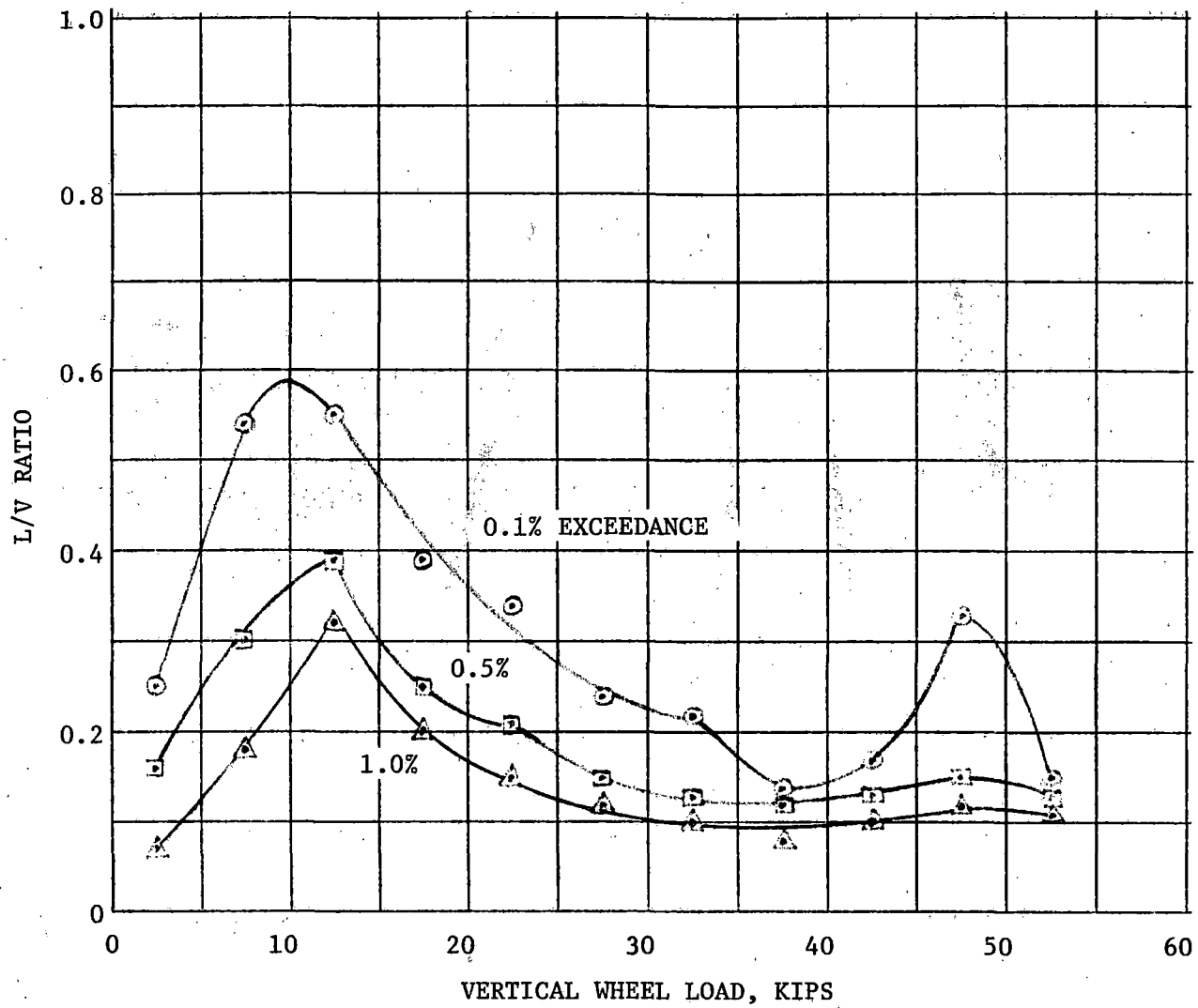


FIGURE 3-11. FREQUENCY OF EXCEEDANCE CURVES FOR L/V RATIO VERSUS VERTICAL WHEEL LOAD, TANGENT BJR TRACK, ALL TRAFFIC, ALL SPEEDS, ALL MEASUREMENT SITES IN TEST SECTION

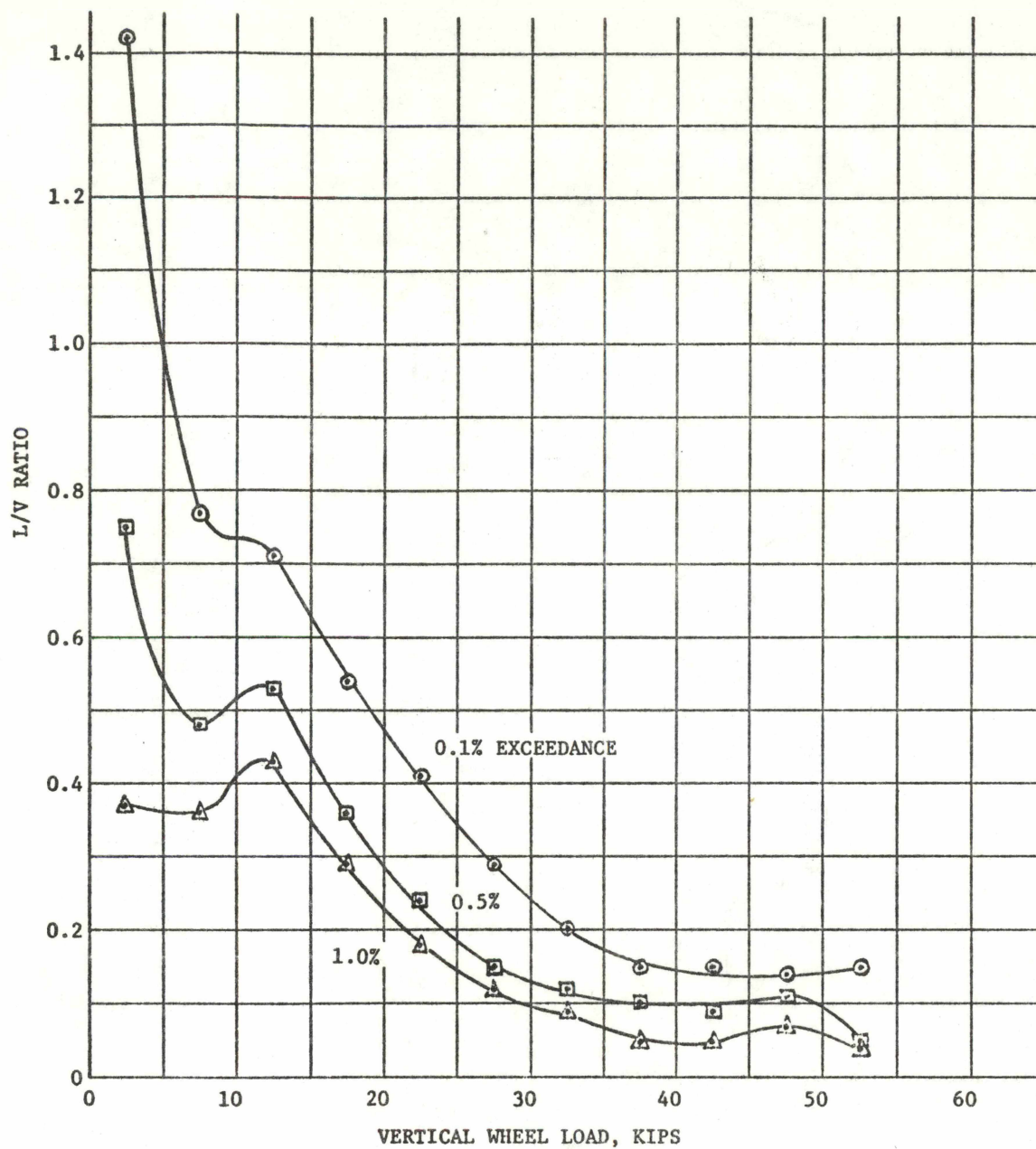


FIGURE 3-12. FREQUENCY OF EXCEEDANCE CURVES FOR L/V RATIO VERSUS VERTICAL WHEEL LOAD, TANGENT CWR TRACK, ALL TRAFFIC, ALL SPEEDS, ALL MEASUREMENT SITES

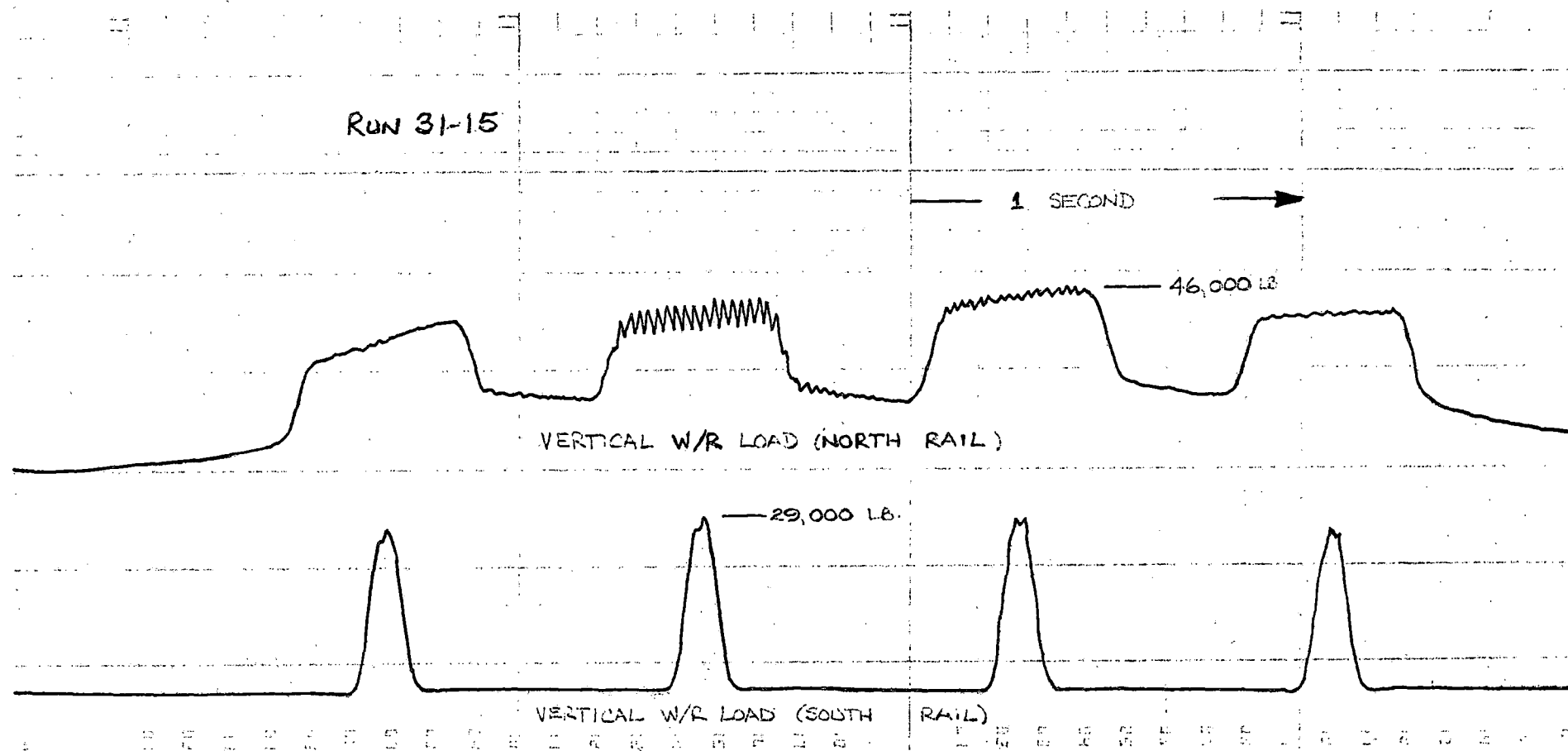


FIGURE 3-13. SLOW ROLL-BY OF LOCOMOTIVE AXLES, TEST SECTION 2 (CWR TRACK), SHOWING VERTICAL WHEEL/RAIL LOADS AT SITE 3 -- TRAILING TRUCK OF 8-AXLE DD-35 LOCOMOTIVE UNIT, WESTBOUND

measurement zones) under the trailing truck of a DD-35 diesel locomotive. The three units were starting a heavy freight train on an 0.5 percent ascending grade and wet rail, and they passed the instrumentation van at about 5 mph. A strong oscillation in vertical load under the second axle, up to 7,000 lb peak-to-peak, can be seen at the track natural frequency of 42 Hz. This oscillation is probably due to incipient wheel slip or chatter of this wheel-set under traction.

### 3.1.3 Frequency-Domain Analysis of Wheel/Rail Loads

Because of the inherent transient nature of the wheel loads from passing axles, it is difficult to determine the frequency content of track loading from wayside data. However, the higher-frequency portion of the spectrum can be estimated by averaging a number of these transients, along with the intervening gaps between load pulses. While frequencies associated with the wheel-pass repetition rate and the shape of the load pulse must be ignored (frequencies under roughly 30 Hz), the resulting spectrum provides a qualitative assessment of the higher-frequency content of the rail loading.

The power spectra of vertical wheel/rail loads from the long measurement zone on CWR track are shown in Figure 3-14 for a representative train, using 50 averages under the locomotive units and freight cars. In Figure 3-14a, the spectrum over a 100-Hz bandwidth shows a strong vertical response in the 41-46 Hz band, with additional lower-amplitude spectral peaks at 51, 57 and 72 Hz. The spectrum over an 800-Hz bandwidth, Figure 3-14b, shows additional important peaks at 110 Hz (which is excited strongly by flat wheel impacts), 140 Hz, and 370 Hz.

The vertical load power spectrum over the 100-Hz bandwidth from the rail joint long measurement zone is shown in Figure 3-15. Because of the reduced vertical stiffness near the joint, the primary track response falls between 32 and 35 Hz, with secondary spectral peaks at 49 and 82 Hz. (The sharp spectral peak at 60 Hz can, of course, be attributed to power supply noise.) Taken over an 800-Hz bandwidth, the spectrum shows additional spectral peaks at 130, 370 and 470 Hz.

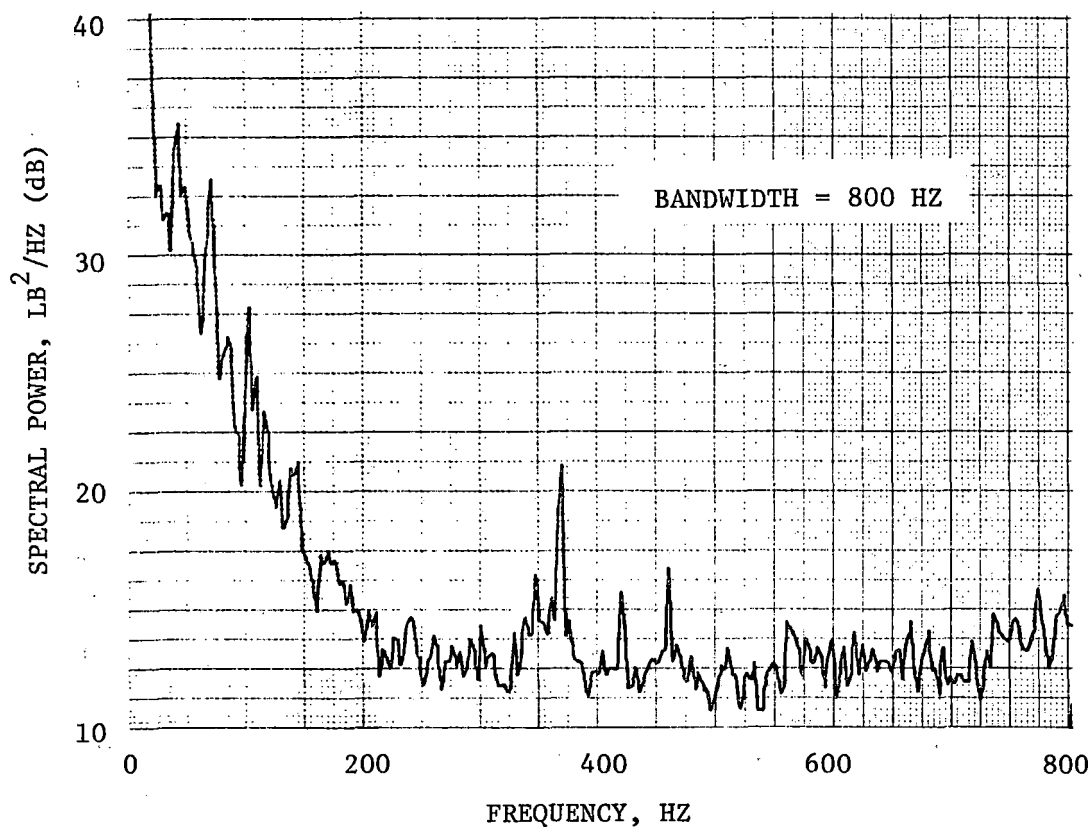
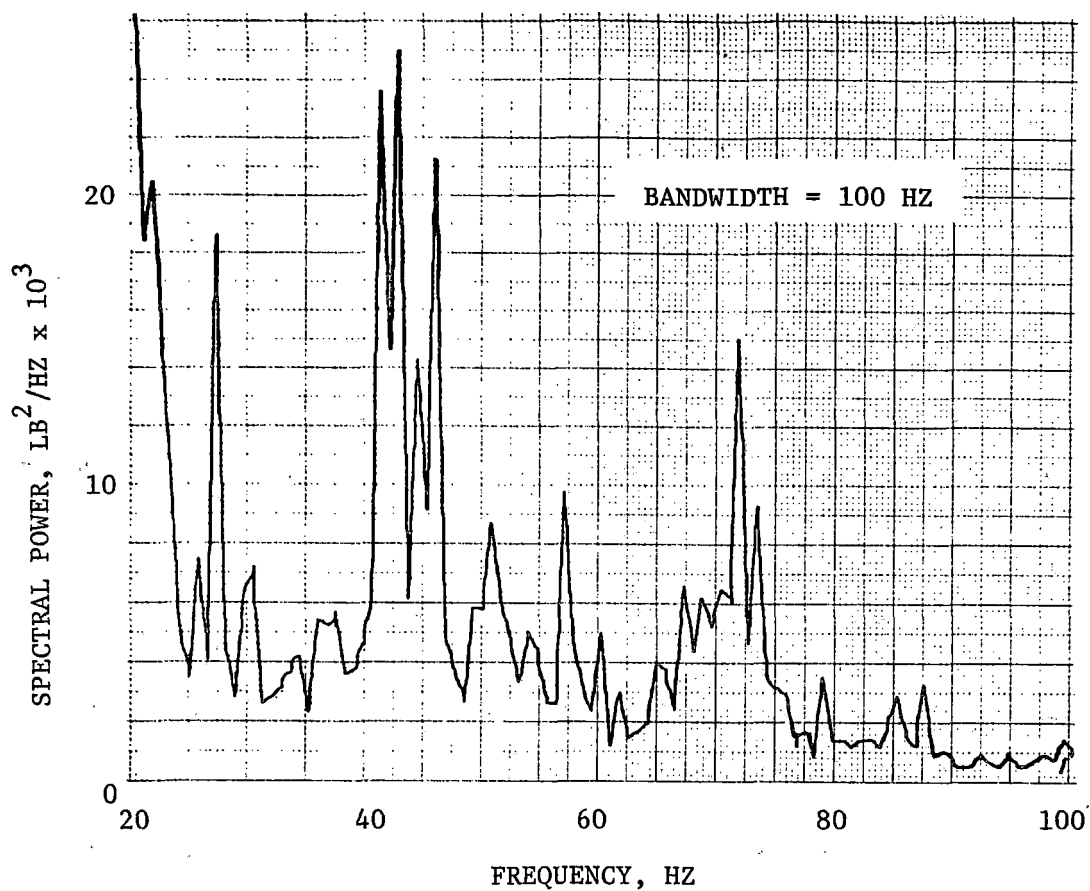


FIGURE 3-14. VERTICAL W/R LOAD FREQUENCY SPECTRA (PSD)  
FOR TYPICAL FREIGHT TRAIN, 68 MPH, CWR TRACK

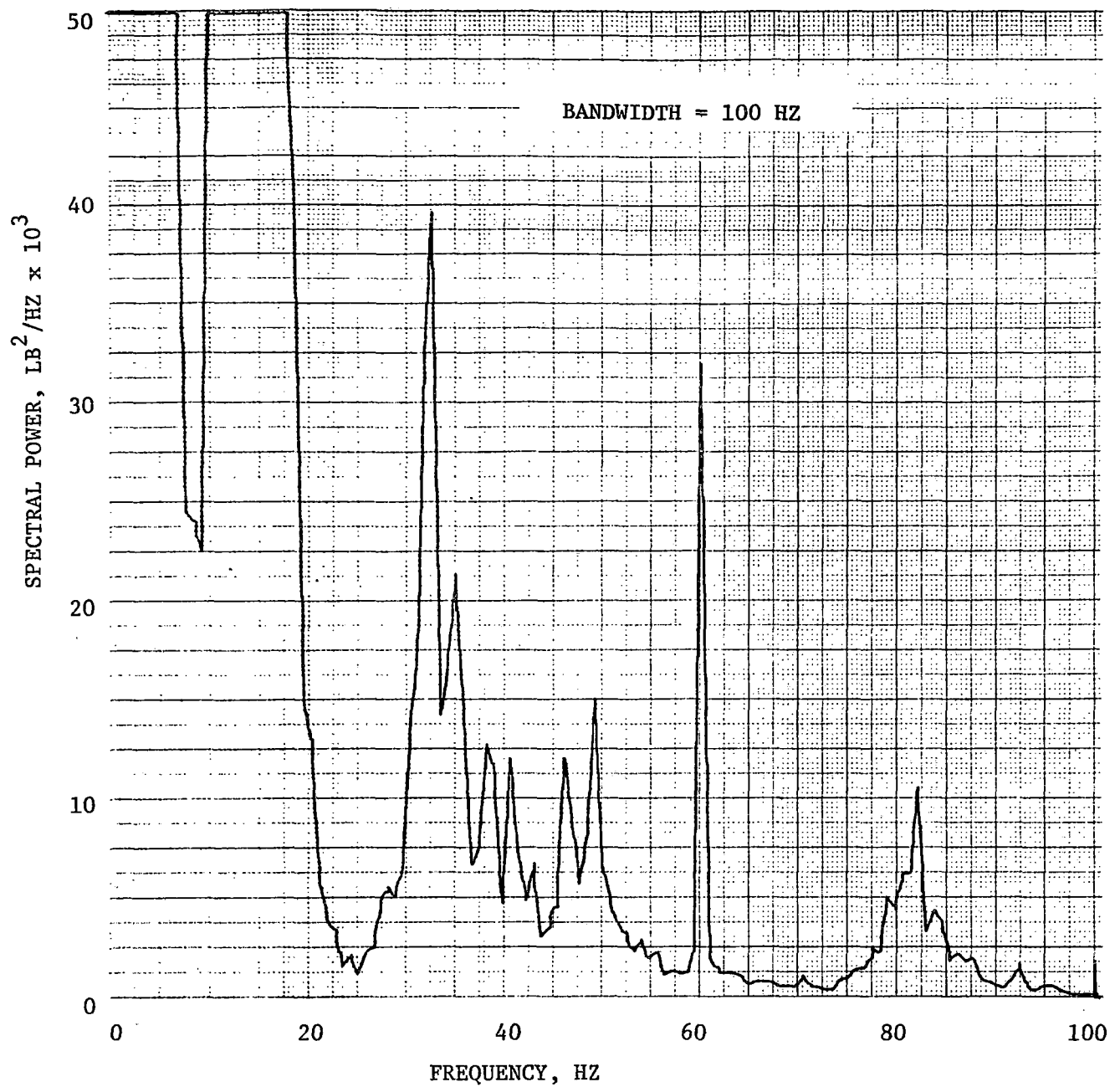


FIGURE 3-15. VERTICAL W/R LOAD FREQUENCY SPECTRUM (PSD) FOR  
TYPICAL FREIGHT TRAIN, 64 MPH, LONG MEASUREMENT  
ZONE AT INSTRUMENTED RAIL JOINT

## 3.2 WHEEL/RAIL IMPACT LOADS

### 3.2.1 Extended Vertical W/R Load Circuit

The extended wheel/rail load circuits shown in Figure 6-12b and 6-12c were designed to record vertical loads through the rail joint zone, and to provide a greater probability of recording wheel flat impact loads by extending the measurement zone to a significant percentage of one wheel circumference. In concept, the two strain gage chevron circuits measure the shear load in the rail web, producing a signal proportional to the wheel load less the tie plate reactions. The vertical loads from the two tie plates between chevrons were added to the chevron signal to generate a signal for measuring the total vertical wheel load.

Measurements from both the standard in-crib chevron circuit (with an effective length of 7 inches) and the extended, joint-zone circuit (with an effective length of 35 inches) are compared in Figure 3-16 under the axles of the test train locomotive (a GP-30 diesel unit) during a slow roll-by of the wayside test site. A good comparison of peak loads from both rails can be seen. However, it can also be seen that the extended-zone circuit signal does not return sharply to zero output as the wheels roll beyond the chevrons. There is a non-zero load typical of the tie plate vertical reactions due to wheel loads near to, but outside the zone. The resulting error signal is a function of wheel vertical load, track structural parameters, and axle spacing. For the 32,000-lb wheel load and 9-ft axle spacing of the GP-30 locomotive, the error signal was found to be insignificant.

Similar results are shown in Figure 3-17 for the instrumented 100-ton hopper car and one truck of an adjacent empty freight car during the same slow roll-by. Note the asymmetrical loading of the hopper car, and the tendency to roll into the joint region, generating higher loads on the south rail. Due to the shorter (6-ft) axle spacing of the freight car truck, the apparent error signal due to the adjacent wheel load is also higher, and may range up to a 10 percent increase over the actual load. The error signal is particularly noticeable in the adjacent empty-car wheel loads.

RUN 17J (10 HZ FILTER)

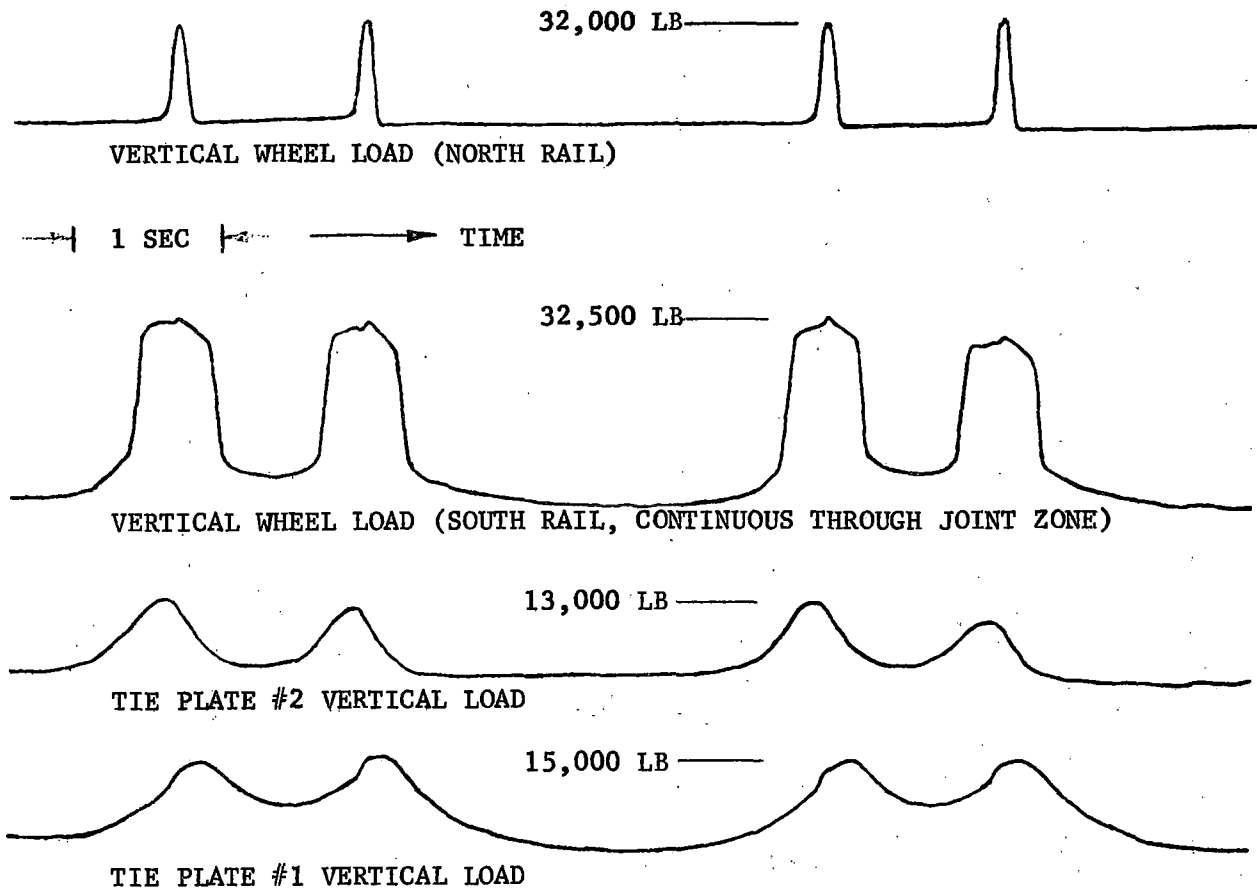


FIGURE 3-16. SLOW ROLL-BY OF TEST TRAIN LOCOMOTIVE (BACKING WEST-BOUND) SHOWING VERTICAL WHEEL AND TIE PLATE LOADS AT SITE 3, TEST SECTION 1 (BJR TRACK)

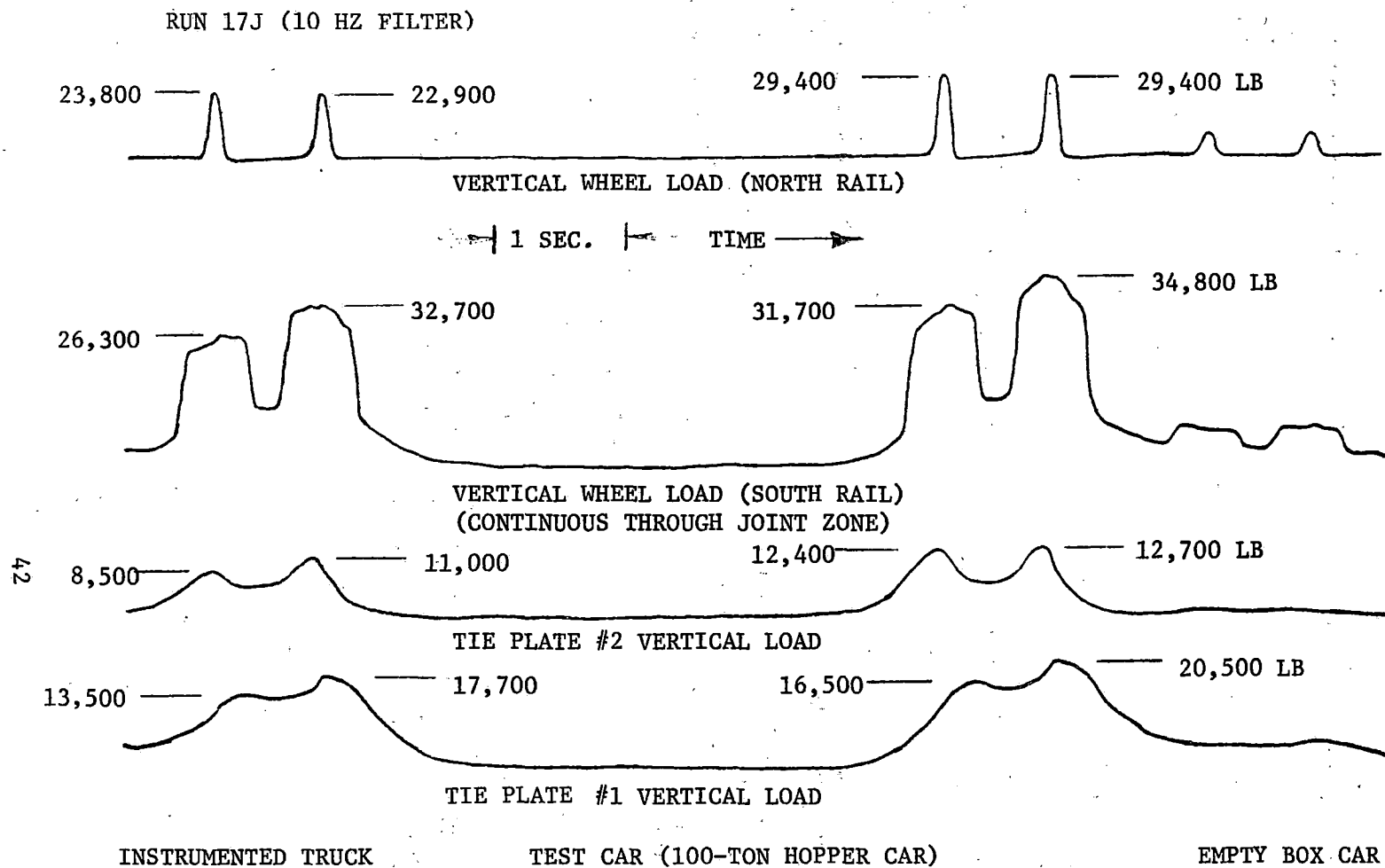


FIGURE 3-17. SLOW ROLL-BY OF TEST CAR (BACKING WESTBOUND) SHOWING VERTICAL WHEEL LOADS AND TIE PLATE LOADS AT SITE 3, TEST SECTION 1 (BJR TRACK)

Since the extended-zone signals are used in this study primarily for the determination of impact load increments, this error signal is of little significance. To determine the impact load increment, the difference between the filtered and unfiltered signal is recorded; and the error signal (which is a low-frequency component) is effectively cancelled.

### 3.2.2 Flat Wheel Impact Loads

Flat wheel impact loads are measured occasionally by the short (in-crib) chevron gage circuits: for example, impact loads at several of the CWR track sites are illustrated in Figure 3-18 for one particularly bad 100-ton freight car. The difference in load signal characteristics between the normal and flatted wheels is particularly graphic at Site 1, axle 2 versus axle 4. The flat wheel impact resembles a half-sine pulse approximately 6 milliseconds in duration.

To assure a greater probability of sampling the flat wheel population, the extended vertical load circuit was used at one CWR track site to provide a zone with an effective length of 35 inches (approximately one-third an average wheel circumference). Four evenly-spaced ties of good quality were chosen for this zone, and the four instrumented tie plates were installed. The newer two-cell plates were installed between the strain gage chevrons, and the older three-cell plates were located on either side to provide some data on the uniformity of support. In spite of care in selection, one of the inner ties provided substantially less support than the other three.

A typical flat wheel response within the extended vertical load zone is shown in Figure 3-19. In this example, the peak wheel flat impact load was 97 kips, with a peak vertical tie plate load of 57 kips directly under the point of impact. A 300-Hz filtering frequency has been used with the oscillograph in reproducing this event (a 4-pole programmable Bessel filter), but negligible higher-frequency content was found in flat wheel

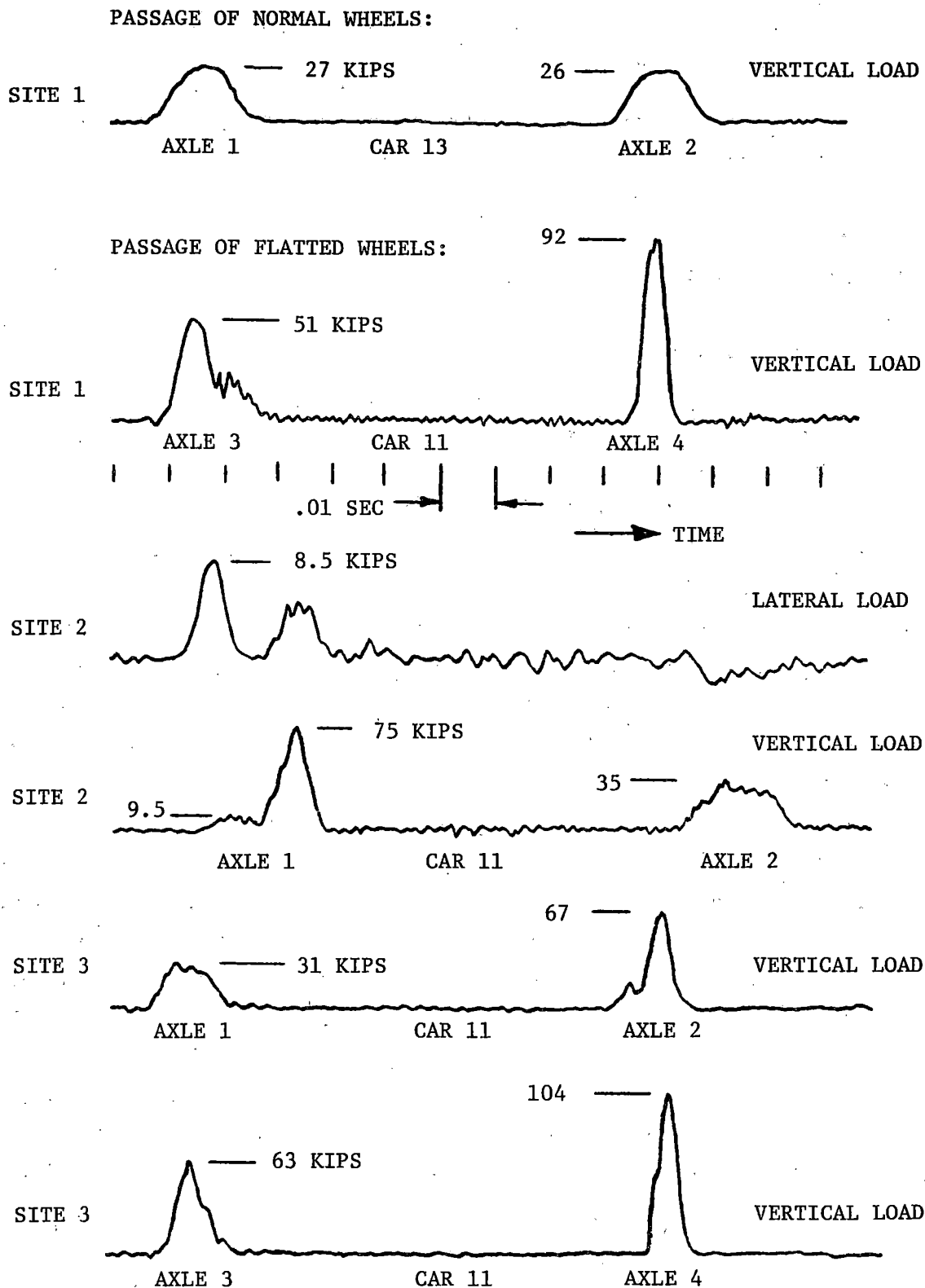


FIGURE 3-18. EXAMPLES OF WHEEL/RAIL LOADS UNDER NORMAL AND FLATTED WHEELS AT SHORT MEASUREMENT SITES, SMOOTH TANGENT TRACK, WESTBOUND FREIGHT TRAIN AT 46 MPH

(300 HZ FILTER)

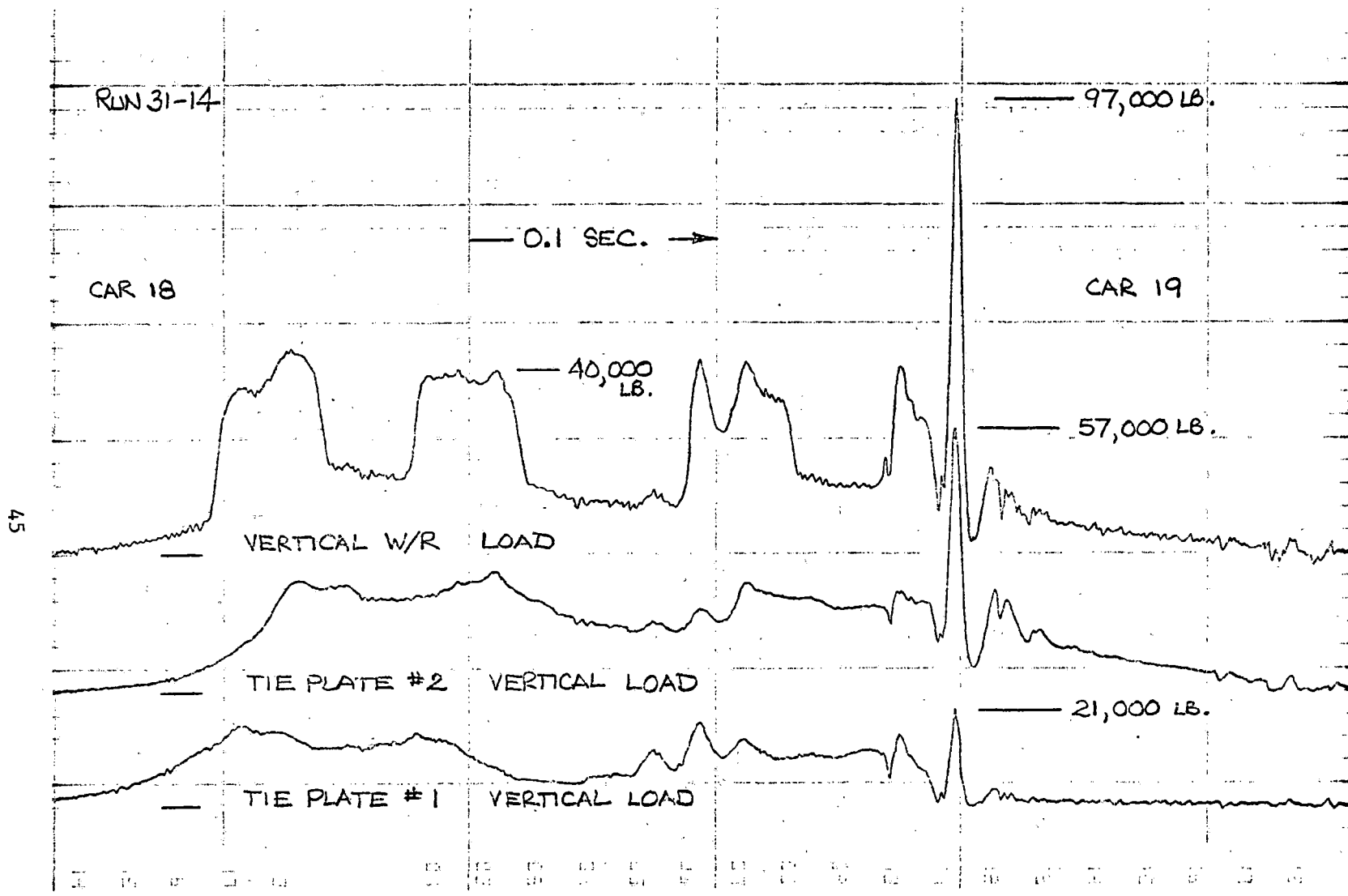


FIGURE 3-19. FLAT WHEEL IMPACT WITHIN VERTICAL CONTINUOUS MEASUREMENT ZONE -- TEST SECTION 2, (CWR TRACK), ADJACENT TRUCKS OF 100-TON COVERED HOPPER CARS IN WHEAT UNIT TRAIN AT 46 MPH

impacts. For example, a 92-kip impact load near the instrumented rail joint was examined through different filter settings:

Run 22-10, Car 14			
Filter Frequency (Hz)	Peak Impact Load (Kips)	Peak Load, Tie Plate 1 (Kips)	Peak Load, Tie Plate 2 (Kips)
30	41	13.2	12.5
100	77	20.5	25
300	90	23	30
1000	92	24	31

This flat wheel impact load occurred on the "running-off" rail within the extended vertical load zone at the instrumented joint (Test Section 1). It was interesting to note that there were no responses at the bolt hole strain gages to this 92-kip impact on the opposite rail end, indicating that the joint bars effectively attenuate any stress waves at these frequencies.

Another example of flat wheel impact loading is shown in Figure 3-20. Filter frequency setting is 1000 Hz. This impact results in a strong 71-Hz response in the track structure, but there is little indication of higher frequency components in the load signal.

In the processing of the vertical W/R load signal from the extended zone, peak loads were detected under each passing wheel for the unfiltered signal (a minimum bandwidth of 1000 Hz), and for the same signal filtered at 30 Hz by a 4-pole Bessel low-pass filter. The difference between these two values was calculated in the data processing and called the dynamic load increment. Exceedance distribution curves for the individual vehicle categories are plotted in Figure 3-21. In these curves, the dynamic load increment is seen to consist of two distinct populations. To provide some insight into the types of distribution functions representing these populations, a print-out of all dynamic load increments greater than 4 kips was generated, and numbers of occurrences in 1-kip bands were determined. Then, the percent of the total wheel population passing through the measurement zone generating dynamic loads exceeding the "cut-off" level was determined. This is plotted in Figure 3-22 for the different vehicle types. Two salient facts are revealed in these curves: first, the percent of "flat wheels" in

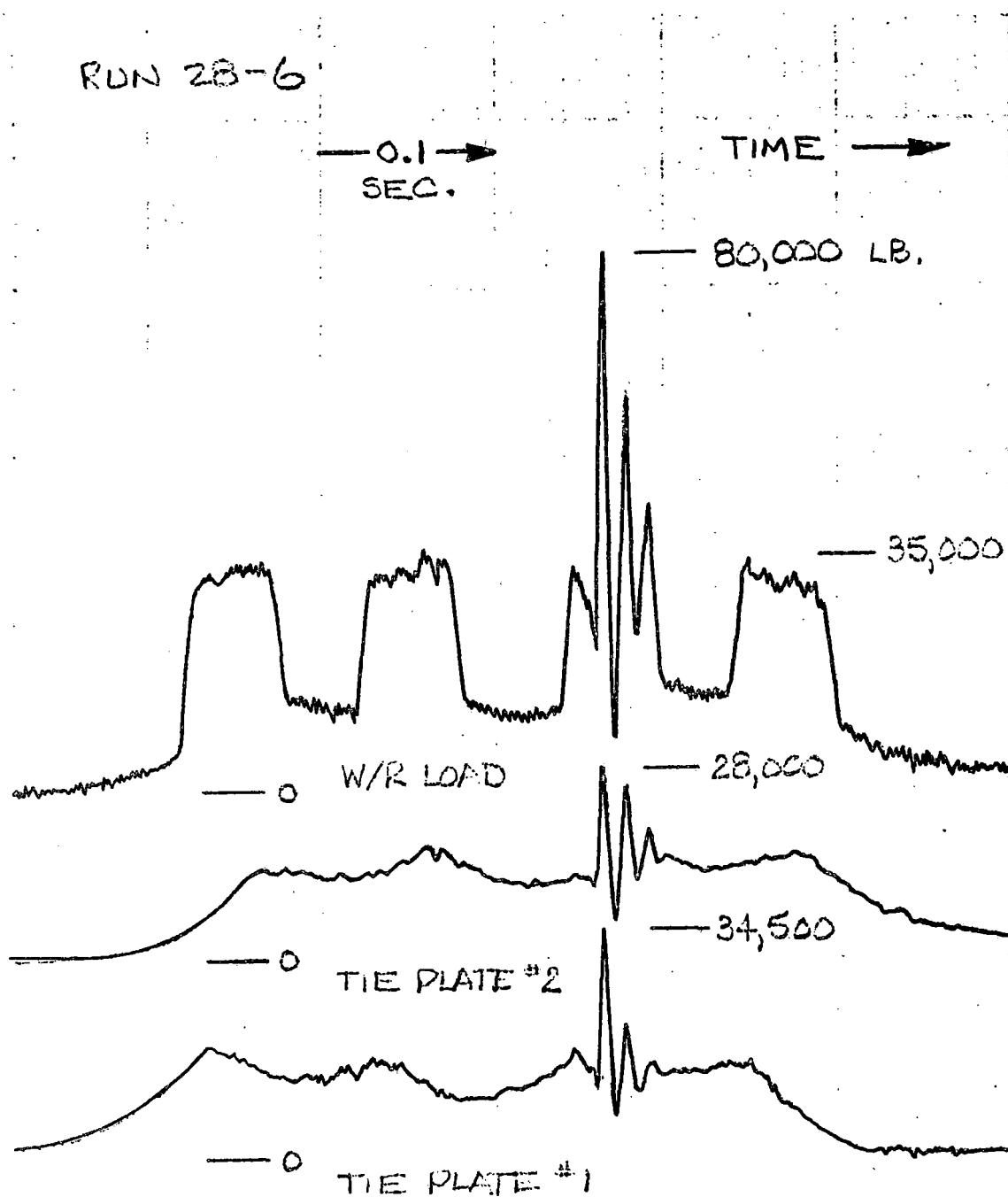


FIGURE 3-20. FLAT WHEEL IMPACT WITHIN VERTICAL CONTINUOUS MEASUREMENT ZONE -- TEST SECTION 2 (CWR TRACK), ADJACENT TRUCKS OF 100-TON HOPPER CARS, WEST-BOUND TRAIN AT 40 MPH

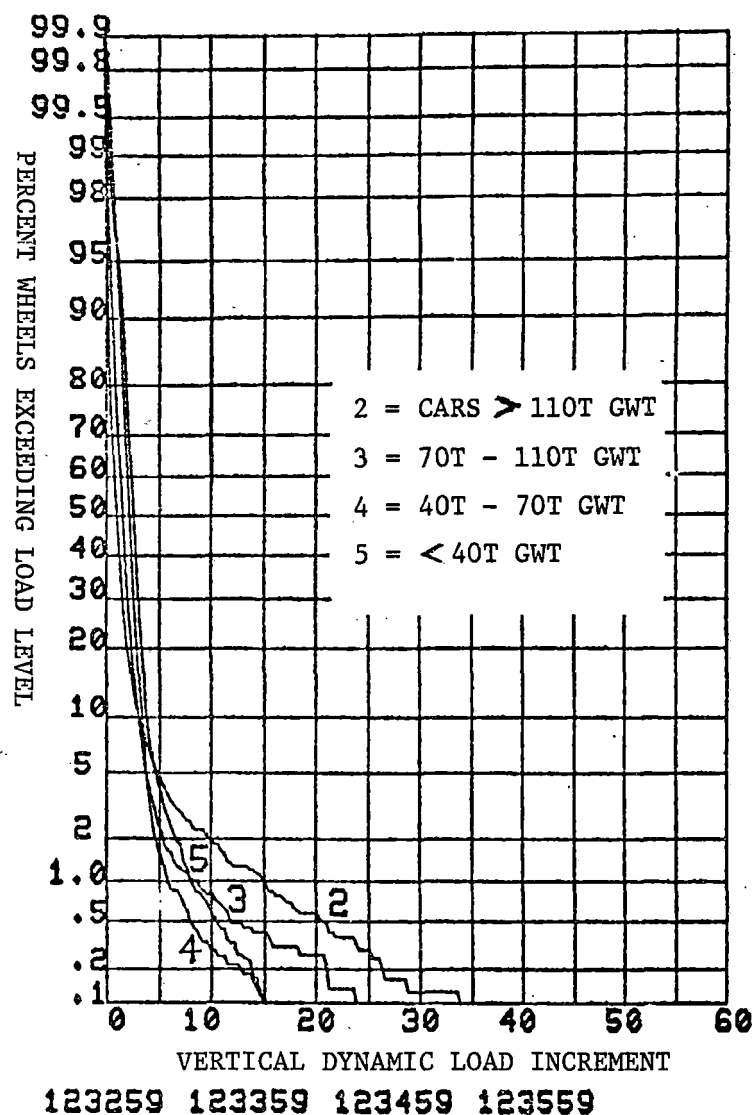
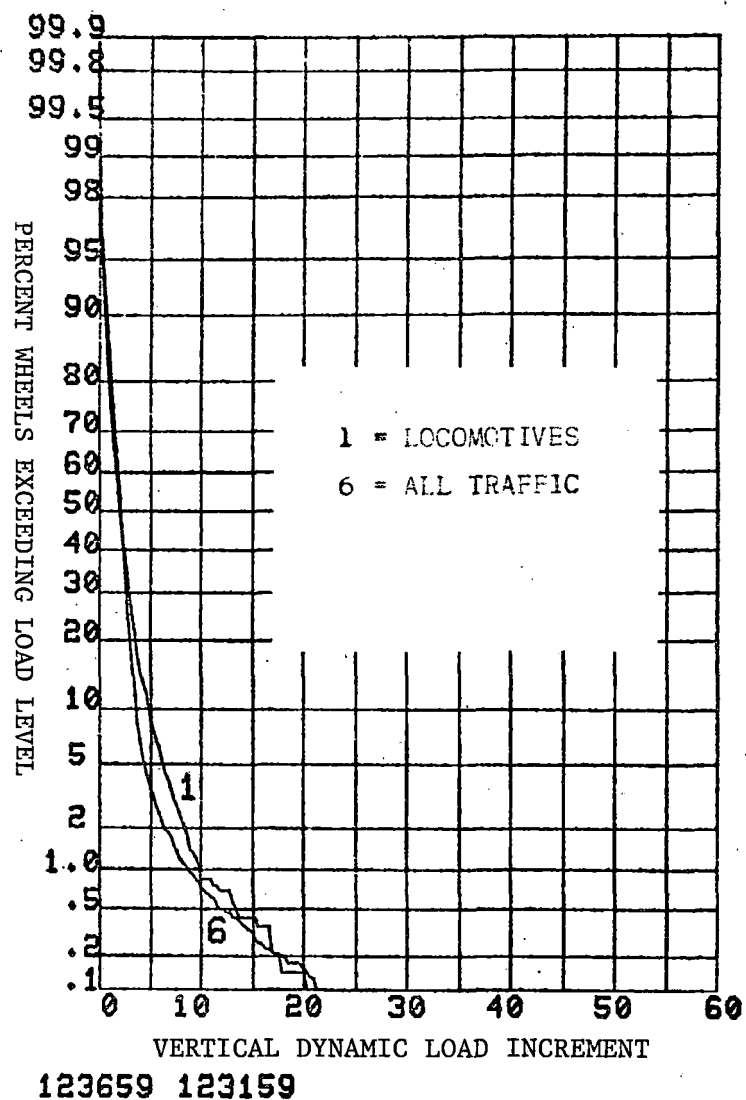


FIGURE 3-21. FREQUENCY OF EXCEEDANCE OF DYNAMIC LOAD INCREMENT  
BY VEHICLE CATEGORIES, ALL SPEEDS

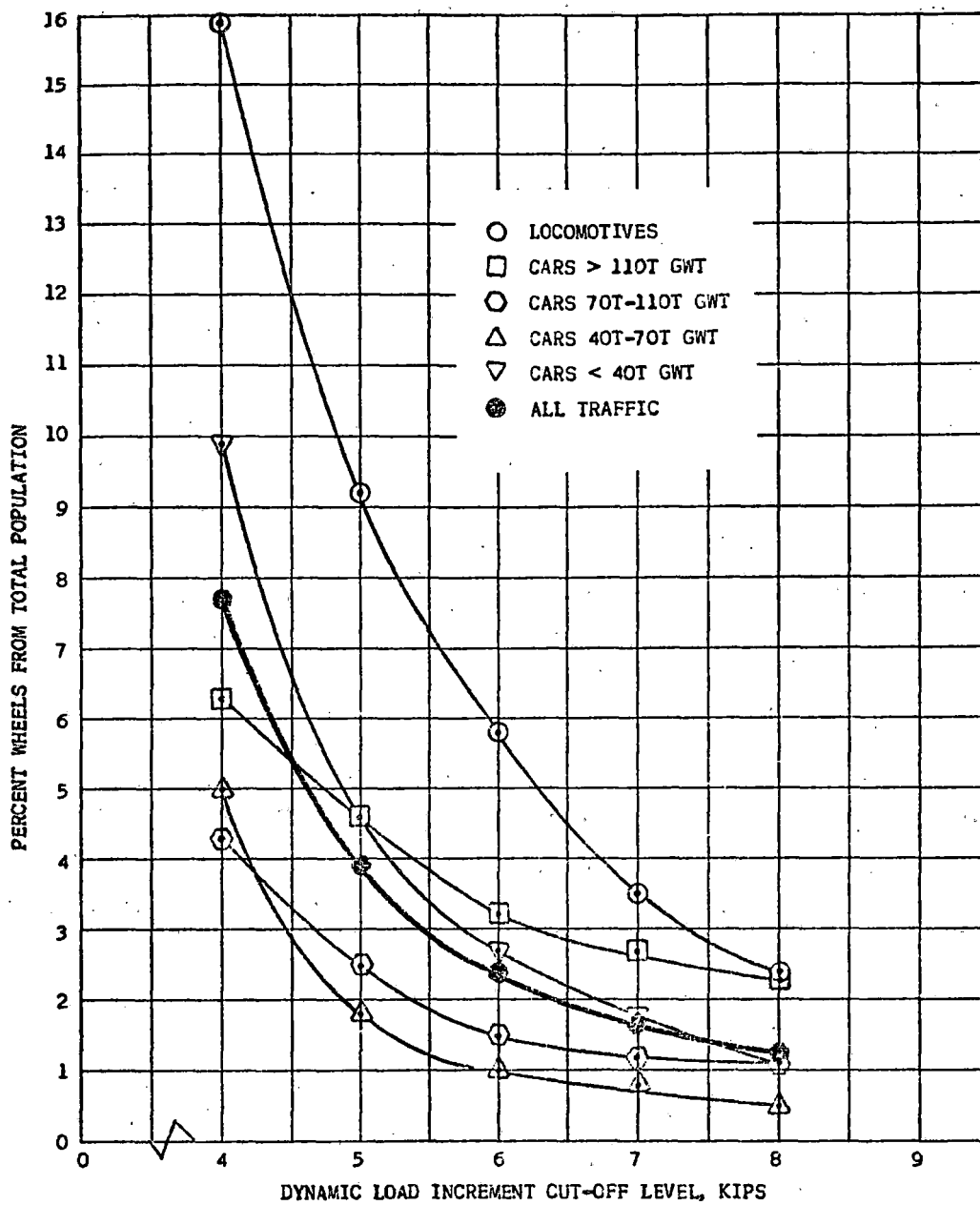


FIGURE 3-22. PERCENT WHEELS FROM TOTAL POPULATION GENERATING DYNAMIC LOAD INCREMENTS ABOVE GIVEN CUT-OFF LEVEL

the population is strongly dependent on the cut-off level; and second, a much greater number of locomotive wheels generate high-frequency load oscillations, possibly due to track response to traction dynamics, than do the unpowered freight car wheels.

Examination of the frequency-of-exceedance plots of Figure 3-21 leads to the conclusion that the bulk of the dynamic load peaks, up to about 5 kips and including about 90 percent of the population, can be approximated by the Rayleigh distribution in the form:

$$E_R(F_{\text{dyn}}) = e^{-(F_{\text{dyn}}^2/2\sigma_{\text{dyn}}^2)}, \text{ the Rayleigh frequency-of-exceedance function.}$$

where  $F_{\text{dyn}} = F_{1\text{kHz}} - F_{30\text{Hz}}$ , the dynamic load increment,  
 $\sigma_{\text{dyn}}$  = standard deviation of dynamic load increment.

Since from Figure 3-20 the impact load appears to be typically a decaying sinusoidal response, the distribution of peaks can be expected to assume the Rayleigh form<sup>(3-6)</sup>.

Above roughly 5 kips, the dynamic load increment frequency-of-exceedance plots fall into an obviously-distinct population. The distribution function that best describes this population is the exponential function, which is a special case of the Weibull distribution. It is commonly used to describe the failure rate of assemblies of components (hydraulic pumps, washing machines, etc.), and takes the form:

$$E_x(F_{\text{dyn}}) = e^{-(F_{\text{dyn}}/\bar{F}_{\text{dyn}})}, \text{ the exponential frequency-of-exceedance function,}$$

where  $\bar{F}_{\text{dyn}}$  = the mean value of flat wheel impact (analogous to the "characteristic time" in failure rate).

With this clue to the nature of the extreme-value distribution, the experimental data from the 7 short measurement sites were used to establish a least-squares best fit (at 5-kip intervals) to exceedance levels above the nominal three-standard-deviation load. The resulting function takes the form:

$$E_x(F_v) = R e^{-(F_v - \bar{F}_v)/\bar{F}_{dyn}}$$

where  $F_v$  = vertical wheel/rail load,  
 $\bar{F}_v$  = mean vertical W/R load for vehicle class (normal distribution)  
 $R$  = portion of wheel population in the extreme-value distribution.

Parameters describing the extreme-value distribution by vehicle class are listed in Table 3-6. A comparison of exceedance levels measured within the 7-inch zones and predicted by the exponential function is given in Table 3-7. Note that up to 75 kips the correlation is very good, but beyond this level a dearth of measured data (2 points out of 157,442 total data points) does not allow accurate comparison.

One of the objectives of the field measurement program was to provide vertical load spectra for "normal" wheels, as well as for flatted wheels alone. The probability of a wheel flat impacting on a short zone can be estimated by assuming the length between -3 dB points is approximately 7 inches for a short zone and 35 inches for the extended zone, and then the number of flatted wheels at a typical short zone becomes:

$$N_{fs}' = N_{TS} (1254/16570) (7/35) = 0.015 N_{TS}$$

where:  $N_{fs}'$  = estimated number of flat wheel impacts at the short zone,  
 $N_{TS}$  = total number of wheels passing the short zone.

This, of course, assumes no multiply-flatted wheels. From this result, we would expect the vertical wheel/rail load spectra from short-zone measurements to begin to deviate from the "normal" spectra at approximately the 1.5 percent frequency-of-exceedance level. This is seen in Figure 3-8.

Representative extreme values of flat wheel impact loads are noted for each vehicle type in Table 3-8, along with the resulting impact factor and speed band of occurrence. It is obvious from this table, comparing the impact factors, that locomotives are less likely to have large wheel flats than heavy freight cars which have similar static vertical wheel loads. Impact factor (defined here as the ratio of dynamic load increment to "static" load) does appear to be an inverse function of vertical wheel load, with values as high as 2.66 under light cars.

TABLE 3-6. PARAMETERS DESCRIBING VERTICAL EXTREME-VALUE  
(FLAT WHEEL) LOADS WITHIN CWR TEST SECTION

Vehicle Type	% Axles in Population	Mean Load, $\bar{F}_v$ (kips)	Exponential Function	
			$F_{dyn}$ (kips)	R
1. Locomotives	8.8	33.5	5.5	0.045
2. Cars > 110T GWT	17.7	32.9	7.4	0.027
3. Cars 70T - 110T	14.3	22.3	5.9	0.058
4. Cars 40T - 70T	29.6	14.1	4.0	0.019
5. Cars <40T	29.6	8.4	4.0	0.110

TABLE 3-7. COMPARISON OF PREDICTED AND MEASURED VERTICAL W/R  
LOAD EXCEEDANCE LEVELS, CWR TRACK (ALL TRAFFIC,  
ALL SPEEDS)

Vertical W/R Load Level, kips	Wheel/Rail Vertical Load Exceedance			
	Predicted	Measured Data		35" Zone (Scaled to 7")
		Average (7 Sites)	Range (7 Sites)	
>50	$8.0 \times 10^{-4}$	$7.1 \times 10^{-4}$	$3.1 \times 10^{-4}$ to $1.6 \times 10^{-3}$	$7.2 \times 10^{-4}$
>55	$3.5 \times 10^{-4}$	$3.8 \times 10^{-4}$	$1.3 \times 10^{-4}$ to $9.0 \times 10^{-4}$	
>60	$1.7 \times 10^{-4}$	$2.0 \times 10^{-4}$	$8.8 \times 10^{-5}$ to $4.5 \times 10^{-4}$	$1.7 \times 10^{-4}$
>65	$8.2 \times 10^{-5}$	$8.9 \times 10^{-5}$	0 to $1.8 \times 10^{-4}$	
>70	$4.0 \times 10^{-5}$	$5.1 \times 10^{-5}$	0 to $9.5 \times 10^{-5}$	$6.0 \times 10^{-5}$
>75	$2.0 \times 10^{-5}$	$1.3 \times 10^{-5}$	0 to $4.4 \times 10^{-5}$	
>80	$9.7 \times 10^{-6}$	$1.3 \times 10^{-5}$	0 to $4.4 \times 10^{-5}$	$1.2 \times 10^{-5}$
>85	$4.7 \times 10^{-6}$	$1.3 \times 10^{-5}$	0 to $4.4 \times 10^{-5}$	
>90	$2.3 \times 10^{-6}$	$1.3 \times 10^{-5}$	0 to $4.4 \times 10^{-5}$	$1.2 \times 10^{-5}$

TABLE 3-8. DISTRIBUTION OF DYNAMIC VERTICAL W/R LOADS AND REPRESENTATIVE  
EXTREME VALUES MEASURED WITHIN EXTENDED (35") ZONE

Vehicle Type	Total Wheels	Wheels ≥ 4 Kips	Vertical W/R Load (Kips)		Impact Factor	Speed Band (mph)
			Filtered Load (30 Hz)	Dynamic Load Increment		
1 (Locomotives)	1487	237 (15.9%)	47.0	20.1	0.43	≥ 60
			39.2	17.0	0.43	≥ 60
			34.8	17.0	0.49	≥ 60
2 (Cars > 110T)	2742	174 (6.3%)	46.9	46.0	0.98	40-49
			44.7	34.9	0.78	50-59
			37.3	33.9	0.91	50-59
3 (Cars 70T-110T)	2306	99 (4.3%)	31.0	38.6	1.25	40-49
			37.3	35.9	0.96	40-49
			29.9	23.9	0.80	40-49
4 (Cars 40T-70T)	5088	255 (5.0%)	23.9	28.1	1.18	50-59
			15.6	22.8	1.46	50-59
			20.2	20.5	1.01	≥ 60
			8.2	14.6	1.78	50-59
5 (Cars < 40T)	4947	489 (9.9%)	11.1	20.0	1.80	50-59
			17.9	19.9	1.11	50-59
			11.6	19.5	1.68	50-59
			4.4	11.7	2.66	50-59
All	16570	1254 (7.7%)				

Speed effects on dynamic loads differ according to both the static vertical load and the wheelset mass, as shown in Table 3-9:

TABLE 3-9. SPEED EFFECTS ON VERTICAL DYNAMIC WHEEL/RAIL LOADS

Speed Band, mph	Dynamic Load Increment at Mean $+(3 \times \text{St'd Dev.})$				
	Locomotives	Cars > 110T	Cars 70T-110T	Cars 40T-70T	Cars < 40 T
<40	5.0	14.3	5.6	3.8	5.7
40-49	7.2	9.9	10.0	6.7	6.1
50-59	8.4	10.0	6.4	7.4	8.2
>60	10.4	8.6	6.6	6.0	6.6

The locomotives with the heaviest wheelset unsprung mass generate monotonically increasing dynamic force peaks, where the freight car dynamic force peaks are highest in the lower speed bands. This, however, may be influenced by the type of equipment run on the higher-speed, priority freight trains and may reflect the better maintenance standards.

### 3.2.3 Rail Joint Impact Loads

An extended vertical load zone was installed at the instrumented rail joint at Test Section 1 to measure wheel/rail loads in the vicinity of this joint. Although this rail joint was chosen initially because it was visually 1/4 to 3/8-inch low, the process of installing the instrumented tie plates (holding the tie up with a tamping bar while spiking) resulted in a nearly-flat joint. In fact, rail surface measurements from a taut string showed the joint to be 1.1 mm (0.04 inch) "proud" under no load. Due to mechanical tamping in the recent past, a number of rail joints in this track section appeared visually to be slightly high relative to the rail midspan region.

A typical example of vertical wheel loads through the joint region is shown in Figure 3-23 for the instrumented hopper car (the high-frequency wheelset as trailing axle on the trailing truck) during a 65-mph test run through the wayside track section. The classical "P<sub>2</sub>" force peak, 10 to 12

RUN 17M (300 HZ FILTER)

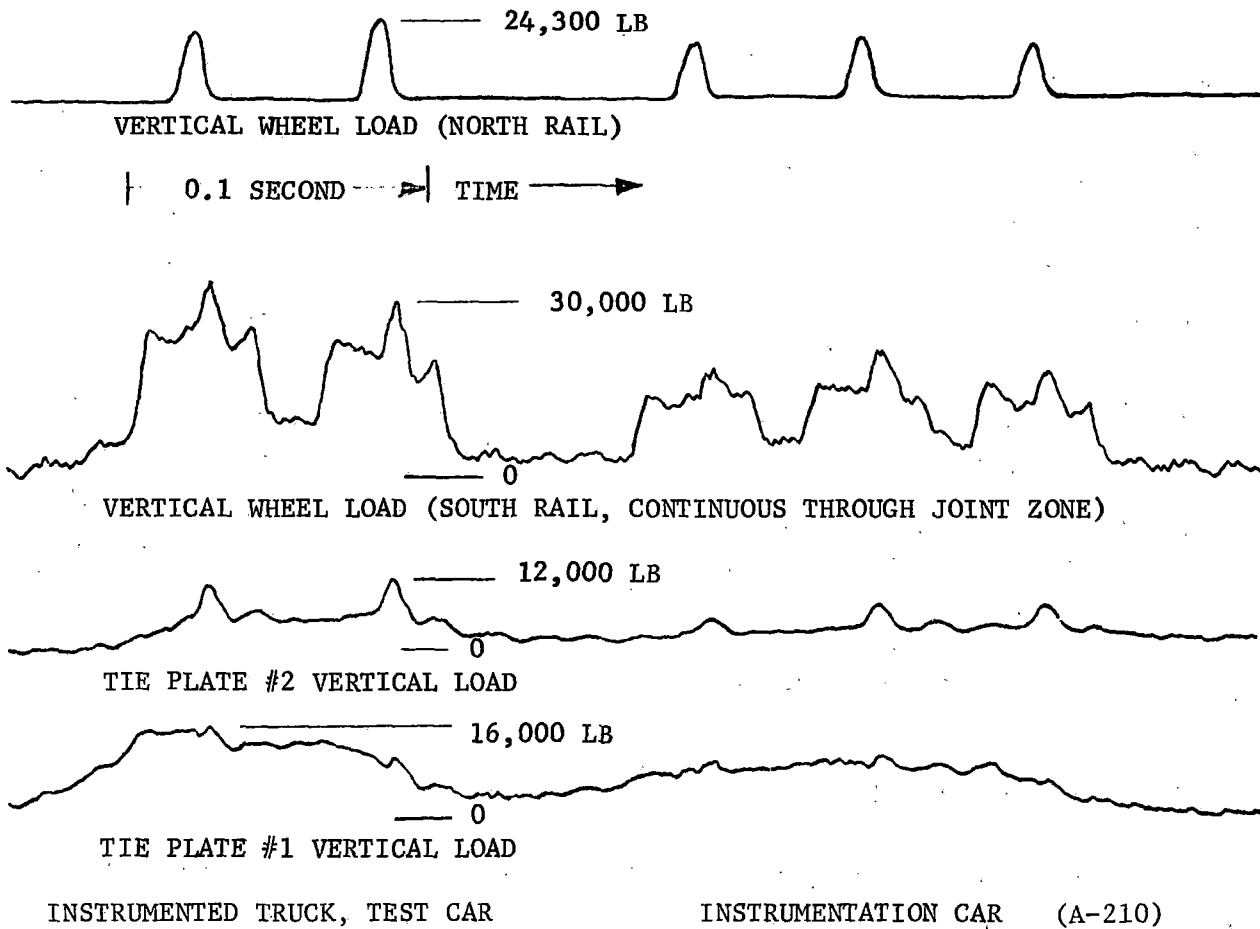


FIGURE 3-23. VERTICAL WHEEL/RAIL LOADS UNDER INSTRUMENTED TRUCK OF TEST CAR (100-TON HOPPER CAR), EASTBOUND AT 65 MPH WITH HIGH-FREQUENCY WHEEL TRAILING, TEST SECTION 1 (BJR TRACK), MEASUREMENT SITE 3

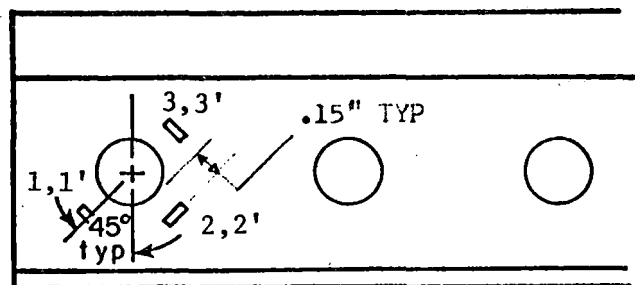
milliseconds in half-cycle duration, can be seen quite plainly, resulting in a wheel load roughly 25 percent higher than the nominal. In this illustration, a 300-Hz filter has been employed; but, the same data through 1000-Hz and 2000-Hz filter settings show no indication of the "P<sub>1</sub>" short-duration impact load. This may be attributed to the essentially flat surface profile and small ( $\sim 1/4$  inch) rail gap at this joint.

Data from a statistical analysis of peak vertical loads within the joint zone are summarized in Table 3-10 for several of the vehicle categories, in comparison with the midspan of the opposite rail (Site 3). From the difference in load between these two locations, the value of joint impact load increment is seen to run typically from 4 to 7 kips over this speed range for locomotive wheels, and from 0 to 15 kips for freight car wheels. Because of a processing problem, data were not available from the lighter vehicle categories. Note that for locomotives and heavy cars, the 3-sigma joint impact load (about 3 axles out of 1000) runs in the 50-kip range, even for a joint with a nearly perfect unloaded surface geometry. (These, however, may be flat wheels.)

### 3.3 TRACK RESPONSE MEASUREMENTS

#### 3.3.1 Rail Joint Bolt Hole Strains

Standard 1/16-inch foil strain gages were applied to the first running-on bolt hole (for westbound trains) of the instrumented joint, oriented as sketched below:



(PRIMED GAGE NOS. ON FIELD SIDE)

TABLE 3-10. COMPARISON OF PEAK VERTICAL W/R LOAD AT JOINT ZONE VS.  
MIDSPAN OF RAIL

Vehicle Type	Speed Band (mph)	Peak Vertical W/R Load					
		Mean		Mean + S*		Mean + 3S	
		Midspan	Joint	Midspan	Joint	Midspan	Joint
Locomotives	< 40	33.5	37.2	37.1	40.8	44.3	48.1
	40-49	34.3	38.0	37.9	42.0	45.0	50.0
	50-59	32.1	38.8	35.8	42.6	43.1	50.3
	≥ 60	33.0	39.2	37.1	44.3	45.2	54.4
Cars ≥ 110T	< 40	34.3	35.8	38.4	40.3	46.5	49.4
	40-49	33.4	36.0	37.3	40.9	45.2	50.6
	50-59	32.4	35.1	36.7	39.7	45.4	49.0
	≥ 60	32.5	37.6	35.9	42.7	42.7	52.8
Cars 70T-110T	< 40	22.5	22.2	25.9	27.5	32.6	38.2
	40-49	25.8	26.0	29.8	34.1	37.9	50.2
	50-59	25.0	26.1	28.9	34.8	36.7	52.5
	≥ 60	23.5	19.1	27.1	29.7	34.2	50.9

\*S = standard deviation estimator.

Gages were applied both to the field and gage sides of the rail and were recorded separately on the FM tape recorder. Calibrated, strain-gaged bolts were used upon reassembly of the joint. Prior to recording several typical freight trains, the bolts were tightened by a member of the section crew with a standard track wrench. Bolt tensions were measured after several trains had passed, using a strain indicator:

Bolt	In Order, East to West					
	59	64	61	60	62	63
Tension (kips)	12.8	17.7	9.2	14.0	11.6	21.0

A typical example of recorded bolt hole strains under the lead truck of an 8-axle DDA-40X diesel unit at 68 mph is shown in Figure 3-24. The bolt hole strains show an almost instantaneous change in strain level with transfer of the wheel vertical load across the joint gap, then a saw-tooth decrease in level (compression at gages 1 and 3, tension at gages 2) as the wheel approaches the bolt hole. Some minor high-frequency, load impact dynamics are superimposed on this fundamental shape. The lower-frequency  $P_2$  force peaks impose rather minor changes in bolt hole strain levels at this particular joint. Bolt hole strains under locomotive axles were found to run typically 600 microstrain maximum for westbound runs. Gages in locations 1F and 2G showed strain reversal (compression to tension, or vice versa) most strongly. For eastbound (running-off) traffic, the strain signature of Figure 3-24 was reversed, with somewhat lower strain peak levels recorded.

For another westbound freight going 69 mph consisting of four 6-axle locomotive units (SD-40-2, U33C, SD-45, SD-40), the following strain values were noted under the locomotive axles:

Gage Location	Bolt Hole Strain, microinch/inch*					
	1F	2F	3F	1G	2G	3G
Maximum strain	-500	490	-580	-670	320	-780
Mean of Peaks	-306	406	-463	-579	262	-587
Standard Deviation of Peaks	95	39	46	54	33	101

\* minus denotes compression

### 3.3.2 Rail Longitudinal Strains

A set of four weldable 1-inch strain gages was applied both at the BJR and CWR tangent track sections (in each case at Site 6) to measure longitudinal strains in the rail. Gages were located at the top edge of the rail

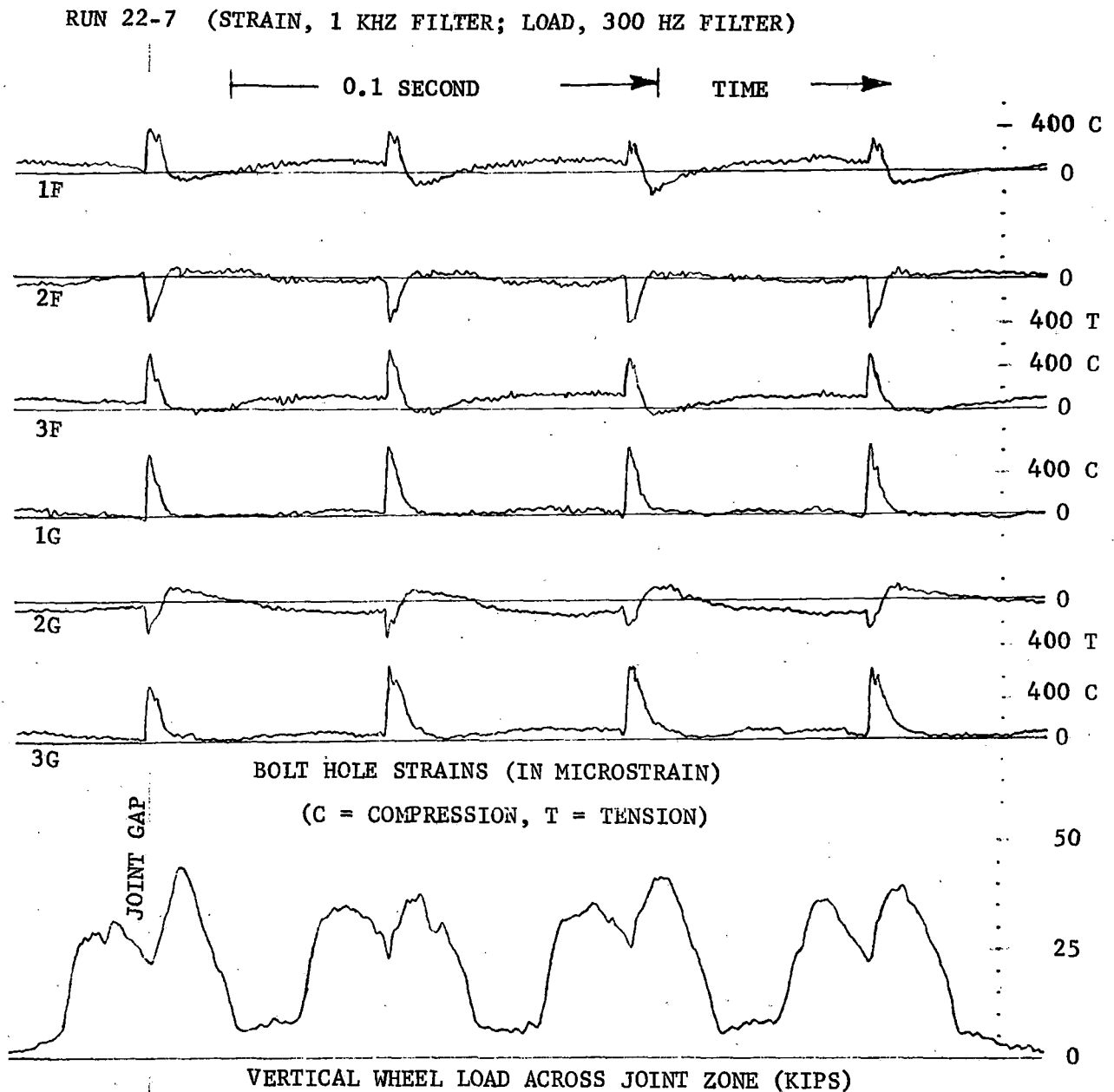


FIGURE 3-24. EXAMPLE OF BOLT HOLE STRAINS AND WHEEL LOAD AT INSTRUMENTED JOINT, TEST SECTION 1 (BJR TRACK), LEAD TRUCK OF TRAILING 8-AXLE (DDA-40X) LOCOMOTIVE UNIT, WESTBOUND AT 68 MPH

base and at the extreme top edge of the rail head fillet. Rail deflections, as well as the standard lateral and vertical W/R force samples, were also recorded from these locations.

An example of wheel loads, longitudinal strains, and rail deflections is shown in Figure 3-25 under the lead truck of a slowly-moving 6-axle locomotive. The rail head longitudinal strain undergoes increased compressive strain due to rail bending as the wheel approaches, then exhibits a sharp reversal directly under the contact patch due to local deflection of the head on the web as a separate elastic foundation. Note that the zero strain line is a relative level: the rail temperature at the time of this recording was 60°F, and the rail was probably in slight tension. Site 6 in the BJR track section turned out to have a lower-than-average track modulus, and this is reflected in the vertical deflection of 0.25 inch, where individual axles of the truck cannot be distinguished.

Measurements of longitudinal strain on the CWR track showed some interesting asymmetries in the head strains, apparently due to wheel contact toward the field side of the rail head. For example, under several locomotive wheels the head/field gage showed a peak of -280 (increased compression) reversing to +430 microstrain under the contact patch, while the head/gage gage showed -350 reduced to -250 microstrain under the contact patch. The base/gage gage showed +400 microstrain (increased tension) under this situation. (The base/field gage was nonoperative due to a high noise level.) Vertical rail deflections at this CWR site were typically 0.15 inch under locomotive wheels, with a lateral deflection of 0.02 inch inward. Longitudinal strains in the rail head were found to decrease (less compression) by 30 to 60 microstrain from the static level after passage of the locomotive axles, possibly due to rail "running" in the direction of traffic. The one operational rail base gage showed an increase of roughly 30 microstrain at the same time.

### 3.3.3 Tie Plate Vertical Loads

Four load-cell tie plates for measuring vertical loads and transverse moments were installed on consecutive ties at the rail joint and CWR

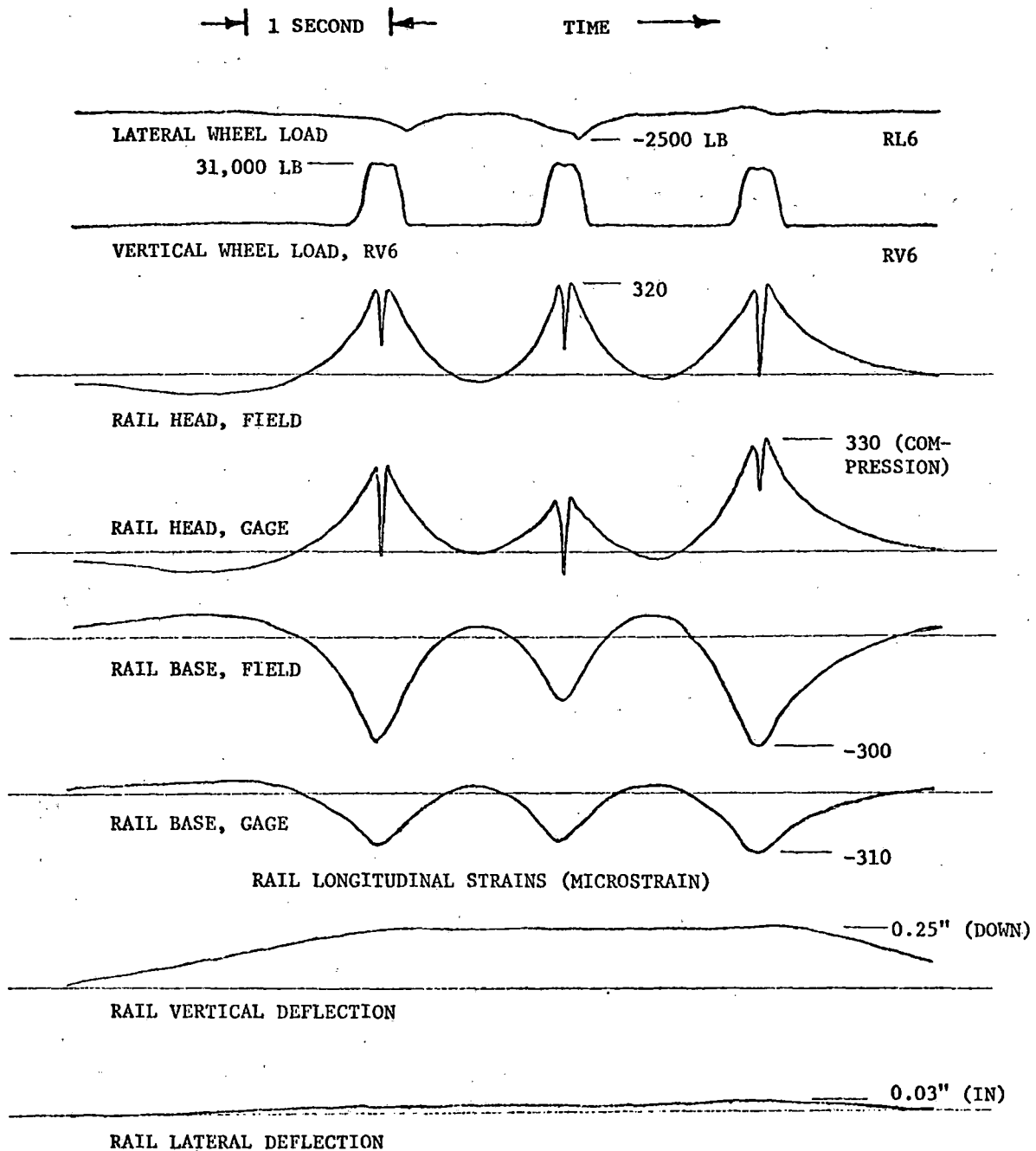


FIGURE 3-25. WHEEL LOADS, LONGITUDINAL STRAINS, AND DEFLECTIONS OF RAIL DURING SLOW ROLL-BY OF LEAD TRUCK OF LOCOMOTIVE, TEST SECTION 1 (BJR), SITE 6

extended vertical load zones. Due to instrumentation problems, data from the two outer tie plates of the rail joint zone were not recorded. Tie plate loads from a few representative trains were recorded from all four tie plates at the CWR test section, however.

Time-domain response of the two inner tie plates has been shown in previous sections (see Figures 3-16, 3-17, 3-19 and 3-20). Loads from all four tie plates under DD-35 locomotives during a slow roll-by were analyzed to check the load distribution at the extended vertical load zone:

Tie Plate*	Tie Plate Load, kips			
	TP3	TP1	TP2	TP4
Max. Load	22.5	17.7	29.7	26.0
Mean Load	18.1	14.4	27.3	19.4
Std Dev.	2.5	1.5	2.6	3.9

\*In order, going west.

The apparent reason for the lower support provided by Tie Plate 1 (even though it was carefully shimmed) was that this tie was a soft wood, while the rest of the ties were hardwood. Oscillations in tie plate load of 3 to 4 kips peak-to-peak due to incipient wheel slip (see Figure 3-13) were noted during this slow roll-by.

#### 3.3.4 Track Deflections

Rail vertical deflections under known vertical loads were measured during the calibration of strain gage circuits. A millimeter scale cemented to the rail web was viewed through a transit, and deflections were measured at several points during the increasing load calibration cycle. Some additional points were measured under slowly-moving locomotive or freight car wheels. The resulting curves in Figure 3-26 show these force/deflection plots for the seven measurement sites for each of the BJR and CWR test sections. The sites, particularly on the BJR track, show a great deal of variability in compliance, as well as the expected nonlinear behavior of increasing tangent stiffness with increasing vertical load. Several of the sites, particularly 1, 2 and 6 on the BJR track, and 4 on the CWR track, exhibited "slack" between rail base and tie plate on the order of 1/10th inch, and an eventual hardening near 2/10ths of an inch. This was illustrated in the rail deflection of Figure 3-25.



Track point-load stiffness values (the change in deflection between 11 and 17 kips) and derived track moduli are listed in Table 3-11 for each of the sites, as well as average values for the test sections. Neither track stiffness nor the amount of initial slack or freeplay under the rail seat seems particularly correlated with whether statistically higher or lower loads were experienced at a particular site.

Dynamic deflection measurements were made under a limited number of trains at Site 6 of both test sections. On the BJR track, a considerable problem was caused by the rail running longitudinally, which required an ad hoc linkage to keep the core of the DCDT from being damaged. This linkage tended to bind up against the transducer support as the rail changed position on the order of an inch. Greater success was experienced at the CWR site, where the rail ran less than one-half inch total. Typical vertical deflections under locomotive axles included an uplift of 0.06 inch ahead of the lead axle, then downward displacements of 0.09 to 0.14 inch. The 42-Hz component of force noted in Figure 3-13 produced a vertical peak-to-peak displacement oscillation of 0.13 inch. Lateral displacements under locomotive wheels ranged from 0.025 to 0.030 inch inward at this site.

Because of the difficult conditions under which force calibrations were conducted, no attempt was made to generate force/deflection curves in the lateral direction. With vertically-unloaded track, however, rail head lateral motions due to translation and rotation were typically on the order of 1/4 inch under the maximum 10 to 12 kip lateral calibration loads.

### 3.3.5 Track Accelerations

Accelerometers were mounted on the rail base (close to the web) and on the tie to measure vertical track acceleration levels under typical traffic. These accelerometers were located at Site 3, north rail (mid-span) on the BJR track, and at Site 3, north rail (at the extended measurement zone) on the CWR track. In addition, an accelerometer was cemented to a tie plate which was in turn sunk into a dried clay patch on the maintenance road, about 10 ft from the track centerline, to measure vertical ground accelerations at the BJR site.

TABLE 3-11. TRACK VERTICAL STIFFNESS MEASUREMENTS AT INDIVIDUAL MEASUREMENT STIES, TANGENT TRACK SECTIONS

Test Section	Test Site	Vertical Stiffness (Kip/in Per Rail) $K_r$	Track Modulus (Lb/in <sup>2</sup> Per Rail) $u$
1 133 lb/yd BJR	1	111	983
	2	188	1990
	3	200	2160
	4	194	2070
	5	316	3970
	6	115	1030
	7	273	3250
	Mean	200	2160
	Std Dev.	75	--
2 133 lb/yd CWR	1	231	2610
	2	273	3250
	3	545	8210
	4	194	2070
	5	273	3250
	6	200	2160
	7	316	3970
	Mean	290	3540
	Std Dev.	120	--

(a) Loads applied at center of crib, one rail.

(b)  $K_r$  calculated from  $(17,000-11,000)/(\Delta Z_{17}-\Delta Z_{11})$ .

(c)  $u = K_r^{4/3}/5422$  lb/in/in.

3.3.5.1 Rail Accelerations, BJR Track. Run 23-1, a mixed freight at 60 mph eastbound with an SD-40-2 diesel unit on the point, was examined in detail to determine acceleration levels. A power spectral density curve for 10 averages (the locomotive units and first few cars) over a 1600-Hz bandwidth is shown in Figure 3-27. The predominant frequency bands for vertical accelerations are seen to be 175-250 Hz, and 500-600 Hz for BJR track. Typically large oscillations noted on the oscillograph, contained amplitudes of -640, +1060, -734 g (after 13 milliseconds), +970 g, at a frequency of 300 Hz under a freight car wheel.

3.3.5.2 Rail Accelerations, CWR Track. Run 31-12, an eastbound van train at 65 mph with a DDA-40X diesel unit on the point, and Run 31-16, a mixed freight westbound at 60 mph again with a DDA-40X on the point, were examined in detail to determine acceleration levels. A PSD plot from Run 31-16 for 10 averages (starting at the locomotive) over a 1600-Hz bandwidth is shown in Figure 3-28. This figure shows a strong spectra peak at 485 Hz. Taking this same data, but with 25 averages over a 3200-Hz bandwidth, brings out the important 780-Hz rail resonant frequency, as shown in Figure 3-29. A scattering of strong spectral peaks between 750 and 1200 Hz can be seen, as well as a strong response between 1500 and 1700 Hz. From the oscillographic records, flat wheels under the locomotives produced oscillations up to +950 g at a frequency just over 1000 Hz.

3.3.5.3 Ground Accelerations, BJR Track. Two runs were examined in detail to determine typical ground response at the BJR track section: Run 22-11, a westbound van train at 65 mph with a DDA-40X locomotive on the point, and Run 22-13, an eastbound empty unit coal train at 48 mph with an SD-45 diesel unit on the point. A linear spectrum of acceleration for 20 averages over a 100-Hz bandwidth shows important spectral peaks at 27, 35, 40 and 60-65 Hz, as shown in Figure 3-30, for the empty unit train. Typically large acceleration peaks from the oscillograph of +0.22, -0.29, +0.24 g at 63 Hz, and +0.40, -0.37, +0.38 g at 80 Hz were noted under empty cars. Ground accelerations under the trailing 6-axle unit of Run 22-11, apparently associated with passage of wheels, reached maxima of -0.45, -0.49 and -0.43 g, with positive maxima of +0.30 g between axles.

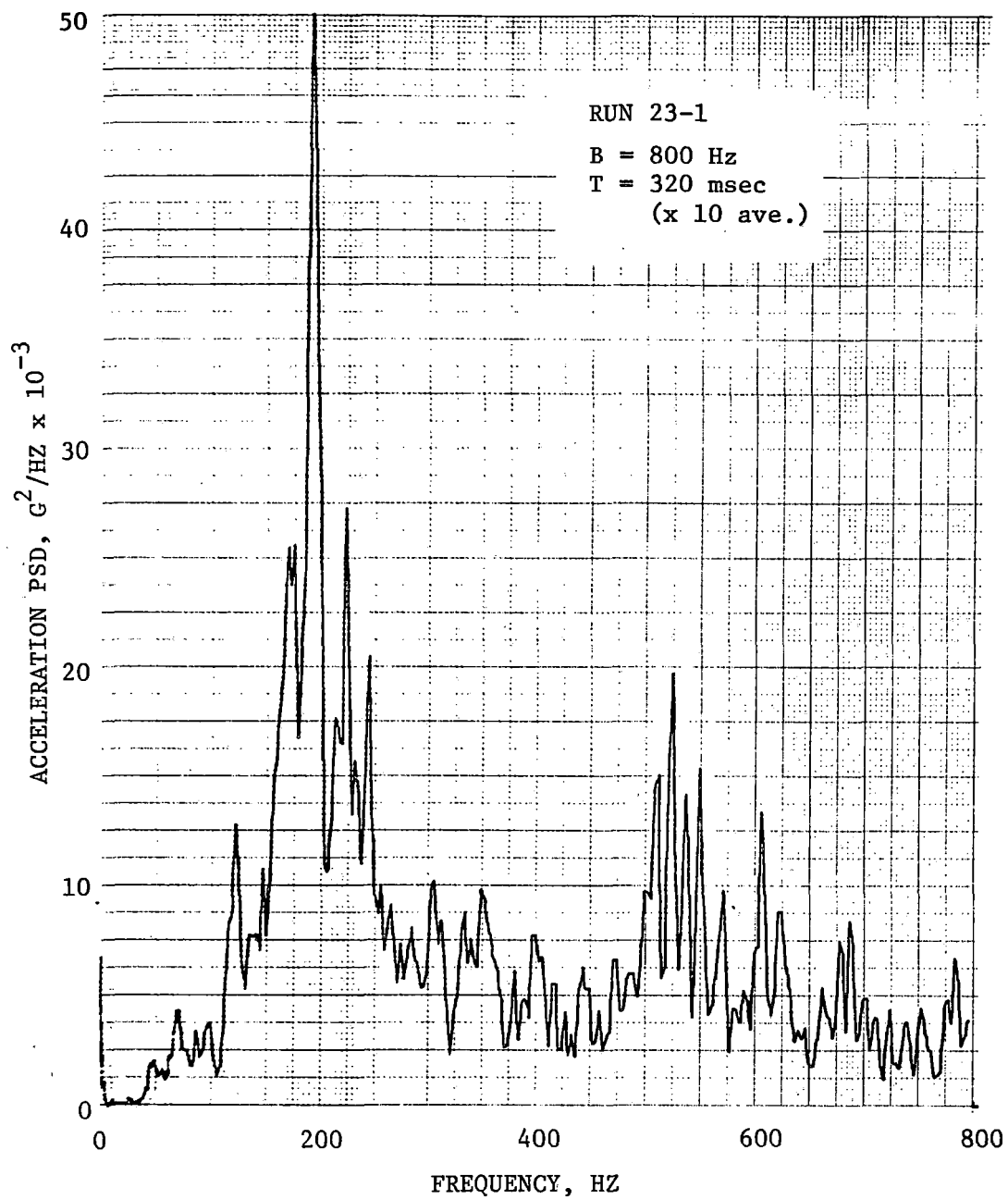


FIGURE 3-27. RAIL VERTICAL ACCELERATION POWER SPECTRAL DENSITY, BJR TRACK UNDER MIXED FREIGHT, 60 MPH (10 AVERAGES, 800-HZ BANDWIDTH)

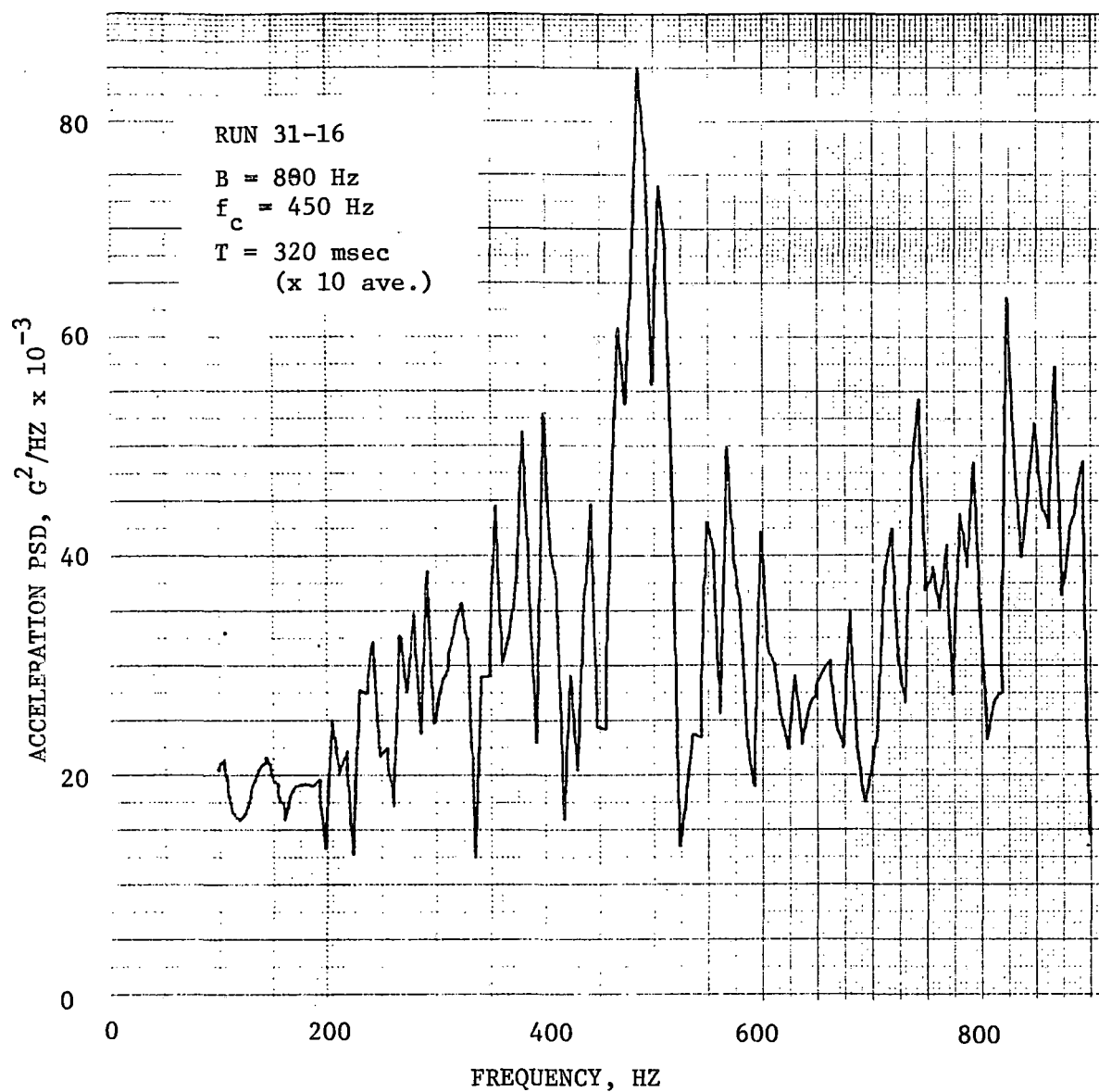


FIGURE 3-28. RAIL VERTICAL ACCELERATION POWER SPECTRAL DENSITY, CWR TRACK UNDER MIXED FREIGHT, 60 MPH (10 AVERAGES, 800-HZ BANDWIDTH)

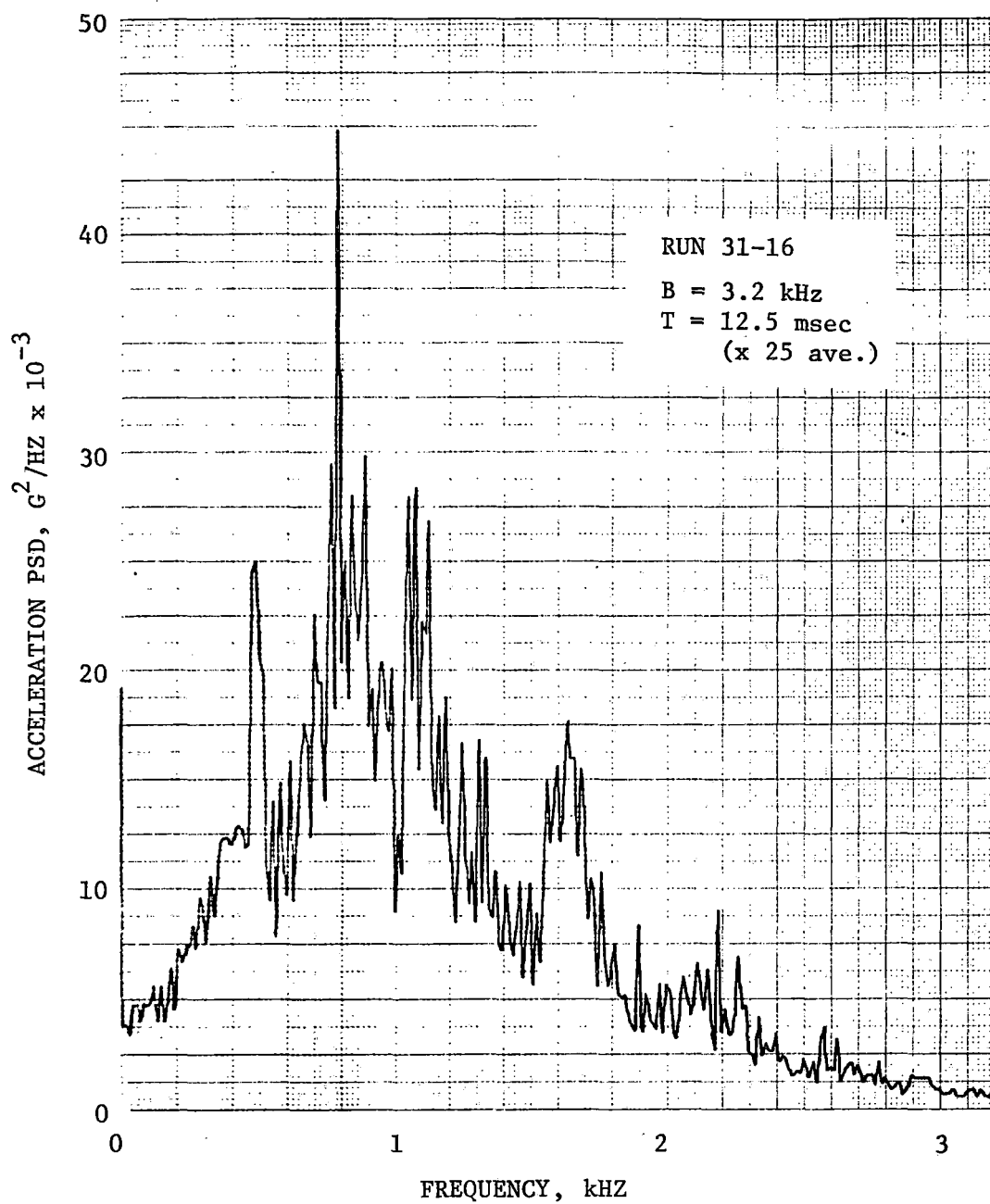


FIGURE 3-29. RAIL VERTICAL ACCELERATION POWER SPECTRAL DENSITY, CWR TRACK UNDER MIXED FREIGHT, 60 MPH (25 AVERAGES, 3200- HZ BANDWIDTH)

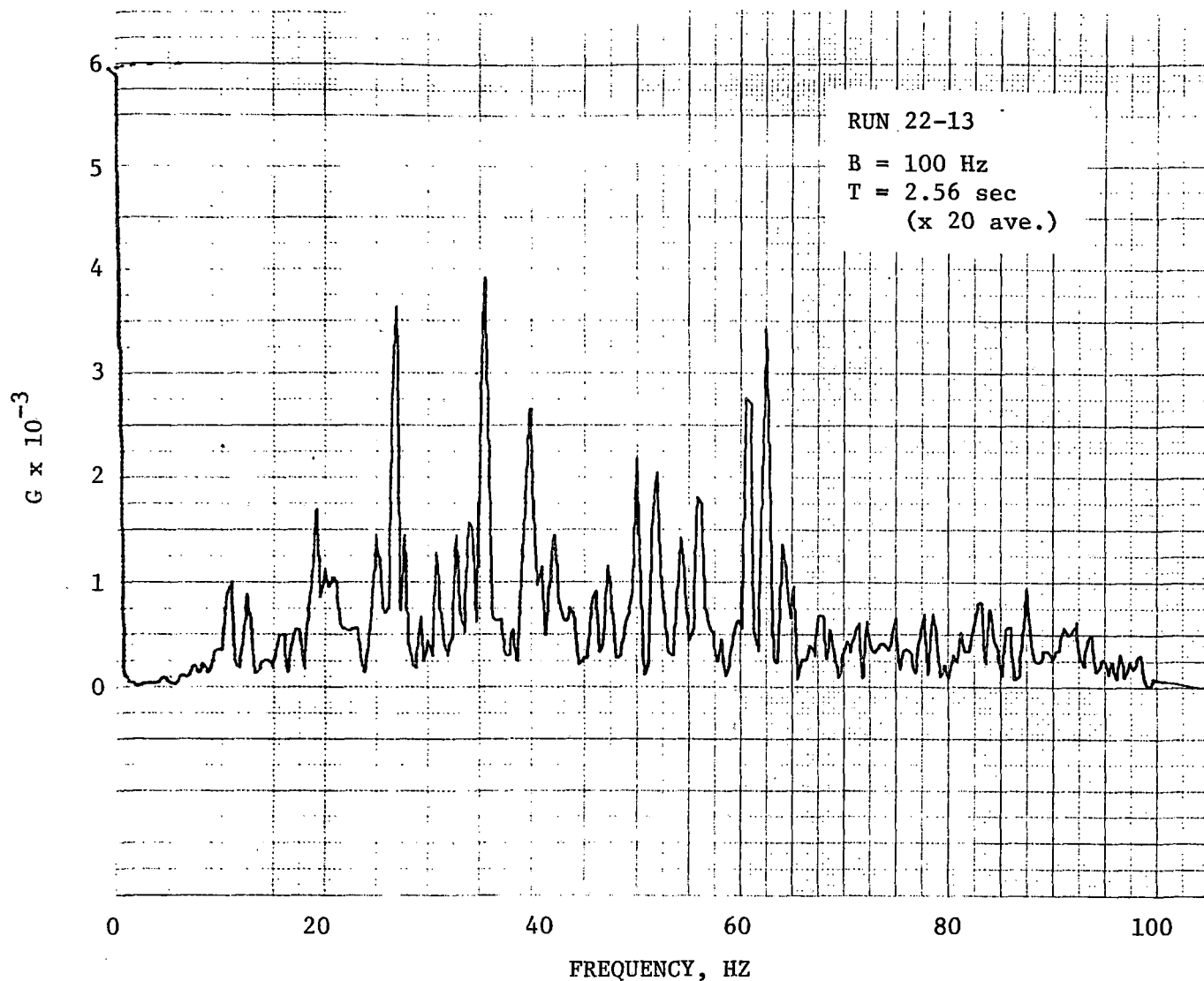


FIGURE 3-30. GROUND VERTICAL ACCELERATION LINEAR SPECTRUM, 10 FT FROM CENTERLINE OF BJR TRACK UNDER EMPTY UNIT TRAIN, 48 MPH (20 AVERAGES, 100-HZ BANDWIDTH)

## 4. RESULTS OF VEHICLE-BORNE MEASUREMENTS

### 4.1 WHEEL/RAIL LOADS

#### 4.1.1 Statistical Analysis of Wheel/Rail Loads

Figures 4-1 through 4-4 present statistical summaries of the load data measured by the instrumented wheel while operating on the BJR and CWR track sections. A set of frequency-of-exceedance distribution curves is presented for the vertical and lateral loads for each traversal of the test site. Each set of distribution curves represents the data obtained from approximately three miles of operation over each of the designated track sections. The results are based upon the classification of eight samples of load data per wheel revolution.

The major statistical parameters are summarized in Table 4-1, which gives the mean values and the standard deviations for the vertical and lateral forces and the L/V ratios. The table also summarizes similar data for the low frequency system so that comparisons can be made between the two systems. The instrumented wheel is on the leading axle of the leading truck (south rail) when operating westbound and on the trailing axle, trailing truck when operating eastbound.

The following general comments can be provided with reference to the vertical load data:

a. There is a gradual increase in the variance of the data about the mean, with increasing speed on both the BJR and CWR track sections.

b. At speeds of 45 mph and above, there is an increase in the variance of the data on BJR with respect to the data on CWR for operations at the same speed.

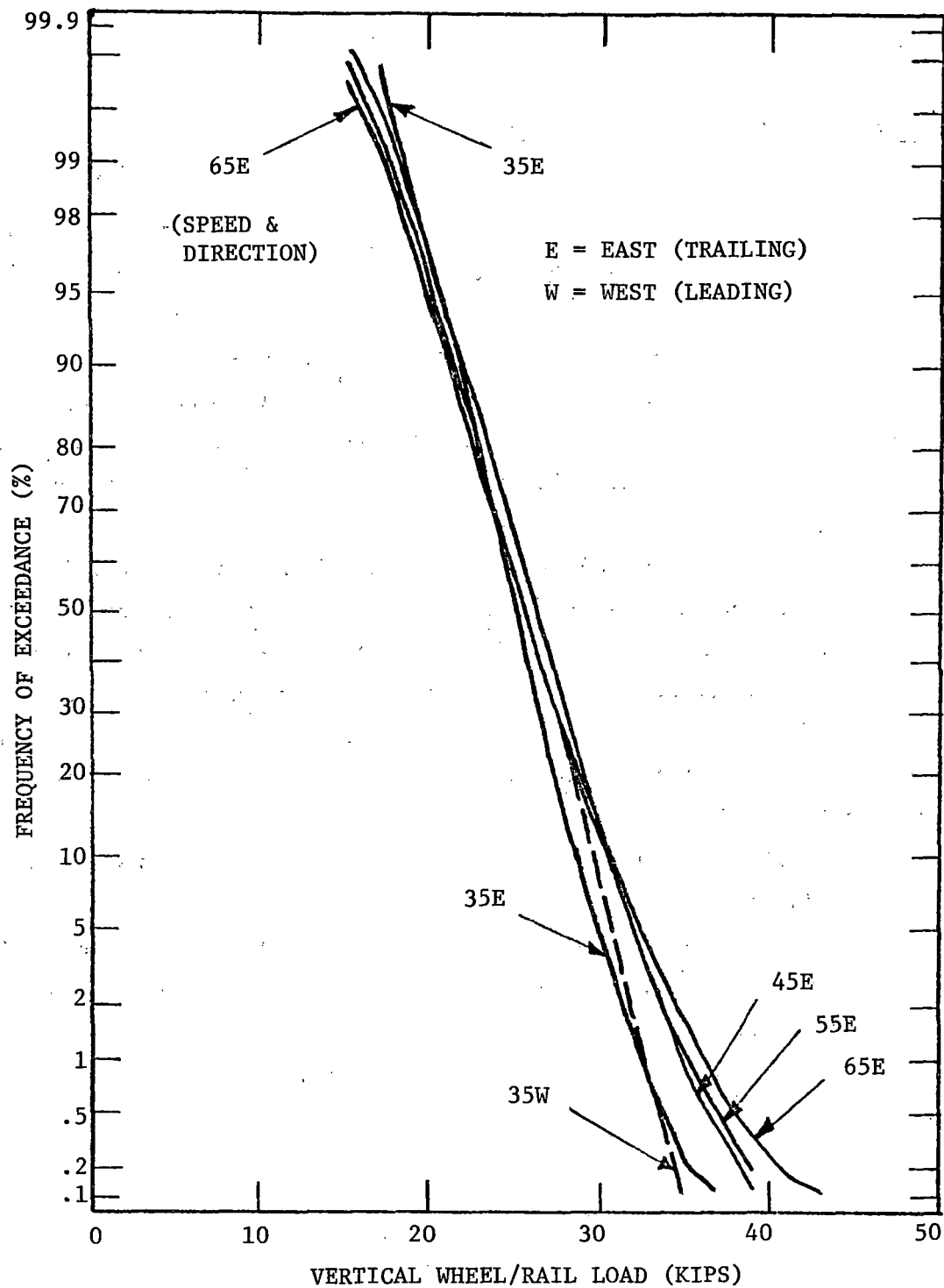


FIGURE 4-1. FREQUENCY-OF-EXCEEDANCE PLOTS FOR VERTICAL WHEEL LOAD FROM INSTRUMENTED WHEEL, TANGENT BJR TRACK

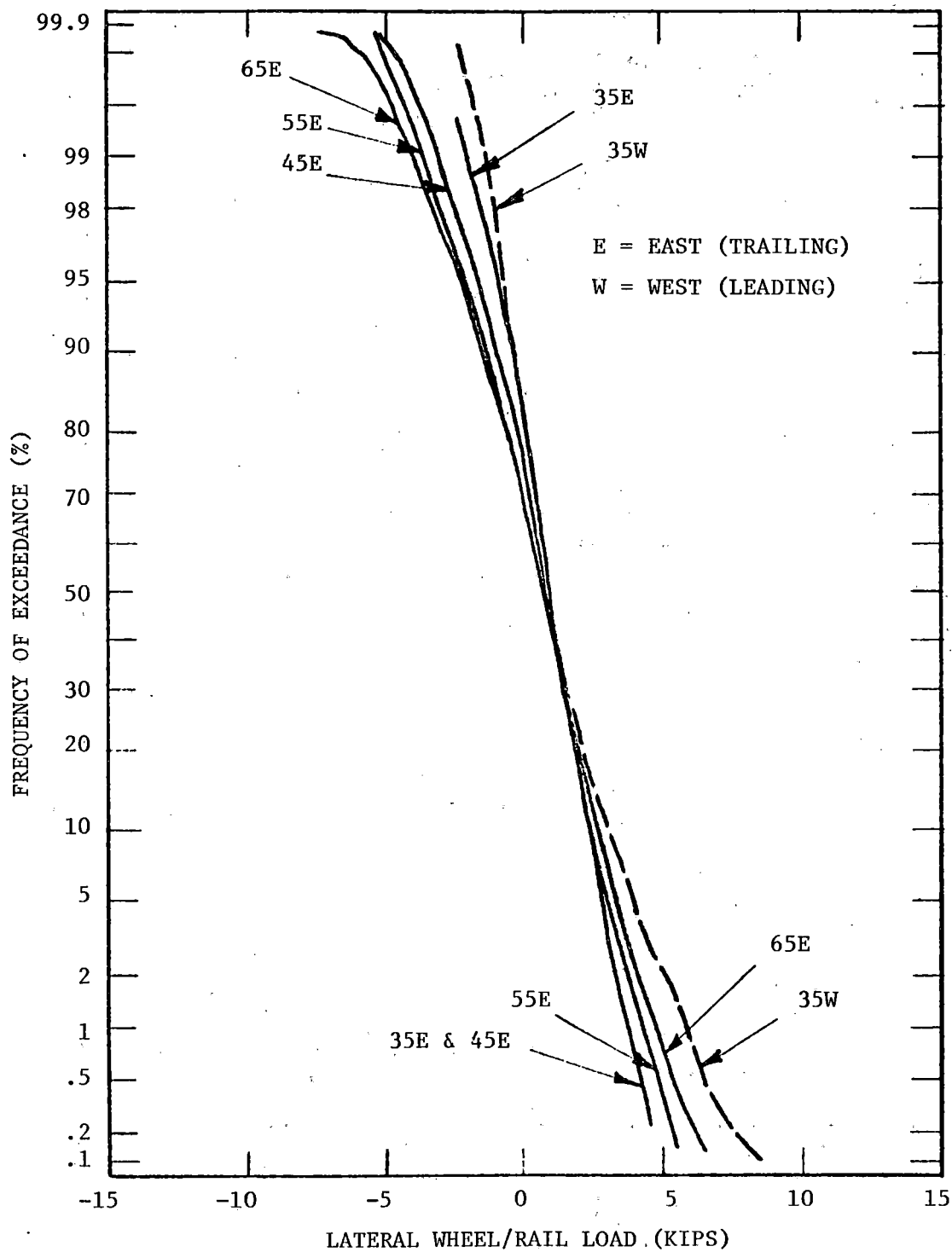


FIGURE 4-2. FREQUENCY-OF-EXCEEDANCE PLOTS FOR LATERAL WHEEL LOAD FROM INSTRUMENTED WHEEL, TANGENT BJR TRACK

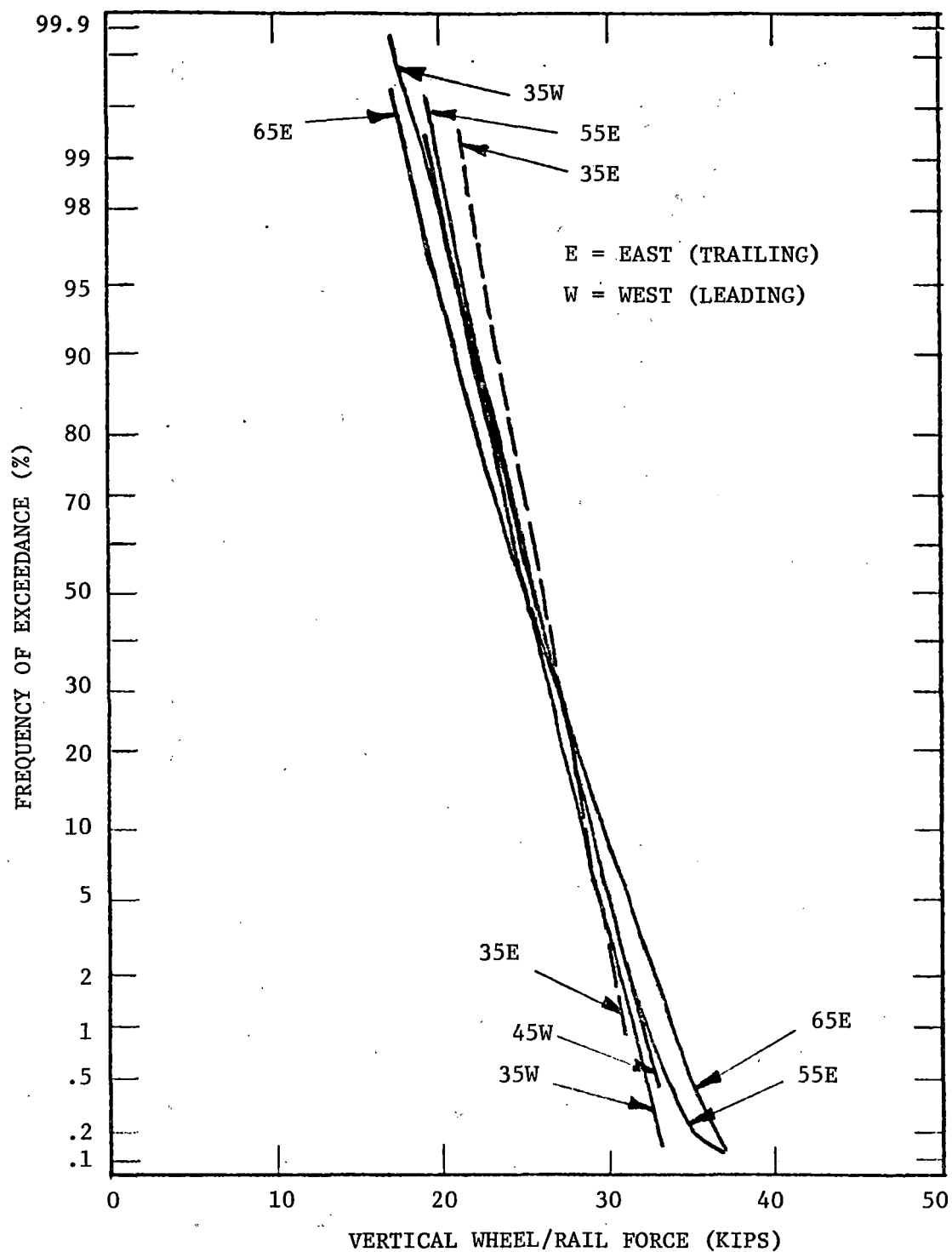


FIGURE 4-3. FREQUENCY-OF-EXCEEDANCE PLOTS FOR VERTICAL WHEEL LOAD FROM INSTRUMENTED WHEEL, TANGENT CWR TRACK

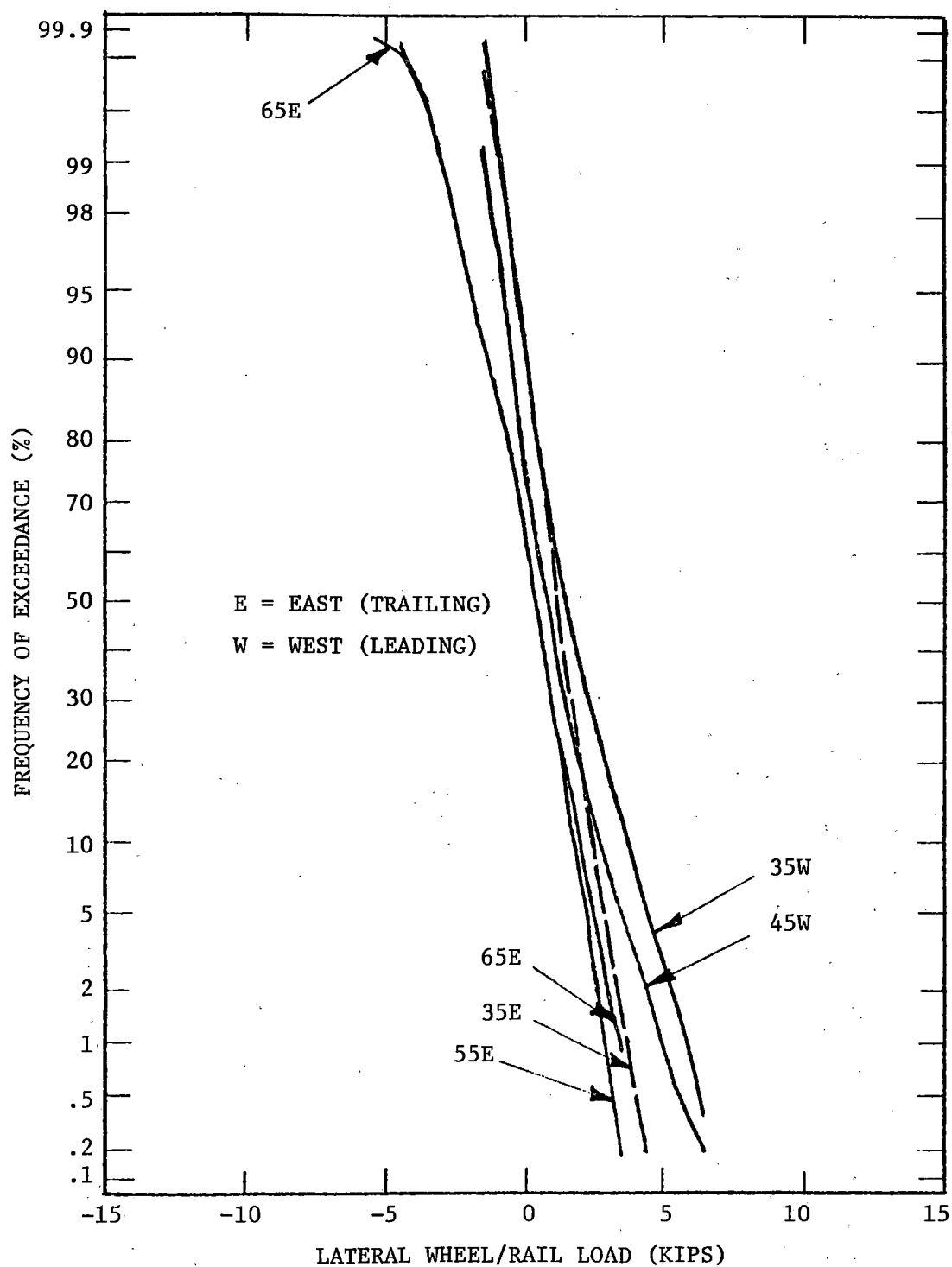


FIGURE 4-4. FREQUENCY-OF-EXCEEDANCE PLOTS FOR LATERAL WHEEL LOAD FROM INSTRUMENTED WHEEL, TANGENT CWR TRACK

TABLE 4-1. STATISTICAL SUMMARY OF WHEEL/RAIL LOAD CHARACTERISTICS FROM  
VEHICLE-BORNE MEASUREMENT SYSTEMS, TANGENT TRACK OPERATION

Load Measurement System	Rough Tangent (BJR) Test Section					Smooth Tangent (CWR) Test Section				
	35 mph EAST	35 mph WEST	45 mph EAST	55 mph EAST	65 mph EAST	35 mph EAST	35 mph WEST	45 mph WEST	55 mph EAST	65 mph EAST
Instrumented Wheel (high frequency system)										
Vertical Load (lb)										
Mean	25030	25620	26040	25710	25620	25930	25050	25450	25520	25160
Std. Deviation	2970	3340	3740	3760	4070	2430	3030	3250	3170	3830
Lateral Load (lb)										
Mean	880	1110	670	590	610	1260	1720	1000	370	320
Std. Deviation	1130	1550	1460	2090	2320	970	1420	1330	1250	1340
L/V Ratio										
Mean	.035	.040	.025	.056	.025	.048	.068	.038	.014	.011
Std. Deviation	.045	.062	.060	.075	.072	.038	.058	.050	.049	.054
Instrumented Axle & Side Frames (low frequency system)										
Vertical Load (lbs, left wheel)										
Mean	25810	25750	25830	25410	25560	25340	27020	26410	26060	26050
Std. Deviation	2390	2570	2620	2670	2920	1760	2030	2100	2210	2400
Lateral Load (lb)										
Mean	130	-240	660	210	350	40	-1070	-810	300	-150
Std. Deviation	1290	1680	1580	1640	1870	1120	1700	1750	1400	1500
L/V Ratio										
Mean	.009	-.008	.031	.014	.021	.004	-.039	-.030	.015	-.001
Std. Deviation	.053	.066	.066	.068	.077	.045	.062	.066	.056	.059

EAST = Trailing Axle, WEST = leading axle

The following general comments can be provided with regard to the lateral load data:

c. There is a greater variance in the data when the wheel is operating on the lead axle of the truck (westbound movement) than when the instrumented wheel is on the trailing axle of the truck (eastbound movement).

d. Considering movements with the instrumented wheel on the trailing axle, there is only a small increase in the variance of the data with increasing speed for operation on CWR, whereas there is a moderate increase in the variance of the data noted with speed for BJR operations.

e. For comparable speeds and directions the variance of the data is greater on BJR than on CWR track.

The cumulative probability distribution curves for the L/V ratio indicate that this parameter stayed within a very narrow range during each of the test runs.

Similar sets of statistical summary curves were developed for the load data measured by the low frequency system. These data sets indicate the same general force magnitudes and trends which were described above for the instrumented wheel system with the exception that the variance of the vertical load data is somewhat less in each case than that recorded by the instrumented wheel system. Curves for vertical load measured by the low-frequency system indicate a normal (straight-line) distribution over the range of data plotted. Curves for lateral load showed the piecewise-linear combination of two normal distributions about approximately zero load, which is similar to the results from trackside instrumentation.

Figures 4-5 and 4-6 present statistical summaries of the lateral load data measured by the instrumented wheel while operating through the curve track test section. Data are presented for the traversal of two curves, the 6°00.4' curve which contained the BCL instrumented track site and the 5°58.7' curve immediately to the west. The instrumented wheel was operating on the low rail within the 6°00.4' curve and on the high rail in the 5°58.7' degree curve. Also, the instrumented wheel was located on the lead axle of the lead truck when operating in a westbound direction and on the trailing axle when operating in an eastbound direction. Data have been obtained only during the period the instrumented wheel was operating in the main body of the curve. The major statistical parameters are summarized in Tables 4-2 and 4-3, which

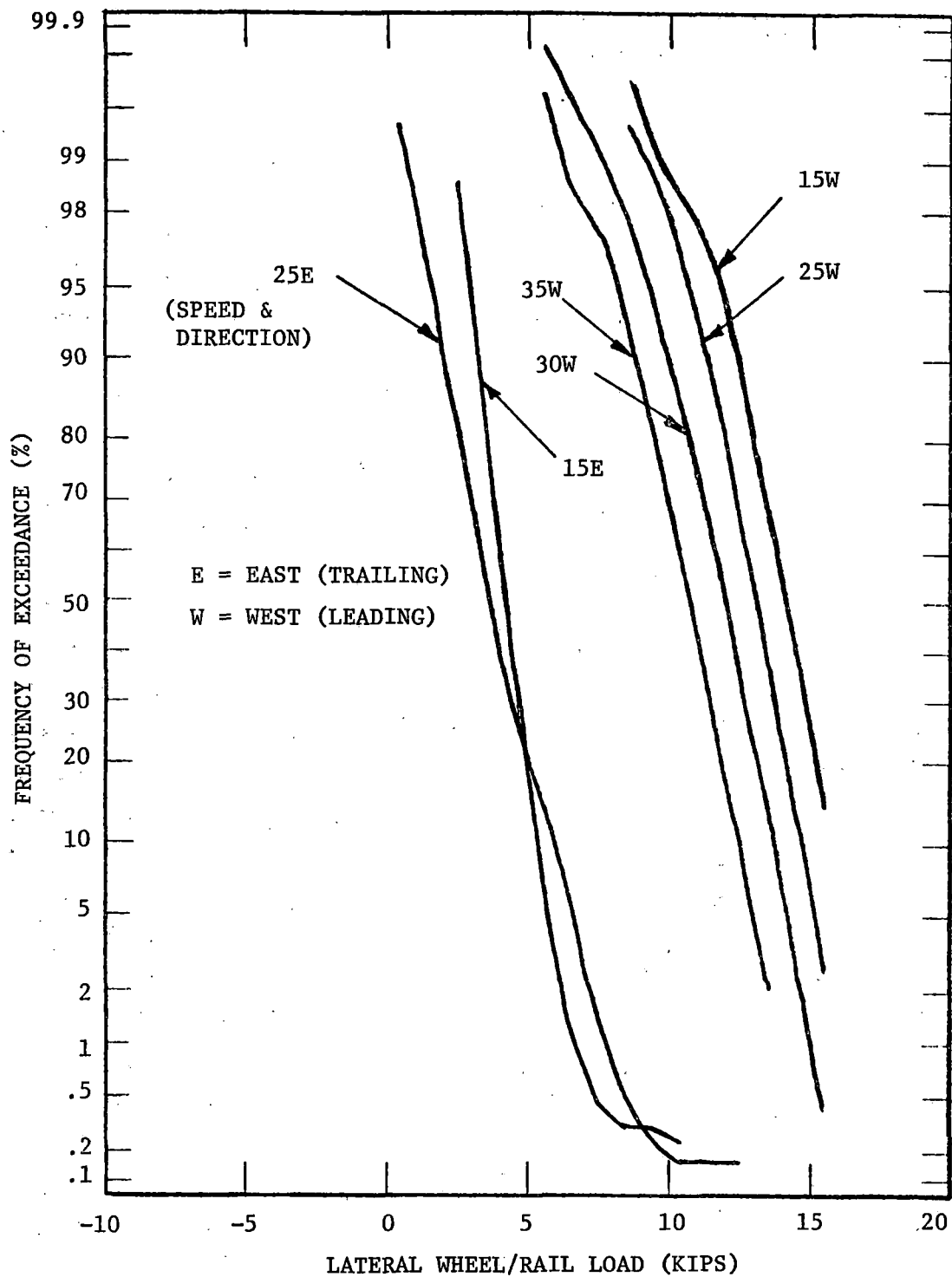


FIGURE 4-5. FREQUENCY-OF-EXCEEDANCE PLOTS FOR LATERAL WHEEL LOAD FROM INSTRUMENTED WHEEL, LOW RAIL OF 6°00' CURVE (6" SUPERELEVATION)

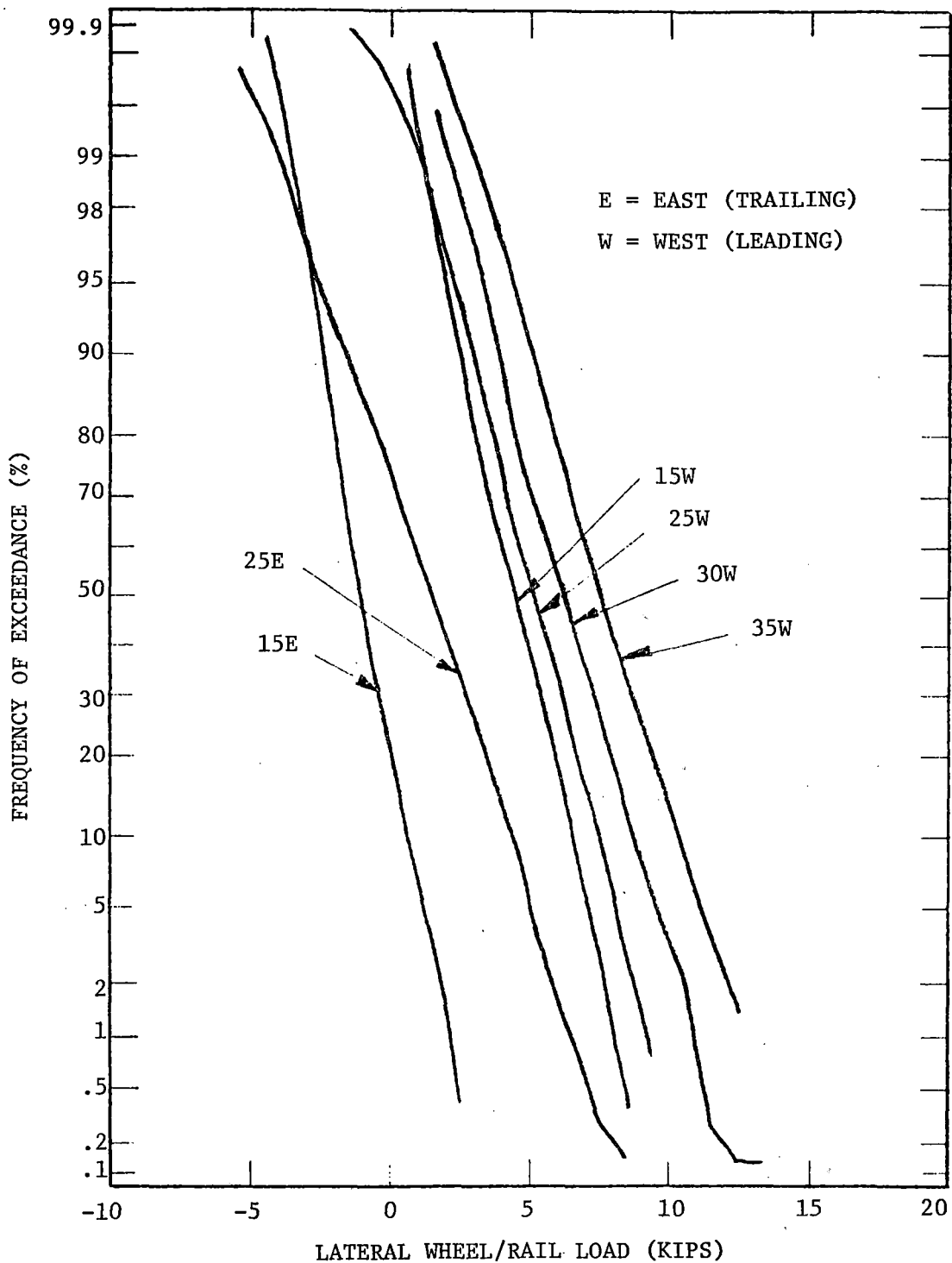


FIGURE 4-6. FREQUENCY-OF-EXCEEDANCE PLOTS FOR LATERAL WHEEL LOAD FROM INSTRUMENTED WHEEL, HIGH RAIL OF  $5^{\circ}59'$  CURVE (6" SUPERELEVATION)

TABLE 4-2. STATISTICAL SUMMARY OF WHEEL/RAIL LOAD DATA FROM INSTRUMENTED  
WHEEL THROUGH CURVED TRACK TEST SECTION (6°, 6" SUPERELEVATION)

Parameter	Test Condition, Speed and Direction											
	15 mph, East		15 mph, West		25 mph, East		25 mph, West		30 mph, West		35 mph, West	
	5°58.7'	6°00.4'	5°58.7'	6°00.4'	5°58.7'	6°00.4'	5°58.7'	6°00.4'	5°58.7'	6°00.4'	5°58.7'	6°00.4'
	High Rail	Low Rail	High Rail	Low Rail	High Rail	Low Rail	High Rail	Low Rail	High Rail	Low Rail	High Rail	Low Rail
Vertical Load (lb)												
Mean	21140	29370	22300	29820	23360	27620	23960	28210	24530	26480	26290	24110
Std. Deviation	3240	3790	3350	3300	3740	3450	3670	3310	3950	3240	4420	3370
Lateral Load (lb)												
Mean	-980	4230	4400	13910	1360	3790	5100	12930	6130	11800	7490	10550
Std. Deviation	1230	990	1650	1800	2300	1600	1870	1690	2060	1770	2220	1720
L/V Ratio												
Mean	-.046	.146	.197	.466	.059	.139	.211	.458	.248	.446	.285	.440
Std. Deviation	.059	.042	.075	.071	.099	.063	.074	.068	.080	.076	.091	.087

East = trailing axle, West = leading axle, Balance speed = 38 mph

TABLE 4-3. COMPARISON OF HIGH- AND LOW-FREQUENCY SYSTEM W/R LOAD MEASUREMENTS THROUGH CURVED TRACK TEST SECTION (6° CURVE, 6" SUPERELEVATION)

Load Measurement System	Test Run, Speed and Direction					
Instrumented Wheel (high frequency system)	25 mph, East		25 mph, West		35 mph, West	
	°58.7'	6°00.4'	5°58.7'	6°00.4'	5°58.7'	6°00.4'
	<u>High Rail</u>	<u>Low Rail</u>	<u>High Rail</u>	<u>Low Rail</u>	<u>High Rail</u>	<u>Low Rail</u>
Vertical Load (lb)						
Mean	23360	27620	23960	28210	26290	24110
Std. Deviation	3740	3450	3670	3310	4420	3370
Lateral Load (lb)						
Mean	1360	3790	5100	12930	7490	10550
Std. Deviation	2300	1600	1870	1690	2220	1720
L/V Ratio						
Mean	.059	.139	.211	.458	.285	.440
Std. Deviation	.099	.063	.074	.068	.091	.087
Instrumented Axle and Side Frames (low frequency system)						
	<u>High Rail</u>	<u>Low Rail</u>	<u>High Rail</u>	<u>Low Rail</u>	<u>High Rail</u>	<u>Low Rail</u>
Vertical Load (lbs, left wheel)						
Mean	22430	27250	22480	28120	26150	24240
Std. Deviation	1900	1960	2130	1880	2240	2050
Lateral Load (lbs, left wheel)						
Mean	-870	3190	-390	8620	7560	6370
Std. Deviation	1580	1010	1510	1000	1760	1330
L/V Ratio						
Mean	-.039	.117	-.019	.307	.289	.263
Std. Deviation	.072	.036	.069	.038	.067	.053
	<u>High Rail</u>	<u>Low Rail</u>	<u>High Rail</u>	<u>Low Rail</u>	<u>High Rail</u>	<u>Low Rail</u>
Vertical Load (lbs, right wheel)						
Mean	29250	23840	29760	22970	25500	27560
Std. Deviation	2440	2042	2680	2050	2590	2380
Lateral Load (lbs, right wheel)						
Mean	4180	-280	3500	3890	7270	13660
Std. Deviation	1000	1210	1320	1120	1730	1950
L/V Ratio						
Mean	.143	-.013	.118	.169	.287	.496
Std. Deviation	.034	.052	.043	.048	.070	.071

East = trailing axle, West = leading axle, Balance speed = 38 mph

give the mean values and the standard deviations for the vertical and lateral forces and the L/V load ratios. The tables also summarize similar data for the low frequency system so that comparisons can be made between the two systems.

The following observations can be made regarding the lateral loads measured on the curved track:

a. the highest lateral loads occurred when the instrumented wheel was on the lead axle, the low rail and at the lowest speed. The load decreased with increasing speed from 13,900 lbs at 15 mph to 10,500 lbs at 35 mph.

b. The load acting on the instrumented wheel while traversing the high rail as the lead outer wheel increased with increasing speed, but was still below the forces developed on the low rail in the 6°00.4' curve.

c. At speeds above 15 mph, there was relatively little change in the variance of the lateral load data with increasing speed.

d. The sharp change in the slope of the curve for the eastbound runs over the 6°00.4' curve are due to a transient load of rather high magnitude which was noted on every eastbound run at a location near a highway underpass.

Figure 4-7 presents statistical summaries of the lateral load data measured from the instrumented axle and side frames (low frequency system) during traversal of the two 6-degree curves. Data are shown for the 25 mph eastbound and westbound runs and the 35 mph westbound run. These data have been analyzed to provide the lateral loads acting at each of the two wheels on the instrumented axle.

Table 4-3 summarizes the data obtained on these runs and permits a comparison with the data derived from the instrumented wheel. It will be noted that the comparison of the vertical load averages is fairly consistent between the two systems, but that in all cases except one the lateral load determined from the instrumented axle is substantially less than that reported by the instrumented wheel. Note that when operating as a lead axle the loads at the low rail are larger than the lateral loads at the high rail at the 25 mph speed, but that at the 35 mph run the highest lateral loads are on the high rail. Also, the standard deviations show that the low-frequency system consistently underestimates the vertical and lateral load variations by as much as a 2 to 1 ratio.

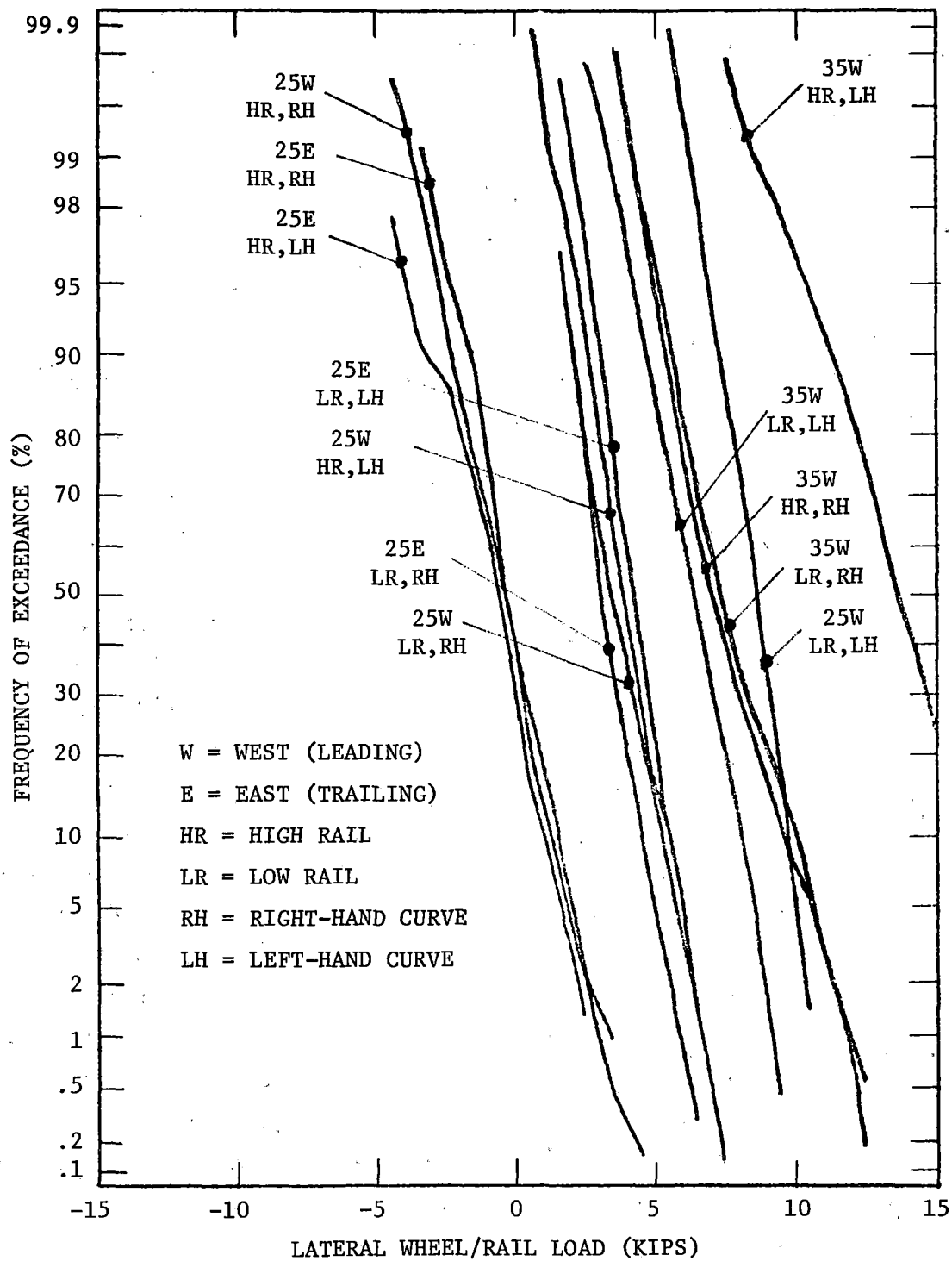


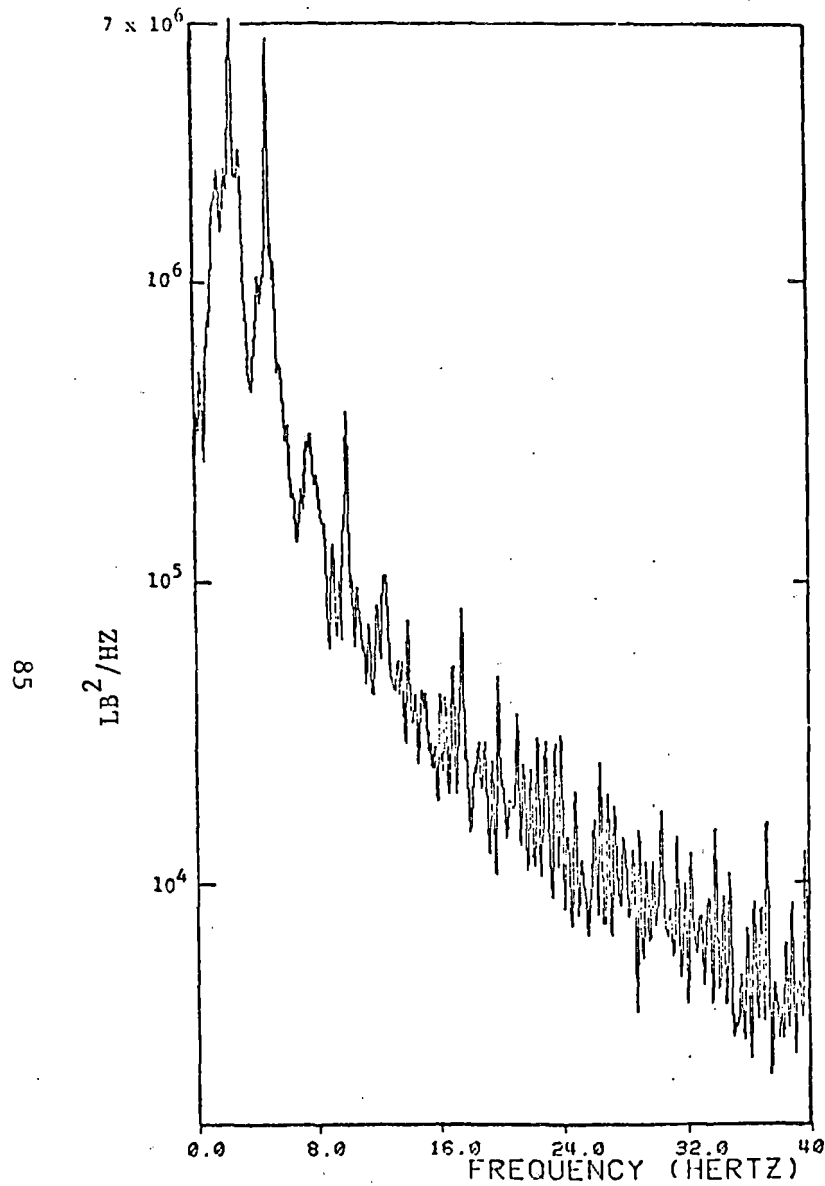
FIGURE 4-7. FREQUENCY-OF-EXCEEDANCE PLOTS OF LATERAL WHEEL LOAD FROM AXLE/SIDE FRAME (LOW-FREQUENCY) MEASUREMENT SYSTEM THROUGH 6° CURVES

#### 4.1.2 Frequency Domain Analysis of Wheel/Rail Loads

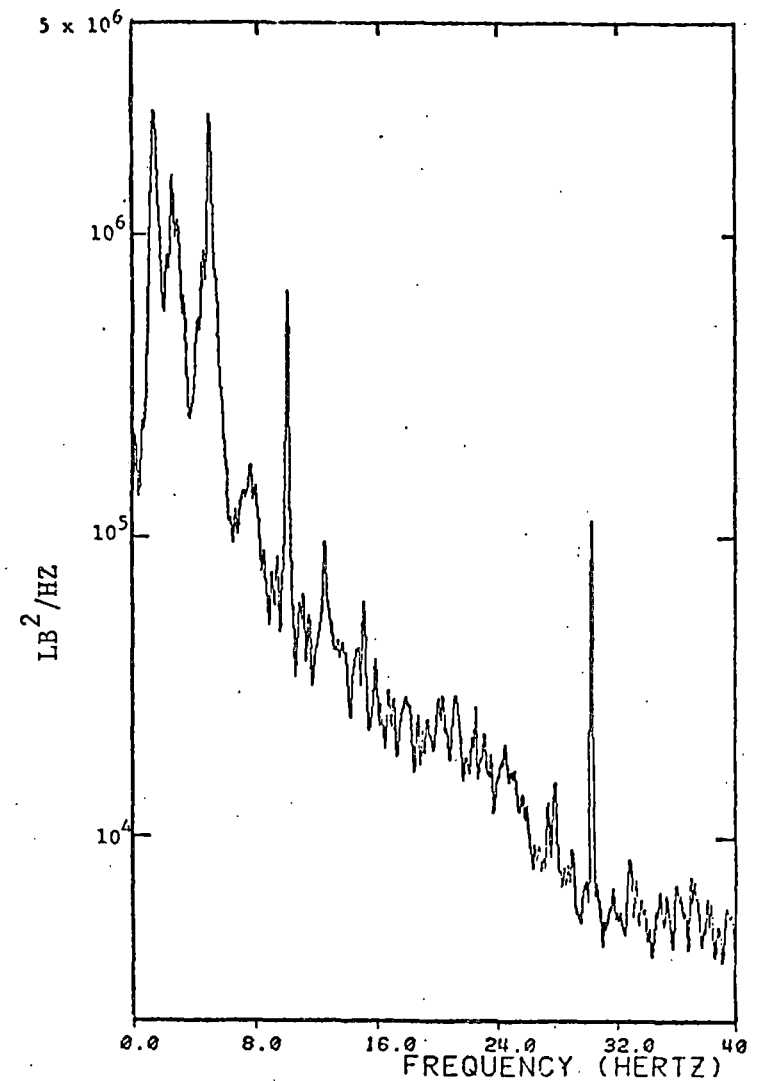
Selected force records have been analyzed to determine the contribution of various frequencies to the variation in wheel/rail forces with time. The frequency dependence is presented in terms of the mean square spectral density. Figure 4-8 shows an example comparison of spectral density plots of the vertical load data obtained from the instrumented wheel while operating on BJR and CWR track. These spectra have been developed from load data sampled 8 times per wheel revolution. This limits the frequency range which can be considered in the spectral analysis as discussed in Section 6.9.4. In Figure 4-8 the effects of rail joints can be seen quite clearly in the resulting spectra. Similar plots of vertical and lateral load spectra were developed for the 35 mph runs (east- and westbound), and the 45, 55 and 65 mph runs (eastbound), and these are contained in Appendix D.

A number of the plots show large values at the wheel rotational frequency and higher harmonics of this frequency. These frequencies are listed in Table 4-4. The peak values at these frequencies do not necessarily represent wheel/rail load phenomena, but are due to the combination of the data from the independent load bridges on the wheel and the artificial coarseness in the data which is introduced by the digitization process. The problem is apparently due to the fact that in a given data set each bridge output will have a different number of points above and below the mean value, even though the dispersion of the points above and below the mean have the same statistical properties. This is due to the calibration value being slightly different for each bridge, which results in a slight variation of the load interval in the digital representation. The mean square spectral density is obtained from an autocorrelation function of the combined load points in the digital data set. The fact that there is a slight difference in the number of positive and negative load values (about the mean) from the load bridges which made up the set causes a bias in the development of autocorrelation function at an interval spacing representative of one wheel revolution.

Most of the vertical load spectral density plots show local maxima at the rail joint passage frequency. This is 1.3, 1.7, 2.1 and 2.4 Hz respectively for 35, 45, 55 and 65 mph. These peaks, which are particularly



a. 65 MPH EASTBOUND, BJR TRACK



b. 65 MPH EASTBOUND, CWR TRACK

FIGURE 4-8. FREQUENCY ANALYSIS OF VERTICAL WHEEL LOAD, DATA FROM INSTRUMENTED WHEEL, TRAILING AXLE OF TRAILING TRUCK

TABLE 4-4. ROTATIONAL FREQUENCIES ASSOCIATED WITH 36-INCH  
DIAMETER INSTRUMENTED WHEEL

Speed (mph)	Frequencies of Harmonics (Hz)			
	1st	2nd	3rd	8 Samples/Rev.
15	2.3	4.7	7.0	18.7
25	3.9	7.8	11.7	31.1
35	5.4	10.9	16.3	43.6
45	7.0	14.0	21.0	56.0
55	8.6	17.1	25.7	68.5
65	10.1	20.2	30.3	80.9

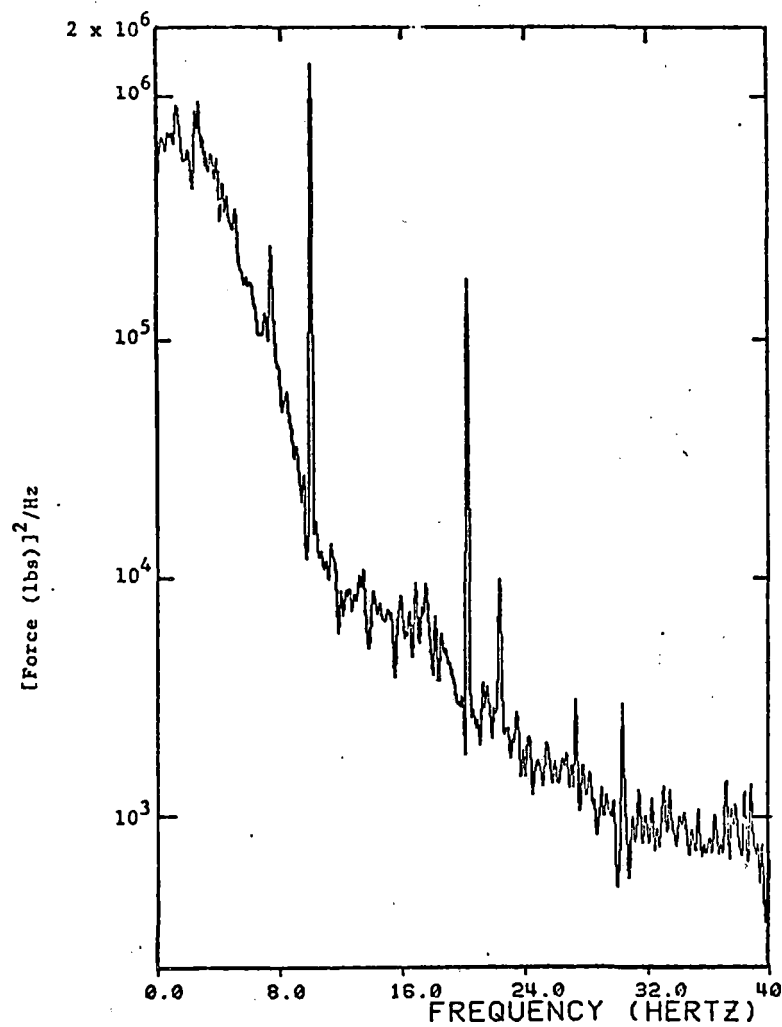
noticeable on the BJR track records, tend to obscure the local peaks associated with the bounce and pitch frequencies of the car (approximately 2.2 and 3.0 Hz respectively). The fact that maxima associated with rail joint passage are evident for the smooth tangent track, which is welded rail, is somewhat surprising. The welded rail, however, was installed in recent years and the subgrade may have a "memory" of the previously jointed track. This phenomena has been reported for other welded-rail tracks.

The lateral load spectral density plots show a lower level of response than the vertical load plots. The data is comparable for BJR and CWR track in the 35 to 45 mph range, but is slightly more intense on the BJR track for the 55 to 65 mph runs. Figure 4-9 presents an example of lateral load spectra (the 65 mph runs) in which the data processing "spikes" show up quite distinctly.

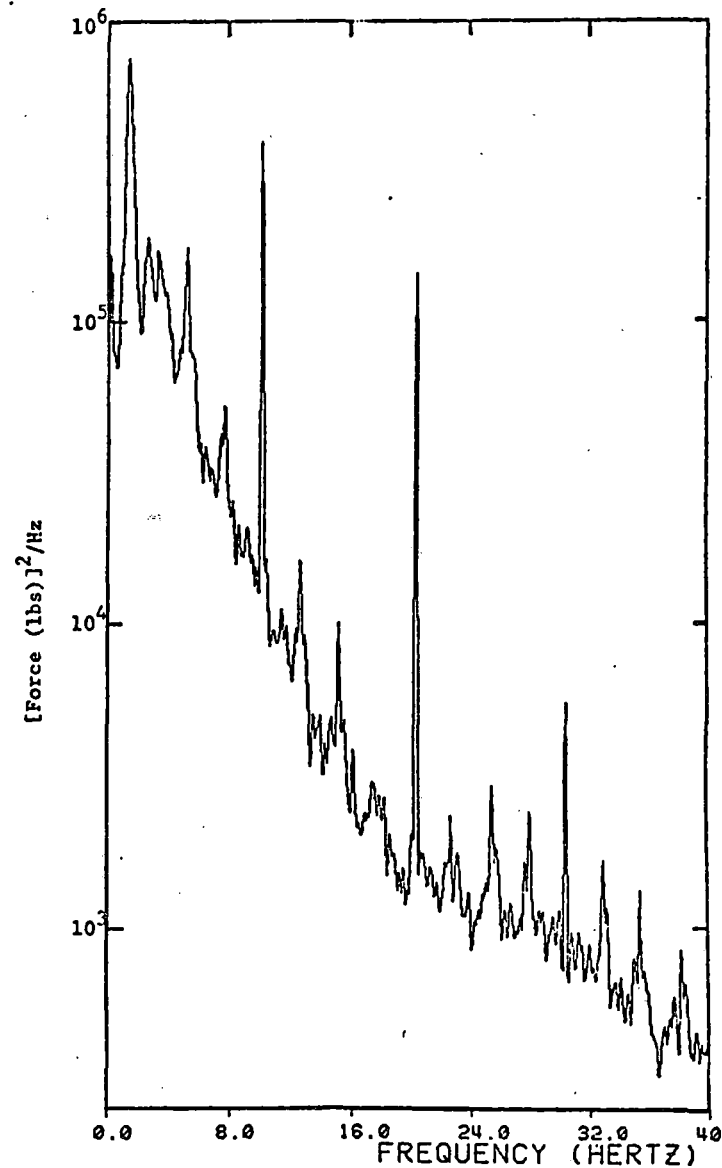
Figures 4-10 and 4-11 present the results of the spectral analysis of vertical load data from the low frequency system for operations on the BJR and CWR track at 35 mph in both directions. These spectral plots have been developed from the side frame vertical load bridge data, and have been obtained directly from the analog data recording using a "real time" spectral analyzer. It is impossible to obtain a meaningful spectral analysis of the low frequency lateral load data because of the low sampling rate at which this data is available.

The spectral data from the runs on the CWR track show local maxima at approximately 1.2, 2.2 and 3.0 Hz which are, respectively, the natural frequencies of the roll, bounce, and pitching modes of the car body. These plots also show local peaks at approximately 5.5 Hz, which is the wheel rotation frequency at 35 mph.

The spectral data from the runs on the BJR track show distinct local peaks at 1.3 Hz and higher multiples of this frequency. This is the frequency of rail joint passage at 35 mph and it is believed that the peaks are due to the transient impact loads at the joint. The effect is most noticeable on the eastbound run, where it obscures the car body roll, pitch, and bounce frequencies. The spectral curve for the westbound run shows evidence of local maxima at 1.2 Hz, which is the natural frequency of car body roll; 2.9 Hz, the natural frequency of car body pitching; and at 5.5 Hz, the wheel rotational frequency, but their effects are somewhat obscured by the harmonics of 1.3 Hz oscillation.

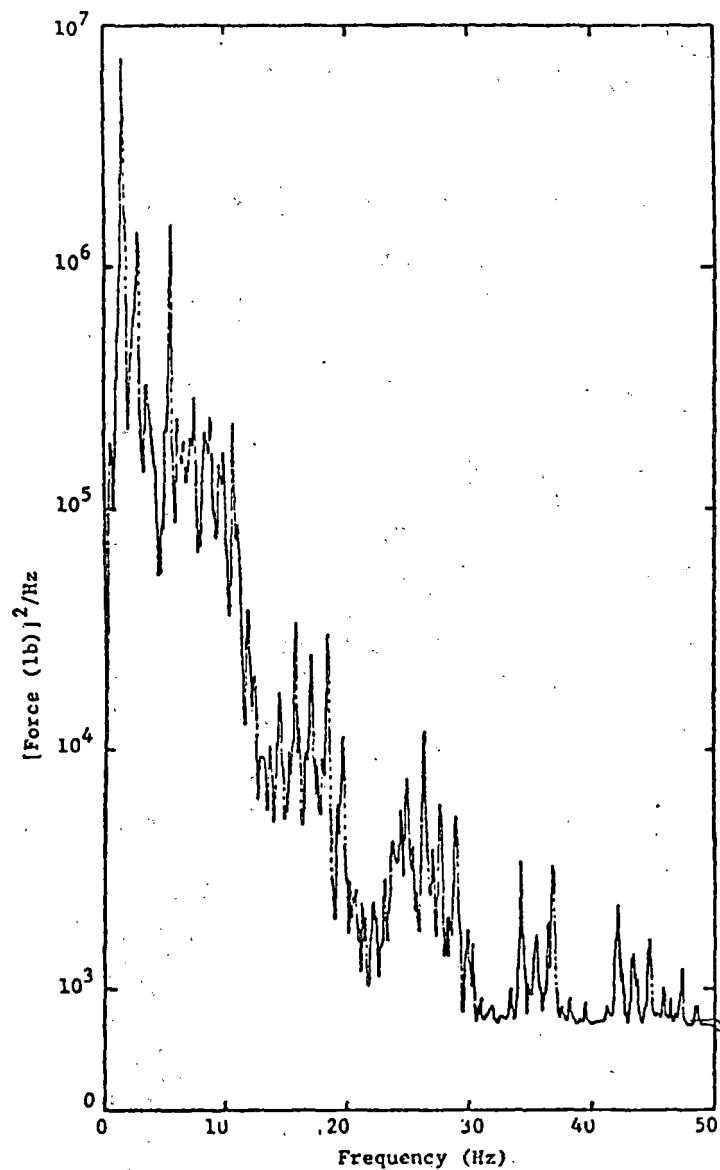


a. 65 MPH EASTBOUND, BJR TRACK

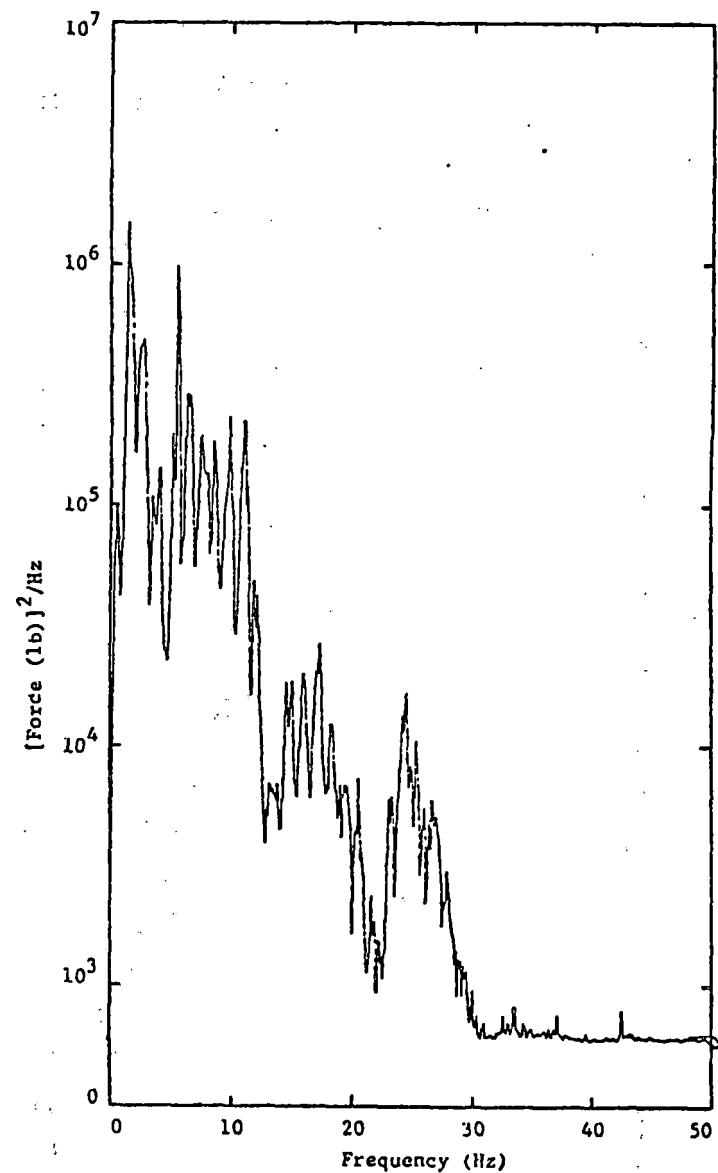


b. 65 MPH EASTBOUND, CWR TRACK

FIGURE 4-9. FREQUENCY ANALYSIS OF LATERAL WHEEL LOAD, DATA FROM INSTRUMENTED WHEEL, TRAILING AXLE OF TRAILING TRUCK

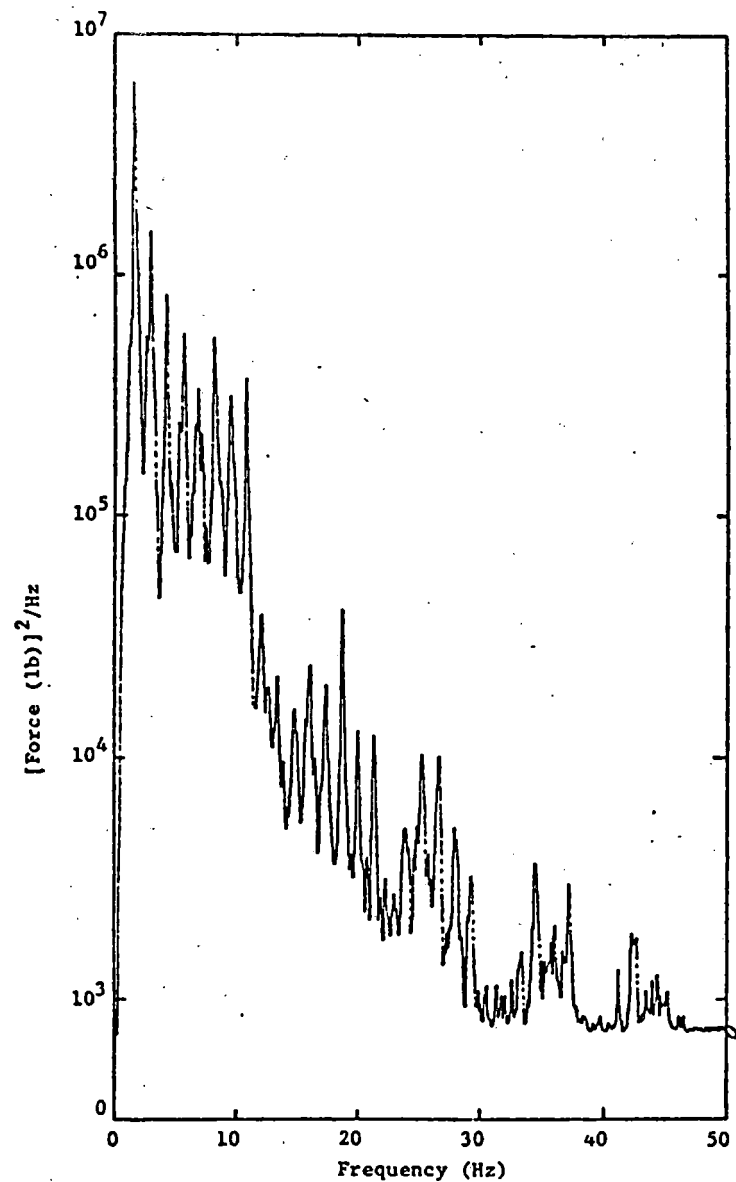


a. 35 MPH WESTBOUND, BJR TRACK

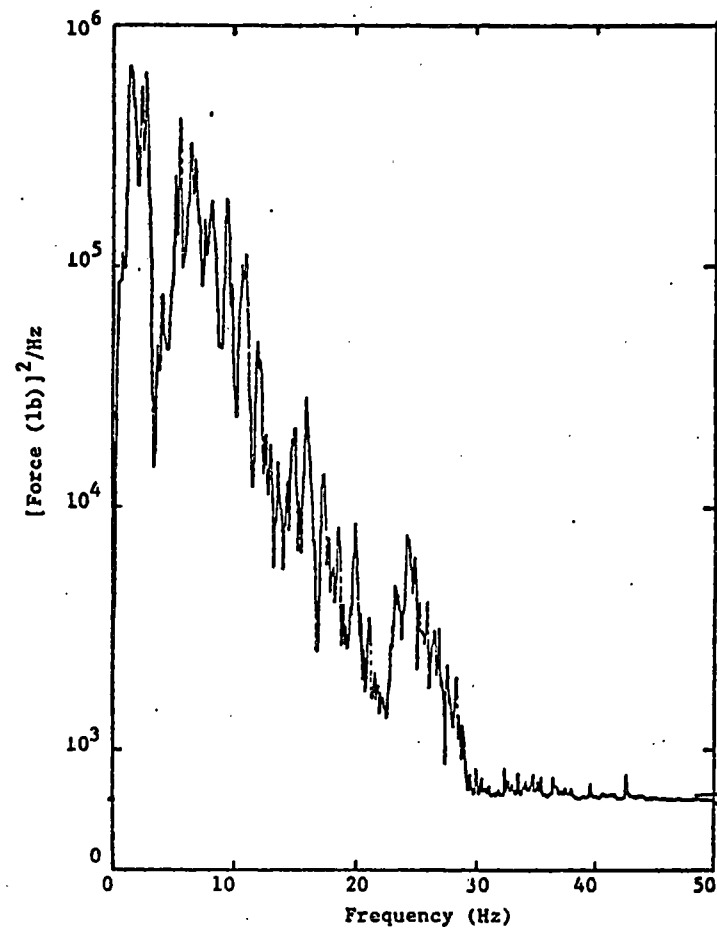


b. 35 MPH WESTBOUND, CWR TRACK

FIGURE 4-10. FREQUENCY ANALYSIS OF VERTICAL SIDE FRAME FORCE,  
WESTBOUND (LEADING TRUCK) RUNS



a. 35 MPH EASTBOUND, BJR TRACK



b. 35 MPH EASTBOUND, CWR TRACK

FIGURE 4-11. FREQUENCY ANALYSIS OF VERTICAL SIDE FRAME FORCE,  
EASTBOUND (TRAILING TRUCK) RUNS

#### 4.1.3 Rail Joint Impact Loads

The rail joint impact load data have been analyzed for the 15, 25, 35, 45, 55 and 65 mph eastbound runs over the BJR track. The data have been analyzed from the vertical load bridges on the high frequency wheel at a sampling rate of 16 samples per wheel revolution (every 7.1"). Fifty successive rail joints which lie between mile post 292.25 to 292.75 have been identified. Note that at this spatial resolution the resulting data describe primarily the "P2" (lower-frequency) force peaks.

Figure 4-12 shows a typical vertical load data record. Note that it is possible to identify each of the 50 rail joint loads. The BCL instrumented rail joint (Site 3) was located at Joint No. 11. Table 4-5 summarizes the maximum vertical forces associated with a traversal of these joints for each of the six eastbound transits of the test zone. Note that certain joints have loads that are consistently higher than the others (e.g., Joints No. 27 and 50). Also note that there is a general tendency for the joint loads to increase with increasing speed. Figure 4-13 presents cumulative probability distribution curves for the data contained in Table 4-5.

Vertical load versus time plots have been generated for a number of joint traversals that resulted in higher load values. Two examples are included in Figures 4-14 and 4-15 for Rail Joint 50 at the two highest speeds. Two different sampling rates were used in generating these plots: 1000 and 4000 samples per second. Note that considerable smoothing (and some attenuation) results at the lower sampling rate. Examination of the signals from individual load-sensing bridges on the wheel plate has shown that there is strong excitation of the wheel vibrational modes, from about 500 Hz on up, in response to impact loads at rail joints. This can be seen particularly in Figure 4-15. The wheel tends to "ring" for 10 to 20 milliseconds at these frequencies after the high transient load. These strains do not accurately represent the impact load itself and, therefore, the analysis of rail joint loads was based on the data obtained at the lower sampling rate. Rail Joint 50 was one of the joints giving a consistently high load for each traverse speed. Note that there is a general tendency for the load histories to exhibit the classical characteristics identified with a dipped rail joint

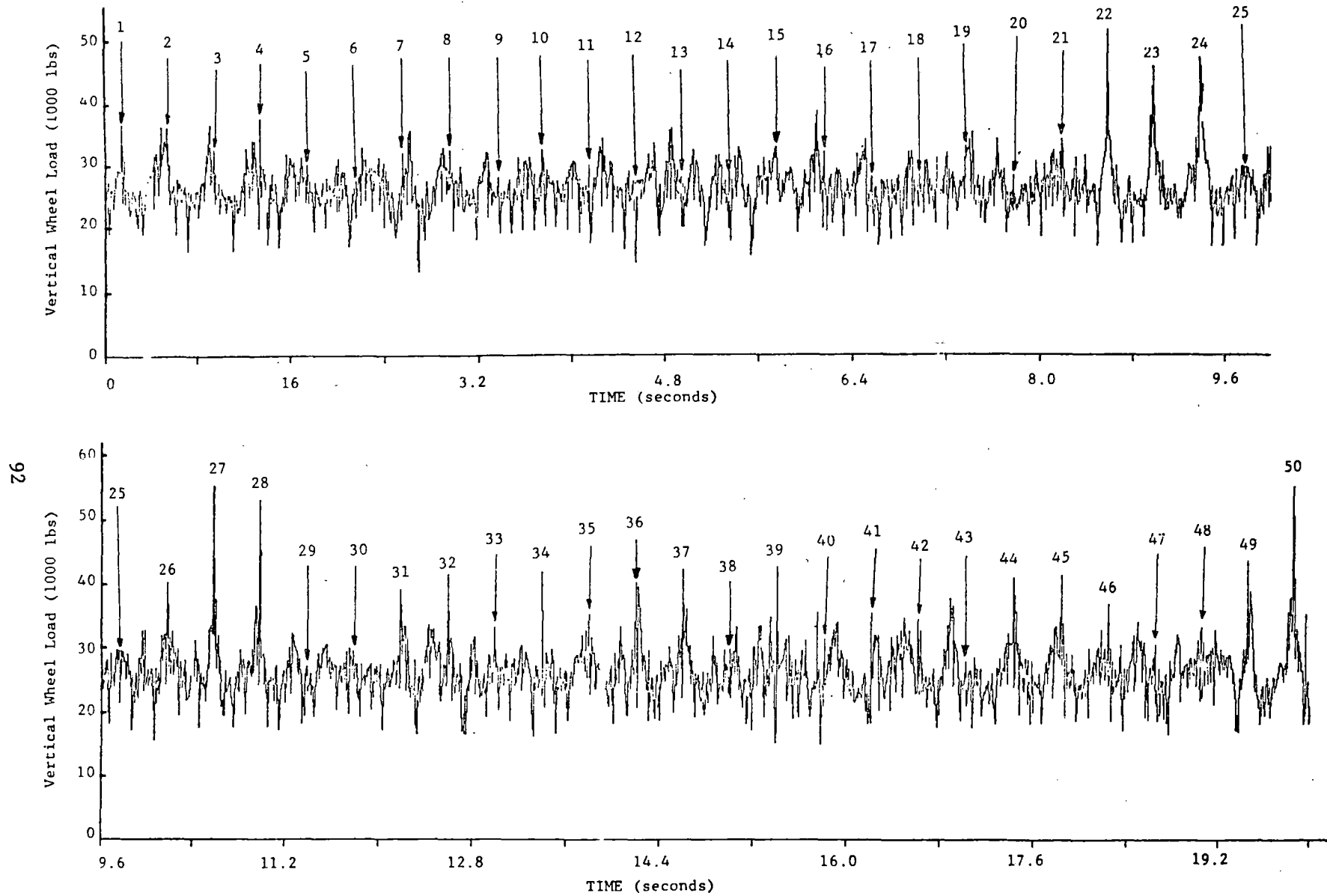


FIGURE 4-12. VERTICAL WHEEL LOAD RECORD FROM INSTRUMENTED WHEEL  
FOR 65 MPH EASTBOUND RUN OVER BJR TRACK

TABLE 4-5. MAXIMUM VERTICAL RAIL JOINT LOADS FOR EASTBOUND  
(TRAILING AXLE) RUNS THROUGH BJR TANGENT SECTION

Maximum Vertical Wheel Load (Kips)						
Rail Joint No.	15 mph	25 mph	35 mph	45 mph	55 mph	65 mph
1	29.2	30.6	28.5	29.2	33.1	35.8
2	27.9	30.9	24.0	27.5	28.1	35.5
3	26.2	25.0	33.7	27.3	30.4	32.0
4	31.6	30.6	30.0	32.4	34.2	36.9
5	29.9	30.0	32.4	29.7	29.5	29.6
6	28.4	32.7	29.3	34.1	30.1	27.0
7	25.4	27.2	26.4	30.5	26.1	31.3
8	28.7	28.8	31.4	26.9	26.5	31.7
9	28.2	33.7	28.5	27.3	30.8	27.5
10	26.5	30.0	27.1	30.7	30.8	31.7
11	28.1	28.5	28.2	29.3	28.7	29.4
12	27.9	27.9	29.4	29.0	26.9	26.7
13	27.5	27.3	28.0	26.4	27.3	27.5
14	26.2	27.1	30.3	28.2	28.1	27.9
15	28.5	27.9	26.5	30.8	31.7	32.1
16	28.6	31.3	29.7	29.8	29.2	31.4
17	28.8	26.6	25.9	32.0	25.5	27.3
18	27.5	27.5	27.3	27.1	31.2	27.7
19	25.1	29.8	28.2	29.3	31.4	32.2
20	26.4	28.4	28.0	27.9	29.5	27.7
21	28.2	29.0	33.1	28.7	29.5	33.4
22	27.6	29.1	32.5	40.3	42.1	57.5
23	30.2	31.6	29.4	30.2	32.8	44.5
24	28.5	32.1	29.2	30.9	35.4	48.0
25	26.3	28.5	31.7	27.6	33.4	29.1
26	29.2	32.3	42.9	32.5	38.1	39.4
27	32.0	31.6	30.0	38.7	56.5	61.8
28	27.9	29.5	24.4	30.2	34.2	52.0
29	26.5	28.0	30.7	26.4	27.9	26.5
30	28.8	26.7	37.1	27.3	28.9	28.8
31	31.3	30.9	27.3	39.1	41.1	38.3
32	28.3	30.6	29.8	35.5	38.1	40.6
33	32.3	33.0	35.0	28.5	36.1	32.5
34	29.3	35.3	34.4	32.0	32.7	40.9
35	27.5	29.9	34.4	34.1	31.7	34.4
36	32.2	37.3	37.6	37.9	42.9	39.5
37	31.3	30.3	30.0	33.4	37.7	41.4
38	29.3	33.3	33.9	37.0	32.2	29.2
39	28.1	29.5	27.5	41.5	33.1	41.9
40	29.2	29.2	33.4	34.8	34.8	30.7
41	27.4	33.1	27.5	36.0	36.7	34.7
42	26.6	29.8	29.5	28.5	28.9	33.7
43	27.7	29.0	31.4	25.5	28.0	27.2
44	29.6	30.6	31.3	29.7	46.4	40.0
45	27.2	28.2	29.0	31.0	34.2	40.6
46	27.6	33.1	27.2	31.2	33.2	36.1
47	29.3	29.3	33.7	28.2	27.9	29.9
48	29.3	29.2	35.1	29.0	30.0	32.7
49	27.9	35.5	36.2	35.5	38.1	42.7
50	39.7	41.2	39.4	46.7	66.3	63.3
Mean	28.7	30.4	30.7	31.5	33.7	35.6
Standard Deviation	2.3	2.9	3.8	4.5	7.4	8.8

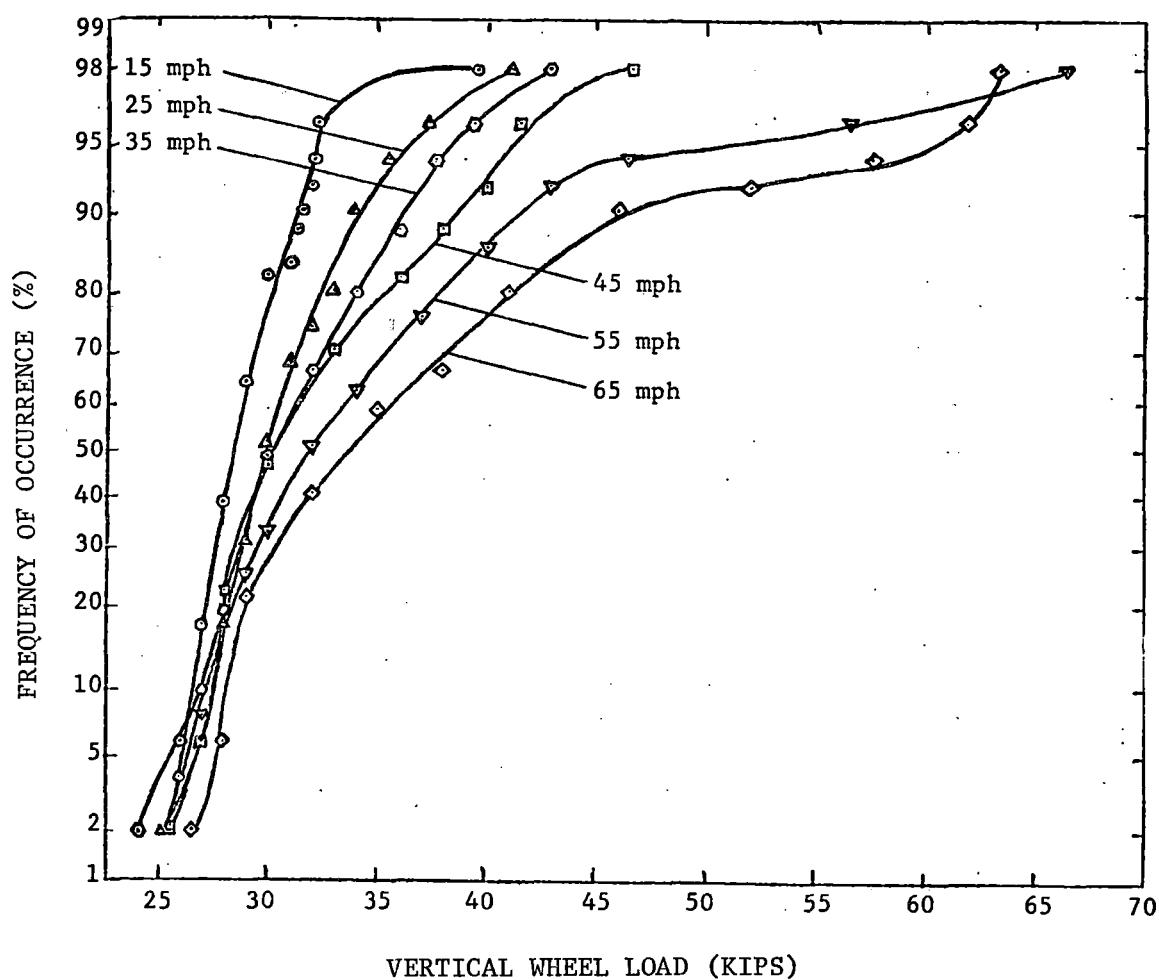
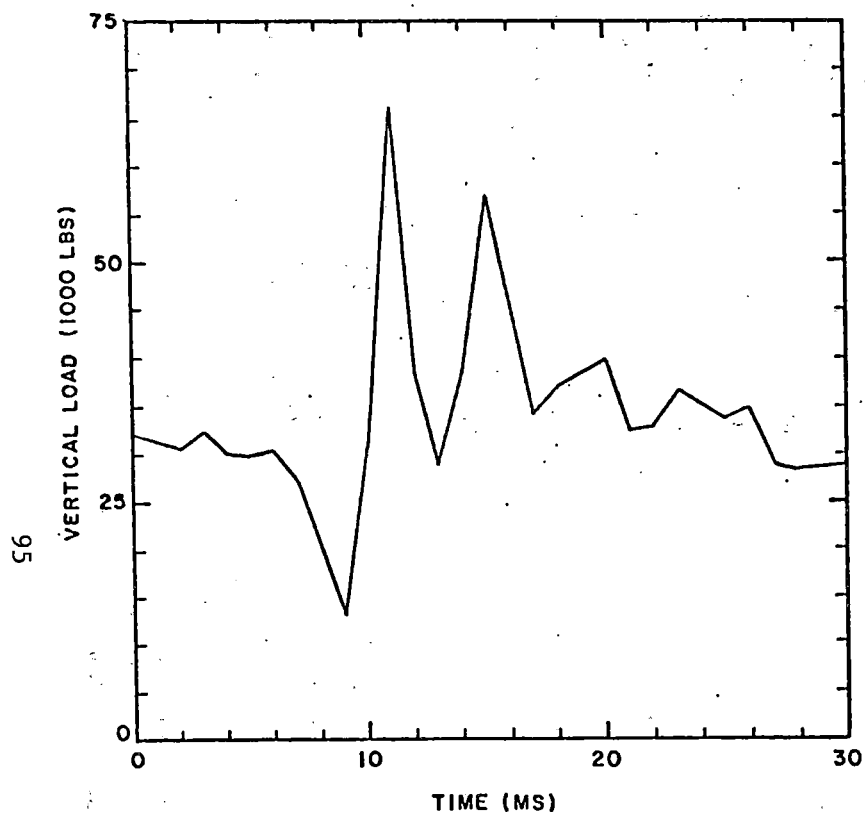
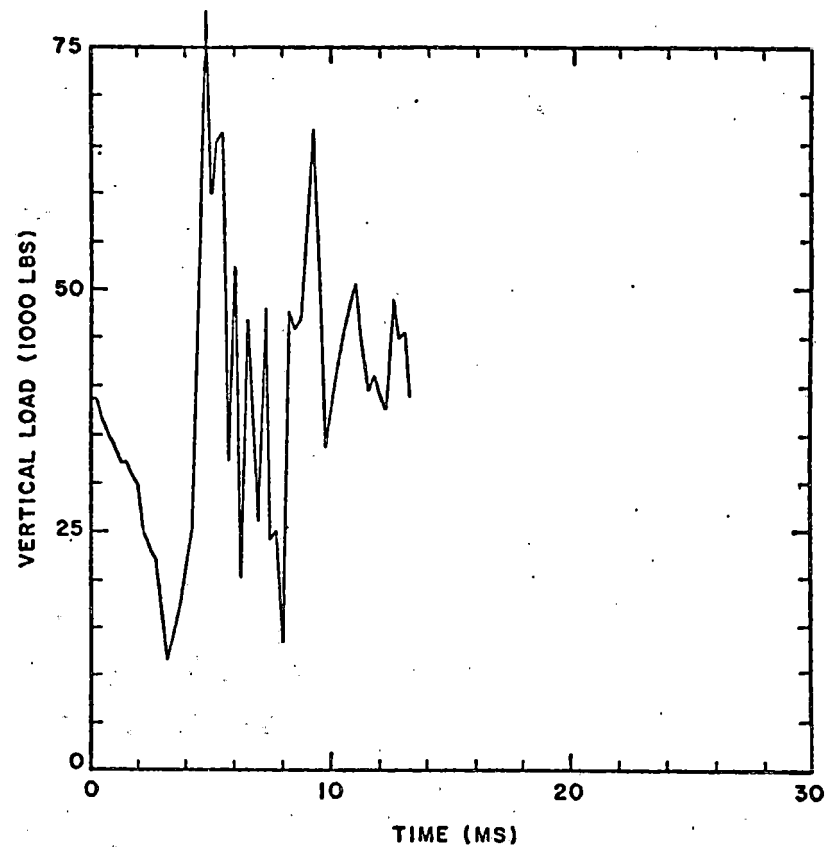


FIGURE 4-13. FREQUENCY OF OCCURRENCE OF PEAK VERTICAL WHEEL LOAD DUE TO JOINT IMPACT VERSUS TRAIN SPEED, 100-TON FREIGHT CAR, TRAILING AXLE, TRAILING TRUCK



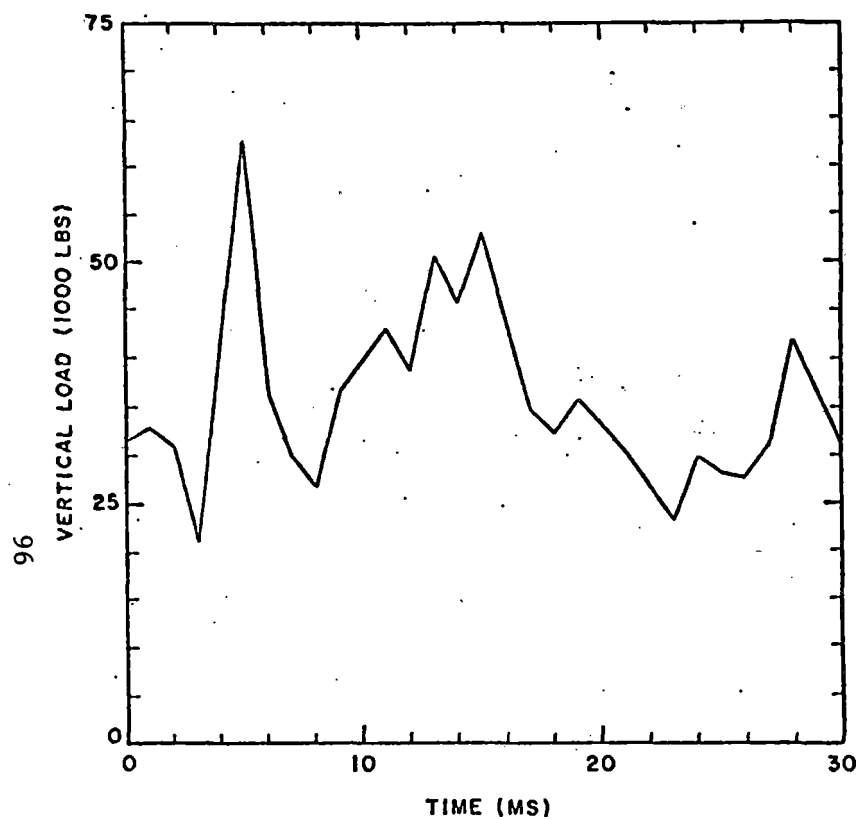
a. 1000 SAMPLES/SECOND



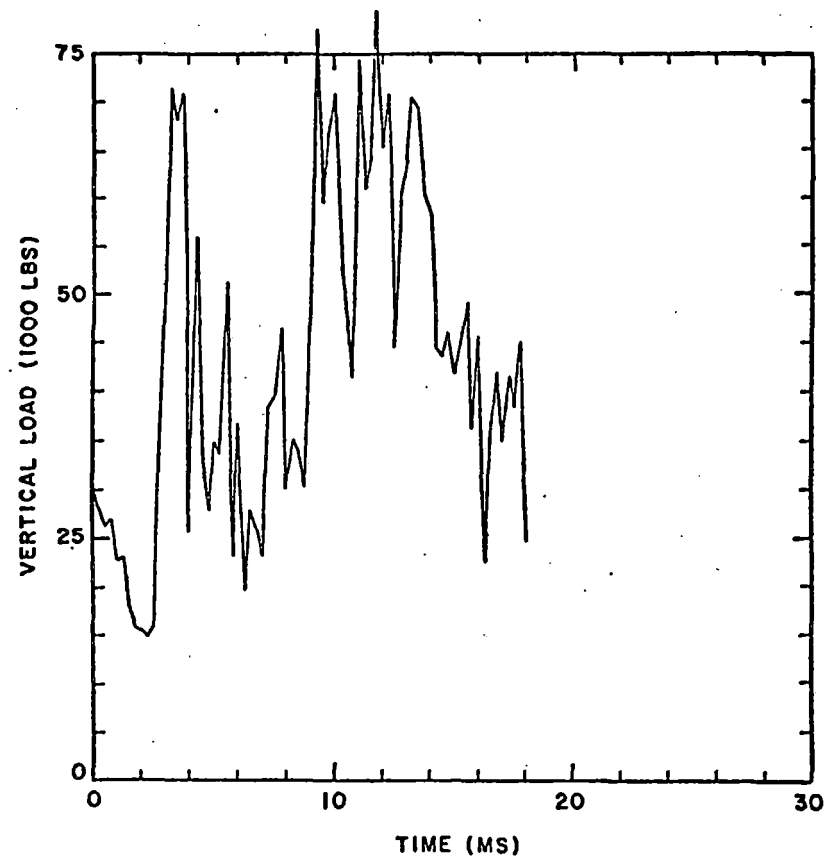
b. 4000 SAMPLES/SECOND

(NOTE: TIME BASE NOT SYNCHRONIZED IN TWO PLOTS)

FIGURE 4-14. VERTICAL WHEEL LOAD ON INSTRUMENTED 100-TON HOPPER CAR TRAVERSING RAIL JOINT #50, EASTBOUND (TRAILING AXLE), 55 MPH



a. 1000 SAMPLES/SECOND



b. 4000 SAMPLES/SECOND

(NOTE: TIME BASE NOT SYNCHRONIZED ON TWO PLOTS)

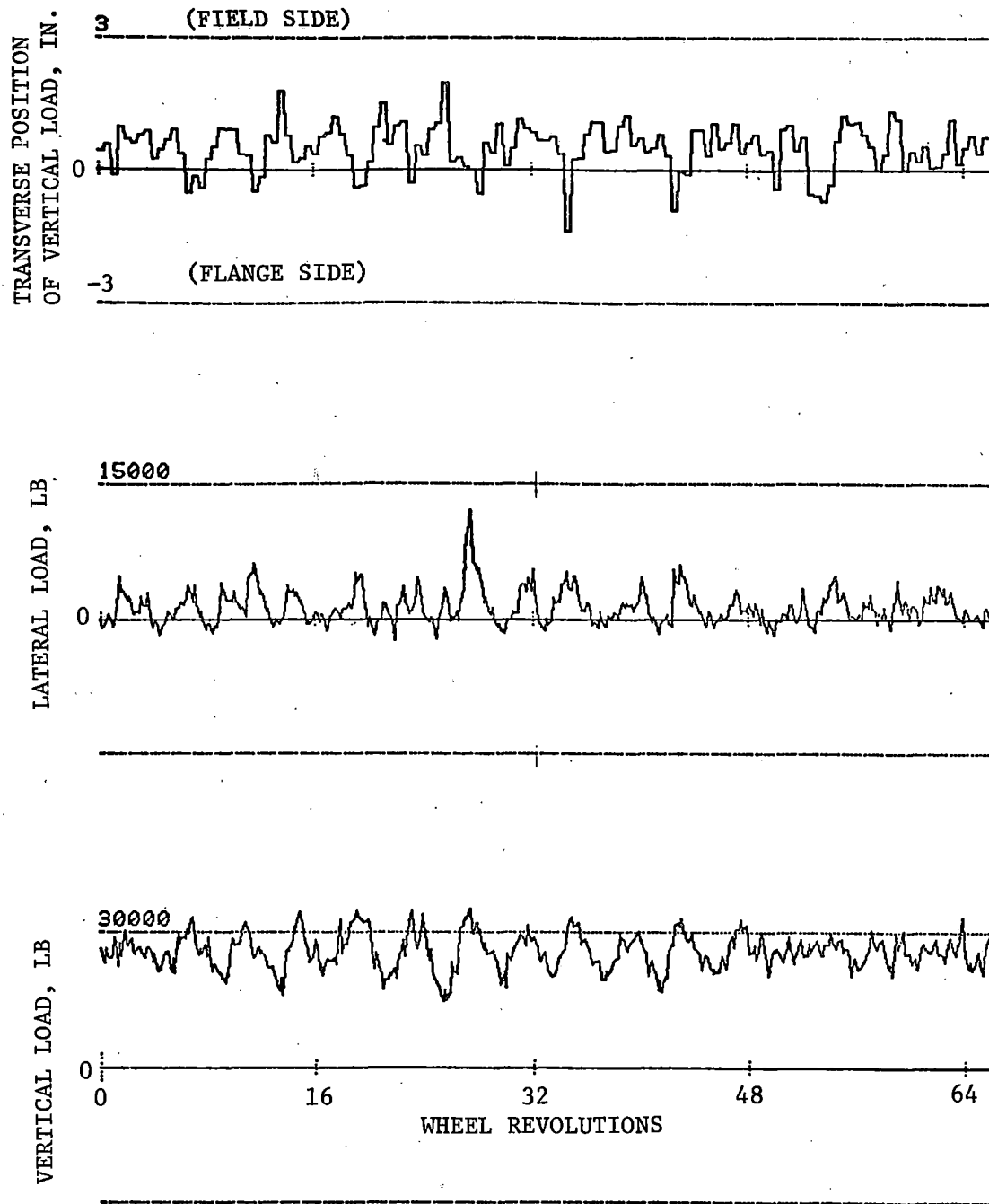
FIGURE 4-15. VERTICAL WHEEL LOAD ON INSTRUMENTED 100-TON HOPPER CAR TRAVERSING RAIL JOINT #50, EASTBOUND (TRAILING AXLE), 65 MPH

traversal. In most cases there is a dip in the load followed by a sharp rise to an initial peak (P1) which is again followed by a sharp dip in the load and then a second rise to a less sharply defined peak (P2) followed by a gradual decay. The duration of the P2 load however, is generally somewhat shorter than the 10-20 milliseconds that has been reported for this component of the load.

#### 4.2 COMPARISON OF W/R LOAD MEASUREMENT SYSTEMS

An example of the outputs from the instrumented wheel are shown in Figure 4-16 over part of the tangent BJR test section during the westbound (instrumented wheel leading) 35-mph test run. This example was chosen to provide a comparison of outputs from the low- and high-frequency systems, primarily for the reasonably high (12,000 lb.) lateral wheel load generated within this sample. The top trace shows the position of the vertical load laterally on the wheel tread relative to the tape line, and it is interesting to note that the high lateral load occurs following a vertical load peak and with the wheel more-or-less centered on the rail. High-frequency and low-frequency load data are compared in Figure 4-17 for this same sample of data (which was taken near Milepost 293.5). The increased high-frequency content and better load resolution can be seen in the vertical load measured by the wheel, as compared with the load average of front and rear wheels from the low-frequency system. From the statistical results in Table 4-1, we have seen that the low frequency system consistently underestimates the vertical dynamic loads.

Several ways of processing the lateral load data will be examined in Section 6.9.3. By filtering (averaging over several sample points), the low-frequency load trends can be salvaged. Another method has been to average the left and right wheel lateral loads (the sum of the loads divided by two, where net axle lateral load is defined as the difference of the loads). This is shown in Figure 4-17 in the top trace, and does have the effect of reducing "noise" to about  $\pm 1,000$  lb. This variable, "average lateral load", is accurate only if the net lateral load on the wheelset is zero, and can be seen in Figure 4-17 to deviate substantially from the actual wheel lateral load due to "absolute value" effects from loads on the opposite wheel.



NEWDATA.2.17B#35WEST.2

FIGURE 4-16. REPRESENTATIVE WHEEL/RAIL LOAD TIME HISTORIES FROM HIGH-FREQUENCY WHEEL (LEADING, SOUTH RAIL), 35 MPH WESTBOUND RUN OF TEST TRAIN, TANGENT BJR TEST SECTION

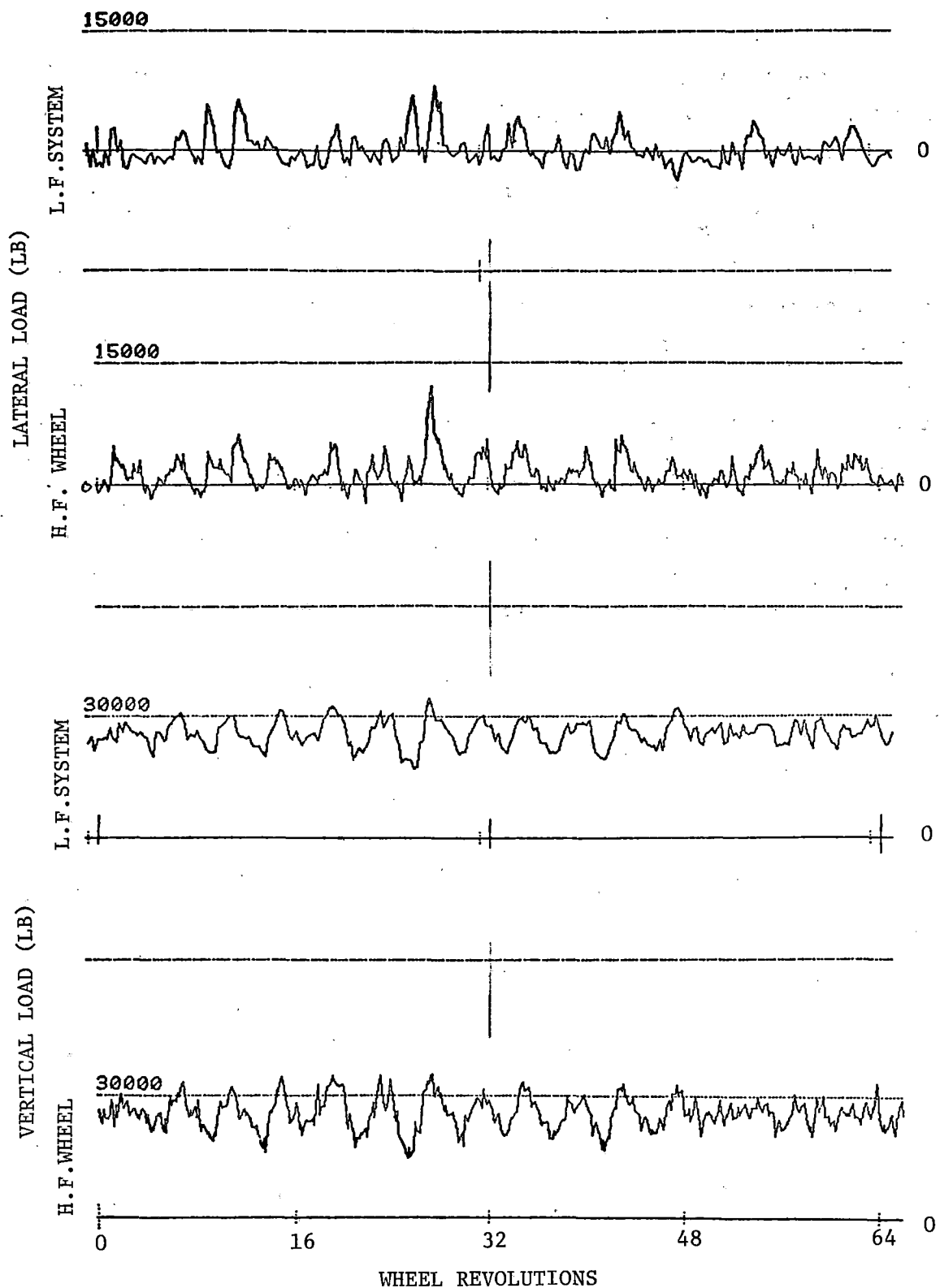


FIGURE 4-17. COMPARISON OF HIGH-FREQUENCY WHEEL AND LOW-FREQUENCY SYSTEM LOADS, 35 MPH WESTBOUND TEST RUN (INSTRUMENTED WHEEL LEADING) THROUGH TANGENT BJR TEST SECTION

Another comparison between wheel lateral load data obtained by the instrumented wheel and the instrumented side frames and axle has been made for the 25 mph eastbound run over the curved track site. On all of the eastbound runs, there was a large transient lateral load that was noted while moving over the 6°00.4' curve approximately 321 ft east of the BCL instrumented track site. The reason for this load is not known, but is probably due to a track geometry error. On the eastbound runs the axle was operating as a trailing axle in the truck and a relatively low quasi-steady lateral load was recorded. Figure 4-18 presents comparisons of the lateral wheel loads indicated by the two systems. The low-frequency system data is presented for both wheels of the axle. The figure indicates that the lateral load acts first against the left wheel, with the lateral load on the opposite wheel probably due to the dynamic response of the wheelset. In this case the low-frequency system has overestimated the lateral load.

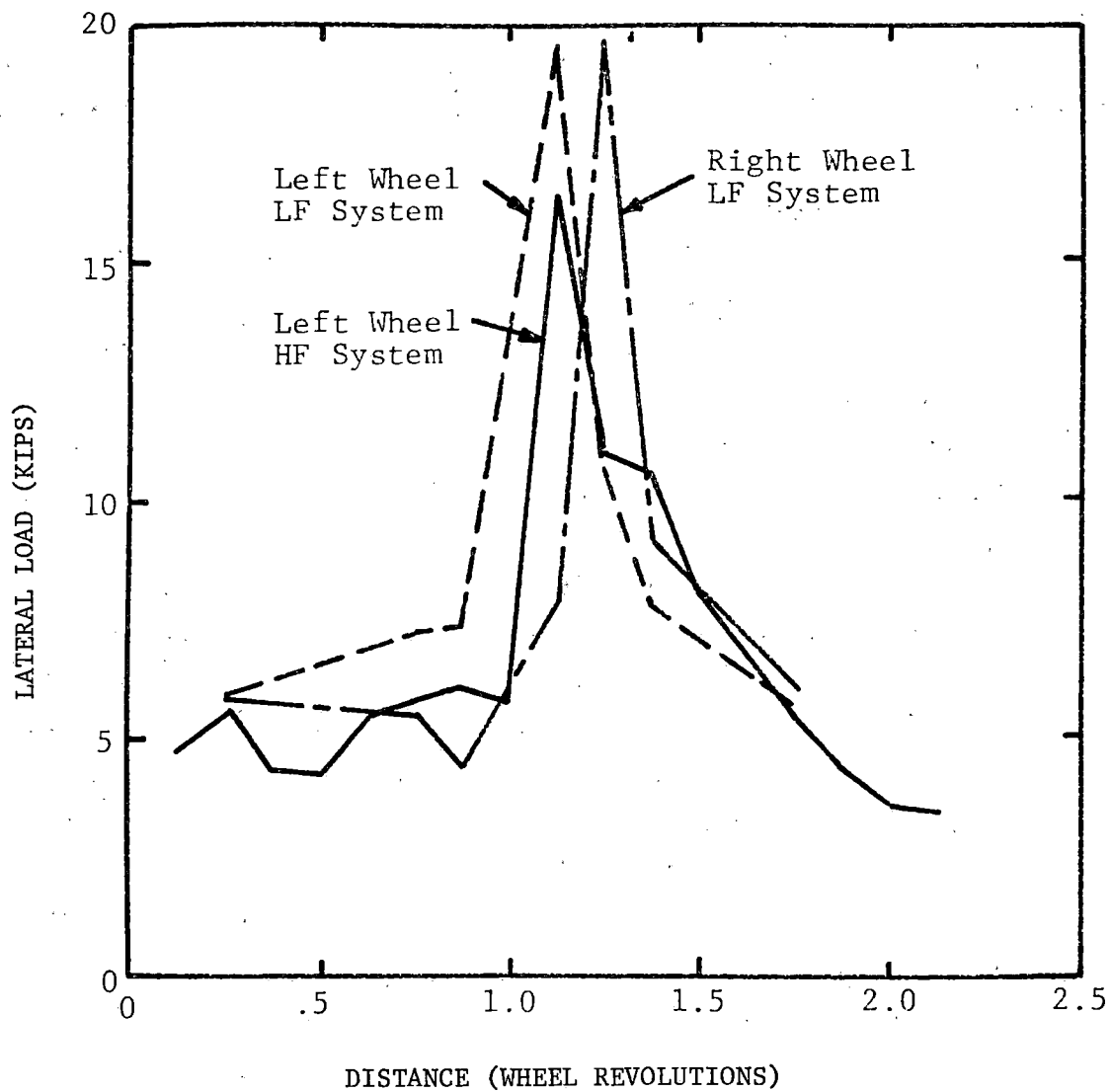


FIGURE 4-18. COMPARISON OF TWO LATERAL LOAD MEASUREMENT SYSTEMS AT TRANSIENT LOAD CONDITION,  $6^{\circ}00.4'$  CURVE, EAST-BOUND AT 25 MPH

## 5. COMPARISON WITH OTHER TEST DATA

### 5.1 WAYSIDE TEST DATA

Some wheel/rail load data from wayside instrumentation have been developed in statistical formats from measurements obtained during the Track-Train Dynamics Program [5-1], the AMTRAK locomotive evaluation tests [5-2], the DOT/TSC Improved Track Structures Research Program [5-3], and the on-going Facility for Accelerated Service Testing (FAST) experiments. Some of these data have limitations due to the comparatively small sample size or inaccuracies in instrumentation. However, these data still provide a useful base for comparison with data from this experimental program.

A comparison of vertical wheel/rail load distributions from existing data with distributions developed during the recent experiments on the UPRR is shown in Figure 5-1. Vertical load distributions reflect, more than anything else, the differences in traffic mix from one location to another. The FAST experiments, for example, produced the highest loads by using a loaded freight train, predominately 100-ton cars. The data base from the Southern Pacific (SP) tangent track, on the other hand, showed the lowest loads from westbound, downgrade freight trains consisting primarily of empty mechanical refrigerator cars and TOFC/COFC flatcars. Data from the Northeast Corridor (NEC) track reflect a relatively large population of passenger cars with static wheel loads in the 15 to 25-kip range. Again, the difference between the two tangent track sections on the UPRR (CWR and BJR, 1978) must be attributed primarily to the higher percentage of loaded 100-ton cars passing the CWR test location during the measurement period.

Lateral load distribution plots from two locations on the Florida East Coast Railway (FEC) concrete tie track are shown in Figure 5-2 in comparison with the plots from the recent Union Pacific test data. While the basic shapes of the curves are similar, a substantial deviation can be noted at the high-load, low-probability end of the plots from FEC data.

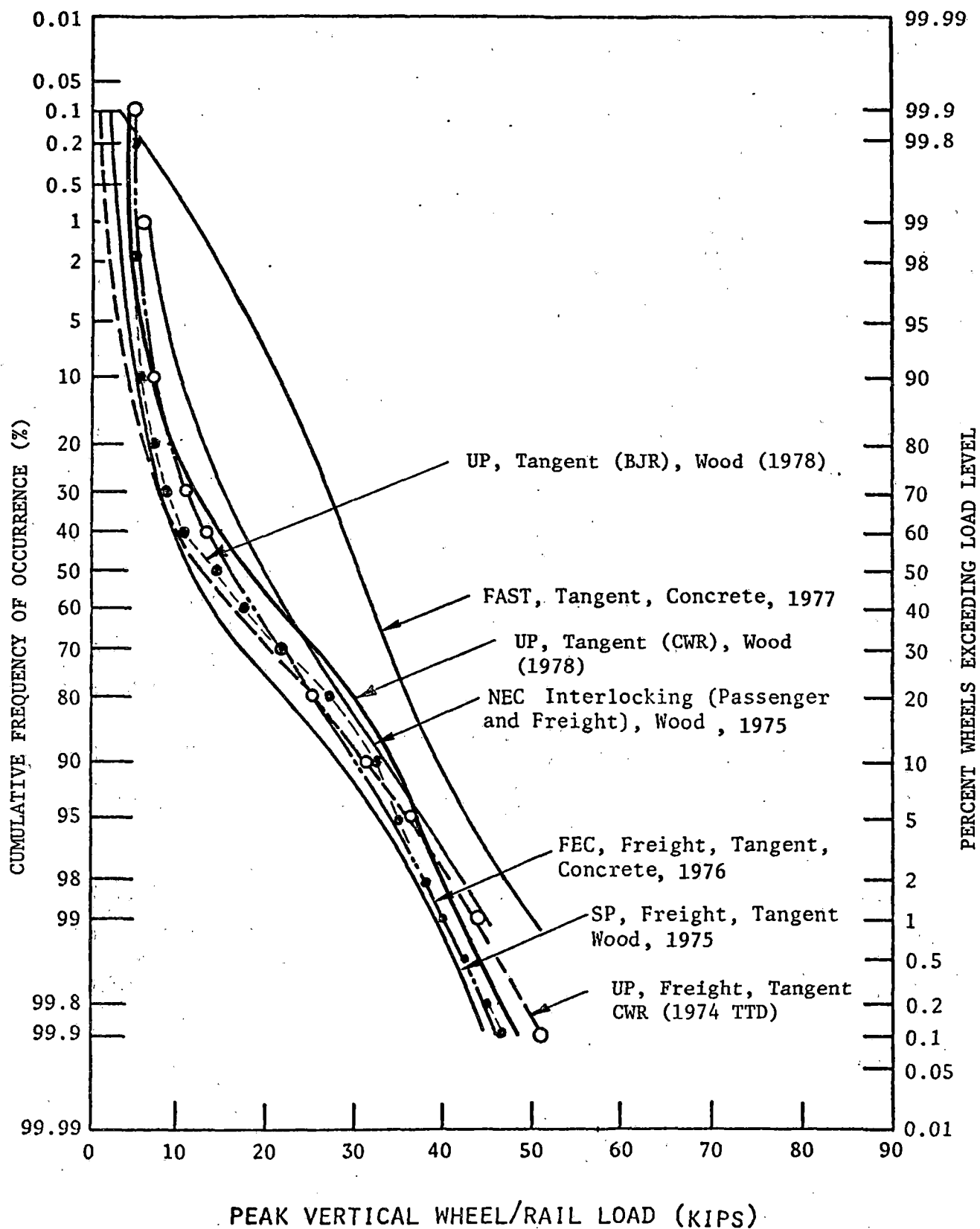


FIGURE 5-1 . COMPARISON OF VERTICAL WHEEL/RAIL LOAD DISTRIBUTIONS FROM PILOT STUDY WITH DATA AVAILABLE FROM OTHER SOURCES

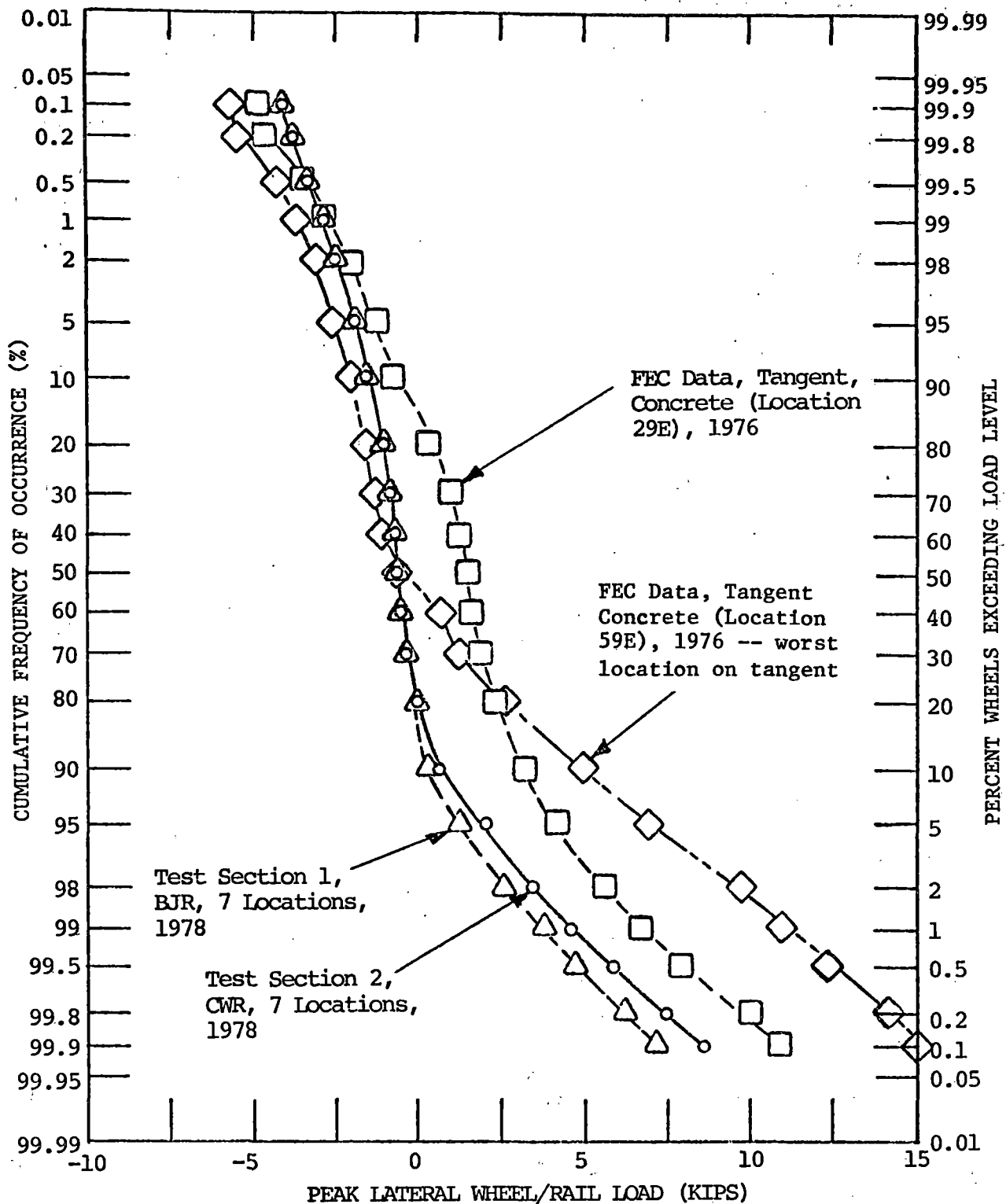


FIGURE 5-2 . COMPARISON OF LATERAL WHEEL/RAIL LOAD DISTRIBUTIONS FROM PILOT STUDY WITH DATA AVAILABLE FROM FLORIDA EAST COAST CONCRETE TIE STUDY

## 5.2 VEHICLE-BORNE TEST DATA

Most previous data defined in statistical formats describing the vertical wheel/rail load spectra have been derived from instrumented side frames or from side frame/bearing adapter load cells [5-4]. Examples of vertical load spectra derived from both the instrumented wheel (high-frequency system) and instrumented side frames during tests conducted under this program are compared in Figure 5-3 with the spectrum obtained during wheel stress tests conducted in 1976 [5-5]. This latter spectrum for operating speeds over 60 mph was also derived from instrumented side frames on a more heavily-loaded 100-ton hopper car running over the Union Pacific's California Division. Spectra from the instrumented side frames are quite similar in shape and slope, although shifted due to the difference in static weight of the cars. The better resolution of both high- and low-amplitude loads due to the improved frequency bandwidth of the instrumented wheel can be seen at the extreme ends of the spectrum, particularly on the BJR track.

Some statistically-processed data from instrumented wheelsets run over the FAST track have also been reviewed. A comparison of lateral loads measured on UPRR curved track during this present program with loads measured during a February 26, 1977 run with FAST Car No. 47 (a loaded 100-ton open-top hopper car) is made in Table 5-1. It is interesting to note that for these runs under the theoretical balance speed, the lead inner wheel develops substantially higher lateral loads than the lead outer wheel. Loads measured by wheel or rail are net lateral loads where, on the high rail, the flange and tread creep forces are opposite in polarity. This accounts for the heavy rail and wheel wear for relatively low net lateral forces.

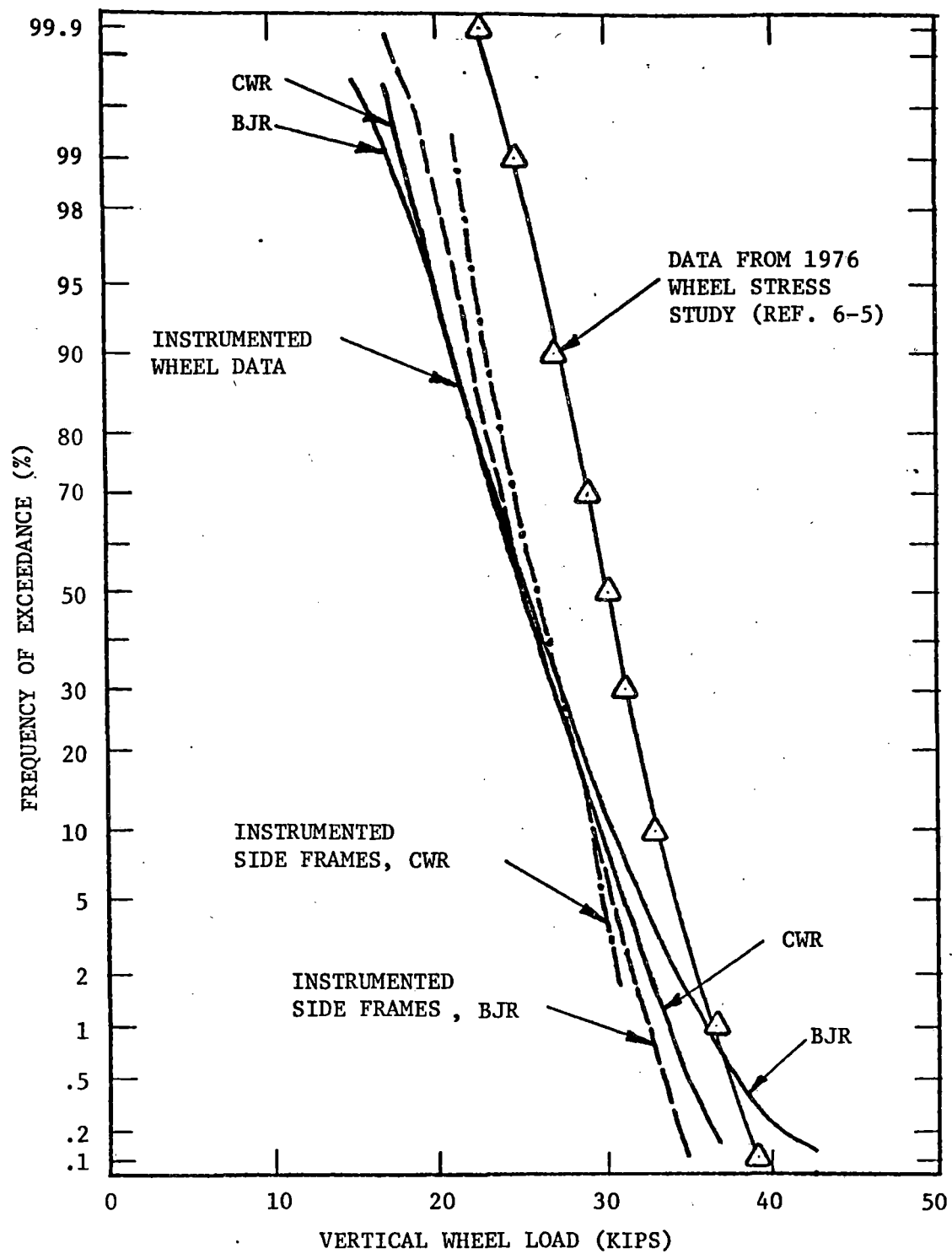


FIGURE 5-3. COMPARISON OF VERTICAL WHEEL LOAD SPECTRA FROM PILOT STUDY WITH 1976 WHEEL STRESS STUDY, OPERATION ON UPRR TRACK AT SPEEDS > 60 MPH

TABLE 5-1. COMPARISON OF LATERAL WHEEL/RAIL LOADS ON UPRR AND FAST CURVED TRACK

Source of Data	Lateral Wheel/Rail Loads on Curve (Kips)							
	Leading Outer		Leading Inner		Trailing Outer		Trailing Inner	
	Mean	Std Dev	Mean	Std Dev	Mean	Std Dev	Mean	Std Dev
Pilot Study, 6°00', 6" SE, 35 mph*	7.5	2.2	10.6	1.7	--	--	--	--
Pilot Study, 6°00', 6" SE, 25 mph	5.1	1.9	12.9	1.7	1.4	2.3	3.8	1.6
FAST, Section 3, 5°00', 4" SE, 30 mph*	6.7	3.2	13.0	2.5	0.4	1.6	2.4	1.7
FAST, Section 7, 5°00', 4" SE, 30 mph*	8.9	2.7	10.0	1.5	-0.3	1.4	3.4	1.8
FAST, Section 17, 5°00', 4" SE, 30 mph*	4.5	2.2	7.6	1.2	--	--	--	--

\*Approximately 4 mph below theoretical balance speed.  
Positive loads = outward on rail.

## 6. PILOT STUDY TEST DESCRIPTION

### 6.1 SITE SELECTION CRITERIA

The criteria for selecting specific track test sections must reflect the overall objectives of the program listed in Section 1.2 and the practical aspects of conducting vehicle-borne and wayside measurements under revenue traffic conditions. Site selection includes the desired revenue traffic and track construction; track geometry or track load category, including factors such as tangent or curved track and grades; train operating characteristics, including speed limits; weather and terrain conditions; and site logistics and accessibility for both the test train and wayside instrumentation van. Test sections for this measurement program were chosen to meet the following specific criteria:

- a. General freight traffic density > 20 MGT/year on a single track,
- b. Train speed limits at least 60 mph for general freight, 70 mph for priority freight,
- c. Tangent CWR and BJR track sections with different geometry roughness, homogeneous over a 3- to 5-mile section,
- d. A track section with curves > 3° and a speed limit 40 to 45 mph,
- e. Test sections accessible to both the test train and the wayside instrumentation van.

The California Division mainline track of the Union Pacific Railroad west of Las Vegas, Nevada, was chosen based on high-speed mixed freight traffic including unit train operations, traffic density of approximately 25 million gross tons per track mile per year on single track, and track construction including long tangent-track sections, curves and grades, and a mixture of CWR and BJR track.

## 6.2 TEST SECTION TRACK GEOMETRY

The selection of the number of different track load categories and the particular types of track for collecting wayside and vehicle-borne measurements during this pilot study was based on the requirements for exercising and evaluating the options of the characterization methodology (see Section 1.1). Three measurement sections were chosen for this study encompassing four distinct track load categories: relatively rough bolted-joint rail (BJR) mainline tangent track, smooth continuous welded rail (CWR) mainline tangent track, curved track, and rail joints.

### 6.2.1 Selection of Test Sections

A track geometry survey was conducted by the Union Pacific Railroad between Salt Lake City, Utah, and Daggett, California (the junction with the AT&SF Railway) on November 7-10, 1977. Union Pacific's EC-1 (Plasser-built) geometry car was utilized for this survey. From a list of 15 potential test sections developed from track charts of the California and Utah Divisions, the final three sections were chosen based on best meeting the selection criteria.

The main purpose in obtaining preliminary track geometry measurements was to locate two tangent track sections having a significant difference in geometry roughness. After examining the EC-1 charts, left and right rail profile traces were chosen as best suited to develop comparative readings. Four candidate tangent track sections were examined by manual analysis for peak-to-peak exceedances within approximately a 50-ft chord length.

The choice from the smoother tangent track sections noted in Table 6-1 was based on a trade-off between technical and operational advantages and disadvantages. While the smoothest site (Milepost 305.4-308.2) had distinct logistical advantages, being readily accessible from the highway and from the yards at Las Vegas, it was approached from both directions by ascending one percent grades, so that train speeds (particularly eastbound) would be lower. The three test sections chosen are described in Table 6-2.

TABLE 6-1. COMPARISON OF TRACK GEOMETRY ROUGHNESS OF CANDIDATE TEST SECTIONS (PEAK-TO-PEAK EXCEEDANCES FROM PLASSER CAR DATA)

		Left Rail Surface		Right Rail Surface	
		$\geq 1/2"$	$\geq 1/4"$	$\geq 1/2"$	$\geq 1/4"$
Rough Tangent	2.8-mi total	16	167	53	292
(mp291.7-294.5)	0.1-mi average	0.6	6.0	1.9	10.4
Smooth Tangent	2.8-mi total	0	43	9	113
(mp305.4-308.2)	0.1-mi average	0	1.5	0.3	4.0
Smooth Tangent	2.8-mi total	0	71	3	148
(mp207.3-210.1)	0.1-mi average	0	2.5	0.1	5.3
Smooth Tangent	2.8-mi total	6	159	35	247
(mp205.0-207.8)	0.1-mi average	0.2	5.7	1.3	8.8

TABLE 6-2. FINAL CHOICE OF TEST SECTIONS FOR W/R LOAD MEASUREMENTS ON UNION PACIFIC RAILROAD

Description	Test Section	Trackside Instrumentation Location	Track	Max. Train Speeds, mph
Rough tangent track	mp 292.0-295.0	mp 292.4	39' BJR	60-70
Smooth tangent track	mp 207.3-210.3	mp 207.9	CWR	60-70
Curved track	mp 349.5-351.5	mp 350.1	6°, 78' BJR	35

### 6.2.2 Track Geometry Measurements

Approximately one week after the EC-1 geometry survey, the U.S. Department of Transportation track geometry measurement vehicle T-3 was run over the same route on a scheduled survey. The track geometry was measured at three chosen test sections. The data were digitized at 2.95-inch intervals and later reformatted for plotting at approximately 6-inch intervals. Six channels of data were recorded: curvature, gage, left and right rail surface profiles, crosslevel, and automatic location detector (ALD). Rail surface profiles were measured by an inertial profilometer system, while crosslevel was measured by a compensated accelerometer system (a combination of an integrated rate gyro and an inclinometer). Track gage was measured using servo-driven magnetic probes; and curvature was derived from the rate of turn of the car body in yaw (a rate gyro on the car body) and vehicle forward speed. Rail alignment per se was not measured.

Track geometry data were processed by ENSCO to provide plots and tabular lists of probability density and distribution function estimates and power spectral density of average profile (sum of left and right rails), crosslevel, gage and curvature. Cross spectral densities for average profile and crosslevel were also generated. These results were generated for each mile of the 3-mile test sections as well as for the total 3-mile length.

Examination of statistical results from these track geometry measurements showed only marginal differences in roughness between the two tangent track sites. For example, in Table 6-3 the standard deviation values are compared for the 3-mile sections and for the one mile sections which include the wayside sites.

These data indicate that the smooth tangent (CWR) test section was rougher in crosslevel than the rough tangent (BJR) section. An examination of the power spectral density plots, however, shows some distinct differences, particularly in the harmonic components of the spectra due to the 39-ft rail lengths. Plotted spectra for the rough and smooth tangent test sections are shown in Figures 6-1 through 6-4. The differences in spectral peaks between rough and smooth sections are given in Table 6-4.

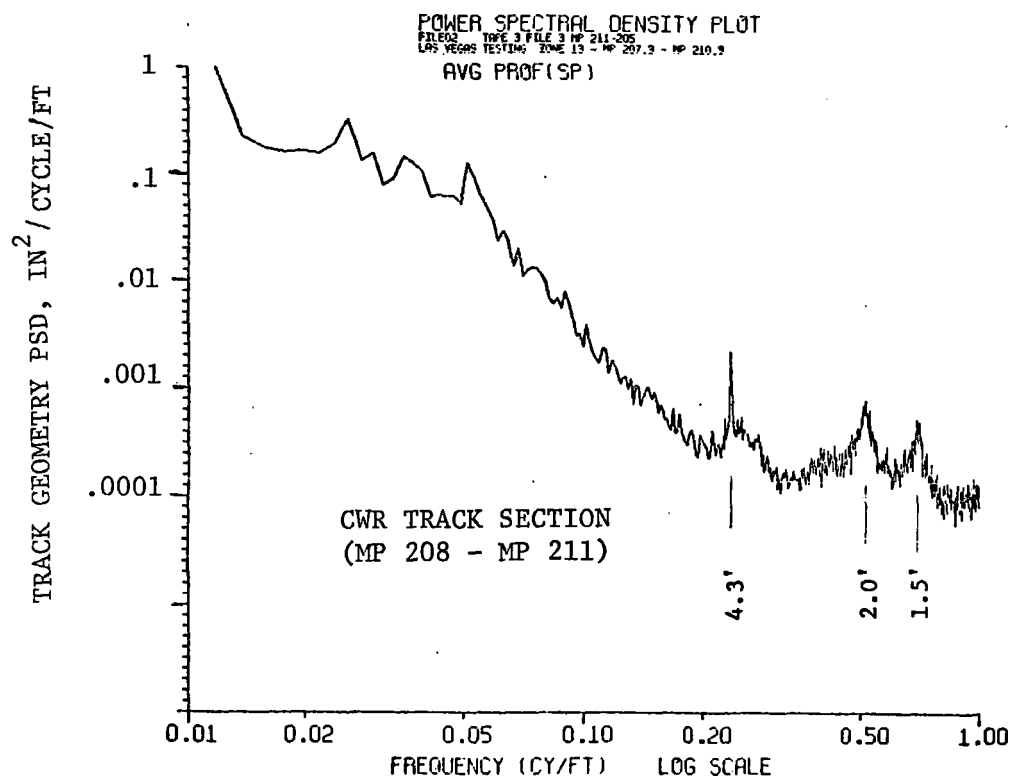
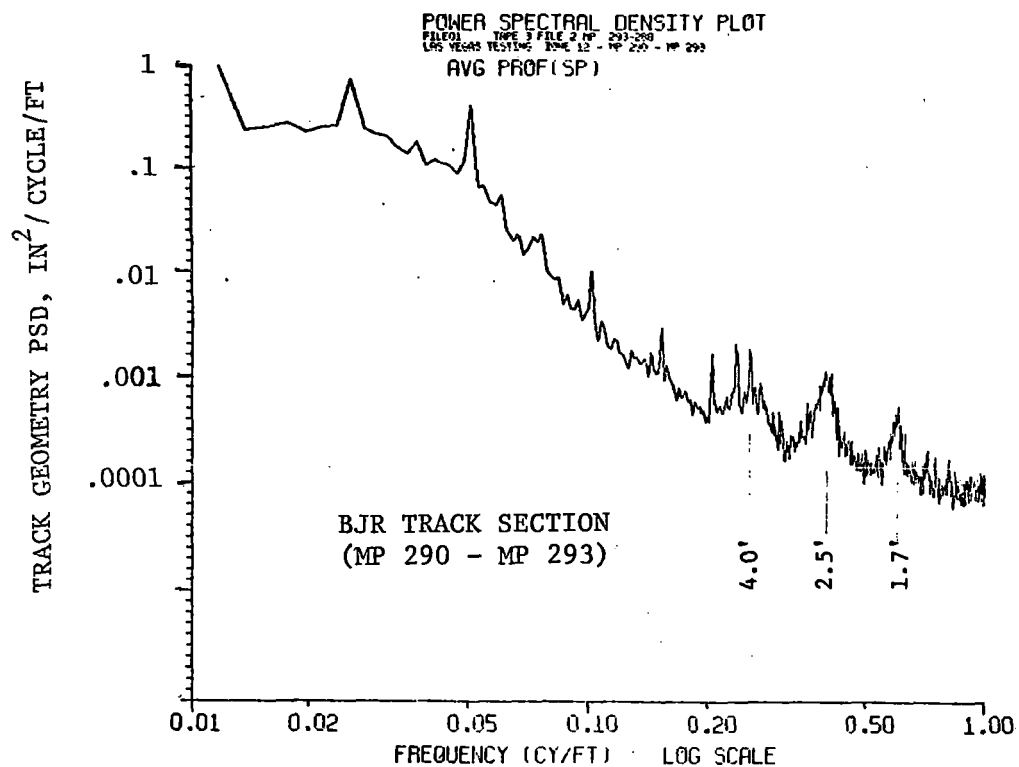


FIGURE 6-1. COMPARISON OF AVERAGE TRACK SURFACE PROFILE GEOMETRY SPECTRA FROM BJR AND CWR SECTIONS

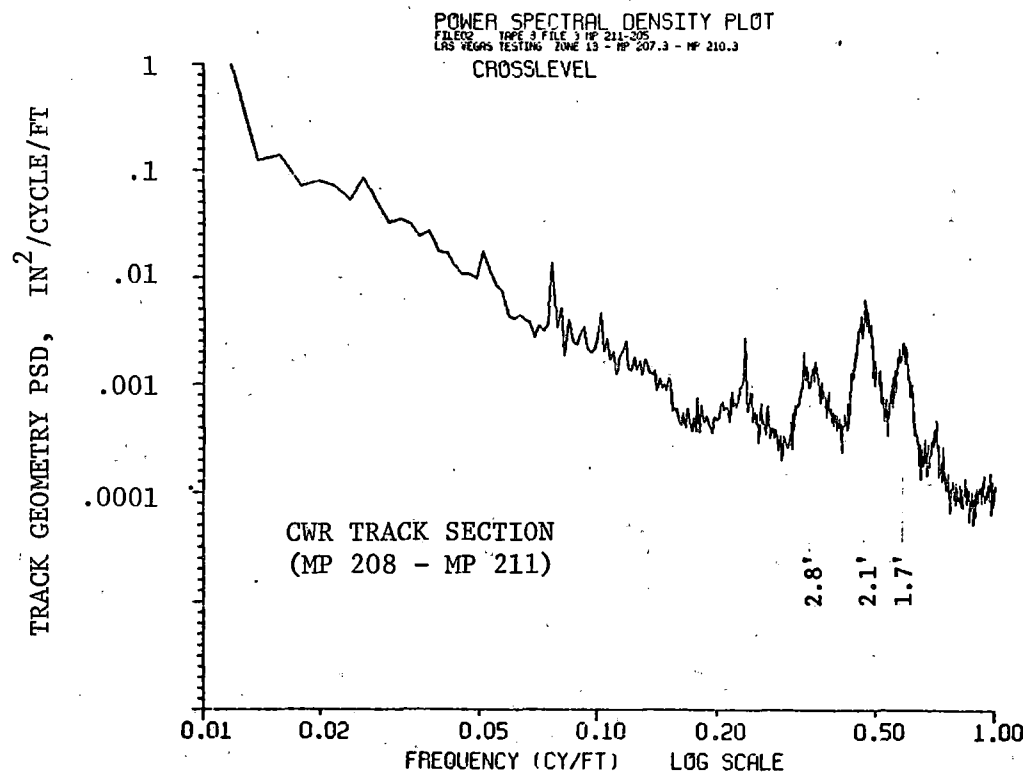
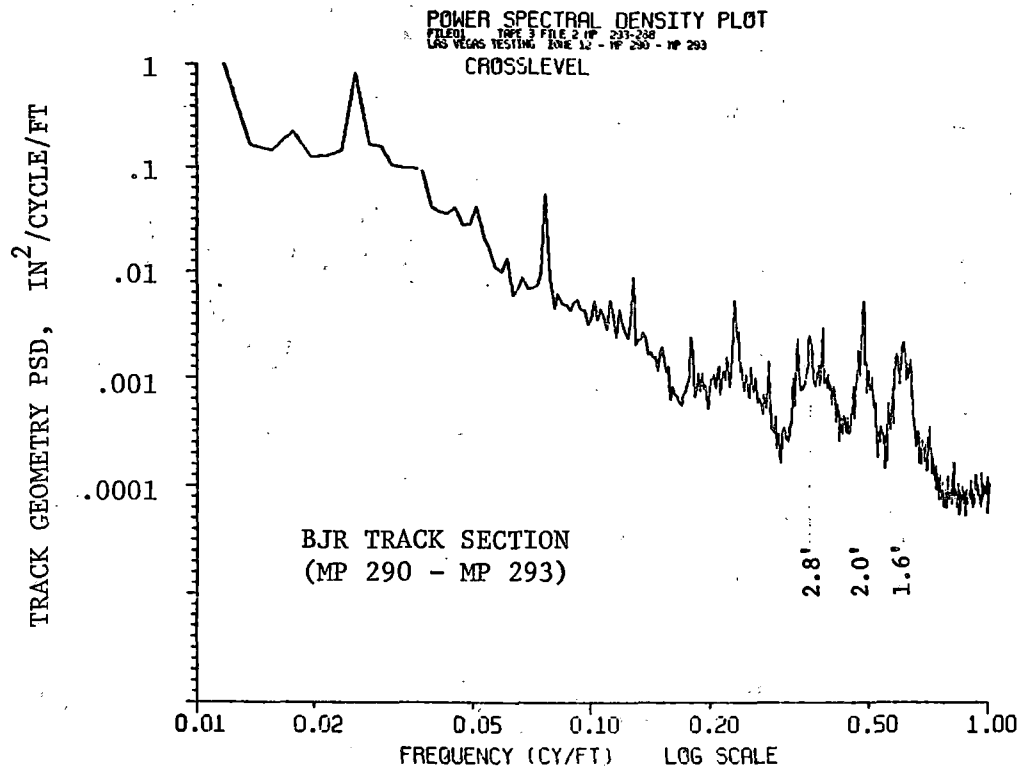


FIGURE 6-2. COMPARISON OF TRACK CROSSLEVEL GEOMETRY SPECTRA FROM BJR AND CWR SECTIONS

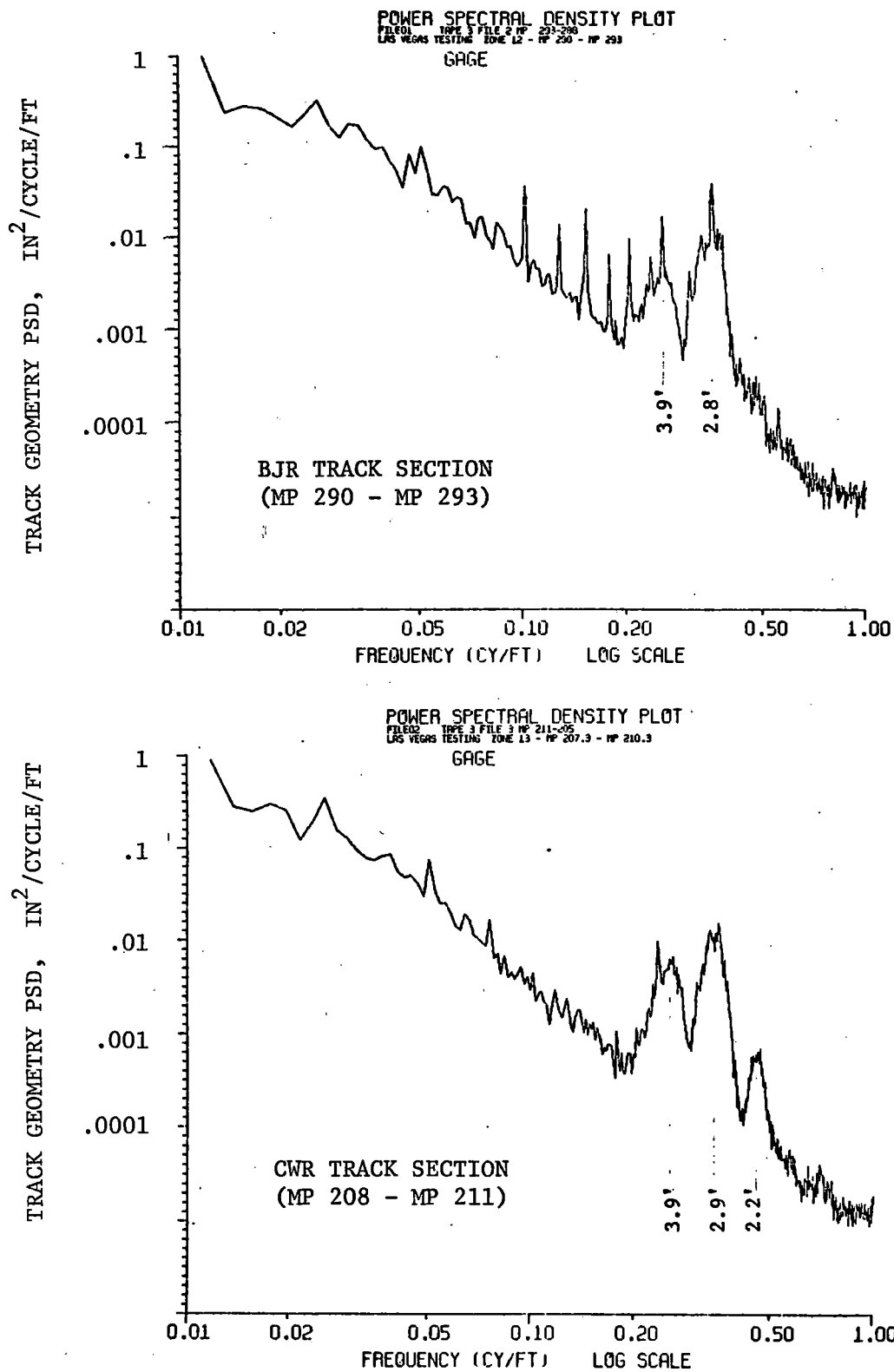


FIGURE 6-3. COMPARISON OF TRACK GAGE GEOMETRY SPECTRA FROM BJR AND CWR SECTIONS

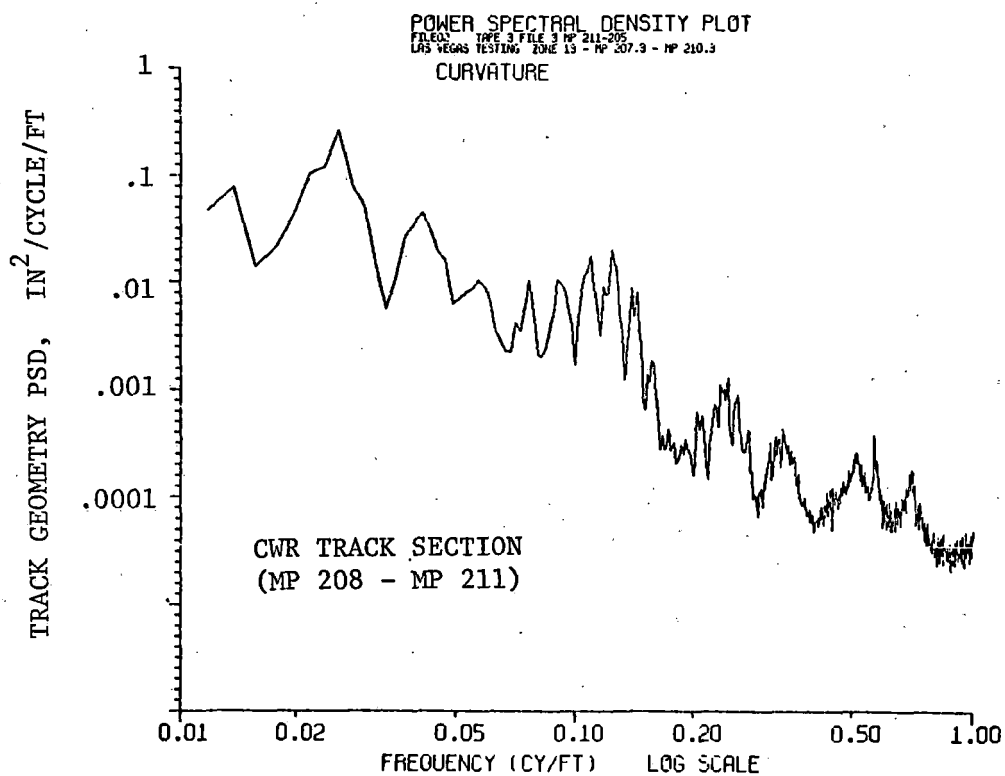
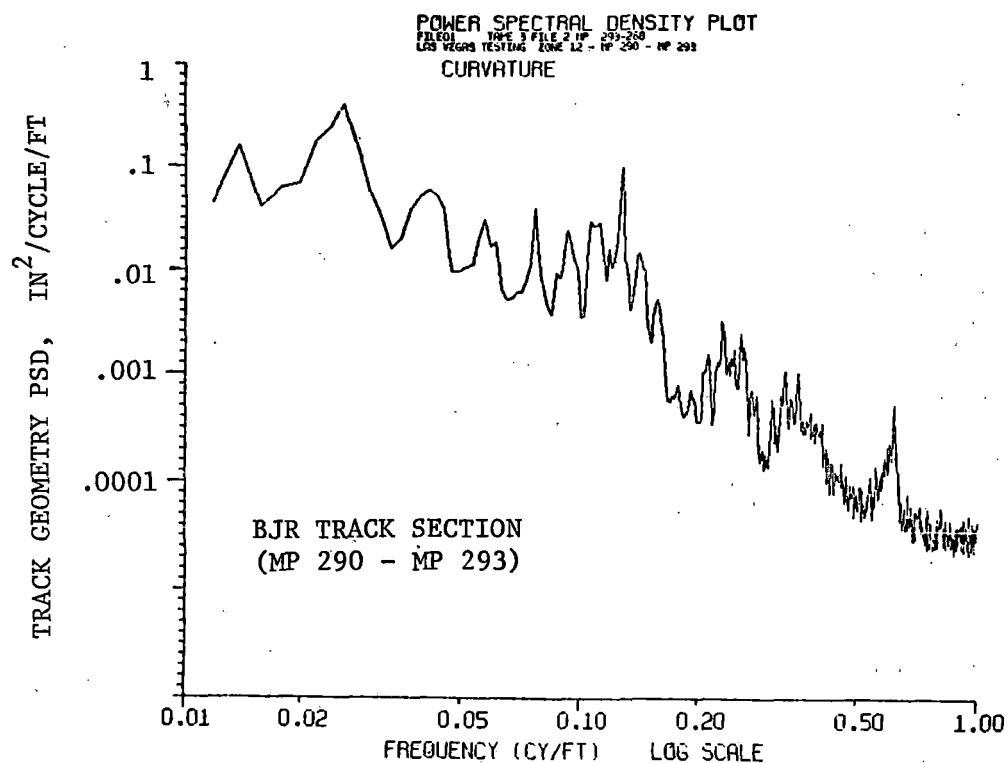


FIGURE 6-4. COMPARISON OF TRACK CURVATURE GEOMETRY SPECTRA FROM BJR AND CWR SECTIONS

TABLE 6-3. COMPARISON OF TRACK GEOMETRY STANDARD DEVIATION VALUES FOR ROUGH AND SMOOTH TANGENT TRACK SECTIONS

Test Section	Standard Deviation Values (inch)			
	Avg. Profile	Crosslevel	Gage	Curvature**
Rough (mp 290-293*)	0.1626	0.1211	0.2203	0.2321
Smooth (mp 207.3-210.3)	0.1402	0.1705	0.1342	0.1891
Rough (mp 292-293)	0.1725	0.0932	0.1336	0.2371
Smooth (mp 207.3-208.3)	0.1366	0.1447	0.1265	0.1839

\*Note that measurements were inadvertently offset from the test zone by 2 miles.

\*\*Inches offset (100' chord). Histograms in 0.025-inch bins, 10880 samples/mile.

TABLE 6-4. DIFFERENCES IN SPECTRAL PEAKS DUE TO HARMONICS OF 39-FT RAIL LENGTH FOR TANGENT TEST SECTIONS

Harmonic	Geometry Power Ratio*			
	Avg. Profile	Crosslevel	Gage	Curvature
39 ft	0.46	0.11	1.14	0.62
19.5	0.32	0.44	0.74	0.65
13	0.59	0.26	0.95	0.25
9.75	0.39	0.89	0.12	1.26
7.8	0.74	0.19	0.17	0.13

\*Ratio of CWR spectral peak to BJR spectral peak

Only gage and curvature showed spectral peaks slightly higher in the smooth tangent section than on the bolted-joint track. Distinctive and somewhat broad spectral peaks may be seen in Figures 6-1 through 6-4 at wavelengths of 1.5 to 2.1 ft, 2.5 to 2.9 ft, and 3.9 to 4.3 ft. These peaks have not been noted in previously-generated spectra [6-3, 6-4] because they were truncated at a wavelength between 5 and 10 ft. The fact that these peaks occur in spectra generated from different types of transducers indicates that they are real, and may be caused by variations in track stiffness due to tie spacing and rail support. These peaks represent amplitudes between 0.005 and 0.010 inch rms.

### 6.3 INSTRUMENTED VEHICLE TEST SECTIONS

The length of track needed for vehicle-borne measurements depends upon several conflicting requirements. The track must have reasonably uniform characteristics of geometry, modulus and construction over its entire length. It must be of sufficient length to provide for averaging a statistically significant number of cycles of the lowest frequency of interest for developing power spectral density curves with good resolution. For example, measurements from a freight car with an assumed 1-Hz natural frequency and a 10 percent damping ratio require a 111-second sample length for a maximum 30-percent random error, a 250-second sample length for a 20-percent random error [6-5].

Tangent track section lengths of 3 miles were chosen, providing a minimum of 166 cycles at the lowest (car rocking) frequency of 1 Hz at the highest test train speed of 65 mph. A curved track section of 2 miles in length provided a minimum of 207 cycles at this lowest frequency at the highest test train speed of 35 mph. From these lengths, mean value estimates will be within a tolerance of 12 percent of one standard deviation, and standard deviation estimates between 0.9 and 1.12 times the actual standard deviation.

#### 6.3.1 BJR Tangent Track

A section of level, tangent track between Mileposts 292 and 295 was chosen for the rough tangent test section. This single-track mainline, consisting of 133 lb/yd bolted-joint rail (BJR), 39-ft lengths with a 19.5-ft joint stagger, is located in a dry lake bed near the California-Nevada border. Grades up to one percent descend into this area from either direction, accounting for generally high revenue train speeds.

Due to heavy winter rains, standing water was found on both sides of the track almost the full length of the test section. Although the lake bed surface tended to dry out quickly, the subgrade under the track probably maintained a high moisture content throughout the year. This section was mechanically surfaced and lined in 1976, but was noticeably rougher (in the opinion of engine crews) than track sections less recently maintained.

This test section is located 40 miles south (westbound) from the Las Vegas yards, providing relatively good access by test train from terminal facilities. Track speed limits of 79 mph for passenger trains and 60 mph for freight trains are listed for the section, and priority freight trains (TOFC/COFC) are run at speeds up to 70 mph.

#### 6.3.2 CWR Tangent Track

A section of tangent track between Mileposts 207.3 and 210.3 was chosen for the smooth tangent test section. This single-track mainline, consisting of 133 lb/yd continuous-welded rail (CWR), is located between the Crucero and Balch (California) sidings in the Mojave River Sink. This is a blowing-sand area where the ballast tends to become sand-infiltrated, resulting in a high track modulus. Following a freight train derailment several years ago attributed to truck hunting and blowing sand under the rail base, the Union Pacific undertook an extensive project to line the track with thick tamarisk tree hedges, 50 to 100 ft either side of track centerline, to control the sand.

The test section is located at the lowest point in the valley, with grades up to one percent descending from either direction into this area, again accounting for generally high revenue train speeds. A ridge within the section results in a one percent descending (eastbound) grade between Milepoints 207.1 and 207.4. This section was also surfaced and lined during 1976. The train speed limits are 79 mph for passenger and 60 mph for freight, and priority freight (TOFC/COFC) is run at speeds up to 70 mph.

During 1976, experiments on freight car lateral dynamics were conducted in this same area by the Union Pacific Railroad and the Association of American Railroads, under the direction of Professors Cooperrider and Law [6-6]. This test section presented some logistical problems since it is 130 miles west of the Las Vegas facilities, and required the test train and crew to tie up at Yermo, California, overnight.

### 6.3.3 Curved Track

A 2-mile curved track section between Mileposts 349.5 and 351.5 was chosen as the third test section. This single-track mainline, consisting of 133 lb/yd BJR in 78-ft lengths, is located on a one percent ascending (east-bound) grade approaching Apex, about 15 miles north of the Las Vegas yards. The section contains the following curves in the eastbound direction:

TABLE 6-5. DESCRIPTION OF CURVES WITHIN CURVED-TRACK TEST SECTIONS, MP 349.5-351.5

Curvature	Direction	Length*	Superelevation**	Balance Speed
5°58.7'	LH	1000 ft	6.0 in	37.9 mph
6°00.4'	RH	1710	6.0	37.8
4°59.9'	LH	1650	5.25	38.7
2°16.6'	RH	435	2.50	39.6

\*In body of curve (from crosslevel, track geometry charts).

\*\*Average from crosslevel.

Train speed limits are 45 mph for passenger and 35 mph for freight, with priority freight trains (TOFC/COFC) run at speeds up to 40 mph. This location is on the Utah Division of the Union Pacific and is readily accessible from the Las Vegas facilities. Train speed limits are dictated by unbalance limits on the curve, but the track specifications meet Class 5 levels of the Track Safety Standards.

## 6.4 WAYSIDE TEST SECTIONS

Wayside test sections were chosen within the 3-mile vehicle test sections based on the criteria of uniformity of track by visual examination, absence of obvious anomalies (such as grade crossings, bridges or culverts, turnouts, etc.), and accessibility. The basic 900-ft wayside test section (600 ft in the curve) was chosen so that the instrumentation van could be more-or-less centered within this length.

### 6.4.1 Rough Tangent Track

The instrumentation van was located approximately at Milepost 292.4 in the rough tangent test section. Locations of the load measurement sites within the wayside zone are shown in Figure 6-5, superimposed on plots of average surface and crosslevel geometry from the T-3 car survey\*. The wayside zone consisted of 133 lb/yd 39-ft BJR on 19.5-ft joint stagger, hardwood ties on an average 20-3/4-inch spacing, on an iron-slag ballast. Standard 1:40-cant tie plates had a 4-spike pattern with two rail and holddown spikes on field and gage sides. Every other crib was boxed with rail anchors, but the anchors were worked loose, so that the rail "ran" (moved longitudinally with reversal of traffic direction) up to 3 inches at the west end of the zone, up to 1 inch at the east end. The subgrade appeared to consist of clay and alkali fines typical of the dry lake bed. A view of the measurement zone with test train and instrumentation van is shown in Figure 6-6.

### 6.4.2 Smooth Tangent Track

The instrumentation van was located at Milepost 207.9 in the smooth tangent test section. Locations of the load measurement sites within the wayside zone are shown in Figure 6-7, superimposed on the track geometry plots. This zone consisted of 133 lb/yd CWR, hardwood ties (somewhat chewed up with

---

\*It is recognized that specific anomalies in the space curve may have changed between November and February due to traffic or due to normal maintenance by the Union Pacific section gang.

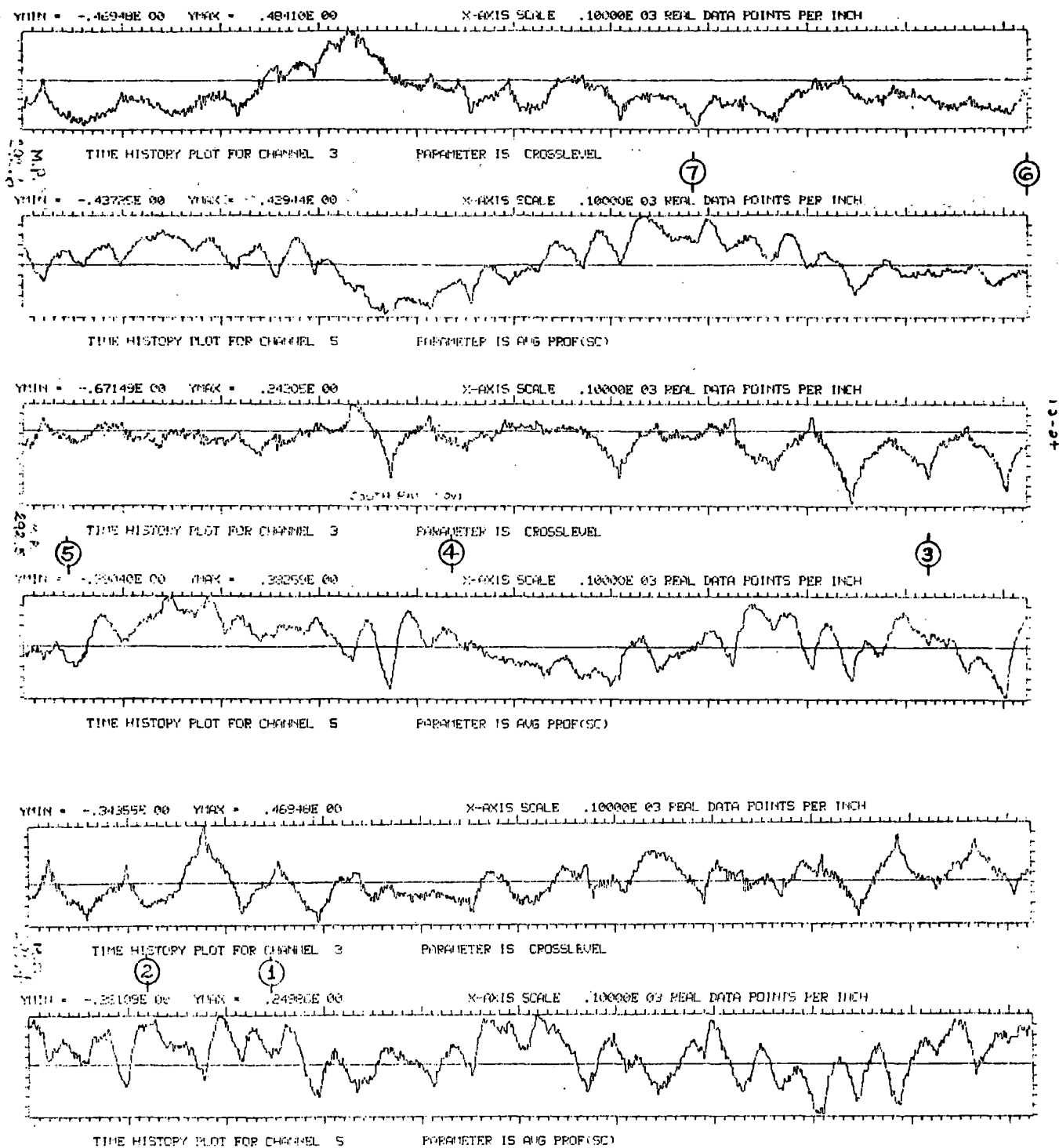


FIGURE 6-5. TRACK AVERAGE SURFACE AND CROSS LEVEL THROUGH TRACKSIDE TEST SECTION 1, ROUGH TANGENT TRACK, M.P. 292.4

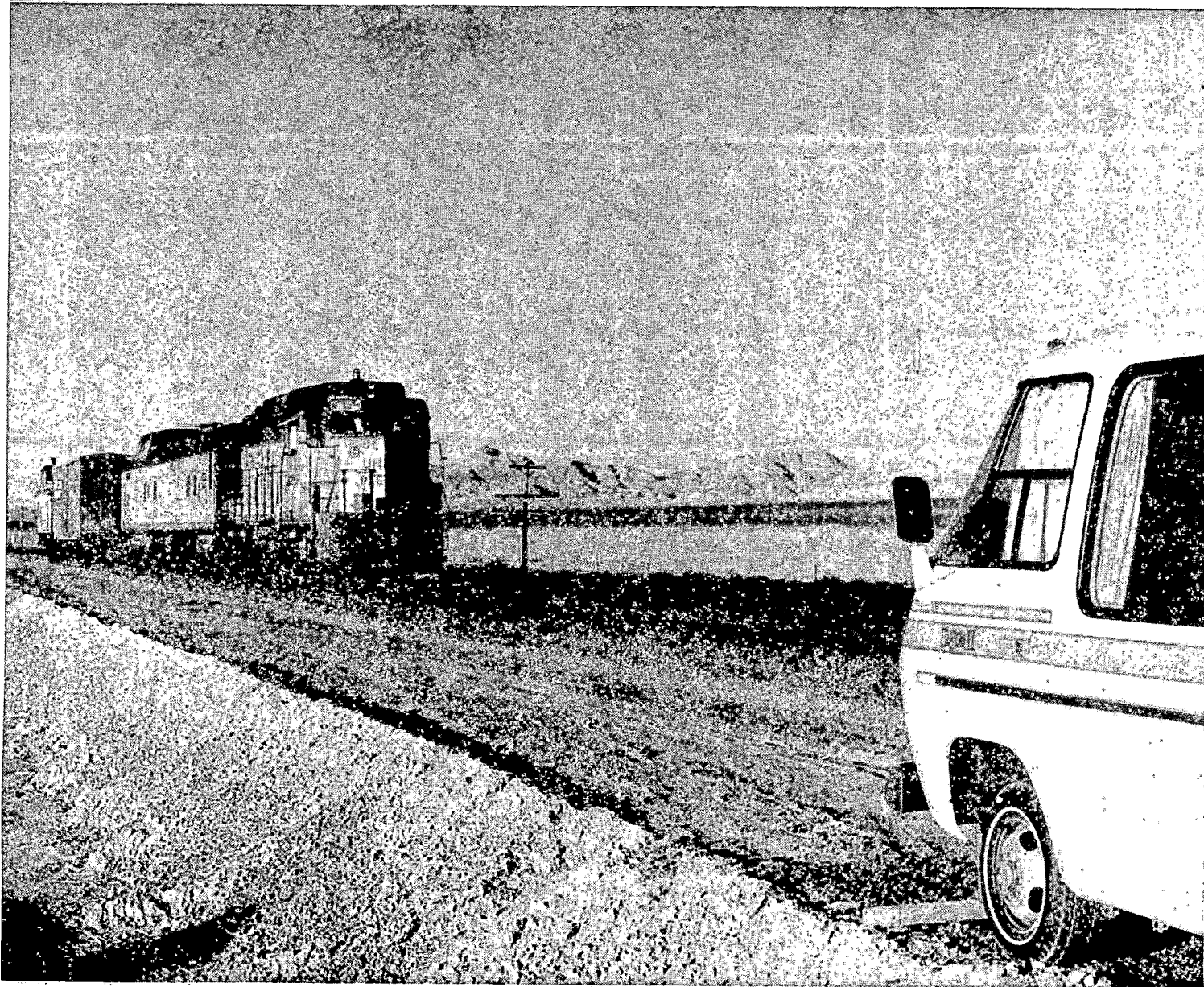


FIGURE 6-6. VIEW OF ROUGH TANGENT TEST SECTION (MP 292.4)

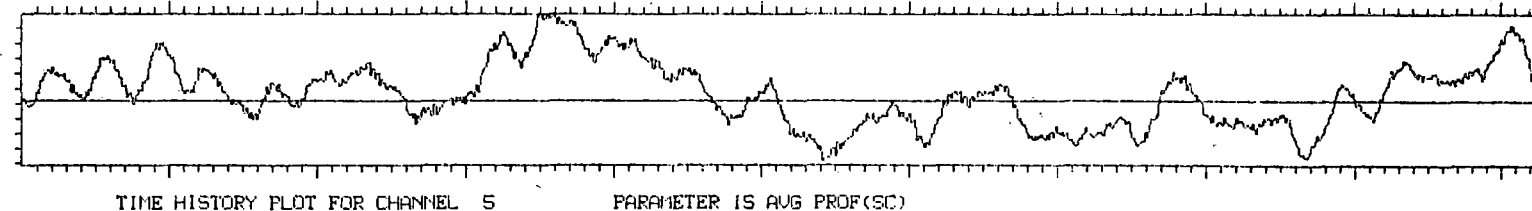
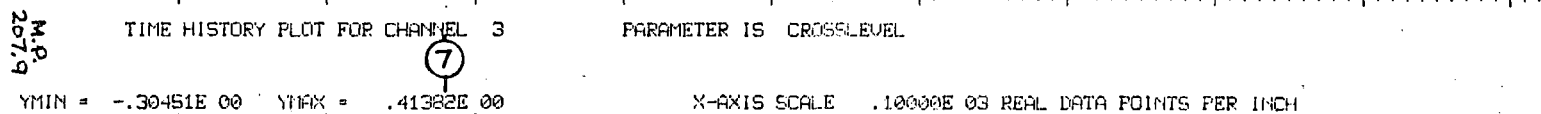
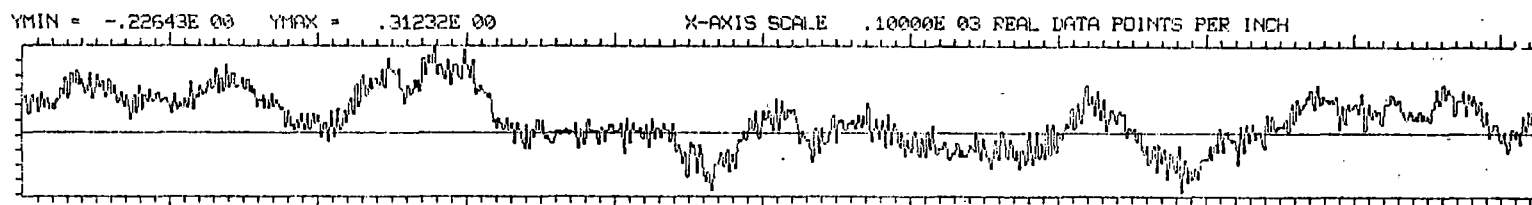
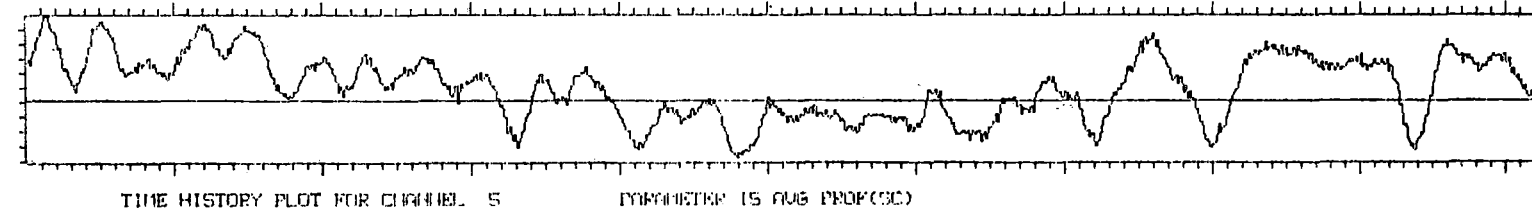
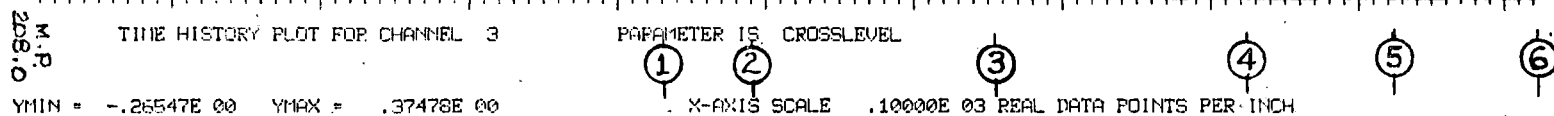
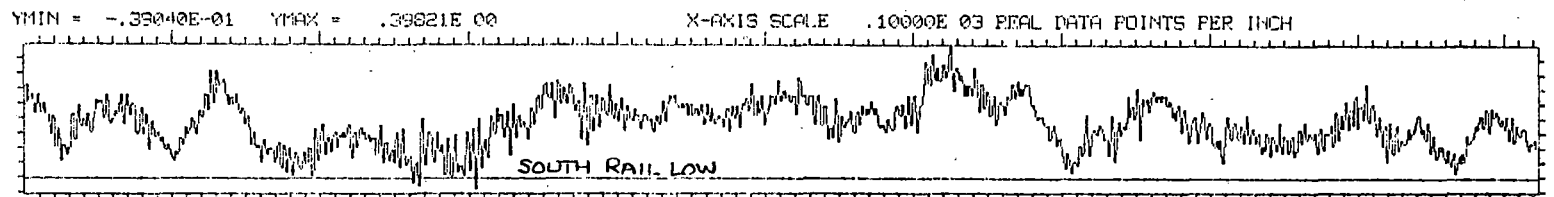


FIGURE 6-7. TRACK AVERAGE SURFACE AND CROSS LEVEL THROUGH TRACKSIDE TEST SECTION 2, SMOOTH TANGENT TRACK, M.P. 207.9

evidence of derailed wheelsets) on an average 21-inch spacing, on an iron-slag ballast thoroughly infiltrated with sand. Older 1:40 tie plates (marked 131 lb) had a spiking pattern of two rail spikes on gage and field side, and a fifth holddown spike on the gage side. Every other tie was boxed with rail anchors, and the rail was running less than 1/2 inch with reversal of traffic direction.

The test zone was within the existing tamarisk tree hedge and was therefore protected from drifting sand. At this point the descending (east-bound) grade was -0.50 percent. A view of the test zone is shown in Figure 6-8.

#### 6.4.3 Curved Track

The instrumentation van was located at Milepost 350.1 on the 6-degree right-hand (eastbound) curve with a one percent ascending grade, well into the body of the curve. The wayside zone consisted of 133 lb/yd 78-ft BJR on hardwood ties with a 20-inch average spacing. Rail joints were found on approximately a 32-ft stagger (low rail joint 32 ft east of the high rail joint). Tie plates consisted of 1:14 CF&I plates on the high rail, 1:40 14-inch plates on the low rail, with 3 rail (two on the inside base) and 2 holddown spikes on the high rail, and 2 rail, 2 holddown spikes on the low rail. Every other crib was anchored at this location.

A lubricator in the vicinity of the instrumented curve was inoperative during the test period. Sustained flange squeal, particularly on long cars, was common; and high rail head wear of 5/16 inch was measured. Most trains negotiated the curve below balance speed, and some flattening of the low rail head profile was noted. Locations of measurement sites are shown superimposed on the track geometry plots in Figure 6-9; and a view of the test zone is shown in Figure 6-10.

### 6.5 WAYSIDE MEASUREMENTS

#### 6.5.1 Instrumentation

Dynamic measurements recorded from wayside transducers were selected to define the wheel/rail load environment and the track response under load



FIGURE 6-8. VIEW OF SMOOTH TANGENT TEST SECTION (MP 207.9)  
LOOKING TOWARD THE WEST

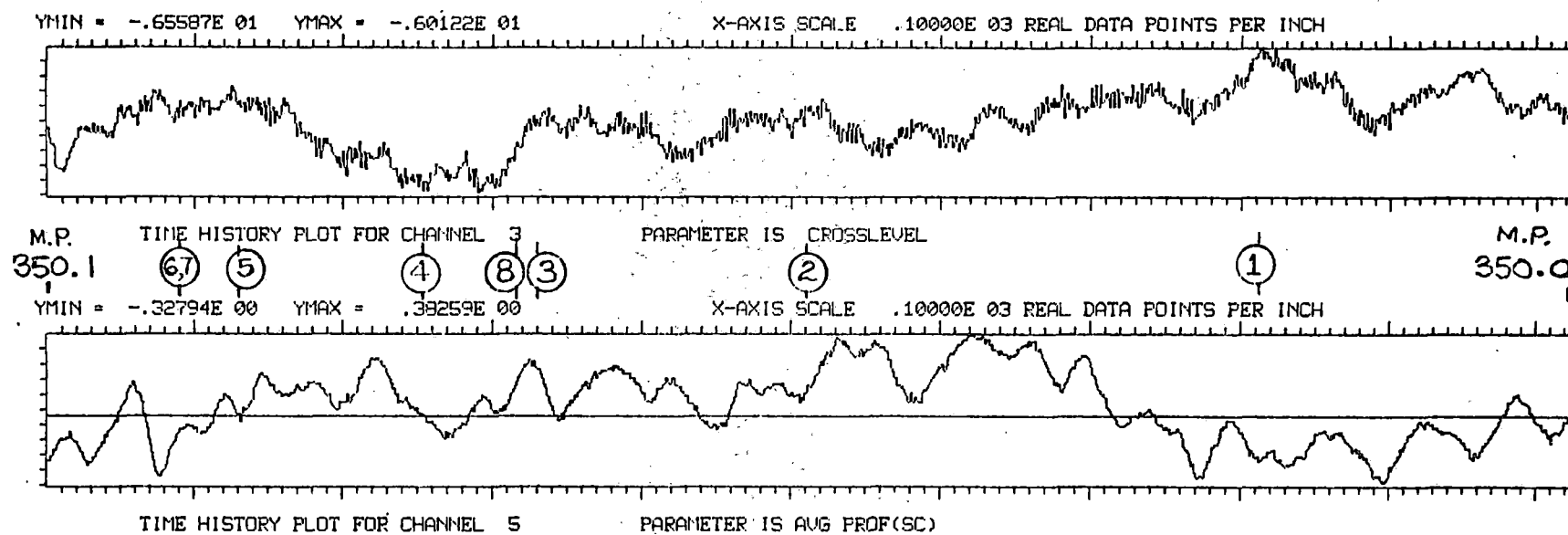


FIGURE 6-9. TRACK AVERAGE SURFACE AND CROSS LEVEL THROUGH TRACK-SIDE TEST SECTION 3, CURVED TRACK, M.P. 350.1

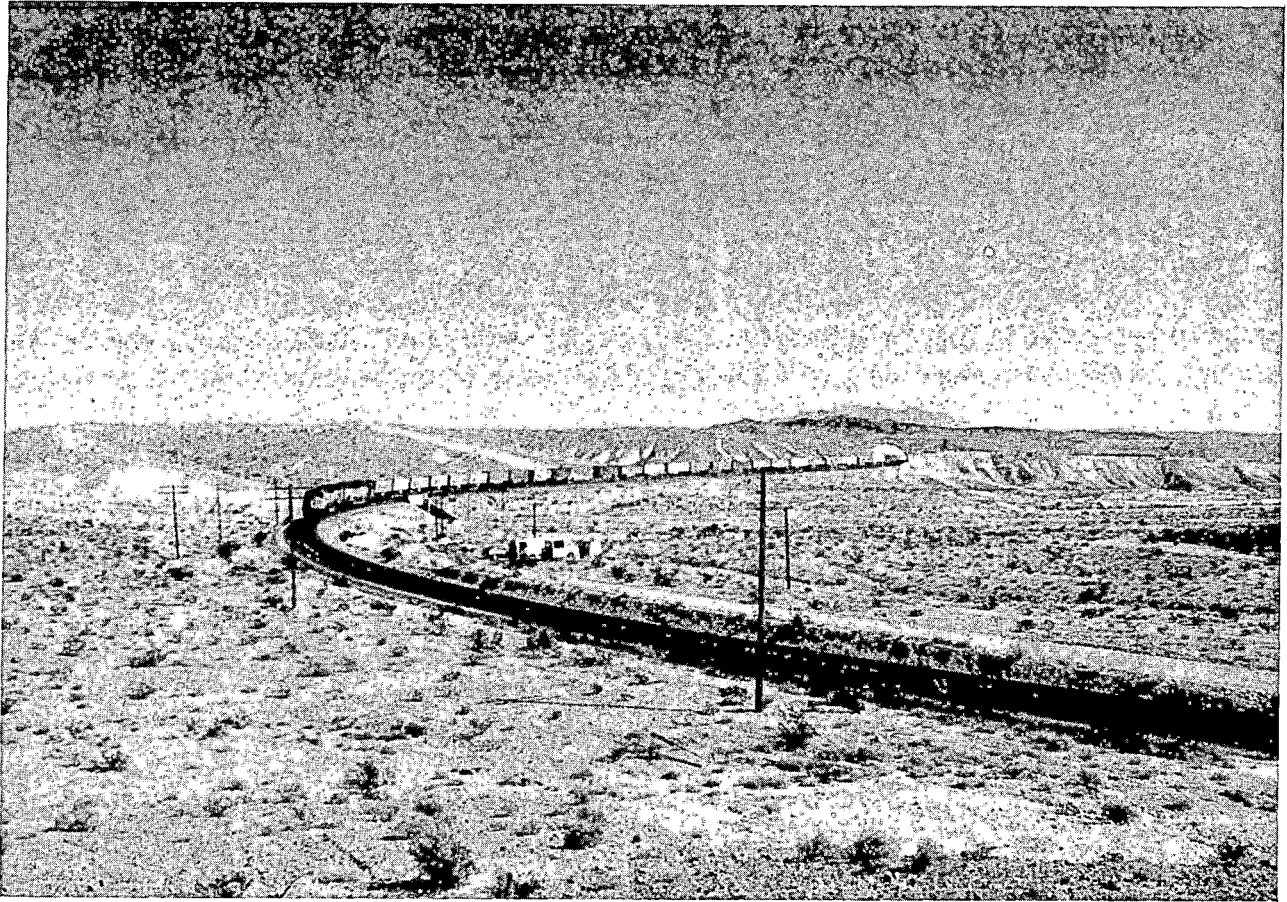
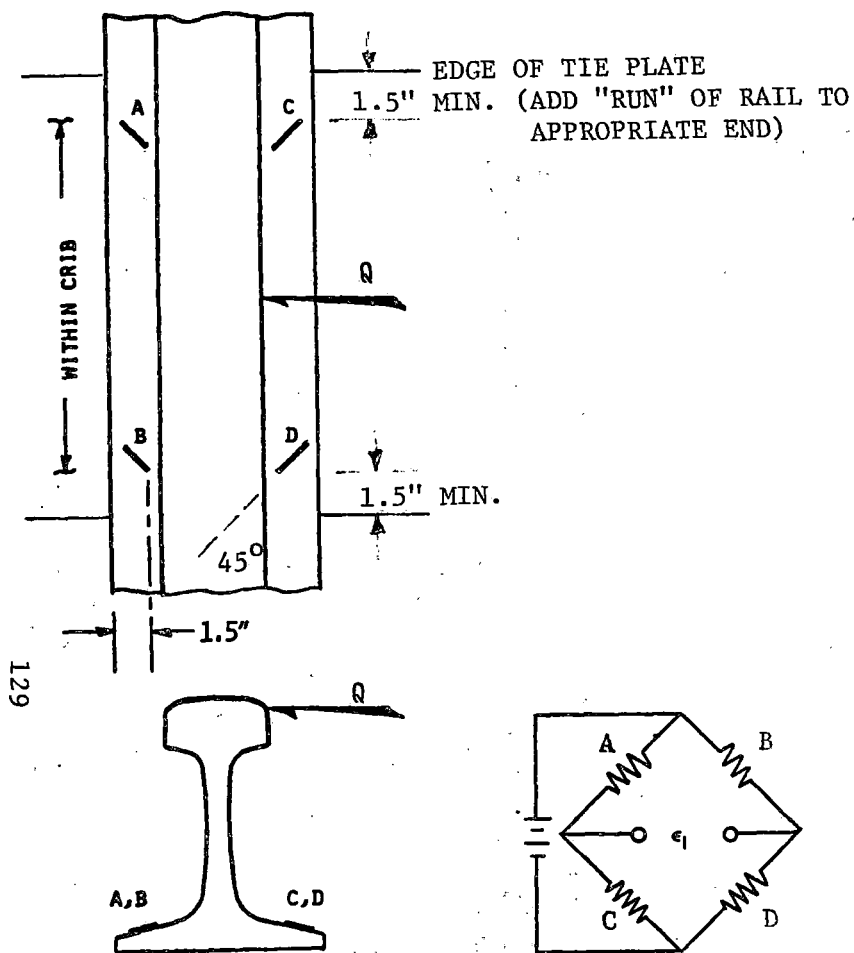


FIGURE 6-10. VIEW OF CURVED TRACK TEST SECTION (MP 350.1)

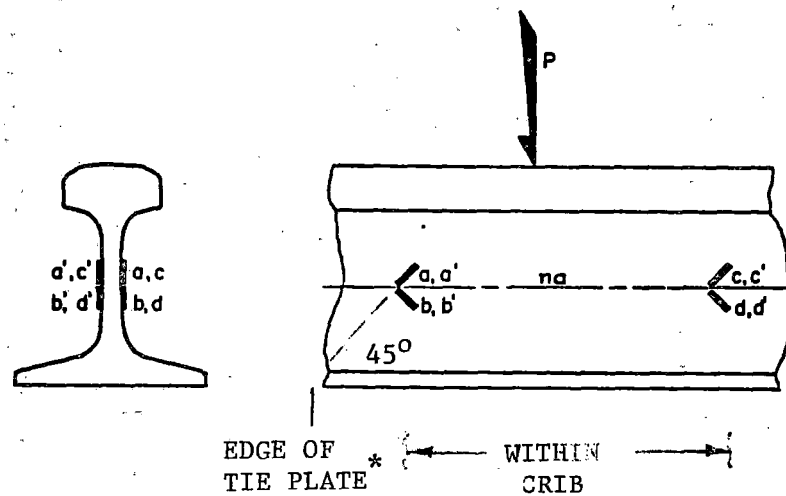
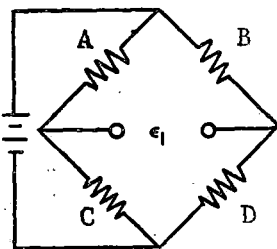
for the given test sections. Transducers for measurement of wheel/rail loads consisted of the strain gage patterns illustrated in Figure 6-11. Weldable strain gages (Ailtech SG-129, Type 6S, with a temperature range from 0° to 180°F, approximately one inch in length) were used for this application. Since the strain gage pattern for vertical load measurement shown in Figure 6-11b provides only a short sample of the passing wheel load (a few milliseconds in duration over a span of several inches), a longer vertical load "window" was used to develop flat wheel statistics. Strain gage chevron patterns were combined with load cell tie plates to generate a vertical load signal over a 35-inch length, approximately one third of a wheel circumference. This configuration was used at one site in Test Section 2, the smooth tangent (CWR) track. A variation of this was used to measure vertical load at a rail joint in Test Section 1, the rough tangent (BJR) track. These transducer configurations are shown in Figure 6-12. A pair of electromagnetic wheel detector transducers was used at each measurement site to provide a logic pulse for data processing.

In addition to vertical and lateral loads on the rail, strain gages were used to measure strains at the first bolt hole of a rail, and longitudinal strains in the head and base of the rail. Bonded strain gages 1/8-inch in length were attached as shown in Figure 6-13 at the joint illustrated in Figure 6-12c, providing bolt hole strains on both sides of the web simultaneous with the vertical load measurement. Strain-gaged and laboratory-calibrated joint bolts were tightened to a nominal level by the section crew, and bolt tension was then measured before and after the bolt hole strain measurements under representative trains. Weldable strain gages were applied to the head fillet and base as shown in Figure 6-14 at Site 6 of both the smooth and rough tangent sections to measure longitudinal rail strains at the center of the crib. Gages were located 1/8 inch from the edges of the head fillet and rail base. Each gage was monitored individually, (using precision 120-ohm resistors to complete the bridge), under a representative sample of trains.

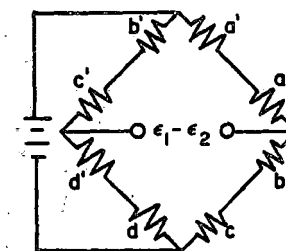
Vertical rail deflections and lateral deflections of the rail head and base were measured at the same location the longitudinal gages were applied



a. LATERAL LOAD-MEASURING CIRCUIT

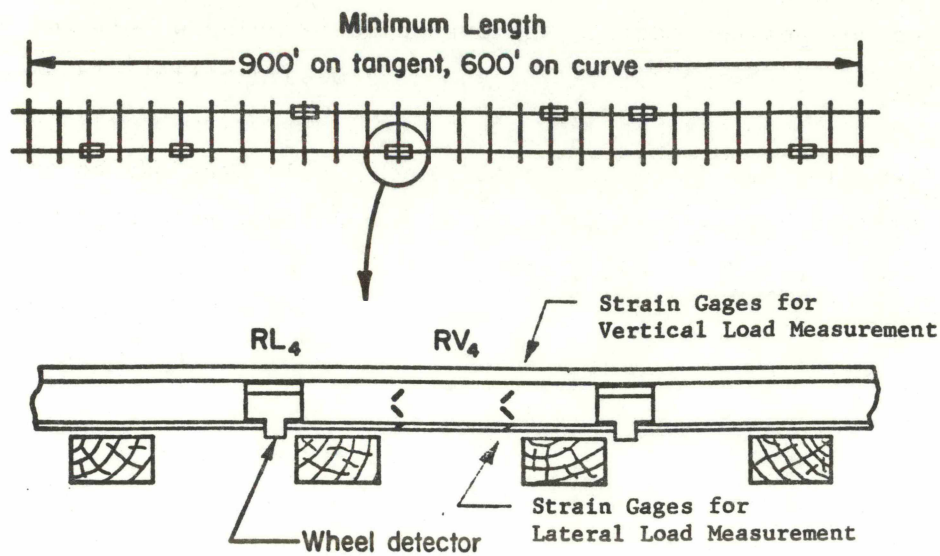


\* PROJECTED LINE OF GAGES TO FALL WITHIN CRIB AREA

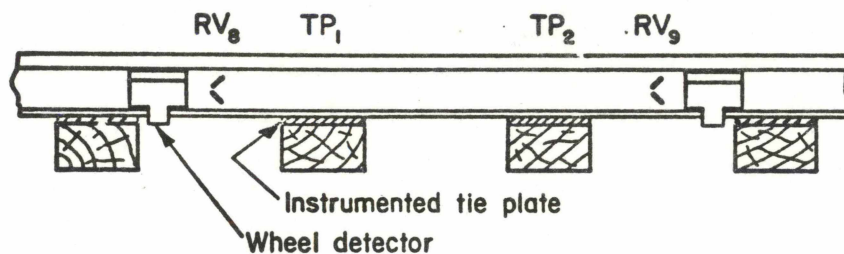


b. VERTICAL LOAD-MEASURING CIRCUIT

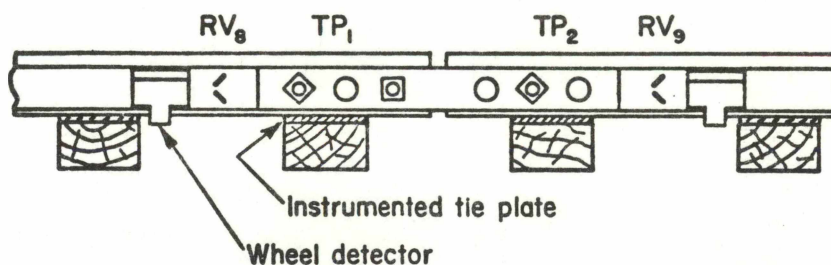
FIGURE 6-11. STRAIN GAGE CIRCUITS FOR MEASURING LATERAL AND VERTICAL WHEEL/RAIL LOADS



(a) RANDOMLY SPACED LOAD MEASUREMENT SITES  
(TEST SECTIONS 1, 2 & 3)

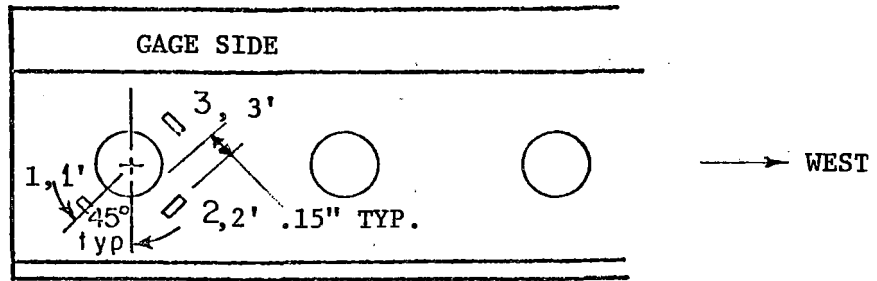


(b) EXTENDED VERTICAL WHEEL/RAIL LOAD MEASUREMENT  
ZONE ON CWR TRACK (TEST SECTION 2)



(c) EXTENDED VERTICAL WHEEL/RAIL LOAD MEASUREMENT  
ZONE AT RAIL JOINT (TEST SECTION 1)

FIGURE 6-12. LAYOUT OF WHEEL/RAIL LOAD TRANSDUCERS FOR  
DIFFERENT WAYSIDE TEST SECTIONS



(PRIMED NUMBER GAGES ON FIELD SIDE)

FIGURE 6-13. RAIL JOINT BOLT HOLE STRAIN GAGES AT SITE 3, TEST SECTION 1 (SOUTH RAIL)

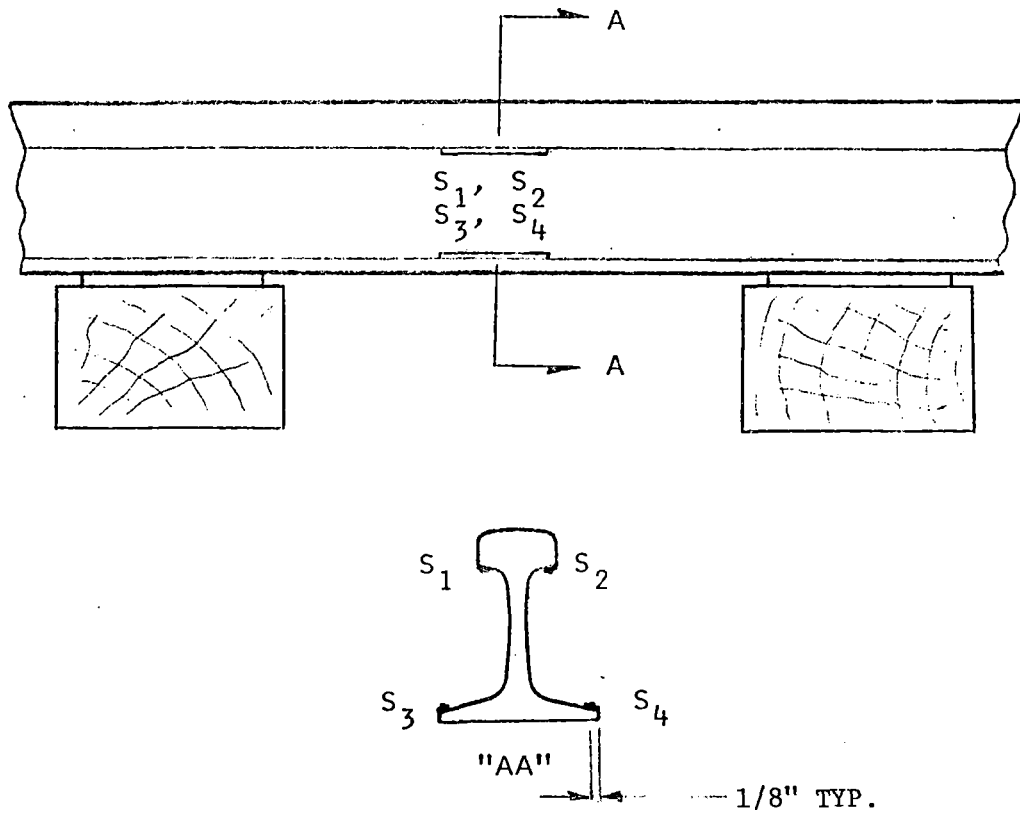


FIGURE 6-14. LOCATION OF LONGITUDINAL STRAIN GAGES ON RAIL, SITE 6, TEST SECTIONS 1 AND 2

(at crib center of Site 6, Test Sections 1 and 2). These deflection measurements were made using direct current differential transformers (DCDTs) with the transformer bodies mounted to an 8-ft "ground rod" driven through the ballast into the subgrade. The DCDT cores were attached to the rail using non-magnetic stainless steel "ready rod" extensions, screwed into phenolic blocks cemented to the rail. This arrangement provided electrical isolation from track circuits, and mechanical isolation from orthogonal motions.

Representative measurements of vertical accelerations of rail, tie and ground were also recorded, using piezoelectric accelerometers (KiaG Swiss Model 808A) and charge amplifiers for the track accelerations, and Unholtz-Dickie Model 75B10T accelerometer and charge amplifier for the ground accelerations. Accelerometers were mounted on phenolic blocks cemented to the rail or tie, or (for ground accelerations) cemented to a tie plate sunk in wetted, then dried clay on the ground roughly 10 feet from the track centerline.

Dynamic measurements are listed in Table 6-6 along with reproduction bandwidths (on oscillographic traces), full-scale transducer ranges, and the type of data base acquired. In addition to these recorded data, auxiliary measurements during tests included rail and ambient temperatures, weather conditions (including relative humidity and wind speed), and commentary on train consist. Train speeds were calculated from the oscillographic charts, using the elapsed time between first and last measurement sites (a known distance).

#### 6.5.2 Data Acquisition System

A block diagram of the wayside data acquisition system is given in Figure 6-15, showing the specific components used in this field experiment. The system consisted of two 14-channel remote signal conditioner/multiplexor units, each contained in a weather-proof, suitcase-sized box that could be placed up to 1000 feet from the instrumentation van; and a 14-channel FM tape recorder (Wide Band Group I configuration) housed in the van. Each group of 14 multiplexed channels was direct-recorded on a single channel of the analog tape, allowing up to ten channels of additional data to be recorded directly on FM. The remaining two tape channels were used for the time code signal and tape synchronization.

TABLE 6-6. WAYSIDE MEASUREMENT FOR CHARACTERIZATION OF WHEEL/RAIL LOADS AND TRACK DYNAMIC PROPERTIES

Measurement	Transducer		Type	Reproduction Bandwidth*	Max. Range	Recorded Channels	Test Section	Data Base
	Identification							
Vertical W/R Load (Sample)	RV <sub>1</sub>	-- RV <sub>7</sub>	A	300 Hz	100,000 lb	7	1,2,3	F
Lateral W/R Load (Sample)	RL <sub>1</sub>	-- RL <sub>7</sub>	A	300 Hz	40,000 lb	7	1,2,3	F
Vertical W/R Load (Extended)	RV <sub>8</sub>	-- RV <sub>9</sub>	A	1000 Hz	100,000 lb	2	2	F
	TP <sub>1</sub>	-- TP <sub>2</sub>	B	1000 Hz	50,000 lb	4	2	F
Vertical W/R Load (Joint)	RV <sub>8</sub>	-- RV <sub>9</sub>	A	1000 Hz	100,000 lb	2	1	F
	TP <sub>1</sub>	-- TP <sub>2</sub>	B	1000 Hz	50,000 lb	4	1	F
Bolt Hole Strain (Joint)	S <sub>1</sub>	-- S <sub>4</sub>	C	1000 Hz	2,000 $\mu$ e	4 max.	1	S
Rail Longitudinal Strain	S <sub>5</sub>	-- S <sub>8</sub>	A	1000 Hz	2,000 $\mu$ e	4	1,2	S
Vertical Tie Plate Load	TP <sub>3</sub>	-- TP <sub>4</sub>	D	100 Hz	50,000 lb	2	1,2	S
Transverse Tie Plate Moment	TP <sub>1</sub>	-- TP <sub>2</sub>	B	100 Hz	+100,000 lb- -40,000 lb-in		1,2	S
Rail Vertical Displacement	DV <sub>1</sub>		E	100 Hz	+0.2 in (up) -0.8	1	1,2	S
Rail Head Lateral Displacement	DL <sub>1</sub>		E	100 Hz	+0.5 in	1	1,2	S
Rail Base Lateral Displacement	DL <sub>2</sub>		E	100 Hz	+0.5 in	1	1,2	S
Rail Vertical Acceleration	AV <sub>1</sub>		F	1000 Hz	+500 g	1	1,2	S
Tie Vertical Acceleration	AV <sub>2</sub>		F	500 Hz	+ 50 g	1	1,2	S
Ground Vertical Acceleration	AV <sub>3</sub>		G	500 Hz	+ 50 g	1	1,2	S

Notes: Transducers - A = Ailtech SG-129-6S weldable strain gage  
 B = 2-cell instrumented tie plate  
 C = Bonded strain gage  
 D = 3-cell instrumented tie plate  
 E = Direct current differential transformer  
 F = Kiag Swiss 808A accelerometer  
 G = Unholtz Dickie 75B10T accelerometer

Data Base - F = Full data for statistical analysis (all trains)  
 S = Representative sample of data (a few typical trains)

\*Data recorded on FM magnetic tape at 2500 Hz min. bandwidth.

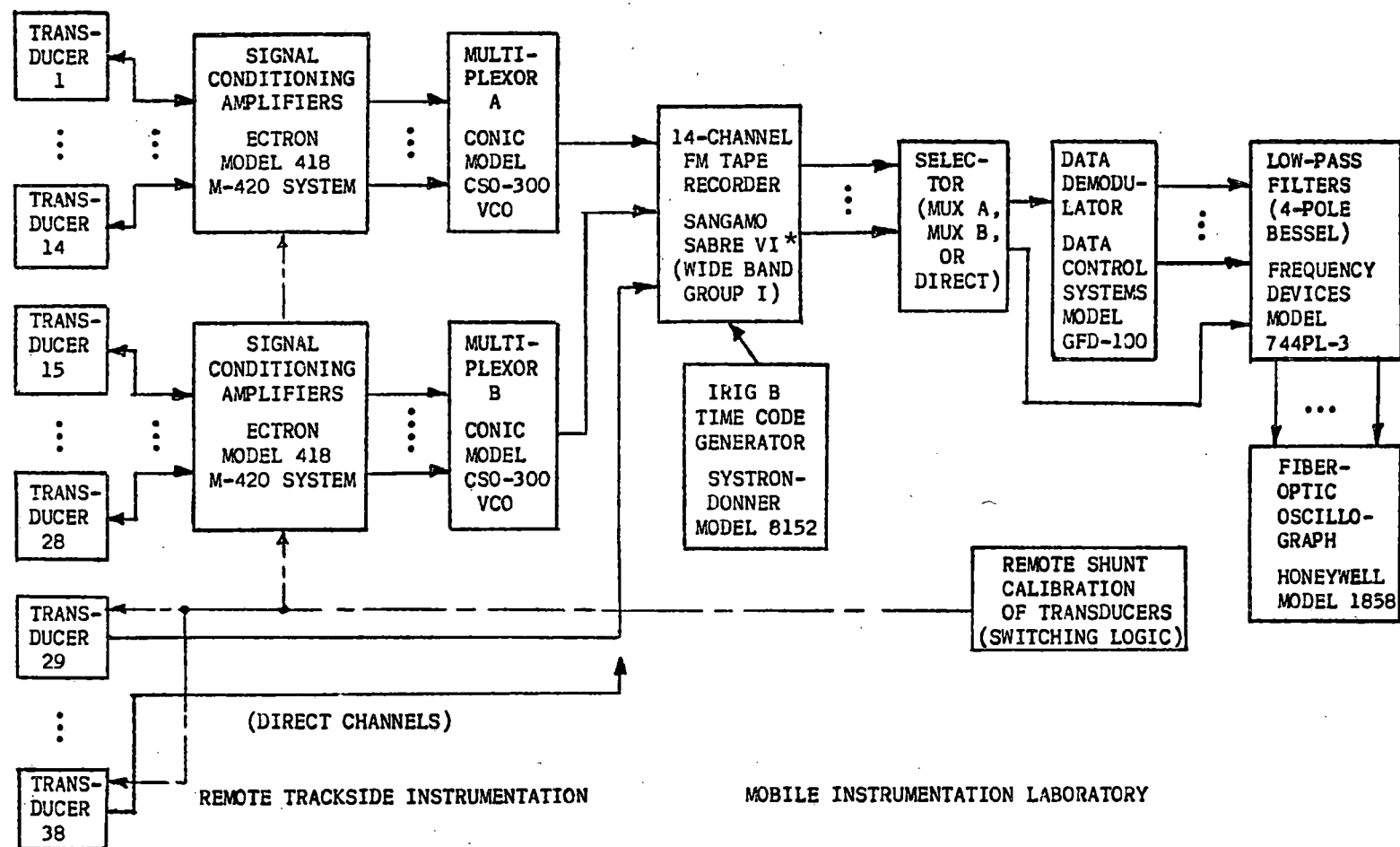


FIGURE 6-15. WAYSIDE MEASUREMENT SYSTEM COMPONENTS

\* Registered Trademark.

Data were monitored during recording at the site by use of a demodulator, switching/filter network, and oscillograph. Data were played out in three passes, first the signals from one multiplex ("Mux A"), then from Mux B, and finally the direct channels, primarily the wheel detector pulses. This quick-look capability was used to check transducer function and data quality for each train pass.

### 6.5.3 Test Section Layout

The basic 900-ft wayside test section (600 ft in the curve) was chosen to represent a minimum of 10 cycles of the longest wavelength of interest in the response of the test vehicle, the 100-ton freight car, based on a 1-Hz response at the highest test speed. Seven randomly-located measurement sites (short zone samples of vertical and lateral wheel/rail load, Figure 6-12a) were instrumented to provide a tolerance band on the resulting mean value estimate of loads (from N sites) within one standard deviation at a 95 percent confidence level. Individual site locations were chosen by reading seven consecutive numbers from a random number table (where 0 to 9999 was proportional to 0 to 900 ft), and assuming a nominal tie spacing. One rail was instrumented at odd-numbered ties, the other rail at even-numbered ties; while the minus or plus increments from rounding off the distance were used to designate the crib ahead or the crib beyond the tie. The following locations were predetermined:

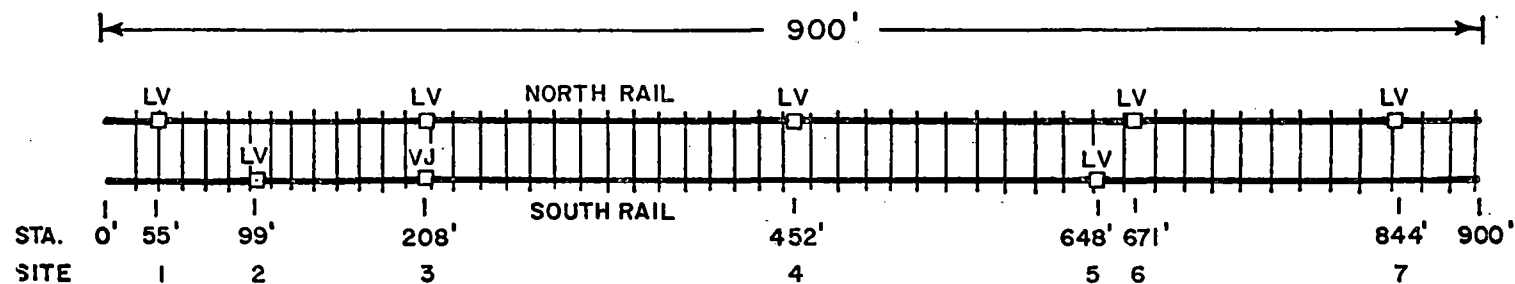
Site	Test Section 1 (Tangent)	Test Section 2 (Tangent)	Test Section 3 (Curved)	
1	Tie No. 19-	Tie No. 182+	Tie No. 70+	} high rail
2	56-	200+	159+	
3	121-	247-	216-	
4	263-	294+	233-	
5	374-	321+	260-	
6	391+	351-	286-	
7	489+	429-	286-	
				} low rail

In the actual field layout of sites, when the predetermined site fell on an unuseable location (a rail joint, an exceptionally narrow crib, etc.), the next useable location beyond this site was then instrumented. Actual locations and dimensional information on the instrumented sites are contained in Table 3-7, and are shown in plan view in Figure 6-16.

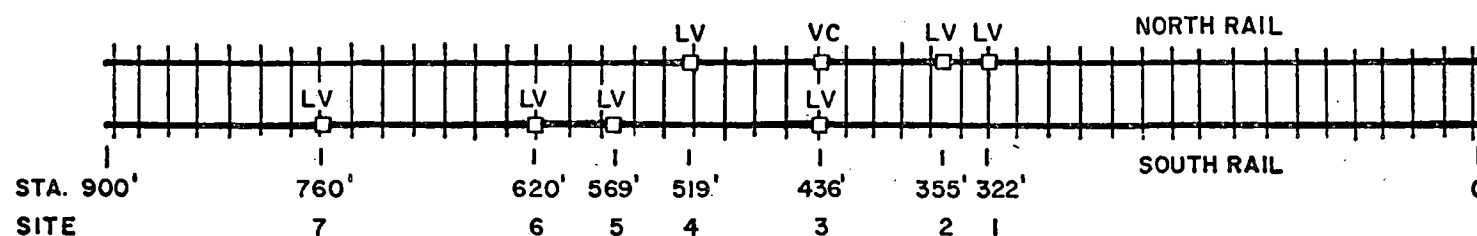
LV = lateral and vertical  
W/R load measurements, short zone

VJ = vertical loads at rail joint

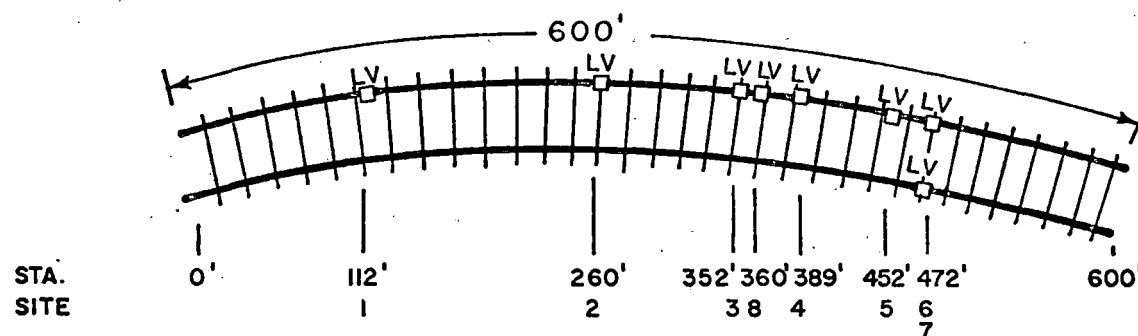
VC = vertical loads, continuous zone



TEST SECTION 1 - ROUGH TANGENT 39' BJR TRACK (M.P. 292.4)



TEST SECTION 2 - SMOOTH TANGENT CWR TRACK (M.P. 207.9)


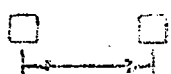


TEST SECTION 3 - CURVED 78' BJR TRACK (M.P. 350.1)

FIGURE 6-16. LAYOUT OF MEASUREMENT SITES WITHIN TEST SECTIONS

TABLE 6-7. DIMENSIONAL LAYOUT OF WHEEL/RAIL LOAD MEASUREMENT TRANSDUCERS ON UPRR TEST SECTIONS

TEST SECTION	TEST SITE	STATION FROM TIE 0	TIE NO.	RAIL	TRACK GAGE	CRIB SPACING	GAGE ZONE <sup>a</sup>	DETECTOR SPACING <sup>b</sup>	NORTH RAIL JOINT <sup>c</sup>	SOUTH RAIL JOINT	RAIL RUN <sup>d</sup>
Rough Tangent	1	35.5 <sup>e</sup>	20/21	N	56-1/2	15"	10-1/4"	42"	0 (+27")		3"
	2	99.0'	56/57	S	56-3/8	15-1/4"	10"	40"		1 (+87")	2-1/2"
	3	208.3'	120/121	N	56-1/4	15"	9-1/2"	52-1/2"		4 (-5")	2"
	4	452.8'	264/265	N	56-1/4	16-3/4"	10-3/4"	40"	11 (-114")		1-1/2"
	5	647.5'	376/377	S	56-5/8	16"	12"	37"		15 (+117")	1-1/4"
	6	671.3'	390/391	N	56-3/4	21-1/2"	16-1/2"	48"	16 (+168")		1-1/4"
	7	843.6'	489/490	N	56-1/2	20"	14-1/2"	43"	21 (-104")		1"
	JNT	208.7'	119/122	S	56-1/4		45"	52-1/2"		4 (±22.5)	2"
Smooth Tangent	1	322.2 <sup>f</sup>	181/182	N	56-1/2	16-1/4"	10-1/4"	43"	no joints	no joints	1/2"
	2	355.0'	200/201	N	56-1/2	19"	9-1/2"	45"			1/2"
	3	436.2'	246/247	S	56-1/2	13-1/4"	7-1/2"	42"			1/2"
	4	519.3'	294/295	N	56-5/8	14-1/2"	8-3/4"	39-1/2"			1/2"
	5	569.3'	322/323	S	56-1/2	16-1/4"	10-1/2"	43-1/2"			1/2"
	6	620.9'	350/351	S	56-3/4	15-1/2"	9-1/2"	44-1/2"			1/2"
	7	760.4'	428/429	S	56-5/8	17-1/2"	12"	48"			1/2"
	CCN	436.2'	245/248	N	56-1/2		38-1/2"	42"			1/2"
Curved Track	1	112.4 <sup>e</sup>	71/72	N <sup>g</sup>		12"	9"	33"	1 (-116")		
	2	260.4'	158/159	N		13"	10"	31-1/2"	3 (-212")	2 (+238")	
	3	352.4'	215/216	N		17-1/4"	14"	36"	4 (-44")		
	4	388.5'	234/235	N		12-1/2"	9-1/2"	32"	4 (+389")	4 (+38")	
	5	451.7'	275/276	N		12-1/2"	9-1/2"	32"	5 (+212")		
	6	471.7'	288/289	N	57-1/4	12-3/4"	9-3/4"	34"	5 (+451")	5 (-64")	
	7	471.7'	288/289	S	(h)	13-3/4"	10-3/4"	34"	5 (+451")	5 (-64")	
	8	360.0'	219/220	N		16-1/2"	13-1/2"	38"	4 (+47")		

Notes: a =  b =  c: Joint No. (±distance to gage)

d: maximum movement of rail with reversal of traffic e: increasing eastbound

f: increasing westbound g: high rail on curve h: 5/8" below running surface

#### 6.5.4 Installation of Transducers

The rail was prepared for weldable strain gage application by grinding smooth patches on both sides of the rail web at each gage pattern location, about 4 inches in width, to remove all rust and mill scale. A small die grinder was then used to finish grind each gage and strain relief strap site. A scribing fixture was used to mark gage locations simultaneously on both sides of the rail web. Weldable gages were then applied using a special electric-discharge spot welder (100 watt-second rating) designed for this purpose. Integral leads from the gages were routed to barrier strips where standard 4-conductor, shielded instrumentation cables from the signal conditioning amplifiers were connected. A bead of RTV rubber was run along the gage sheath up to the strain relief structure to reduce potential vibration levels. A typical gage installation with wheel detectors is shown in Figure 6-17.

Instrumented tie plates were installed by UPRR section gangs using a track jack to lift the rail slightly, removing the standard tie plate, then slipping the load cell tie plate into place and spiking it. The newer two-cell plates were used within the vertical load zone, while the older three-cell plates were used on either side of the zone, providing four consecutive instrumented tie plates. A view of both types of tie plate is given in Figure 6-18 prior to installation at the rail joint. Strain gaged bolts and one of the vertical load zone chevron patterns can be seen in this photograph.

#### 6.5.5 Calibration

The field calibration of vertical and lateral W/R force circuits was accomplished by means of a calibration head and two hand-operated hydraulic jacks: one applying a lateral force reacted against the opposite rail head; the other applying a vertical force reacted against the side sill, cross bearer or other structure of a locomotive or car. The calibration head, shown in Figure 6-19, consists of two contact patches simulating the vertical and lateral (flange) contact of an AAR freight car wheel profile. Vertical and lateral load cells, laboratory calibrated, built into the calibration head, provide the force signals for the X axis of an X-Y plot. The lateral load



FIGURE 6-17. TYPICAL INSTALLATION OF VERTICAL AND LATERAL  
WHEEL/RAIL LOAD MEASUREMENT GAGE PATTERNS

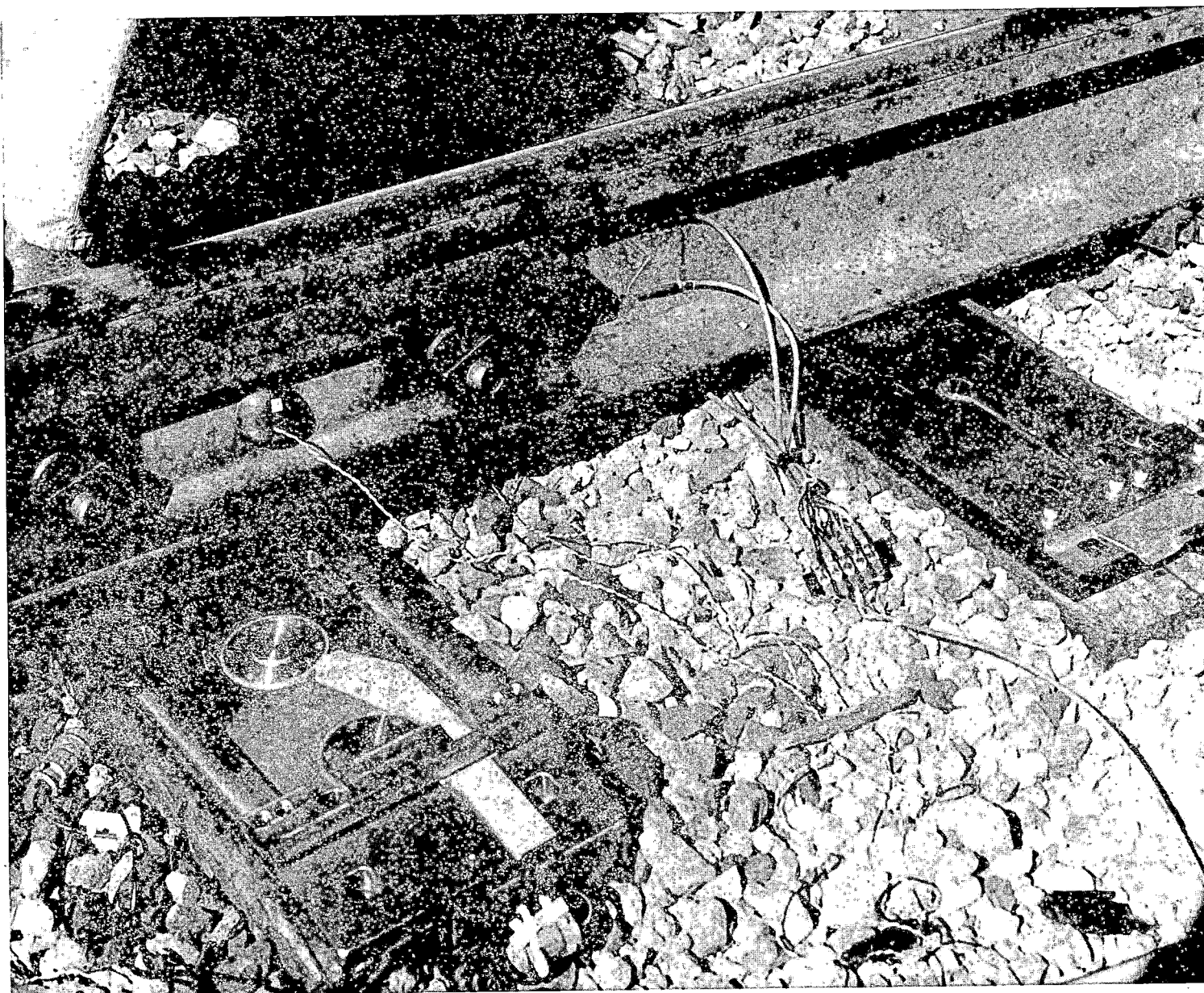


FIGURE 6-18. VIEW OF LOAD CELL TIE PLATES DURING INSTALLATION AT INSTRUMENTED RAIL JOINT

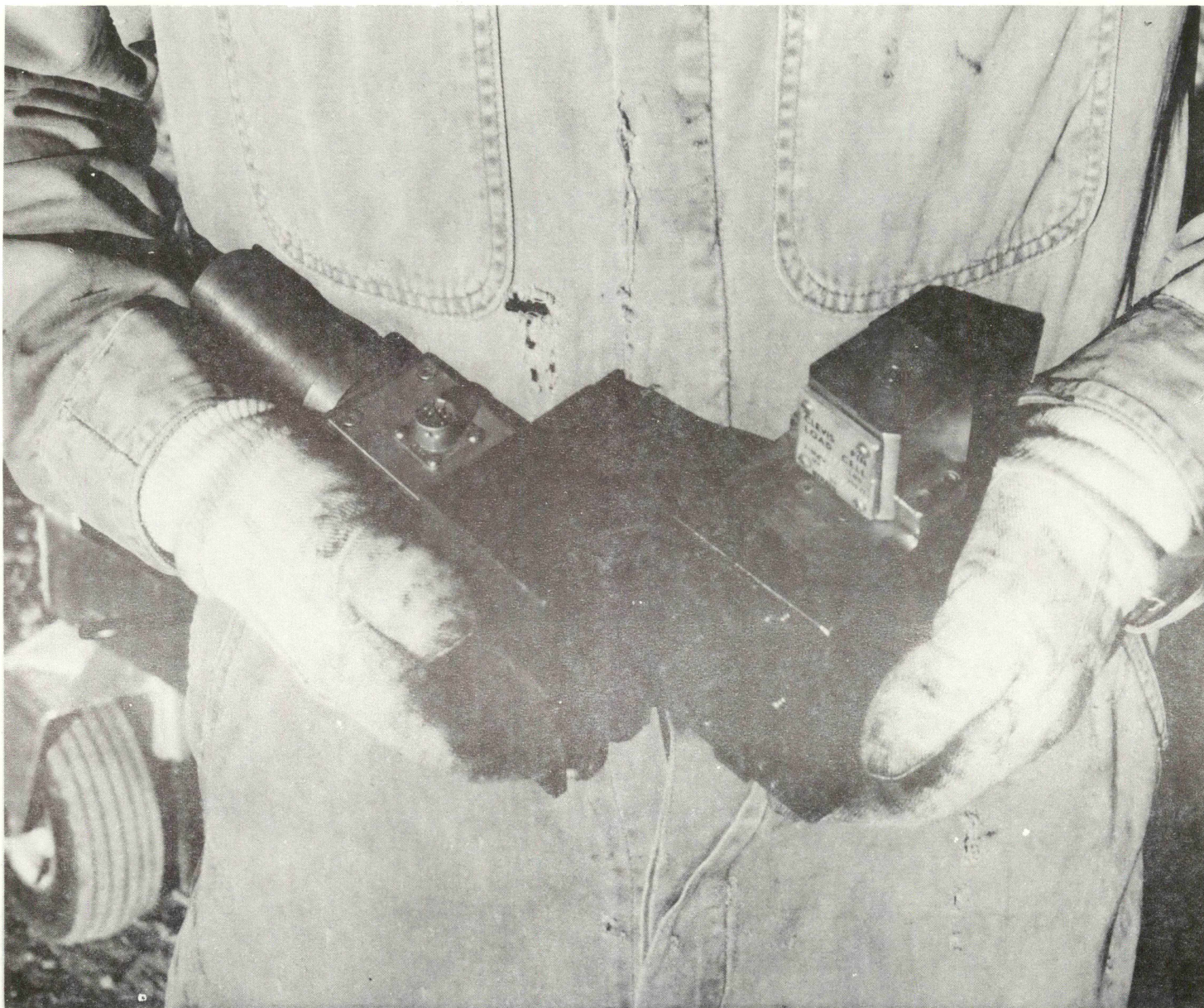


FIGURE 6-19 CALIBRATION HEAD WITH LOAD CELLS USED FOR  
FIELD CALIBRATION OF STRAIN GAGE PATTERNS

cell consists of a strain-gaged clevis pin, while the vertical load cell loads through a spherical washer, thus reducing bending and orthogonal loads.

The calibration procedure, after spotting the accessible structure of car or locomotive over the site, was to center the calibration head on the vertical/lateral measurement zone. The vertical load was then increased to its maximum value (about 24,000 lb) and plotted by one pen of the dual-pen X-Y plotter. This is shown by the plot marked "vertical load circuit" in Figure 6-20. Next, the lateral load was cycled to its maximum value (about 12,000 lb) and back to zero with the vertical load held at its maximum, as plotted by the second pen in Figure 6-20. The pens were then zero-shifted upward on the page, and the change in output from the lateral circuit was plotted as the vertical load was released, providing some estimate of the apparent cross talk (with the vertical load contacting about 0.3 in. toward the gage surface).<sup>\*</sup> A small stabilizing vertical force (2 to 3 kips) was then applied, and an "unloaded" lateral calibration plotted. Note that the vertical load increased from 3 kips to almost 7 kips due to rotation of the rail under lateral loading. Each "curlicue" in the X-Y plot indicates the end of one stroke on the hand pump of the hydraulic jack.

Strain gage circuit outputs were plotted as a percentage of the 100 percent shunt calibration step, which was provided by shunting two opposite arms of the bridge by pairs of precision resistors (200K ohm lateral, 301K ohm vertical). During tests the shunt calibration was recorded after each train, with calibrations and channel identification provided through a remote switching unit.

Calibration of each load cell used in the instrumented tie plates was done in the laboratory prior to the field experiments using a Baldwin-Southwark test machine. Shunt calibration levels were established for specific resistor sizes using the same cable lengths in the laboratory as in the field. A Budd Model P-350 strain indicator and a precision calibrator were used to establish equivalent strain levels for shunt calibration of the bolt hole and longitudinal strain gages. Displacement transducers were calibrated by moving the bodies of the DCDTs a known distance (using a precision scale) relative

---

<sup>\*</sup>Note that this test is not the same as plotting lateral output due to vertical loads at several lateral positions across the rail head, as was done in the laboratory.

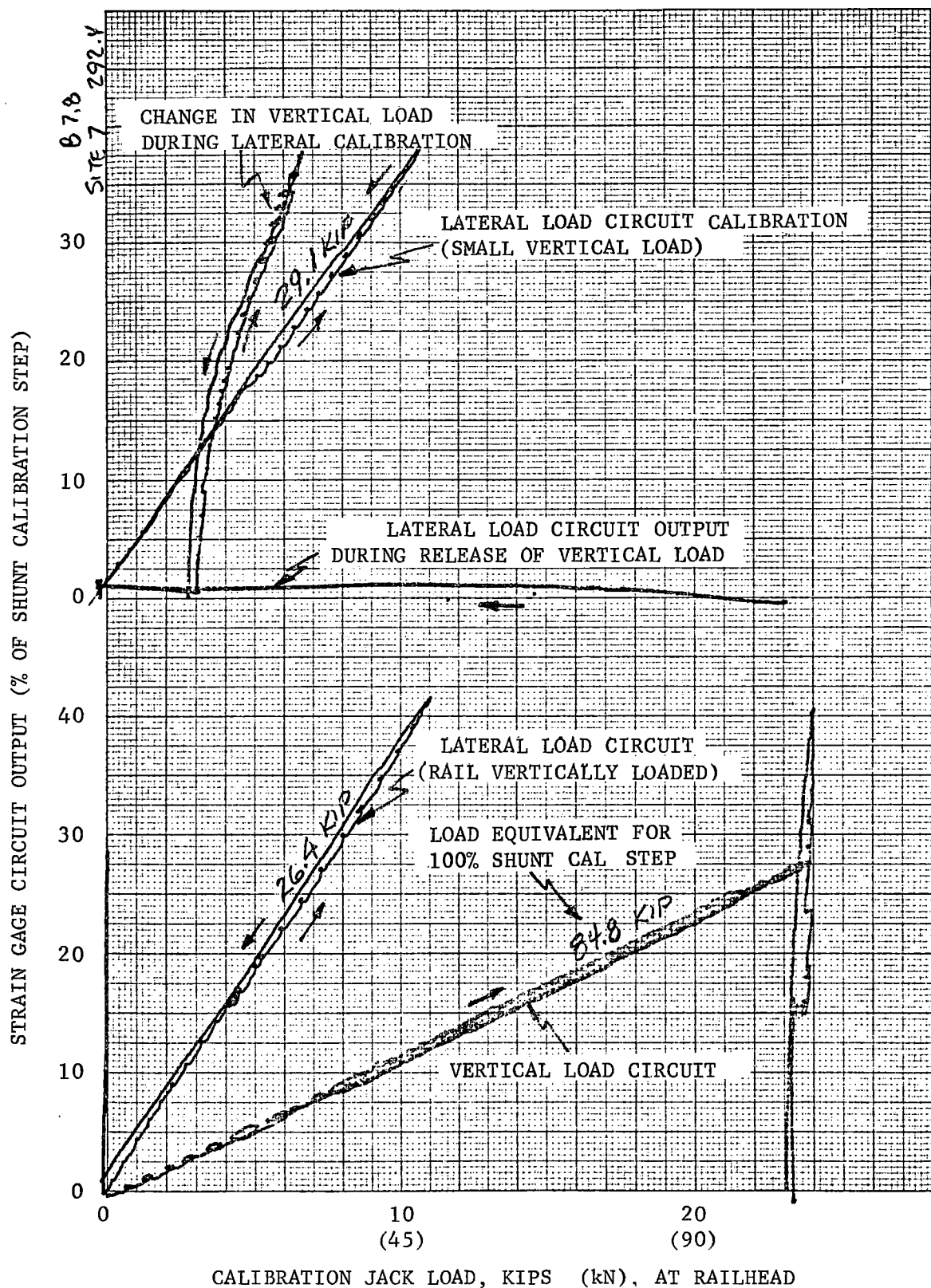


FIGURE 6-20. EXAMPLE OF X-Y PLOT OF STRAIN GAGE CIRCUIT OUTPUT VERSUS CALIBRATION LOAD INPUT (FROM LOAD CELL), WHEEL/RAIL LOAD STUDY FIELD EXPERIMENTS

to the cores, and recording the change in voltage level. Accelerometers were calibrated using a General Radio Model 1557A calibrator. For all channels, a system end-to-end calibration was performed: i.e., from transducer input to recorded output.

During the vertical load circuit calibrations, rail deflections were monitored through a transit to provide static vertical displacement under three or four levels of vertical load, up to a maximum of about 24,000 lb. A millimeter target cemented to the rail web was used during these measurements. These measurements provided estimates of track vertical stiffness and modulus.

#### 6.5.6 Wayside Test Operations

Once operational, the test facility was manned on a 24-hour basis to record all revenue traffic through the section. With approximately 14 trains a day, the facility was operated for six days to acquire sufficient data for statistical confidence in the important data subcategories.

Each revenue train recorded on magnetic tape was identified by a train ID number both on edge-track voice channel and in the log book, along with pertinent information on date, time, tape count, ambient conditions, and data quality. A typical page from the log book is shown in Figure 6-21. Train ID number was based on the day of the month of February (March 2 became "30" to avoid confusion). Oscillographic recordings were examined for data quality, particularly for problems in the wheel detector pulse trains (note, for example, the occasional wheel detector pulse inversions logged in Figure 6-21). Train speed and axle count for the train were determined from these traces.

TEST SITE SMOOTH TANGENT PAGE 23  
MILE POST 207.9 TEST SETUP \_\_\_\_\_ DATE MAR 2, 78  
TAPE RECORDER #1 REEL 7 TAPE RECORDER #2 REEL 6

---

TRAIN ID NO. 30-8 LEAD UNIT NO. 3625 DIRECTION WEST  
TIME: START RUN 1 1 TAPE #1 1527 TAPE #2 1.5  
START TRAIN 1 1  
END TRAIN 1 1  
END RUN 16116 118 1852 4.0

SPEED: IN 47 MPH TEMP: AMB 69 °F WIND: 0 MPH, DIRECTION \_\_\_\_\_  
OUT 46 MPH RAIL 82 °F RELATIVE HUMIDITY 69 %

AXLE COUNT: LOCO 28 CAT. \_\_\_\_\_, CAT. \_\_\_\_\_, 308 TOTAL 336  
COMMENTS: LOADED UNIT TRAIL 2 (MIS STATED RUN NO. ON TAPE)  
READJUSTED MUX 6 MIN STAUFFER CHEMICALS HORROR  
WD 5 CARS 6-14 INJECTED B5, 8, 11 NOISY REST OF MUX 8 CLEAN

---

TRAIN ID NO. 30-9 LEAD UNIT NO. 6905 DIRECTION WEST  
TIME: START RUN 1 1 TAPE #1 1852 TAPE #2 4.0  
START TRAIN 1 1  
END TRAIN 1 1  
END RUN 17109 111 2053 5.5

SPEED: IN 63 MPH TEMP: AMB 68 °F WIND: 0 MPH, DIRECTION \_\_\_\_\_  
OUT 62 MPH RAIL 78 °F RELATIVE HUMIDITY 73 %

AXLE COUNT: LOCO 22 CAT. \_\_\_\_\_, CAT. \_\_\_\_\_, 204 TOTAL 226  
COMMENTS: LOADED VAN  
WD 1, 7 → CAR 20 (2/3 INJURY)

---

TRAIN ID NO. 30-10 LEAD UNIT NO. 6916 DIRECTION WEST  
TIME: START RUN 1 1 TAPE #1 2053 TAPE #2 5.5  
START TRAIN 1 1  
END TRAIN 1 1  
END RUN 19109 148 2256 7.2

SPEED: IN 65 MPH TEMP: AMB 62 °F WIND: 3-10 MPH, DIRECTION W  
OUT 61 MPH RAIL 62 °F RELATIVE HUMIDITY 70 %

AXLE COUNT: LOCO 20 CAT. \_\_\_\_\_, CAT. \_\_\_\_\_, 188 TOTAL 208  
COMMENTS: WD 1 → CARS 2, 7, 22, 33, 46 INJECTED 2/3

FIGURE 6-21. TYPICAL PAGE FROM FIELD DATA LOG BOOK

## 6.6 WAYSIDE DATA ANALYSIS TECHNIQUES AND FORMATS

Analysis of the wheel/rail loads and associated data from wayside instrumentation was conducted by three different techniques: an examination of time-domain (oscillographic chart) data, a frequency analysis by Fast Fourier Transform (FFT) techniques, and a statistical analysis of peak loads from each passing wheel. Each technique and associated data formats are described below.

### 6.6.1 Time-Domain Data Analysis

Wheel loads measured by the short zone strain gage patterns on the rail are essentially samples of the passing continuous load from each wheel. From laboratory tests, the "influence zones" of these gage patterns have been charted:

<u>Distance Along Rail From Crib Center</u>	<u>Ratio of Measured to Actual Load</u>	
	<u>Vertical</u>	<u>Lateral</u>
0 inch (center)	1.00	1.00
<u>+1</u>	0.98	0.98
<u>+2</u>	0.92	0.94
<u>+3</u>	0.84	0.88
<u>+4</u>	0.66	0.82
<u>+5</u> (edge of chevron)	0.41	0.73

It can be seen that the lateral (base chevron) gage pattern has a much wider influence zone and will produce a signal due to lateral wheel loads well beyond the instrumented crib area. This is illustrated in Figure 6-22, which compares vertical and lateral load traces from one of the measurement sites under the wheels of several freight cars. Since only the maximum value of the sample is of real interest, the width of the influence zone is of no consequence, as long as it is significantly shorter than the axle spacing of trucks. However, because of the short duration of the vertical pulse (on the order of 10 milliseconds for high-speed freight trains), a recording bandwidth greater than 100 Hz is necessary. For the wheel load data, a minimum

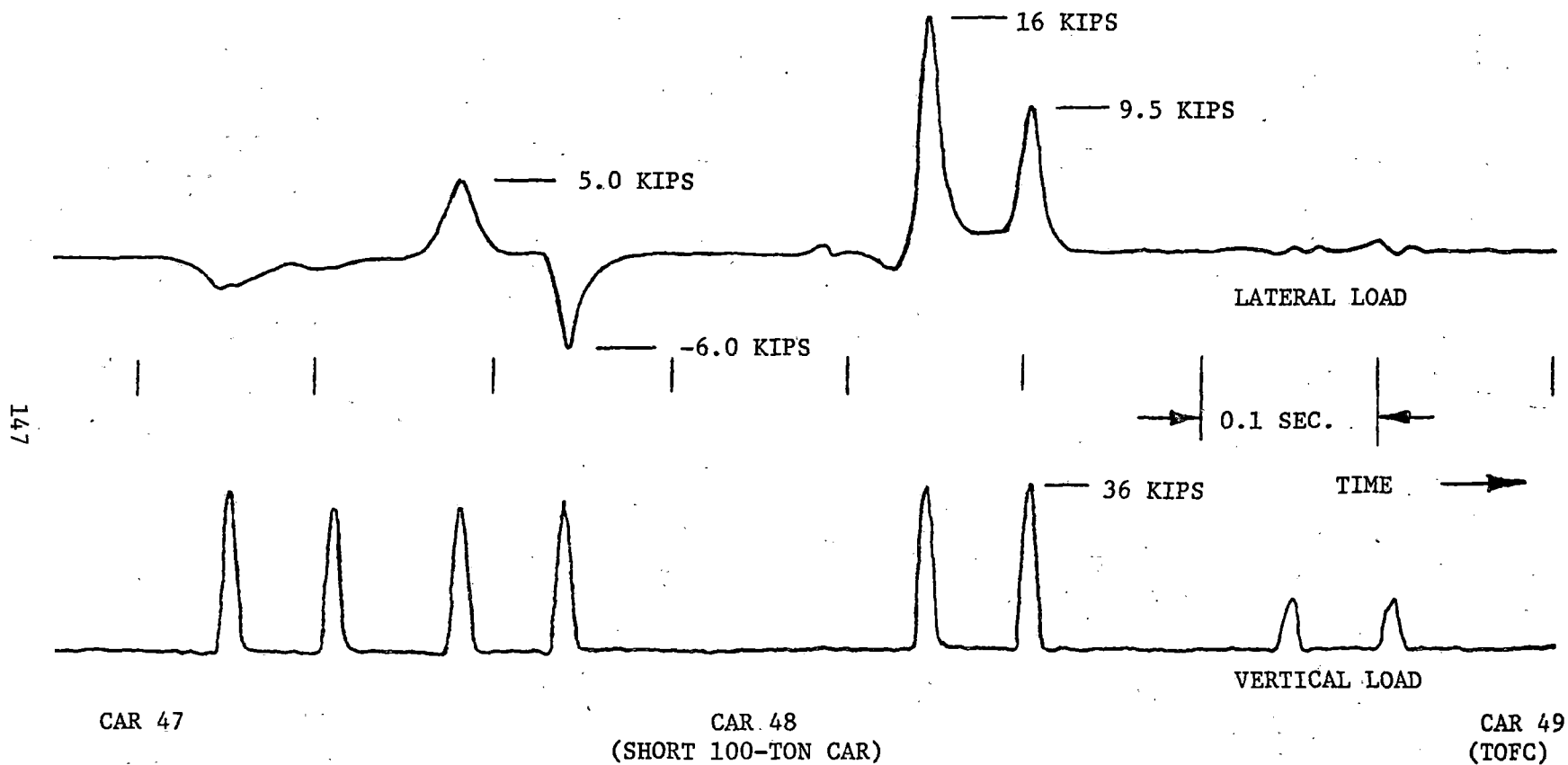


FIGURE 6-22. EXAMPLE OF LATERAL AND VERTICAL WHEEL/RAIL LOADS GENERATED AT SHORT MEASUREMENT SITE (SITE 5), SMOOTH TANGENT TRACK (CWR), WESTBOUND FREIGHT TRAIN AT 67 MPH

FM tape recording bandwidth of 2500 Hz was used; and a 4-pole Bessel filter set at 300 Hz was used for the oscillograph recordings.

Because of the longer influence zones, time history traces from the "continuous" vertical load zones and the instrumented tie plates were found to provide a more graphic description of the passing wheel loads. For example, Figure 6-23 shows the rail joint impact loads developed under the lead axles of the test train locomotive during a high-speed run. The decreasing load at the joint gap and the "P2" impact load on the running-on rail and tie plate are clearly visible. Tie plate loads display the typically long influence zone associated with the rail as a beam on an elastic foundation.

In addition to wheel loads and tie plate loads, rail strain, deflection and acceleration data were analyzed by means of the oscillographic traces run at chart speeds up to 40 inches per second and bandwidths to 2000 Hz.

#### 6.6.2 Frequency-Domain Data Analysis

A Hewlett-Packard 5420A digital signal analyzer was used to generate frequency analyses of wheel loads, and track and ground accelerations for the frequency analysis of data. Wayside data are recurrent transient events, rather than continuous signals, so that a number of these events must be averaged to bring out spectral peaks. Spectra from the analyzer were plotted on 10 x 15 inch graph paper using an X-Y plotter. An example of a typical frequency-domain format is given in Figure 6-24, in which the power spectrum of rail acceleration under the locomotive units (6-axle SD-40 locomotives) is shown for bolted-joint track.

#### 6.6.3 Statistical Data Analysis

The instrumentation used in the wheel/rail load experiments included pairs of wheel detectors at each measurement site to generate a logic pulse when any wheel was within the "window" between the detectors. These logic pulses were used to control analog peak detector pairs for each of the vertical and lateral load circuits. The trailing edge of the wheel pulse

RUN 17M (300HZ FILTER)

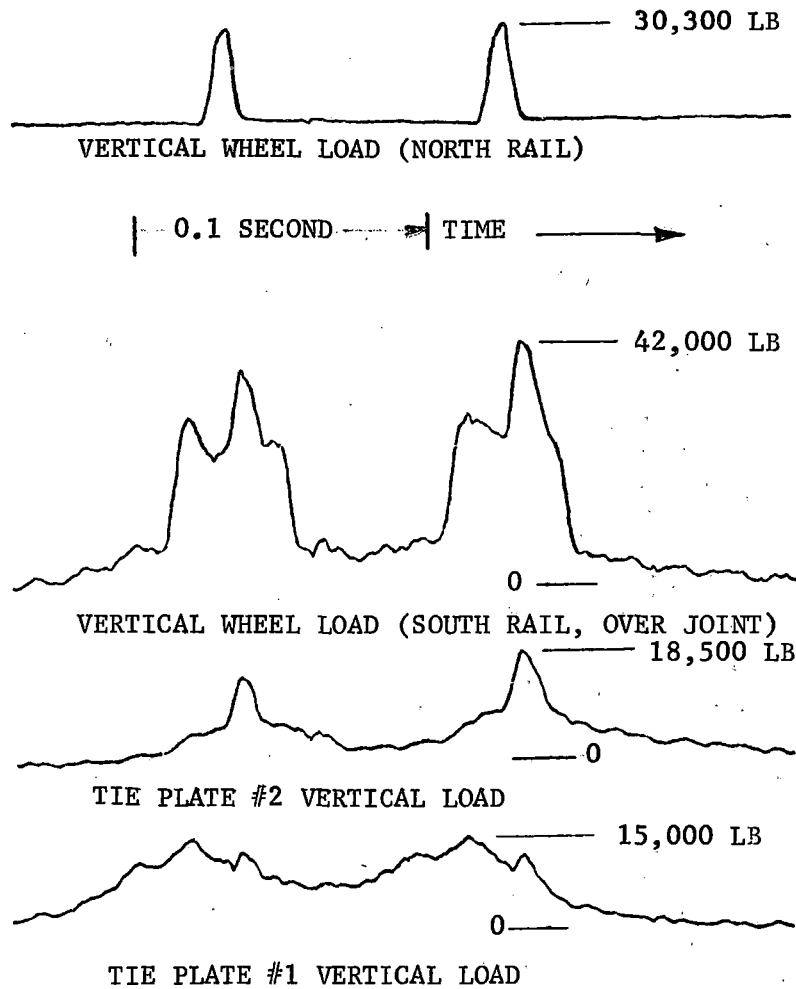


FIGURE 6-23. VERTICAL WHEEL/RAIL LOADS UNDER LEAD TRUCK OF TEST TRAIN LOCOMOTIVE (GP-30), EASTBOUND AT 65 MPH, TEST SECTION 1 (BJR TRACK), SITE 3

RUN 23-1

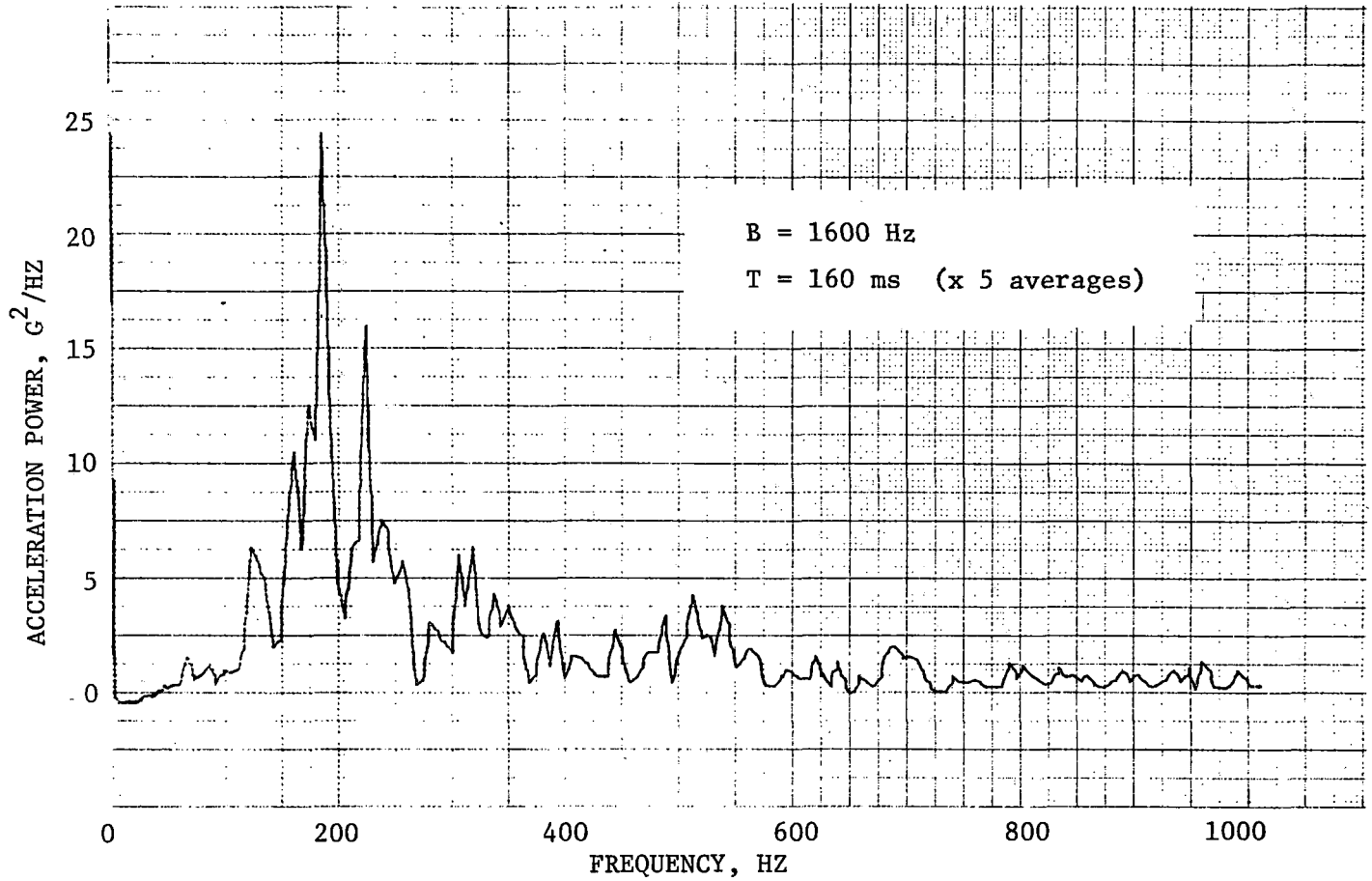


FIGURE 6-24. POWER SPECTRUM OF RAIL ACCELERATION UNDER LOCOMOTIVE UNITS, 60 MPH, BOLTED-JOINT RAIL AT MIDSPAN

generated a control pulse to a microprocessor to attach and store digital values (through an a/d converter) of the peak lateral and vertical load voltages, then reset the peak detectors. Since the lateral load can have either positive (toward flanging) or negative maxima, the lateral signal was split, one path through an absolute value circuit to the peak detector, and the other path through a sample/hold amplifier controlled by the peak detector status line. This provided a signed value for the microprocessor. A block diagram of this analog-to-digital conversion stage is shown in Figure 6-25.

Further steps in the processing of data are shown in the block diagram of Figure 6-26. The second step in the data processing procedure, Program KEYPUT, converted digital voltages into physical units (pounds) from calibration factors, calculated either an L/V ratio or the difference between unfiltered and filtered vertical "continuous" load, and assigned an identifying key number to each set of three values (L, V, and L/V) describing test section, measurement site, vehicle type, speed band, and data type.

The final step in the data processing was to perform the statistical calculations needed to obtain mean values, standard deviations, probability densities and probability distributions for the peak value data from each subcategory (key number). Statistical calculations were made by dividing the total expected data range into 200 equal intervals ("bins") and summing the number of peak values (axles) falling into each interval. These data were stored on a disk file according to the subcategory identification (key) number. Graphs of frequency-of-occurrence histograms and percent exceedance were then plotted on an interactive graphics terminal using the identification numbers for single subcategories or combinations of categories. An option to increase the interval size and reduce the number of intervals for plotting is included in the program. Fifty intervals were used for all the plots in this study.

The format for statistical analysis results shown in Figure 6-27 has typical plots of the exceedance distribution function (left-hand graph) and the frequency-of-occurrence histogram (right-hand graph) for a measurement of peak vertical wheel/rail loads. These data are the peak loads on one rail

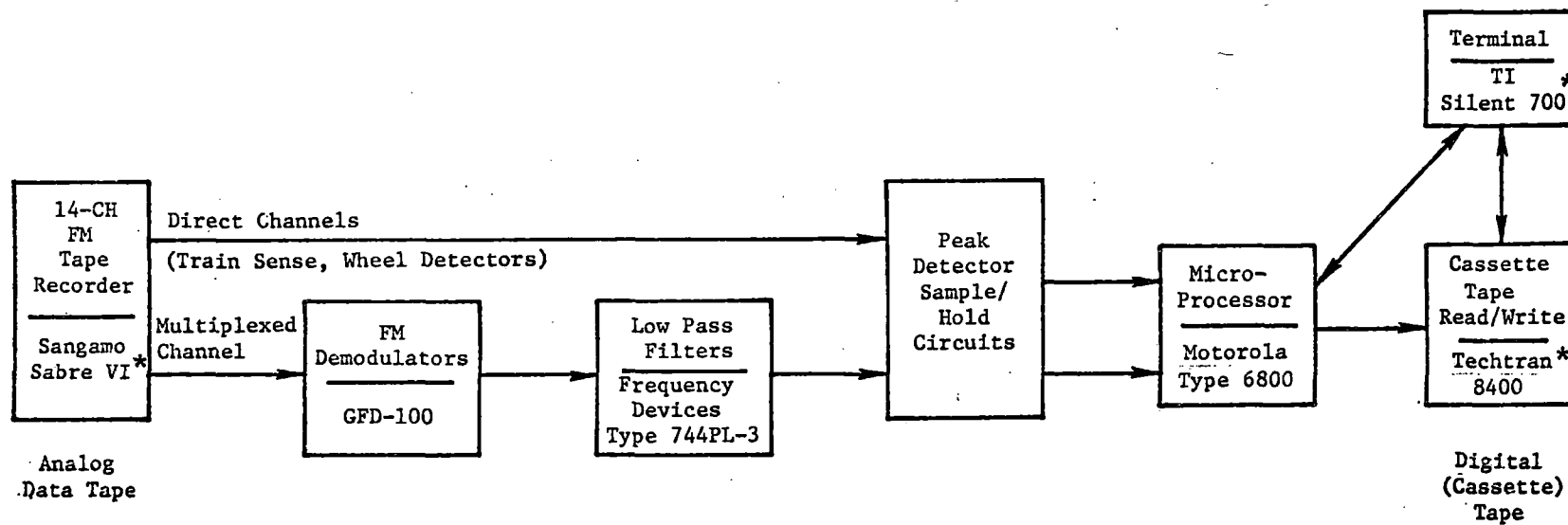


FIGURE 6-25. ANALOG/DIGITAL DATA CONVERSION SYSTEM

\* Registered Trademark

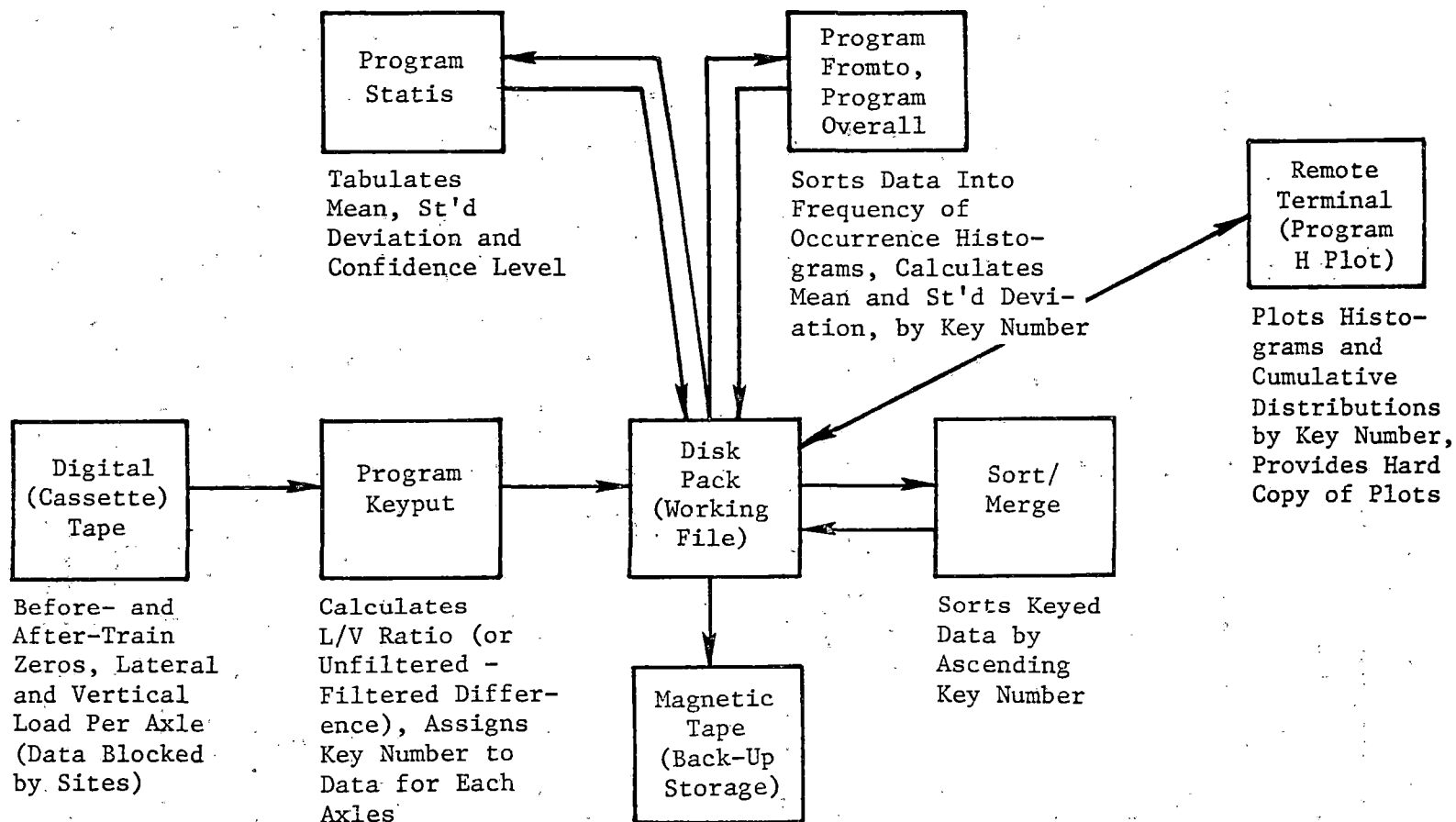
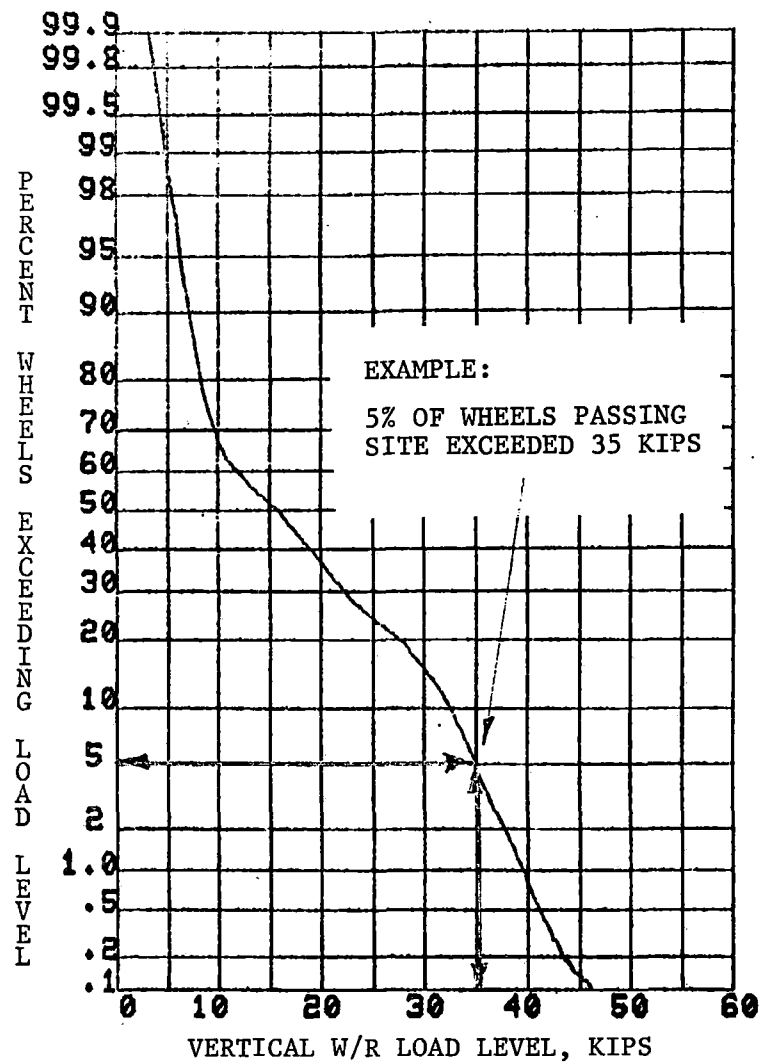


FIGURE 6-26. DATA PROCESSING ON CDC 6500 DIGITAL COMPUTER SYSTEM



113652 ← KEY NUMBER

- CHANNEL (2=VERTICAL LOAD)
- SPEED BAND (5=ALL SPEEDS)
- VEHICLE (6=ALL CARS & LOCOMOTIVES)
- MEASUREMENT SITE
- TEST SECTION (1=TANGENT BJR TRACK)
- EXPERIMENT

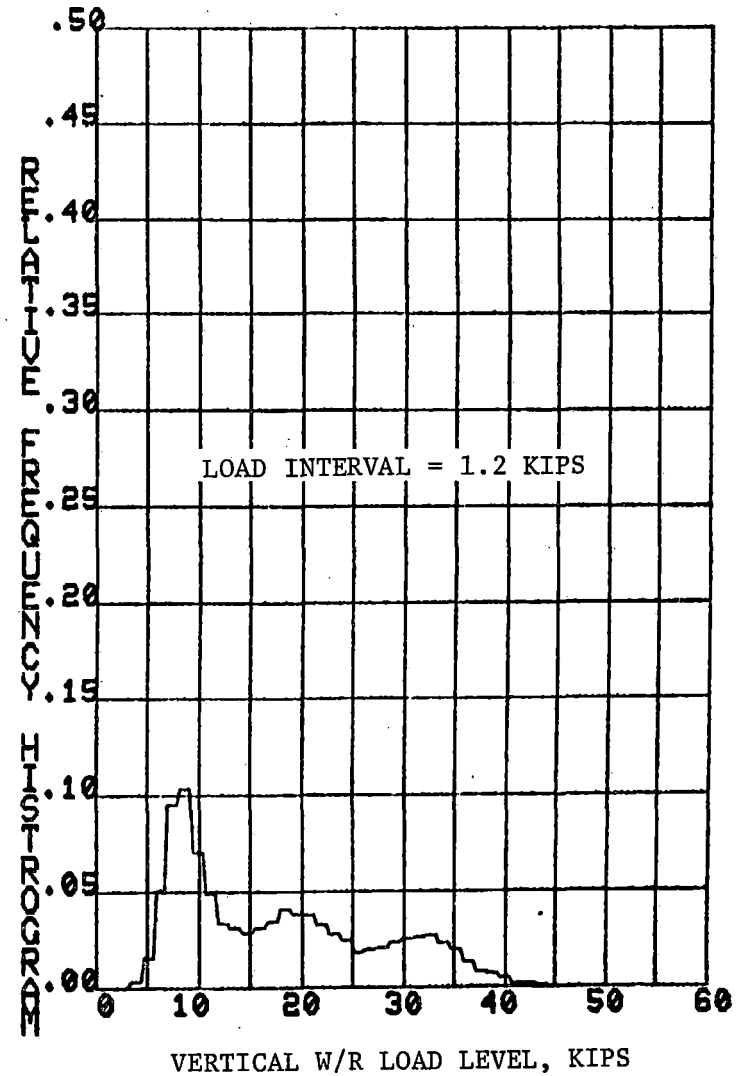


FIGURE 6-27. EXAMPLE OF W/R LOAD STATISTICAL CURVES

for all cars and all speeds (all traffic) at one measurement location. The frequency-of-occurrence histogram shows the ratio of the number of peak loads within each of the 50, 1.2-kip load intervals which cover the total range of 60 kips. It is important to note that the quantitative results for the histogram depend on the selected load interval  $W_N$ , and are therefore not unique. Increasing the load interval (reducing the number of intervals) will increase the number of occurrences at a particular load level. This improves the averaging used for the estimate but reduces the resolution--a tradeoff decision. Load intervals which are too small for the data base cause irregularities in the density curve at extreme loads because of an insufficient number of data points to provide a reliable average for these low probability events.

The exceedance distribution function shown in Figure 6-27 gives the percentage of wheels for which peak loads exceed a specified load level. This is calculated from the integral of the frequency of occurrence function, and therefore the quantitative results are unique and do not depend on the load interval used to generate the histogram. The vertical axis for the exceedance distribution function is expanded to provide greater resolution of the extreme values. Insufficient data points to provide a reliable estimate for low probability events appear in the distribution function as horizontal segments which show there were no data points at that load level. The accuracy of the low probability estimates at these points is questionable.

Statistical data having a normal (Gaussian) distribution will appear as the familiar bell-shaped curve on the frequency of occurrence histogram and as a straight line on the scale used for the probability of exceedance plot. Three distinct straight-line segments in the exceedance curve and three peaks in the histogram of Figure 6-27 indicate that vertical wheel/rail load data consist of a mixture of at least three nominally-Gaussian populations: empty cars (about 8 kips wheel load), medium-weight cars (about 18 kips wheel load), and heavy cars and locomotives (about 33 kips wheel load).

## 6.7 INSTRUMENTED VEHICLE DESCRIPTION

A 100-ton-capacity open-top hopper car (Union Pacific Class H-90-4) was chosen for these tests because it represents a substantial portion of the vehicle population in North American railroad traffic. It produces high static vertical wheel loads, and (under certain conditions) can develop high dynamic vertical and lateral wheel/rail loads.

Characteristics of the specific car used in these tests are listed in Table 6-8. Crushed rock was used as a cargo, but was inadvertently loaded asymmetrically so that the instrumented truck was under roughly 10 tons less than full design load. The calculated center of mass of the cargo was therefore shifted 28 inches toward the non-instrumented truck. Barber S-2 freight trucks with centerplate extension pads (CPEP), 6.5 x 12 inch journals, and 36-inch diameter wheels were provided with the car. Wheelsets prepared in the laboratory by IITRI were substituted in place of the original wheelsets on the instrumented truck. Brake shoes were disabled on this truck to avoid excessive thermal inputs.

## 6.8 VEHICLE-BORNE MEASUREMENTS

### 6.8.1 Instrumentation

Two different measurement systems, designated the low frequency and high frequency systems, were used to measure forces at the wheel/rail interface. The low frequency load measurement system was used to determine the lateral and vertical forces at the wheel/rail interfaces for each of the four wheels of the truck. This system's use is based on the assumption that the wheel/axle set can be considered as a rigid free body on which there are acting five unknown load components; the lateral and vertical forces at each of the wheel/rail interfaces and the lateral force from the truck frame acting along the centerline of the axle. Two additional load components are the vertical loads at the two journal bearings which were determined by using instrumented side frames. The high-frequency system utilized strain gages mounted on a wheel plate of one wheel of the truck.

TABLE 6-8. DESCRIPTION OF INSTRUMENTED 100-TON HOPPER CAR

Parameter	Value	Units
Truck unsprung component weights		
Wheels, axles, journals, adapters	6,300	lb
Side frames	2,100	
Springs (1/2 each)	200	
Brakes	700	
Total per truck	9,300	lb
Truck sprung component weights		
Bolster	1,500	lb
Springs (1/2 each)	200	
Total per truck	1,700	lb
Hopper car structural weight	44,000	lb
Cargo weight (crushed stone)	161,500	lb
Total weight, loaded car	227,500	lb
Average wheel load - instrumented truck	25,800	lb
non-instrumented truck	31,075	lb
Mass center (c.g.) heights above rail		
Truck unsprung components	18	in.
Truck sprung components	18	in.
Car body structure	64.5	in.
Cargo	82	in.
Truck center distance	434	in.
Truck wheelbase	70	in.
Car overall length	540	in.
Vertical spring rate per truck (3-11/16")	49,940	lb/in.
Nominal friction shoe load - instrumented truck	5,180	lb
(4 per truck) - non-instrumented	6,240	lb

The plan for the vehicle-borne instrumentation system was based on the following constraints:

- use of three analog recorders, 14 channels each
- use of two available wheel/axle sets with 40 slip ring positions each (20 each journal)
- grouping the channels of related information on a single recorder to simplify subsequent digitization and data processing.

Strain measurements were taken using conventional compensated welded strain gages (Micromeasurements LWK-06-W250B-350). The instrumentation channels are listed in Table 6-9. The locations of the gages are indicated in Figure 6-28.

6.8.1.1 Side Frame Vertical Load Gages. Four strain gages were used on each side frame, one on each of the two tension members as illustrated in Figure 6-29. These gages were wired into a four-active-arm bridge. The output of these bridges as a function of load was determined by calibration loads applied to the truck.

6.8.1.2 Axle Bending Moment Gages. The positions of the bending moment bridges are shown in Figure 6-30. The strain gage bridges consisted of two active gages mounted at diametrically opposite positions on the axle and two dummy gages to complete the bridge. Each pair of active gages provided a measurement of the bending moment twice per revolution when the plane of the gages was oriented in the vertical direction. Two bridges were used at each position oriented at 90 degree intervals around the axle.

6.8.1.3 Wheel Plate Strain Gage Bridges (Vertical Load). Vertical loads were determined by a series of equally spaced, radially oriented strain gage bridges mounted on the wheel plate. Each of the four-active-arm bridges utilized gages applied on radii 180 degrees apart on both the inside and outside wheel plate. The gage locations were chosen so that the output of the bridge was independent of the lateral position of the point of vertical load application on the tread and so that the output of the bridge was insensitive

TABLE 6-9. INSTRUMENTATION DATA CHANNELS

Gage Channel	Type of Transducer	Measured Parameter	Location
1	Strain Gage Bridge (four active arms)	Vertical Load	Left Side Frame
2			Right Side Frame
3	Strain Gage Bridge (two active arms)	Axle Bending Moment	First Axle 0°
4			Left Side 90°
5	Strain Gage Bridge (two active arms)	Axle Bending Moment	First Axle 0°
6			Right Side 90°
7	Switch	Wheel Rotational Position	First Axle
8	Strain Gage Bridge (two active arms)	Axle Bending Moment	Second Axle 0°
9			Left Side 90°
10	Strain Gage Bridge (two active arms)	Axle Bending Moment	Second Axle 0°
11			Left Side 90°
12	Switch	Wheel Rotational Position	First Axle
13 thru 20	Wheel Plate Strain Gage Bridge (four active arms)	Vertical Load	First Axle, Left Side. Bridges at 22.5° Spacing
21 thru 24	Wheel Plate Strain Gage Bridge (four active arms)	Lateral Load	First Axle, Left Side. Bridges at 45° Spacing
25 thru 26	Wheel Plate Strain Gage Bridge (two active arms)	Position of Vertical Load	First Axle, Left Side
27 thru 28	Accelerometer	Vertical Acceleration	Center Sill near B end. Center sill near A End
29 thru 30	Accelerometer	Vertical Acceleration--two gage outputs combined one gage each side at B end body bolster	Gage Outputs Summed, each side Gage outputs difference, each side
31	Event Marker (Correlation Switch)	Passage of Fixed Site, etc.	--
32	Time Code	--	--

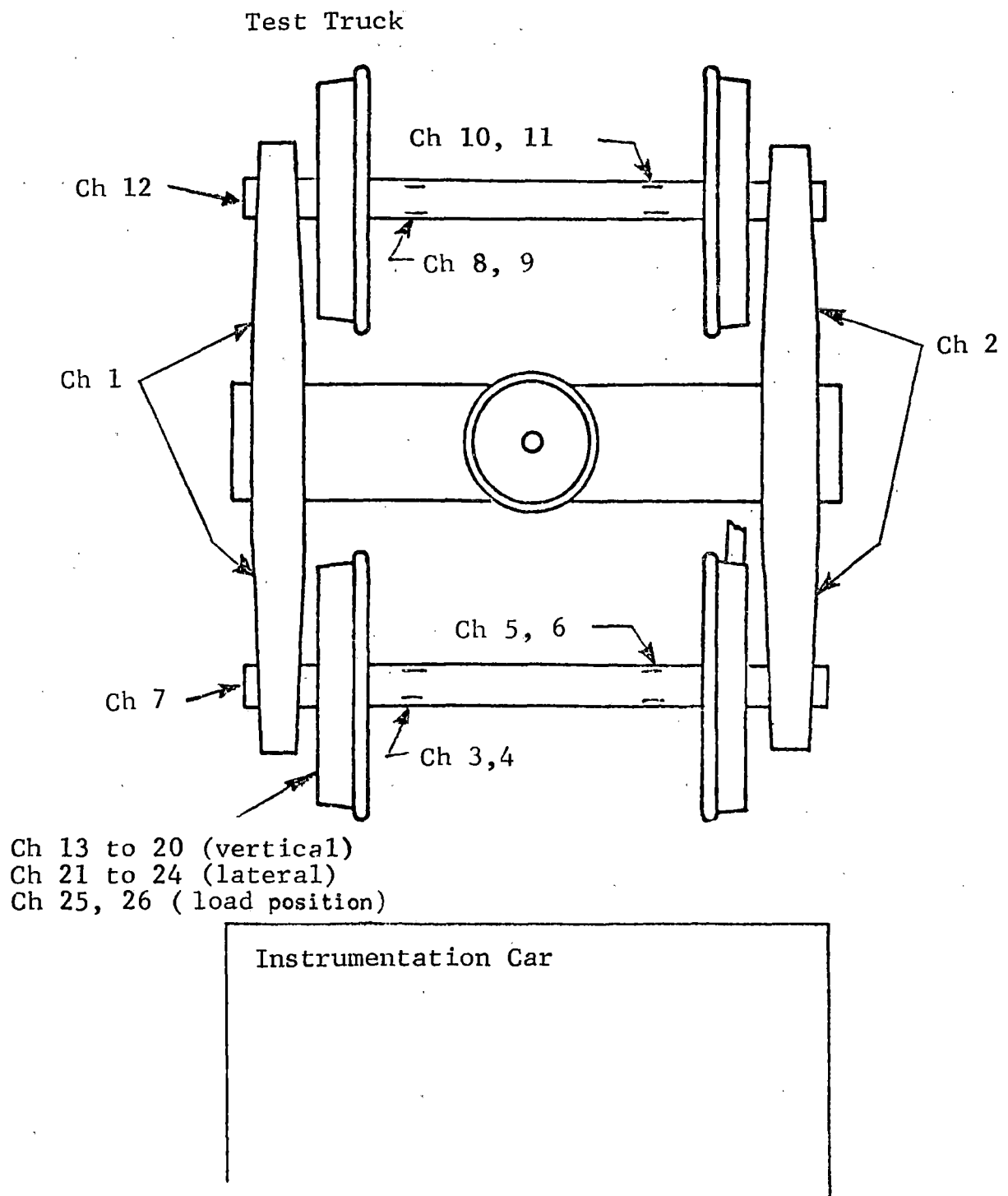


FIGURE 6-28. TRANSDUCER PLACEMENT ON TEST TRUCK

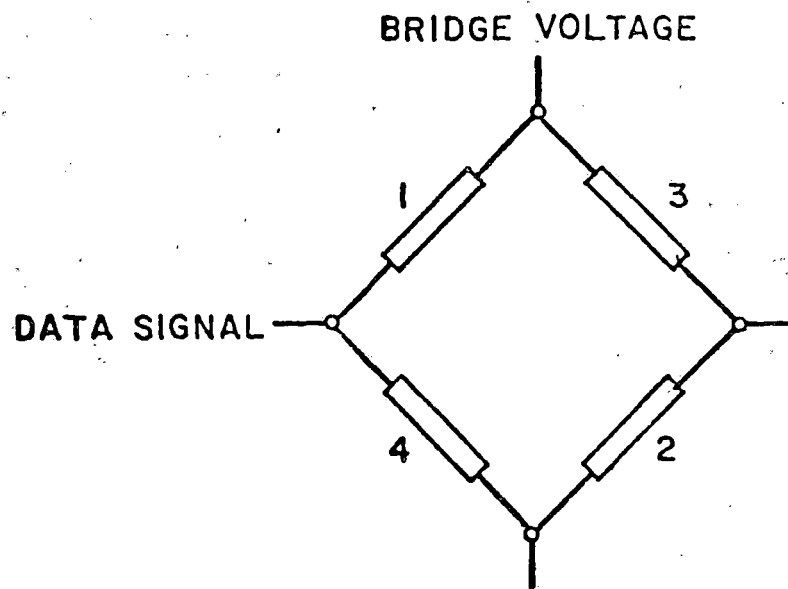
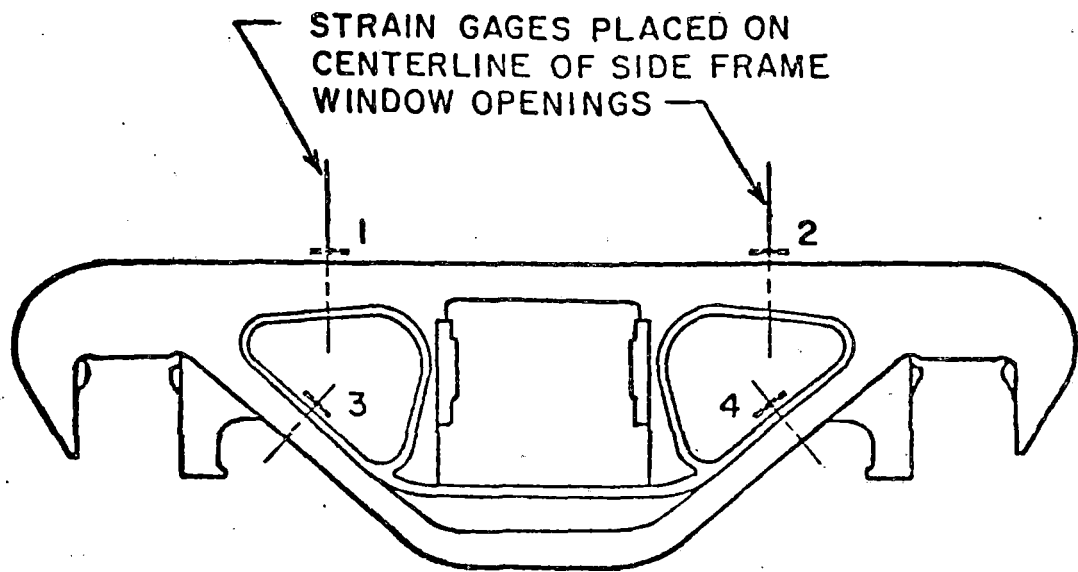


FIGURE 6-29. TRUCK SIDE FRAMES STRAIN-GAGED FOR VERTICAL  
LOAD MEASUREMENTS (LOW-FREQUENCY SYSTEM)

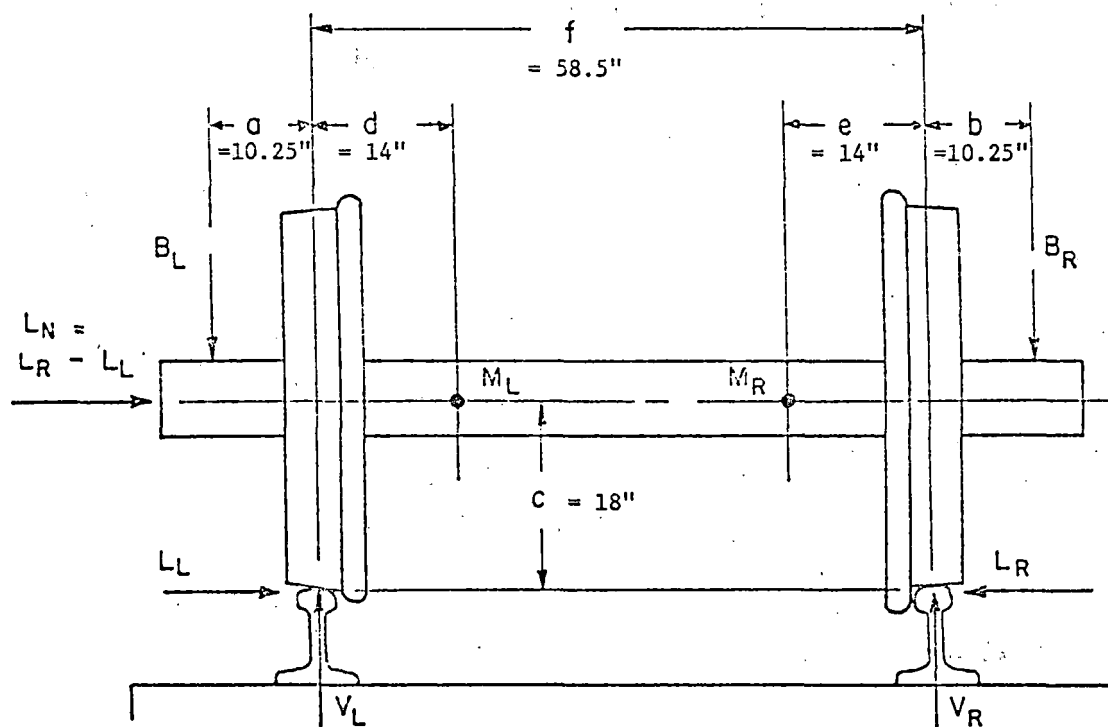


FIGURE 6-30. DIAGRAM OF INSTRUMENTED WHEEL/AXLE SET SHOWING POSITIONS OF AXLE BENDING MOMENT BRIDGES  $M_L$  AND  $M_R$

to lateral load. This required attenuating the output of the gages on the inside plate (C and D) by a factor of 0.70. The gage placement and bridge connections are indicated in Figure 6-31. Eight strain gage bridges spaced at 22.5 degrees were used.

6.8.1.4 Wheel Plate Strain Gage Bridges (Lateral Load). Lateral loads were determined by a series of equally spaced, radially oriented strain gage bridges mounted on the inside wheel plate. These gages were located on the inside plate surface, applied at equal radii 180 degrees apart, and wired into four-active arm bridges as shown in Figure 6-32. Gages E and E' and F and F' were at the same nominal position on the wheel to increase sensitivity of the bridge. This bridge is sensitive to cross talk caused by transverse movement of the line of action of the vertical load. The output of the bridge was modified during data processing to compensate for this effect by making use of a bridge which is indicative of the position of the vertical load (see below). Four radially oriented strain gage bridges spaced at 45 degrees were used.

6.8.1.5 Wheel Plate Strain Gage Bridges (Vertical Load Position). The interaction of the vertical load position with the lateral load bridge output can be corrected in the data processing by determining the position of the load and using this information to provide a suitable correction factor for the lateral bridge output. A suitable bridge for determining the load position was installed as indicated in Figure 6-31, but consisting only of the gages on the inside plate, C, D, (A and B would be dummy gages). The output of this bridge is sensitive to vertical load position and proportional to total vertical load. Since the vertical load is established independently, it can be used to correct the reading of this bridge and the resultant output used to determine the vertical load position. This in turn is used to correct the lateral load output.

6.8.1.6 Wheel Position Indicators. Wheel position signals were obtained for each axle using a specially-cut toothed wheel attached to the axle in conjunction with a proximity sensor.

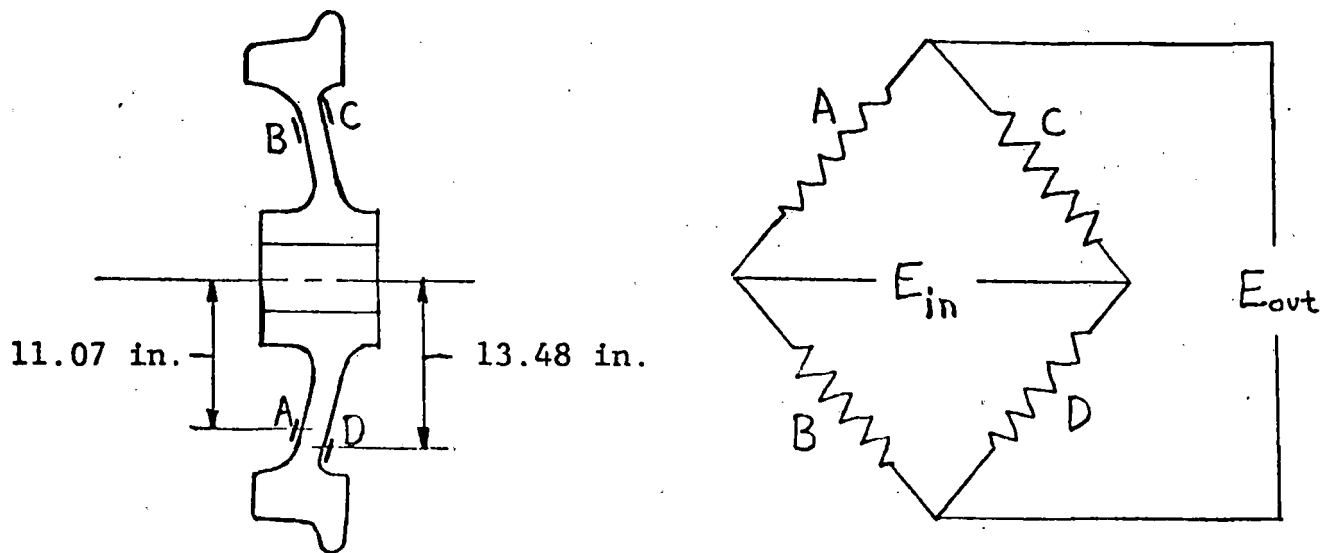


FIGURE 6-31. VERTICAL LOAD MEASUREMENT STRAIN-GAGE BRIDGE

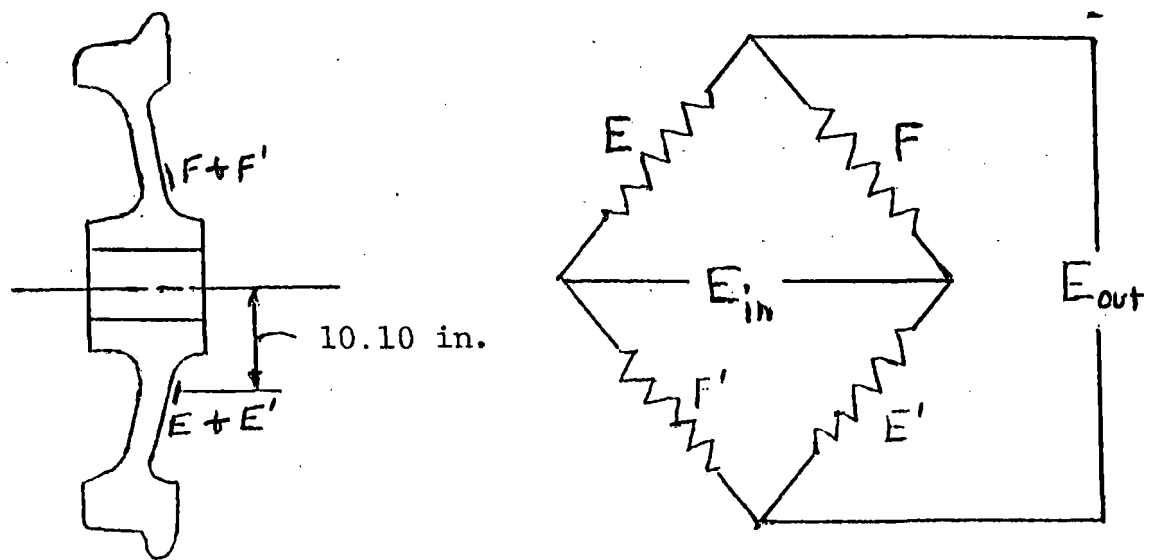


FIGURE 6-32. LATERAL LOAD MEASUREMENT STRAIN-GAGE BRIDGE

6.8.1.7 Accelerometers. Two accelerometers were mounted on the center sill, one at either end of the car oriented in the transverse direction of the horizontal plane. The data from these gages were recorded on separate channels and were used to determine yaw and lateral motions of the car.

Two vertically oriented accelerometers were installed over the test truck, one on each side of the car to establish roll motions, or at either end of the car to establish bounce and pitch motions. The accelerometer outputs were summed to describe bounce motions and the difference of the outputs was used to describe roll or pitch motions of the car.

6.8.1.8 Event Marker, Correlation Switch. One channel was used to record a precise reference of the passage of the wayside load measurement site. This was done with an inductive pickup of magnetic wheel detectors installed adjacent to the rail.

6.8.1.9 Time Code. A precise time reference was established with an IRIG B time code generator and recorded on each data tape.

6.8.1.10 Signal Conditioning. The strain gage circuits for the gages applied to the axles and wheels utilized amplifiers mounted directly on the axle to provide a significant increase in the signal-to-noise ratio. The principal source of noise was the slip rings. The amplifiers brought the signal level to the order of + 5 volts for expected strains. The amplifier chosen for this purpose was the Analog Devices AD520J.

Slip rings were used to transmit the data signals from the wheels and axles. Each wheel set had two 20-circuit slip ring assemblies. The axles contain central axial holes and radial ports so that power and signal leads could be routed from the sensors to the slip rings. The slip rings were fitted with electrical connectors so that they could be disconnected for shipping and maintenance.

### 6.8.2 Data Acquisition System

Three 14 channel frequency modulation (FM) analog recorders were used to record the data. The first and second recorders used the IRIG intermediate band FM system with a tape speed of 7.5 ips and a bandwidth of 2500 Hz. The third recorder was operated at a 1.875 ips tape speed and a bandwidth of 625 Hz. The recorders and associated signal conditioning equipment were housed in the UP instrumentation car which was run as part of the test train consist.

The recorder gage channel assignments resulted in the following instrumentation array:

#### Recorder 1

- 4 vertical bridges, first axle, left wheel
- 4 lateral bridges, first axle, left wheel (on same diametral lines as above)
- 2 lateral wheel position bridges, first axle, left wheel
- 1 time code
- 1 wheel rotation angle
- 1 correlation switch (with wayside data system)

13

#### Recorder 2

- 8 vertical bridges, first axle, left wheel (includes 4 vertical bridges listed on recorder 1 above)
- 4 accelerometers on car body (one channel multiplexed)
- 2 side frame vertical force, one each right and left sides (multiplexed channels)
- 1 time code
- 1 wheel rotation angle

16 (13 channels on the recorder)

#### Recorder 3

- 2 side frame vertical force, one each right and left sides
- 4 axle mounted bending moment bridges, 2 each right and left side, leading axle
- 4 axle mounted bending moment bridges, 2 each right and left side, trailing axle
- 1 time code
- 2 wheel rotation angle, one each axle
- 1 correlation switch (with wayside data system)

14

The data channels on the first recorder were grouped to obtain high frequency vertical, lateral and L/V information. The data channels on the second recorder were grouped to develop high frequency vertical load parameters. Car body motions were described by the four accelerometer channels. The two side frame channels provided low frequency vertical load data. The data channels on the third recorder were grouped to develop low frequency vertical and lateral load data.

### 6.8.3 Installation and Calibration

Pretest calibrations were conducted to determine the response of the transducers to lateral and vertical load. Lateral and vertical loads were applied to the wheel with the high frequency load measurement transducers and on both wheel/axle sets to calibrate the axle-mounted strain gages. This work was done at IITRI prior to the shipment of the equipment to the field. Calibration reference signals were generated by shunting strain gages with precise known values of resistance which were related to specific loads.

The vertical load calibration of the side frames was conducted in the field at the time the tests were performed. First, the test car, equipped with the test truck, was weighed (loaded) to establish a reference signal level. The car was then jacked free of the truck and the change in the signal level of the side frame bridge noted.

A dynamic calibration was attempted in the field to determine the natural frequencies of vibration of the instrumented truck and car. An inclined shim was placed on the rail and the car rolled over the shims at approximately 5 mph. The test was unsuccessful because a shim of sufficient height to excite a vibrating response would not stay on the rail, but rather was kicked out of the way by the advancing wheel. Subsequent frequency analysis of the wheel plate-mounted vertical load bridges while operating over jointed rail, where there was considerable joint impact excitation of the system, has revealed a local peak at 190 Hz, which is probably the fundamental mode of the side frame, and a local peak at 570 Hz, which is probably the fundamental frequency of the wheel.

## 6.9 VEHICLE-BORNE DATA ANALYSIS TECHNIQUES AND DATA FORMATS

The techniques used to analyze the load data are described as follows.

### 6.9.1 Vertical Load at Rail Joints

The data channels for the eight vertical load bridges of the instrumented wheel, which were recorded on the second recorder, were digitized at 1,000 samples per second. A computer program was then developed to scale the data from each bridge and determine the maximum load recorded as it passed through its zone of greatest sensitivity twice per wheel revolution. This permitted the construction of a function giving the vertical load 16 times per wheel revolution (one sample every 7.07 inches). Plots of this load data versus time showed the transient loads associated with passage over each rail joint.

The data for the highest indicated rail joint loads and other selected joint loads of specific interest (e.g., the BCL instrumented rail joint) were processed further to obtain a one-millisecond resolution time history of the load during traversal of the rail joint area. This involved scaling up the data put out by adjacent bridges on the wheel when the wheel-rail contact point was between the bridge lines. A computer program was not developed to provide this intermediate data because of the time resolution problem in identifying the exact position of the bridge for proper scaling of the data. This problem is more acute at the highest test speeds. For example, at 65 mph there is an approximate interval of 6.2 ms between bridge maxima. With a 1,000-sample per second representation of the data, this means either six or seven samples in the interval. This complicates the logic required to automate the data reduction. In view of the limited number of joint loads where the detailed time resolution was required, it was more efficient to calculate the load data directly from the digitized record rather than develop the software to perform this calculation automatically.

### 6.9.2 Statistical Load Parameters From Instrumented Wheel

The data channels on the first recorder, which included 4 vertical load channels, 4 lateral load channels and 2 vertical load position channels, were digitized at 400 samples per second. Separate digital records were established on a disc file for each of these data channels and for each of the test runs over the 3 test track sites. Each data set represented approximately 3 miles movement of the test car. This was the length of the designated test areas at each site. The digital data were then appropriately scaled and processed to provide vertical and lateral load data points eight times per wheel revolution and vertical load positional information twice per wheel revolution. The positional data were then used to apply a correction factor to the lateral load data to compensate for cross talk between the vertical load position and the output of the lateral bridge. A separate digital data file was then established for the load and load position data obtained on each of the test runs. These data were subsequently used for statistical and frequency analyses.

### 6.9.3 Load Parameters From Instrumented Side Frames and Axles

The data channels from the instrumented side frames and axles were recorded on the third recorder. These data channels were sampled at 200 samples per second for the derivation of wheel/rail load data. The following assumptions were required for the analysis of these load parameters:

- a. the wheel/axle set was assumed to be in static equilibrium,
- b. the line-of-action of the forces acting on the wheel/axle set were assumed to be at fixed positions, and
- c. the vertical load acting on the journals was assumed to be one-half of the load registered by the side frame load bridges.

Figure 3-24 defines the loads acting on the wheel/axle set and the assumed positions of their lines of action. The loads at the wheel/rail interface may then be calculated using the following relationships [6-1]:

$$V_L = B_L + \frac{(M_R - M_L)}{(f - e - d)} + W_W \quad (6-1)$$

$$V_R = B_R + \frac{(M_L - M_R)}{(f - e - d)} + W_W \quad (6-2)$$

$$L_L = \frac{1}{c} \left[ \frac{M_R d - M_L (f - e)}{(f - e - d)} - B_L a \right] \quad (6-3)$$

$$L_R = \frac{1}{c} \left[ \frac{M_L e - M_R (f - d)}{(f - e - d)} - B_R b \right] \quad (6-4)$$

where  $W_W$  is one half the weight of the wheel/axle set.

Substituting the following values:

$$a = b = 10.25 \text{ inches}$$

$$c = 18 \text{ inches}$$

$$d = e = 14 \text{ inches}$$

$$f = 58.5 \text{ inches}$$

The expressions for the loads become:

$$V_L = B_L + (0.033)(M_R - M_L) + W_W \quad (6-5)$$

$$V_R = B_R + (0.033)(M_L - M_R) + W_W \quad (6-6)$$

$$L_L = (0.026)M_R - (0.081)M_L - (0.57)B_L \quad (6-7)$$

$$L_R = (0.026)M_L - (0.081)M_R - (0.57)B_R \quad (6-8)$$

Two moment bridges were used at each of the moment bridge positions on the axle. They were oriented 90 degrees apart so that axle bending moment data would be obtained at maximum bridge sensitivity 4 times per wheel revolution. Bending moment data at intermediate locations may be obtained by assuming a sinusoidal variation in bridge output at bridge orientations off the vertical axis. This permits definition of load parameters at the sampling rate of the data channels. Vertical and lateral load data from runs through the curved track test section were analyzed successfully using Equations 6-5 through 6-8.

Several problems were encountered in the reduction and analysis of the data from the instrumented side frames and axles operating on the tangent track sections. Attempts to derive wheel/rail load information at each data sample showed wide variation from one sample to the next. This was primarily due to variations in the axle bending moment data which appeared to be superimposed on the once-per-revolution sinusoidal variation of the bridge output. Attempts to process the data point-by-point were then abandoned and the load data were read at points corresponding to the vertical orientation of the bridges when they were at their maximum sensitivity for measurement of the axle bending moment in the vertical plane. The load data derived in this manner also showed wide swings in load values (on the order of  $\pm 5000$  lb.) from one set of data points to the next. The variations in the axle bending moment data were probably due to continuous shifts in the lines-of-action of the forces and the dynamic effects where inertial loads were involved.

The major problem appears to be due to the assumptions made regarding the lines of action of the forces acting on the axle. For example, consider Equation 6-3, the formula for the lateral load on the left wheel based upon assumed measurements of the journal load and the moments in the axle. Note that the calculated load is quite sensitive to the value that is assumed for "a", which is the distance between the line-of-action of the vertical load acting on the journal and the line-of-action of the vertical force at the wheel/rail interface. The normal tolerances between the side frame and the roller bearing adapter would allow up to  $\pm 3/8$  inch motion of the side frame relative to the roller bearing. In addition, the top of the roller bearing adapter is flat for 3 in. and the bottom of the pedestal opening on the side frame is flat for a width of 3-1/2 in., making it possible for the load to be transferred over at least a 3 in. width with a slight shift of the loads acting on the side frame. Using typical values for measured moments and wheel loads, it can be shown that a one-inch movement in the line-of-action of the journal load with respect to the wheel/rail contact point can result in an error of 1700 lbs in the measurement of the lateral load.

Another approach in processing the load data on tangent track from the instrumented side frames and the axles is to make the assumption that there is no net lateral load on the axle. The development of a net lateral load on a wheel/axle set would usually be due to transient loads associated

with the impact of the flange with the rail during the hunting action of the wheel/axle set. Dynamic flange forces primarily involve equilibrium between the lateral wheel/rail force and the inertial loads of the wheel/axle set, and cannot be quantitatively described if the assumption of static equilibrium is made for the interpretation of the data. Thus the quasi-static net lateral forces are the only ones amenable to definition by the transducers.

By making the assumption of no net lateral load, one can solve for lateral wheel loads where static equilibrium exists, such as when the lateral wheel flange force on one side of the axle is opposed by the frictional forces on the tread of the opposite wheel. Only one of the moment bridges,  $M_R$  or  $M_L$ , is required for the definition of the lateral force. The equations for lateral and vertical loads under these conditions then become:

$$V_L = \frac{B_L(f+a) - B_R(a)}{f} + W_W \quad (6-9)$$

$$V_R = \frac{B_R(f+a) - B_L(a)}{f} + W_W \quad (6-10)$$

$$L_L = \frac{1}{c} \left[ M_L - B_L(a+d) + V_L(d) - W_W(d) \right] \quad (6-11)$$

$$L_R = \frac{1}{c} \left[ M_R - B_R(a+d) + V_R(d) - W_W(d) \right] \quad (6-12)$$

where  $W_W$  is one-half the weight of the wheel/axle net.

Note that the vertical load equations are independent of the moment data. The use of these equations to derive vertical load data gave results which appeared to be free of extraneous oscillations and which were more representative of the true vertical wheel/rail load than when the previous equations were used to process the data. Consequently, these equations were used for the reduction of all tangent-track data from the instrumented side frames and axle system. The lateral load data that were derived using Equations 6-11 and 6-12 still exhibited variations in load values from one point to the next, but these were much less than were calculated when using the original equations, 6-5 through 6-8.

#### 6.9.4 Mean Square Spectral Density

Two different techniques were used to develop plots of mean square spectral density from load and acceleration data. The vertical load data from the instrumented side frames, which is representative of vertical wheel load data, were processed directly from the analog data tape using a Spectral Dynamics real-time analyzer. Several frequency ranges were used for the reduction of this data. At the 0-50 Hz range, 2.7 minutes of data were included in each sample.

The frequency analysis of the load data from the instrumented wheel utilized the data sets giving load data 8 times per wheel revolution (every 14.1 inches) for 3 miles of operation. These data sets were analyzed using a computer program for determining mean square spectral density. All of the data points from the 3 miles of operation at each track test site were utilized in this analysis. The use of data sampled 8 times per wheel revolution limits the range of frequencies that can be included in the analysis\*. For example, at 35 mph the limitation of the frequency analysis is from 0 to 22 Hz. At 65 mph the frequency range increases to 0 to 40 Hz.

#### 6.9.5 Data Formats

Three basic formats have been used for the presentation of load data: time-history plots, cumulative probability distribution plots, and mean-square spectral density plots. Plots of load parameters versus time have been used to describe the transient vertical loads measured during the traversal of a rail joint and to make comparisons between the instrumented wheel system and the instrumented side frames and axles system at specific test locations.

Cumulative probability distribution curves have been utilized to show the statistical variations in the vertical and lateral wheel/rail forces and the lateral to vertical load ratio for passage over the three test track sites. This format was also used to show the variation of rail joint impact forces on a selected portion of the rough tangent track site. Force data

---

\*The basic theorem of C. E. Shannon states that the sampling rate must be twice the maximum frequency described in the data.

were segregated into 1000 lb ranges for determination of the cumulative probability distribution functions. The lateral to vertical load ratio data was segregated into 0.1 ranges for determination of the cumulative probability distribution functions.

Mean-square spectral density plots have been used to summarize the frequency content of vertical and lateral load and car body acceleration data obtained on the rough tangent and smooth tangent track sites. These plots show  $[(\text{force})^2/\text{Hz}]$  or  $[g^2/\text{Hz}]$  versus frequency.

## 7. EVALUATION OF LOAD MEASUREMENT SYSTEMS

### 7.1 WAYSIDE INSTRUMENTATION ERROR ANALYSIS

#### 7.1.1 Lateral Load Measurements

Previous experience with using rail strain gage circuits to measure lateral wheel/rail loads has demonstrated the difficulty in selecting a circuit which minimizes the effect of vertical load on the lateral load measurement. In order to investigate this "cross talk" in greater detail, BCL conducted a series of laboratory experiments [7-1] using a 39-ft length of 131 lb/yd rail in a special fixture capable of simulating variable tie support conditions. The rail was gaged extensively to map strain distributions for various combinations of lateral and vertical loads. The output of the previously used lateral load circuit based on ORE experiments was found to have the form:

$$e = C_L L + C_x V y,$$

where

L = lateral load

V = vertical load

y = lateral position (toward gage surface) of vertical  
load on rail running surface

$C_L, C_x$  = circuit constants.

Several load-measuring circuits were evaluated during these laboratory experiments to select an improved circuit for this program. These included rail base longitudinal gages (similar to an ORE/DB circuit), rail head fillet and base longitudinal gages (similar to an ORE/SNCF circuit), and a rail base chevron circuit (see Figure 6-11). All three circuits were applied to a section of rail in the crib area between two ties and used standard, one-inch weldable gages. While all three strain gage patterns showed a marked reduction in cross talk error due to vertical load, the base chevron circuit was chosen for the field experiments because of its superior linearity and lower change in sensitivity with vertical load and support conditions. A summary comparison of the circuits is given in Table 7-1.

TABLE 7-1. COMPARATIVE EVALUATION OF LATERAL WHEEL/RAIL LOAD-MEASURING STRAIN GAGE CIRCUITS

176

Criteria	Web Vertical Over Tie (Fully- Supported)	Web Vertical Between Ties	Base Chevron	Base Longitudinal	Head and Base Longitudinal
Sensitivity #	Good	Good	Good	Good	Excellent
Microvolts/volt per kip	21	19	17	31 (1/2 bridge)	74
Linearity (0 to 10 Kips at 5Kips, Error =	Fair + 9%	Excellent -1%	Good -5%	Poor +61%	Poor + 32%
Crosstalk*	Poor	Poor	Good	Fair	Good
Lb per 1000 lb V at Flange Contact Point	580	780	-56/-132 <sup>a</sup>	133	-13/-179 <sup>b</sup>
Sensitivity to Support	Fair	Poor	Good	Poor	Poor
Clips off, field -		-7%	-11%	+89%	+46%
Clips snugged -		-49%	+10%	-46%	-32%
Sensitivity to Vertical Position of Lateral Load	Fair	Fair	Good	Fair	Good
Z = -.44" to -.81"	+18%	+19%	+8%	-12%	-10%
Change in Sensitivity under Vertical Load	Good	Poor	Good	Fair	Good
30 Kip V, Y = 0	-4%	-49%	-3%	+19%	+3% <sup>c</sup>
# Clips loose on adjacent ties (nominal condition)					
* Sensitivity for lateral load applied at Z = -.44"					
a Near edge of chevron pattern					
b Due to localized head bending strains					
c Disregarding localized effects in head (gages centered on head at X = 1.75")					

As part of the normal field test procedure, each of the lateral load circuits was calibrated with and without simultaneous vertical load, as described in Section 6.5.5. From the lateral calibration X-Y plots, circuit characteristics were determined for each site, including sensitivity (equivalent load for the precision shunt resistor calibration), linearity, hysteresis, and apparent cross talk and maximum deviation from zero under the vertical calibration load. Circuit characteristics, along with site physical parameters, are listed in Table 7-2.

Lateral circuit sensitivity was based on a straight-line approximation of the field calibration X-Y plot as shown in Figure 6-20. Sensitivity determined under a vertical load of 21 to 25 kips for lateral loads from 0 to between 10 and 14 kips was used in data analysis. Since this sensitivity is subject to some error in calculation due to linearity and hysteresis in the X-Y plots, as well as some change in sensitivity under varying vertical load, an approximate tolerance must be established for this factor. From the mean-square summation of the range of sensitivities for each X-Y plot under higher vertical loads, a mean error of  $\pm 1.2\%$  with a standard deviation of 2.0% was established. Therefore, the lateral loads (based on circuit sensitivity error alone) will fall within a tolerance band of  $\pm 3.2$  percent at one standard deviation, or  $\pm 5.2$  percent at the 95-percent confidence level.

Some scatter in circuit sensitivity was noted from the calibrations, particularly in Test Section 1, the last three sites of which were found to have high sensitivity (low equivalent load for the shunt calibration). A careful check of the circuits and calibration system did not indicate any mechanical or electrical reason for these unusual sensitivities. (In the laboratory, the circuit shunt calibration equivalent load with 200K resistors was 34,800 lb with a 10-in. gage zone dimension.)

Lateral circuit error is also dependent upon four additional factors: circuit noise, linearity error, hysteresis, and cross talk from vertical load. Calculation of the mean and unbiased standard deviations (Table 7-2) of error values observed during calibrations showed the following:

	<u>Mean</u>	<u>Std. Deviation</u>
Circuit noise (peak), Kips	0.4	0.2
Linearity error, Kips	-0.1	0.6
Hysteresis, Kips	0.60	0.30
Apparent cross talk (Kips per kip of vertical load)	-0.04	0.02

TABLE 7-2. DESCRIPTION OF PHYSICAL PARAMETERS FOR LATERAL WHEEL/RAIL LOAD MEASUREMENT CIRCUITS

Parameter	Test Section 1, 133 lb/yd 39-ft BJR Tangent						
	Site 1	Site 2	Site 3	Site 4	Site 5	Site 6	Site 7
Calibration Equivalent Load (kips) <sup>(a)</sup>							
Under large vertical load <sup>(b)</sup>	37.6	31.0	34.0	36.0	21.6	20.2	26.4
Under small vertical load <sup>(c)</sup>		32.2	34.0	37.6	22.5	21.5	29.1
Linearity error (kips) <sup>(d)</sup>	+0.7	+0.7	+0.4	+1.1	-0.2	-0.6	-0.3
Apparent cross talk (kips/kip V) <sup>(e)</sup>	-0.06	-0.02	-0.03	-0.07	-0.05	-0.07	-0.02
Circuit noise (kips peak-peak)	0.9	0.5	0.7	0.9	0.3	1.4	0.3
Hysteresis (kips peak-peak)	0.8	0.2	1.1	1.1	0.4	0.8	0.4
Track vertical stiffness (kips/in) <sup>(f)</sup>	274	206	227	227	435	200	317
Rail initial vertical deflection (in.) (under 5kip load)	.102	.116	.037	.066	.038	.104	.040
Gage zone dimension (in.) <sup>(g)</sup>	10-1/4	10	9-1/2	10-3/4	12	16-1/2	14-1/2
Crib spacing (in.)	15	15-1/4	15	16-3/4	16	21-1/2	20
Rail longitudinal run (in.) <sup>(h)</sup>	3	2-1/2	2	1-1/2	1-1/4	1-1/4	1

Parameter	Test Section 2, 133 lb/yd CWR Tangent						
	Site 1	Site 2	Site 3	Site 4	Site 5	Site 6	Site 7
Calibration Equivalent Load (kips) <sup>(a)</sup>							
Under large vertical load <sup>(b)</sup>	29.2	28.8	40.2	39.2	29.4	33.2	32.6
Under small vertical load <sup>(c)</sup>	29.2	31.0	37.4	39.0	31.2	33.5	29.4
Linearity error (kips) <sup>(d)</sup>	-0.3	-0.3	-0.4	-0.1	-0.9	-0.7	-0.5
Apparent cross talk (kips/kip V) <sup>(e)</sup>	0	-0.06	0	-0.03	-0.04	-0.03	-0.02
Circuit noise (kips peak-peak)	0.8	0.6	0.8	0.9	0.8	2.0	0.6
Hysteresis (kips peak-peak)	0.3	0.4	0.6	0.1	0.7	0.8	0.6
Track vertical stiffness (kips/in) <sup>(f)</sup>	281	299	588	256	278	190	250
Rail initial vertical deflection (in.) (under 5kip load)	.067	.067	.038	.104	.047	.057	.027
Gage zone dimension (in.) <sup>(g)</sup>	10-1/4	9-1/2	7-1/2	8-3/4	10-1/2	9-1/2	12
Crib spacing (in.)	16-1/4	19	13-1/4	14-1/2	16-1/4	15-1/2	17-1/2
Rail longitudinal run (in.) <sup>(h)</sup>	1/2	1/2	1/2	1/2	1/2	1/2	1/2

Parameter	Test Section 3, 133 lb/yd 78' BJR, 6° CURVE		Statistics (All Sites)	
	Site 7		Mean	Std. Dev.
Calibration Equivalent Load (kips) <sup>(a)</sup>				
Under large vertical load <sup>(b)</sup>	36.0		31.7	5.9
Under small vertical load <sup>(c)</sup>	36.0		32.9	6.9
Linearity error (kips) <sup>(d)</sup>	-0.3		-0.1	0.6
Apparent cross talk (kips/kip V) <sup>(e)</sup>	-		-0.04	0.02
Circuit noise (kips peak-peak)	0.5		0.8	0.4
Hysteresis (kips peak-peak)	0.6		0.6	0.3
Track vertical stiffness (kips/in) <sup>(f)</sup>	-			
Rail initial vertical deflection (in.) (under 5 kip load)	-			
Gage zone dimension (in.) <sup>(g)</sup>	10-3/4			
Crib spacing (in.)	13-3/4			
Rail longitudinal run (in.) <sup>(h)</sup>	-			

Notes: a. 100 percent shunt calibration using 4 200K resistors.  
b. Vertical load between 21,000 and 25,000 lb.  
c. Vertical load between 2,000 and 7,000 lb. at Section 1. No vertical load at Test Sections 2 or 3.  
d. Linearity = maximum deviation (kips) from straight line over lateral load range of 0 to 12 kips.  
e. Lateral circuit output due to vertical calibration load, kips per kip vertical load.  
f. Tangent stiffness per rail at 20,000-lb vertical load, kips/in.  
g. In.  $\frac{1}{16}$  to  $\frac{1}{8}$   
h. Longitudinal motion of rail in plates on reversal of traffic.

By assuming the first three to be random errors and taking a root-mean-square summation, the lateral loads can be predicted to fall within an uncertainty band of  $\pm 1.2$  kips (at one standard deviation). The maximum additional cross talk error on lateral load can be expected to range up to  $\pm 0.6$  kips under light wheel loads, and up to  $\pm 1.8$  kips under heavy wheel loads, at one standard deviation. For high positive (flanging) lateral load, this term is subtractive, tending to underestimate the actual lateral load.

#### 7.1.2 Vertical Load Measurements

The vertical wheel/rail load-measuring circuit used in these field tests (see Figure 6-11) consisted of two 4-gage chevron patterns oriented at 45 degrees about the neutral axis of the rail to measure the principal strains due to the vertical shear force in the rail web. These circuits were also evaluated in the laboratory during tests of the lateral load circuits. A maximum variation in signal equivalent to 700 lb under a 30,000 lb load ( $-2.3$  percent) was recorded in varying the lateral position of the vertical load on the rail head from 0.53 inch toward the field side to 1.00 inch toward the gage side. Cross talk caused by a 10,000 lb lateral load was less than 200 lb.

Vertical load circuit characteristics are listed in Table 7-3. Site physical parameters are the same as those listed in Table 7-2 for the lateral circuits. The most notable feature of the vertical load circuits was the excellent linearity and low hysteresis--the calibration X-Y plot shown in the example curves of Figure 6-20 shows the highest hysteresis of any circuit, and most calibration curves deviated less than a pen line width during the complete cycle. Vertical circuits were set up for a full-scale range of 100,000 lb, with approximately a 15 percent overrange capability on amplifiers and recorder. Due to force limitations of the calibration jack, circuits were tested in situ to maximum loads between 18,000 and 24,000 lb. The extreme linearity in this range, however, provides confidence in the measurements well beyond the range of calibration.

TABLE 7-3. DESCRIPTION OF PHYSICAL PARAMETERS, VERTICAL WHEEL/RAIL LOAD-MEASURING CIRCUITS

Parameter	Test Section 1, 133 lb/yd 39-ft BJR Tangent						
	Site 1	Site 2	Site 3	Site 4	Site 5	Site 6	Site 7
Calibration Equivalent Load (kips) <sup>(a)</sup>	86.0	80.8	84.0	95.9	82.8	73.6	84.8
Linearity Error <sup>(b)</sup>	*	*	*	1.0	*	1.0	0.8
Circuit Noise (p-p)	1.8	1.7	1.8	1.4	1.8	2.6	4.0
Hysteresis (p-p)	0.5	*	*	0.5	*	0.7	0.7
(Values in kips)							
Parameter	Test Section 2, 133 lb/yd CWR Tangent						
	Site 1	Site 2	Site 3	Site 4	Site 5	Site 6	Site 7
Calibration Equivalent Load (kips) <sup>(a)</sup>	82.0	88.8	85.0	82.0	83.6	79.6	84.0
Linearity Error <sup>(b)</sup>	0.6	*	*	*	*	*	*
Circuit Noise (p-p)	1.7	2.2	1.8	2.1	1.5	2.5	2.3
Hysteresis (p-p)	*	*	0.8	*	*	*	*
Parameter	Test Section 3 6° Curve			Statistics (all sites)			
	Site 7			Mean	Std. Dev.		
Calibration Equivalent Load (kips) <sup>(a)</sup>	87.9			84.1	4.9		
Linearity Error <sup>(b)</sup>	*			0.6	0.2		
Circuit Noise (p-p)	2.0			1.9	0.7		
Hysteresis (p-p)	*			0.5	0.1		

\*Less than X-Y plotter pen line width (< 0.5 kip).

(a) 100 percent shunt calibration using 4310K resistors.

(b) Maximum deviation from straight line, 0 to approximately 20 kips (laboratory tests to 30 kips showed circuit linearity within  $\pm 0.5$  percent).

Basing the vertical circuit error analysis on the same four factors used for the lateral circuit, the mean and unbiased standard deviation values observed during tests showed the following:

	<u>Mean</u>	<u>St'd Deviation</u>
Circuit noise (peak, kips)	1.0	0.4
Linearity error (kips)	0.6	0.2
Hysteresis (kips)	0.5	0.1

Combining the circuit noise, linearity, and hysteresis errors by an rms summation, the vertical load measurements are expected to be within an uncertainty band of  $\pm 1.7$  kips at one standard deviation, plus an additional error up to  $\pm 0.5$  kips due to cross talk and load position on the rail head.

Because of the excellent linearity and repeatability of the vertical load calibration X-Y plots, the circuit sensitivity error is estimated to be within  $\pm 1$  percent. Digitization errors for both vertical and lateral load data analysis are small: 50 lb per digit for the vertical, and 12.5 lb per digit for the lateral channels.

### 7.1.3 Extended Vertical Load Circuits

The extended-length vertical load measurement zones consisting of two strain gage chevron patterns and load-cell tie plates are described in Section 6.5 and have been discussed in Sections 3.2.2 and 3.2.3 on flat wheel and rail joint impact loads. Because of interference between the joint bars and the calibration head, a direct calibration using a known vertical load was not possible at the instrumented joint. The load cell tie plates were, of course, pre-calibrated in the laboratory using a Baldwin-Southwark test machine. The two chevron circuits were therefore set in sensitivity to the mean value of 84.1 kips equivalent for the 100 percent shunt calibration step, based on the calibration for the other 15 vertical load circuits. The combined result was verified during the slow roll-by of the test train (see Figure 3-16). For the CWR track extended-length zone, difficulties in obtaining a "calibration train" (a freight car against which to react the vertical calibration load) until the last evening of tests precluded on-site calibration of the zone. This summation circuit was therefore set up in the same manner as the joint zone, and verified against the 24 locomotive wheel loads during a slow roll-by of the calibration train.

In evaluating the extended vertical load measurement zone signals, it was observed that the tie plates were loaded (as expected) by wheels well beyond the limits of the zone. The rail shear force measured by the chevron gage patterns did not, however, completely cancel this external loading as had been anticipated when considering the rail as a free body. The more complex loading paths within the track structure cause an error signal that is a function of axle spacing (distance to the adjacent wheel load), vertical wheel load, and the "balance" of seating of the several tie plates within and adjacent to the zone. For the 9-ft axle spacing of the GP-30 locomotive, this error is small (see Figure 3-16), but for the 6-ft axle spacing of the 100-ton freight car, the error may range up to 10 percent of the adjacent wheel load (see Figure 3-17).

Circuit noise levels for the extended measurement zones were higher than the short-zone circuits due to the combined effects of four individual load cells and two separate strain gage bridges. Noise levels of 2.5 kips and 2.1 kips, peak-to-peak, were typical at the instrumented rail joint and CWR zones, respectively. No estimates of linearity, hysteresis, or sensitivity variations along the zone were possible without in situ calibrations.

Frequency analysis of vertical loads from both the rail joint and CWR extended-length zones shows very little energy above 500 Hz. In the joint zone there is little evidence of a "P1" impact force component, although there is a minor spectral component of force at 1370 Hz. Examination of bolt-hole strains (Figure 3-26) shows a minor dynamic oscillation with a 1.5-millisecond period, about 670 Hz, that may be due to joint gap impact. Similarly, there is little evidence of the 800-Hz vibration that shows up so strongly in rail vertical acceleration. If the rail head is considered as a beam supported by the rail web acting as a continuous foundation, the resulting dynamic system is approximately a 4.6-lb mass with a natural frequency of 6.7 kHz. However, a laboratory-controlled determination of the system transfer function is needed to determine whether (a) the measurement system severely attenuates frequency components above 500 Hz, or (b) the frequency components of force above 500 Hz are negligible.

## 7.2 VEHICLE-BORNE INSTRUMENTATION ERROR ANALYSIS

The errors associated with the measurement of vertical and lateral loads at the wheel/rail interface may be estimated by determining the relative importance of random variations in the test parameters associated with each measurement. The analysis is based on the fact that the measured load,  $L$ , is a function of several independent variables,  $x_1, x_2, x_3, \dots, x_n$ .

$$L = f(x_1, x_2, x_3, \dots) \quad (7-1)$$

It may be shown that:

$$\sigma_{EL}^2 = \left[ \frac{dL}{dx_1} \right]^2 \sigma_{EX_1}^2 + \left[ \frac{dL}{dx_2} \right]^2 \sigma_{EX_2}^2 \dots \quad (7-2)$$

where  $\sigma_{EL}^2$  is the variance of the error associated with  $L$ , and

$\sigma_{EX_1}^2, \sigma_{EX_2}^2 \dots$  are the variances of the errors associated with the independent variables

Equation (7.2), known as the Propagation of Error formula, is used to estimate the errors associated with the measurement of vertical and lateral loads with the two vehicle-borne instrumentation systems. The quantity  $\epsilon_{X_1}$  is defined as,

$$\epsilon_{X_1}^2 = \left[ \frac{dL}{dx_1} \right]^2 \sigma_{X_1}^2$$

in this presentation as a means of showing the relative importance of various parameters contributing to the error of load measurement.

A detailed analysis of the vehicle-borne instrumentation errors is contained in Appendix E. Estimated errors at the one-standard-deviation level are summarized below in Table 7.4. As discussed in Section 6.9, one of the major sources of error in the low-frequency system is the variation in lateral position at the side frame/bearing adapter interface of the line of action of the vertical force. The calculation of vertical load from the low-frequency system is relatively insensitive to this error, but the calculation of lateral load is influenced quite strongly by variations in this dimension.

TABLE 7-4. SUMMARY OF VEHICLE-BORNE LOAD MEASUREMENT ERRORS  
AT THE ONE-STANDARD-DEVIATION LEVEL

Error Source	W/R Load Error Contributions, 1b rms#			
	Instrumented Wheel		Side Frame/Axle	
	Vertical	Lateral	Vertical	Lateral
System electrical noise	860	210	150	340
Digitization error	150	38	26	61
Bridge nonlinearity, hysteresis	72	120	62	320
Bridge calibration errors		410		930
Sensitivity error, position of load	410			
Cross talk error	280*			
Corss talk correction error (position)		820		
(calibration)		180		
(load)		34		
Calibration error, vertical load			1000	780
Positional errors, side frames, wheel/ rail			810	2100
Total (rms) error	1000	970	1300	2500
Estimated maximum bandwidth, Hz	200	200	10	10

\*At nominal 5000-1b lateral load.

#See Appendix E.

### 7.3 COMPARISON OF WAYSIDE AND VEHICLE-BORNE MEASUREMENTS

Table 7-5 summarizes the measurements taken simultaneously by wayside and vehicle-borne transducers at the single operational (low-rail) wayside site on the curved track. Ranges of expected error for these measurements are included in this table, based on the one-standard-deviation errors estimated above. For the rail lateral load circuit, cross talk was considered a random error with a maximum expected value of  $0.06 \times 25 = 1.5$  kips under the instrumented wheel, and a probable (random) error of 1.05 kips. This results in a maximum expected error band of  $\pm 1.7$  kips. Wheel/rail forces through the curve are predominantly quasi-static in nature, and rapid fluctuations in load between samples (once every 14 inches from the wheel, every 28 inches from the side frame/axle system) are less likely. As a result, there is a reasonably good correspondence between wheel and rail, although the rail reads consistently low on leading-axle runs, and high on trailing-axle runs. Before correction of instrumented-wheel cross talk by wheel position, the rail measurement was consistently high on leading-axle runs:

<u>Speed (mph)</u>	<u>Lateral W/R Load (kips)</u>		
	<u>Rail</u>	<u>Uncorrected Wheel</u>	<u>Corrected Wheel</u>
26	10.9	9.1	11.9
31	9.4	7.3	12.6
38	8.0	7.1	11.3

TABLE 7-5. COMPARISON OF WAYSIDE AND VEHICLE WHEEL/RAIL LOAD PEAKS AT LOW RAIL INSTRUMENTED SITE, 6° CURVE, 6" SUPERELEVATION

BCL RUN NO.	SPEED (MPH)	DIRECTION	LATERAL W/R LOADS (KIPS)					
			RAIL		WHEEL		SIDEFRAME/AXLE	
			MEASURED	RANGE (ERROR)	MEASURED	RANGE (ERROR)	MEASURED	RANGE (ERROR)
R1	15	E*	4.6	2.9-6.3	3.5	2.5-4.5		
R2	40	W	7.8	6.1-9.5				
R3	26	W	10.9	9.2-12.6	11.9	10.9-12.9	5.8	3.3-8.3
R4	27	E	3.3	1.6-5.0	2.0	1.0-3.0	0.3	-2.2-2.8
R5	15	W			13.0	12.0-14.0		
R6	31	W	9.4	7.7-11.1	12.6	11.6-13.6	9.9	7.4-12.4
R7	20	E	3.3	1.6-5.0				
R8	38	W	8.0	6.3-9.7	11.3	10.3-11.3	8.8	6.3-11.3

BCL RUN NO.	SPEED (MPH)	DIRECTION	VERTICAL W/R LOADS (KIPS)					
			RAIL		WHEEL		SIDEFRAME/AXLE	
			MEASURED	RANGE (ERROR)	MEASURED	RANGE (ERROR)	MEASURED	RANGE (ERROR)
R1	15	E	29.2	27.4-31.0	26.4	25.4-27.4		
R2	40	W	23.8	22.0-25.6				
R3	26	W	27.3	25.5-29.1	26.4	25.4-27.4	25.0	23.7-26.3
R4	27	E	28.2	26.4-30.0	27.1	26.1-28.1	22.3	21.0-23.6
R5	15	W			26.8	25.8-27.8		
R6	31	W	24.6	22.8-26.4	25.0	24.0-26.0	27.1	25.8-28.4
R7	20	E	27.7	25.9-29.5				
R8	38	W	23.5	21.7-25.3	21.7	20.7-22.7	29.2	27.9-30.5

\*Instrumented wheel on trailing axle eastbound, leading axle westbound.

Cross talk in the low-rail circuit will tend to subtract from the actual load on leading-axle runs, since the lead outer wheel is expected to be flanging on the high rail, and the low-rail wheel is expected to contact about 1/4 inch in from the center of the rail. Lateral loads from the side frame/axle system were consistently lower than wheel load measurements, although for the two higher-speed leading-axle runs the measurements corresponded rather closely with the rail measurements.

A preliminary analysis of the comparison between wayside lateral load circuits used for locomotive evaluation tests at the TTC in Pueblo, Colorado provides a more definitive evaluation of these circuits. Comparing lateral loads recorded by the ASEA/SJ wheelset in a lead-axle position on an SDP40F locomotive against 14 rail circuits in one test section for five of the high-speed runs, the rail circuits were found on the average 0.4 kips high, with a standard deviation of 2.4 kips on the difference between wheel and rail. Loads at most of these curved-track positions ranged from 10 to 30 kips.

A comparison of wayside and vehicle-borne measurements on the south rail of the tangent BJR track section (under the instrumented wheel) is given in Table 7-6. Again the problem arises in sampling the wheel/rail load from on-board instrumentation only 8 times per wheel revolution, or every 14.1 inches; rapid changes in the loads can cause a significant difference between values measured at the center of the rail circuit and at the center of the wheel circuit, up to  $\pm 7$  inches apart. For example, vertical wheel load oscillations at the track structure/unsprung mass natural frequency near 40 Hz (which, from tests on the Northeast Corridor of the ASEA Rc-4A locomotive with instrumented wheelsets, was found to be an important load component) can change from a maximum to zero in 6.6 inches at 60 mph. For this reason, additional high-resolution plots (1000 samples per second) were reconstructed by combining bridge signals with the inverse transfer function for high-speed runs through wayside Site 3, the instrumented joint zone. An example of the excellent comparison between rail and wheel circuit outputs is given in Figure 7-1, where the circled points representing trackside data have been derived (as accurately as possible) from Figure 3-23. The transient vertical load associated with passage of this particular rail joint (which is Joint #11 in Figure 4-12) contains only the "P2" component from joint deflection, since this joint was essentially flat when vertically unloaded.

TABLE 7-6. COMPARISON OF WAYSIDE AND VEHICLE WHEEL/RAIL LOAD PEAKS THROUGH TANGENT BJR TEST SECTION, SOUTH RAIL (M.P. 292.4)

BCL RUN NO.	17F	17G	17I	17M	Note
SPEED (MPH)	38	37	49	68	(a)
DIRECTION	E	W	E	E	(b)
SITE NO. 2					
LATERAL, RAIL (KIPS)	0.4	-0.2	1.0	0.9	(c)
WHEEL	0.6	0.1	0.9	0.4	(d)
LF SYSTEM	-0.1	-2.5	0.0	0.3	(g)
VERTICAL, RAIL (KIPS)	27.5	29.9	26.7	26.4	
WHEEL	25.7	26.9	27.7	26.3	(d)
LF SYSTEM	25.5	29.3	25.8	25.0	
SITE NO. 3 (INST. JOINT)					
VERTICAL, RAIL (MAX.)	27.5	30.0	30.0	30.0	(e)
(MIN.)	22.5	23.0	24.0	20.0	(f)
WHEEL (MAX.)	27.5	25.2 <sup>(d)</sup>	33.0	31.3	(e)
(MIN.)	21.4		23.0	19.2	(f)
LF SYSTEM	25.0	25.3	27.7	23.0	
SITE NO. 5					
LATERAL, RAIL (KIPS)	0.3	-0.5	0.0	0.8	
WHEEL	0.3	2.4	2.1	-0.8	
LF SYSTEM	0.3	-1.4	0.5	-0.4	(g)
VERTICAL, RAIL (KIPS)	26.5	28.6	24.5	24.1	
WHEEL	25.9	26.0	19.9	21.8	(d)
LF SYSTEM	24.0	26.5	23.4	20.9	

Notes: (a) Speed through instrumented trackside sites  
 (b) Instrumented wheel on south rail, leading West, trailing East  
 (c) Positive lateral force toward flanging  
 (d) Vertical load sampled every 1/8th wheel revolution (14.1 inches)  
 (e) Maximum impact past joint  
 (f) Minimum load at joint  
 (g) LF (low frequency) system.

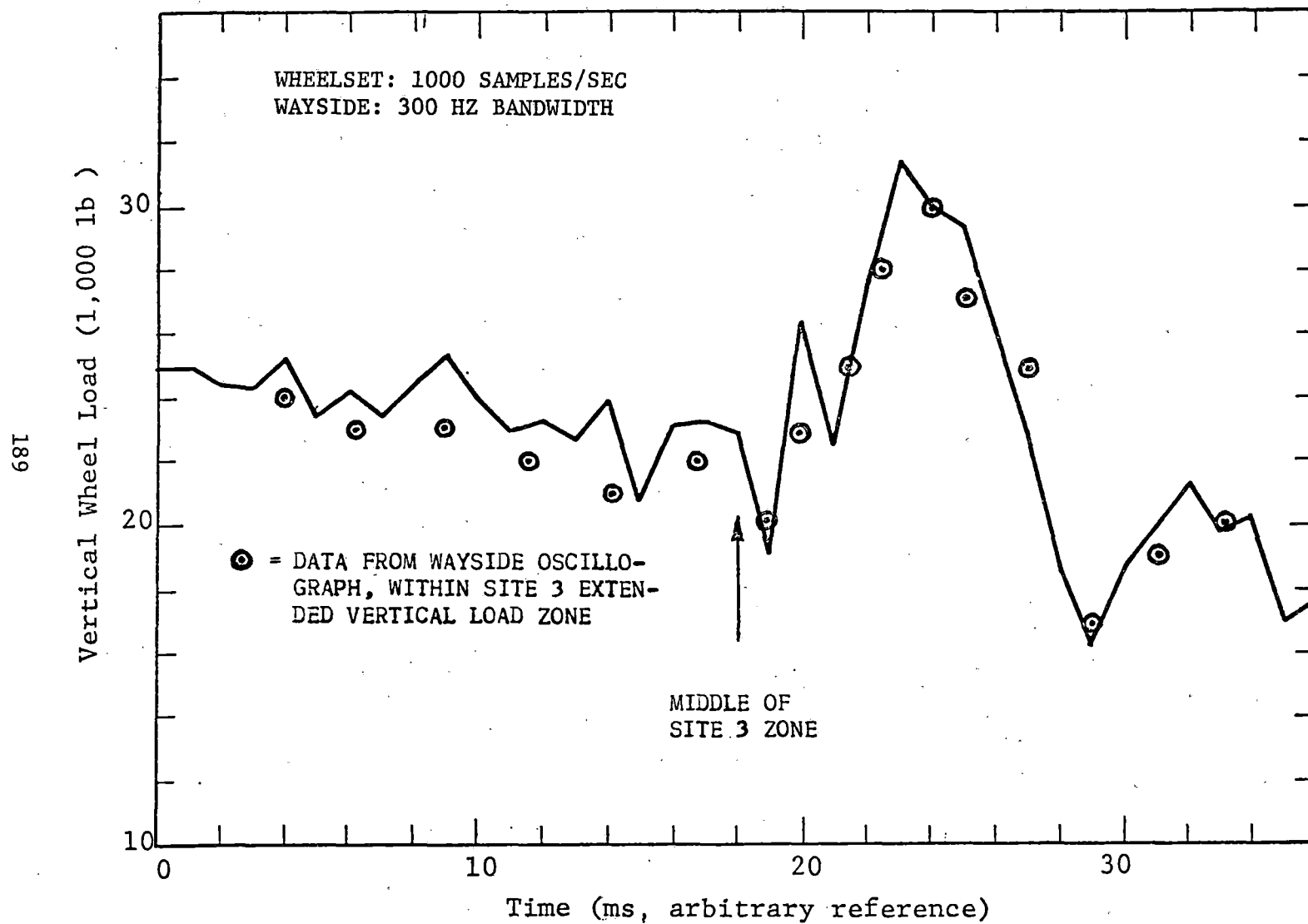


FIGURE 7-1. COMPARISON OF HIGH-FREQUENCY WHEELSET DATA WITH WAYSIDE DATA, VERTICAL WHEEL LOAD AT SITE 3, 65 MPH TEST RUN

## 7.4 RECOMMENDATIONS FOR IMPROVED INSTRUMENTATION

### 7.4.1 Wayside Instrumentation

One major problem was encountered with the weldable strain gages (Ailtech SG-129/30) at the curved track test section. After only a few days, gage failures--both open-circuit and dielectric breakdowns--increased to the point where the high-rail circuits could not be maintained operational. Only the low-rail circuit functioned without failure throughout the test period. Circumstantial evidence indicated that the weldable strain gages were failing in fatigue under the high vibration levels induced in the high rail by flange squeal (a lubricator near this curve was not functioning). Substantial head wear was noted on the high rail, and sustained flange squeal, particularly with the longer cars, was common. We suspect that the nonsupported (and normally unstrained) portion of the gage sheath between the welding flange and the strain relief structure was microphonic, resonating at the flange squeal frequency. This apparently resulted in breakdown of the MgO dielectric, a radical change in gage factor, and shorting or fatigue failure of the gage element.

As a precautionary measure, a bead of RTV rubber was run the length of each gage, including the strain relief structure, to reduce vibration levels at the two tangent-track installations. The failure rate reduced to 10 percent on the BJR section and 3 percent on the CWR section over the 10-day test periods, but it is not clear whether this was caused by the use of RTV or the reduced rail vibration on tangent track.

Modified weldable gages having larger-diameter sheaths have been used previously on Northeast Corridor electrified track after gage failures attributed to dielectric breakdown were experienced. These modified gages were also used successfully on curved track during the Florida East Coast Railway concrete-tie experiments when standard gages failed, and they have also been used in the recent locomotive tests at the Transportation Test Center in Pueblo, Colorado. It cannot be said for certain that these modified gages would survive the flange squeal environment on a shorter-radius curve, however.

The electrodynamic wheel detector transducers and associated circuitry for providing data-processing wheel pulses were also a source of problems. The apparent reason for these problems was the wide variability in transducer voltage level for different wheels and speeds, resulting in missing or inverted pulses and consequent data processing difficulties. This experience indicates the need for a data recording/processing system which is not dependent upon track-mounted hardware for logic signals. In the recent locomotive evaluation tests at the TTC, Battelle has been evaluating on-site data processing using a microprocessor to determine the presence of a wheel using only the vertical load signal. This has worked well for heavy cars, but may require additional development to detect light wheel loads with noise (wheel flats) superimposed. This is the recommended approach for future wayside measurement programs.

#### 7.4.2 Vehicle-Borne Instrumentation

The test wheels which were available to this project were conventional, regular production, wrought-steel wheels and as such contained several slight irregularities which would be desirable to avoid on future instrumented wheel sets. The wheel exhibited a slight variation in the thickness of the plate around a circumferential line and a slight tilting of the plate so that the axis of the plate did not coincide with the axis of the tread of the wheel. As a result, the outputs of the load sensing bridges were not equal for a constant load application. Therefore, provisions had to be made to provide variable gain factors for each bridge. The effects of wheel plate irregularity can be eliminated by machining the wheel, and it is recommended that machined wheels be used for any system which is intended as a standardized measurement tool.

Another irregularity was that the wheel was unbalanced. An unbalanced wheel gives rise to a speed-dependent, nonaxisymmetric strain field. This results in a cyclic once-per-revolution variation in strain which can be explained in the following manner. The unbalanced mass of the wheel can be envisioned as being located at a point on the rim. When this point is away from the rail the unbalanced force will be carried through the plate to the hub causing a strain field in the plate. However, when the center of the unbalance rotates to a point where it is near the rail, the unbalanced load

will be transmitted directly to the rail at the wheel-rail interface, eliminating the load path through the plate and its associated strain field. Thus, a once per revolution strain field variation occurs in the plate, which affects the output of the load sensing bridges. The effects of this phenomenon were compensated by a speed-dependent calibration, but it would be better to minimize the unbalanced condition by using a machined wheel.

The dynamic characteristics of the wheel/rail load measurement systems have not been determined directly. A comparison of vertical loads from the instrumented wheel and the side frame/axle system (see Appendix D) shows apparent sideframe resonances in the 5 to 10 Hz range and a substantial attenuation by the low-frequency system above 10 Hz. However, the extent of load attenuation between the wheel/rail interface and the strain gage patterns on the wheel plate due to the wheel rim mass is not known. Attempts to use a wedge to generate an impact between the instrumented wheel and the rail circuit were unsuccessful in the field. It is recommended, therefore, that laboratory tests be conducted on an instrumented wheel to determine the transfer function between the wheel/rail contact patch and the strain gage bridge. A transient force impulse on the order of 10 milliseconds duration and 10,000 lb peak is recommended to provide good signal-to-noise ratio, and a two-channel real-time analyzer can be used to generate the amplitude and phase information.

The processing of data from the instrumented wheel proved to be inefficient, and improved methods for combining the signals from individual strain gage bridges are needed. A system to process vertical and lateral load signals in real time and provide continuous load signals, such as that demonstrated by the Swedish State Railways (SJ) on the recent ASEA locomotive tests on the Northeast Corridor, is recommended. A processing system that uses a sample/hold arrangement between bridges is not as desirable, due to the occasional unrealistically-high L/V ratio that may be calculated.

## APPENDIX A

### STATISTICAL ANALYSIS OF WHEEL/RAIL LOAD DATA

The tables in this appendix summarize all of the statistical data for mean values and standard deviations for each speed and car weight subcategory of the W/R load data base. The content of these tables is identified in the following sections.

Data Key. A 6-digit identification (key) number is used for each data category. The format for this key number is shown below with the possible combinations for numerical indices.

(A) EXPERIMENT NUMBER	(B) SECTION NUMBER	(C) MEASUREMENT SITE NUMBER	(D) VEHICLE NUMBER	(E) SPEED BAND (MPH)	(F) DATA CHANNEL
1=Pilot Study	1=BJR tangent	1 ... 7	1=locomotives	1=<40	1=lateral load
	2=CWR tangent	(see Figure 3-16)	2 = car >110T	2=40-49	2=vertical load
	3=6° curve	8=pooled data (all sites)	3=car 70T-110T	3=50-59	3=L/V ratio
			4=car 40T-70T	4=>60	4=joint vertical
			5=car <40T	On curve:	5=joint vertical (filtered)
			6=all vehicles	1=<35	6=joint dynamic load increment
				2=>35	7=CWR vertical
				5=all speed speeds	8=CWR vertical (filtered)
					9=CWR dynamic load increment

For example, the key number 113542 would designate vertical load data from the BJR test section, Site No. 3, empty cars (<40T GWT) in the >60 mph speed band. Battelle's interactive graphics program HPILOT can be used to plot individual curves for the probability density and distribution functions for any of the key numbers in the table. It is also possible to combine any of the categories for a specific data channel to give averages for these combinations.

Axle Count. The column labeled AXLES in Table A-1 gives the total number N of data points (one peak value for each axle) in the specified category.

Mean Load. The column labeled MEAN gives the mean value estimate  $\bar{p}$  of all peak load data  $p_i$  in that category using the equation

$$\bar{p} = \frac{1}{N} \sum_{i=1}^N p_i \quad (A-1)$$

Standard Deviation. The standard deviation (STD DEV)  $\sigma$  is calculated for each category from

$$\sigma^2 = \frac{1}{(N-1)} \sum_{i=1}^N (p_i - \bar{p})^2 \quad (A-2)$$

Confidence Limits. Confidence limits (percent) are calculated for the mean value estimates based on an assumed normal distribution for the sampling distribution of mean values. The true mean value  $\bar{p}_t$  is expected to be within a tolerance band of the estimated mean value as given by

$$\bar{p}_t = \bar{p} \pm \frac{\sigma t_{n;\alpha/2}}{\sqrt{N}}, \quad (A-3)$$

where  $t_{n;\alpha/2}$  is the student t probability distribution function which is readily available in statistical tables. The confidence statement for the range, or tolerance band, given by Equation (A-3) is that the true mean value  $\bar{p}_t$  will be in the specified range with a confidence level of 100 (1 -  $\alpha$ ) percent. Confidence limits in percent are listed for tolerance bands of  $\pm$  percent CONF (10) and  $\pm$  20 percent CONF (20) of the mean value.

Tolerance Bands. The columns labeled TOL (95) and TOL (90) give the mean value tolerance bands as a  $\pm$  percent of mean value for confidence limits of 95 and 90 percent, respectively. Data having large standard deviations and mean values close to zero typically show the lowest confidence levels and the largest tolerance bands.

TABLE A-1. STATISTICAL SUMMARY OF WAYSIDE WHEEL/RAIL LOAD DATA

KEY	AXLES	MEAN	STD DEV	CONF.(10%)	CONF.(20%)	TOI (95%)	TOI (90%)
111111	125.	-.135E+04	.681E+03	97.2	100.0	8.9	7.5
111112	125.	.333E+05	.358E+04	100.0	100.0	1.9	1.6
111113	125.	-.369E-01	.214E-01	94.4	100.0	10.3	8.6
111121	280.	-.146E+04	.695E+03	99.9	100.0	5.6	4.7
111122	280.	.346E+05	.350E+04	100.0	100.0	1.2	1.0
111123	280.	-.388E-01	.211E-01	99.8	100.0	6.4	5.4
111131	584.	-.109E+04	.947E+03	99.4	100.0	7.1	5.9
111132	584.	.334E+05	.360E+04	100.0	100.0	.9	.7
111133	584.	-.288E-01	.282E-01	98.6	100.0	8.0	6.7
111141	675.	-.129E+04	.968E+03	99.9	100.0	5.7	4.7
111142	675.	.338E+05	.380E+04	100.0	100.0	.8	.7
111143	675.	-.347E-01	.288E-01	99.8	100.0	6.3	5.3
111151	1664.	-.125E+04	.911E+03	100.0	100.0	3.5	2.9
111152	1664.	.338E+05	.369E+04	100.0	100.0	.5	.4
111153	1664.	-.335E-01	.272E-01	100.0	100.0	3.9	3.3
111211	281.	-.165E+04	.798E+03	99.9	100.0	5.7	4.8
111212	281.	.335E+05	.406E+04	100.0	100.0	1.4	1.2
111213	281.	-.461E-01	.252E-01	99.8	100.0	6.4	5.4
111221	550.	-.118E+04	.890E+03	99.8	100.0	6.3	5.3
111222	550.	.336E+05	.390E+04	100.0	100.0	1.0	.8
111223	550.	-.316E-01	.258E-01	99.6	100.0	6.8	5.7
111231	384.	-.126E+04	.991E+03	98.7	100.0	7.9	6.6
111232	384.	.335E+05	.413E+04	100.0	100.0	1.2	1.0
111233	384.	-.346E-01	.295E-01	97.8	100.0	8.6	7.2
111241	148.	-.109E+04	.144E+04	64.0	93.2	21.5	18.0
111242	148.	.338E+05	.392E+04	100.0	100.0	1.9	1.6
111243	148.	-.297E-01	.383E-01	65.3	93.9	20.9	17.5
111251	1363.	-.129E+04	.994E+03	100.0	100.0	4.1	3.4
111252	1363.	.336E+05	.400E+04	100.0	100.0	.6	.5
111253	1363.	-.352E-01	.289E-01	100.0	100.0	4.4	3.7
111311	98.	-.923E+03	.540E+03	90.7	99.9	11.7	9.8
111312	98.	.221E+05	.460E+04	100.0	100.0	4.2	3.5
111313	98.	-.431E-01	.252E-01	90.7	99.9	11.7	9.8
111321	697.	-.104E+04	.710E+03	100.0	100.0	5.1	4.3
111322	697.	.260E+05	.371E+04	100.0	100.0	1.1	.9
111323	697.	-.388E-01	.284E-01	100.0	100.0	5.4	4.6
111331	992.	-.103E+04	.903E+03	100.0	100.0	5.4	4.6
111332	992.	.250E+05	.356E+04	100.0	100.0	.9	.7
111333	992.	-.403E-01	.350E-01	100.0	100.0	5.4	4.5
111341	975.	-.750E+03	.112E+04	96.3	100.0	9.4	7.9
111342	975.	.243E+05	.343E+04	100.0	100.0	.9	.7
111343	975.	-.303E-01	.474E-01	95.4	100.0	9.8	8.2
111351	2762.	-.931E+03	.944E+03	100.0	100.0	3.8	3.2
111352	2762.	.249E+05	.370E+04	100.0	100.0	.6	.5
111353	2762.	-.365E-01	.385E-01	100.0	100.0	3.9	3.3
111411	149.	-.636E+03	.461E+03	90.6	99.9	11.7	9.8
111412	149.	.152E+05	.287E+04	100.0	100.0	3.1	2.6
111413	149.	-.477E-01	.316E-01	93.2	100.0	10.7	9.0
111421	631.	-.637E+03	.606E+03	99.1	100.0	7.4	6.2
111422	631.	.166E+05	.331E+04	100.0	100.0	1.6	1.3
111423	631.	-.436E-01	.364E-01	99.7	100.0	6.5	5.5
111431	1546.	-.638E+03	.755E+03	99.9	100.0	5.9	5.0
111432	1546.	.166E+05	.339E+04	100.0	100.0	1.0	.9
111433	1546.	-.429E-01	.479E-01	100.0	100.0	5.6	4.7
111441	2841.	-.645E+03	.103E+04	99.9	100.0	5.9	4.9

KEY	AXLES	MEAN	STD. DEV.	CONF.(10%)	CONF.(20%)	IDL(95%)	IDL(90%)
111442	2841.	.130E+05	.334E+04	100.0	100.0	.7	.6
111443	2841.	-.400E-01	.613E-01	99.9	100.0	5.6	4.7
111451	5167.	-.642E+03	.900E+03	100.0	100.0	3.8	3.2
111452	5167.	.174E+05	.343E+04	100.0	100.0	.5	.5
111453	5167.	-.415E-01	.543E-01	100.0	100.0	3.6	3.0
111511	732.	-.465E+03	.270E+03	100.0	100.0	4.2	3.5
111512	732.	.931E+04	.193E+04	100.0	100.0	1.5	1.3
111513	732.	-.688E-01	.299E-01	100.0	100.0	3.2	2.6
111521	1884.	-.611E+03	.564E+03	99.8	100.0	6.2	5.2
111522	1884.	.101E+05	.227E+04	100.0	100.0	1.0	.9
111523	1884.	-.575E-01	.554E-01	100.0	100.0	4.3	3.6
111531	4549.	-.357E+03	.862E+03	99.5	100.0	7.0	5.9
111532	4549.	.111E+05	.661E+04	100.0	100.0	1.7	1.5
111533	4549.	-.491E-01	.837E-01	100.0	100.0	5.0	4.2
111541	1594.	-.207E+03	.105E+04	56.9	88.4	24.9	20.9
111542	1594.	.961E+04	.239E+04	100.0	100.0	1.2	1.0
111543	1594.	-.424E-01	.103E+00	89.9	99.9	11.9	10.0
111551	8759.	-.351E+03	.816E+03	100.0	100.0	4.9	4.1
111552	8759.	.105E+05	.506E+04	100.0	100.0	1.0	.9
111553	8759.	-.513E-01	.797E-01	100.0	100.0	3.3	2.7
111611	1385.	-.838E+03	.698E+03	100.0	100.0	4.4	3.7
111612	1385.	.179E+05	.110E+05	100.0	100.0	3.2	2.7
111613	1385.	-.572E-01	.309E-01	100.0	100.0	2.8	2.4
111621	4042.	-.733E+03	.751E+03	100.0	100.0	3.2	2.7
111622	4042.	.188E+05	.101E+05	100.0	100.0	1.7	1.4
111623	4042.	-.473E-01	.447E-01	100.0	100.0	2.9	2.4
111631	8055.	-.590E+03	.914E+03	100.0	100.0	3.4	2.6
111632	8055.	.166E+05	.950E+04	100.0	100.0	1.3	1.1
111633	8055.	-.447E-01	.684E-01	100.0	100.0	3.3	2.6
111641	6233.	-.630E+03	.110E+04	100.0	100.0	4.3	3.6
111642	6233.	.189E+05	.817E+04	100.0	100.0	1.1	.9
111643	6233.	-.383E-01	.701E-01	100.0	100.0	4.6	3.8
111651	19715.	-.649E+03	.939E+03	100.0	100.0	2.0	1.7
111652	19715.	.179E+05	.941E+04	100.0	100.0	.7	.6
111653	19715.	-.441E-01	.630E-01	100.0	100.0	2.0	1.7
112111	136.	.147E+02	.176E+04	.8	1.6	2027.3	1697.7
112112	136.	.345E+05	.376E+04	100.0	100.0	1.8	1.5
112113	136.	.564E-02	.515E-01	10.2	20.1	154.6	129.5
112121	304.	.595E+03	.149E+04	51.4	83.6	28.2	23.6
112122	304.	.339E+05	.316E+04	100.0	100.0	1.1	.9
112123	304.	.221E-01	.442E-01	61.7	91.8	22.5	18.9
112131	595.	-.345E+02	.188E+04	3.6	7.1	438.6	367.9
112132	595.	.352E+05	.369E+04	100.0	100.0	.8	.7
112133	595.	.375E-02	.527E-01	13.8	27.1	113.3	95.0
112141	670.	.485E+03	.167E+04	54.8	86.8	26.1	21.9
112142	670.	.343E+05	.422E+04	670.	100.0	.9	.8
112143	670.	.187E-01	.478E-01	68.9	95.7	19.4	16.3
112151	1705.	.286E+03	.174E+04	50.2	82.4	28.9	24.3
112152	1705.	.346E+05	.386E+04	100.0	100.0	.5	.4
112153	1705.	.131E-01	.499E-01	72.0	96.9	18.2	15.2
112211	413.	-.217E+03	.139E+04	24.9	47.5	61.8	51.8
112212	413.	.358E+05	.405E+04	100.0	100.0	1.1	.9
112213	413.	-.153E-02	.384E-01	6.5	12.9	242.7	203.6
112221	758.	.529E+03	.160E+04	63.7	93.1	21.6	18.1
112222	758.	.347E+05	.357E+04	100.0	100.0	.7	.6

KEY	AXLES	MEAN	STD DEV	CONE(10:)	CONE(20:)	TOL(95:)	TOL(90:)
112223	758.	.200E-01	.477E-01	75.3	97.9	17.0	14.2
112231	384.	.251E+03	.173E+04	22.3	43.0	62.2	58.1
112232	384.	.330E+05	.374E+04	100.0	100.0	1.1	1.0
112233	384.	.113E-01	.546E-01	31.4	56.1	48.7	40.8
112241	160.	.553E+03	.221E+04	24.8	47.2	62.5	52.4
112242	160.	.313E+05	.573E+04	100.0	100.0	2.9	2.4
112243	160.	.212E-01	.601E-01	34.3	62.5	44.4	37.2
112251	1715.	.289E+03	.168E+04	52.4	84.5	27.5	23.1
112252	1715.	.343E+05	.419E+04	100.0	100.0	.6	.5
112253	1715.	.130E-01	.494E-01	72.3	97.0	18.0	15.1
112311	100.	.364E+03	.103E+04	27.5	51.7	56.3	47.1
112312	100.	.234E+05	.352E+04	100.0	100.0	3.0	2.5
112313	100.	.179E-01	.457E-01	30.5	56.6	50.5	42.2
112321	824.	.392E+03	.145E+04	56.2	87.9	25.3	21.2
112322	824.	.279E+05	.491E+04	100.0	100.0	1.2	1.0
112323	824.	.181E-01	.533E-01	67.0	94.8	20.1	16.9
112331	994.	.237E+03	.142E+04	40.2	70.8	37.2	31.2
112332	994.	.269E+05	.468E+04	100.0	100.0	1.1	.9
112333	994.	.122E-01	.538E-01	52.6	84.8	27.4	23.0
112341	996.	.564E+03	.153E+04	75.4	98.0	16.9	14.2
112342	996.	.221E+05	.472E+04	100.0	100.0	1.3	1.1
112343	956.	.259E-01	.694E-01	76.0	98.1	16.7	14.0
112351	2914.	.397E+03	.146E+04	85.7	99.7	13.4	11.2
112352	2914.	.254E+05	.541E+04	100.0	100.0	.8	.6
112353	2914.	.187E-01	.595E-01	91.1	99.9	11.5	9.7
112411	164.	.297E+03	.650E+03	44.0	75.6	33.8	28.3
112412	164.	.154E+05	.300E+04	100.0	100.0	3.0	2.5
112413	164.	.161E-01	.419E-01	37.7	67.4	40.1	33.6
112421	824.	.452E+03	.105E+04	78.1	98.6	16.0	13.4
112422	824.	.170E+05	.380E+04	100.0	100.0	1.5	1.3
112423	824.	.231E-01	.612E-01	72.2	97.0	18.1	15.2
112431	1578.	.224E+03	.110E+04	58.0	89.3	24.3	20.4
112432	1578.	.174E+05	.476E+04	100.0	100.0	1.3	1.1
112433	1578.	.995E-02	.619E-01	47.7	79.8	30.7	25.8
112441	2872.	.562E+03	.139E+04	96.9	100.0	9.1	7.6
112442	2872.	.175E+05	.352E+04	100.0	100.0	.7	.6
112443	2872.	.293E-01	.795E-01	95.2	100.0	9.9	8.3
112451	5438.	.439E+03	.126E+04	99.0	100.0	7.6	6.4
112452	5438.	.173E+05	.396E+04	100.0	100.0	.6	.5
112453	5438.	.224E-01	.717E-01	97.8	100.0	8.5	7.2
112511	804.	.644E+02	.273E+03	49.7	81.9	29.3	24.6
112512	804.	.935E+04	.225E+04	100.0	100.0	1.7	1.4
112513	604.	.627E-02	.302E-01	44.3	76.0	33.4	28.0
112521	1978.	.279E+03	.824E+03	86.8	99.7	13.0	10.9
112522	1978.	.997E+04	.201E+04	100.0	100.0	.9	.7
112523	1978.	.151E-01	.804E-01	59.5	90.4	23.5	19.7
112531	4844.	.167E+03	.941E+03	78.3	98.7	15.9	13.3
112532	4844.	.111E+05	.652E+04	100.0	100.0	1.7	1.4
112533	4844.	.130E-03	.785E-01	.9	1.8	1706.9	1432.5
112541	1692.	.419E+03	.132E+04	80.9	99.1	15.0	12.6
112542	1692.	.103E+05	.285E+04	100.0	100.0	1.3	1.1
112543	1692.	.224E-01	.105E+00	61.9	92.0	22.4	18.8
112551	9318.	.228E+03	.968E+03	97.7	100.0	8.6	7.2
112552	9318.	.106E+05	.502E+04	100.0	100.0	1.0	.8
112553	9318.	.679E-02	.022E-01	57.5	88.9	24.6	20.6

KEY	AXLES	MEAN	STD DEV	CONF(10%)	CONF(20%)	IQL(95%)	IQL(90%)
112611	1617.	.303E+02	.963E+03	10.1	20.0	154.0	129.9
112612	1617.	.197E+05	.123E+05	100.0	100.0	3.0	2.5
112613	1617.	-.288E-03	.378E-01	2.4	4.9	641.6	538.2
112621	4688.	.390E+03	.119E+04	97.5	100.0	4.7	7.3
112622	4688.	.199E+05	.107E+05	100.0	100.0	1.5	1.3
112623	4688.	.183E-01	.663E-01	94.1	100.0	10.4	8.7
112631	8395.	.176E+03	.117E+04	83.1	95.4	14.2	12.0
112632	8395.	.165E+05	.100E+05	100.0	100.0	1.3	1.1
112633	8395.	.417E-02	.706E-01	41.2	72.2	36.2	30.4
112641	6390.	.516E+03	.145E+04	99.5	100.0	5.9	5.8
112642	6390.	.184E+05	.802E+04	100.0	100.0	1.1	.9
112643	6390.	.256E-01	.828E-01	98.7	100.0	7.9	6.7
112651	21090.	.315E+03	.126E+04	100.0	100.0	5.4	4.5
112652	21090.	.182E+05	.938E+04	100.0	100.0	.7	.6
112653	21090.	.135E-01	.724E-01	99.3	100.0	7.3	6.1
113111	136.	-.624E+03	.153E+04	36.5	65.7	41.5	34.8
113112	136.	.335E+05	.359E+04	100.0	100.0	1.8	1.5
113113	136.	-.161E-01	.425E-01	34.2	62.3	44.6	37.4
113114	70.	.372E+05	.362E+04	100.0	100.0	2.3	1.9
113115	70.	.348E+05	.351E+04	100.0	100.0	2.4	2.0
113116	70.	.261E+04	.864E+03	98.6	100.0	7.9	6.6
113121	321.	-.482E+03	.146E+04	44.7	76.4	33.2	27.8
113122	321.	.343E+05	.356E+04	100.0	100.0	1.1	1.0
113123	321.	-.101E-01	.419E-01	33.5	61.4	45.4	38.0
113124	144.	.380E+05	.399E+04	100.0	100.0	1.7	1.4
113125	144.	.339E+05	.378E+04	100.0	100.0	1.6	1.5
113126	144.	.439E+04	.139E+04	100.0	100.0	5.2	4.4
113131	458.	-.973E+03	.124E+04	90.6	99.9	11.7	9.8
113132	458.	.321E+05	.366E+04	100.0	100.0	1.0	.9
113133	458.	-.273E-01	.326E-01	85.8	99.7	13.4	11.2
113134	258.	.388E+05	.384E+04	100.0	100.0	1.2	1.0
113135	258.	.346E+05	.337E+04	100.0	100.0	1.2	1.0
113136	258.	.445E+04	.140E+04	100.0	100.0	3.9	3.2
113141	706.	-.666E+03	.118E+04	86.6	99.7	13.1	11.0
113142	706.	.330E+05	.407E+04	100.0	100.0	.9	.8
113143	706.	-.176E-01	.365E-01	72.8	96.9	15.4	12.9
113144	382.	.392E+05	.508E+04	100.0	100.0	1.3	1.1
113145	382.	.342E+05	.445E+04	100.0	100.0	1.3	1.1
113146	382.	.521E+04	.158E+04	100.0	100.0	3.1	2.6
113151	1621.	-.713E+03	.130E+04	97.3	100.0	8.9	7.5
113152	1621.	.331E+05	.389E+04	100.0	100.0	.6	.5
113153	1621.	-.187E-01	.395E-01	94.3	100.0	10.3	8.6
113154	854.	.387E+05	.449E+04	100.0	100.0	.8	.7
113155	854.	.343E+05	.397E+04	100.0	100.0	.8	.7
113156	854.	.463E+04	.161E+04	100.0	100.0	2.3	2.0
113211	414.	-.115E+04	.905E+03	99.0	100.0	7.6	6.4
113212	414.	.343E+05	.408E+04	100.0	100.0	1.2	1.0
113213	414.	-.236E-01	.258E-01	97.6	100.0	8.7	7.3
113214	394.	.358E+05	.453E+04	100.0	100.0	1.3	1.1
113215	394.	.337E+05	.415E+04	100.0	100.0	1.2	1.0
113216	394.	.239E+04	.167E+04	99.5	100.0	6.9	5.8
113221	879.	-.929E+03	.105E+04	99.1	100.0	7.5	6.3
113222	879.	.334E+05	.393E+04	100.0	100.0	.8	.7
113223	879.	-.239E-01	.297E-01	98.3	100.0	8.2	6.9
113224	500.	.360E+05	.485E+04	100.0	100.0	1.2	1.0

KEY	AXLES	MEAN	STD. DEV.	CONF (10%)	CONF (20%)	TOL (95%)	TOL (90%)
113225	500.	.312E+05	.372E+04	100.0	100.0	1.0	.9
113226	500.	.509E+04	.244E+04	100.0	100.0	4.2	3.5
113231	284.	-.906E+03	.117E+04	80.7	99.0	15.1	12.6
113232	284.	.324E+05	.434E+04	100.0	100.0	1.6	1.3
113233	284.	-.243E-01	.358E-01	74.6	97.7	17.2	14.4
113234	276.	.351E+05	.463E+04	100.0	100.0	1.6	1.3
113235	276.	.301E+05	.335E+04	100.0	100.0	1.3	1.1
113236	276.	.523E+04	.235E+04	100.0	100.0	5.3	4.5
113241	200.	-.776E+03	.121E+04	63.3	92.8	21.8	18.3
113242	200.	.325E+05	.341E+04	100.0	100.0	1.5	1.2
113243	200.	-.199E-01	.381E-01	54.0	86.0	26.6	22.3
113244	100.	.376E+05	.506E+04	100.0	100.0	2.7	2.2
113245	100.	.320E+05	.433E+04	100.0	100.0	2.7	2.2
113246	100.	.578E+04	.143E+04	100.0	100.0	4.9	4.1
113251	1777.	-.959E+03	.107E+04	100.0	100.0	5.2	4.3
113252	1777.	.333E+05	.403E+04	100.0	100.0	.6	.5
113253	1777.	-.246E-01	.311E-01	99.9	100.0	5.9	4.9
113254	1270.	.359E+05	.476E+04	100.0	100.0	.7	.6
113255	1270.	.318E+05	.407E+04	100.0	100.0	.7	.6
113256	1270.	.434E+04	.251E+04	100.0	100.0	3.2	2.7
113311	100.	-.454E+03	.641E+03	52.0	84.0	28.0	23.4
113312	100.	.225E+05	.336E+04	100.0	100.0	3.0	2.5
113313	100.	-.186E-01	.267E-01	51.2	83.3	28.5	23.8
113314	76.	.222E+05	.533E+04	99.9	100.0	5.5	4.6
113315	76.	.201E+05	.192E+04	100.0	100.0	2.2	1.6
113316	76.	.304E+04	.152E+04	91.5	99.9	11.4	9.5
113321	889.	-.529E+03	.106E+04	86.3	99.7	13.2	11.1
113322	889.	.258E+05	.402E+04	100.0	100.0	1.0	.9
113323	889.	-.194E-01	.408E-01	84.4	99.5	13.8	11.6
113324	515.	.260E+05	.807E+04	100.0	100.0	2.7	2.3
113325	515.	.232E+05	.454E+04	100.0	100.0	1.7	1.4
113326	515.	.408E+04	.168E+04	100.0	100.0	3.6	3.0
113331	782.	-.706E+03	.867E+03	97.7	100.0	8.6	7.2
113332	782.	.250E+05	.390E+04	100.0	100.0	1.1	.9
113333	782.	-.265E-01	.367E-01	95.6	100.0	9.7	8.2
113334	656.	.261E+05	.881E+04	100.0	100.0	2.6	2.2
113335	656.	.234E+05	.412E+04	100.0	100.0	1.4	1.1
113336	656.	.430E+04	.256E+04	100.0	100.0	4.6	3.8
113341	1163.	-.397E+03	.105E+04	80.2	99.0	15.2	12.8
113342	1163.	.235E+05	.358E+04	100.0	100.0	.9	.7
113343	1163.	-.162E-01	.474E-01	75.7	98.0	16.8	14.1
113344	630.	.191E+05	.106E+05	100.0	100.0	4.4	3.7
113345	630.	.199E+05	.370E+04	100.0	100.0	1.5	1.2
113346	630.	.329E+04	.204E+04	100.0	100.0	4.1	4.1
113351	2934.	-.521E+03	.100E+04	99.5	100.0	7.0	5.9
113352	2934.	.245E+05	.394E+04	100.0	100.0	.6	.5
113353	2934.	-.200E-01	.424E-01	98.9	100.0	7.7	6.4
113354	1877.	.235E+05	.974E+04	100.0	100.0	1.9	1.6
113355	1877.	.220E+05	.437E+04	100.0	100.0	.9	.8
113356	1877.	.385E+04	.219E+04	100.0	100.0	2.6	2.2
113411	164.	-.213E+03	.359E+03	55.3	87.0	25.9	21.7
113412	164.	.147E+05	.277E+04	100.0	100.0	2.9	2.4
113413	164.	-.194E-01	.248E-01	68.1	95.3	19.8	16.6
113414	56.	.450E+04	.616E+04	41.3	72.1	36.6	30.6
113415	56.	.137E+05	.305E+04	99.9	100.0	6.0	5.0

KEY	AXLES	MEAN	STD DEV	CONE (10%)	CONE (20%)	TOL (95%)	TOL (90%)
113416 #	56.	.979E+03	.837E+03	39.3	69.5	38.7	32.3
113421	820.	-.166E+03	.720E+03	46.1	78.1	31.9	26.8
113422	820.	.162E+05	.344E+04	100.0	100.0	1.5	1.2
113423	820.	-.146E-01	.501E-01	59.5	90.4	23.5	19.7
113424	448.	.844E+04	.863E+04	96.1	100.0	9.5	8.0
113425	448.	.139E+05	.366E+04	100.0	100.0	2.4	2.0
113426 #	448.	.143E+04	.154E+04	94.9	100.0	10.0	8.4
113431	1160.	-.349E+03	.806E+03	85.9	99.7	13.3	11.2
113432	1160.	.161E+05	.394E+04	100.0	100.0	1.4	1.2
113433	1160.	-.265E-01	.637E-01	84.3	99.5	13.9	11.6
113434	864.	.102E+05	.945E+04	99.9	100.0	6.2	5.2
113435	864.	.151E+05	.416E+04	100.0	100.0	1.8	1.5
113436 #	864.	.167E+04	.181E+04	99.3	100.0	7.2	6.1
113441	3108.	-.188E+03	.114E+04	64.2	93.4	21.3	17.9
113442	3108.	.180E+05	.375E+04	100.0	100.0	.7	.6
113443	3108.	-.142E-01	.645E-01	78.1	98.6	16.0	13.4
113444	1858.	.115E+05	.950E+04	100.0	100.0	3.8	3.2
113445	1858.	.155E+05	.364E+04	100.0	100.0	1.1	.9
113446 #	1858.	.201E+04	.191E+04	100.0	100.0	4.3	3.6
113451	5252.	-.221E+03	.101E+04	83.8	99.9	12.3	10.3
113452	5252.	.172E+05	.385E+04	100.0	100.0	.6	.5
113453	5252.	-.171E-01	.616E-01	95.6	100.0	9.7	8.2
113454	3226.	.106E+05	.942E+04	100.0	100.0	3.1	2.6
113455	3226.	.152E+05	.332E+04	100.0	100.0	.9	.7
113456 #	3226.	.181E+04	.184E+04	100.0	100.0	3.5	2.9
113511	804.	-.163E+03	.229E+03	95.6	100.0	9.7	8.2
113512	804.	.891E+04	.183E+04	100.0	100.0	1.4	1.2
113513	804.	-.351E-01	.273E-01	100.0	100.0	5.4	4.5
113514	356.	.168E+04	.889E+03	100.0	100.0	5.5	4.6
113515	356.	.758E+04	.149E+04	100.0	100.0	2.0	1.7
113516 #	356.	.304E+03	.794E+02	100.0	100.0	2.7	2.3
113521	2050.	-.785E+02	.622E+03	43.2	74.7	34.3	28.8
113522	2050.	.966E+04	.202E+04	100.0	100.0	.9	.8
113523	2050.	-.249E-01	.658E-01	91.4	99.9	11.4	9.6
113524	772.	.415E+04	.449E+04	99.0	100.0	7.6	6.4
113525	772.	.794E+04	.169E+04	100.0	100.0	1.5	1.3
113526 #	772.	.841E+03	.939E+03	96.7	100.0	7.9	6.6
113531 *	3722.	-.159E+03	.841E+03	75.1	97.9	17.0	14.3
113532 *	3722.	.105E+05	.698E+04	100.0	100.0	2.1	1.8
113533 *	3722.	-.306E-01	.865E-01	96.9	100.0	9.1	7.6
113534 *	1298.	.521E+04	.440E+04	100.0	100.0	4.6	3.9
113535 *	1298.	.771E+04	.156E+04	100.0	100.0	1.1	.9
113536 #	1298.	.114E+04	.111E+04	100.0	100.0	5.3	4.4
113541	1314.	.435E+02	.113E+04	11.1	21.9	140.9	118.2
113542	1314.	.941E+04	.268E+04	100.0	100.0	1.5	1.3
113543	1314.	-.182E-01	.115E+00	43.4	74.9	34.1	28.6
113544	498.	.423E+04	.501E+04	94.0	100.0	10.4	8.7
113545	498.	.844E+04	.237E+04	100.0	100.0	2.5	2.1
113546 #	498.	.963E+03	.119E+04	92.8	100.0	10.9	9.1
113551	7890.	-.105E+03	.812E+03	74.8	97.8	17.1	14.4
113552	7890.	.995E+04	.509E+04	100.0	100.0	1.1	.9
113553	7890.	-.275E-01	.834E-01	99.7	100.0	6.7	5.6
113554	2924.	.434E+04	.441E+04	100.0	100.0	3.7	3.1
113555	2924.	.788E+04	.177E+04	100.0	100.0	.8	.7
113556 #	2924.	.928E+03	.104E+04	100.0	100.0	4.1	3.4

# Suspected data processing problem

KEY	AXLES	MEAN	STD DEV	CONE (10:1)	CONE (20:1)	TOL (95:1)	TOL (90:1)
113611	1618.	-.477E+03	.802E+03	98.3	100.0	8.2	6.9
113612	1618.	-.189E+05	.118E+05	100.0	100.0	3.0	2.6
113613	1618.	-.293E-01	.291E-01	100.0	100.0	4.8	4.1
113614	952.	-.202E+05	.167E+05	100.0	100.0	5.3	4.4
113615	952.	-.217E+05	.127E+05	100.0	100.0	3.7	3.1
113616	#	-.157E+04	.152E+04	99.7	100.0	6.6	5.5
113621	4959.	-.351E+03	.947E+03	99.1	100.0	7.5	6.3
113622	4959.	-.194E+05	.104E+05	100.0	100.0	1.5	1.2
113623	4959.	-.211E-01	.529E-01	99.5	100.0	7.0	5.9
113624	2379.	-.184E+05	.150E+05	100.0	100.0	3.3	2.8
113625	2379.	-.186E+05	.102E+05	100.0	100.0	2.2	1.8
113626	#	-.276E+04	.243E+04	100.0	100.0	3.5	3.0
113631	6406.	-.351E+03	.932E+03	99.7	100.0	6.5	5.5
113632	6406.	-.158E+05	.961E+04	100.0	100.0	1.5	1.2
113633	6406.	-.288E-01	.736E-01	99.8	100.0	6.3	5.2
113634	3352.	-.156E+05	.139E+05	100.0	100.0	3.0	2.5
113635	3352.	-.166E+05	.953E+04	100.0	100.0	1.9	1.6
113636	#	-.248E+04	.238E+04	100.0	100.0	3.2	2.7
113641	6491.	-.249E+03	.115E+04	91.8	99.9	11.3	9.5
113642	6491.	-.193E+05	.789E+04	100.0	100.0	1.0	.8
113643	6491.	-.159E-01	.725E-01	92.3	100.0	11.1	9.3
113644	3468.	-.156E+05	.135E+05	100.0	100.0	2.9	2.4
113645	3468.	-.178E+05	.803E+04	100.0	100.0	1.5	1.3
113646	#	-.255E+04	.222E+04	100.0	100.0	2.9	2.4
113651	19474.	-.327E+03	.101E+04	100.0	100.0	4.3	3.6
113652	19474.	-.182E+05	.963E+04	100.0	100.0	.7	.5
113653	19474.	-.226E-01	.660E-01	100.0	100.0	4.1	3.4
113654	10151.	-.167E+05	.144E+05	100.0	100.0	1.7	1.4
113655	10151.	-.180E+05	.968E+04	100.0	100.0	1.0	.9
113656	#	-.249E+04	.230E+04	100.0	100.0	1.8	1.5
114111	132.	-.350E+03	.165E+04	19.2	37.3	81.3	68.1
114112	132.	-.306E+05	.347E+04	100.0	100.0	2.0	1.6
114113	132.	-.778E-02	.550E-01	12.9	25.5	121.6	101.8
114121	352.	-.285E+03	.156E+04	26.8	50.6	57.5	48.2
114122	352.	-.310E+05	.308E+04	100.0	100.0	1.0	.9
114123	352.	-.609E-02	.507E-01	17.8	34.7	87.3	73.2
114131	596.	-.207E+03	.174E+04	22.8	43.8	67.6	56.7
114132	596.	-.320E+05	.357E+04	100.0	100.0	.9	.8
114133	596.	-.291E-02	.553E-01	10.2	20.3	152.7	128.1
114141	761.	-.285E+03	.164E+04	36.8	66.1	41.0	34.4
114142	761.	-.311E+05	.401E+04	100.0	100.0	.9	.8
114143	761.	-.505E-02	.547E-01	20.1	36.9	77.1	64.6
114151	1841.	-.264E+03	.166E+04	50.5	92.8	28.7	24.1
114152	1841.	-.313E+05	.370E+04	100.0	100.0	.5	.5
114153	1841.	-.475E-02	.542E-01	29.3	54.8	52.1	43.7
114211	409.	-.150E+04	.100E+04	99.7	100.0	6.5	5.4
114212	409.	-.295E+05	.330E+04	100.0	100.0	1.1	.9
114213	409.	-.479E-01	.341E-01	99.5	100.0	6.9	5.8
114221	934.	-.735E+03	.143E+04	88.5	99.8	12.5	10.4
114222	934.	-.304E+05	.387E+04	100.0	100.0	.8	.7
114223	934.	-.210E-01	.457E-01	84.0	99.5	14.0	11.7
114231	380.	-.552E+03	.153E+04	51.9	84.1	27.9	23.4
114232	380.	-.298E+05	.419E+04	100.0	100.0	1.4	1.2
114233	380.	-.144E-01	.512E-01	41.6	72.6	35.9	30.1
114241	212.	-.194E+03	.162E+04	13.9	27.3	112.8	94.6

KEY	AXES	MEAN	STD DEV	CONF(10%)	CONF(20%)	YOL(95%)	YOL(90%)
114242	212.	.268E+05	.437E+04	100.0	100.0	2.5	2.1
114243	212.	-.408E-02	.597E-01	7.3	15.8	193.0	165.9
114251	1935.	-.201E+03	.145E+04	98.5	100.0	8.0	6.8
114252	1935.	.297E+05	.411E+04	100.0	100.0	.6	.5
114253	1935.	-.239E-01	.484E-01	96.7	100.0	9.2	7.7
114311	100.	-.198E+03	.127E+04	12.4	24.6	126.5	105.9
114312	100.	.205E+05	.484E+04	100.0	100.0	4.7	3.9
114313	100.	-.853E-02	.664E-01	10.2	20.2	154.5	129.2
114321	1008.	-.270E+03	.127E+04	50.1	82.3	29.0	24.4
114322	1008.	.233E+05	.383E+04	100.0	100.0	1.0	.9
114323	1008.	-.101E-01	.543E-01	44.6	76.3	33.2	27.8
114331	994.	-.245E+03	.129E+04	44.9	76.7	32.9	27.6
114332	994.	.235E+05	.411E+04	100.0	100.0	1.1	.9
114333	994.	-.613E-02	.569E-01	34.7	63.2	43.6	36.6
114341	1216.	.206E+03	.143E+04	38.5	68.5	39.0	32.7
114342	1216.	.202E+05	.344E+04	100.0	100.0	1.0	.8
114343	1216.	.115E-01	.724E-01	42.2	73.4	35.3	29.6
114351	3318.	-.857E+02	.135E+04	28.4	53.4	53.8	45.1
114352	3318.	.221E+05	.412E+04	100.0	100.0	.6	.5
114353	3318.	-.153E-02	.634E-01	11.1	22.0	140.6	118.0
114411	158.	-.106E+03	.647E+03	16.2	31.8	96.2	80.6
114412	158.	.134E+05	.275E+04	100.0	100.0	3.2	2.7
114413	158.	-.148E-01	.488E-01	29.6	55.2	51.9	43.5
114421	916.	.235E+01	.908E+03	.6	1.2	2507.4	2103.6
114422	916.	.146E+05	.313E+04	100.0	100.0	1.4	1.2
114423	916.	-.560E-02	.623E-01	21.4	41.3	72.2	60.6
114431	1572.	.444E+02	.107E+04	13.1	25.8	119.1	99.9
114432	1572.	.151E+05	.362E+04	100.0	100.0	1.2	1.0
114433	1572.	-.147E-02	.759E-01	6.1	12.2	254.5	213.5
114441	3304.	.190E+03	.119E+04	64.4	93.5	21.2	17.8
114442	3304.	.153E+05	.311E+04	100.0	100.0	.7	.6
114443	3304.	.746E-02	.811E-01	40.3	71.0	37.1	31.1
114451	5950.	.115E+03	.111E+04	57.7	89.1	24.5	20.5
114452	5950.	.151E+05	.327E+04	100.0	100.0	.6	.5
114453	5950.	.250E-02	.766E-01	19.9	38.5	77.9	65.4
114511	796.	-.670E+02	.320E+03	44.6	76.3	33.2	27.8
114512	796.	.893E+04	.162E+04	100.0	100.0	1.3	1.1
114513	796.	-.234E-01	.362E-01	93.2	100.0	10.7	9.0
114521	2132.	-.178E+01	.633E+03	1.0	2.1	1506.9	1264.6
114522	2132.	.923E+04	.227E+04	100.0	100.0	1.0	.9
114523	2132.	-.162E-01	.670E-01	73.6	97.4	17.6	14.7
114531	4804.	-.207E+02	.855E+03	13.3	26.2	117.1	98.2
114532	4804.	.100E+05	.546E+04	100.0	100.0	1.5	1.3
114533	4804.	-.136E-01	.846E-01	73.5	97.4	17.6	14.8
114541	1771.	.799E+01	.867E+03	3.1	6.2	505.6	424.1
114542	1771.	.914E+04	.256E+04	100.0	100.0	1.3	1.1
114543	1771.	-.176E-01	.672E-01	60.6	91.1	23.0	19.3
114551	9503.	-.150E+02	.780E+03	14.8	29.2	104.8	87.9
114552	9503.	.959E+04	.423E+04	100.0	100.0	.9	.7
114553	9503.	-.158E-01	.784E-01	95.0	100.0	10.0	8.4
114611	1595.	-.470E+03	.102E+04	93.3	100.0	10.7	9.0
114612	1595.	.172E+05	.987E+04	100.0	100.0	2.8	2.4
114613	1595.	-.266E-01	.436E-01	98.5	100.0	8.0	6.7
114621	5342.	-.198E+03	.109E+04	81.6	99.2	14.8	12.4
114622	5342.	.180E+05	.926E+04	100.0	100.0	1.4	1.2

KEY	AXLES	MEAN	STD DEV	CONF (10%)	CONF (20%)	TOL (95%)	TOL (90%)
114623	5342.	-0.134E-01	.598E-01	89.9	99.9	12.0	10.0
114631	8346.	-0.726E+02	.108E+04	45.9	77.9	32.1	26.9
114632	8346.	.150E+05	.876E+04	100.0	100.0	1.2	1.0
114633	8346.	-0.994E-02	.771E-01	76.1	98.1	16.6	14.0
114641	7264.	.876E+02	.124E+04	45.1	77.0	32.7	27.4
114642	7264.	.166E+05	.721E+04	100.0	100.0	1.0	.8
114643	7264.	.375E-03	.791E-01	3.2	6.4	485.2	407.2
114651	22547.	-0.789E+02	.115E+04	69.9	96.1	19.0	15.9
114652	22547.	.164E+05	.858E+04	100.0	100.0	.7	.6
114653	22547.	-0.662E-02	.725E-01	92.6	100.0	11.0	9.2
115111	132.	.225E+03	.934E+03	21.9	41.9	71.5	59.8
115112	132.	.361E+05	.363E+04	100.0	100.0	1.7	1.5
115113	132.	.110E-01	.254E-01	37.9	67.7	39.9	33.4
115121	351.	.433E+03	.103E+04	57.1	88.6	24.8	20.8
115122	351.	.359E+05	.365E+04	100.0	100.0	1.1	.9
115123	351.	.167E-01	.287E-01	72.4	97.0	18.0	15.1
115131	596.	.223E+03	.110E+04	38.1	68.0	39.5	33.1
115132	596.	.354E+05	.357E+04	100.0	100.0	.8	.7
115133	596.	.111E-01	.312E-01	61.3	91.6	22.7	19.0
115141	770.	.535E+03	.116E+04	79.8	98.9	15.4	12.9
115142	770.	.361E+05	.399E+04	100.0	100.0	.8	.7
115143	770.	.199E-01	.324E-01	91.1	99.9	11.5	9.7
115151	1849.	.393E+03	.111E+04	87.2	99.8	12.9	10.8
115152	1849.	.359E+05	.378E+04	100.0	100.0	.5	.4
115153	1849.	.158E-01	.311E-01	97.1	100.0	9.0	7.5
115211	409.	-0.302E+03	.111E+04	41.8	72.9	35.7	29.9
115212	409.	.366E+05	.415E+04	100.0	100.0	1.1	.9
115213	409.	-0.221E-02	.307E-01	11.6	22.9	134.9	113.1
115221	934.	.240E+03	.885E+03	59.2	90.2	23.7	19.9
115222	934.	.318E+05	.423E+04	100.0	100.0	.8	.7
115223	934.	.120E-01	.274E-01	81.9	99.2	14.7	12.3
115231	380.	.344E+03	.113E+04	44.8	76.5	33.1	27.7
115232	380.	.334E+05	.362E+04	100.0	100.0	1.1	.9
115233	380.	.149E-01	.344E-01	60.2	90.9	23.2	19.5
115241	212.	.228E+03	.115E+04	22.8	43.7	68.0	57.0
115242	212.	.301E+05	.765E+04	100.0	100.0	3.4	2.9
115243	212.	.993E-02	.369E-01	30.4	56.5	50.4	42.2
115251	1935.	.144E+03	.104E+04	45.8	77.7	32.1	27.0
115252	1935.	.339E+05	.494E+04	100.0	100.0	.6	.5
115253	1935.	.936E-02	.313E-01	81.1	99.1	14.9	12.5
115311	100.	.493E+03	.124E+04	30.9	57.3	49.8	41.6
115312	100.	.239E+05	.367E+04	100.0	100.0	3.0	2.6
115313	100.	.234E-01	.547E-01	33.1	60.6	46.3	38.8
115321	1008.	.286E+03	.933E+03	67.0	94.8	20.1	16.9
115322	1008.	.275E+05	.544E+04	100.0	100.0	1.2	1.0
115323	1008.	.126E-01	.350E-01	74.5	97.8	17.1	14.3
115331	994.	.168E+03	.111E+04	36.8	66.2	40.9	34.3
115332	994.	.269E+05	.496E+04	100.0	100.0	1.1	1.0
115333	994.	.858E-02	.426E-01	47.5	79.6	30.9	25.9
115341	1216.	.576E+03	.115E+04	91.8	99.9	11.3	9.4
115342	1216.	.228E+05	.424E+04	100.0	100.0	1.0	.9
115343	1216.	.263E-01	.488E-01	94.0	100.0	10.4	8.8
115351	3318.	.363E+03	.109E+04	94.4	100.0	10.2	8.6
115352	3318.	.255E+05	.528E+04	100.0	100.0	.7	.6
115353	3318.	.167E-01	.440E-01	97.2	100.0	8.9	7.5

KEY	AXLES	MEAN	STD DEV	CONF (10%)	CONF (20%)	TOL (95%)	TOL (90%)
115411	156.	.338E+03	.579E+03	53.2	85.2	27.1	22.7
115412	156.	.156E+05	.289E+04	100.0	100.0	2.9	2.5
115413	156.	.189E-01	.361E-01	48.6	80.8	30.2	25.3
115421	916.	.374E+03	.852E+03	81.6	99.2	14.8	12.4
115422	916.	.174E+05	.405E+04	100.0	100.0	1.5	1.3
115423	916.	.187E-01	.471E-01	77.1	98.4	16.3	13.7
115431	1572.	.141E+03	.861E+03	48.3	80.5	30.3	25.4
115432	1572.	.171E+05	.480E+04	100.0	100.0	1.4	1.2
115433	1572.	.346E-02	.547E-01	19.8	38.4	78.1	65.5
115441	3304.	.437E+03	.101E+04	98.7	100.0	7.9	6.7
115442	3304.	.181E+05	.386E+04	100.0	100.0	.7	.6
115443	3304.	.214E-01	.557E-01	97.3	100.0	8.9	7.4
115451	5948.	.346E+03	.951E+03	99.5	100.0	7.0	5.9
115452	5948.	.176E+05	.417E+04	100.0	100.0	.6	.5
115453	5948.	.162E-01	.543E-01	97.8	100.0	8.5	7.2
115511	531.	.108E+03	.304E+03	58.8	89.9	23.9	20.1
115512	531.	.961E+04	.226E+04	100.0	100.0	2.0	1.7
115513	531.	-.203E-02	.326E-01	11.4	22.6	136.7	114.6
115521	2129.	.129E+03	.537E+03	73.2	97.3	17.7	14.8
115522	2129.	.991E+04	.300E+04	100.0	100.0	1.3	1.1
115523	2129.	-.146E-02	.501E-01	10.7	21.2	145.8	122.4
115531	* 4803.	.225E+02	.734E+03	16.8	32.9	92.2	77.4
115532	* 4803.	.105E+05	.683E+04	100.0	100.0	1.8	1.6
115533	* 4803.	-.127E-01	.766E-01	74.9	97.8	17.1	14.3
115541	1772.	.224E+03	.822E+03	74.9	97.6	17.1	14.3
115542	1772.	.975E+04	.313E+04	100.0	100.0	1.5	1.3
115543	1772.	.447E-02	.725E-01	20.5	39.7	75.5	63.3
115551	9235.	.907E+02	.699E+03	78.8	98.7	15.7	13.2
115552	9235.	.101E+05	.535E+04	100.0	100.0	1.1	.9
115553	9235.	-.619E-02	.689E-01	61.2	91.6	22.7	19.1
115611	1328.	.494E+02	.850E+03	16.8	32.8	92.5	77.6
115612	1328.	.223E+05	.127E+05	100.0	100.0	3.1	2.6
115613	1328.	.358E-02	.353E-01	28.9	54.1	53.0	44.4
115621	5338.	.240E+03	.788E+03	97.4	100.0	8.8	7.4
115622	5338.	.204E+05	.109E+05	100.0	100.0	1.4	1.2
115623	5338.	.822E-02	.432E-01	83.6	98.5	14.1	11.8
115631	8345.	.911E+02	.865E+03	66.4	94.6	20.4	17.1
115632	8345.	.165E+05	.104E+05	100.0	100.0	1.4	1.1
115633	8345.	-.416E-02	.662E-01	43.3	74.8	34.2	28.7
115641	7274.	.413E+03	.103E+04	99.9	100.0	5.7	4.8
115642	7274.	.191E+05	.859E+04	100.0	100.0	1.0	.9
115643	7274.	.176E-01	.574E-01	99.1	100.0	7.5	6.3
115651	22285.	.229E+03	.914E+03	100.0	100.0	5.2	4.4
115652	22285.	.186E+05	.103E+05	100.0	100.0	.7	.6
115653	22285.	.637E-02	.577E-01	90.1	99.9	11.9	10.0
116111	132.	-.110E+04	.869E+03	85.4	99.6	13.5	11.3
116112	132.	.327E+05	.403E+04	100.0	100.0	2.1	1.8
116113	132.	-.307E-01	.289E-01	77.5	98.4	16.2	13.6
116121	352.	-.803E+03	.633E+03	98.2	100.0	8.3	6.9
116122	352.	.338E+05	.395E+04	100.0	100.0	1.2	1.0
116123	352.	-.198E-01	.190E-01	94.9	100.0	10.1	8.4
116131	596.	-.550E+03	.744E+03	92.8	100.0	10.9	9.1
116132	596.	.304E+05	.387E+04	100.0	100.0	1.0	.9
116133	596.	-.146E-01	.243E-01	85.8	99.7	13.4	11.2
116141	770.	-.629E+03	.706E+03	98.6	100.0	7.9	6.7

KEY	AXLES	MEAN	STD DEV	CONF (10%)	CONF (20%)	TOL (95%)	TOL (90%)
116142	770.	.336E+05	.536E+04	100.0	100.0	1.1	.9
116143	770.	-.144E-01	.215E-01	93.7	100.0	10.5	8.8
116151	1850.	-.670E+03	.734E+03	100.0	100.0	5.0	4.2
116152	1350.	.326E+05	.481E+04	100.0	100.0	.7	.6
116153	1850.	-.167E-01	.230E-01	99.8	100.0	6.3	5.3
116211	409.	-.225E+04	.121E+04	100.0	100.0	5.2	4.4
116212	409.	.330E+05	.534E+04	100.0	100.0	1.6	1.3
116213	409.	-.687E-01	.465E-01	99.7	100.0	6.6	5.5
116221	930.	-.160E+04	.865E+03	100.0	100.0	3.5	2.9
116222	930.	.366E+05	.414E+04	100.0	100.0	.7	.6
116223	930.	-.393E-01	.231E-01	100.0	100.0	3.8	3.2
116231	380.	-.150E+04	.102E+04	99.6	100.0	6.8	5.7
116232	380.	.380E+05	.471E+04	100.0	100.0	1.3	1.0
116233	380.	-.346E-01	.262E-01	99.0	100.0	7.6	6.4
116241	212.	-.169E+04	.145E+04	90.8	99.9	11.6	9.7
116242	212.	.371E+05	.794E+04	100.0	100.0	2.9	2.4
116243	212.	-.415E-01	.408E-01	86.0	99.7	13.3	11.1
116251	1931.	-.173E+04	.109E+04	100.0	100.0	2.8	2.4
116252	1931.	.362E+05	.534E+04	100.0	100.0	.7	.6
116253	1931.	-.448E-01	.345E-01	100.0	100.0	3.4	2.9
116311	100.	-.970E+03	.883E+03	72.5	97.0	18.1	15.1
116312	100.	.211E+05	.534E+04	100.0	100.0	5.0	4.2
116313	100.	-.536E-01	.537E-01	67.9	95.1	19.9	16.6
116321	1008.	-.104E+04	.797E+03	100.0	100.0	4.7	4.0
116322	1008.	.287E+05	.403E+04	100.0	100.0	.9	.7
116323	1008.	-.338E-01	.278E-01	100.0	100.0	5.1	4.3
116331	992.	-.650E+03	.887E+03	97.9	100.0	8.5	7.1
116332	992.	.267E+05	.483E+04	100.0	100.0	1.1	.9
116333	992.	-.212E-01	.322E-01	96.2	100.0	9.5	7.9
116341	1202.	-.639E+03	.896E+03	98.6	100.0	7.9	6.7
116342	1202.	.253E+05	.513E+04	100.0	100.0	1.1	1.0
116343	1202.	-.235E-01	.367E-01	97.4	100.0	8.8	7.4
116351	3302.	-.776E+03	.884E+03	100.0	100.0	3.9	3.3
116352	3302.	.266E+05	.502E+04	100.0	100.0	.6	.5
116353	3302.	-.269E-01	.343E-01	100.0	100.0	4.3	3.6
116411	158.	-.578E+03	.563E+03	80.1	98.9	15.3	12.8
116412	158.	.146E+05	.314E+04	100.0	100.0	3.4	2.8
116413	158.	-.490E-01	.436E-01	84.0	99.5	14.0	11.7
116421	916.	-.581E+03	.629E+03	99.5	100.0	7.0	5.9
116422	916.	-.179E+05	.405E+04	100.0	100.0	1.5	1.2
116423	916.	-.358E-01	.361E-01	99.7	100.0	6.5	5.5
116431	1554.	-.298E+03	.651E+03	92.8	100.0	10.9	9.1
116432	1554.	.155E+05	.450E+04	100.0	100.0	1.4	1.2
116433	1554.	-.256E-01	.415E-01	98.5	100.0	8.1	6.8
116441	3327.	-.382E+03	.872E+03	98.8	100.0	7.8	6.5
116442	3327.	.182E+05	.486E+04	100.0	100.0	.9	.8
116443	3327.	-.243E-01	.468E-01	99.7	100.0	6.5	5.5
116451	5955.	-.396E+03	.783E+03	100.0	100.0	5.0	4.2
116452	5955.	.174E+05	.477E+04	100.0	100.0	.7	.6
116453	5955.	-.271E-01	.442E-01	100.0	100.0	4.1	3.5
116511	796.	-.227E+03	.229E+03	99.5	100.0	7.0	5.9
116512	796.	.899E+04	.186E+04	100.0	100.0	1.4	1.2
116513	796.	-.428E-01	.272E-01	100.0	100.0	4.4	3.7
116521	2132.	-.283E+03	.315E+03	100.0	100.0	4.7	4.0
116522	2132.	.928E+04	.220E+04	100.0	100.0	1.0	.8

KEY	AXLES	MEAN	STD. DEV.	CONF.(10%)	CONF.(20%)	TOL.(95%)	TOL.(90%)
116523	2132.	-.486E-01	.360E-01	100.0	100.0	3.1	2.6
116531	4802.	-.319E+03	.607E+03	100.0	100.0	5.4	4.5
116532	4802.	.983E+04	.747E+04	100.0	100.0	2.2	1.6
116533	4802.	-.495E-01	.472E-01	100.0	100.0	2.7	2.3
116541	1718.	-.127E+03	.710E+03	54.1	86.2	26.5	22.2
116542	1718.	.891E+04	.279E+04	100.0	100.0	1.5	1.2
116543	1718.	-.348E-01	.626E-01	97.8	100.0	8.5	7.1
116551	9448.	-.268E+03	.558E+03	100.0	100.0	4.2	3.5
116552	9448.	.947E+04	.560E+04	100.0	100.0	1.2	1.0
116553	9448.	-.460E-01	.472E-01	100.0	100.0	2.1	1.7
116611	1595.	-.901E+03	.112E+04	99.9	100.0	6.1	5.1
116612	1595.	.184E+05	.114E+05	100.0	100.0	3.0	2.6
116613	1595.	-.497E-01	.388E-01	100.0	100.0	3.8	3.2
116621	5338.	-.742E+03	.787E+03	100.0	100.0	2.8	2.4
116622	5338.	.208E+05	.115E+05	100.0	100.0	1.5	1.2
116623	5338.	-.401E-01	.327E-01	100.0	100.0	2.2	1.8
116631	8324.	-.425E+03	.736E+03	100.0	100.0	3.7	3.1
116632	8324.	.157E+05	.106E+05	100.0	100.0	1.5	1.2
116633	8324.	-.395E-01	.445E-01	100.0	100.0	2.5	2.1
116641	7229.	-.429E+03	.894E+03	100.0	100.0	4.8	4.0
116642	7229.	.194E+05	.925E+04	100.0	100.0	1.1	.9
116643	7229.	-.261E-01	.430E-01	100.0	100.0	4.2	3.6
116651	22486.	-.535E+03	.849E+03	100.0	100.0	2.1	1.7
116652	22486.	.183E+05	.107E+05	100.0	100.0	.8	.6
116653	22486.	-.357E-01	.434E-01	100.0	100.0	1.6	1.3
117111	62.	-.843E+03	.715E+03	64.3	93.2	21.5	18.0
117112	62.	.337E+05	.511E+04	100.0	100.0	3.9	3.2
117113	62.	-.204E-01	.209E-01	55.3	86.9	26.1	21.8
117121	292.	-.689E+03	.814E+03	85.1	99.6	13.6	11.4
117122	292.	.339E+05	.372E+04	100.0	100.0	1.3	1.1
117123	292.	-.164E-01	.248E-01	74.1	97.6	17.4	14.6
117131	448.	-.737E+03	.130E+04	75.9	98.3	16.4	13.7
117132	448.	.344E+05	.373E+04	100.0	100.0	1.0	.8
117133	448.	-.167E-01	.379E-01	64.9	93.7	21.1	17.7
117141	654.	-.599E+03	.133E+04	74.9	97.8	17.1	14.3
117142	654.	.341E+05	.366E+04	100.0	100.0	.8	.7
117143	654.	-.130E-01	.395E-01	60.0	90.7	23.3	19.6
117151	1456.	-.670E+03	.122E+04	96.4	100.0	9.3	7.8
117152	1456.	.341E+05	.377E+04	100.0	100.0	.6	.5
117153	1456.	-.151E-01	.359E-01	69.2	99.9	12.2	10.2
117211	259.	-.138E+04	.104E+04	96.6	100.0	9.2	7.7
117212	259.	.330E+05	.429E+04	100.0	100.0	1.6	1.3
117213	259.	-.383E-01	.317E-01	94.8	100.0	10.1	8.5
117221	744.	-.914E+03	.780E+03	99.9	100.0	6.1	5.2
117222	744.	.310E+05	.434E+04	100.0	100.0	1.0	.8
117223	744.	-.260E-01	.241E-01	99.7	100.0	6.7	5.6
117231	198.	-.745E+03	.109E+04	66.5	94.5	20.4	17.1
117232	198.	.309E+05	.546E+04	100.0	100.0	2.5	2.1
117233	198.	-.195E-01	.366E-01	54.6	66.5	26.3	22.0
117241	168.	-.454E+03	.109E+04	40.9	71.7	35.7	30.7
117242	168.	.291E+05	.497E+04	100.0	100.0	2.6	2.2
117243	168.	-.142E-01	.338E-01	41.3	72.2	36.3	30.4
117251	1369.	-.922E+03	.962E+03	100.0	100.0	5.5	4.6
117252	1369.	.311E+05	.471E+04	100.0	100.0	.8	.7
117253	1369.	-.259E-01	.299E-01	99.9	100.0	6.1	5.1

KEY	AXLES	MEAN	STD DEV	CONF (10%)	CONF (20%)	TOL (95%)	TOL (90%)
117311	1.	-.100E+03	0.	100.0	100.0	0.0	0.0
117312	1.	-.256E+05	0.	100.0	100.0	0.0	0.0
117313	1.	-.500E-02	0.	100.0	100.0	0.0	0.0
117321	744.	-.481E+03	.813E+03	89.3	99.9	12.2	10.2
117322	744.	.247E+05	.376E+04	100.0	100.0	1.1	.9
117323	744.	-.179E-01	.335E-01	85.5	99.6	13.4	11.3
117331	610.	-.307E+03	.111E+04	50.7	82.9	28.6	24.0
117332	610.	.247E+05	.456E+04	100.0	100.0	1.5	1.2
117333	610.	-.105E-01	.461E-01	42.6	73.9	34.9	29.3
117341	996.	-.250E+03	.990E+03	57.5	88.9	24.6	20.6
117342	996.	.219E+05	.348E+04	100.0	100.0	1.0	.6
117343	996.	-.112E-01	.438E-01	58.0	89.3	24.3	20.4
117351	2351.	-.338E+03	.976E+03	90.7	99.9	11.7	9.8
117352	2351.	.235E+05	.412E+04	100.0	100.0	.7	.6
117353	2351.	-.131E-01	.416E-01	87.4	99.8	12.8	10.7
117411	55.	-.482E+02	.347E+03	8.2	16.2	194.7	162.5
117412	55.	.127E+05	.209E+04	100.0	100.0	4.4	3.7
117413	55.	-.107E-01	.271E-01	23.0	44.1	68.2	56.9
117421	674.	-.172E+03	.634E+03	51.9	84.1	27.8	23.4
117422	674.	.155E+05	.354E+04	100.0	100.0	1.7	1.4
117423	674.	-.146E-01	.417E-01	63.8	93.1	21.5	18.1
117431	963.	-.120E+03	.727E+03	39.2	69.5	38.3	32.1
117432	963.	.156E+05	.481E+04	100.0	100.0	1.9	1.6
117433	963.	-.128E-01	.557E-01	52.4	84.6	27.5	23.1
117441	2668.	-.116E+03	.849E+03	51.8	84.1	27.8	23.4
117442	2668.	.165E+05	.357E+04	100.0	100.0	.8	.7
117443	2668.	-.111E-01	.539E-01	71.2	96.6	19.5	15.5
117451	4360.	-.125E+03	.788E+03	70.3	96.3	18.8	15.8
117452	4360.	.161E+05	.390E+04	100.0	100.0	.7	.6
117453	4360.	-.120E-01	.523E-01	87.0	99.8	12.9	10.9
117511	302.	-.851E+02	.209E+03	52.1	84.2	27.8	23.3
117512	302.	.953E+04	.182E+04	100.0	100.0	2.2	1.8
117513	302.	-.235E-01	.239E-01	91.2	99.9	11.5	9.6
117521	1917.	-.273E+02	.530E+03	17.9	34.8	86.9	72.9
117522	1917.	.913E+04	.250E+04	100.0	100.0	1.2	1.0
117523	1917.	-.199E-01	.570E-01	87.3	99.8	12.8	10.8
117531 *	4271.	-.123E+02	.777E+03	8.3	16.4	188.8	158.4
117532 *	4271.	.961E+04	.604E+04	100.0	100.0	1.9	1.6
117533 *	4271.	-.152E-01	.810E-01	78.1	98.6	19.9	13.4
117541	1708.	.618E+02	.745E+03	26.8	50.7	57.3	48.0
117542	1708.	.893E+04	.281E+04	100.0	100.0	1.5	1.3
117543	1708.	-.118E-01	.811E-01	45.4	77.3	32.5	27.2
117551	8198.	-.308E+01	.706E+03	3.2	6.3	496.2	416.5
117552	8198.	.936E+04	.472E+04	100.0	100.0	1.1	.9
117553	8198.	-.159E-01	.747E-01	94.6	100.0	10.2	8.5
117611	679.	-.647E+03	.934E+03	92.8	100.0	10.9	9.1
117612	679.	.210E+05	.120E+05	100.0	100.0	4.3	3.6
117613	679.	-.278E-01	.286E-01	98.9	100.0	7.7	6.5
117621	4371.	-.322E+03	.748E+03	99.6	100.0	6.9	5.8
117622	4371.	.181E+05	.100E+05	100.0	100.0	1.6	1.4
117623	4371.	-.195E-01	.451E-01	99.6	100.0	6.8	5.7
117631	6490.	-.128E+03	.890E+03	75.5	98.0	16.9	14.2
117632	6490.	.143E+05	.961E+04	100.0	100.0	1.6	1.4
117633	6490.	-.147E-01	.715E-01	90.1	99.9	11.9	10.0
117641	6194.	-.149E+03	.938E+03	78.8	98.7	15.7	13.2

KEY	AXLES	MEAN	STD DEV	CONF.(10%)	CONF.(20%)	TOL(95%)	TOL(90%)
117602	6194.	.175E+05	.826E+04	100.0	100.0	1.2	1.0
117603	6194.	-.116E-01	.597E-01	87.4	99.8	12.8	10.6
117651	17734.	-.203E+03	.895E+03	99.8	100.0	6.4	5.4
117652	17734.	.166E+05	.956E+04	100.0	100.0	.8	.7
117653	17734.	-.153E-01	.606E-01	99.9	100.0	5.8	4.9
118111	855.	-.545E+03	.139E+04	74.8	97.8	17.1	14.4
118112	855.	.335E+05	.413E+04	100.0	100.0	.8	.7
118113	855.	-.128E-01	.423E-01	62.3	92.3	22.2	18.6
118121	2252.	-.362E+03	.133E+04	80.3	99.0	15.2	12.8
118122	2252.	.339E+05	.381E+04	100.0	100.0	.5	.4
118123	2252.	-.685E-02	.400E-01	58.3	89.5	24.1	20.3
118131	3873.	-.452E+03	.141E+04	95.3	100.0	9.9	8.3
118132	3873.	.333E+05	.407E+04	100.0	100.0	.4	.3
118133	3873.	-.992E-02	.426E-01	85.3	99.6	13.5	11.3
118141	5006.	-.339E+03	.141E+04	91.1	99.9	11.5	9.7
118142	5006.	.337E+05	.444E+04	100.0	100.0	.4	.3
118143	5006.	-.628E-02	.428E-01	70.1	96.2	19.9	15.6
118151	11986.	-.395E+03	.140E+04	99.8	100.0	6.3	5.3
118152	11986.	.336E+05	.419E+04	100.0	100.0	.2	.2
118153	11986.	-.802E-02	.422E-01	96.3	100.0	9.4	7.9
118211	2594.	-.117E+04	.130E+04	100.0	100.0	4.3	3.6
118212	2594.	.337E+05	.477E+04	100.0	100.0	.5	.5
118213	2594.	-.324E-01	.418E-01	100.0	100.0	5.0	4.2
118221	5729.	-.646E+03	.132E+04	100.0	100.0	5.3	4.5
118222	5729.	.334E+05	.449E+04	100.0	100.0	.3	.3
118223	5729.	-.153E-01	.395E-01	99.7	100.0	6.7	5.6
118231	2390.	-.603E+03	.145E+04	95.8	100.0	9.7	8.1
118232	2390.	.332E+05	.491E+04	100.0	100.0	.6	.5
118233	2390.	-.137E-01	.445E-01	86.6	99.7	13.1	11.0
118241	1312.	-.499E+03	.164E+04	72.9	97.2	17.8	15.0
118242	1312.	.315E+05	.670E+04	100.0	100.0	1.2	1.0
118243	1312.	-.114E-01	.495E-01	59.6	90.4	23.5	19.7
118251	12025.	-.735E+03	.140E+04	100.0	100.0	3.4	2.9
118252	12025.	.332E+05	.496E+04	100.0	100.0	.3	.2
118253	12025.	-.182E-01	.429E-01	100.0	100.0	4.2	3.5
118311	599.	-.279E+03	.113E+04	45.6	77.4	32.4	27.2
118312	599.	.223E+05	.445E+04	100.0	100.0	1.6	1.3
118313	599.	-.136E-01	.557E-01	45.1	76.9	32.8	27.5
118321	6178.	-.367E+03	.117E+04	98.6	100.0	7.9	6.7
118322	6178.	.263E+05	.468E+04	100.0	100.0	.4	.4
118323	6178.	-.120E-01	.452E-01	96.3	100.0	9.4	7.9
118331	6358.	-.354E+03	.119E+04	92.2	100.0	8.3	7.0
118332	6358.	.256E+05	.461E+04	100.0	100.0	.4	.4
118333	6358.	-.119E-01	.479E-01	95.2	100.0	9.9	8.3
118341	7764.	-.899E+02	.129E+04	46.1	78.1	31.9	26.8
118342	7764.	.229E+05	.437E+04	100.0	100.0	.4	.4
118343	7764.	-.208E-02	.579E-01	24.9	47.4	61.8	51.9
118351	20859.	-.257E+03	.123E+04	99.8	100.0	6.5	5.4
118352	20859.	.247E+05	.480E+04	100.0	100.0	.3	.2
118353	20859.	-.833E-02	.516E-01	98.1	100.0	8.4	7.0
118411	1004.	-.138E+03	.656E+03	49.6	81.8	29.4	24.6
118412	1004.	.147E+05	.299E+04	100.0	100.0	1.3	1.1
118413	1004.	-.153E-01	.462E-01	70.5	96.4	18.7	15.7
118421	5697.	-.825E+02	.895E+03	51.3	83.6	28.2	23.7
118422	5697.	.165E+05	.381E+04	100.0	100.0	.6	.5

KEY	AXLES	MEAN	STU DEV	CONF(10%)	CONF(20%)	TOL(95%)	TOL(90%)
118423	5657.	-.895E-02	.546E-01	78.5	98.7	15.8	13.3
118431	9945.	-.133E+03	.927E+03	84.8	99.6	13.7	11.5
118432	9945.	.163E+05	.436E+04	100.0	100.0	.5	.4
118433	9945.	-.131E-01	.610E-01	96.8	100.0	9.2	7.7
118441	21424.	-.146E+02	.116E+04	14.7	28.8	106.1	89.1
118442	21424.	.174E+05	.391E+04	100.0	100.0	.3	.3
118443	21424.	-.414E-02	.683E-01	62.5	32.4	22.1	18.5
118451	38070.	-.590E+02	.105E+04	72.5	97.1	17.2	15.1
118452	38070.	.169E+05	.404E+04	100.0	100.0	.2	.2
118453	38070.	-.750E-02	.642E-01	97.7	100.0	8.6	7.2
118511	4765.	-.131E+03	.323E+03	99.5	100.0	7.0	5.9
118512	4765.	.918E+04	.196E+04	100.0	100.0	.6	.5
118513	4765.	-.303E-01	.370E-01	100.0	100.0	3.5	2.9
118521	14222.	-.540E+02	.628E+03	63.5	96.0	19.1	16.0
118522	14222.	.960E+04	.238E+04	100.0	100.0	.4	.3
118523	14222.	-.217E-01	.644E-01	100.0	100.0	4.9	4.1
118531 *	31795.	-.938E+02	.828E+03	95.7	100.0	9.7	8.1
118532 *	31795.	.104E+05	.660E+04	100.0	100.0	.7	.6
118533 *	31795.	-.241E-01	.796E-01	100.0	100.0	3.6	3.0
118541	11569.	.635E+02	.982E+03	51.4	33.6	26.2	23.6
118542	11569.	.944E+04	.280E+04	100.0	100.0	.5	.5
118543	11569.	-.136E-01	.923E-01	83.6	99.8	12.4	10.4
118551	62351.	-.584E+02	.794E+03	93.4	100.0	10.7	9.0
118552	62351.	.994E+04	.505E+04	100.0	100.0	.4	.3
118553	62351.	-.221E-01	.767E-01	100.0	100.0	2.7	2.3
118611	9817.	-.453E+03	.994E+03	100.0	100.0	4.3	3.6
118612	9817.	.191E+05	.117E+05	100.0	100.0	1.2	1.0
118613	9817.	-.268E-01	.418E-01	100.0	100.0	3.1	2.6
118621	34078.	-.235E+03	.100E+04	100.0	100.0	4.5	3.8
118622	34078.	.194E+05	.105E+05	100.0	100.0	.6	.5
118623	34078.	-.158E-01	.547E-01	100.0	100.0	3.7	3.1
118631	54361.	-.179E+03	.990E+03	100.0	100.0	4.6	3.9
118632	54361.	.159E+05	.986E+04	100.0	100.0	.5	.4
118633	54361.	-.192E-01	.700E-01	100.0	100.0	3.1	2.6
118641	47075.	-.558E+02	.119E+04	69.0	95.8	19.3	16.2
118642	47075.	.185E+05	.829E+04	100.0	100.0	.4	.3
118643	47075.	-.654E-02	.711E-01	95.4	100.0	9.8	8.2
118651	145331.	-.171E+03	.107E+04	100.0	100.0	3.2	2.7
118652	145331.	.178E+05	.979E+04	100.0	100.0	.3	.2
118653	145331.	-.148E-01	.658E-01	100.0	100.0	2.3	1.9
121111	36.	-.400E+03	.107E+04	17.6	34.2	90.9	75.6
121112	36.	.343E+05	.384E+04	100.0	100.0	3.8	3.1
121113	36.	-.667E-02	.317E-01	10.0	19.8	160.8	133.8
121121	402.	-.343E+03	.102E+04	49.9	82.2	29.2	24.5
121122	402.	.340E+05	.357E+04	100.0	100.0	1.0	.9
121123	402.	-.493E-02	.314E-01	24.7	47.1	62.4	52.4
121131	842.	.919E+02	.103E+04	20.4	39.4	76.1	63.8
121132	842.	.345E+05	.474E+04	100.0	100.0	.9	.8
121133	842.	.755E-02	.316E-01	51.2	93.5	28.3	23.7
121141	844.	.219E+03	.111E+04	43.4	74.9	34.2	28.7
121142	844.	.341E+05	.540E+04	100.0	100.0	1.1	.9
121143	844.	.113E-01	.336E-01	67.1	94.9	20.1	16.9
121151	2124.	.517E+02	.108E+04	17.4	34.0	89.0	74.7
121152	2124.	.342E+05	.482E+04	100.0	100.0	.6	.5
121153	2124.	.643E-02	.329E-01	63.2	92.8	21.8	18.3

KEY	AXLES	MEAN	STD DEV	CONF(10%)	CONF(20%)	TOL(95%)	TOL(90%)
121211	80.	-.269E+03	.706E+03	26.6	50.2	59.4	48.9
121212	80.	.335E+05	.350E+04	100.0	100.0	2.3	1.9
121213	80.	-.453E-02	.209E-01	15.4	30.1	102.4	85.7
121221	2016.	-.391E+03	.974E+03	92.8	100.0	10.9	9.1
121222	2016.	.342E+05	.412E+04	100.0	100.0	.5	.4
121223	2016.	-.683E-02	.282E-01	72.4	97.0	18.0	15.1
121231	1932.	-.402E+03	.112E+04	88.6	99.8	12.4	10.4
121232	1932.	.357E+05	.409E+04	100.0	100.0	.5	.4
121233	1932.	-.612E-02	.321E-01	59.8	90.6	23.4	19.6
121241	188.	-.121E+03	.112E+04	11.7	23.2	133.7	112.0
121242	188.	.337E+05	.382E+04	100.0	100.0	1.6	1.4
121243	188.	.126E-02	.355E-01	3.9	7.8	404.9	339.3
121251	4216.	-.381E+03	.105E+04	98.2	100.0	8.3	6.9
121252	4216.	.349E+05	.416E+04	100.0	100.0	.4	.3
121253	4216.	-.610E-02	.303E-01	80.9	99.1	15.0	12.6
121311	87.	-.138E+03	.621E+03	16.4	32.0	95.9	80.2
121312	87.	.241E+05	.300E+04	100.0	100.0	2.7	2.2
121313	87.	-.293E-02	.284E-01	7.7	15.2	206.3	172.6
121321	1258.	-.493E+02	.914E+03	15.2	29.8	102.5	86.0
121322	1258.	.258E+05	.374E+04	100.0	100.0	.8	.7
121323	1258.	.974E-03	.362E-01	7.6	15.1	205.6	172.5
121331	1344.	.139E+03	.123E+04	32.0	59.1	47.5	39.9
121332	1344.	.250E+05	.356E+04	100.0	100.0	.8	.6
121333	1344.	.793E-02	.484E-01	45.1	77.0	32.7	27.4
121341	718.	.309E+03	.139E+04	45.0	76.8	32.8	27.5
121342	718.	.239E+05	.309E+04	100.0	100.0	.9	.8
121343	718.	.144E-01	.543E-01	52.3	84.5	27.6	23.1
121351	3407.	.982E+02	.116E+04	37.9	67.8	39.6	33.2
121352	3407.	.251E+05	.359E+04	100.0	100.0	.5	.4
121353	3407.	.645E-02	.456E-01	59.1	90.1	23.7	19.9
121411	132.	-.227E+02	.352E+03	5.9	11.8	267.1	223.6
121412	132.	.167E+05	.331E+04	100.0	100.0	3.4	2.9
121413	132.	-.335E-02	.207E-01	14.7	29.0	106.3	89.0
121421	1038.	.110E+03	.614E+03	43.5	75.0	34.1	28.6
121422	1038.	.173E+05	.431E+04	100.0	100.0	1.5	1.3
121423	1038.	.565E-02	.384E-01	36.5	65.7	41.4	34.7
121431	2074.	.443E+03	.129E+04	88.1	99.8	12.6	10.5
121432	2074.	.157E+05	.326E+04	100.0	100.0	.9	.8
121433	2074.	.255E-01	.849E-01	82.9	99.4	14.3	12.0
121441	3862.	.552E+03	.160E+04	96.8	100.0	9.2	7.7
121442	3862.	.176E+05	.351E+04	100.0	100.0	.6	.5
121443	3862.	.310E-01	.979E-01	95.1	100.0	10.0	8.4
121451	7106.	.445E+03	.140E+04	99.2	100.0	7.3	6.2
121452	7106.	.170E+05	.366E+04	100.0	100.0	.5	.4
121453	7106.	.251E-01	.873E-01	98.4	100.0	8.1	6.8
121511	44.	.169E+03	.234E+03	36.6	65.7	42.0	35.0
121512	44.	.886E+04	.141E+04	100.0	100.0	4.8	4.0
121513	44.	.506E-02	.256E-01	10.4	20.5	154.1	128.5
121521	519.	.244E+03	.389E+03	84.6	99.6	13.7	11.5
121522	519.	.918E+04	.195E+04	100.0	100.0	1.8	1.5
121523	519.	.126E-01	.414E-01	51.3	83.5	28.3	23.7
121531	5273.	.412E+03	.113E+04	99.2	100.0	7.4	6.2
121532	5273.	.973E+04	.231E+04	100.0	100.0	.6	.5
121533	5273.	.260E-01	.112E+00	90.8	99.9	11.6	9.8
121541	1495.	.670E+03	.179E+04	85.2	99.6	13.5	11.4

KEY	AXLES	MEAN	STD DEV	CONE (10%)	CONE (20%)	TOL (95%)	TOL (90%)
121542	1495.	.976E+04	.254E+04	100.0	100.0	1.3	1.1
121543	1495.	.438E-01	.170E+00	62.2	95.4	19.6	16.5
121551	7331.	.451E+03	.126E+04	99.8	100.0	6.4	5.4
121552	7331.	.969E+04	.233E+04	100.0	100.0	.6	.5
121553	7331.	.286E-01	.123E+00	95.4	100.0	9.8	8.3
121611	379.	-.115E+03	.615E+03	28.3	53.2	54.2	45.4
121612	379.	.227E+05	.910E+04	100.0	100.0	4.0	3.4
121613	379.	-.284E-02	.246E-01	17.8	34.7	87.5	73.4
121621	5233.	-.143E+03	.890E+03	75.4	92.0	16.9	14.2
121622	5233.	.263E+05	.941E+04	100.0	100.0	1.0	.8
121623	5233.	-.402E-03	.347E-01	6.7	13.3	233.5	195.9
121631	11465.	.225E+03	.120E+04	95.4	100.0	9.8	8.2
121632	11465.	.188E+05	.110E+05	100.0	100.0	1.1	.9
121633	11465.	.170E-01	.880E-01	96.2	100.0	9.5	7.9
121641	7107.	.495E+03	.157E+04	99.2	100.0	7.4	6.2
121642	7107.	.189E+05	.819E+04	100.0	100.0	1.0	.8
121643	7107.	.289E-01	.109E+00	97.5	100.0	8.8	7.4
121651	24184.	.219E+03	.128E+04	99.2	100.0	7.4	6.2
121652	24184.	.205E+05	.103E+05	100.0	100.0	.6	.5
121653	24184.	.164E-01	.868E-01	99.7	100.0	6.7	5.6
122111	24.	.156E+03	.133E+04	4.5	9.0	360.8	298.9
122112	24.	.379E+05	.248E+04	100.0	100.0	2.8	2.3
122113	24.	.875E-02	.361E-01	9.3	18.5	174.4	144.5
122121	402.	-.511E+02	.123E+04	6.6	13.2	236.7	198.5
122122	402.	.378E+05	.349E+04	100.0	100.0	.9	.8
122123	402.	.326E-02	.330E-01	15.7	30.8	99.0	83.0
122131	792.	.477E+02	.113E+04	9.4	18.8	165.3	138.7
122132	792.	.366E+05	.450E+04	100.0	100.0	.9	.7
122133	792.	.588E-02	.311E-01	40.5	71.2	36.9	30.9
122141	780.	.152E+03	.111E+04	29.8	55.5	51.3	43.1
122142	780.	.371E+05	.462E+04	100.0	100.0	.9	.7
122143	780.	.883E-02	.298E-01	59.2	90.2	23.7	19.9
122151	1998.	.700E+02	.115E+04	21.4	41.3	72.1	60.5
122152	1998.	.371E+05	.437E+04	100.0	100.0	.5	.4
122153	1998.	.654E-02	.311E-01	65.2	94.0	20.9	17.5
122211	76.	-.505E+03	.920E+03	36.6	65.8	41.7	34.8
122212	76.	.379E+05	.370E+04	100.0	100.0	2.2	1.9
122213	76.	-.964E-02	.243E-01	26.9	50.8	57.7	48.2
122221	2024.	-.631E+03	.114E+04	98.7	100.0	7.8	6.6
122222	2024.	.379E+05	.435E+04	100.0	100.0	.5	.4
122223	2024.	-.121E-01	.298E-01	93.3	100.0	10.7	9.0
122231	1828.	-.818E+03	.124E+04	99.5	100.0	6.9	5.8
122232	1828.	.376E+05	.420E+04	100.0	100.0	.5	.4
122233	1828.	-.170E-01	.335E-01	97.0	100.0	9.0	7.6
122241	160.	-.277E+03	.129E+04	21.4	41.3	72.6	60.8
122242	160.	.370E+05	.494E+04	100.0	100.0	2.1	1.7
122243	160.	-.172E-02	.348E-01	5.0	9.9	315.9	264.6
122251	4088.	-.698E+03	.119E+04	100.0	100.0	5.2	4.4
122252	4088.	.377E+05	.430E+04	100.0	100.0	.3	.3
122253	4088.	-.138E-01	.318E-01	99.5	100.0	7.0	5.9
122311	92.	-.363E+03	.725E+03	36.7	66.0	41.4	34.7
122312	92.	.276E+05	.377E+04	100.0	100.0	2.8	2.4
122313	92.	-.110E-01	.273E-01	29.8	55.6	51.7	43.2
122321	1262.	-.221E+03	.898E+03	61.7	91.9	22.5	18.9
122322	1262.	.282E+05	.445E+04	100.0	100.0	.9	.7

KEY	AXLES	MEAN	STD. DEV.	CONF.(10%)	CONF.(20%)	CONF.(95%)	CONF.(99%)
122323	1262.	-.545E-02	.333E-01	43.5	75.5	33.8	28.3
122331	1199.	.121E+01	.128E+04	.3	.5	6005.5	5038.7
122332	1199.	.266E+05	.367E+04	100.0	100.0	.8	.7
122333	1199.	.220E-02	.493E-01	12.3	24.2	127.1	106.6
122341	656.	.509E+02	.135E+04	7.7	15.3	202.8	170.2
122342	656.	.256E+05	.370E+04	100.0	100.0	1.1	.9
122343	656.	.348E-02	.517E-01	13.7	27.0	113.8	95.5
122351	3209.	-.863E+02	.115E+04	32.8	60.3	46.3	38.5
122352	3209.	.271E+05	.413E+04	100.0	100.0	.5	.4
122353	3209.	-.922E-03	.440E-01	5.5	16.3	165.0	138.5
122411	52.	-.250E+03	.464E+03	30.1	55.9	51.7	43.1
122412	52.	.159E+05	.359E+04	99.8	100.0	6.3	5.3
122413	52.	-.197E-01	.286E-01	37.9	67.6	40.3	33.7
122421	1072.	-.210E+03	.585E+03	76.1	98.1	16.7	14.0
122422	1072.	.189E+05	.460E+04	100.0	100.0	1.5	1.2
122423	1072.	-.135E-01	.307E-01	84.9	99.6	13.7	11.5
122431	1845.	.114E+03	.123E+04	30.9	57.4	49.3	41.3
122432	1845.	.167E+05	.420E+04	100.0	100.0	1.2	1.0
122433	1845.	.141E-02	.756E-01	6.4	12.7	244.8	205.4
122441	3463.	.920E+02	.146E+04	29.0	54.3	52.7	44.2
122442	3463.	.194E+05	.454E+04	100.0	100.0	.8	.7
122443	3463.	.105E-02	.797E-01	6.2	12.3	253.6	213.0
122451	6432.	.452E+02	.128E+04	22.2	42.8	69.4	58.2
122452	6432.	.185E+05	.461E+04	100.0	100.0	.6	.5
122453	6432.	-.143E-02	.725E-01	12.6	24.9	123.6	103.7
122511	32.	-.813E+02	.239E+03	15.1	29.6	106.2	88.3
122512	32.	.110E+05	.209E+04	99.4	100.0	6.9	5.7
122513	32.	-.177E-01	.224E-01	34.2	62.1	45.7	38.0
122521	508.	-.935E+02	.393E+03	40.8	71.6	36.6	30.7
122522	508.	.103E+05	.218E+04	100.0	100.0	1.8	1.5
122523	508.	-.231E-01	.381E-01	82.8	99.4	14.4	12.0
122531	4563.	.108E+02	.992E+03	5.9	11.7	265.3	222.6
122532	4563.	.968E+04	.232E+04	100.0	100.0	.7	.6
122533	4563.	-.193E-01	.907E-01	85.0	99.6	13.6	11.4
122541	1456.	.392E+03	.181E+04	59.0	90.1	23.8	19.9
122542	1456.	.104E+05	.247E+04	100.0	100.0	1.2	1.0
122543	1456.	.119E-01	.155E+00	23.0	44.2	67.0	56.2
122551	6559.	.868E+02	.121E+04	44.0	75.7	33.6	28.2
122552	6559.	.989E+04	.236E+04	100.0	100.0	.6	.5
122553	6559.	-.127E-01	.107E+00	66.5	94.6	20.3	17.1
122611	276.	-.303E+03	.805E+03	46.7	78.8	31.5	26.4
122612	276.	.272E+05	.104E+05	100.0	100.0	4.5	3.8
122613	276.	-.113E-01	.281E-01	49.5	81.7	29.5	24.7
122621	5268.	-.351E+03	.970E+03	99.1	100.0	7.5	6.3
122622	5268.	.290E+05	.104E+05	100.0	100.0	1.0	.8
122623	5268.	-.107E-01	.326E-01	98.3	100.0	8.2	6.9
122631	10227.	-.117E+03	.118E+04	68.5	95.5	19.5	16.4
122632	10227.	.200E+05	.120E+05	100.0	100.0	1.2	1.0
122633	10227.	-.107E-01	.733E-01	86.0	99.7	13.3	11.1
122641	6515.	.153E+03	.150E+04	58.9	90.0	23.8	20.0
122642	6515.	.206E+05	.909E+04	100.0	100.0	1.1	.9
122643	6515.	.458E-02	.958E-01	30.0	56.0	50.8	42.6
122651	22286.	-.957E+02	.125E+04	74.7	97.8	17.1	14.4
122652	22286.	.224E+05	.115E+05	100.0	100.0	.7	.6
122653	22286.	-.623E-02	.739E-01	79.2	98.8	15.6	13.1

KEY	AXLES	MEAN	STD. DEV.	CONF.(10%)	CONF.(20%)	TOL.(95%)	TOL.(90%)
123111	24.	-.338E+03	.627E+03	20.6	39.7	78.5	65.0
123112	24.	.326E+05	.294E+04	100.0	100.0	3.7	3.0
123113	24.	-.563E-02	.195E-01	11.1	22.0	146.2	121.1
123117	24.	.376E+05	.273E+04	100.0	100.0	3.0	2.5
123118	24.	.365E+05	.227E+04	100.0	100.0	2.6	2.2
123119	24.	.153E+04	.115E+03	47.7	79.3	31.9	26.4
123121	34.	-.265E+03	.899E+03	41.5	72.5	36.0	30.2
123122	34.	.342E+05	.324E+04	100.0	100.0	1.0	.8
123123	34.	-.354E-02	.274E-01	18.9	36.8	82.1	68.8
123127	251.	.385E+05	.698E+04	100.0	100.0	2.3	1.9
123128	251.	.377E+05	.410E+04	100.0	100.0	1.4	1.1
123129	251.	.169E+04	.183E+04	85.5	99.6	13.5	11.3
123131	618.	-.208E+03	.129E+04	35.6	64.4	42.5	35.6
123132	618.	.337E+05	.446E+04	100.0	100.0	.9	.8
123133	618.	-.225E-02	.416E-01	12.3	24.3	126.9	106.5
123137	552.	.399E+05	.529E+04	100.0	100.0	1.1	.9
123138	552.	.376E+05	.455E+04	100.0	100.0	1.0	.8
123139	552.	.255E+04	.195E+04	99.8	100.0	6.4	5.4
123141	782.	-.248E+03	.111E+04	46.7	78.7	31.5	26.4
123142	782.	.332E+05	.500E+04	100.0	100.0	1.1	.8
123143	782.	-.269E-02	.344E-01	17.3	33.8	89.8	75.4
123147	660.	.418E+05	.497E+04	100.0	100.0	.9	.8
123148	660.	.383E+05	.439E+04	100.0	100.0	.9	.7
123149	660.	.372E+04	.223E+04	100.0	100.0	4.6	3.8
123151	1968.	-.235E+03	.115E+04	63.5	93.0	21.6	18.2
123152	1968.	.336E+05	.450E+04	100.0	100.0	.6	.5
123153	1968.	-.269E-02	.364E-01	25.7	48.8	59.8	50.2
123157	1487.	.405E+05	.560E+04	100.0	100.0	.7	.6
123158	1487.	.379E+05	.439E+04	100.0	100.0	.6	.5
123159	1487.	.291E+04	.220E+04	100.0	100.0	3.8	3.2
123211	76.	-.114E+04	.683E+03	84.9	99.5	13.7	11.5
123212	76.	.311E+05	.331E+04	100.0	100.0	2.4	2.0
123213	76.	-.336E-01	.214E-01	82.5	99.2	14.6	12.2
123217	76.	.361E+05	.626E+04	100.0	100.0	4.0	3.3
123218	76.	.343E+05	.381E+04	100.0	100.0	2.5	2.1
123219	76.	.206E+04	.407E+04	34.0	62.0	45.1	37.7
123221	1720.	-.891E+03	.984E+03	100.0	100.0	5.2	4.4
123222	1720.	.311E+05	.399E+04	100.0	100.0	.6	.5
123223	1720.	-.253E-01	.319E-01	99.9	100.0	6.0	5.0
123227	1210.	.365E+05	.574E+04	100.0	100.0	.9	.7
123228	1210.	.351E+05	.467E+04	100.0	100.0	.8	.6
123229	1210.	.176E+04	.270E+04	97.7	100.0	8.6	7.2
123231	1904.	-.922E+03	.130E+04	99.8	100.0	6.3	5.3
123232	1904.	.324E+05	.427E+04	100.0	100.0	.6	.5
123233	1904.	-.244E-01	.416E-01	99.0	100.0	7.7	6.4
123237	1356.	.372E+05	.542E+04	100.0	100.0	.8	.7
123238	1356.	.354E+05	.459E+04	100.0	100.0	.7	.6
123239	1356.	.209E+04	.264E+04	99.6	100.0	6.7	5.6
123241	160.	-.112E+04	.219E+04	48.1	80.2	30.6	25.6
123242	160.	.307E+05	.447E+04	100.0	100.0	2.3	1.9
123243	160.	-.352E-01	.741E-01	45.2	76.9	32.8	27.5
123247	100.	.358E+05	.486E+04	100.0	100.0	2.7	2.3
123248	100.	.333E+05	.441E+04	100.0	100.0	2.6	2.2
123249	100.	.273E+04	.196E+04	83.2	99.3	14.3	12.0
123251	3860.	-.921E+03	.121E+04	100.0	100.0	4.2	3.5

KEY	AXLES	MEAN	STD DEV	CONF (10%)	CONF (20%)	TOL (95%)	TOL (90%)
123252	3860.	.317E+05	.420E+04	100.0	100.0	.4	.3
123253	3860.	.254E-01	.394E-01	100.0	100.0	4.9	4.1
123257	2742.	.368E+05	.559E+04	100.0	100.0	.6	.5
123258	2742.	.351E+05	.462E+04	100.0	100.0	.5	.4
123259	2742.	.197E+04	.270E+04	100.0	100.0	5.1	4.3
123311	92.	.783E+03	.569E+03	81.0	99.0	15.1	12.6
123312	92.	.226E+05	.310E+04	100.0	100.0	2.8	2.4
123313	92.	.352E-01	.263E-01	79.7	96.8	15.5	13.0
123317	92.	.254E+05	.380E+04	100.0	100.0	3.1	2.6
123318	92.	.237E+05	.388E+04	100.0	100.0	3.4	2.8
123319	92.	.202E+04	.120E+04	89.0	99.8	12.3	10.3
123321	1256.	.287E+03	.887E+03	74.8	97.8	17.1	14.4
123322	1256.	.244E+05	.479E+04	100.0	100.0	1.1	.9
123323	1256.	.551E-02	.354E-01	65.9	94.3	20.6	17.3
123327	892.	.275E+05	.515E+04	100.0	100.0	1.2	1.0
123328	892.	.256E+05	.441E+04	100.0	100.0	1.1	1.0
123329	892.	.222E+04	.258E+04	99.0	100.0	7.6	6.4
123331	1306.	.796E+02	.121E+04	18.8	36.5	82.6	69.3
123332	1306.	.225E+05	.368E+04	100.0	100.0	.9	.7
123333	1306.	.307E-02	.570E-01	15.4	30.3	100.7	84.5
123337	850.	.255E+05	.397E+04	100.0	100.0	1.0	.9
123338	850.	.236E+05	.376E+04	100.0	100.0	1.1	.9
123339	850.	.221E+04	.140E+04	100.0	100.0	4.3	3.6
123341	644.	.865E+02	.138E+04	12.7	25.0	123.1	103.2
123342	644.	.208E+05	.379E+04	100.0	100.0	1.4	1.2
123343	644.	.358E-02	.624E-01	11.6	22.9	134.9	113.2
123347	472.	.261E+05	.329E+04	100.0	100.0	1.1	1.0
123348	472.	.235E+05	.325E+04	100.0	100.0	1.3	1.0
123349	472.	.282E+04	.127E+04	100.0	100.0	4.1	3.4
123351	3298.	.180E+03	.113E+04	63.8	93.2	21.5	18.0
123352	3298.	.229E+05	.435E+04	100.0	100.0	.6	.5
123353	3298.	.652E-02	.507E-01	53.9	86.0	26.6	22.3
123357	2306.	.264E+05	.444E+04	100.0	100.0	.7	.6
123358	2306.	.243E+05	.406E+04	100.0	100.0	.7	.6
123359	2306.	.233E+04	.194E+04	100.0	100.0	3.4	2.8
123411	52.	.282E+03	.422E+03	36.8	56.0	41.7	34.8
123412	52.	.142E+05	.353E+04	99.4	100.0	6.9	5.8
123413	52.	.256E-01	.262E-01	51.6	83.5	28.5	23.8
123417	52.	.160E+05	.299E+04	100.0	100.0	5.2	4.3
123418	52.	.139E+05	.313E+04	99.8	100.0	6.3	5.2
123419	52.	.231E+04	.493E+03	99.9	100.0	5.9	5.0
123421	960.	.140E+03	.607E+03	52.4	84.6	27.5	23.1
123422	960.	.158E+05	.418E+04	100.0	100.0	1.7	1.4
123423	960.	.136E-01	.395E-01	71.3	96.7	18.4	15.4
123427	784.	.192E+05	.519E+04	100.0	100.0	1.9	1.6
123428	784.	.170E+05	.480E+04	100.0	100.0	2.0	1.7
123429	784.	.253E+04	.138E+04	100.0	100.0	3.8	3.2
123431	2048.	.264E+02	.121E+04	7.9	15.7	197.9	166.1
123432	2048.	.142E+05	.348E+04	100.0	100.0	1.1	.9
123433	2048.	.712E-02	.943E-01	26.8	50.6	57.3	48.1
123437	1244.	.184E+05	.372E+04	100.0	100.0	1.1	.9
123438	1244.	.158E+05	.338E+04	100.0	100.0	1.2	1.0
123439	1244.	.282E+04	.152E+04	100.0	100.0	3.0	2.5
123441	3556.	.733E+02	.136E+04	25.1	47.9	61.1	51.3
123442	3556.	.160E+05	.361E+04	100.0	100.0	.7	.6

KEY	AXLES	MEAN	STD DEV	CONF(10%)	CONF(20%)	TOL(95%)	TOL(90%)
123443	3556.	-.167E-02	.907E-01	8.3	17.4	178.1	149.5
123447	3008.	.210E+05	.347E+04	100.0	100.0	.6	.5
123449	3008.	.182E+05	.350E+04	100.0	100.0	.7	.6
123449	3008.	.298E+04	.101E+04	100.0	100.0	1.2	1.0
123451	6616.	.251E+02	.123E+04	13.2	26.0	118.2	99.2
123452	6616.	.154E+05	.374E+04	100.0	100.0	.6	.5
123453	6616.	-.528E-02	.862E-01	38.2	68.1	39.3	33.0
123457	5088.	.200E+05	.402E+04	100.0	100.0	.6	.5
123458	5088.	.174E+05	.385E+04	100.0	100.0	.6	.5
123459	5088.	.287E+04	.122E+04	100.0	100.0	1.2	1.0
123511	32.	-.222E+03	.223E+03	42.2	73.1	36.3	30.2
123512	32.	.872E+04	.123E+04	100.0	100.0	5.1	4.2
123513	32.	-.434E-01	.233E-01	70.0	95.7	19.4	16.1
123517	32.	.117E+05	.166E+04	100.0	100.0	5.1	4.2
123518	32.	.907E+04	.133E+04	99.9	100.0	5.3	4.4
123519	32.	.287E+04	.928E+03	91.0	99.9	11.7	9.7
123521	500.	-.817E+02	.297E+03	46.2	78.1	31.9	26.8
123522	500.	.885E+04	.162E+04	100.0	100.0	1.6	1.3
123523	500.	-.252E-01	.339E-01	90.3	99.9	11.8	9.9
123527	368.	.110E+05	.351E+04	100.0	100.0	3.3	2.7
123528	368.	.917E+04	.190E+04	100.0	100.0	2.1	1.8
123529	368.	.256E+04	.117E+04	100.0	100.0	4.7	3.9
123531	4987.	-.817E+01	.110E+04	4.2	8.4	372.4	312.5
123532	4987.	.895E+04	.239E+04	100.0	100.0	.7	.6
123533	4987.	-.270E-01	.124E+00	87.5	99.8	12.8	10.7
123537	3187.	.129E+05	.368E+04	100.0	100.0	1.0	.8
123538	3187.	.991E+04	.281E+04	100.0	100.0	1.0	.8
123539	3187.	.329E+04	.162E+04	100.0	100.0	1.7	1.4
123541	1456.	.117E+03	.155E+04	22.7	43.7	67.9	56.9
123542	1456.	.875E+04	.251E+04	100.0	100.0	1.5	1.2
123543	1456.	-.176E-01	.167E+00	31.2	57.8	48.8	41.0
123547	1360.	.136E+05	.252E+04	100.0	100.0	1.0	.8
123548	1360.	.104E+05	.230E+04	100.0	100.0	1.2	1.0
123549	1360.	.336E+04	.108E+04	100.0	100.0	1.7	1.4
123551	6975.	.118E+02	.117E+04	6.7	13.4	233.1	195.7
123552	6975.	.890E+04	.237E+04	100.0	100.0	.6	.5
123553	6975.	-.250E-01	.130E+00	89.1	99.9	12.2	10.3
123557	4947.	.129E+05	.343E+04	100.0	100.0	.7	.6
123558	4947.	.999E+04	.263E+04	100.0	100.0	.7	.6
123559	4947.	.325E+04	.147E+04	100.0	100.0	1.3	1.1
123611	276.	-.683E+03	.660E+03	91.3	99.9	11.5	9.6
123612	276.	.226E+05	.860E+04	100.0	100.0	4.5	3.8
123613	276.	-.313E-01	.259E-01	95.5	100.0	9.8	8.2
123617	276.	.261E+05	.101E+05	100.0	100.0	4.6	3.8
123618	276.	.242E+05	.998E+04	100.0	100.0	4.9	4.1
123619	276.	.214E+04	.233E+04	87.2	99.8	12.9	10.8
123621	4780.	-.452E+03	.900E+03	99.9	100.0	5.6	4.7
123622	4780.	.241E+05	.892E+04	100.0	100.0	1.0	.9
123623	4780.	-.172E-01	.353E-01	99.9	100.0	5.8	4.9
123627	3505.	.278E+05	.105E+05	100.0	100.0	1.2	1.0
123628	3505.	.261E+05	.103E+05	100.0	100.0	1.3	1.1
123629	3505.	.213E+04	.226E+04	100.0	100.0	3.5	3.0
123631	11063.	-.182E+03	.123E+04	86.1	99.8	12.6	10.6
123632	11063.	.174E+05	.103E+05	100.0	100.0	1.1	.9
123633	11063.	-.182E-01	.975E-01	95.1	100.0	10.0	8.4

KEY	AXLES	MEAN	STU DEV	CONF (10:1)	CONF (20:1)	CONF (35:1)	CONF (50:1)
123637	7189.	.220E+05	.113E+05	100.0	100.0	1.2	1.0
123638	7189.	.195E+05	.114E+05	100.0	100.0	1.4	1.1
123639	7189.	.280E+04	.191E+04	100.0	100.0	1.6	1.3
123641	6598.	.417E+00	.142E+04	.2	.4	8235.7	6911.6
123642	6598.	.172E+05	.813E+04	100.0	100.0	1.1	1.0
123643	6598.	.631E-02	.106E+00	37.0	66.5	40.7	34.2
123647	5600.	.223E+05	.900E+04	100.0	100.0	1.1	.9
123648	5600.	.194E+05	.887E+04	100.0	100.0	1.2	1.0
123649	5600.	.314E+04	.130E+04	100.0	100.0	1.1	.9
123651	22717.	.192E+03	.124E+04	98.1	100.0	8.4	7.0
123652	22717.	.186E+05	.963E+04	100.0	100.0	.7	.6
123653	22717.	.147E-01	.906E-01	98.6	100.0	8.0	6.7
123657	16570.	.234E+05	.106E+05	100.0	100.0	.7	.6
123658	16570.	.209E+05	.107E+05	100.0	100.0	.8	.7
123659	16570.	.276E+04	.186E+04	100.0	100.0	1.0	.9
124111	24.	.625E+03	.170E+04	14.2	27.9	114.6	95.0
124112	24.	.323E+05	.241E+04	100.0	100.0	3.2	2.6
124113	24.	.241E-01	.543E-01	17.0	33.2	95.3	79.0
124121	346.	.464E+03	.140E+04	46.2	78.1	31.9	26.8
124122	346.	.322E+05	.337E+04	100.0	100.0	1.1	.9
124123	346.	.186E-01	.451E-01	55.8	87.5	25.6	21.4
124131	794.	.545E+03	.149E+04	69.6	96.0	19.1	16.0
124132	794.	.319E+05	.357E+04	100.0	100.0	.8	.7
124133	794.	.210E-01	.482E-01	78.0	98.6	16.0	13.4
124141	802.	.625E+03	.161E+04	72.9	97.2	17.8	15.0
124142	802.	.321E+05	.411E+04	100.0	100.0	.9	.7
124143	802.	.232E-01	.519E-01	79.5	98.9	15.5	13.0
124151	1966.	.564E+03	.153E+04	89.8	99.9	12.0	10.1
124152	1966.	.320E+05	.375E+04	100.0	100.0	.5	.4
124153	1966.	.215E-01	.493E-01	94.7	100.0	10.1	8.5
124211	76.	.270E+03	.109E+04	17.0	33.3	92.3	77.2
124212	76.	.308E+05	.446E+04	100.0	100.0	3.3	2.8
124213	76.	.530E-02	.337E-01	10.8	21.5	145.6	121.7
124221	1987.	.194E+03	.133E+04	48.3	80.5	30.2	25.4
124222	1987.	.317E+05	.392E+04	100.0	100.0	.5	.5
124223	1987.	.194E-02	.427E-01	16.0	31.4	96.9	81.4
124231	1884.	.336E+03	.127E+04	75.0	97.9	17.0	14.3
124232	1884.	.318E+05	.413E+04	100.0	100.0	.6	.5
124233	1884.	.584E-02	.403E-01	47.0	79.1	31.2	26.2
124241	188.	.979E+02	.159E+04	6.7	13.4	233.0	195.3
124242	188.	.290E+05	.410E+04	100.0	100.0	2.0	1.7
124243	188.	.805E-02	.590E-01	14.8	29.1	105.5	88.4
124251	4135.	.247E+03	.132E+04	77.2	96.4	16.2	13.6
124252	4135.	.316E+05	.408E+04	100.0	100.0	.4	.3
124253	4135.	.332E-02	.425E-01	38.5	66.5	39.0	32.7
124311	90.	.135E+03	.736E+03	13.6	27.1	114.2	95.5
124312	90.	.231E+05	.408E+04	100.0	100.0	3.7	3.1
124313	90.	.467E-02	.326E-01	10.8	21.3	146.5	122.5
124321	1217.	.248E+03	.117E+04	54.0	86.0	26.6	22.3
124322	1217.	.236E+05	.378E+04	100.0	100.0	.9	.8
124323	1217.	.131E-01	.509E-01	63.0	92.7	21.9	18.3
124331	1254.	.567E+02	.113E+04	14.1	27.7	110.7	92.8
124332	1254.	.219E+05	.322E+04	100.0	100.0	.8	.7
124333	1254.	.358E-02	.530E-01	18.9	36.8	81.9	68.8
124341	708.	.367E+03	.151E+04	48.1	80.3	30.4	25.5

KEY	AXLES	MEAN	STD DEV	CONF(10%)	CONF(20%)	TOL(95%)	TOL(90%)
124342	708.	.216E+05	.325E+04	100.0	100.0	1.1	.9
124343	708.	.163E-01	.710E-01	45.8	77.7	32.2	27.0
124351	3269.	.190E+03	.124E+04	62.0	92.1	22.3	18.8
124352	3269.	.225E+05	.359E+04	100.0	100.0	.5	.5
124353	3269.	.965E-02	.565E-01	67.1	94.9	20.1	16.9
124411	48.	-.147E+03	.413E+03	19.3	37.5	81.7	68.1
124412	48.	.145E+05	.470E+04	96.3	100.0	9.4	7.8
124413	48.	-.156E-01	.300E-01	28.0	52.6	55.7	46.5
124421	1037.	.614E+02	.791E+03	19.7	38.3	78.5	65.9
124422	1037.	.157E+05	.383E+04	100.0	100.0	1.5	1.2
124423	1037.	.359E-03	.514E-01	1.8	3.6	872.4	732.0
124431	2004.	.285E+03	.126E+04	68.9	95.7	19.3	16.2
124432	2004.	.134E+05	.339E+04	100.0	100.0	1.1	.9
124433	2004.	.122E-01	.974E-01	42.6	73.9	34.9	29.3
124441	3700.	.471E+03	.164E+04	91.9	100.0	11.2	9.4
124442	3700.	.161E+05	.352E+04	100.0	100.0	.7	.6
124443	3700.	.233E-01	.104E+00	82.6	99.3	14.4	12.1
124451	6789.	.349E+03	.143E+04	95.5	100.0	9.8	8.2
124452	6789.	.152E+05	.374E+04	100.0	100.0	.6	.5
124453	6789.	.163E-01	.960E-01	83.7	99.5	14.0	11.8
124511	8.	.106E+03	.198E+03	11.7	23.0	155.4	124.5
124512	8.	.870E+04	.299E+04	56.3	85.6	23.7	23.0
124513	8.	-.125E-02	.260E-01	1.0	2.1	1737.6	1392.2
124521	497.	.104E+03	.495E+03	36.2	65.3	41.8	35.0
124522	497.	.847E+04	.203E+04	100.0	100.0	2.1	1.8
124523	497.	-.509E-02	.614E-01	14.7	28.8	106.2	89.1
124531	4701.	.212E+03	.121E+04	77.2	98.4	16.3	13.6
124532	4701.	.794E+04	.217E+04	100.0	100.0	.8	.7
124533	4701.	-.504E-02	.138E+00	19.7	38.2	78.6	65.9
124541	1479.	.453E+03	.173E+04	68.6	95.6	19.5	16.4
124542	1479.	.856E+04	.235E+04	100.0	100.0	1.4	1.2
124543	1479.	.164E-01	.178E+00	27.7	52.2	55.3	46.4
124551	6685.	.257E+03	.131E+04	89.2	99.9	12.2	10.2
124552	6685.	.812E+04	.222E+04	100.0	100.0	.7	.5
124553	6685.	-.297E-03	.144E+00	1.3	2.7	1164.7	977.5
124611	246.	-.970E+02	.971E+03	12.4	24.6	125.8	105.4
124612	246.	.242E+05	.798E+04	100.0	100.0	4.1	3.5
124613	246.	-.409E-02	.365E-01	13.9	27.4	112.1	94.0
124621	5084.	.380E+02	.116E+04	18.4	35.8	84.2	70.7
124622	5084.	.243E+05	.889E+04	100.0	100.0	1.0	.8
124623	5084.	.323E-02	.494E-01	35.9	64.9	42.1	35.3
124631	10637.	.135E+03	.127E+04	73.0	97.3	17.8	14.9
124632	10637.	.166E+05	.103E+05	100.0	100.0	1.2	1.0
124633	10637.	.103E-02	.105E+00	8.0	16.0	134.0	162.8
124641	6877.	.464E+03	.165E+04	98.1	100.0	8.4	7.0
124642	6877.	.173E+05	.772E+04	100.0	100.0	1.1	.9
124643	6877.	.207E-01	.117E+00	85.9	99.7	13.3	11.2
124651	22844.	.210E+03	.138E+04	97.9	100.0	8.5	7.1
124652	22844.	.186E+05	.977E+04	100.0	100.0	.7	.6
124653	22844.	.738E-02	.995E-01	73.8	97.5	17.5	14.7
125111	24.	-.875E+03	.795E+03	40.5	70.8	38.3	31.8
125112	24.	.359E+05	.258E+04	100.0	100.0	3.0	2.5
125113	24.	-.197E-01	.214E-01	34.4	62.4	45.8	38.0
125121	345.	-.859E+03	.990E+03	89.2	99.9	12.2	10.2
125122	345.	.357E+05	.319E+04	100.0	100.0	.9	.8

KEY	AXLES	MEAN	STD. DEV.	CONF (10%)	CONF (20%)	TOL (95%)	TOL (90%)
125123	345.	-.195E-01	.277E-01	81.0	99.1	15.0	12.6
125131	784.	-.715E+03	.924E+03	97.1	100.0	9.0	7.6
125132	794.	.333E+05	.392E+04	100.0	100.0	.8	.7
125133	794.	-.172E-01	.287E-01	90.9	99.9	11.6	9.7
125141	804.	-.621E+03	.115E+04	87.5	99.8	12.8	10.7
125142	804.	.320E+05	.474E+04	100.0	100.0	1.0	.9
125143	804.	-.162E-01	.418E-01	72.9	97.2	17.8	14.9
125151	1967.	-.704E+03	.103E+04	99.7	100.0	6.5	5.4
125152	1967.	.332E+05	.436E+04	100.0	100.0	.6	.5
125153	1967.	-.173E-01	.345E-01	97.4	100.0	8.8	7.4
125211	76.	-.126E+04	.623E+03	91.8	99.9	11.3	9.4
125212	76.	.328E+05	.325E+04	100.0	100.0	2.3	1.9
125213	76.	-.348E-01	.102E-01	89.9	99.9	12.0	10.0
125221	1849.	-.138E+04	.935E+03	100.0	100.0	3.1	2.6
125222	1849.	.331E+05	.481E+04	100.0	100.0	.7	.6
125223	1849.	-.382E-01	.288E-01	100.0	100.0	3.4	2.9
125231	1884.	-.142E+04	.110E+04	100.0	100.0	3.5	2.9
125232	1884.	.355E+05	.417E+04	100.0	100.0	.5	.4
125233	1884.	-.350E-01	.306E-01	100.0	100.0	3.9	3.3
125241	149.	-.905E+03	.135E+04	58.7	89.7	24.1	20.2
125242	149.	.335E+05	.497E+04	100.0	100.0	2.4	2.0
125243	149.	-.243E-01	.466E-01	45.8	77.6	32.4	27.1
125251	3958.	-.138E+04	.103E+04	100.0	100.0	2.3	2.0
125252	3958.	.343E+05	.466E+04	100.0	100.0	.4	.4
125253	3958.	-.361E-01	.306E-01	100.0	100.0	2.6	2.2
125311	89.	-.877E+03	.598E+03	83.0	99.3	14.4	12.0
125312	89.	.240E+05	.283E+04	100.0	100.0	2.5	2.1
125313	89.	-.358E-01	.243E-01	83.2	99.3	14.3	12.0
125321	1067.	-.854E+03	.888E+03	99.8	100.0	6.2	5.2
125322	1067.	.253E+05	.577E+04	100.0	100.0	1.4	1.1
125323	1067.	-.319E-01	.325E-01	99.9	100.0	6.1	5.1
125331	1250.	-.496E+03	.104E+04	90.7	99.9	11.7	9.8
125332	1250.	.252E+05	.395E+04	100.0	100.0	.9	.7
125333	1250.	-.184E-01	.403E-01	89.3	99.9	12.2	10.2
125341	676.	-.299E+03	.145E+04	40.8	71.6	36.7	30.7
125342	676.	.240E+05	.402E+04	100.0	100.0	1.3	1.1
125343	676.	-.112E-01	.594E-01	40.2	70.8	37.3	31.3
125351	3082.	-.586E+03	.111E+04	99.7	100.0	6.7	5.6
125352	3082.	.249E+05	.468E+04	100.0	100.0	.7	.6
125353	3082.	-.220E-01	.423E-01	99.6	100.0	6.8	5.7
125411	51.	-.353E+03	.414E+03	45.4	77.1	33.0	27.5
125412	51.	.147E+05	.302E+04	93.9	100.0	5.8	4.8
125413	51.	-.278E-01	.229E-01	61.1	91.1	23.1	19.3
125421	921.	-.522E+03	.540E+03	99.7	100.0	6.7	5.6
125422	921.	.180E+05	.497E+04	100.0	100.0	1.8	1.5
125423	921.	-.320E-01	.307E-01	99.8	100.0	6.2	5.2
125431	2002.	-.225E+03	.995E+03	68.8	95.7	19.4	16.3
125432	2002.	.158E+05	.393E+04	100.0	100.0	1.1	.9
125433	2002.	-.189E-01	.708E-01	76.7	98.3	16.4	13.8
125441	3650.	-.131E+03	.127E+04	46.5	78.5	31.6	26.5
125442	3650.	.182E+05	.449E+04	100.0	100.0	.8	.7
125443	3650.	-.108E-01	.774E-01	60.1	90.8	23.2	19.5
125451	6624.	-.215E+03	.112E+04	88.3	99.8	12.5	10.5
125452	6624.	.174E+05	.453E+04	100.0	100.0	.6	.5
125453	6624.	-.163E-01	.708E-01	94.0	100.0	10.4	8.8

KEY	AXLES	MEAN	STD. DEV	CONF (10%)	CONF (20%)	TOL (95%)	TOL (90%)
125511	31.	-.153E+03	.217E+03	30.3	56.1	52.0	43.2
125512	31.	-.993E+04	.165E+04	99.8	100.0	6.1	5.1
125513	31.	-.292E-01	.234E-01	50.8	82.5	29.4	24.4
125521	438.	-.199E+03	.418E+03	68.1	95.3	19.7	16.5
125522	438.	.105E+05	.463E+04	100.0	100.0	4.1	3.5
125523	438.	-.280E-01	.315E-01	93.7	100.0	10.5	8.8
125531	4591.	-.992E+02	.812E+03	59.2	90.2	23.7	19.9
125532	4591.	-.880E+04	.266E+04	100.0	100.0	.9	.7
125533	4591.	-.388E-01	.101E+00	99.1	100.0	7.6	6.3
125541	1255.	-.266E+02	.122E+04	6.1	12.2	254.8	213.8
125542	1255.	.857E+04	.279E+04	100.0	100.0	1.8	1.5
125543	1255.	-.332E-01	.136E+00	61.3	91.6	22.7	19.0
125551	6315.	-.920E+02	.890E+03	58.9	90.0	23.8	20.0
125552	6315.	.886E+04	.290E+04	100.0	100.0	.2	.7
125553	6315.	-.369E-01	.106E+00	99.4	100.0	7.1	5.9
125611	271.	-.803E+03	.684E+03	94.6	100.0	10.2	8.5
125612	271.	.242E+05	.903E+04	100.0	100.0	4.5	3.7
125613	271.	-.318E-01	.227E-01	97.9	100.0	8.5	7.1
125621	4620.	-.937E+03	.920E+03	100.0	100.0	2.8	2.4
125622	4620.	.263E+05	.934E+04	100.0	100.0	1.0	.9
125623	4620.	-.332E-01	.307E-01	100.0	100.0	2.7	2.2
125631	10521.	-.453E+03	.106E+04	100.0	100.0	4.5	3.7
125632	10521.	.187E+05	.113E+05	100.0	100.0	1.2	1.0
125633	10521.	-.303E-01	.771E-01	100.0	100.0	4.9	4.1
125641	6534.	-.206E+03	.129E+04	80.4	99.0	15.1	12.7
125642	6534.	.190E+05	.821E+04	100.0	100.0	1.0	.9
125643	6534.	-.161E-01	.869E-01	86.6	99.7	13.1	11.0
125651	21946.	-.486E+03	.113E+04	100.0	100.0	3.1	2.6
125652	21946.	.205E+05	.105E+05	100.0	100.0	.7	.6
125653	21946.	-.267E-01	.731E-01	100.0	100.0	3.6	3.0
126111	24.	.125E+02	.136E+04	.4	.7	4589.1	3802.0
126112	24.	.339E+05	.196E+04	100.0	100.0	2.4	2.0
126113	24.	.375E-02	.389E-01	3.7	7.4	437.9	362.8
126121	370.	-.163E+03	.151E+04	16.5	32.2	94.6	79.3
126122	370.	.337E+05	.325E+04	100.0	100.0	1.0	.8
126123	370.	-.103E-02	.449E-01	3.5	7.0	447.1	374.9
126131	794.	-.110E+03	.121E+04	20.2	39.1	76.6	64.3
126132	794.	.345E+05	.404E+04	100.0	100.0	.8	.7
126133	794.	.970E-03	.360E-01	6.0	12.0	258.9	217.2
126141	804.	.117E+03	.163E+04	16.1	31.5	96.8	81.2
126142	804.	.350E+05	.435E+04	100.0	100.0	.9	.7
126143	804.	.801E-02	.481E-01	36.3	65.5	41.6	34.9
126151	1992.	-.270E+02	.146E+04	6.6	13.1	237.1	199.0
126152	1992.	.345E+05	.405E+04	100.0	100.0	.5	.4
126153	1992.	.348E-02	.431E-01	28.1	52.8	54.5	45.8
126211	76.	-.787E+03	.658E+03	70.0	96.0	19.1	16.0
126212	76.	.341E+05	.396E+04	100.0	100.0	2.7	2.2
126213	76.	-.180E-01	.191E-01	58.7	89.6	24.2	20.2
126221	1632.	-.706E+03	.133E+04	96.8	100.0	9.2	7.7
126222	1632.	.336E+05	.422E+04	100.0	100.0	.6	.5
126223	1632.	-.167E-01	.399E-01	90.8	99.9	11.6	9.8
126231	1884.	-.878E+03	.127E+04	99.7	100.0	6.5	5.5
126232	1884.	.343E+05	.396E+04	100.0	100.0	.5	.4
126233	1884.	-.212E-01	.377E-01	98.5	100.0	8.0	6.8
126241	188.	-.713E+03	.113E+04	61.1	91.4	22.8	19.1

KEY	AXLES	MEAN	STD DEV	CONF(10%)	CONF(20%)	CONF(95%)	IOL(90%)
126242	188.	.316E+05	.454E+04	100.0	100.0	2.1	1.7
126243	188.	-.190E-01	.371E-01	51.6	83.7	23.2	23.6
126251	3780.	-.793E+03	.128E+04	100.0	100.0	5.2	4.3
126252	3780.	.340E+05	.414E+04	100.0	100.0	.4	.3
126253	3780.	-.190E-01	.384E-01	99.8	100.0	6.4	5.4
126311	92.	-.460E+03	.591E+03	54.3	86.1	26.6	22.2
126312	92.	.249E+05	.330E+04	100.0	100.0	2.7	2.3
126313	92.	-.159E-01	.229E-01	49.3	81.4	23.8	25.0
126321	1170.	-.408E+03	.105E+04	61.7	95.2	14.7	12.3
126322	1170.	.255E+05	.482E+04	100.0	100.0	1.1	.9
126323	1170.	-.140E-01	.398E-01	77.1	98.4	16.3	13.7
126331	1250.	-.252E+03	.106E+04	60.2	90.9	23.2	19.5
126332	1250.	.239E+05	.354E+04	100.0	100.0	.8	.7
126333	1250.	-.952E-02	.444E-01	55.2	87.1	25.9	21.7
126341	680.	-.107E+03	.147E+04	15.1	29.6	103.4	86.7
126342	680.	.239E+05	.347E+04	100.0	100.0	1.1	.9
126343	680.	-.463E-02	.596E-01	16.0	31.4	37.1	81.4
126351	3192.	-.285E+03	.115E+04	83.7	99.5	14.0	11.8
126352	3192.	.245E+05	.412E+04	100.0	100.0	.6	.5
126353	3192.	-.103E-01	.462E-01	79.2	98.8	15.6	13.1
126411	52.	-.712E+02	.415E+03	9.8	19.4	162.4	135.5
126412	52.	.148E+05	.347E+04	99.7	100.0	5.5	5.4
126413	52.	-.788E-02	.271E-01	16.5	32.3	95.8	79.9
126421	1012.	-.249E+03	.679E+03	75.7	98.0	16.8	14.1
126422	1012.	.171E+05	.436E+04	100.0	100.0	1.6	1.3
126423	1012.	-.182E-01	.379E-01	87.2	99.8	12.9	10.8
126431	2004.	-.826E+02	.985E+03	25.2	54.7	52.2	43.8
126432	2004.	.156E+05	.352E+04	100.0	100.0	1.0	.8
126433	2004.	-.115E-01	.654E-01	56.7	88.3	25.0	21.0
126441	3676.	.194E+03	.147E+04	57.8	89.1	24.4	20.5
126442	3676.	.193E+05	.382E+04	100.0	100.0	.6	.5
126443	3676.	.700E-02	.805E-01	40.2	70.8	37.2	31.2
126451	6744.	.434E+02	.125E+04	22.4	43.1	68.8	57.7
126452	6744.	.178E+05	.417E+04	100.0	100.0	.6	.5
126453	6744.	-.237E-02	.717E-01	21.4	41.3	72.1	60.5
126511	32.	-.109E+02	.198E+03	2.5	4.9	652.5	542.4
126512	32.	.975E+04	.123E+04	100.0	100.0	4.5	3.8
126513	32.	-.125E-01	.227E-01	24.3	46.3	55.3	54.3
126521	492.	-.131E+02	.361E+03	6.4	12.8	243.7	204.4
126522	492.	.930E+04	.190E+04	100.0	100.0	1.8	1.5
126523	492.	-.156E-01	.423E-01	58.5	89.7	24.1	20.2
126531	4704.	-.476E+02	.103E+04	25.0	47.5	61.6	51.7
126532	4704.	.109E+05	.235E+04	100.0	100.0	.6	.5
126533	4704.	-.197E-01	.860E-01	88.3	99.8	12.5	10.5
126541	1486.	.330E+03	.158E+04	56.0	89.3	24.3	20.4
126542	1486.	.120E+05	.299E+04	100.0	100.0	1.1	1.1
126543	1486.	.993E-02	.118E+00	25.5	48.4	60.3	50.6
126551	6714.	.387E+02	.115E+04	21.7	41.9	71.1	59.7
126552	6714.	.110E+05	.256E+04	100.0	100.0	.6	.5
126553	6714.	-.128E-01	.924E-01	74.4	97.7	17.3	14.5
126611	276.	-.394E+03	.727E+03	61.9	92.0	22.4	18.8
126612	276.	.246E+05	.932E+04	100.0	100.0	4.5	3.8
126613	276.	-.129E-01	.254E-01	60.0	90.7	23.4	19.6
126621	4676.	-.417E+03	.112E+04	98.9	100.0	7.7	6.4
126622	4676.	.255E+05	.949E+04	100.0	100.0	1.1	.9

KEY	AXLES	MEAN	STD. DEV.	CONE.(103)	CONE.(203)	TOL.(953)	TOL.(903)
126623	4676.	-150E-01	.404E-01	98.9	100.0	7.7	6.5
126631	10636.	-230E+03	.113E+04	96.5	100.0	9.3	7.8
126632	10636.	.192E+05	.102E+05	100.0	100.0	1.0	.8
126633	10636.	-157E-01	.686E-01	98.1	100.0	8.3	7.0
126641	6834.	.160E+03	.152E+04	61.6	91.8	22.5	18.9
126642	6834.	.203E+05	.771E+04	100.0	100.0	.9	.8
126643	6834.	.589E-02	.848E-01	43.4	74.9	34.2	28.7
126651	22422.	-152E+03	.127E+04	92.7	100.0	10.9	9.2
126652	22422.	.209E+05	.965E+04	100.0	100.0	.6	.5
126653	22422.	-892E-02	.698E-01	94.4	100.0	10.2	8.6
127111	24.	.388E+03	.166E+04	9.0	17.9	180.7	149.7
127112	24.	.357E+05	.257E+04	100.0	100.0	3.0	2.5
127113	24.	.159E-01	.463E-01	13.2	26.1	122.6	101.6
127121	342.	.343E+03	.135E+04	36.1	65.2	41.9	35.1
127122	342.	.353E+05	.341E+04	100.0	100.0	1.0	.9
127123	342.	.143E-01	.384E-01	50.9	83.1	28.5	23.9
127131	718.	.378E+03	.119E+04	60.5	91.1	23.1	19.4
127132	718.	.331E+05	.417E+04	100.0	100.0	.9	.8
127133	718.	.161E-01	.367E-01	75.9	98.1	16.7	14.0
127141	752.	.590E+03	.123E+04	81.2	99.1	14.9	12.5
127142	752.	.313E+05	.426E+04	100.0	100.0	1.0	.8
127143	752.	.225E-01	.401E-01	87.6	99.8	12.7	10.7
127151	1836.	.459E+03	.125E+04	88.4	99.8	12.5	10.5
127152	1836.	.328E+05	.432E+04	100.0	100.0	.6	.5
127153	1836.	.184E-01	.388E-01	95.8	100.0	9.6	8.1
127211	76.	-349E+02	.579E+03	4.2	8.3	379.2	317.0
127212	76.	.323E+05	.360E+04	100.0	100.0	2.5	2.1
127213	76.	.349E-02	.180E-01	13.4	26.3	118.1	98.7
127221	1720.	-399E+03	.104E+04	88.8	99.8	12.3	10.4
127222	1720.	.317E+05	.414E+04	100.0	100.0	.6	.5
127223	1720.	-848E-02	.333E-01	70.9	96.5	18.6	15.6
127231	1802.	-381E+03	.108E+04	86.7	99.7	13.0	10.9
127232	1802.	.318E+05	.369E+04	100.0	100.0	.6	.5
127233	1802.	-736E-02	.339E-01	64.3	93.4	21.3	17.9
127241	188.	-346E+02	.105E+04	3.6	7.2	438.6	367.7
127242	188.	.289E+05	.447E+04	100.0	100.0	2.2	1.9
127243	188.	.150E-02	.398E-01	4.1	8.2	380.9	319.2
127251	3786.	-365E+03	.106E+04	96.7	100.0	9.2	7.7
127252	3786.	.317E+05	.408E+04	100.0	100.0	.4	.3
127253	3786.	-721E-02	.338E-01	81.0	99.1	14.9	12.5
127311	90.	.200E+02	.601E+03	2.5	5.0	629.7	526.8
127312	90.	.242E+05	.331E+04	100.0	100.0	2.9	2.4
127313	90.	.242E-02	.261E-01	7.0	13.9	225.9	189.0
127321	1264.	-828E+02	.938E+03	23.4	44.9	65.8	55.2
127322	1264.	.244E+05	.481E+04	100.0	100.0	1.1	.9
127323	1264.	-188E-02	.398E-01	13.4	26.3	116.6	97.9
127331	1096.	.149E+03	.109E+04	34.9	63.5	43.3	36.4
127332	1096.	.219E+05	.362E+04	100.0	100.0	.8	.8
127333	1096.	.741E-02	.502E-01	37.5	67.2	40.1	33.6
127341	642.	.329E+03	.128E+04	48.4	80.6	30.2	25.4
127342	642.	.212E+05	.381E+04	100.0	100.0	1.4	1.2
127343	642.	.147E-01	.598E-01	46.6	78.7	31.5	26.5
127351	3092.	.876E+02	.109E+04	34.4	62.8	44.0	36.5
127352	3092.	.229E+05	.440E+04	100.0	100.0	.7	.6
127353	3092.	.498E-02	.484E-01	43.3	74.7	34.3	28.8

KEY	AXLES	MEAN	STD DEV	CONF.(10%)	CONF.(20%)	TOL.(95%)	TOL.(99.8%)
127411	52.	.154E+02	.405E+03	2.2	4.3	733.0	611.7
127412	52.	.147E+05	.353E+04	99.6	100.0	6.7	5.6
127413	52.	-.486E-02	.274E-01	10.1	20.1	157.2	131.2
127421	1063.	-.598E+02	.544E+03	26.1	49.5	58.8	49.4
127422	1063.	.162E+05	.409E+04	100.0	100.0	1.5	1.3
127423	1063.	-.796E-02	.383E-01	50.2	82.5	28.9	24.3
127431	1741.	.164E+03	.106E+04	48.2	80.4	30.3	25.4
127432	1741.	.139E+05	.368E+04	100.0	100.0	1.2	1.0
127433	1741.	.487E-02	.799E-01	20.0	38.8	77.2	64.8
127441	3469.	.305E+03	.134E+04	81.9	99.2	14.7	12.3
127442	3469.	.165E+05	.401E+04	100.0	100.0	.8	.7
127443	3469.	.138E-01	.915E-01	62.6	92.5	22.0	18.5
127451	6325.	.202E+03	.177E+04	83.0	99.4	14.3	12.0
127452	6325.	.157E+05	.409E+04	100.0	100.0	.6	.5
127453	6325.	.754E-02	.816E-01	53.7	85.8	26.7	22.4
127511	32.	-.266E+02	.296E+03	4.0	8.0	404.4	336.2
127512	32.	.889E+04	.123E+04	100.0	100.0	5.0	4.2
127513	32.	-.118E-01	.346E-01	15.2	29.8	105.7	87.9
127521	477.	-.399E+02	.381E+03	18.1	35.3	85.8	72.0
127522	477.	.867E+04	.240E+04	100.0	100.0	2.5	2.1
127523	477.	-.209E-01	.515E-01	62.4	92.3	22.2	18.6
127531	4161.	.258E+03	.114E+04	85.6	99.7	13.4	11.2
127532	4161.	.805E+04	.214E+04	100.0	100.0	.8	.7
127533	4161.	.426E-02	.128E+00	17.0	33.3	91.0	76.4
127541	1334.	.567E+03	.167E+04	78.5	96.7	15.8	13.3
127542	1334.	.790E+04	.254E+04	100.0	100.0	1.7	1.4
127543	1334.	.356E-01	.199E+00	49.7	50.9	30.0	25.2
127551	6004.	.302E+03	.125E+04	93.3	100.0	10.5	8.8
127552	6004.	.807E+04	.226E+04	100.0	100.0	.7	.6
127553	6004.	.914E-02	.143E+00	37.9	67.7	39.6	33.3
127611	274.	.369E+02	.712E+03	6.8	13.6	229.6	192.5
127612	274.	.239E+05	.919E+04	100.0	100.0	4.6	3.8
127613	274.	.858E-03	.288E-01	3.9	7.8	399.7	335.1
127621	4866.	-.155E+03	.947E+03	74.7	97.8	17.1	14.4
127622	4866.	.244E+05	.914E+04	100.0	100.0	1.1	.9
127623	4866.	-.627E-02	.333E-01	73.4	97.4	17.6	14.8
127631	9518.	.116E+03	.114E+04	68.1	95.4	19.7	16.5
127632	9518.	.171E+05	.105E+05	100.0	100.0	1.2	1.0
127633	9518.	.343E-02	.945E-01	27.6	52.1	55.4	46.5
127641	6385.	.386E+03	.140E+04	97.2	100.0	8.9	7.5
127642	6385.	.173E+05	.786E+04	100.0	100.0	1.1	.9
127643	6385.	.191E-01	.116E+00	81.2	99.1	14.9	12.5
127651	21043.	.134E+03	.120E+04	89.6	99.9	12.1	10.1
127652	21043.	.189E+05	.995E+04	100.0	100.0	.7	.6
127653	21043.	.591E-02	.927E-01	64.5	93.6	21.2	17.8
128111	180.	-.842E+02	.135E+04	6.7	13.3	235.7	197.5
128112	180.	.346E+05	.333E+04	100.0	100.0	1.4	1.2
128113	180.	.229E-02	.344E-01	6.2	12.4	252.7	211.7
128121	2551.	-.129E+03	.128E+04	38.7	68.8	38.7	32.5
128122	2551.	.347E+05	.376E+04	100.0	100.0	.4	.4
128123	2551.	.915E-03	.378E-01	9.7	19.3	160.4	134.6
128131	5552.	-.101E+01	.125E+04	.5	1.0	3264.2	2739.4
128132	5552.	.340E+05	.444E+04	100.0	100.0	.3	.3
128133	5552.	.441E-02	.386E-01	60.6	91.2	23.0	19.3
128141	5568.	.117E+03	.136E+04	47.8	79.9	30.6	25.7

KEY	AXLES	MEAN	SID DEV	CONF.(10:)	CONF.(20:)	TOL(95:)	TOL(90:)
128142	5568.	.336E+05	.502E+04	100.0	100.0	.4	.3
128143	5568.	.776E-02	.426E-01	82.6	99.3	14.4	12.1
128151	13851.	.217E+02	.131E+04	15.5	30.4	100.4	84.3
128152	13851.	.339E+05	.428E+04	100.0	100.0	.2	.2
128153	13851.	.509E-02	.402E-01	86.4	99.7	13.1	11.0
128211	536.	-.607E+03	.883E+03	28.6	99.8	12.3	10.4
128212	536.	.332E+05	.431E+04	100.0	100.0	1.1	.9
128213	536.	-.146E-01	.266E-01	79.4	98.8	15.5	13.0
128221	12948.	-.647E+03	.117E+04	100.0	100.0	3.1	2.6
128222	12948.	.335E+05	.477E+04	100.0	100.0	.2	.2
128223	12948.	-.153E-01	.357E-01	100.0	100.0	4.0	3.4
128231	13118.	-.738E+03	.125E+04	100.0	100.0	2.9	2.4
128232	13118.	.342E+05	.459E+04	100.0	100.0	.2	.2
128233	13118.	-.167E-01	.373E-01	100.0	100.0	3.8	3.2
128241	1221.	-.412E+03	.148E+04	66.8	94.7	20.2	17.0
128242	1221.	.319E+05	.520E+04	100.0	100.0	.9	.8
128243	1221.	-.907E-02	.507E-01	46.8	78.8	31.4	26.4
128251	27823.	-.679E+03	.122E+04	100.0	100.0	2.1	1.8
128252	27823.	.337E+05	.472E+04	100.0	100.0	.2	.1
128253	27823.	-.157E-01	.372E-01	100.0	100.0	2.8	2.3
128311	632.	-.393E+03	.711E+03	83.5	99.4	14.1	11.9
128312	632.	.244E+05	.369E+04	100.0	100.0	1.2	1.0
128313	632.	-.146E-01	.305E-01	77.7	98.5	16.1	13.5
128321	8494.	-.223E+03	.102E+04	95.5	100.0	9.8	8.2
128322	8494.	.253E+05	.482E+04	100.0	100.0	.4	.3
128323	8494.	-.641E-02	.407E-01	85.3	99.6	13.5	11.3
128331	8699.	-.711E+02	.117E+04	42.8	74.1	34.7	29.1
128332	8699.	.239E+05	.398E+04	100.0	100.0	.4	.3
128333	8699.	-.150E-02	.500E-01	22.0	42.3	70.2	58.9
128341	4724.	.638E+02	.143E+04	31.3	58.0	48.6	40.8
128342	4724.	.230E+05	.395E+04	100.0	100.0	.5	.4
128343	4724.	.435E-02	.504E-01	37.9	67.8	39.6	33.2
128351	22549.	-.105E+03	.118E+04	81.9	99.3	14.6	12.3
128352	22549.	.243E+05	.440E+04	100.0	100.0	.2	.2
128353	22549.	-.245E-02	.490E-01	55.5	87.4	25.6	21.5
128411	439.	-.133E+03	.423E+03	49.1	81.3	29.7	24.5
128412	439.	.154E+05	.369E+04	100.0	100.0	2.3	1.9
128413	439.	-.128E-01	.270E-01	67.9	95.2	19.8	16.6
128421	7103.	-.138E+03	.663E+03	92.0	100.0	11.2	9.4
128422	7103.	.170E+05	.448E+04	100.0	100.0	.6	.5
128423	7103.	-.109E-01	.404E-01	97.7	100.0	8.6	7.2
128431	13718.	.104E+03	.117E+04	70.0	96.2	18.9	15.9
128432	13718.	.150E+05	.380E+04	100.0	100.0	.4	.4
128433	13718.	.960E-03	.833E-01	10.7	21.3	145.2	121.8
128441	25376.	.226E+03	.147E+04	98.6	100.0	8.0	6.7
128442	25376.	.176E+05	.416E+04	100.0	100.0	.3	.2
128443	25376.	.938E-02	.905E-01	90.1	99.9	11.9	10.0
128451	46636.	.132E+03	.129E+04	97.2	100.0	8.9	7.5
128452	46636.	.167E+05	.425E+04	100.0	100.0	.2	.2
128453	46636.	.360E-02	.825E-01	65.4	94.0	20.8	17.5
128511	211.	-.268E+02	.271E+03	11.4	22.6	137.1	114.9
128512	211.	.945E+04	.177E+04	100.0	100.0	2.5	2.1
128513	211.	-.162E-01	.301E-01	56.6	88.1	25.2	21.1
128521	3431.	-.657E+01	.416E+03	7.4	14.7	211.9	177.8
128522	3431.	.932E+04	.262E+04	100.0	100.0	.9	.8

KEY	AXLES	MEAN	STD DEV	CONF (101)	CONF (201)	TOL (951)	TOL (901)
128523	3431.	-.146E-01	.460E-01	93.7	100.0	10.5	8.3
128531	32980.	.108E+03	.108E+04	93.1	100.0	10.8	9.0
128532	32980.	.918E+04	.253E+04	100.0	100.0	.3	.2
128533	32980.	-.110E-01	.115E+00	91.8	99.9	11.3	9.5
128541	9961.	.364E+03	.165E+04	97.2	100.0	8.9	7.5
128542	9961.	.945E+04	.291E+04	100.0	100.0	.6	.5
128543	9961.	.102E-01	.164E+00	46.7	78.8	31.4	26.4
128551	46583.	.154E+03	.120E+04	99.4	100.0	7.1	5.9
128552	46583.	.925E+04	.262E+04	100.0	100.0	.3	.2
128553	46583.	-.674E-02	.124E+00	76.0	98.1	16.7	14.0
128611	1998.	-.327E+03	.791E+03	93.5	100.0	10.6	8.9
128612	1998.	.241E+05	.924E+04	100.0	100.0	1.7	1.4
128613	1998.	-.129E-01	.301E-01	94.5	100.0	10.2	8.6
128621	34527.	-.336E+03	.103E+04	100.0	100.0	3.2	2.7
128622	34527.	.258E+05	.954E+04	100.0	100.0	.4	.3
128623	34527.	-.109E-01	.395E-01	100.0	100.0	3.8	3.2
128631	74067.	-.717E+02	.120E+04	89.7	99.9	12.0	10.1
128632	74067.	.183E+05	.109E+05	100.0	100.0	.4	.4
128633	74067.	-.752E-02	.886E-01	97.9	100.0	8.5	7.1
128641	46850.	.212E+03	.150E+04	99.8	100.0	6.4	5.4
128642	46850.	.187E+05	.824E+04	100.0	100.0	.4	.3
128643	46850.	.838E-02	.104E+00	91.3	100.0	11.2	9.4
128651	157442.	-.485E+02	.128E+04	86.9	99.7	13.0	10.9
128652	157442.	.201E+05	.103E+05	100.0	100.0	.3	.2
128653	157442.	-.361E-02	.856E-01	90.6	99.9	11.7	9.6
137111	★ 180.	.490E+04	.325E+04	95.5	100.0	9.8	8.2
137112	180.	.292E+05	.444E+04	100.0	100.0	2.2	1.9
137113	180.	.174E+00	.118E+00	95.1	100.0	10.0	8.4
137121	256.	.460E+04	.429E+04	91.2	99.9	11.5	9.6
137122	256.	.271E+05	.445E+04	100.0	100.0	2.0	1.7
137123	256.	.171E+00	.159E+00	91.2	99.9	11.5	9.6
137151	436.	.472E+04	.390E+04	98.8	100.0	7.8	6.5
137152	436.	.279E+05	.456E+04	100.0	100.0	1.5	1.3
137153	436.	.172E+00	.144E+00	98.7	100.0	7.9	6.6
137211	202.	.494E+04	.338E+04	96.1	100.0	9.5	8.0
137212	202.	.282E+05	.376E+04	100.0	100.0	1.9	1.6
137213	202.	.181E+00	.126E+00	95.9	100.0	9.6	8.0
137221	393.	.471E+04	.443E+04	96.5	100.0	9.3	7.8
137222	393.	.284E+05	.312E+04	100.0	100.0	1.1	.9
137223	393.	.167E+00	.150E+00	97.2	100.0	8.9	7.5
137251	595.	.479E+04	.410E+04	99.5	100.0	6.9	5.8
137252	595.	.283E+05	.335E+04	100.0	100.0	1.0	.8
137253	595.	.172E+00	.143E+00	99.7	100.0	6.7	5.6
137311	320.	.353E+04	.252E+04	99.7	100.0	7.8	6.6
137312	320.	.219E+05	.357E+04	100.0	100.0	1.8	1.5
137313	320.	.166E+00	.119E+00	98.7	100.0	7.9	6.6
137321	312.	.346E+04	.267E+04	97.7	100.0	8.6	7.2
137322	312.	.210E+05	.312E+04	100.0	100.0	1.7	1.4
137323	312.	.166E+00	.125E+00	98.1	100.0	8.4	7.0
137351	632.	.350E+04	.259E+04	99.9	100.0	5.8	4.9
137352	632.	.215E+05	.338E+04	100.0	100.0	1.2	1.0
137353	632.	.166E+00	.122E+00	99.9	100.0	5.7	4.8
137411	442.	.234E+04	.176E+04	99.5	100.0	7.0	5.9
137412	442.	.139E+05	.346E+04	100.0	100.0	2.3	2.0
137413	442.	.165E+00	.118E+00	99.6	100.0	6.7	5.6

★ Only Site 7 (low rail) operational on 6° curve

KEY	AXLES	MEAN	STD DEV	CONF (10%)	CONF (20%)	TOL (95%)	TOL (90%)
137421	954.	.237E+04	.199E+04	100.0	100.0	5.3	4.5
137422	954.	.149E+05	.277E+04	100.0	100.0	1.2	1.0
137423	954.	.158E+00	.134E+00	100.0	100.0	5.4	4.5
137451	1396.	.236E+04	.192E+04	100.0	100.0	4.3	3.6
137452	1396.	.146E+05	.304E+04	100.0	100.0	1.1	.9
137453	1396.	.160E+00	.129E+00	100.0	100.0	4.2	3.6
137511	1272.	.994E+03	.970E+03	100.0	100.0	5.4	4.5
137512	1272.	.855E+04	.176E+04	100.0	100.0	1.1	1.0
137513	1272.	.105E+00	.116E+00	99.9	100.0	6.0	5.1
137521	848.	.873E+03	.109E+04	98.0	100.0	3.4	7.0
137522	848.	.799E+04	.203E+04	100.0	100.0	1.7	1.4
137523	848.	.924E-01	.137E+00	95.0	100.0	10.0	8.4
137551	2120.	.946E+03	.102E+04	100.0	100.0	4.6	3.9
137552	2120.	.833E+04	.190E+04	100.0	100.0	1.0	.8
137553	2120.	.100E+00	.125E+00	100.0	100.0	5.3	4.4
137611	2416.	.220E+04	.241E+04	100.0	100.0	4.4	3.7
137612	2416.	.145E+05	.811E+04	100.0	100.0	2.2	1.9
137613	2416.	.136E+00	.122E+00	100.0	100.0	3.6	3.0
137621	2763.	.257E+04	.301E+04	100.0	100.0	4.4	3.7
137622	2763.	.165E+05	.802E+04	100.0	100.0	1.8	1.5
137623	2763.	.141E+00	.143E+00	100.0	100.0	3.8	3.2
137651	5179.	.240E+04	.275E+04	100.0	100.0	3.1	2.6
137652	5179.	.156E+05	.812E+04	100.0	100.0	1.4	1.2
137653	5179.	.139E+00	.133E+00	100.0	100.0	2.6	2.2
138111	180.	.490E+04	.325E+04	95.5	100.0	9.8	8.2
138112	180.	.292E+05	.444E+04	100.0	100.0	2.2	1.9
138113	180.	.174E+00	.118E+00	95.1	100.0	10.0	8.4
138121	256.	.460E+04	.429E+04	91.2	99.9	11.5	9.6
138122	256.	.271E+05	.445E+04	100.0	100.0	2.0	1.7
138123	256.	.171E+00	.159E+00	91.2	99.9	11.5	9.6
138151	436.	.472E+04	.390E+04	98.8	100.0	7.8	6.5
138152	436.	.279E+05	.456E+04	100.0	100.0	1.5	1.3
138153	436.	.172E+00	.144E+00	98.7	100.0	7.9	6.6
138211	202.	.494E+04	.338E+04	96.1	100.0	9.5	8.0
138212	202.	.282E+05	.376E+04	100.0	100.0	1.9	1.6
138213	202.	.181E+00	.126E+00	95.9	100.0	9.6	8.0
138221	393.	.471E+04	.443E+04	96.5	100.0	9.3	7.8
138222	393.	.284E+05	.312E+04	100.0	100.0	1.1	.9
138223	393.	.167E+00	.150E+00	97.2	100.0	8.9	7.5
138251	595.	.479E+04	.410E+04	99.5	100.0	6.9	5.8
138252	595.	.283E+05	.335E+04	100.0	100.0	1.0	.8
138253	595.	.172E+00	.143E+00	99.7	100.0	6.7	5.6
138311	320.	.353E+04	.252E+04	98.7	100.0	7.8	6.6
138312	320.	.219E+05	.357E+04	100.0	100.0	1.3	1.5
138313	320.	.166E+00	.119E+00	98.7	100.0	7.9	6.6
138321	312.	.346E+04	.267E+04	97.7	100.0	8.6	7.2
138322	312.	.210E+05	.312E+04	100.0	100.0	1.7	1.4
138323	312.	.166E+00	.125E+00	98.1	100.0	8.4	7.0
138351	632.	.350E+04	.259E+04	99.9	100.0	5.8	4.9
138352	632.	.215E+05	.338E+04	100.0	100.0	1.2	1.0
138353	632.	.166E+00	.122E+00	99.9	100.0	5.7	4.8
138411	442.	.234E+04	.176E+04	99.5	100.0	7.0	5.9
138412	442.	.139E+05	.346E+04	100.0	100.0	2.3	2.0
138413	442.	.165E+00	.118E+00	99.6	100.0	6.7	5.6
138421	954.	.237E+04	.199E+04	100.0	100.0	5.3	4.5

KEY	AXLES	MEAN	STD DEV	CONF (10%)	CONF (20%)	TOL (95%)	TOL (90%)
138422	954.	.149E+05	.277E+04	100.0	100.0	1.2	1.0
138423	954.	.158E+00	.134E+00	100.0	100.0	5.4	4.5
138451	1396.	.236E+04	.192E+04	100.0	100.0	4.3	3.6
138452	1396.	.146E+05	.304E+04	100.0	100.0	1.1	.9
138453	1396.	.160E+00	.129E+00	100.0	100.0	4.2	3.6
138511	1272.	.994E+03	.970E+03	100.0	100.0	5.4	4.5
138512	1272.	.855E+04	.178E+04	100.0	100.0	1.1	1.0
138513	1272.	.105E+00	.116E+00	99.9	100.0	6.0	5.1
138521	848.	.873E+03	.109E+04	98.0	100.0	8.4	7.0
138522	848.	.799E+04	.203E+04	100.0	100.0	1.7	1.4
138523	848.	.924E-01	.137E+00	95.0	100.0	10.0	8.4
138551	2120.	.946E+03	.102E+04	100.0	100.0	4.6	3.9
138552	2120.	.833E+04	.190E+04	100.0	100.0	1.0	.8
138553	2120.	.100E+00	.125E+00	100.0	100.0	5.3	4.4
138611	2416.	.220E+04	.241E+04	100.0	100.0	4.4	3.7
138612	2416.	.145E+05	.811E+04	100.0	100.0	2.2	1.9
138613	2416.	.136E+00	.122E+00	100.0	100.0	3.6	3.0
138621	2763.	.257E+04	.301E+04	100.0	100.0	4.4	3.7
138622	2763.	.165E+05	.802E+04	100.0	100.0	1.8	1.5
138623	2763.	.141E+00	.143E+00	100.0	100.0	3.8	3.2
138651	5179.	.240E+04	.275E+04	100.0	100.0	3.1	2.6
138652	5179.	.156E+05	.812E+04	100.0	100.0	1.4	1.2
138653	5179.	.139E+00	.133E+00	100.0	100.0	2.6	2.2

226

Note 1: Approximately 6% of axles in Categories 11(i)53(j)...for example, 111531...were inadvertently from Vehicle Category 3 (70T to 110T GWT).

## OUTLYING VERTICAL LOAD VALUES, GT 60 KIPS

## OUTLYING LATERAL LOAD VALUES, GT 12 KIPS

KEY NUMBER	LATERAL LOAD	VERTICAL LOAD	L/V RATIO	KEY NUMBER	LATERAL LOAD	VERTICAL LOAD	L/V RATIO
112141.	-3331.	76150.	-.0444	111441.	14300.	19400.	.7369
112211.	-1116.	62320.	-.0179	112241.	12450.	41800.	.2981
113121.	-3637.	60800.	-.0598	112241.	16420.	37860.	.3431
113331.	-249.	80500.	-.0031	112331.	12740.	34990.	.3641
113441.	-851.	104300.	-.0082	112331.	12120.	25660.	.4723
116231.	-1943.	67400.	-.0156	112441.	12050.	30760.	.3917
116241.	-6167.	64380.	-.0958	116541.	13460.	16980.	.7927
116241.	-1651.	65710.	-.0251	121331.	13300.	44310.	.2961
116241.	-2271.	67970.	-.0334	121341.	12160.	29080.	.4182
116241.	-3317.	63110.	-.0552	121441.	12450.	16730.	.7442
116241.	-1269.	65900.	-.0193	121441.	12920.	22680.	.5697
116531.	-3261.	63190.	-.0542	121441.	14910.	18320.	.8139
117111.	-2880.	63990.	-.0450	121441.	15260.	18760.	.8134
117231.	-1221.	61670.	-.0312	121441.	14650.	18120.	.8085
121131.	-1901.	67130.	-.0301	121441.	15940.	20290.	.7856
121141.	-201.	70550.	-.0123	121441.	15430.	23240.	.6661
121221.	2601.	60280.	.0432	121441.	14670.	22210.	.6605
121221.	-4694.	90460.	-.0519	121441.	16270.	21080.	.7718
121231.	-898.	71720.	-.0125	121441.	12740.	19770.	.6444
121211.	-1803.	61550.	-.0293	121441.	12720.	17730.	.7174
122131.	3709.	66710.	.0556	121531.	12120.	13620.	.8899
122131.	-1699.	61190.	-.0278	122541.	12730.	18110.	.7029
122141.	2557.	62600.	.0409	123241.	13610.	32490.	.4189
122221.	-1144.	67140.	-.0170	123431.	12320.	20510.	.6292
122221.	-767.	61130.	-.0126	123441.	12840.	17580.	.7304
122221.	-1324.	64650.	-.0205	124431.	12830.	23180.	.5535
122221.	8276.	72610.	.1140	124441.	12720.	18700.	1.1610
122231.	-444.	63600.	-.0070	124441.	20150.	19080.	1.0570
12231.	-1676.	73840.	-.0227	124441.	20870.	14390.	1.4500
122331.	-1064.	60760.	-.0175	124441.	19860.	13720.	1.4420
123131.	3798.	67760.	.0561	124441.	21370.	14150.	1.5100
123221.	-2904.	61980.	-.0469	124441.	19830.	14870.	1.3340
123221.	-4216.	97820.	-.0431	125341.	15080.	32440.	.4649
123221.	4603.	62170.	.0740	126441.	14310.	23450.	.6102
124221.	-2540.	60320.	-.0421	127341.	12450.	26900.	.4628
124321.	-1811.	60720.	-.0298	127441.	14510.	24340.	.5962
125221.	-43.	60480.	-.0007	137111.	14280.	29360.	.4864
125231.	-3604.	65310.	-.0552	137111.	12130.	28380.	.4274
125231.	-1919.	70460.	-.0272	137111.	13130.	25650.	.5119
126131.	-1052.	61540.	-.0173	137121.	12970.	26610.	.4874
126221.	-131.	63300.	-.0021	137121.	12740.	29950.	.4254
127121.	3983.	66000.	.0604	137121.	15250.	25660.	.5938
127221.	3539.	66670.	.0515	137121.	16760.	30620.	.5474
127221.	-1282.	64870.	-.0198	137121.	16330.	28250.	.5770
127221.	-118.	74350.	-.0016	137121.	13430.	40280.	.3334
127231.	-420.	63700.	-.0066	137121.	12760.	30010.	.4252
0.	0.	0.	0.0000	137121.	14570.	25150.	.5793
				137121.	12540.	25320.	.4838
				137121.	15560.	31950.	.4870
				137121.	12720.	26280.	.4840
				137121.	13060.	25050.	.5214

OUTLYING L/V VALUES, GT 0.9

KEY NUMBER LATERAL LOAD VERTICAL LOAD L/V RATIO

113531.	5668.	5827.	.9727
121531.	5828.	4047.	1.4400
121531.	7746.	8192.	.9456
121541.	3120.	3358.	.9291
121541.	4668.	3998.	1.1680
121541.	5934.	5633.	1.0530
121541.	9167.	10120.	.9058
123531.	2389.	2543.	.9394
123541.	9008.	7660.	1.1760
123541.	7225.	7112.	1.0160
123541.	8364.	7772.	1.0760
123541.	8831.	7819.	1.1290
123541.	7619.	7577.	.9929
123541.	6933.	6029.	1.1500
123541.	9683.	8437.	1.1480
124441.	21720.	18700.	1.1610
124441.	20160.	19080.	1.0570
124441.	20870.	14390.	1.4500
124441.	19860.	13770.	1.4420
124441.	21370.	14150.	1.5100
124441.	19830.	14870.	1.3340
124531.	5367.	5748.	.9337
124531.	8397.	5700.	1.4730
125531.	2032.	1796.	1.1310
125531.	6012.	5978.	1.0060
125541.	5663.	5508.	1.0290
127531.	8641.	7513.	1.1500
127531.	6603.	6230.	1.0600
127541.	5853.	3880.	1.5090
127541.	6144.	6465.	.9503
127541.	10420.	7917.	1.3160
127541.	7794.	8230.	.9470
127541.	7912.	8616.	.9183
127541.	9851.	10010.	.9841
127541.	5757.	5670.	1.0150
127541.	1362.	1428.	.9538
127541.	3611.	3934.	.9179
127541.	4203.	2778.	1.5130 *
0.	0.	0.	0.0000

228

## APPENDIX B

### FREQUENCY OF EXCEEDANCE CURVES COMPARING VARIATIONS IN WHEEL/RAIL LOAD MEASUREMENTS AMONG WAYSIDE MEASUREMENT SITES

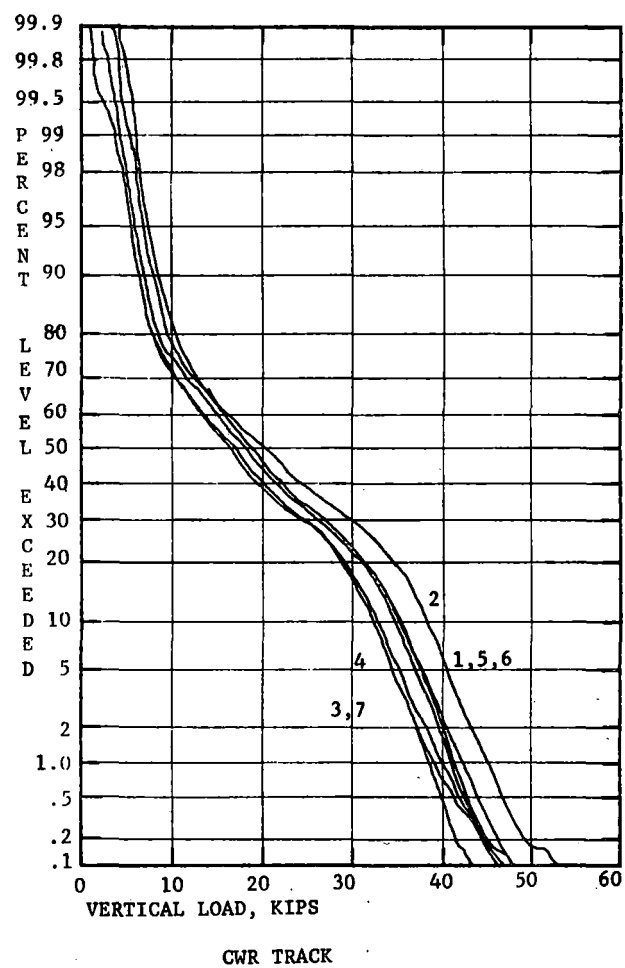
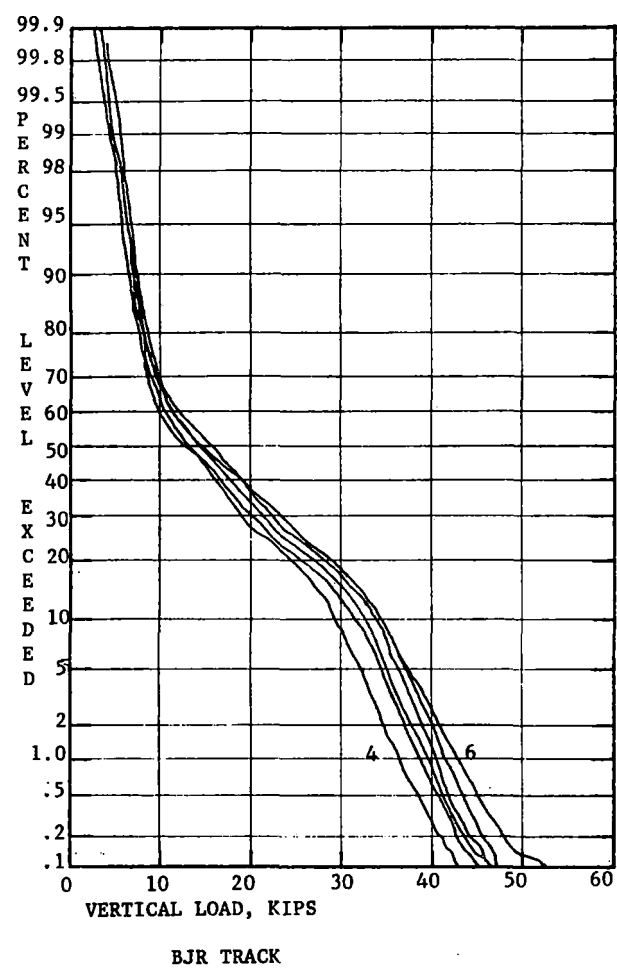


FIGURE B-1. VARIATIONS IN VERTICAL W/R LOAD STATISTICS AMONG MEASUREMENT SITES, ALL TRAFFIC, ALL SPEEDS

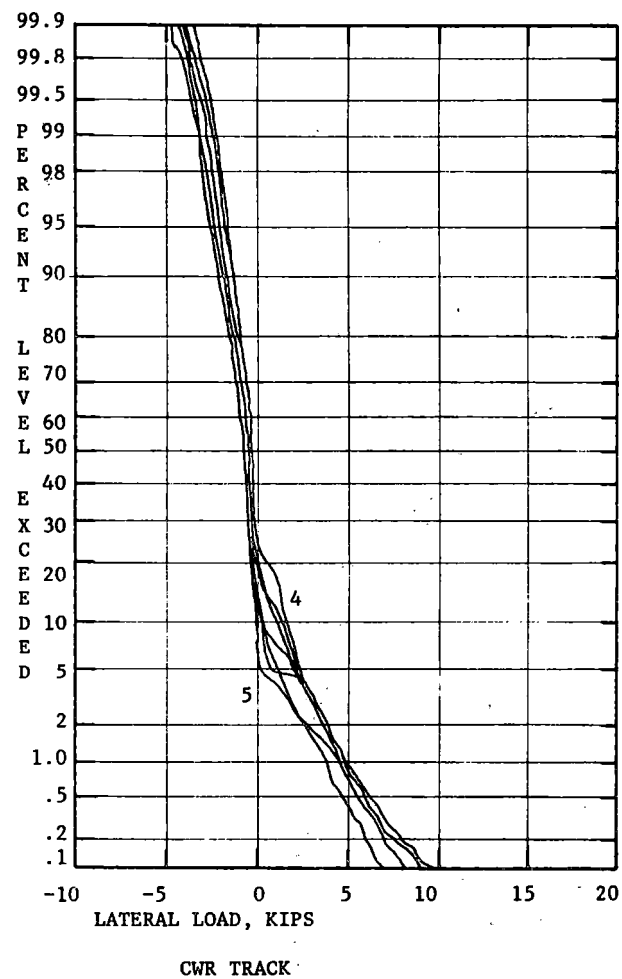
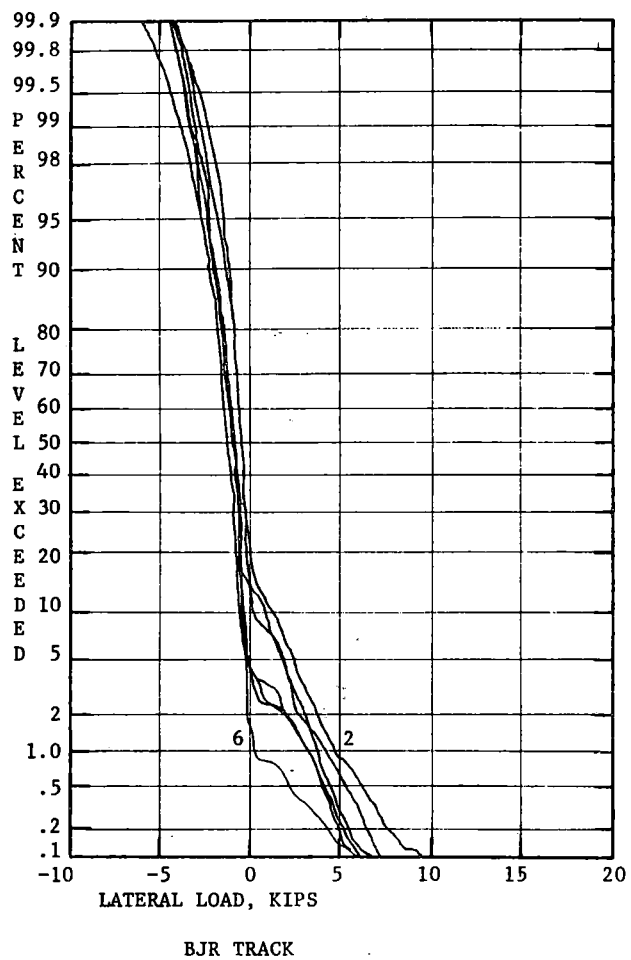
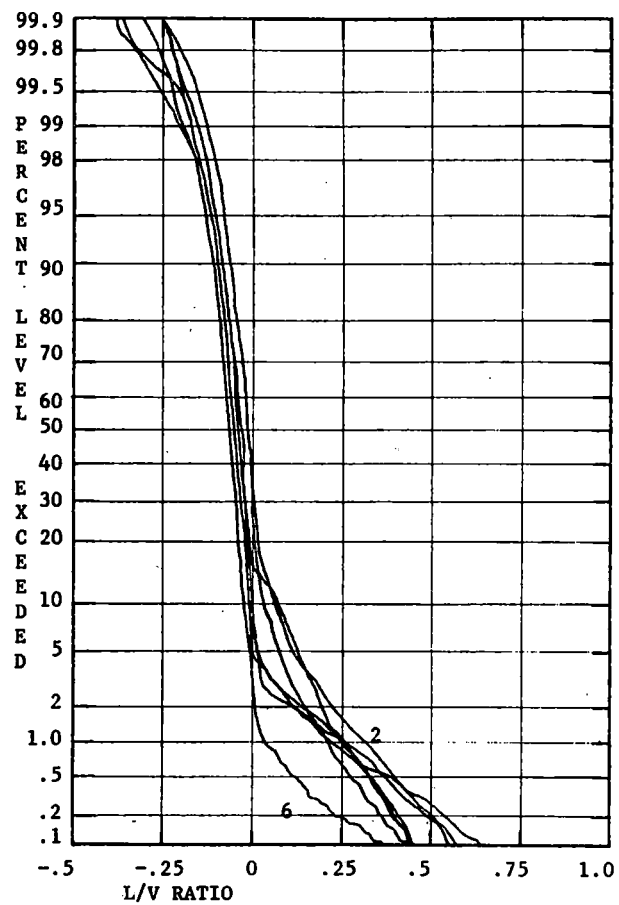
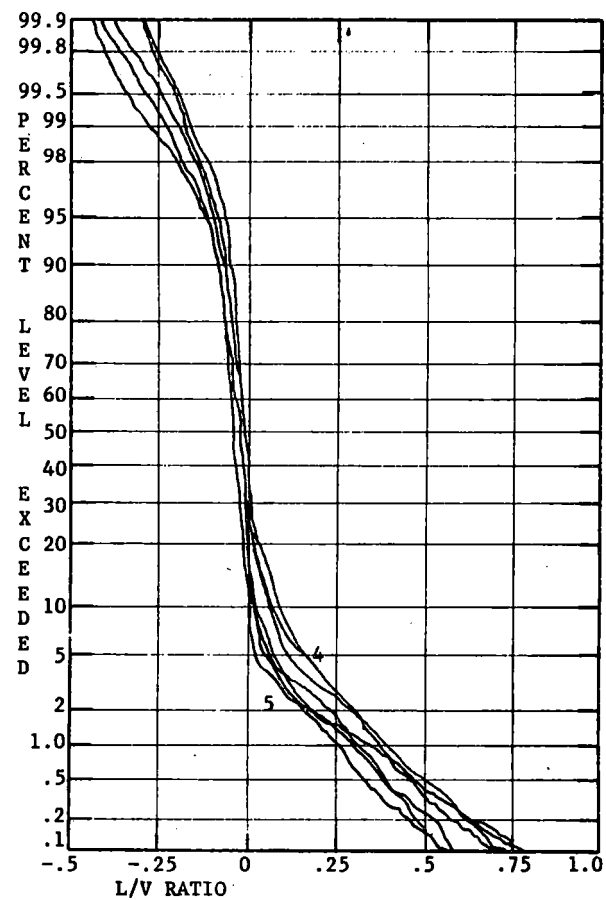


FIGURE B-2. VARIATIONS IN LATERAL W/R LOAD STATISTICS AMONG MEASUREMENT SITES, ALL TRAFFIC, ALL SPEEDS



BJR TRACK



CWR TRACK

FIGURE B-3. VARIATIONS IN L/V RATIO STATISTICS AMONG MEASUREMENT SITES,  
ALL TRAFFIC, ALL SPEEDS

## APPENDIX C

### FREQUENCY OF OCCURRENCE OF LATERAL LOAD AND L/V RATIO VERSUS VERTICAL LOAD, WAYSIDE DATA

TABLE C-1. FREQUENCY OF OCCURRENCE OF LATERAL VS. VERTICAL W/R LOAD

L	VERTICAL LOAD, KIPS																			
	* 5.	10.	15.	20.	25.	30.	35.	40.	45.	50.	55.	60.	65.	70.	75.	80.	85.	90.	95.	100.
-16000.	0.	0.	0.	0.	0.	0.	0.	0.	0.	0.	0.	0.	0.	0.	0.	0.	0.	0.	0.	0.
-14000.	0.	0.	0.	0.	0.	0.	0.	0.	0.	0.	0.	0.	0.	0.	0.	0.	0.	0.	0.	0.
-12000.	0.	0.	0.	0.	0.	0.	0.	0.	0.	0.	0.	0.	0.	0.	0.	0.	0.	0.	0.	0.
-10000.	0.	0.	0.	0.	0.	0.	0.	0.	0.	0.	0.	0.	0.	0.	0.	0.	0.	0.	0.	0.
-8000.	0.	0.	0.	0.	0.	0.	0.	0.	0.	0.	0.	0.	0.	0.	0.	0.	0.	0.	0.	0.
-6000.	0.	0.	0.	0.	0.	0.	0.	0.	0.	0.	0.	0.	0.	0.	0.	0.	0.	0.	0.	0.
-4000.	0.	0.	0.	0.	0.	0.	0.	0.	0.	0.	0.	0.	0.	0.	0.	0.	0.	0.	0.	0.
-2000.	0.	0.	0.	0.	0.	0.	0.	0.	0.	0.	0.	0.	0.	0.	0.	0.	0.	0.	0.	0.
0.	0.	0.	0.	0.	0.	0.	0.	0.	0.	0.	0.	0.	0.	0.	0.	0.	0.	0.	0.	0.
2000.	0.	0.	0.	0.	0.	0.	0.	0.	0.	0.	0.	0.	0.	0.	0.	0.	0.	0.	0.	0.
4000.	0.	0.	0.	0.	0.	0.	0.	0.	0.	0.	0.	0.	0.	0.	0.	0.	0.	0.	0.	0.
6000.	0.	0.	0.	0.	0.	0.	0.	0.	0.	0.	0.	0.	0.	0.	0.	0.	0.	0.	0.	0.
8000.	0.	0.	0.	0.	0.	0.	0.	0.	0.	0.	0.	0.	0.	0.	0.	0.	0.	0.	0.	0.
10000.	0.	0.	0.	0.	0.	0.	0.	0.	0.	0.	0.	0.	0.	0.	0.	0.	0.	0.	0.	0.
12000.	0.	0.	0.	0.	0.	0.	0.	0.	0.	0.	0.	0.	0.	0.	0.	0.	0.	0.	0.	0.
14000.	0.	0.	0.	0.	0.	0.	0.	0.	0.	0.	0.	0.	0.	0.	0.	0.	0.	0.	0.	0.
16000.	0.	0.	0.	0.	0.	0.	0.	0.	0.	0.	0.	0.	0.	0.	0.	0.	0.	0.	0.	0.
18000.	0.	0.	0.	0.	0.	0.	0.	0.	0.	0.	0.	0.	0.	0.	0.	0.	0.	0.	0.	0.
20000.	0.	0.	0.	0.	0.	0.	0.	0.	0.	0.	0.	0.	0.	0.	0.	0.	0.	0.	0.	0.
22000.	0.	0.	0.	0.	0.	0.	0.	0.	0.	0.	0.	0.	0.	0.	0.	0.	0.	0.	0.	0.

## a. TANGENT BJR TRACK SECTION

L	VERTICAL LOAD, KIPS																			
	* 5.	10.	15.	20.	25.	30.	35.	40.	45.	50.	55.	60.	65.	70.	75.	80.	85.	90.	95.	100.
-16000.	0.	0.	0.	0.	0.	0.	0.	0.	0.	0.	0.	0.	0.	0.	0.	0.	0.	0.	0.	0.
-14000.	0.	0.	0.	0.	0.	0.	0.	0.	0.	0.	0.	0.	0.	0.	0.	0.	0.	0.	0.	0.
-12000.	0.	0.	0.	0.	0.	0.	0.	0.	0.	0.	0.	0.	0.	0.	0.	0.	0.	0.	0.	0.
-10000.	0.	0.	0.	0.	0.	0.	0.	0.	0.	0.	0.	0.	0.	0.	0.	0.	0.	0.	0.	0.
-8000.	0.	0.	0.	0.	0.	0.	0.	0.	0.	0.	0.	0.	0.	0.	0.	0.	0.	0.	0.	0.
-6000.	0.	0.	0.	0.	0.	0.	0.	0.	0.	0.	0.	0.	0.	0.	0.	0.	0.	0.	0.	0.
-4000.	0.	0.	0.	0.	0.	0.	0.	0.	0.	0.	0.	0.	0.	0.	0.	0.	0.	0.	0.	0.
-2000.	0.	0.	0.	0.	0.	0.	0.	0.	0.	0.	0.	0.	0.	0.	0.	0.	0.	0.	0.	0.
0.	0.	0.	0.	0.	0.	0.	0.	0.	0.	0.	0.	0.	0.	0.	0.	0.	0.	0.	0.	0.
2000.	0.	0.	0.	0.	0.	0.	0.	0.	0.	0.	0.	0.	0.	0.	0.	0.	0.	0.	0.	0.
4000.	0.	0.	0.	0.	0.	0.	0.	0.	0.	0.	0.	0.	0.	0.	0.	0.	0.	0.	0.	0.
6000.	0.	0.	0.	0.	0.	0.	0.	0.	0.	0.	0.	0.	0.	0.	0.	0.	0.	0.	0.	0.
8000.	0.	0.	0.	0.	0.	0.	0.	0.	0.	0.	0.	0.	0.	0.	0.	0.	0.	0.	0.	0.
10000.	0.	0.	0.	0.	0.	0.	0.	0.	0.	0.	0.	0.	0.	0.	0.	0.	0.	0.	0.	0.
12000.	0.	0.	0.	0.	0.	0.	0.	0.	0.	0.	0.	0.	0.	0.	0.	0.	0.	0.	0.	0.
14000.	0.	0.	0.	0.	0.	0.	0.	0.	0.	0.	0.	0.	0.	0.	0.	0.	0.	0.	0.	0.
16000.	0.	0.	0.	0.	0.	0.	0.	0.	0.	0.	0.	0.	0.	0.	0.	0.	0.	0.	0.	0.
18000.	0.	0.	0.	0.	0.	0.	0.	0.	0.	0.	0.	0.	0.	0.	0.	0.	0.	0.	0.	0.
20000.	0.	0.	0.	0.	0.	0.	0.	0.	0.	0.	0.	0.	0.	0.	0.	0.	0.	0.	0.	0.
22000.	0.	0.	0.	0.	0.	0.	0.	0.	0.	0.	0.	0.	0.	0.	0.	0.	0.	0.	0.	0.

## b. TANGENT CWR TRACK SECTION

\* high end of interval (i.e., 0-5 kip band)

TABLE C-2. FREQUENCY OF OCCURRENCE OF L/V VS. VERTICAL  
WHEEL/RAIL LOAD FROM WAYSIDE DATA

L/V	VERTICAL LOAD, KIPS																			
	* 5.	10.	15.	20.	25.	30.	35.	40.	45.	50.	55.	60.	65.	70.	75.	80.	85.	90.	95.	100.
-.4	9.	32.	2.	0.	0.	0.	0.	0.	0.	0.	0.	0.	0.	0.	0.	0.	0.	0.	0.	0.
-.3	22.	90.	11.	3.	0.	0.	0.	0.	0.	0.	0.	0.	0.	0.	0.	0.	0.	0.	0.	0.
-.2	82.	359.	94.	29.	7.	14.	2.	0.	1.	0.	0.	0.	0.	0.	0.	0.	0.	0.	0.	0.
-.1	238.	4197.	1160.	531.	282.	218.	126.	44.	14.	2.	0.	0.	0.	0.	0.	0.	0.	0.	0.	0.
0	587.	35822.	18654.	15165.	11451.	9666.	10817.	5531.	1245.	196.	30.	11.	7.	4.	0.	1.	1.	0.	0.	1.
.1	99.	6022.	4189.	4221.	3039.	1758.	2180.	1300.	231.	27.	7.	1.	0.	0.	0.	0.	0.	0.	0.	0.
.2	6.	483.	671.	849.	533.	259.	200.	95.	25.	4.	1.	0.	0.	0.	0.	0.	0.	0.	0.	0.
.3	5.	260.	395.	232.	111.	43.	24.	4.	2.	0.	0.	0.	0.	0.	0.	0.	0.	0.	0.	0.
.4	1.	137.	268.	65.	21.	4.	6.	1.	0.	1.	0.	0.	0.	0.	0.	0.	0.	0.	0.	0.
.5	0.	83.	111.	26.	9.	2.	0.	0.	0.	0.	0.	0.	0.	0.	0.	0.	0.	0.	0.	0.
.6	0.	46.	41.	8.	3.	0.	0.	0.	0.	0.	0.	0.	0.	0.	0.	0.	0.	0.	0.	0.
.7	0.	20.	16.	1.	0.	0.	0.	0.	0.	0.	0.	0.	0.	0.	0.	0.	0.	0.	0.	0.
.8	0.	10.	4.	3.	0.	0.	0.	0.	0.	0.	0.	0.	0.	0.	0.	0.	0.	0.	0.	0.
.9	0.	3.	2.	0.	0.	0.	0.	0.	0.	0.	0.	0.	0.	0.	0.	0.	0.	0.	0.	0.
1.0	0.	1.	0.	0.	0.	0.	0.	0.	0.	0.	0.	0.	0.	0.	0.	0.	0.	0.	0.	0.
1.1	0.	0.	0.	0.	0.	0.	0.	0.	0.	0.	0.	0.	0.	0.	0.	0.	0.	0.	0.	0.
1.2	0.	0.	0.	0.	0.	0.	0.	0.	0.	0.	0.	0.	0.	0.	0.	0.	0.	0.	0.	0.
1.3	0.	0.	0.	0.	0.	0.	0.	0.	0.	0.	0.	0.	0.	0.	0.	0.	0.	0.	0.	0.
1.4	0.	0.	0.	0.	0.	0.	0.	0.	0.	0.	0.	0.	0.	0.	0.	0.	0.	0.	0.	0.
1.5	0.	0.	0.	0.	0.	0.	0.	0.	0.	0.	0.	0.	0.	0.	0.	0.	0.	0.	0.	0.
1.6	0.	0.	0.	0.	0.	0.	0.	0.	0.	0.	0.	0.	0.	0.	0.	0.	0.	0.	0.	0.
1.7	0.	0.	0.	0.	0.	0.	0.	0.	0.	0.	0.	0.	0.	0.	0.	0.	0.	0.	0.	0.
1.8	0.	0.	0.	0.	0.	0.	0.	0.	0.	0.	0.	0.	0.	0.	0.	0.	0.	0.	0.	0.
1.9	0.	0.	0.	0.	0.	0.	0.	0.	0.	0.	0.	0.	0.	0.	0.	0.	0.	0.	0.	0.
2.0	0.	0.	0.	0.	0.	0.	0.	0.	0.	0.	0.	0.	0.	0.	0.	0.	0.	0.	0.	0.

a. TANGENT BJR TRACK SECTION

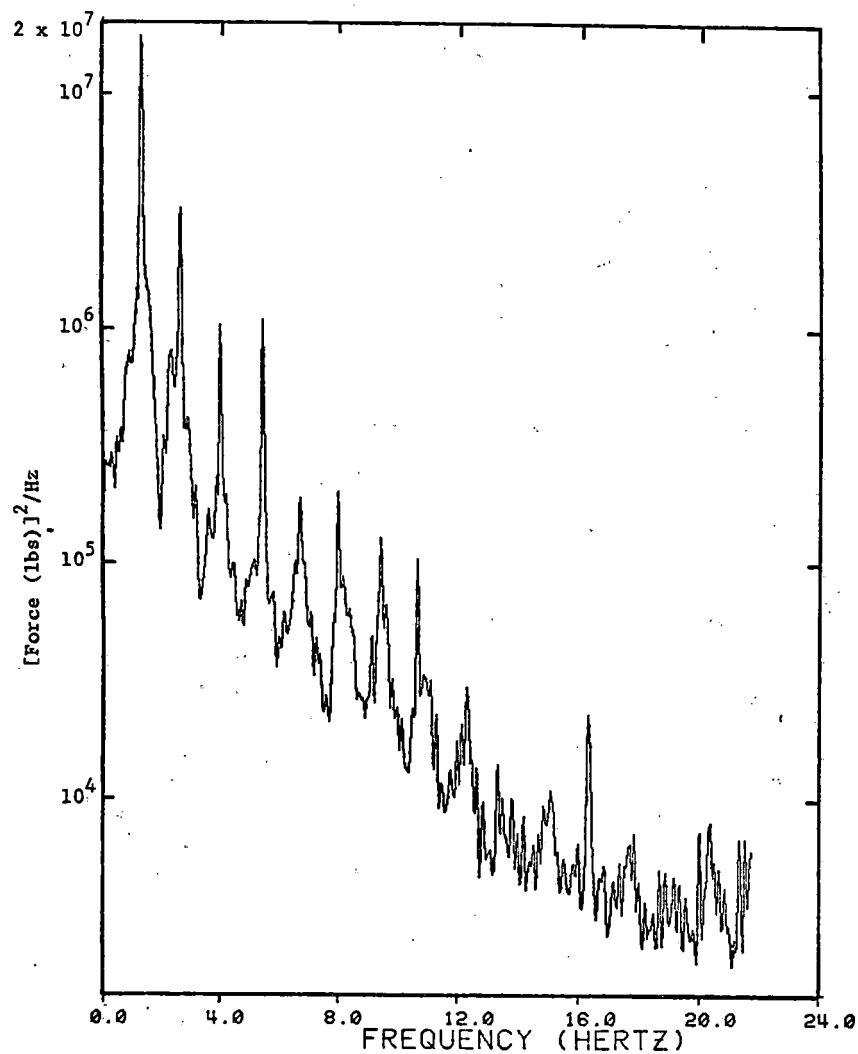
L/V	VERTICAL LOAD, KIPS																			
	* 5.	10.	15.	20.	25.	30.	35.	40.	45.	50.	55.	60.	65.	70.	75.	80.	85.	90.	95.	100.
-.4	133.	34.	1.	1.	0.	0.	0.	0.	0.	0.	0.	0.	0.	0.	0.	0.	0.	0.	0.	0.
-.3	122.	207.	33.	2.	0.	1.	0.	0.	0.	0.	0.	0.	0.	0.	0.	0.	0.	0.	0.	0.
-.2	295.	753.	168.	32.	8.	1.	1.	0.	0.	0.	0.	0.	0.	0.	0.	0.	0.	0.	0.	0.
-.1	469.	3804.	1257.	490.	266.	204.	131.	82.	9.	1.	0.	0.	0.	0.	0.	0.	0.	0.	0.	0.
0	916.	21631.	17705.	15621.	13274.	11799.	15397.	9182.	2318.	308.	44.	23.	15.	2.	5.	0.	0.	0.	1.	1.
.1	198.	5949.	5804.	6367.	4647.	3372.	3539.	1802.	439.	67.	7.	4.	3.	4.	0.	0.	0.	0.	0.	0.
.2	14.	790.	1016.	1073.	632.	327.	256.	181.	17.	5.	0.	1.	0.	0.	1.	0.	0.	0.	0.	0.
.3	22.	505.	783.	376.	167.	51.	23.	9.	3.	0.	0.	0.	0.	0.	0.	0.	0.	0.	0.	0.
.4	16.	311.	609.	193.	49.	22.	5.	0.	0.	0.	0.	0.	0.	0.	0.	0.	0.	0.	0.	0.
.5	7.	165.	249.	76.	20.	3.	2.	0.	0.	0.	0.	0.	0.	0.	0.	0.	0.	0.	0.	0.
.6	3.	88.	117.	32.	5.	0.	0.	0.	0.	0.	0.	0.	0.	0.	0.	0.	0.	0.	0.	0.
.7	1.	47.	72.	11.	4.	0.	0.	0.	0.	0.	0.	0.	0.	0.	0.	0.	0.	0.	0.	0.
.8	1.	29.	23.	5.	2.	0.	0.	0.	0.	0.	0.	0.	0.	0.	0.	0.	0.	0.	0.	0.
.9	2.	16.	14.	3.	0.	0.	0.	0.	0.	0.	0.	0.	0.	0.	0.	0.	0.	0.	0.	0.
1.0	4.	6.	2.	0.	0.	0.	0.	0.	0.	0.	0.	0.	0.	0.	0.	0.	0.	0.	0.	0.
1.1	0.	7.	0.	1.	0.	0.	0.	0.	0.	0.	0.	0.	0.	0.	0.	0.	0.	0.	0.	0.
1.2	2.	5.	0.	1.	0.	0.	0.	0.	0.	0.	0.	0.	0.	0.	0.	0.	0.	0.	0.	0.
1.3	0.	0.	0.	0.	0.	0.	0.	0.	0.	0.	0.	0.	0.	0.	0.	0.	0.	0.	0.	0.
1.4	0.	1.	1.	0.	0.	0.	0.	0.	0.	0.	0.	0.	0.	0.	0.	0.	0.	0.	0.	0.
1.5	1.	1.	2.	0.	0.	0.	0.	0.	0.	0.	0.	0.	0.	0.	0.	0.	0.	0.	0.	0.
1.6	2.	0.	1.	0.	0.	0.	0.	0.	0.	0.	0.	0.	0.	0.	0.	0.	0.	0.	0.	0.
1.7	0.	0.	0.	0.	0.	0.	0.	0.	0.	0.	0.	0.	0.	0.	0.	0.	0.	0.	0.	0.
1.8	0.	0.	0.	0.	0.	0.	0.	0.	0.	0.	0.	0.	0.	0.	0.	0.	0.	0.	0.	0.
1.9	0.	0.	0.	0.	0.	0.	0.	0.	0.	0.	0.	0.	0.	0.	0.	0.	0.	0.	0.	0.
2.0	0.	0.	0.	0.	0.	0.	0.	0.	0.	0.	0.	0.	0.	0.	0.	0.	0.	0.	0.	0.

b. TANGENT CWR TRACK SECTION

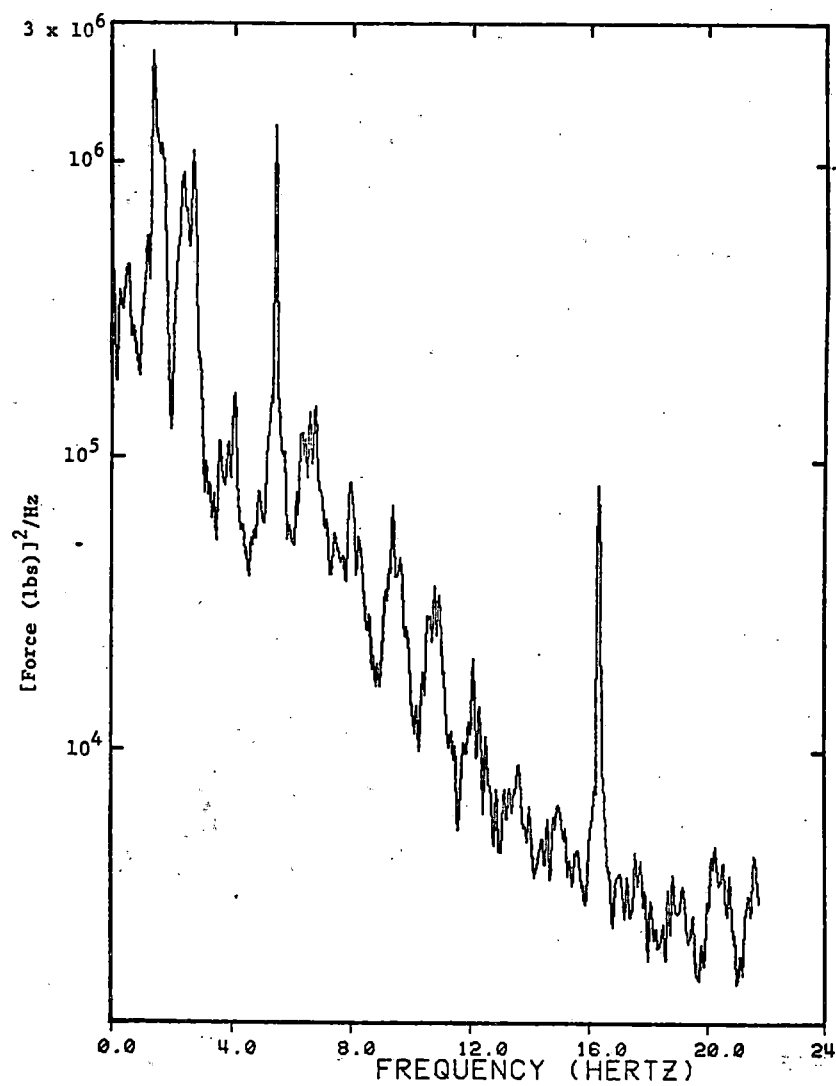
\* high end of interval (i.e., 0-5 kip band)

APPENDIX D

FREQUENCY ANALYSIS OF VEHICLE-BORNE WHEEL/RAIL LOAD DATA

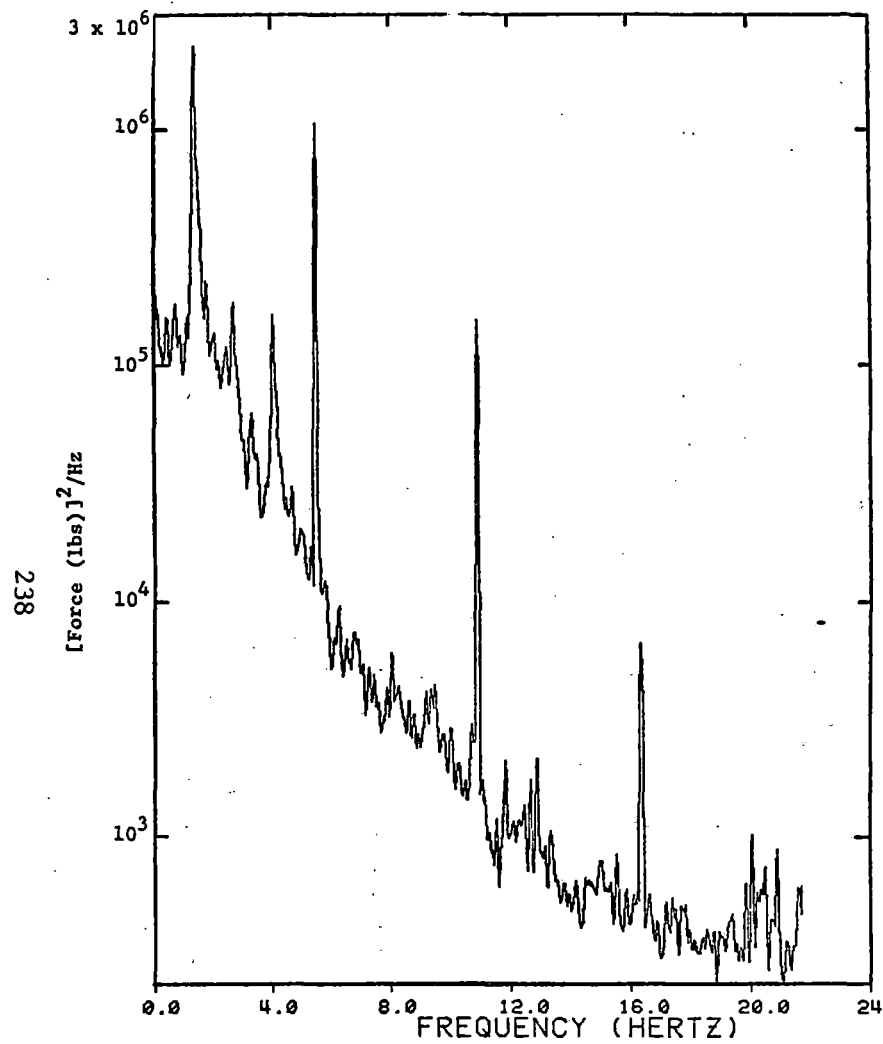


a. BJR TRACK

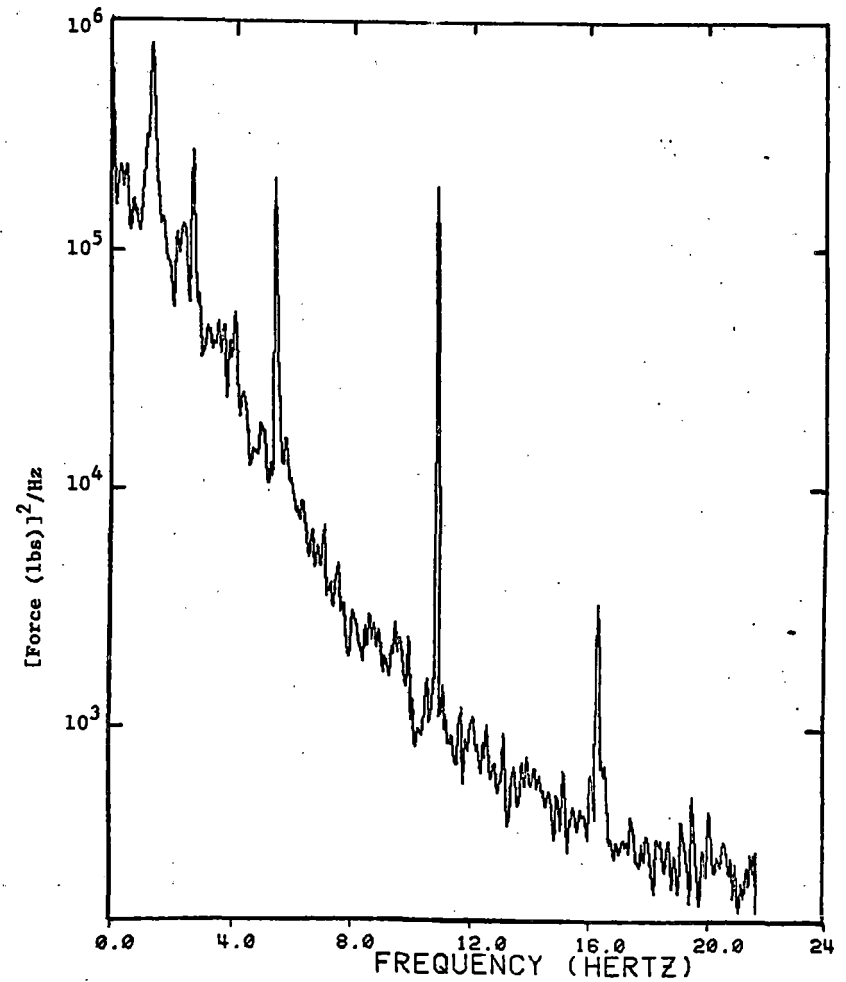


b. CWR TRACK

FIGURE D-1. FREQUENCY ANALYSIS OF VERTICAL WHEEL LOAD FROM INSTRUMENTED WHEEL, 35 MPH EASTBOUND (TRAILING AXLE) RUNS

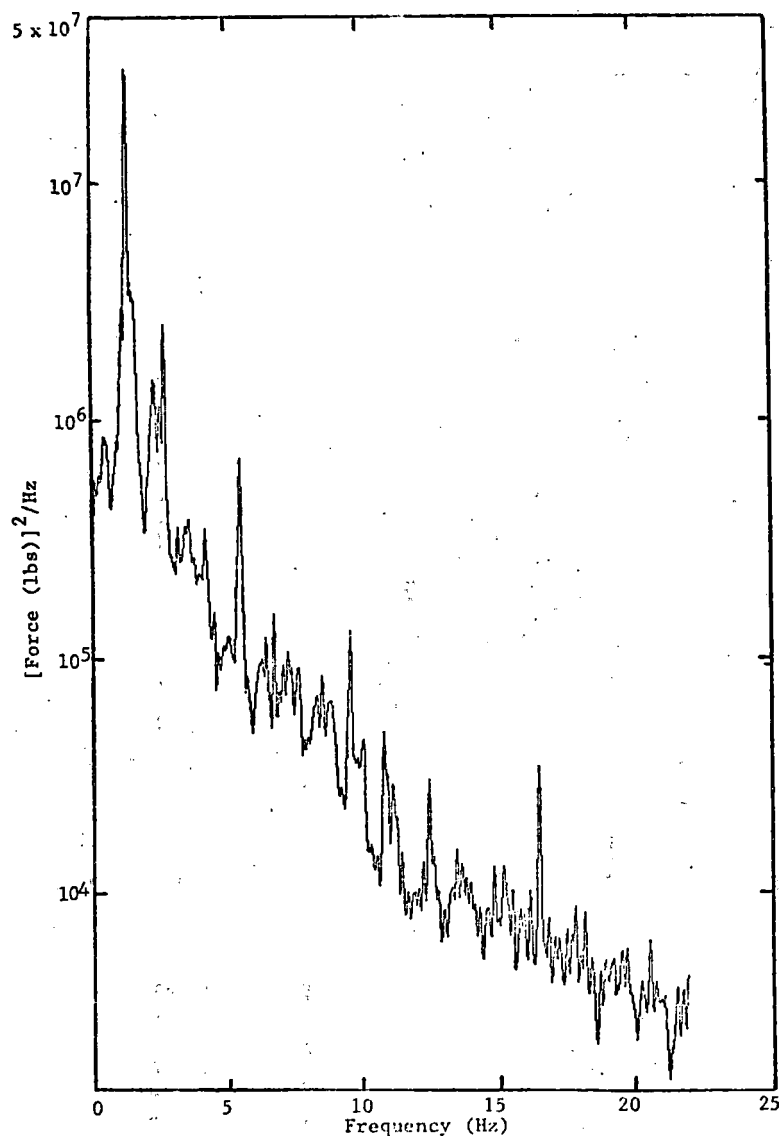


a. BJR TRACK

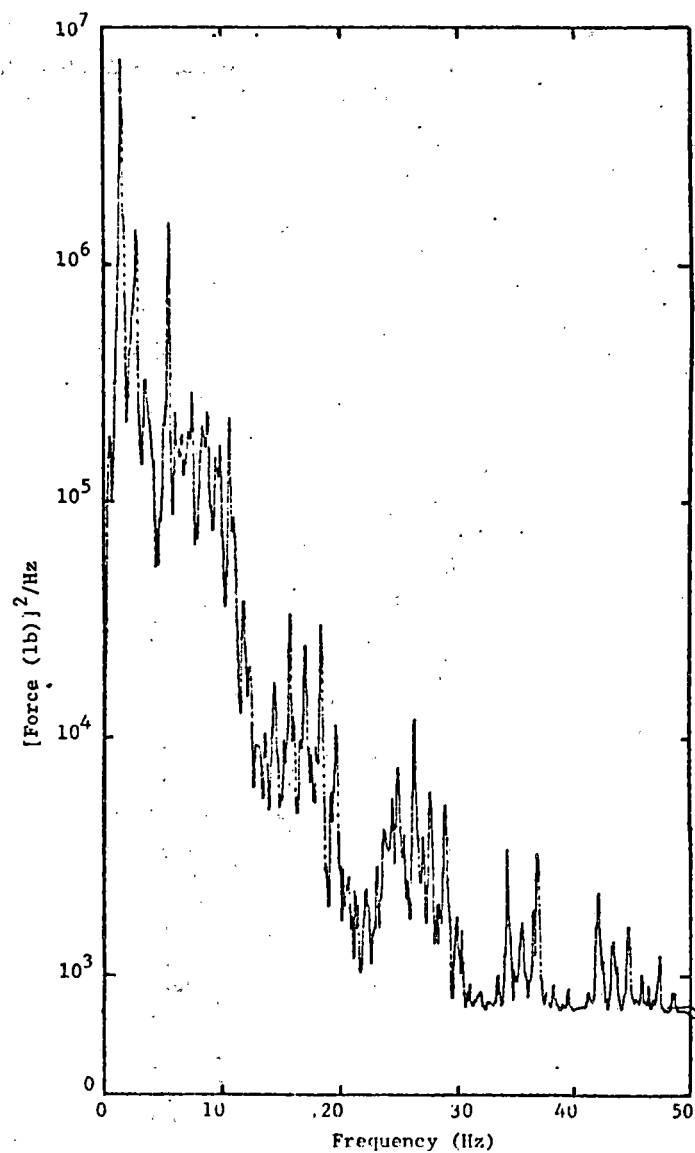


b. CWR TRACK

FIGURE D-2. FREQUENCY ANALYSIS OF LATERAL WHEEL LOAD FROM INSTRUMENTED WHEEL, EASTBOUND (TRAILING AXLE) RUNS, 35 MPH

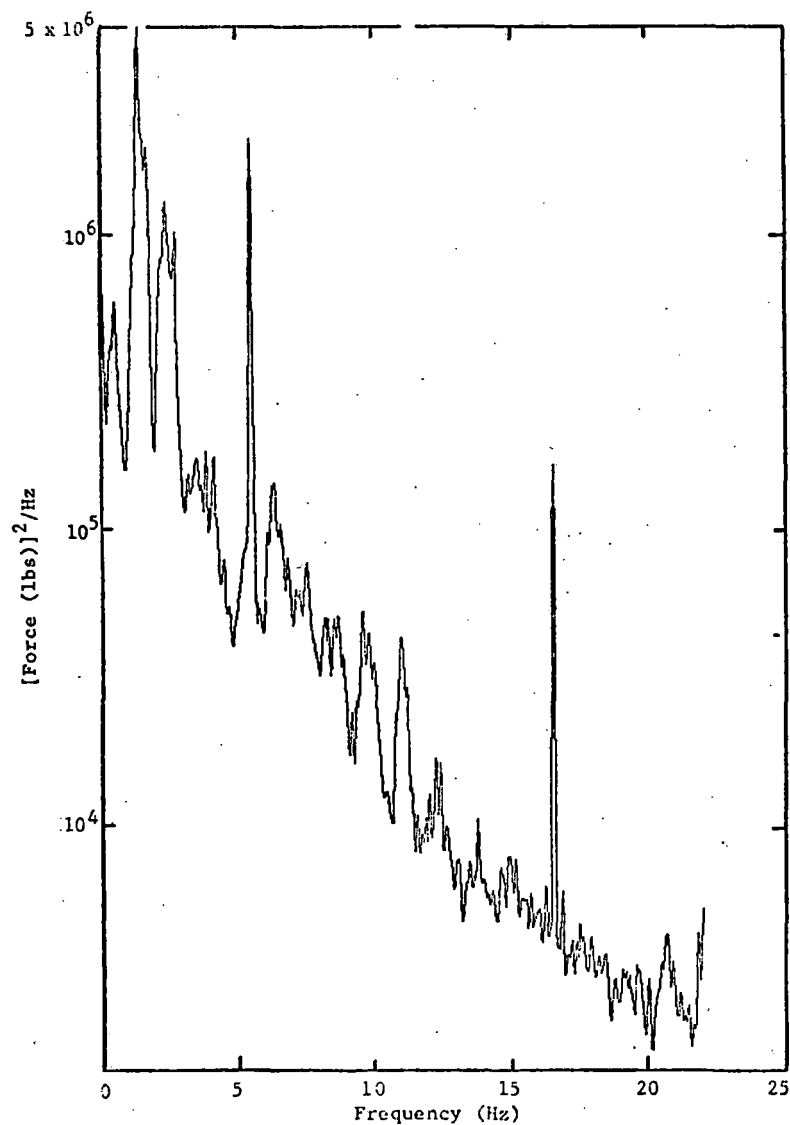


a. INSTRUMENTED WHEEL

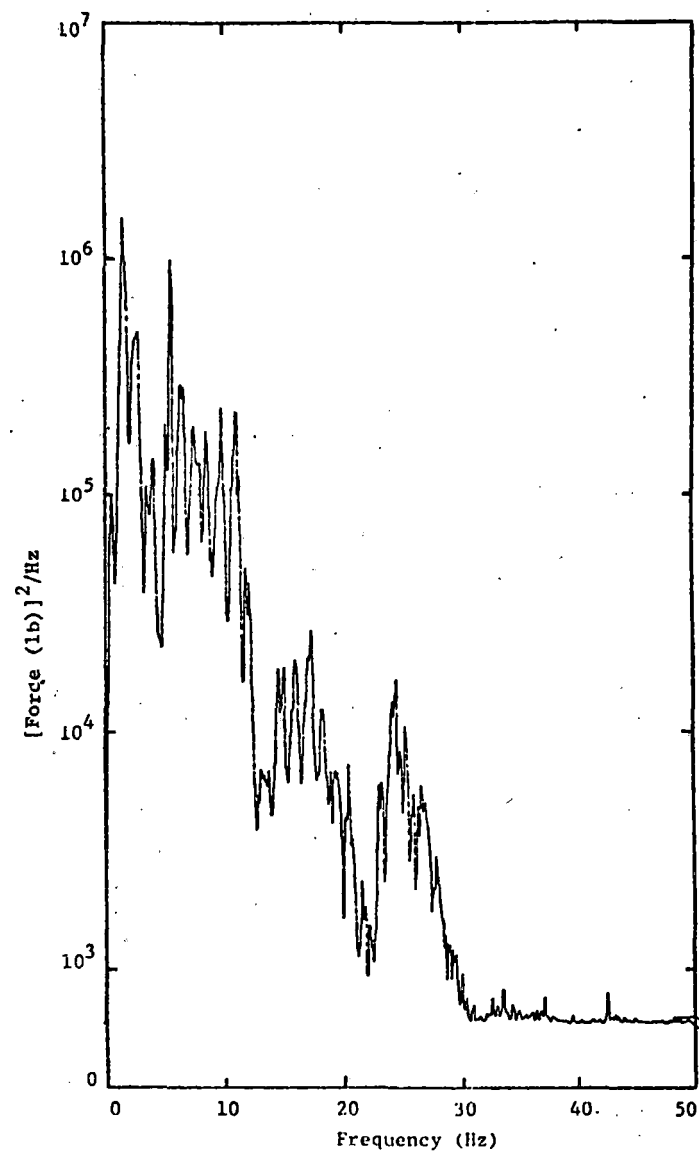


b. INSTRUMENTED SIDE FRAMES

FIGURE D-3. COMPARISON OF FREQUENCY ANALYSIS OF VERTICAL WHEEL/RAIL LOAD FROM HIGH-FREQUENCY AND LOW-FREQUENCY SYSTEMS, WESTBOUND (LEADING AXLE) RUN, 35 MPH ON BJR TRACK SECTION

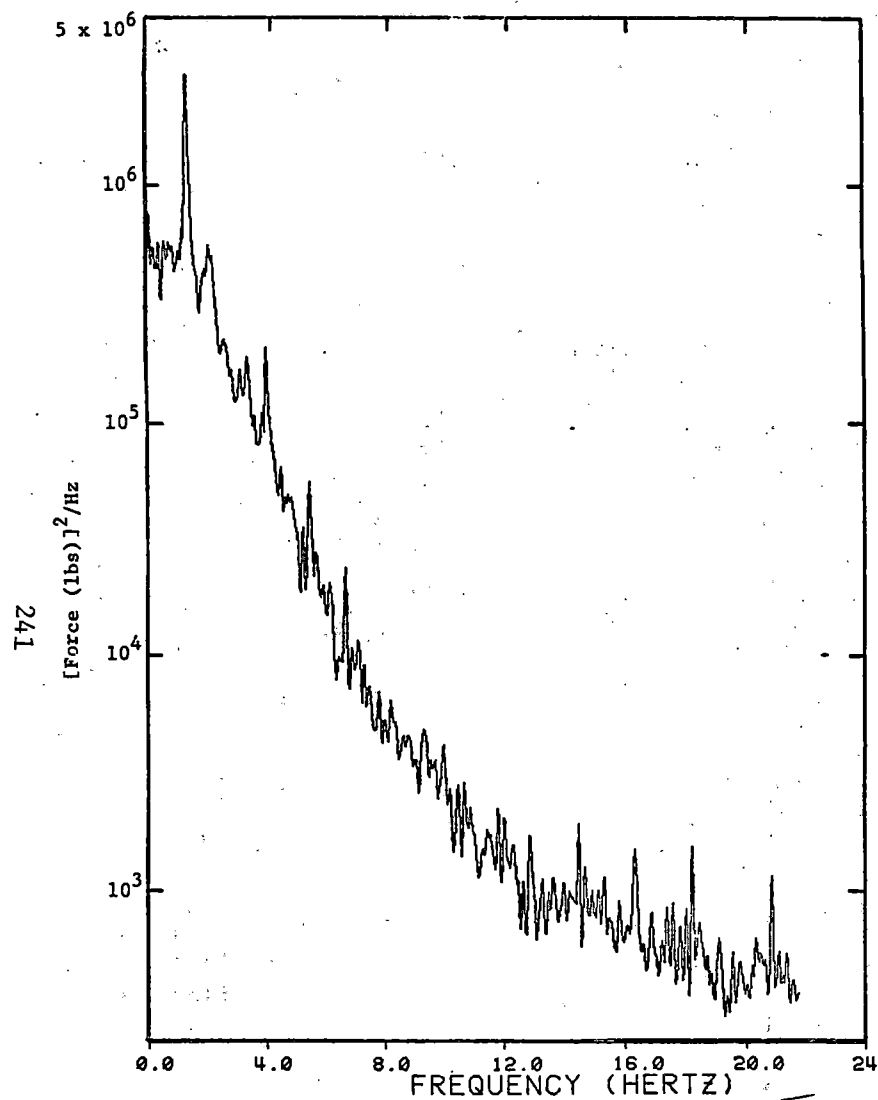


a. INSTRUMENTED WHEEL

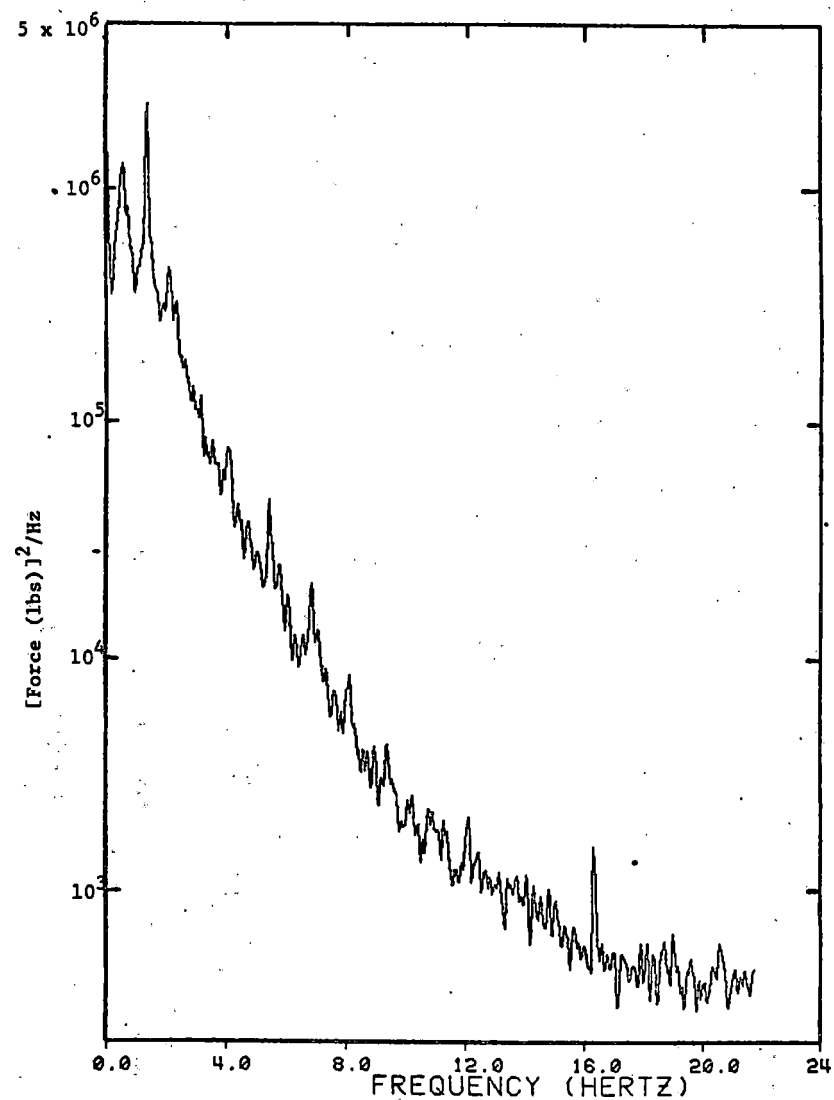


b. INSTRUMENTED SIDE FRAMES

FIGURE D-4. COMPARISON OF FREQUENCY ANALYSIS OF VERTICAL WHEEL/RAIL LOAD FROM HIGH-FREQUENCY AND LOW-FREQUENCY SYSTEMS, WESTBOUND (LEADING AXLE) RUN, 35 MPH ON CWR TRACK

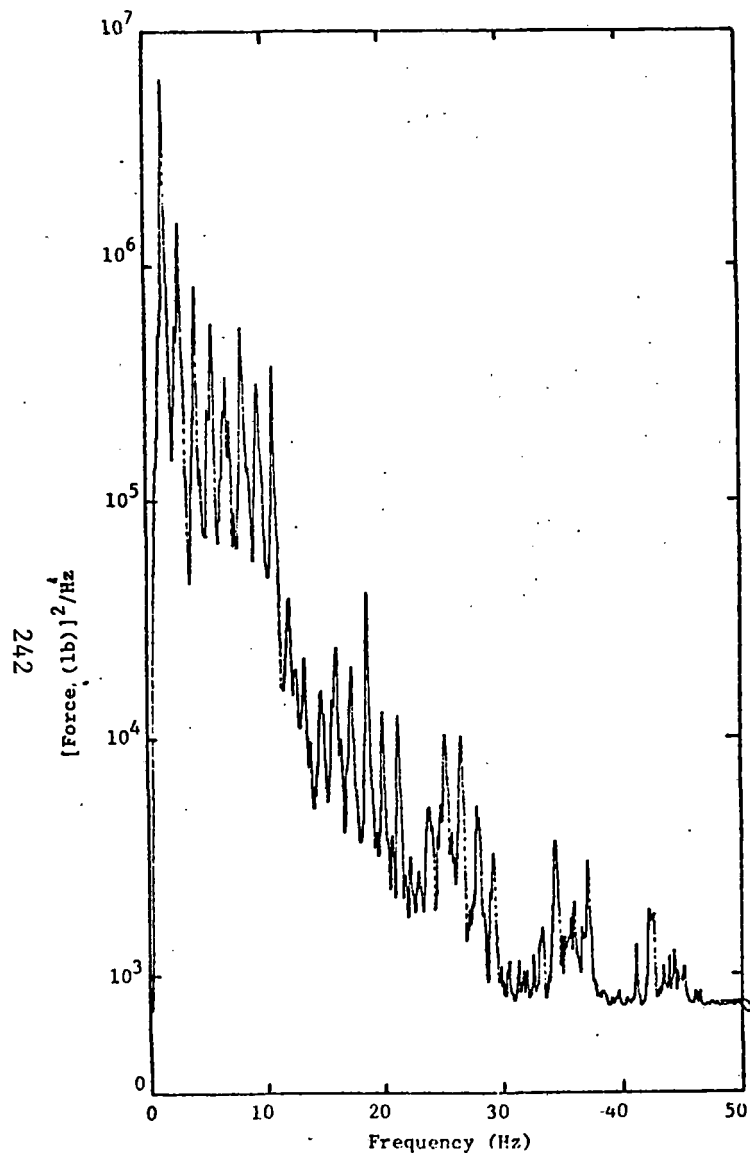


a. BJR TRACK

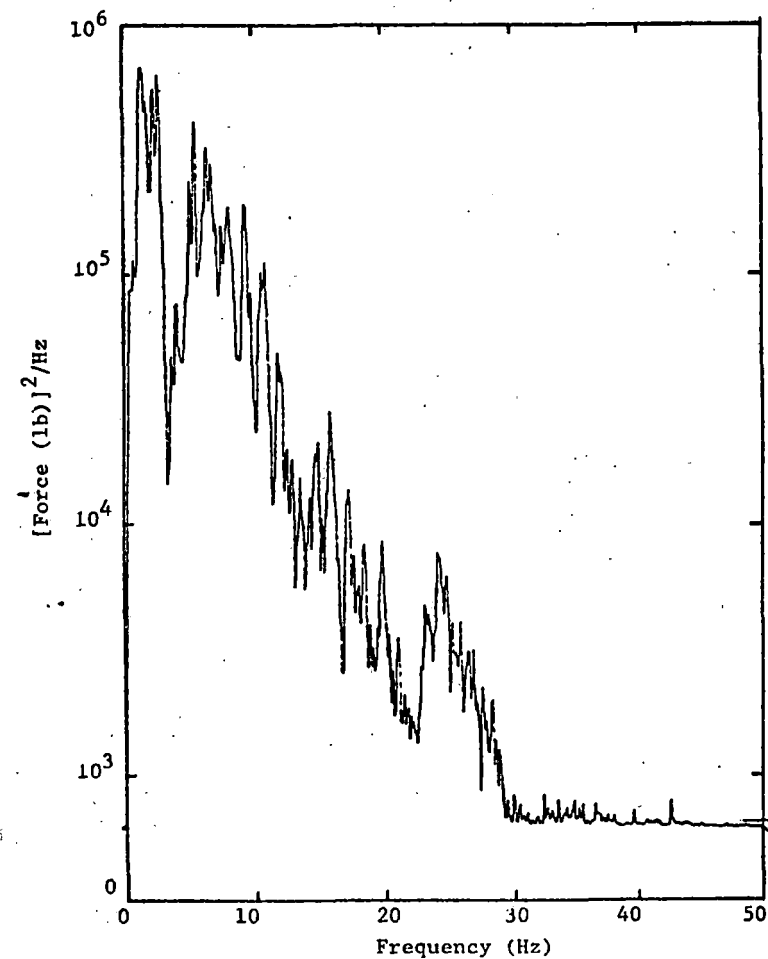


b. CWR TRACK

FIGURE D-5. FREQUENCY ANALYSIS OF LATERAL WHEEL LOAD FROM INSTRUMENTED WHEEL, WESTBOUND (LEADING AXLE) RUNS AT 35 MPH

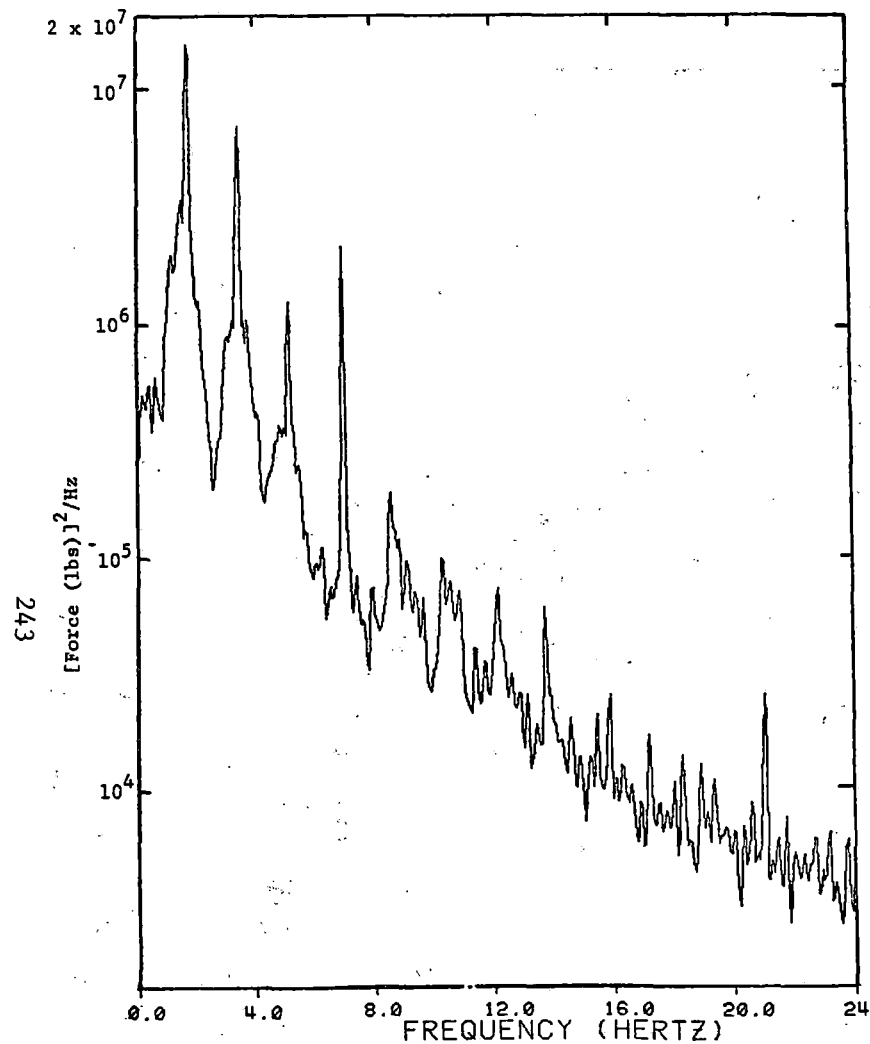


a. BJR TRACK

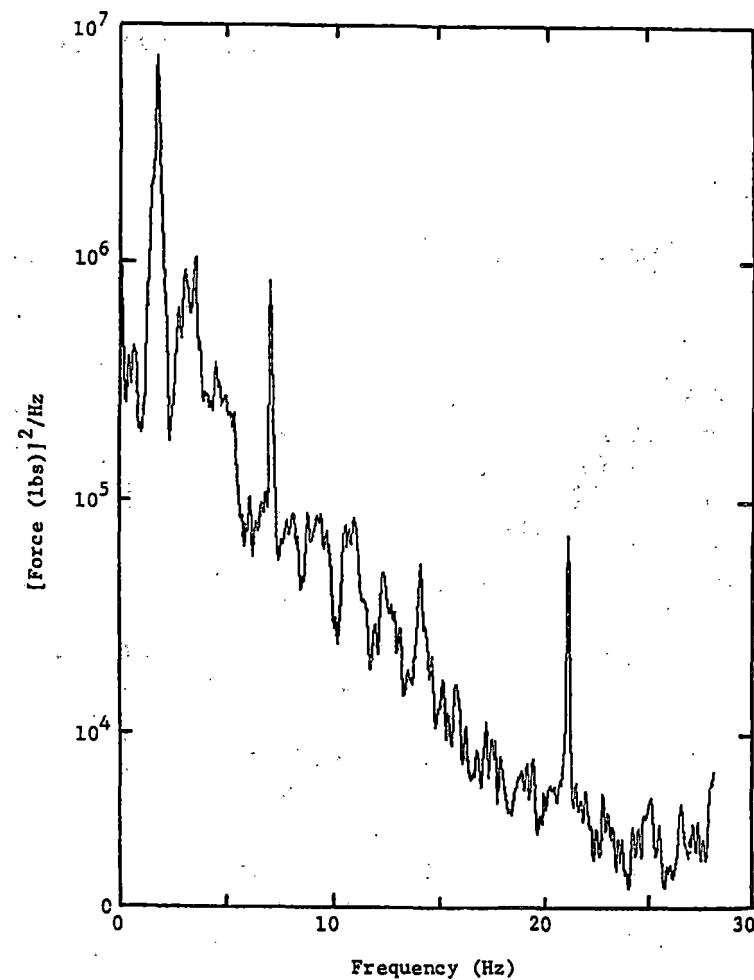


b. CWR TRACK

FIGURE D-6. FREQUENCY ANALYSIS OF VERTICAL WHEEL/RAIL FORCE FROM INSTRUMENTED SIDE FRAMES, EASTBOUND (TRAILING AXLE) RUNS AT 35 MPH

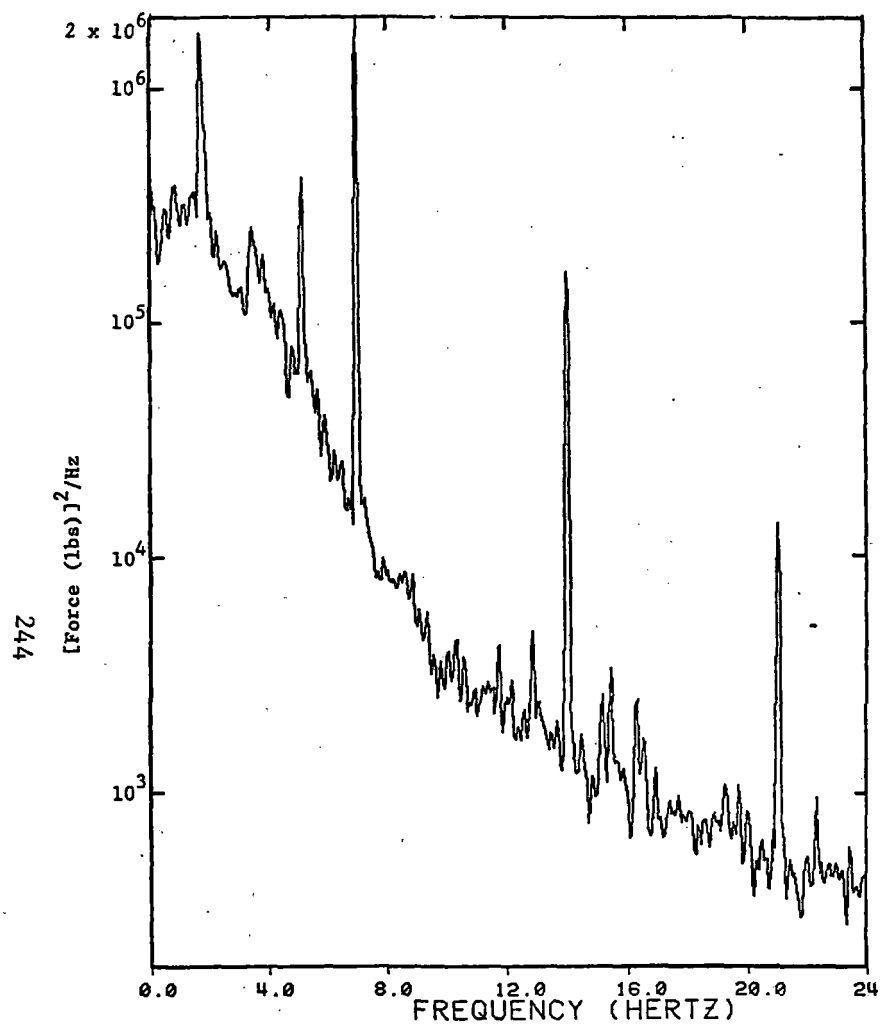


a. BJR TRACK, TRAILING AXLE

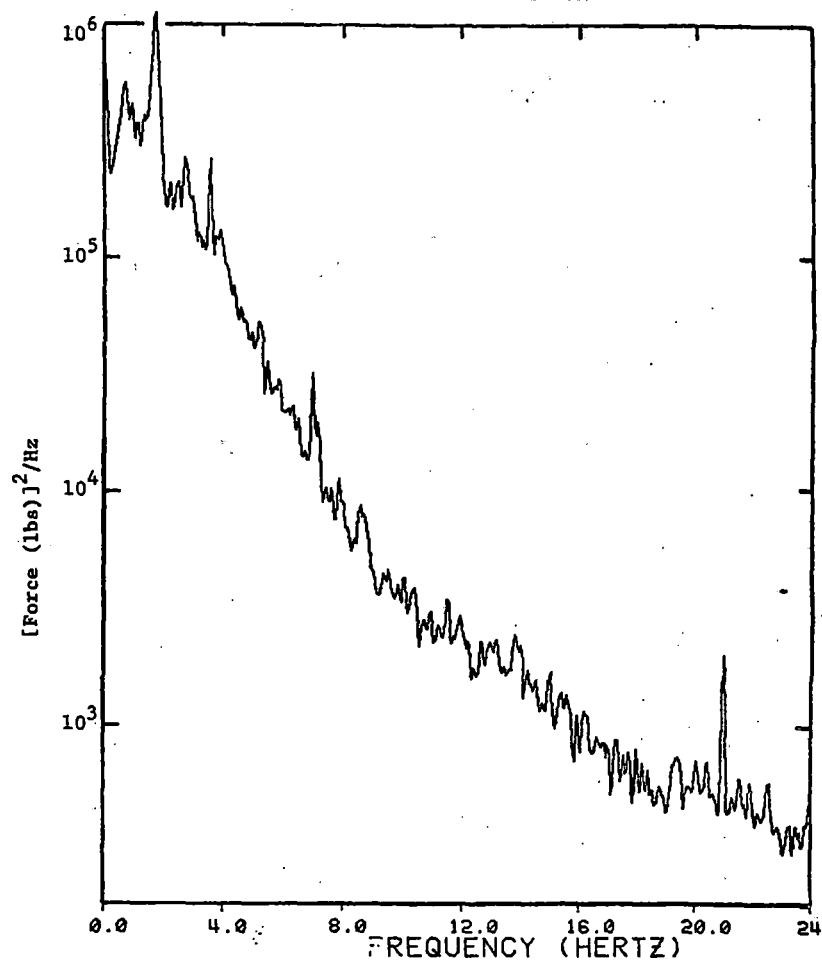


b. CWR TRACK, LEADING AXLE

FIGURE D-7. FREQUENCY ANALYSIS OF VERTICAL WHEEL LOAD FROM INSTRUMENTED WHEEL,  
45 MPH RUNS

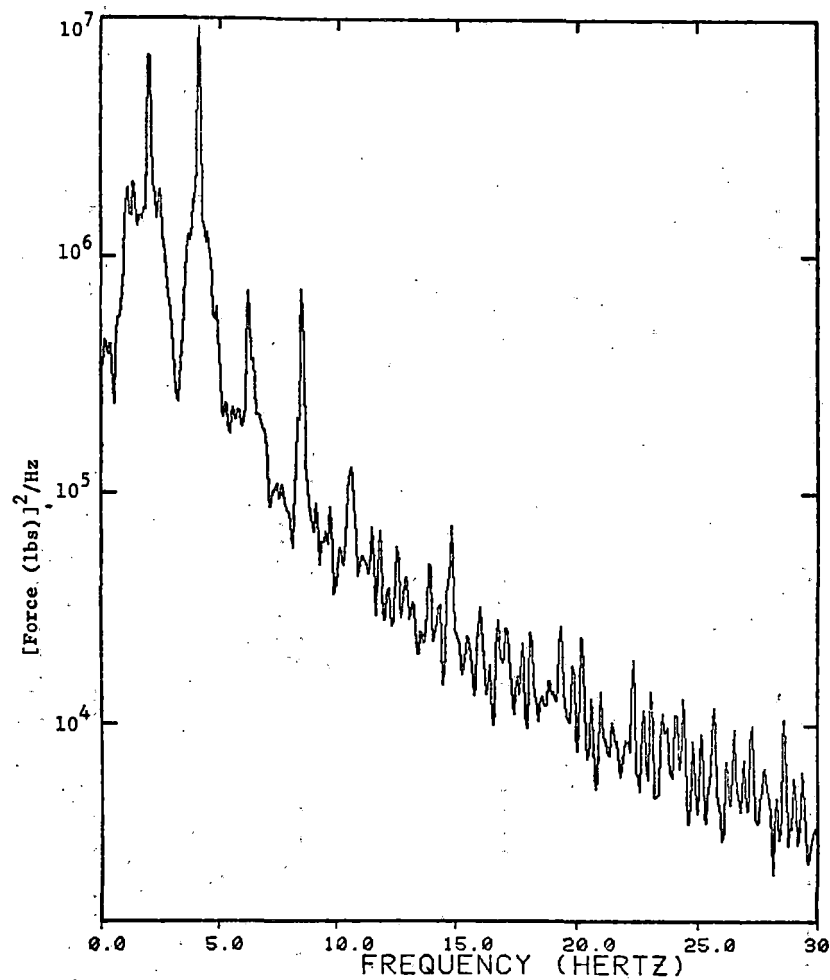


a. BJR TRACK, TRAILING AXLE

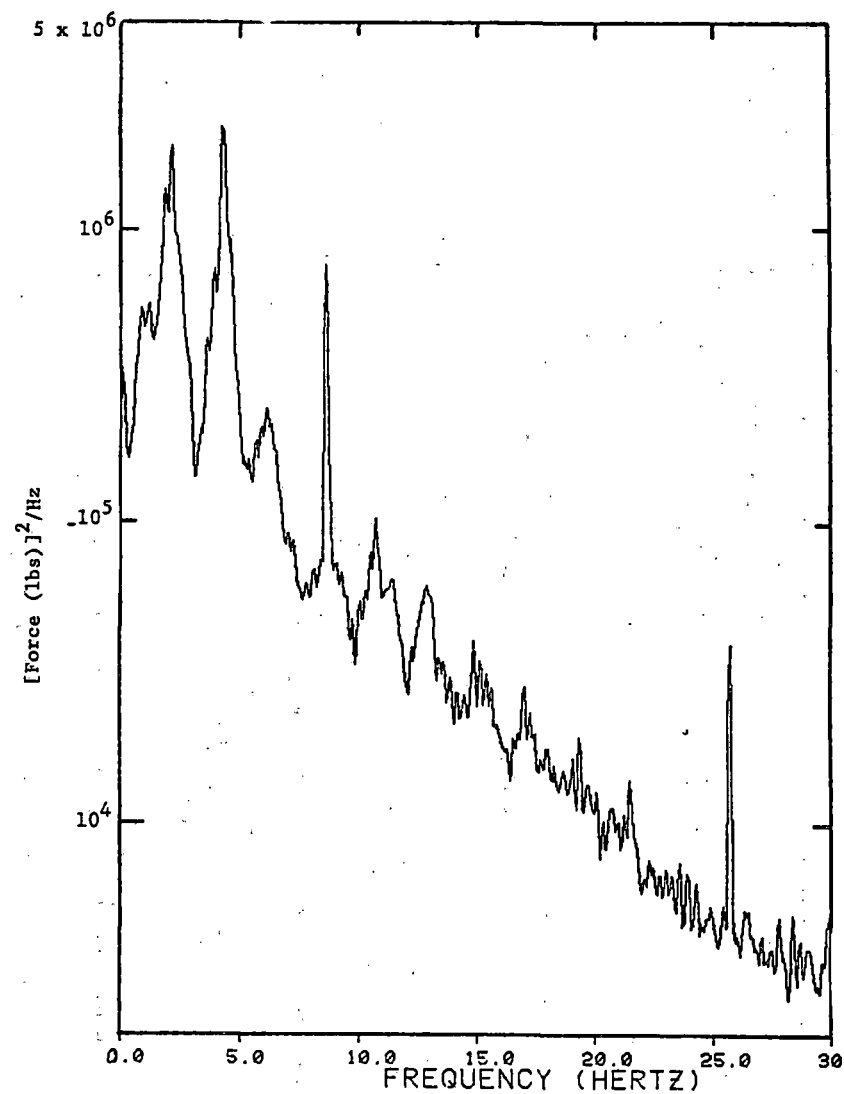


b. CWR TRACK, LEADING AXLE

FIGURE D-8. FREQUENCY ANALYSIS OF LATERAL WHEEL LOAD FROM INSTRUMENTED WHEEL,  
45 MPH RUNS

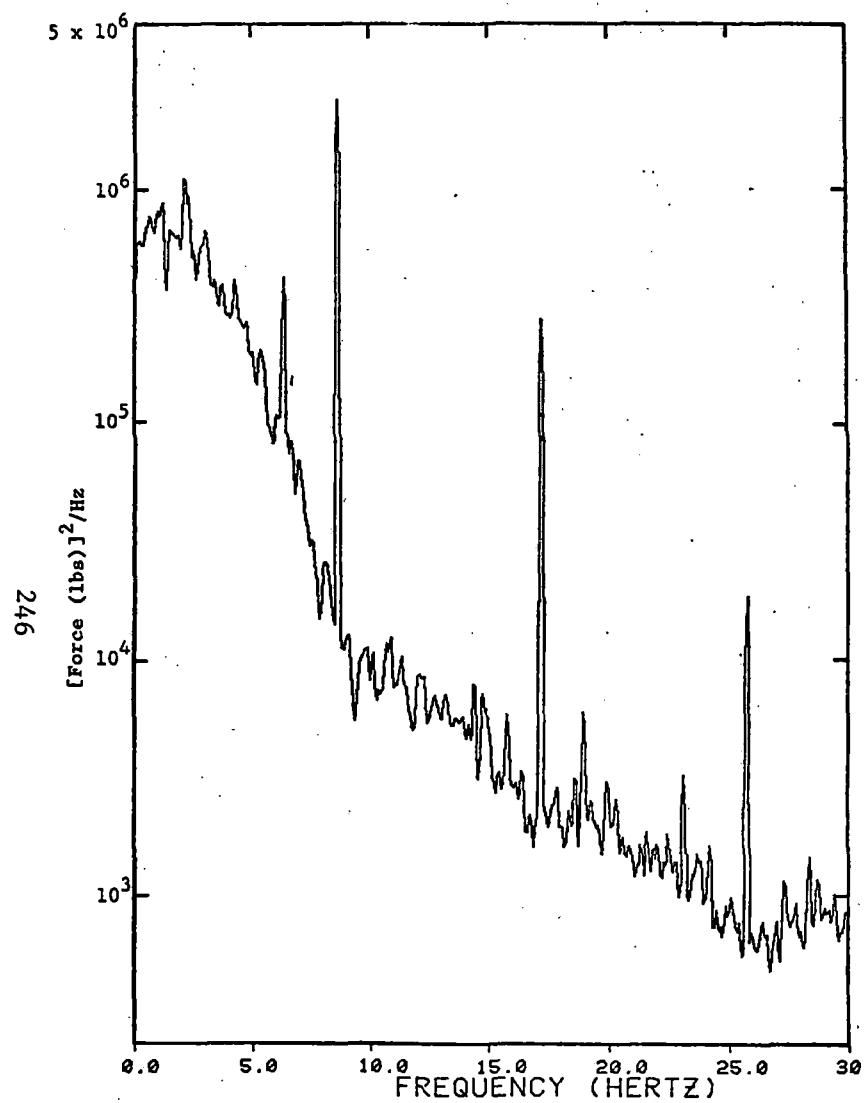


a. BJR TRACK

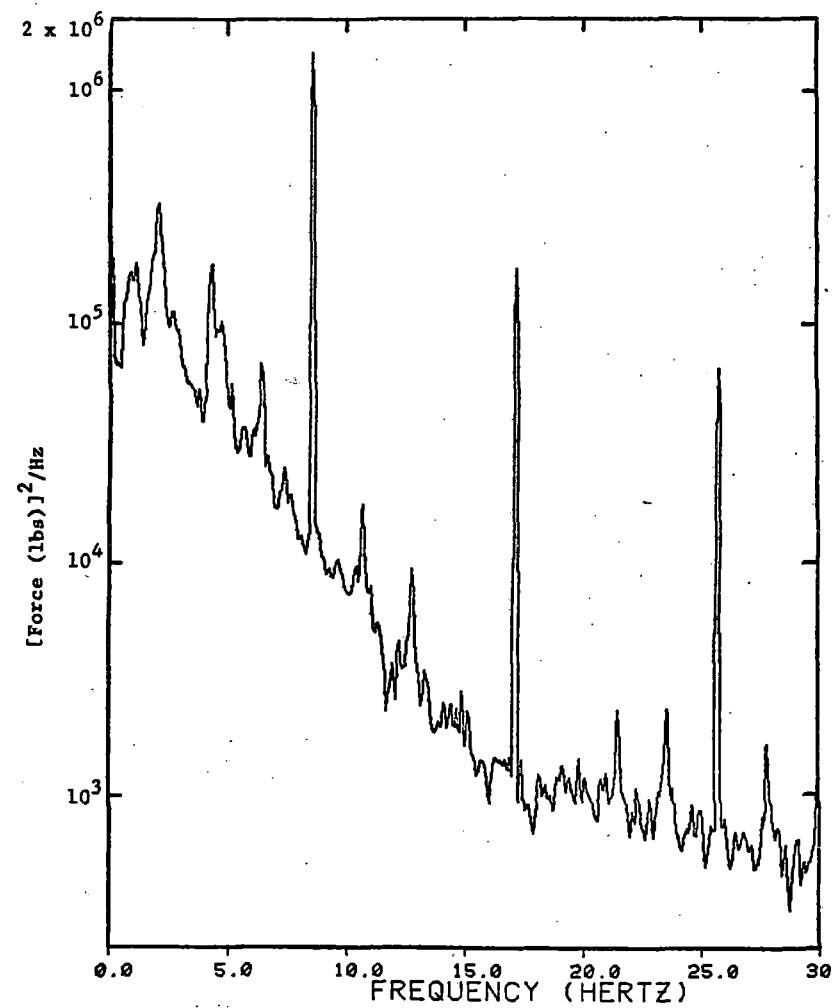


b. CWR TRACK

FIGURE D-9. FREQUENCY ANALYSIS OF VERTICAL WHEEL LOAD FROM INSTRUMENTED WHEEL, EASTBOUND (TRAILING AXLE) RUNS AT 55 MPH



a. BJR TRACK



b. CWR TRACK

FIGURE D-10. FREQUENCY ANALYSIS OF LATERAL WHEEL LOAD FROM INSTRUMENTED WHEEL, EASTBOUND (TRAILING AXLE) RUNS AT 55 MPH

## APPENDIX E

### VEHICLE-BORNE INSTRUMENTATION ERROR ANALYSIS

#### E.1 Basis of Analysis

The error analysis described in this section examines the sources of error in the measurement of wheel/rail loads, and by means of the Propagation of Error formula quantifies these errors so that the relative importance of different parameters can be assessed. Only static effects are included, since dynamic calibration tests were not part of the test plan. Where appropriate, reference is made to calibration factors and bridge output voltages which are typical values associated with the tests. These parameters are stated in terms of the voltages recorded on magnetic tape. The specific values of the calibration constants are determined with reference to the signals obtained from precision calibration resistors which were recorded both during static calibration tests and during road tests.

#### E.2 Instrumented Wheel Vertical Load Measurement

The vertical load is established as the product of the measured output voltage from the vertical strain gage bridges and the calibration factor:

$$V_H = E_V C_V$$

where  $V_H$  is the measured vertical load,

$E_V$  is the voltage output from the vertical load transducer,

$C_V$  is the calibration factor relating voltage to load.

The variance associated with the measurement of  $V_H$  can be found by expressing the relationship in the form:

$$\sigma_{V_H}^2 = \left( \frac{dV}{dE_V} \right)^2 \sigma_{E_V}^2 + \left( \frac{dV}{dC_V} \right)^2 \sigma_{C_V}^2 \quad (E-1)$$

The total expected error in the measurement of  $V_H$  is then estimated by determining the error associated with  $E_V$  and  $C_V$ . There are likely to be several independent sources of error associated with each of these parameters. These must be identified separately and combined for a determination of  $\sigma_{E_V}^2$  and  $\sigma_{C_V}^2$ , respectively. The variance associated with  $E_V$  is equal to the sum of the variances of the independent factors influencing  $E_V$ .

#### E.2.1 Errors Associated With Measurement of Bridge Voltage

The factors which affect the accuracy of the vertical wheel load bridge voltage measurements are the system electrical noise, error due to signal digitization, and the nonlinearity of bridge response.

E.2.1.1 System Electrical Noise. Measurements were made of the system electrical noise at the time the strain gages were integrated with the tape recorders. It was found that the RMS value of the system noise ranged between 6.8 to 9.4 mV with a mean value of 7.8 mV.

E.2.1.2 Digitization Error. The data were recorded in analog form and subsequently digitized. The digitization interval was 5 mV, which means that the reported signal could be as much as 2.5 mV away from the true signal voltage. If it is assumed that all possible differences between the actual and reported signal voltages are equally probable within the 0-2.5 mV range, then the RMS error in the reported signal would be 1.4 mV.

E.2.1.3 Nonlinearity of Bridge Response. Hysteresis effects are considered as part of the nonlinearity of bridge response for this discussion. The output of the vertical load bridges generally showed a high degree of linearity with increasing load and showed very little evidence of hysteresis. Figure E-1 shows a typical plot of bridge output as a function of vertical load. The maximum deviation of the signal from a straight line representation

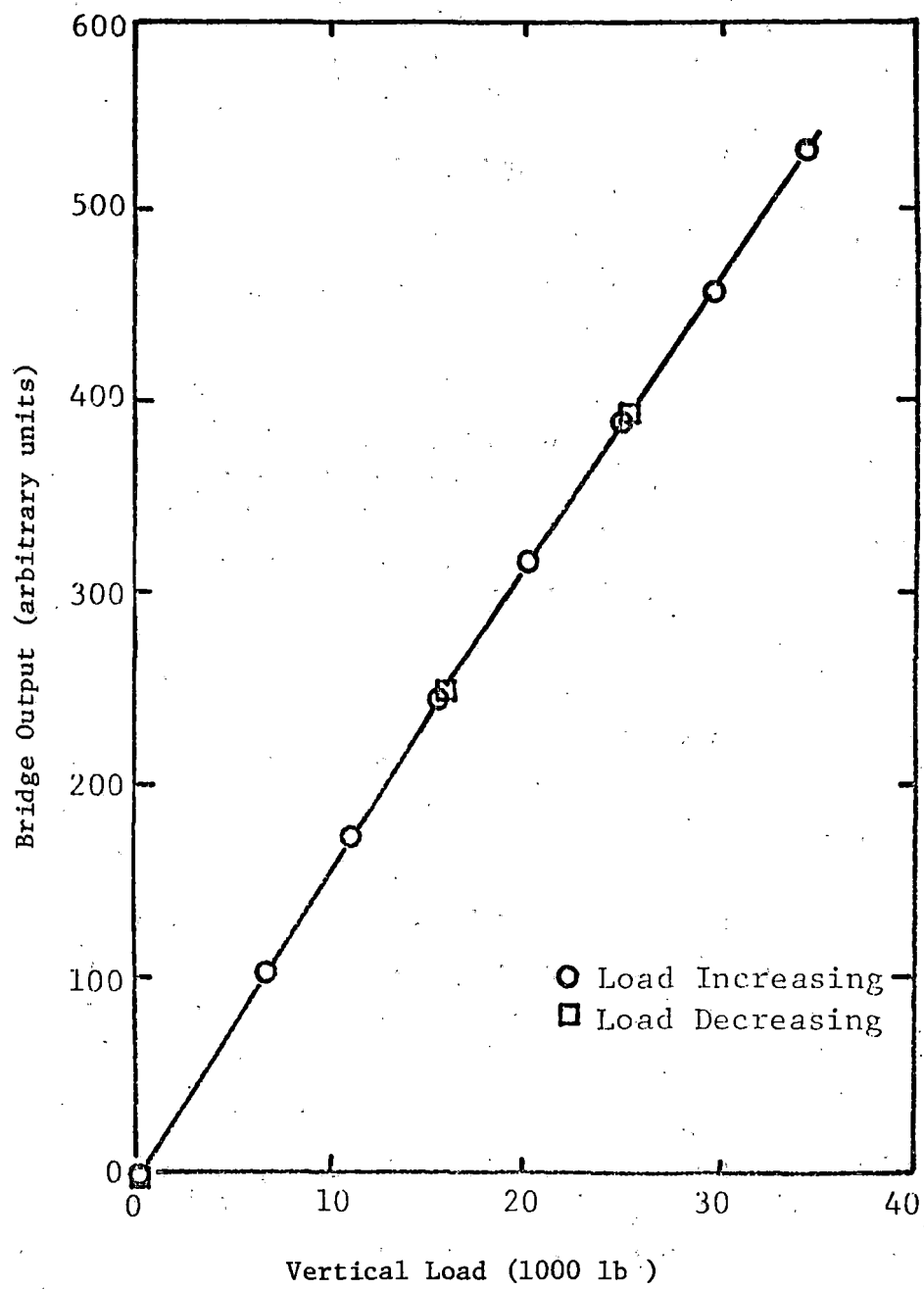


FIGURE E-1. RESULTS FROM CALIBRATION OF VERTICAL WHEEL LOAD BRIDGE

of the data has been determined in the 0-30,000 lbs load range. The maximum signal deviation is 0.41 percent of the full-load signal. A typical value for the calibration constant was 110 lbs/mV so that the maximum signal deviation is:

$$\frac{30,000}{110} (0.0041) = 1.1 \text{ mV.}$$

If it is assumed that all signal variations in the range 0-1.1 mV are equally probable, the RMS value of the error would be:

$$\frac{1.1}{\sqrt{3}} = 0.65 \text{ mV.}$$

E.2.1.4 Summary of Bridge Voltage Errors. The variance of the bridge signal may then be determined as the sum of the variances associated with the individual factors listed above:

$$\sigma_{E_V}^2 = (7.8)^2 + (1.4)^2 + (0.65)^2$$
$$\sigma_{E_V}^2 = (8.0 \text{ mV})^2.$$

The dominant source of error is that associated with system electrical noise.

## E.2.2 Errors Associated With Bridge Calibration

Two factors are considered which contribute to error associated with the vertical bridge calibration constant,  $C_V$ . These are the variation of vertical bridge output with respect to the lateral position of vertical load and the variation of vertical bridge output caused by lateral load.

E.2.2.1 Variation of Vertical Bridge Output With Resepect to Lateral Position of Vertical Load. The vertical load bridge configuration used on the wheel was designed to provide accurate load measurement as the lateral position of the vertical load changed. The extent to which there was some variation in this output represents error in the measurement of vertical load. Data were developed for all 8 vertical load bridges from both directions of loading, at tape line and  $\pm 1$  inch lateral position, at full load (32,000 lb).

The standard deviation of these values about the mean is 0.016. The values of the calibration constants for the vertical wheel bridges were approximately 110 lb/mV so that the standard deviation of the calibration constant due to this effect would be 1.76 lbs/mV.

#### E.2.2.2 Variation of Vertical Bridge Output Caused by Lateral Load.

The vertical load bridge used on the wheel was designed to provide load measurement independent of lateral load applied to the wheel. The extent to which there was some variation in output caused by lateral load effects represents error in the measurement of vertical load.

This characteristic of the vertical bridges is illustrated by the following data from the calibration tests. The data shows the change in vertical output signal associated with the application of an 8800-lb lateral test load.

<u>Vertical Bridge No.</u>	<u>Position of Lateral Load Application</u>	<u>Vertical Bridge Signal Change (Percent of 25,800 lbs Vertical Load Signal)</u>
1-9	1	0
3-11	3	0
5-13	5	-2.5
7-15	7	-1.2
1-9	9	+2.5
3-11	11	-2.5
5-13	13	-1.2
7-15	15	-2.5

The RMS value of the percent change in the vertical bridge signal is 1.87 percent. This is based on a lateral load test load of 8800 lbs. It would seem more reasonable to select a lower value of lateral load for the representation of this source of error in the system evaluation. A value of 5,000 lbs lateral load has been selected for this evaluation. This change is then expressed as an error in the calibration factor. The RMS value of the error of the calibration factor becomes:

$$(0.0187) \left( \frac{5000}{8800} \right) (110) = 1.17 \text{ lb/mV.}$$

E.2.2.3 Summary of Calibration Errors. The variance associated with the bridge calibration is the sum of the variances associated with the individual factors listed above.

$$\sigma_{C_V}^2 = (1.76)^2 + (1.17)^2 = (2.11 \text{ lb/mV})^2$$

### E.2.3 Vertical Wheel Load Summary and Discussion

The results from Sections E.2.1 and E.2.2 can be combined according to Equation E.1 to determine the variance from all the errors associated with the measurement of the load. The derivatives in Equation E.1 serve to relate the various independent parameters in the same units as the load parameter, i.e.,

$$\sigma_{V_H}^2 = (C_V)^2 \sigma_{E_V}^2 + (E_V)^2 \sigma_{C_V}^2 \quad (E-2)$$

They are evaluated using the following typical operating magnitudes that were observed during the course of the tests.

$$E_V = 235 \text{ mV}$$

$$C_V = 110 \text{ lbs/mV}$$

Substituting in Equation E.2 the variance of the vertical wheel load error is:

$$\begin{aligned} \sigma_{V_H}^2 &= (110)^2 (8.0)^2 + (235)^2 (2.11)^2 \\ &= (880 \text{ lbs})^2 + (500 \text{ lbs})^2 \\ &= (1000 \text{ lbs})^2. \end{aligned}$$

The dominant source of error is due to system electrical circuit noise. This is the result of the use of a relatively low gain factor such that the static wheel load signal was approximately 235 mV. This resulted in the system noise being a larger percentage of the signal than if a higher gain factor had been used.

There were two principal considerations in the choice of the gain factor. First, a static wheel load about 25 percent greater had been expected. The car did not contain a full load and the load was not properly centered. Second, transient load effects with peak loads up to 2 or 3 times the static load were anticipated and it was desired that these data points be included well within the linear range of the tape recorder. On future measurement programs it would be desirable to optimize the range over which the signal is recorded so as to minimize the effects of electrical noise.

### E.3 Instrumented Wheel Vertical Load Position Measurement

The position sensing bridge which was installed on the wheel was used to establish the transverse position of the radial line-of-action of the vertical load. Knowledge of the load position is used to correct the output of the lateral load bridge.

The position,  $P$ , is a function of the ratio of the output voltage of the position sensing bridge and the vertical load sensing bridge:

$$P = k_1 \left[ \frac{E_p}{E_v} \right] - k_2 \quad (E-3)$$

where

$P$  is the position of the vertical load relative to the tape line,

$k_1$  and  $k_2$  are constants obtained from the calibration,

$E_p$  is the measured output voltage of the load position sensing bridge,

$E_v$  is the measured output voltage of the vertical load sensing bridge.

Errors associated with each of the above parameters will limit the accuracy to which  $P$  can be established. The variance associated with the measurement of  $P$  is defined as  $\sigma_p^2$  and is found from:

$$\begin{aligned} \sigma_p^2 = & \left( \frac{dP}{dE_v} \right)^2 \sigma_{E_v}^2 + \left( \frac{dP}{dE_p} \right)^2 \sigma_{E_p}^2 + \left( \frac{dP}{dk_1} \right)^2 \sigma_{k_1}^2 \\ & + \left( \frac{dP}{dk_2} \right)^2 \sigma_{k_2}^2 \end{aligned} \quad (E-4)$$

Evaluating the derivatives the equation becomes:

$$\sigma_p^2 = \left[ \frac{k_1 E_p}{E_v^2} \right]^2 \sigma_{E_v}^2 + \left[ \frac{k_1}{E_v} \right]^2 \sigma_{E_p}^2 = \left[ \frac{E_p}{E_v} \right]^2 \sigma_{k_1}^2 + \sigma_{k_2}^2 \quad (E-5)$$

The probable errors associated with each of the parameters in the equation are then estimated.

### E.3.1 Errors Associated With the Measurement of Vertical Bridge Voltage, $E_V$

The three factors described in Section E.2.1 apply, resulting in a variance in the measurement of  $E_V$  of:

$$\sigma_{E_V}^2 = (8.0 \text{ mV})^2.$$

### E.3.2 Errors Associated With the Measurement of Position Bridge Voltage, $E_P$

The factors which affect the accuracy of the positional bridge voltage measurements are the system electrical noise, error due to signal digitization, and the nonlinearity of bridge response. The RMS values of the system noise and digitization errors are the same as reported for the other bridge voltage measurements, namely, 7.8 and 1.4 mV respectively.

E.3.2.1 Nonlinearity of Bridge Response. The output of the position bridge was similar to the output of the vertical load bridge showing a high degree of linearity and minor hysteresis effects. The maximum signal deviation from a straight line representation of the data over a 0-30,000 lb load range was determined to be 0.84 percent of the full load signal. A typical value for the output signal was 195 mV so that the maximum signal deviation due to nonlinearity effects would be 1.6 mV. If it is assumed that all signal variations in the range 0-1.6 mV are equally probable, the RMS value of the error would be:

$$\frac{1.6}{\sqrt{3}} = 0.92 \text{ mV}.$$

E.3.2.2 Summary of Bridge Voltage Errors. The variance associated with the bridge signal may then be determined as the sum of the variances associated with the individual factors listed above.

$$\sigma_{E_P}^2 = (7.8)^2 + (1.4)^2 + (0.92)^2$$
$$\sigma_{E_P}^2 = (8.0 \text{ mV})^2.$$

The dominant source of error is from the system electrical noise. The problem is the same as that described for the vertical load bridge, namely, the relatively low load on the test wheel and the desire to provide a linear recording range for high dynamic loads.

### E.3.3 Errors Associated With Bridge Calibration

The parameters  $k_1$  and  $k_2$  in Equation E.3 are derived from calibration data and the extent to which there are errors associated with their determination there will be errors in the establishment of the position of the vertical load,  $P$ . Slightly different values for  $k_1$  and  $k_2$  were obtained for each of the position bridges during the calibration tests. The major source of error associated with these constants is that only one (average) set of constants for Equation E.3 was utilized in the data reduction process. While variations in  $k_1$  and  $k_2$  from one bridge to the next would represent systematic rather than random errors, an estimate for their contribution to the total error for  $P$  can be obtained by considering their variation as random. Based on the calibration tests the average values for  $k_1$  and  $k_2$  are listed as follows:

$$k_1 = 6.09 \text{ in.}$$

$$k_2 = 4.73 \text{ in.}$$

with RMS deviations of 0.26 in. and 0.21 in. for  $k_1$  and  $k_2$  respectively.

### E.3.4 Wheel Load Position Summary and Discussion

The results from Sections E.3.1 to E.3.3 can be combined according to Equation E.4 to determine the variance from all the errors associated with the measurement of  $P$ . The derivatives in Equation E.4 serve to relate the various independent parameters in the same units as the position parameter. They are evaluated using the following typical operating magnitudes that were observed during the course of the tests.

$$E_p = 195 \text{ mV}$$

$$E_v = 235 \text{ mV}$$

$$k_1 = 6.09 \text{ in.}$$

$$k_2 = 4.73 \text{ in.}$$

Substituting in Equation E.5 the variance of the positional error is determined as follows:

$$\begin{aligned}\sigma_p^2 &= \left[ \frac{6.09(195)}{(235)^2} \right]^2 (8.0)^2 + \left[ \frac{6.09}{235} \right]^2 (8.0)^2 + \left[ \frac{195}{235} \right]^2 (0.26)^2 + (0.21)^2 \\ \sigma_p^2 &= (0.17 \text{ in.})^2 + (0.21 \text{ in.})^2 + (0.22 \text{ in.})^2 + (0.21 \text{ in.})^2 \\ \sigma_p^2 &= (0.41 \text{ in.})^2 .\end{aligned}$$

The variance of the error in the measurement of P is therefore  $(0.41 \text{ in.})^2$ . The error is divided almost equally between the four major parameters, the bridge voltages  $E_p$  and  $E_v$  and the calibration constants,  $k_1$  and  $k_2$ . The total error is greater than desired. This is due to the relatively low bridge voltage in relationship to system noise, a problem discussed earlier, and the use of a single set of calibration constants to relate positional data to the bridge outputs. The accuracy could be improved by using a different set of relationships for each bridge and the use of a better wheel cross sectional configuration so that there is less variation in bridge output from point to point around the wheel.

#### E.4 Instrumented Wheel Lateral Load Measurement

The lateral wheel/rail load,  $L_H$ , is established from the experimental measurements by the following equation:

$$L_H = E_L C_{L1} + (P + k_3) C_{L2} \left( \frac{V_H}{32,000} \right) . \quad (E-6)$$

where

$E_L$  is the measured output voltage from the lateral load bridge,  
 $C_{L1}$  is a calibration constant relating the output voltage to force,  
 $P$  is the lateral position of the vertical wheel/rail load with respect to the tape line of the wheel,  
 $k_3$  is a constant derived from the calibration of the wheel,  
 $C_{L2}$  is a calibration constant relating the position of the vertical load to a modification of the lateral load.

The dominant source of error is from the system electrical noise. The problem is the same as that described for the vertical load bridge, namely, the relatively low load on the test wheel and the desire to provide a linear recording range for high dynamic loads.

### E.3.3 Errors Associated With Bridge Calibration

The parameters  $k_1$  and  $k_2$  in Equation E.3 are derived from calibration data and the extent to which there are errors associated with their determination there will be errors in the establishment of the position of the vertical load,  $P$ . Slightly different values for  $k_1$  and  $k_2$  were obtained for each of the position bridges during the calibration tests. The major source of error associated with these constants is that only one (average) set of constants for Equation E.3 was utilized in the data reduction process. While variations in  $k_1$  and  $k_2$  from one bridge to the next would represent systematic rather than random errors, an estimate for their contribution to the total error for  $P$  can be obtained by considering their variation as random. Based on the calibration tests the average values for  $k_1$  and  $k_2$  are listed as follows:

$$k_1 = 6.09 \text{ in.}$$

$$k_2 = 4.73 \text{ in.}$$

with RMS deviations of 0.26 in. and 0.21 in. for  $k_1$  and  $k_2$  respectively.

### E.3.4 Wheel Load Position Summary and Discussion

The results from Sections E.3.1 to E.3.3 can be combined according to Equation E.4 to determine the variance from all the errors associated with the measurement of  $P$ . The derivatives in Equation E.4 serve to relate the various independent parameters in the same units as the position parameter. They are evaluated using the following typical operating magnitudes that were observed during the course of the tests.

$$E_p = 195 \text{ mV}$$

$$E_v = 235 \text{ mV}$$

$$k_1 = 6.09 \text{ in.}$$

$$k_2 = 4.73 \text{ in.}$$

Substituting in Equation E.5 the variance of the positional error is determined as follows:

$$\begin{aligned}\sigma_P^2 &= \left[ \frac{6.09(195)}{(235)^2} \right]^2 (8.0)^2 + \left[ \frac{6.09}{235} \right]^2 (8.0)^2 + \left[ \frac{195}{235} \right]^2 (0.26)^2 + (0.21)^2 \\ \sigma_P^2 &= (0.17 \text{ in.})^2 + (0.21 \text{ in.})^2 + (0.22 \text{ in.})^2 + (0.21 \text{ in.})^2 \\ \sigma_P^2 &= (0.41 \text{ in.})^2 .\end{aligned}$$

The variance of the error in the measurement of P is therefore  $(0.41 \text{ in.})^2$ . The error is divided almost equally between the four major parameters, the bridge voltages  $E_p$  and  $E_v$  and the calibration constants,  $k_1$  and  $k_2$ . The total error is greater than desired. This is due to the relatively low bridge voltage in relationship to system noise, a problem discussed earlier, and the use of a single set of calibration constants to relate positional data to the bridge outputs. The accuracy could be improved by using a different set of relationships for each bridge and the use of a better wheel cross sectional configuration so that there is less variation in bridge output from point to point around the wheel.

#### E.4 Instrumented Wheel Lateral Load Measurement

The lateral wheel/rail load,  $L_H$ , is established from the experimental measurements by the following equation:

$$L_H = E_L C_{L1} + (P + k_3) C_{L2} \left( \frac{V_H}{32,000} \right) . \quad (E-6)$$

where

$E_L$  is the measured output voltage from the lateral load bridge,  
 $C_{L1}$  is a calibration constant relating the output voltage to force,  
 $P$  is the lateral position of the vertical wheel/rail load with respect to the tape line of the wheel,  
 $k_3$  is a constant derived from the calibration of the wheel,  
 $C_{L2}$  is a calibration constant relating the position of the vertical load to a modification of the lateral load.

Equation E.6 accounts for the interaction of the position of the vertical load with the lateral bridge output. Errors associated with each of the above parameters will limit the accuracy to which  $L_H$  can be established. The variance associated with the measurement of  $L_H$  can be found:

$$\begin{aligned} \sigma_{L_H}^2 = & \left( \frac{dL_H}{dE_L} \right)^2 \sigma_{E_L}^2 + \left( \frac{dL_H}{dC_{L1}} \right)^2 \sigma_{C_{L1}}^2 + \left( \frac{dL_H}{dP} \right)^2 \sigma_P^2 \\ & + \left( \frac{dL_H}{dk_3} \right)^2 \sigma_{k_3}^2 + \left( \frac{dL_H}{dC_{L2}} \right)^2 \sigma_{C_{L2}}^2 + \left( \frac{dL_H}{dV_H} \right)^2 \sigma_{V_H}^2 \end{aligned} \quad (E-7)$$

Evaluating the derivatives the equation becomes:

$$\begin{aligned} \sigma_{L_H}^2 = & (C_{L1})^2 \sigma_{E_L}^2 + (E_L)^2 \sigma_{C_{L1}}^2 + \left( \frac{C_{L2} V_H}{32,000} \right)^2 \sigma_P^2 \\ & + \left( \frac{C_{L2} V_H}{32,000} \right)^2 \sigma_{k_3}^2 + (P + k_3)^2 \left( \frac{V_H}{32,000} \right)^2 \sigma_{C_{L2}}^2 \\ & + \left( \frac{(P+k_3)C_{L2}}{32,000} \right)^2 \sigma_{V_H}^2 \end{aligned} \quad (E-8)$$

The probable errors associated with each of the parameters in the equation are then estimated.

#### E.4.1 Errors Associated with Measurement of Lateral Bridge Voltage, $E_L$

The factors which affect the accuracy of the lateral bridge voltage measurements are the system electrical noise, error due to signal digitization, and the nonlinearity of bridge response. The RMS values of the system noise and digitization errors are the same as reported for other bridge voltage measurements, namely, 7.8 mV and 1.4 mV respectively.

E.4.1.1 Nonlinearity of Bridge Response. The output of the lateral load bridges showed a high degree of linearity with minor hysteresis effects. The maximum signal deviation from a straight line representation of the data over a 0 - 8800 lb load range was determined to be 2.5 percent of the full load signal. A typical value for the output signal was 325 mV so that the maximum signal deviation due to nonlinearity effects would be 8.0 mV. If it is assumed that all signal variations in the range 0-8 mV are equally probable, the RMS value of the error would be

$$\frac{8.0}{\sqrt{3}} = 4.6 \text{ mV.}$$

E.4.1.2 Summary of Bridge Voltage Errors. The variances associated with the bridge signal may then be determined as the sum of the variances associated with the individual factors listed above.

$$\begin{aligned}\sigma_{E_L}^2 &= (7.8)^2 + (1.4)^2 + (4.6)^2 \\ \sigma_{E_L}^2 &= (9.2 \text{ mV})^2.\end{aligned}$$

E.4.2 Errors Associated With Bridge Calibration Factor,  $C_L$

Only one source of error is identified with respect to the bridge calibration factor, namely, the variation in the output of the different lateral bridges around the wheel. The assumption was made in the analysis of the data that the output of each bridge could be determined from the average  $C_L$  constant for the lateral bridges. Analysis of the data from the calibration tests showed that the average of the calibration constant was 27 lbs/mV with an RMS variation 1.25 lbs/mV.

E.4.3 Error Associated With Measurement of Position of Vertical Load, P

The variance in the measurement of P is given in Section E.3.4 to be  $(0.41 \text{ in})^2$ .

#### E.4.4 Error Associated With the Calibration Constants " $k_3$ " and " $C_{L2}$ "

The constants  $k_3$  and  $C_{L2}$  relate the positional information to be a correction of the indicated lateral load. These constants have been derived from the calibration test data. The constant " $k_3$ " designates the lateral position on the wheel, with respect to the tape line, where a vertical load has no affect on the lateral load bridge ( $k_3$  is positive measured toward flange). In the analysis of the data  $k_3$  and  $C_{L2}$  were treated as being the same for each bridge although there were some differences in their magnitude from one bridge to the next. This led to error in the calculation of the positional load correction term. The standard deviation in the value for  $k_3$  was 0.09 in., and in the value for  $C_{L2}$  was 52.3 lbs/in.

#### E.4.5 Error Associated With the Measurement of $V_H$

The variance of the error associated with  $V_H$  is given in Section E.2.3 as  $(1000 \text{ lb})^2$ .

#### E.4.6 Wheel Lateral Load Summary and Discussion

The results from Sections E.4.1 to E.4.5 can be combined according to Equation E.7 to determine the variance from all the errors associated with the measurement of the load. The derivatives in Equation E.7 serve to relate the various independent parameters in the same units as the lateral load parameter. They are evaluated using the following typical operating magnitudes that were observed during the course of the tests.

$$\begin{aligned}E_L &= 325 \text{ mV} \\C_{L1} &= 27 \text{ lb/mV} \\C_{L2} &= 2500 \text{ lbs/in.} \\V_H &= 25,800 \text{ lbs.} \\P &= 0.1 \text{ in.} \\a &= 0.34 \text{ in.}\end{aligned}$$

Substituting these values in Equation E.8 the variance of the lateral wheel load is calculated to be:

$$\begin{aligned}
 \sigma_{L_H}^2 &= (27)^2 (9.2)^2 + (325)^2 (1.25)^2 + \left[ \frac{(2500)(25,800)}{(32,000)} \right]^2 (0.41)^2 \\
 &\quad + \left[ \frac{(2500)(25,800)}{(32,000)} \right]^2 (0.09)^2 + \left[ (0.44) \frac{25,800}{32,000} \right]^2 (52.3)^2 \\
 &\quad + \left[ \frac{(0.44)(2500)}{32,000} \right]^2 (1000)^2 \\
 \sigma_{L_H}^2 &= (248 \text{ lb})^2 + (406 \text{ lb})^2 + (820 \text{ lb})^2 + (181 \text{ lb})^2 \\
 &\quad + (19 \text{ lb})^2 + (34 \text{ lb})^2 \\
 \sigma_{L_H}^2 &= (970 \text{ lbs})^2 .
 \end{aligned}$$

The major source of error is due to inaccuracies in the positional information, P, of the line-of-action of the vertical load. As discussed in Section E.3.4, there are a number of ways in which the accuracy of this parameter could improve. Note that the second most important contribution to lateral load error is due to inaccuracies in the lateral load calibration constant. The error here is proportional to the signal level and, hence, is proportional to the magnitude of the lateral load. The equation has been evaluated at a relatively large lateral load (8800 lbs where  $E_L = 325 \text{ mV}$ ) to obtain the  $(406 \text{ lb})^2$  variance estimate of this parameter.

#### E.5 Side Frame Vertical Wheel Load Measurement

The vertical wheel/rail load,  $L_V$ , is established from the experimental side frame gage measurements by the following equation:

$$V_L = (S + E_{BL} C_{BL}) \left(1 + \frac{a_l}{f}\right) - (S + E_{BR} C_{BR}) \left(\frac{a_r}{f}\right) . \quad (E-9)$$

where

S is the static wheel load (both wheels on an axle are assumed to have the same load),

$E_{BL}$  and  $E_{BR}$  are the voltage outputs from the left and right side frame bridges,

$C_{BL}$  and  $C_{BR}$  are the calibration factors relating the side frame bridge voltages to journal bearing loads,

$a_l$  and  $a_r$  are the lateral distances between the line-of-action of the vertical side frame and wheel/rail loads (left and right hand respectively) as illustrated in Figure 3.3,

$f$  is the distance between the left and right hand wheel/rail contact points as illustrated in Figure 3.3.

Errors associated with each of the above parameters will limit the accuracy to which  $V_L$  can be established. The variance associated with the measurement of  $V_L$  can be found:

$$\begin{aligned} \sigma_{V_L}^2 = & \left( \frac{dV_L}{dS} \right)^2 \sigma_S^2 + \left( \frac{dV_L}{dE_{BL}} \right)^2 \sigma_{E_{BL}}^2 + \left( \frac{dV_L}{dC_{BL}} \right)^2 \sigma_{C_{BL}}^2 \\ & + \left( \frac{dV_L}{da_l} \right)^2 \sigma_{a_l}^2 + \left( \frac{dV_L}{da_r} \right)^2 \sigma_{a_r}^2 + \left( \frac{dV_L}{df} \right)^2 \sigma_f^2 \\ & + \left( \frac{dV_L}{dE_{BR}} \right)^2 \sigma_{E_{BR}}^2 + \left( \frac{dV_L}{dC_{BR}} \right)^2 \sigma_{C_{BR}}^2 \end{aligned} \quad (E-10)$$

Evaluating the derivatives the equation becomes:

$$\begin{aligned} \sigma_{V_L}^2 = & \left[ 1 + \frac{a_l}{f} - \frac{a_r}{f} \right]^2 \sigma_S^2 + \left[ C_{BL} \left( 1 + \frac{a_l}{f} \right) \right]^2 \sigma_{E_{BL}}^2 \\ & + \left[ E_{BL} \left( 1 + \frac{a_l}{f} \right) \right]^2 \sigma_{C_{BL}}^2 + \left[ \frac{(S + E_{BL} C_{BL})}{f} \right]^2 \sigma_{a_l}^2 \\ & + \left[ \frac{(S + E_{BR} C_{BR})}{f} \right]^2 \sigma_{a_r}^2 + \left[ (S + E_{BL} C_{BL}) a_l \right. \\ & \left. - (S + E_{BR} C_{BR}) a_r \right]^2 \left[ \frac{1}{f^2} \right]^2 \sigma_f^2 \\ & + \left[ C_{BL} \left( \frac{a_r}{f} \right) \right]^2 \sigma_{E_{BR}}^2 + \left[ E_{BR} \left( \frac{a_r}{f} \right) \right]^2 \sigma_{C_{BR}}^2. \end{aligned} \quad (E-11)$$

The probable error associated with each of the parameters in the equation is then estimated.

### E.5.1 Error Associated With the Measurement of Bridge Voltage, $E_{BL}$ and $E_{BR}$

The factors which affect the accuracy of the side frame vertical load bridge voltage measurements are the system electrical noise, error due to signal digitization, and the nonlinearity of bridge response. The RMS values of the system noise and digitization errors are the same as reported for other bridge voltage measurements, namely, 7.8 mV and 1.4 mV respectively.

E.5.1.1 Nonlinearity of Bridge Response. The side frames were instrumented in the field and it was not possible to run standard calibration tests to determine the specific characteristics of the bridge. The calibration constant was determined by jacking the test car to remove the load and noting the change in bridge output voltage.

Data from calibration tests of other side frames using this type of strain gage bridge can be utilized to provide an estimate of the expected non-linearity error. The analysis of typical data from 4 instrumented side frames shows an RMS error of 1.3 percent of full scale load application. A typical signal level for the side frames would be on the order of 250 mV so that the RMS signal due to nonlinearity effects can be estimated to be 3.3 mV (adjusted for the fact that the side frame output must be divided by two for wheel load representation).

E.5.1.2 Summary of Bridge Voltage Errors. The variances associated with the bridge signal may then be determined as the sum of the variances associated with the individual factors listed above.

$$\begin{aligned}\sigma_{E_{BL}}^2 &= \sigma_{E_{BR}}^2 = (7.8)^2 + (1.4)^2 + (3.3)^2 \\ &= (8.6 \text{ mV})^2 .\end{aligned}$$

### E.5.2 Errors Associated With Bridge Calibration Factors, $C_{BL}$ and $C_{BR}$

The factors which affect the accuracy of the side frame bridge calibration factors include crosstalk from lateral load effects, changes due to

off-center vertical load application, and errors associated with the establishment of a reference load during the calibration tests. Because the side frames were instrumented in the field, where there was no opportunity to perform detailed calibration tests, it was not possible to ascertain crosstalk from lateral load effects or changes in signal output from off-center load application. Therefore, no estimate of the errors caused by these effects are included in this analysis. One would expect that the lateral load crosstalk error would be relatively small because, with the side frame, one is dealing with the lateral load acting from the bolster, which is usually smaller than the lateral wheel/rail load acting through the wheel/axle set.

The largest source of error associated with the bridge calibration factors results from the uncertainty of the weight of the car when it was jacked off the truck. It had been anticipated that the static wheel load could be established for the loaded car by means of a truck scale, but it was found that the truck scale could only be used to give the weight of the entire car. The loads on individual trucks could not be ascertained. Furthermore, the load was not centered in the car so that one could not assume that the four side frames were equally loaded. Therefore, the calibration load had to be estimated from the output of the wheel plate vertical load gages. As described in Section E.2.3 the variance of the vertical wheel measurement was  $(1,000 \text{ lbs})^2$ . It follows that the RMS error of the calibration load would be 890 lbs. The nominal (side frame) calibration load was 23,050 lbs. (These figures are stated in terms of equivalent wheel load, assuming the side frame load is equally divided between the two axles.) Under the operating conditions of the test the side frame bridge calibration factors were set at approximately 16 mV/lbs which then implies an RMS deviation of 0.62 mV/lb for the calibration factors.

#### E.5.3 Error Associated With Static Wheel Load, S

See preceding section. The static wheel load was established from the vertical wheel plate gages with a variance of  $(1000 \text{ lbs})^2$ .

#### E.5.4 Error Associated With Lateral Positions of Vertical Loads: $a_l$ , $a_r$ and $f$

The positions assumed for the vertical side-frame/roller-bearing-adapter loads and the vertical wheel/rail loads are illustrated in Figures 6-30. The distances,  $a_l$ ,  $a_r$  and  $f$  are subject to some variation during the operation of the wheel set because of local variations in track geometry and because of relative motion between truck components. There is no precise method of determining these dimensional variations. For this error analysis, estimates have been made based on a review of nominal dimensional relationships and tolerances.

A cross section through the side frame pedestal and the roller bearing adapter is shown in Figure E-2. It shows that the side frame is flat for 3-1/2 in. and then blends into a 15 inch radius. The top surface of the roller bearing has a crown in this direction defined by a 60 inch radius. Thus, a slight rotation of the side frame relative to the bearing adapter will cause a significant lateral motion of the point of contact between these two members. Furthermore, the tolerances between the side frame lug and the recess in the roller bearing adapter is such that up to  $\pm 17/64$  in. motion of the side frame relative to the roller bearing adapter can be anticipated.

The exact position of the wheel/rail contact point depends on a number of factors including the variation in track gage and the states of wear on both the tread of the wheels and the rails. Generally, it would be expected that the wheel/rail contact surface would fall within 1 to 2 inches of the inside surface of the wheels.

A greater variation would be anticipated in the distance between the side frame/bearing adapter, wheel/rail contact point than between the two wheel/rail contact points. In the first case, the 2 load positions are independent, whereas in the second case the two load positions would be somewhat related to one another (i.e., as the wheel/axle set moves within the gage clearance an inward movement of the wheel/rail contact point on one wheel would result in an outward movement of the wheel/rail contact point on the opposite wheel).

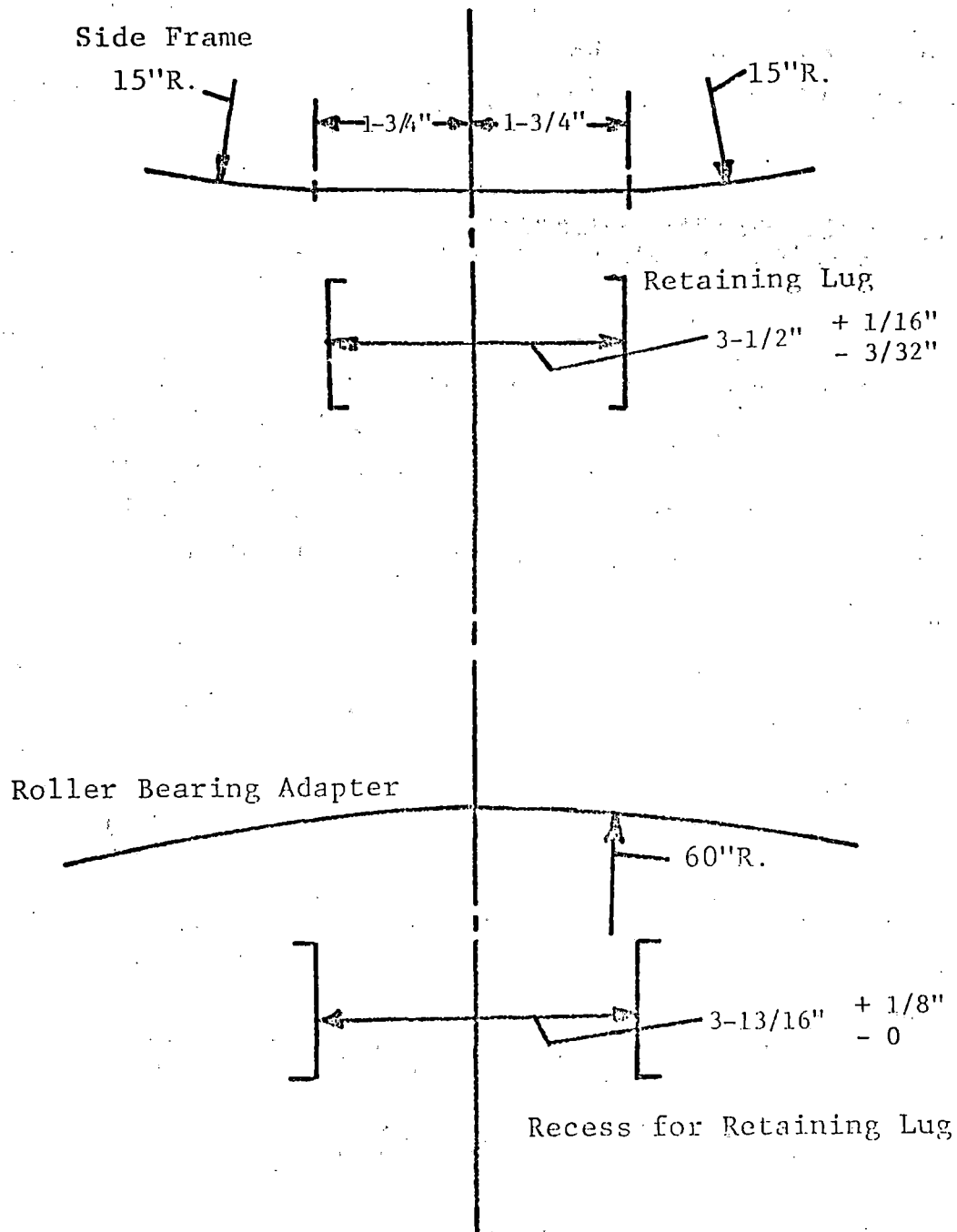


FIGURE E-2. SECTION THROUGH SIDE-FRAME-PEDESTAL/ROLLER-BEARING-ADAPTER INTERFACE

The assessment of the errors caused by assuming that the distances  $f$ ,  $a_l$ , and  $a_r$  are constant has been estimated in this analysis by assuming that the RMS error in  $f$  is 0.75 in. and that the RMS variations in  $a_l$  and  $a_r$  are 1.25 in.

#### E.5.5 Side Frame Measurement of Wheel/Rail Vertical Load, Summary and Discussion

The results from Sections E.5.1 to E.5.4 can be combined according to Equation E.10 to determine the variance from all the effects of the errors associated with the measurement of the load. The derivatives in Equation E.10 serve to relate the variances of the independent parameters in the same units as the vertical wheel load parameter. They are evaluated using the following typical operating magnitudes that were observed during the course of the tests.

$$\begin{aligned} S &= 25,800 \text{ lbs} \\ E_{BL} &= 250 \text{ mV} \\ E_{BR} &= -250 \text{ mV} \\ C_{BL} &= 16 \text{ lbs/mV} \\ C_{BR} &= 16 \text{ lbs/mV} \\ a_l &= 10.25 \text{ in.} \\ a_r &= 10.25 \text{ in.} \\ f &= 58.5 \text{ in.} \end{aligned}$$

Substituting Equation E.11 the variance of the vertical wheel load is calculated to be:

$$\begin{aligned} \sigma_{V_L}^2 &= (1000)^2 + [16(1.18)]^2(8.6)^2 + [250(1.18)]^2(0.62)^2 \\ &\quad + \left[\frac{29,800}{58.5}\right]^2(1.25)^2 + \left[\frac{21,800}{58.5}\right]^2(1.25)^2 \\ &\quad + \left[\frac{(8000)(10.25)}{(58.5)^2}\right]^2(0.75)^2 + [16(0.18)]^2(8.6)^2 \\ &\quad + [250(0.18)]^2(0.62)^2 \end{aligned}$$

$$\begin{aligned}\sigma_V^2 &= (1000 \text{ lb})^2 + (162 \text{ lb})^2 + (183 \text{ lb})^2 + (637 \text{ lb})^2 \\ &\quad + (466 \text{ lb})^2 + (18 \text{ lb})^2 + (25 \text{ lb})^2 + (28 \text{ lb})^2 \\ &= (1300 \text{ lb})^2\end{aligned}$$

The largest source of error is due to the establishment of the static wheel load. The next largest source of error is due to dimensional variations between the side frame/bearing adapter and the wheel/rail contact points. The wheel load error could be improved by better calibration procedures, but the effects of dimensional errors would be more difficult to control.

The error associated with the measurement of bridge voltage is much less important for side frame vertical load measurement than for the vertical wheel load measurement. This results from the use of a more sensitive calibration factor with the side frame, e.g., 16 lbs/mV, compared to 110 lbs/mV for the instrumented wheel. The side frame load signals can be recorded with reference to the mean load (zero voltage case) where the signal voltage records the plus-minus variations in the dynamic loads about the mean. The instrumented wheel bridges cannot be treated in this way because the wheel load signal goes from a full load positive value to a full load negative value once per wheel revolution. With the wheel, the zero signal represents a no-load condition.

There is another source of error which has not been considered in this discussion of the instrumented side frame, namely, that the instrumented side frame provides a signal which averages the two journal loads. When dealing with low frequency vertical load phenomena, such as fluctuations due to fundamental car body response motions (e.g., car-body roll, bounce, etc.) this is a reasonable assumption. When dealing with high frequency phenomena such as the traversal of rail corrugations or rail crossings, there would probably be a substantial difference between the actual wheel/rail load and the reported load. There would also be a substantial error for high-frequency measurements due to mass attenuation effects because the major fraction of the unsprung mass would lie between the gage locations and the wheel/rail interface.

## E.6 Side Frame and Axle Lateral Wheel Load Measurements

The lateral wheel/rail load,  $L_L$ , is established from experimental measurements made on the instrumented side frames and axle using the following equation. In this discussion only the lateral load on the left wheel of the axle is considered. The analysis for the lateral wheel load on the right wheel would be similar.

$$L_L = \frac{1}{c} \left[ \frac{E_{ML} C_{ML} (f-d) - E_{MR} C_{MR} (d)}{f - 2d} - a (S + E_{BL} C_{BL}) \right] \quad (E-12)$$

where

$E_{ML}$  and  $E_{MR}$  are the voltage outputs from the left and right axle bending moment bridges,

$C_{ML}$  and  $C_{MR}$  are the calibration factors relating bending moment bridge voltages to bending moments,

$a$ ,  $f$ ,  $d$  and  $c$  are dimensions defining load lines-of-action

(see Figure 6-30). Note  $(f-2d)$  is a constant equal to 30.5 in.

$S$  is the static wheel load,

$E_{BL}$  is the voltage output from the left vertical side frame bridge

$C_{BL}$  is the calibration factor relating side frame bridge voltage to journal bearing loads.

Errors associated with each of the above parameters will limit the accuracy to which  $L_L$  can be established. The variance associated with the measurement of  $L_L$  can be found:

$$\begin{aligned} \sigma_{L_L}^2 = & \left( \frac{dL_L}{dE_{ML}} \right)^2 \sigma_{E_{ML}}^2 + \left( \frac{dL_L}{dC_{ML}} \right)^2 \sigma_{C_{ML}}^2 + \left( \frac{dL_L}{dE_{MR}} \right)^2 \sigma_{E_{MR}}^2 \\ & + \left( \frac{dL_L}{dC_{MR}} \right)^2 \sigma_{C_{MR}}^2 + \left( \frac{dL_L}{dc} \right)^2 \sigma_c^2 + \left( \frac{dL_L}{df} \right)^2 \sigma_f^2 + \left( \frac{dL_L}{dd} \right)^2 \sigma_d^2 \quad (E-13) \\ & + \left( \frac{dL_L}{da} \right)^2 \sigma_a^2 + \left( \frac{dL_L}{dS} \right)^2 \sigma_S^2 + \left( \frac{dL_L}{dE_{BL}} \right)^2 \sigma_{E_{BL}}^2 + \left( \frac{dL_L}{dC_{BL}} \right)^2 \sigma_{C_{BL}}^2 \end{aligned}$$

Evaluating the derivatives, the equation becomes:

$$\begin{aligned}
 \sigma_{L_L}^2 = & \left[ \frac{C_{ML}(f-d)}{30.5c} \right]^2 \sigma_{E_{ML}}^2 + \left[ \frac{E_{ML}(f-d)}{30.5c} \right]^2 \sigma_{C_{ML}}^2 \\
 & + \left[ \frac{C_{MR}(d)}{30.5c} \right]^2 \sigma_{E_{MR}}^2 + \left[ \frac{E_{MR}(d)}{30.5c} \right]^2 \sigma_{C_{MR}}^2 \\
 & + \left[ \frac{1}{c} \right]^2 \left[ \frac{E_{ML}C_{ML}(f-d) - E_{MR}C_{MR}(d)}{30.5} a(S + E_{BL}C_{BL}) \right]^2 \sigma_c^2 \\
 & + \left[ \frac{E_{ML}C_{ML}}{30.5c} \right]^2 \sigma_f^2 + \left[ \frac{E_{ML}C_{ML} + E_{MR}C_{MR}}{30.5c} \right]^2 \sigma_d^2 \\
 & + \left[ \frac{S + E_{BL}C_{BL}}{c} \right]^2 \sigma_a^2 + \left[ \frac{a}{c} \right]^2 \sigma_S^2 + \left[ \frac{aC_{BL}}{c} \right]^2 \sigma_{E_{BL}}^2 \\
 & + \left[ \frac{aE_{BL}}{c} \right]^2 \sigma_{C_{BL}}^2
 \end{aligned} \tag{E-14}$$

The probable errors associated with each of the parameters in the equation are then estimated.

#### E.6.1 Errors Associated With the Measurement of Axle Bending Moment Bridge Voltage, $E_{ML}$ and $E_{MR}$

The factors which affect the accuracy of the axle bending moment bridge voltage measurements are the system electrical noise, error due to signal digitization, and the nonlinearity of bridge response. The RMS values of the system noise and digitization errors are the same as reported for other bridge voltage measurements, namely, 7.8 mV and 1.4 mV respectively.

E.6.1.1 Nonlinearity of Bridge Response. Insufficient data were obtained during the calibration tests of the axle bending moment gages to permit determination of the nonlinearity of bridge response. An assumption is made that the RMS error due to non-linearity effects can be estimated as one percent of the full load signal. A typical signal level for the axle bending moment

bridges under moderate lateral wheel load conditions (7000 lbs) would be approximately 730 mV. Therefore, an estimate for the RMS bridge voltage error due to nonlinear effects would be 7.3 mV.

E.6.1.2 Summary of Bridge Voltage Errors. The variances in the errors associated with the bridge signal may then be determined as the sum of the variances associated with the individual factors listed above.

$$\begin{aligned}\sigma_{E_{ML}}^2 &= \sigma_{E_{MR}}^2 = (7.8 \text{ mV})^2 + (1.4 \text{ mV})^2 + (7.3 \text{ mV})^2 \\ &= (10.8 \text{ mV})^2.\end{aligned}$$

E.6.2 Errors Associated With Axle Bending.  
Moment Bridge Calibration Factor,  
 $C_{ML}$  and  $C_{MR}$

Only one source of error is identified with respect to the bridge calibration factor, namely, the variation in the output of the different bridges on the axle. The assumption was made in the analysis of the data that the output of each bridge could be determined from the average bending moment calibration constant. Analysis of the data from the calibration tests showed that the average value of the calibration constant was 510 in-lbs/mV, with an RMS variation of 15 in-lbs/mV.

E.6.3 Error Associated With the Horizontal  
Position of Lateral Wheel/Rail Loads, c

The positions assumed for the line-of-action of the lateral load at the wheel/rail interface and the net lateral load acting on the wheel/axle set are illustrated in Figure 6-30. The vertical position of the lateral wheel/rail load can vary approximately 1/2 inch, ranging from a frictional load on the tread of the wheel to a load acting through a contact point on the side of the flange when the wheel is forced up against the rail. The assumed position of the net lateral load (the difference between the right wheel lateral and the left wheel lateral load) is illustrated at the center line of the axle. It should be obvious that slight movements in the line-of-action about this location

are possible. No data has been found to indicate the variation of this distance. For this analysis the assumption has been made that the RMS deviation of  $c$  is 1/2 inch. This allows a preliminary calculation of the relative importance of different sources of error.

#### E.6.4 Errors Associated With Lateral Positions of Vertical Loads, $a_l$ , $a_r$ , $f$ and $d$

The errors associated with the locations of the vertical loads through the side frame/bearing adapter interface and the wheel/rail contact point are described in Section E.5.4. The values established there for the variance of  $a_l$ ,  $a_r$ , and  $f$  are used in this analysis of lateral wheel load. The parameter  $d$ , the lateral distance between the wheel/rail contact point and the moment gages on the axle (see Figure 6.30) is estimated to have an RMS deviation of 0.75 inches.

#### E.6.5 Error Associated With Static Wheel Load Estimate, $S$

The errors associated with the static wheel load were described in Section E.2.3 where an RMS value of 1,000 lbs. was estimated.

#### E.6.6 Errors Associated With Side Frame Bridge Voltage Measurements, $E_{BL}$

The errors associated with the measurement of  $E_{BL}$  were described in Section E.5.1 where an RMS value of 8.6 mV was estimated.

#### E.6.7 Errors Associated With Side Frame Bridge Calibration Factor, $C_{BL}$

The errors associated with  $C_{BL}$  were described in Section E.5.2 where an RMS value of 0.62 mV/in. was estimated.

#### E.6.8 Side Frame and Axle Measurement of Wheel/Rail Lateral Load, Summary and Discussion

The results from Sections E.6.1 to E.6.7 can be combined according to Equation E.13 to determine the variance from all the effects of the errors associated with the measurement of the load. The derivatives in Equation E.13 serve to relate the variance of the independent parameters in the same units as the lateral wheel load parameter. They are evaluated using the following typical operating magnitudes that were observed during the course of the tests.

$$\begin{aligned} E_{ML} &= 730 \text{ mV} \\ E_{MR} &= 660 \text{ mV} \\ C_{ML} &= C_{MR} = 510 \text{ lb/mV} \\ f &= 58.5 \text{ in.} \\ d &= 14 \text{ in.} \\ c &= 18 \text{ in.} \\ a &= 10.25 \text{ in.} \\ S &= 25,800 \text{ lbs} \\ E_{BL} &= 0 \\ C_{BL} &= 16 \text{ lb/mV.} \end{aligned}$$

Substituting Equation E.14 the variance of the lateral wheel load is calculated to be:

$$\begin{aligned} \sigma_{L_L}^2 &= \left[ \frac{510(44.5)}{18(30.5)} \right]^2 (10.8)^2 + \left[ \frac{730(44.5)}{18(30.5)} \right]^2 (15)^2 \\ &+ \left[ \frac{510(14)}{30.5(18)} \right]^2 (10.8)^2 + \left[ \frac{660(14)}{30.5(18)} \right]^2 (15)^2 \\ &+ \left[ \frac{1}{(18)^2} \right]^2 \left[ \frac{(510)(730)(44.5) - (660)(510)(14)}{30.5} \right. \\ &\quad \left. - 10.25(25,800) \right]^2 (0.5)^2 + \left[ \frac{730(510)}{30.5(18)} \right]^2 (0.75)^2 \\ &+ \left[ \frac{730(510) + 660(510)}{(30.5)(18)} \right]^2 (0.75)^2 + \left[ \frac{25,800}{18} \right]^2 (1.25)^2 \\ &+ \left[ \frac{14}{18} \right]^2 + \left[ \frac{14(16)}{18} \right]^2 (8.6)^2 \end{aligned}$$

$$\begin{aligned}\sigma_{L_L}^2 &= (446 \text{ lb})^2 + (888 \text{ lb})^2 + (140 \text{ lb})^2 + (252 \text{ lb})^2 \\ &\quad + (192 \text{ lb})^2 + (509 \text{ lb})^2 + (968 \text{ lb})^2 + (1792 \text{ lb})^2 \\ &\quad + (778 \text{ lb})^2 + (107 \text{ lb})^2 \\ \sigma_{L_L}^2 &= (2500 \text{ lb})^2 .\end{aligned}$$

The largest source of error is in the estimate for the distance,  $a$ , between the position of the vertical load at the bearing adapter and the wheel/rail contact point. The RMS variation of this distance was estimated to be 1.25 in. If this uncertainty could be reduced the probable error could be significantly reduced.

The next most important error is due to the estimate for the distance,  $d$ , between the position of the axle bending moment gages and the wheel/rail contact point. The third most important source of error is associated with the calibration constant of the axle bending moment bridges. As explained earlier, the accuracy could be improved by using separate calibration constants for each bridge. Also, not enough calibration data was obtained so that nonlinearity effects had to be estimated. The fourth most important source of error was associated with the static wheel load assumption. This problem has been discussed in earlier sections.

Note that the effect of the error of  $c$ , the distance between the lateral journal load and the lateral wheel/rail load is relatively small (variance,  $[192 \text{ lb}]^2$ ) so that the estimate of the RMS variation of 0.5 in. for  $c$  does not have a significant influence on the error analysis.

## APPENDIX F

### REPORT OF NEW TECHNOLOGY

This report includes the development and evaluation of instrumentation and data processing hardware and software for making wheel/rail load measurements. Laboratory and field experiments have resulted in an improved rail-mounted circuit for measuring lateral wheel/rail loads, and this improved circuit is currently in use at the Transportation Test Center. The use of a finite-element computer model in developing an instrumented wheelset for measuring vertical and lateral wheel loads represents a unique contribution to this area of technology. Similarly, the advances in data processing developed under this program will provide an improved capability for handling wayside wheel/rail load measurements.

## REFERENCES

- [3-1] Shioya, A., et al, "On the Test of a Device for the Measurement of Static Imbalance of Wheel Load as a Part of Automated Arrival Inspection System in Freight Car Yard", Quarterly Reports RTRI, Vol. 15 No. 3, 1974, pp 170-171.
- [3-2] Johnson, M. R., "Summarization and Comparison of Freight Car Truck Load Data", ASME Paper No. 77-WA/RT-3, November 1977.
- [3-3] Ahlbeck, D. R., et al, "Evaluation of Analytical and Experimental Methodologies for the Characterization of Wheel/Rail Loads", Report No. FRA-OR&D-76-276, November 1976.
- [3-4] Satoh, Y., "Dynamic Effect of a Flat Wheel on Track Deformation", Bulletin of Permanent Way Society of Japan, Vol 12, No. 7, July 1964.
- [3-5] 20th Monthly Progress Report, Contract No. DOT-TSC-1051, Appendix A. On file at DOT/TSC March 14, 1977.
- [3-6] Broch, J. T., "Effects of Spectrum Non-Linearities Upon the Peak Distribution of Random Signals", B&K Technical Review, No. 3, 1963, pp 5-31.
- [5-1] Ahlbeck, D. R., Harrison, H., Prause, R. H., and Johnson, M. R., "Evaluation of Analytical and Experimental Methodologies for the Characterization of Wheel/Rail Loads", Report No. FRA-OR&D-76-276, November 1976, pp 60-65.
- [5-2] Ibid, pp 66-71.
- [5-3] Prause, R. H., et al, "An Analytical and Experimental Evaluation of Concrete Crosstie and Fastener Loads", Report No. FRA/ORD-77/71, December 1977.
- [5-4] Johnson, M. R., "Analysis of Railroad Car Truck and Wheel Fatigue, Part 1, Service Load Data and Procedures for the Development of Fatigue Performance Criteria", Report No. FRA-OR&D-75-68, May 1975.
- [5-5] Johnson, M. R., "Summarization and Comparison of Freight Car Truck Load Data", ASME Paper No. 77-WA/RT-3, November 1977.
- [6-1] Ahlbeck, D. R., and Doyle, G. R., "Comparative Analysis of Dynamics of Freight and Passenger Rail Vehicles", Report No. FRA/ORD-77/04, November 1976.
- [6-2] Corbin, J., et al, "Statistical Representations of Track Geometry", Final Report, Vol II, Appendixes, FRA/ORD-80/1,II, January 1980.
- [6-3] Bendat, J. S. and Piersol, A. G., Measurement and Analysis of Random Data, John Wiley & Sons, 2nd Edition, 1972, pp 188 and 210.

- [6-4] Cooperrider, N. K., "Theoretical and Experimental Research on Freight Car Lateral Dynamics", Paper presented at Heavy Haul Railways Conference, Perth, Western Australia, September 1978, Session 310, Paper E.5, Work under Contract DOT-OS-40018.
- [6-5] Peterson, L. A., Freeman, W. H. and Wandrisco, J. M., "Measurement and Analysis of Wheel-Rail Forces", ASME Paper No. 71-WA/RT-4, November 1971.
- [7-1] Harrison, H. D. and Ahlbeck, D. R., "A Laboratory Evaluation of a Lateral Rail Force Measuring Circuit", Summary Report, Battelle-Columbus Laboratories. On file at DOT/TSC, May 23, 1978.

**Measurements of Wheel/Rail Loads on Class  
5 Track (Final Report), 1980**

US DOT, FRA, Donald R Ahlbeck, Milton R  
Johnson, Harold D Harrison, James M Tuten

PROPERTY OF FRA  
RESEARCH & DEVELOPMENT  
LIBRARY

OWNER

DATE

100-413-111

100-413-111

100-413-111

100-413-111